



**HAL**  
open science

# Uptake and reactivity of sulfur dioxide gas onto Icelandic volcanic dusts

Darya Urupina

► **To cite this version:**

Darya Urupina. Uptake and reactivity of sulfur dioxide gas onto Icelandic volcanic dusts. Theoretical and/or physical chemistry. Ecole nationale supérieure Mines-Télécom Lille Douai, 2020. English. NNT : 2020MTLD0022 . tel-03663357

**HAL Id: tel-03663357**

**<https://theses.hal.science/tel-03663357>**

Submitted on 10 May 2022

**HAL** is a multi-disciplinary open access archive for the deposit and dissemination of scientific research documents, whether they are published or not. The documents may come from teaching and research institutions in France or abroad, or from public or private research centers.

L'archive ouverte pluridisciplinaire **HAL**, est destinée au dépôt et à la diffusion de documents scientifiques de niveau recherche, publiés ou non, émanant des établissements d'enseignement et de recherche français ou étrangers, des laboratoires publics ou privés.

N° d'ordre :

IMT LILLE DOUAI



UNIVERSITE DE LILLE



## THESE

présentée en vue  
d'obtenir le grade de

## DOCTEUR

en

Discipline : Chimie théorique, physique, analytique  
Spécialité : Optique et Lasers, Physico-chimie, Atmosphère

par

**Darya URUPINA**

DOCTORAT DE L'UNIVERSITE DE LILLE  
DELIVRE PAR IMT LILLE DOUAI

Titre de la thèse :

### **Uptake and reactivity of sulfur dioxide gas onto Icelandic volcanic dusts**

Soutenue le 15 décembre 2020 devant le jury d'examen :

<b>Rapportrice</b>	Paola FORMENTI	DR CNRS, LISA, CNRS / Université Paris Est Créteil
<b>Rapporteur</b>	Yuri BEDJANIAN	DR CNRS, ICARE, CNRS / Université d'Orléans
<b>Membre</b>	Karine DEBOUDT	Professeure, LPCA, Université du Littoral Côte d'Opale
<b>Membre</b>	Denis PETITPREZ	Professeur, PC2A, Université de Lille
<b>Membre</b>	Antoine ROUSSEAU	DR CNRS, LPP, CNRS / Ecole Polytechnique
<b>Encadrant de thèse</b>	Emmanouil ROMANIAS	Maitre Assistant, SAGE, IMT Lille Douai
<b>Directeur de thèse</b>	Frédéric THEVENET	Professeur, SAGE, IMT Lille Douai

Laboratoire d'accueil : CERI-EE, Unité de Recherche SAGE, IMT Lille Douai

Ecole Doctorale SMRE 104 (ULille, UPHF, Centrale Lille, Chimie Lille, IMT Lille Douai)



## **Acknowledgements**





*“Learning never exhausts the mind.”*

*Leonardo da Vinci*

I would like to dedicate this work to the wonderful teachers that guided the journey to this thesis. Especially, I'm thankful to Dr Sargon Albazi for his help and precious advice. Many thanks go to my first chemistry teacher Valentina Nikolaevna Fomenko and my Triton College professor Dr Preet Saluja. I'm especially grateful to my supervisors Dr Frederic Thevenet and Dr Emmanouil Romanias for making me a part of the team and letting me explore the subject in the way that was fulfilling and challenging, but never overpowering and suffocating. I would like to acknowledge my colleague Dr Jerome Lasne for his help with both practical aspects of this thesis and administrative challenges of doing a PhD in France.

Pursuing a doctoral degree in France was also about discovery of a new country and in this context I'm grateful to my French teacher Ioana Thiery and my colleagues, especially Raphael Brun, for helping me overcome the language barrier and for being supportive in my cultural quest.

I am also very thankful to my friends here in France and in other parts of the world for their support and for always believing in me. Finally, I am forever grateful to my family for never stopping me in my adventures. Even though far away, I know that I can count on you.

## **Thesis Outline**

General Introduction.....3

Chapter I. Context, state of the art, objectives and strategy.....9

Chapter II. Materials and methods.....73

Chapter III. Investigation of the uptake of SO<sub>2</sub> on natural v-dust: gas-phase approach.....103

Chapter IV. *In-situ* monitoring of SO<sub>2</sub> uptake on natural v-dust by DRIFT spectroscopy: toward surface reaction pathways.....135

Chapter V. HPLC method development and validation for the quantification of sulfites and sulfates on the surface of natural dusts.....155

Chapter VI. How atmospherically relevant is to use mineral proxies to mimic the reactivity of natural dust samples? A reactivity study using SO<sub>2</sub> as probe molecule.....187

Chapter VII. Investigating the distributions of sulfites and sulfates on the surface of natural volcanic dusts.....205

Chapter VIII. Connections between the three experimental approaches: coated wall flow-tube, DRIFT optical cell, and HPLC.....231

General conclusions and perspectives.....243

Valorization.....259

Annex 1.....251

Annex 2.....254

## **General Introduction**



## Environmental context

The heterogeneous interactions of gas-phase species with solid surfaces is a crucial research field to understand the chemical evolution of the atmosphere of Earth. Explosive volcanic eruptions are powerful events that have a capacity to alter Earth's climate. They provide an ample environment for heterogeneous interactions. The development of volcanic plumes and the subsequent transport of volcanic dusts and gasses in the atmosphere are widely addressed. However, these atmospheric systems are not studied from a heterogeneous physical chemistry point of view, while the budget of volcanic gasses, especially SO<sub>2</sub> can be considerably influenced by reactive uptake processes on atmospheric aerosols, especially volcanic dusts. Thus, one area that could particularly benefit from understanding heterogeneous interactions is climate modelling. But, most importantly, this research contributes to the understanding of heterogeneous chemistry occurring in the Earth's atmosphere.

Volcanic dust is a highly variable source of natural particles in the atmosphere, and during the period of high volcanic activity it can provide a large surface for heterogeneous interactions with other atmospheric compounds. Emissions from volcanic eruptions range from 33 million tons (Mt) on an average year to over 100,000 Mt of ash after a major volcanic eruption, as was the case for the eruption of Mount Tambora in 1815. With respect to atmospheric chemistry the most significant impact would be expected to come from smaller particles as they can be carried over thousands of kilometers before eventually being deposited onto the land or the ocean.

Iceland is considered to be one of the most volcanically active areas on the planet. There are about 30 active volcanic systems and volcanic eruptions occurring every 3-5 years on average. Frequent dust events in Iceland transport dust over long distances, often exceeding 2,500 km, towards High Arctic (>80° N) and Europe. Located only 1000 km from mainland Europe, it makes a particularly interesting case study due to its proximity to densely populated European countries.

In this research a greater understanding of the role of interactions of SO<sub>2</sub> gas with volcanic particles is pursued through focused laboratory studies in order to better understand fundamental processes involved. **This thesis has a multifaceted approach to address specifically the interactions of SO<sub>2</sub> gas with Icelandic volcanic dust.** A brief description of the content of each chapter of the manuscript is given below.

This work was achieved in the frame of Labex CaPPA, funded by ANR through the PIA under contract ANR-11-LABX-0005-01, and CPER CLIMIBIO project, both funded by the Hauts-de-France Regional Council and the European Regional Development Fund (ERDF). The author acknowledges IMT Lille Douai for funding this PhD.

## Structure of this Ph.D. thesis

In Chapter 1, an overview of the volcanism in relation to atmospheric chemistry is discussed. Next, fundamentals of heterogeneous chemistry are introduced. Finally, the objectives of the thesis and the structure of the manuscript are defined.

In Chapter 2, the origins and the characterization of five volcanic Icelandic dusts and other samples of interest used during that work are detailed. A second part of this chapter is dedicated to the experimental strategy and experimental methods employed to investigate the heterogeneous interactions of the volcanic dust with SO<sub>2</sub> gas.

In Chapter 3, the uptake of 75 ppb SO<sub>2</sub> gas by five Icelandic volcanic dusts is investigated under atmospherically relevant conditions using a coated-wall flow-tube reactor. More specifically, steady state uptake coefficients and the transient number of molecules initially taken up are experimentally determined. In addition, the influence of humidity and UV light on the uptake of SO<sub>2</sub> gas are thoroughly studied. Finally, atmospheric implications are addressed and discussed.

In Chapter 4, the formation of the surface sulfur species is monitored by DRIFTS using Hagavatn as a representative volcanic dust sample and employing 175 ppm SO<sub>2</sub>. As a result of these investigations and based on the literature, a mechanism for the formation of surface sulfur-based species is proposed. The role of humidity on the uptake process is assessed by performing the DRIFTS experiments under dry conditions and 30% RH.

In Chapter 5, to quantify the amount of sulfur-based products formed on the surface of volcanic dusts and to study the kinetics of the transformation, a simple, accurate and precise reversed-phase liquid chromatography method is developed and validated. The developed method can be used both for laboratory studies and for field measurements.

In Chapter 6, the question of how atmospherically relevant is the use of proxies to mimic the reactivity of natural dust samples is addressed. For this matter, the sample pool is enlarged by introducing in addition to the five volcanic dusts, three desert dusts and a number of mineral oxides and clays commonly used as proxies. The samples are aged for one hour with 175 ppm SO<sub>2</sub> under ambient conditions.

In Chapter 7, the influence of humidity and elemental composition on the formation of sulfur species on the surface of five volcanic dusts and three desert dusts after ageing the samples with 175 ppm SO<sub>2</sub> are investigated using the developed HPLC method. Next, the time profiles of sulfur species obtained for up to 24 hours are constructed and the stability of the formed species is discussed. Finally, the validity of ageing



at elevated concentrations of 175 ppm SO<sub>2</sub> is addressed by performing a long-term 5-day ageing of a selected Myrdalssandur dust at 75 ppb.

In Chapter 8, the consistency of the different results obtained with contrasted instrumental techniques during this work, such as flow tube, DRIFTS, and HPLC, is discussed. This final part aims at taking a step back to evaluate the relevant techniques or groups of techniques to address accurately a heterogeneous atmospheric system.



2010 Eruption of Iceland's Eyjafjallajökull volcano. Image Credit: NASA



Tongariro National Park, New Zealand Photo by Jens Johnsson on Unsplash



Acatenango, Guatemala Photo by Caitlin Wynne on Unsplash



## **Chapter I. Context, state of the art, objectives and strategy**

## Table of content of Chapter 1

1	Volcanic eruptions.....	16
1.1	Volcanoes .....	16
1.2	Volcanic Conduits and Plumes .....	20
2	Volcanic ash.....	22
2.1	Properties of volcanic ash.....	22
2.1.1	Composition.....	22
2.1.2	Size distribution .....	23
2.2	Impact of volcanic ash on global processes.....	24
2.2.1	Impact on stratospheric and tropospheric chemistry.....	24
2.2.2	Impact on climate.....	25
2.2.3	Other impacts.....	26
3	Gasses emitted after volcanic eruptions: focus on SO <sub>2</sub> .....	26
3.1	Impact of volcanic gasses on global processes.....	28
3.1.1	Impact of volcanic gasses on stratospheric and tropospheric chemistry.....	28
3.1.2	Impact of volcanic gasses on climate.....	29
3.1.3	Impact of volcanic gasses on health.....	29
4	Iceland: a study-case?.....	29
5	Fundamentals of heterogeneous reactions.....	31
5.1	Physical chemistry approach .....	31
5.1.1	Models for adsorption description .....	33
5.1.2	Experimentally determined kinetic parameters.....	35
5.2	Laboratory techniques for studying heterogeneous reactions.....	36
5.2.1	Coated wall flow-tube reactor.....	36
5.2.2	Knudsen cell .....	38
5.2.3	Diffuse reflectance infrared Fourier transform spectroscopy .....	40
5.2.4	Reactors using suspended aerosol and typical instrumentation .....	42

5.3	Laboratory techniques for surface characterization.....	45
5.3.1	Scanning electron microscopy (SEM) .....	46
5.3.2	BET .....	46
5.3.3	Inductively coupled plasma mass spectrometry.....	46
5.3.4	X-ray photoelectron spectroscopy .....	46
5.3.5	X-ray powder diffraction spectroscopy .....	47
6	Groundwork for investigation of the interactions of volcanic dust with SO <sub>2</sub> volcanic gas.....	48
6.1	Review of SO <sub>2</sub> interactions with single metal oxides, CaCO <sub>3</sub> and natural dust samples .....	48
6.1.1	γ-Al <sub>2</sub> O <sub>3</sub> .....	49
6.1.2	α-Al <sub>2</sub> O <sub>3</sub> and MgO .....	51
6.1.3	Fe <sub>2</sub> O <sub>3</sub> .....	52
6.1.4	TiO <sub>2</sub> .....	52
6.1.5	CaCO <sub>3</sub> .....	52
6.2	Oxidation of sulfites to sulfates .....	52
6.3	Role of humidity .....	54
6.4	Role of the UV light .....	56
6.4.1	Photocatalysis .....	56
6.4.2	Photochemistry .....	57
6.5	Influence of SO <sub>2</sub> -covered particles on other species .....	58
6.6	Atmospheric implications.....	58
6.7	Limitations of the present research and directions for further work.....	59
7	Thesis objectives and strategy.....	64
	References .....	66

## List of Tables of Chapter 1

Table 1 The seven types of volcanoes (McCall, 2004) .....	17
Table 2 Criteria for Estimation of the Volcanic Explosivity Index (VEI) (“The volcanic explosivity index (VEI) an estimate of explosive magnitude for historical volcanism,” 1982) .....	18
Table 3 Major types of magma (Langmann, 2013) .....	19
Table 4 Surface composition of volcanic ash analyzed by XPS. Adapted from Maters et al. (Maters et al., 2016) ....	22
Table 5 Average High-Temperature Volcanic gas Composition in Mole%. Adapted from Hoshyaripour et al. (Hoshyaripour et al., 2012) .....	27
Table 6 Reactive surface sites on the volcanic ash. Adapted from E.C. Maters (Maters et al., 2016) .....	48
Table 7 Possible nature of adsorbed species. Adapted from Datta et al., 1985 and Lo et al., 2010 .....	50
Table 8 IR vibration modes of water using FT-IR. Adapted from Grassian et al., 2003.....	54
Table 9 Methods and preferred uptake values for reactions of SO <sub>2</sub> with mineral dust and various mineral oxides ....	61

## List of Figures of Chapter 1

Figure 1: The earliest known record of a volcanic eruption. Çatalhöyük mural in central Turkey is thought to represent a volcanic eruption of Hasan Dağ Volcano dating around 6,200 BC. Adapted from “Mountains of fire: the nature of volcanoes” (Decker and Decker, 1991). .....	14
Figure 2: Illustration of the various processes involved in a Plinian eruption. Adapted from “Expansion and quenching of vesicular magma fragments in Plinian eruptions” (Kaminski and Jaupart, 1997). .....	20
Figure 3: Model of the Plinian volcanic eruption after 30 min. Temperature distribution in degrees Celsius. Adapted from “Injection of gases into the stratosphere by explosive volcanic eruptions” (Textor et al., n.d.). .....	21
Figure 4: Ash particle size distribution. Adapted from (Langmann, 2013). .....	23
Figure 5: Ash plume from Iceland’s Eyjafjallajökull Volcano, April 15 2010 (“Ash Plume across the North Atlantic,” 2010) .....	30
Figure 6: Potential energy of chemisorption and physisorption vs. distance from surface. Adapted from “How does adsorption work?” (“How does adsorption work?,” n.d.). .....	32
Figure 7: Langmuir adsorption isotherm, adapted from “Langmuir adsorption model” (“Langmuir adsorption model,” 2018) .....	34
Figure 8: Schematic drawing of a coated wall flow tube reactor. ....	36
Figure 9: Schematic drawing of a Knudsen Cell. ....	38
Figure 10: Schematic drawing of a DRIFTS apparatus. ....	40
Figure 11: Absorption difference spectra recorded during the reaction of mineral dust with 20 ppm of SO <sub>2</sub> . Product spectra (a) after addition of SO <sub>2</sub> , (b) after pumping sample for 10 min without SO <sub>2</sub> , (c) after pumping sample overnight and (d) after heating of sample to 373 K. Adapted from “The kinetics and mechanism of SO <sub>2</sub> oxidation by O <sub>3</sub> on mineral dust” (Ullerstam et al., 2002). .....	42
Figure 12: Components of an HPLC system. Adapted from “HPLC Troubleshooting Guide” (“HPLC Troubleshooting Guide,” n.d.). ....	44
Figure 13: Schematic of the Aerodyne aerosol mass spectrometer (AMS). Adapted from “Aerosol mass spectrometry” (“Aerosol mass spectrometry,” 2020). .....	45
Figure 14: Mechanism of adsorption of SO <sub>2</sub> , NO and NH <sub>3</sub> on the surface of Fe(0.1)-Mn(0.4)/TiO <sub>2</sub> catalytic surface. Adapted from “DRIFT Study of the SO <sub>2</sub> Effect on Low-Temperature SCR Reaction over Fe–Mn/TiO <sub>2</sub> ” (Jiang et al., 2010). .....	58

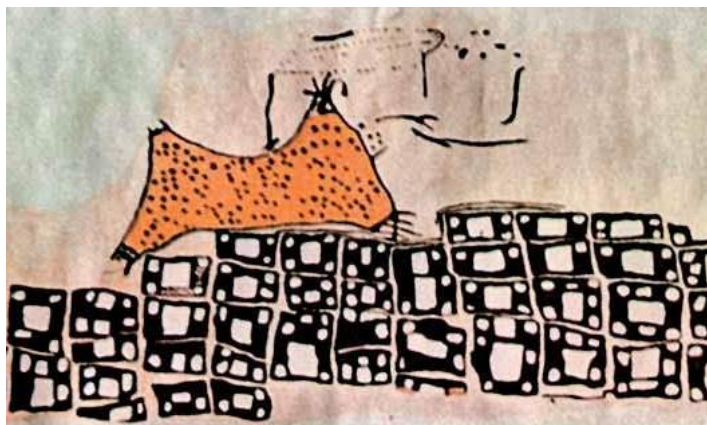


*Figure 1: The earliest known record of a volcanic eruption. Çatalhöyük mural in central Turkey is thought to represent a volcanic eruption of Hasan Dağ Volcano dating around 6,200 BC. Adapted from “Mountains of fire: the nature of volcanoes” (Decker and Decker, 1991).*

Volcanic eruptions have always fascinated and intrigued humankind. Countless myths, based on the volcanic events witnessed by many cultures, provide meaning, explanation and soothing for the observed catastrophic events (Palmer, n.d.). Through centuries volcanoes are feared, respected and venerated. Hence, an African volcano Oldonyo-Lengai, literally meaning “Mountain of God” is cherished by Maasai tribe as the giver of all good things (“Volcano Myths and Rituals,” 2017). In Hawaii, volcanic eruptions are seen as beneficial and viewed as an act of creation (“Volcano Myths and Rituals,” 2017). In this respect, Hawaiians might not be too far away from the reality. As inhospitable as volcanic environment might seem, it was recently suggested that it contains the very ingredients necessary for the emergence of the first organic molecules - a fundamental step in the prebiotic assembly of life. According to this theory, volcanic lightning can serve as an energy source, porous volcanic particles can provide a large reactive surface, while volcanic plumes themselves are rich in gases necessary for the abiotic synthesis (Springsklee, 2020). In a more widely accepted scenario for the origin of life, hydrothermal environments (e.g. the presence of fresh mafic minerals, such as olivine, in contact with liquid water) are the most likely conditions to promote synthesis of organic molecules (Camprubí et al., 2019).

Volcanic eruptions vividly demonstrate how fragile humans are when forced to face the power of Nature. Large volcanic eruptions of the past have significantly influenced Earth’s climate by injecting vast amounts of particulate matter and volcanic gases into the atmosphere. Volcanic emissions can cause both regional and global changes to climate by affecting monsoon circulation, causing either excess or limited rainfall thus leading to floods and droughts (Stevenson et al., 2003), (Highwood and Stevenson, 2003), (“Tambora and the ‘Year Without a Summer’ of 1816,” 2016). Failed crops often result in famine and civil unrest. At times, in the aftermath the volcanic eruptions, whole cultures vanish or people are forced to migrate (Highwood and Stevenson, 2003). Volcanic eruptions comprise one of the most significant natural



hazards threatening people living in the proximity, as well as effecting livelihoods of the humankind on the global scale. Significant volcanic eruptions of the past vividly demonstrate how closely Earth and human systems are connected to each other.

The oldest known record of a volcanic eruption is a wall painting at Çatalhöyük, a village in central Turkey. It is thought to represent a volcanic eruption of Hasan Dağ Volcano dating around 6,200 BC (Figure 1) (Decker and Decker, 1991). One of the first written records of meteorological data is preserved in Babylonian astronomical diaries written on cuneiform tablets spanning from 652 to 61 BC and now housed in the British Museum. These records, unparalleled in resolution and scope until early modern period (weather observations are given in sub-daily resolution for all seasons), provide information about wind directions, atmospheric clarity, temperature, and precipitation, etc. together with socio-economic data, such as agricultural prices and major societal stresses (Ludlow et al., 2020). In the view of recently available and much-improved ice-core chronologies of explosive volcanism for the first millennium BC, scientists were able to link extreme weather anomalies and climatic shocks described in these diaries to major ice-core volcanic signals (Ludlow et al., 2020). Here is a representative excerpt from Astronomical diary dating 173 BC: “The 24th, the north wind blew, the cold became severe... around noon, the disk of the sun looked like that of the moon...” (Ludlow et al., 2020). According to Sigl et al. the majority of such observations were found to occur closely in time with volcanic deposition on the revised ice-core timescale (Sigl et al., 2015). Volcanic eruptions were implicated as catalysts in the major 6th century pandemics, famines, and socioeconomic disruptions in Eurasia and Mesoamerica (Sigl et al., 2015). Overall, after investigating volcanic records for the past 2,500 years, cooling was proportional to the magnitude of volcanic forcing and persisted for up to ten years after some of the largest eruptive episodes (Sigl et al., 2015).

On June 8, 1783, a 27-kilometer-long fissure tore through the highlands in southeastern Iceland marking the beginning of one of the major eruptive events in human history. The 8-month long Laki fissure eruption in Iceland in 1783-1784 released approximately 15 km<sup>2</sup> of basaltic magma and 122 million tons of sulfur dioxide, 60 % of which got emitted in the first six weeks of the eruption (Stevenson et al., 2003), (Highwood and Stevenson, 2003). Dry fog and haze covered much of the Northern Hemisphere and reached as far as Asia (Highwood and Stevenson, 2003). Rise in the concentration of SO<sub>2</sub> caused respiratory difficulties and troublesome headaches (Schmidt et al., 2011). Crop failure and livestock loss lead to famine in Iceland, where about 21 % of the population died (Schmidt et al., 2011). Famine and plague pandemics ravaged across the Middle East (Stothers, 1999). One study linked this powerful volcanic eruption in Iceland to the dying out of the entire Inuit population in Northwest Alaska (Highwood and Stevenson, 2003).

On April 10, 1815 the Indonesian island of Sumbawa became the epicenter of the largest volcanic eruption in the last millennium – eruption of Mount Tambora. The 1815 eruption of Mount Tambora in

Indonesia produced a staggering 100,000 million tons of primary aerosol in a single eruption killing around 100,000 people in Indonesia and as many as 200,000 worldwide (Andreae, 1995), (“Tambora and the ‘Year Without a Summer’ of 1816,” 2016). The eruption lowered the global temperature by 1 to 1.5 °C (Savarino, 2020). The year of the eruption in the Northern Hemisphere was known as a year without summer, snow storms were witnessed in New England as late as June (“Tambora and the ‘Year Without a Summer’ of 1816,” 2016). Climate anomalies brought crop failure leading to the worst famine in Europe in the 19<sup>th</sup> century followed by epidemics of cholera and typhus (“Tambora and the ‘Year Without a Summer’ of 1816,” 2016).

A number of eruptions marked 20<sup>th</sup> century. Eruption of Mount Pinatubo on June 15, 1991 injected 20 millions of tons of sulfur dioxide into the stratosphere lowering the average global temperature by 0.5 °C, an effect that lasted for 2 years (Andreae, 1995), (Durant et al., 2010). More recently, Eyjafjallajökull released  $8 \pm 4$  million tons of volcanic ash and 0.39 million tons of SO<sub>2</sub> in the upper troposphere and lower stratosphere, which led to prolonged disruptions of aviation and billions of dollars in economic loss by the transportation industry (Thorsteinsson et al., 2012), (Schmidt et al., 2014), (Gislason et al., 2011). Concerns about health risks were particularly high due to contamination of drinking water with fluoride (Gislason et al., 2011).

At this point I would like to invite the reader to take a closer look at what is happening during volcanic eruption. In the following sections, I’ll investigate the lifecycle of the volcanic emissions in both particular and gaseous phase, paying closer attention to the interaction of volcanic ash particles with sulfur dioxide, one of the most abundant gases found in the plume of the volcano.

## **1 Volcanic eruptions**

All the matter present on Earth can be viewed as a collection of 94 individual elements that in their original form or in the form of various molecules migrate continuously from one reservoir to another in the process known as geochemical cycling. Reservoirs include atmosphere, hydrosphere, biosphere, soil, and lithosphere. Most of the mass of the planet is concentrated in the Deep Earth part of the lithosphere which has a very limited exchange with the other reservoirs. Volcanic eruptions provide a main way for such exchange (Daniel J. Jacob, 1999).

### **1.1 Volcanoes**

Volcanoes are major components of the Earth’s surface geology. They do not occur everywhere on Earth, but are most often situated along the edges of the rigid lithospheric plates that move along the Earth’s surface at the speed of few centimeters per year (McCall, 2004). In relationship to each other, lithospheric

plates can either move away from each other and thus diverge or converge and collide. When a continental plate collides with an oceanic plate, it forces the latter underneath itself creating subduction zone. Where two continental plates collide with each other they are forced upwards creating fold mountains, such as Himalayas. Most volcanoes on Earth are found in subduction zones. Yet, another type of volcanoes found on our planet is related to neither converging nor diverging plates and is a result of a hot spot, which is a hot narrow plume of molten material in the Earth's mantle (McCall, 2004).

At any given moment as many as 20 volcanoes around the globe might be erupting (Langmann, 2013). Eruption can be defined as a sudden occurrence of a violent discharge of gases and volcanic materials. There are two major types of volcanic eruptions: fissure eruption and central eruption. In fissure eruptions, lava flows through long linear volcanic vents. This type of eruption is usually not explosive. In fissure eruptions, fluid basaltic lava forms extensive plateaus. The Laki eruption in 1783 was of this type. More commonly though, volcanoes form a crater with a central vent through which volcanic material is emitted. There are seven types of volcanoes classified according to the type of the eruption in Table 1. One must keep in mind though that most volcanoes show some deviation from the classical definition (McCall, 2004).

*Table 1: The seven types of volcanoes (McCall, 2004)*

<b>Type</b>	<b>Characteristics</b>
Icelandic	Fissure eruptions, releasing free-flowing basaltic magma; quiet, gas-poor; great volumes of lava flowing as sheets over large areas to build plateaus
Hawaiian	Fissure, caldera, and pit-crater eruptions; mobile lavas with some gas; quiet to moderately active eruptions, occasional rapid emissions of gas ; mainly basaltic; minor amounts of ash, builds up lava domes
Strombolian	Stratovolcanoes with summit craters; moderate, rhythmic to nearly continuous explosions, resulting from spasmodic gas escape, light colored clouds, mostly steam reach to moderate heights
Vulcanian	Stratovolcanoes with central vents; associated lavas more viscous; lavas form crust over vents between eruptions, trapping the gas below its surface; explosive eruptions; dark ash-laden clouds, convoluted and cauliflower-shaped rise vertically to moderate heights, depositing ash along the flanks of the volcano
Vesuvian	Stratovolcanoes; extremely violent expulsion of gas-charged magma; vent tends to be emptied to a considerable depth; repeated cauliflower clouds that reach great heights and deposit ash
Plinian	More violent than Vesuvian eruption; last major phase is uprush of gas that carries cloud vertically upward in a column for kilometers; narrow at the base but expands outwards at upper elevations; clouds generally low in ash
Peléan	Results from high viscosity lava and delayed explosiveness; conduit of stratovolcano is usually blocked by dome or plug; gas and lava escape from lateral openings or by destruction of upper plug; ash, gas and blocks move with high velocity downslope in one or more blasts

A useful way to evaluate volcanic explosion was proposed by Chris Newhall of the US Geological Society and Stephen Self at the University of Hawaii who devised a Volcanic Explosivity Index in 1982, summarized in Table 2 (“The volcanic explosivity index (VEI) an estimate of explosive magnitude for historical volcanism,” 1982).

Table 2: Criteria for Estimation of the Volcanic Explosivity Index (VEI) (“The volcanic explosivity index (VEI) an estimate of explosive magnitude for historical volcanism,” 1982)

General description	Non-explosive	Small	Moderate	Moderate-large	Large	Very large			
	0	1	2	3	4	5	6	7	8
Volume of tephra	<10 <sup>4</sup>	10 <sup>4</sup> -10 <sup>6</sup>	10 <sup>6</sup> -10 <sup>7</sup>	10 <sup>7</sup> -10 <sup>8</sup>	10 <sup>8</sup> -10 <sup>9</sup>	10 <sup>9</sup> -10 <sup>10</sup>	10 <sup>10</sup> -10 <sup>11</sup>	10 <sup>11</sup> -10 <sup>12</sup>	>10 <sup>12</sup>
Cloud column height (km)*	<0.1	0.1-1	1-5	3-15	10-25	>25			
Qualitative description	Gentle, effusive		Explosive		Cataclysmic, paroxysmal, colossal				
Classification	Hawaiian		Vulcanian			Ultra-Plinian			
		Strombolian			Plinian				
Tropospheric injection	minor	minor	moderate	substantial					
Stratospheric injection	none	none	none	possible	definite	significant			
Maximum explosivity	lava flows	explosion or nuée ardente							
		phreatic							
	dome or mudflow								
Total historic eruptions	487	623	3176	733	119	19	5	2	0

\* For VEI 0-2 data are in km above crater; for VEI 3-8 data are in km above the sea level.

The explosiveness of the volcano can be linked to the explosivity of magma (Geishi, 2004). Explosive eruptions occur when magma containing dissolved gases rises rapidly through the conduit. As pressure rapidly decreases the magma-gas mixture accelerates through the vent till it leaves it in explosive manner (Langmann, 2013). Lava is usually a product of a non-explosive moderate eruption. By contrast, volcanic ash is produced as a result of explosive eruption. Explosive magma depends on many factors, such as viscosity, decompression speed, and gas content (Geishi, 2004). Viscous magma contains a higher amount of silica that is able to form chain-like structures (Geishi, 2004). Elements such as magnesium can disrupt those chains, so that magma becomes less viscous. Water has a similar effect on the magma viscosity (Geishi, 2004). Viscosity is also controlled by the temperature making the magma of higher temperature more fluid. There are three major types of magma: basaltic, andesitic, and rhyolitic. They differ in viscosity, melting temperature and amount of volatile gases content (Table 3) (Langmann, 2013). The most viscous magma is rhyolite, which is similar in composition to granite (McCall, 2004). Higher fragmentation of magma and surrounding rock during eruption is observed with magma of rhyolitic composition as it contains

the highest amount of silica and dissolved gas (Kaminski and Jaupart, 1997). As a result, it produces the most explosive eruptions and thus the highest amount of fine volcanic ash. Having said that, highly explosive Plinian basaltic eruptions do occur and can be induced by rapid crystallization due to high undercooling and high decompression rates of the ascending magma (Arzilli, 2020). This implies that all types of volcanic systems on Earth have the potential to produce powerful explosive eruptions.

*Table 3: Major types of magma (Langmann, 2013)*

<b>Magma type</b>	<b>SiO<sub>2</sub> (wt %)</b>	<b>(°C)</b>	<b>Viscosity and gas content</b>	<b>Amount of volcanic ash</b>
Basaltic	45–55	1000–1200	Low	Low
Andesitic	55–65	800–1000	Intermediate	Intermediate
Rhyolitic	65–75	650–1000	High	High

In addition to explosive eruptions a significant amount of volcanic ash can be created as a result of phreatomagmatic eruptions and pyroclastic flows. A phreatomagmatic eruption is a result of magma interaction with external water, such as a glacier or a crater lake. Initially, water chills the magma interface, which shatters as a result. Water then penetrates through the shattered glass and turns into superheated steam that further shatters the magma. The process ends in a violent explosive eruption that creates particularly fine-grained ash. Pyroclastic flows are a result of the collapse of the part of the volcano leading to high-speed tephra flows that contribute to fragmentation through collision and milling processes (Langmann, 2013).

## 1.2 Volcanic Conduits and Plumes

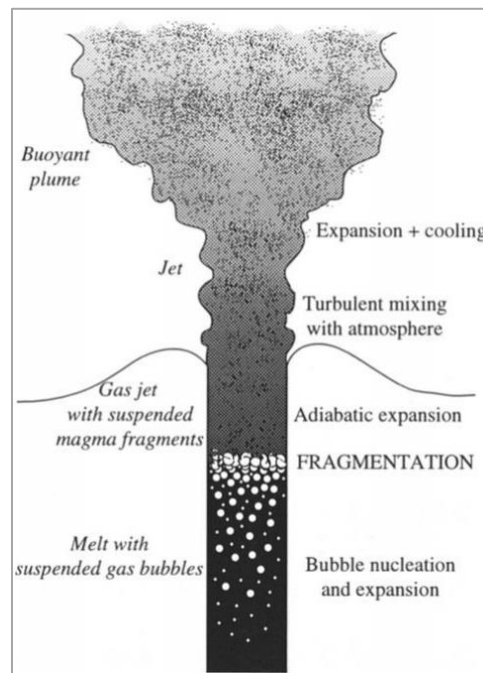


Figure 2: Illustration of the various processes involved in a Plinian eruption. Adapted from “Expansion and quenching of vesicular magma fragments in Plinian eruptions” (Kaminski and Jaupart, 1997).

Figure 2 illustrates various processes involved in an explosive eruption. Gas-tephra mixture is generated by fragmentation at some depth in the conduit. Fragmentation depth varies from several hundred meters to almost 4000 meters (Ayris et al., 2013). Above the fragmentation level in subterranean conduit gas-tephra mixture undergoes pressure release and small amounts of cooling due to adiabatic expansion. After leaving the conduit the mixture is subjected to large amounts of cooling because of mixing with cold atmospheric air (Kaminski and Jaupart, 1997). Thus, the first stage in the existence of ash can be characterized by the conditions of constant high temperature of 650-1200 °C and a high decompression rate of 0.7 to 10 MPa/s, while the second stage is characterized by variable temperature (1200 to -70°C) and pressure (Langmann, 2013), (Kaminski and Jaupart, 1997).

While magma makes its way to the surface through the volcanic conduit, different processes happen: fragmentation, quenching of glass material contained in volcanic ash, as well as homogeneous and heterogeneous modifications of the ash surface. Volcanic ash interacts with the volatiles that are released during fragmentation. Ayris et al. estimate that, for a voluminous explosive eruption (>10 km<sup>3</sup> of magma), SO<sub>2</sub> scavenging efficiency varies from less than 1 % to 73 %, depending mostly on the depth of the magma chamber, but also tephra crystallinity and water content (Ayris et al., 2013). Further modifications are expected to take place on the surface of the volcanic particles as they are transported in the atmosphere.

Volcanic plume formed during explosive eruptions expands vertically from the vent of the volcano to the level of neutral buoyancy, which is defined as the height at which a rising parcel of air is at the same temperature as its environment. While ascending through the volcanic plume volcanic ash undergoes an extreme temperature gradient from 1000°C to 0°C in a matter of just a few minutes (Ayris et al., 2013). As can be deduced from the model of the explosive Plinian eruption in the plume itself, the exposure of ash to the gases is brief and temperatures in excess of 500 cannot be sustained for more than 10 seconds (Figure 3) (Textor et al., 2003). Nevertheless, it is assumed that in the process volcanic ash scavenging accounts for about 30 - 40 % of sulfur and 10 – 20 % of chlorine emitted during eruption (Langmann, 2013).

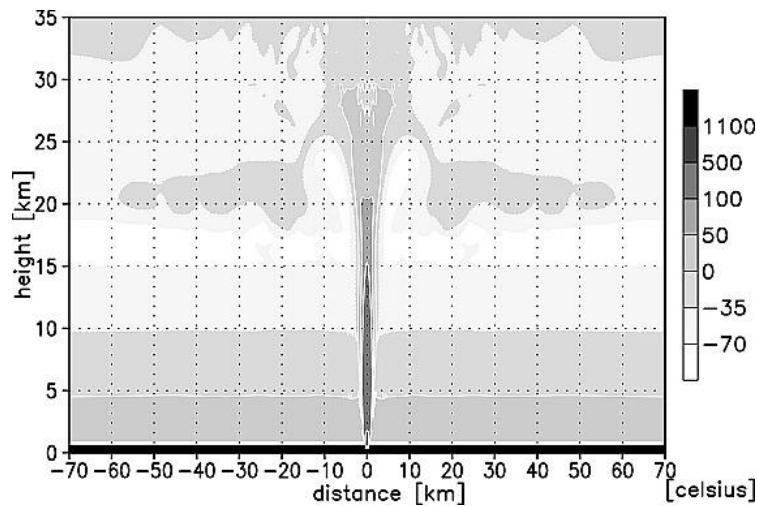


Figure 3: Model of the Plinian volcanic eruption after 30 min. Temperature distribution in degrees Celsius. Adapted from “Injection of gases into the stratosphere by explosive volcanic eruptions” (Textor et al., 2003). The volcanic conditions at the base of the volcanic plume: height - 600 m above sea level, diameter - 750 m, vertical velocity - 400 m/s, and temperature - 1100 K.

Volcanic plumes can be far-reaching. They can carry volcanic ash to a distance of thousands of kilometers before eventually being deposited onto land or into the ocean by gravitational settling and wet deposition (Langmann et al., 2010). For example, several volcanic dust plumes originating from Iceland were observed to exceed 1000 km traveling distance spreading towards Europe, North America and Arctic (Dagsson-Waldhauserova et al., 2014). Once settled, volcanic dust can then be once again remobilized by the wind and entrained into the atmosphere. Nevertheless, the physico-chemical processes that govern modifications in the plume and in the cloud are poorly understood and need further investigation.

In the following sections I would like to explore what happens to the volcanic ash after its emission in the atmosphere. I will concentrate on its interactions with the most important gas emitted during eruption: sulfur dioxide. First, characterization of volcanic ash and sulfur dioxide as well as their impact on the atmosphere will be introduced (Section 2 and Section 3). Second, the system of study will be chosen (Section 4). Third, the fundamentals of heterogeneous reactivity and laboratory techniques used will be presented (Section 5). Forth, literature concerning heterogeneous reactivity between volcanic dust, mineral dust, and

individual oxides with SO<sub>2</sub> will be reviewed (Section 6). Finally, the thesis objectives will be defined (Section 7).

## 2 Volcanic ash

Volcanic eruptions are a highly variable source of solid particles in the atmosphere. At 33 to 256 million tons a year, volcanic emissions are the fourth major contributor to the flux of primary solid particles of natural origin (Andreae, 1995) (Durant et al., 2010). However, during the years of high volcanic activity explosive volcanic eruptions can inject much higher amounts of particular matter, dwarfing all other sources of solid particles in the atmosphere. For example, the eruption of Mount Tambora produced 100,000 million tons of ash (Andreae, 1995).

All fragmental magmatic material issued from a volcano is called tephra and is often classified by size, the smallest kind being ash and dust. Most of the literature on volcanology refers to volcanic dust as smaller kind of volcanic ash (less than 0.25 mm in diameter for volcanic dust vs 0.25-4 mm for the volcanic ash) (McCall, 2004). **Some literary sources distinguish between volcanic dust, being a material which was re-suspended from old tephra deposits, and “fresh unaltered volcanic ash” (Dagsson-Waldhauserova et al., 2015). In this manuscript the terms volcanic dust and volcanic ash are interchangeable. When unaltered volcanic dust is discussed it will be clearly stated.**

### 2.1 Properties of volcanic ash

#### 2.1.1 Composition

Just as with mineral dust, the main components of volcanic ash are oxygen and silicon (Langmann, 2013). Other elements found in volcanic ash include iron, aluminum, magnesium, calcium, and titanium (Maters et al., 2016). Surface composition of volcanic ash from Eyjafjallajökull, Tungurahua, Pinatubo and Chaitén volcanoes using XPS is reflected in Table 4.

*Table 4: Surface composition of volcanic ash analyzed by XPS. Adapted from “Controls on the surface chemical reactivity of volcanic ash investigated with probe gases” (Maters et al., 2016).*

Ash Source	O	Si	Al	Fe	Mg	Ca	Na	K	Ti	Cl	F
<b>Eyjafjallajökull</b>	56.4	25.5	7.2	3.0	3.4	1.5	1.4	0.5	0.5	0.3	0.3
<b>Tungurahua</b>	56.7	30.7	7.2	0.8	0.8	1.3	1.3	0.5	0.2	0.2	0.3
<b>Pinatubo</b>	54.8	31.2	8.4	0.7	2.0	0.8	1.0	0.9	n.d. <sup>a</sup>	0.1	0.2
<b>Chaitén</b>	60.2	29.8	7.0	0.3	0.4	0.8	1.2	0.2	n.d.	0.1	n.d.

n.d.: not determined



The mineral composition of the volcanic ash reflects the composition of magma from which it was generated (Langmann, 2013). These minerals are formed in magma through the process of crystallization, cooling and decompressing as magma raises to the surface (Langmann, 2013). Silicate is the main component of minerals found in volcanic ash, such as feldspar, olivine, pyroxene, hornblende, and biotite (Langmann, 2013). The individual mineral grains and crystals are imbedded in the glass (Dagsson-Waldhauserova et al., 2015).

### 2.1.2 Size distribution

Volcanic ash consists of fragments of 4 mm or smaller in diameter (McCall, 2004). The particle size controls the fraction that is transported to large distances with the coarser particles being deposited much faster (Langmann, 2013).

Volcanic ash particles are hard and sharp, and remain so, even after days of interaction with each other and with water in clouds (Gislason et al., 2011). The morphology of volcanic dust particles is assumed to be spherical with a density from 2000 to 3000 kg/m<sup>3</sup>. Density depends on the composition (basaltic, rhyolitic, etc.), amount of crystallization, and porosity of the particles. The specific surface area (SSA) reported varies from under 2 to 10 m<sup>2</sup>/g (Langmann, 2013). These values are comparable to those measured for desert dusts, where a value of 10.5 m<sup>2</sup>/g was reported for Gobi dust and 14.5 m<sup>2</sup>/g for M'Bour dust (Joshi et al., 2017). As for other airborne materials, such as soot (SSA=98-122 m<sup>2</sup>/g) and montmorillonite clays (SSA=225 m<sup>2</sup>/g) the specific surface area of volcanic ash is smaller in comparison (Romanías et al., 2015), (Lasne et al., 2018).

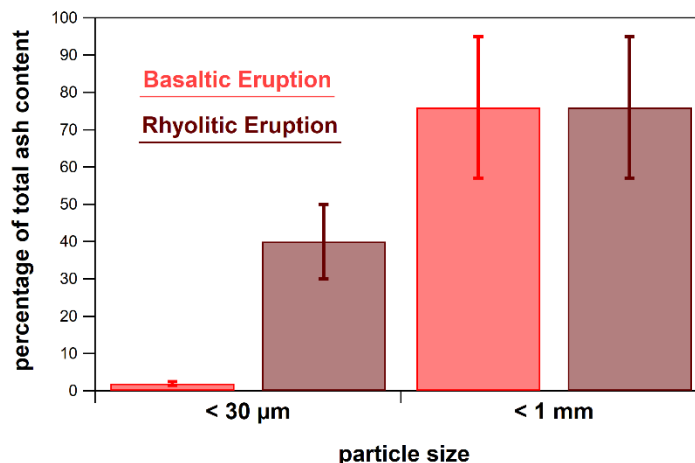


Figure 4: Ash particle size distribution. Adapted from (Langmann, 2013)

The size distribution of the volcanic particles varies greatly depending on the formation process (Figure 4). Statistically, the ash particles that are smaller than 1 mm compose 55 to 97 % of total ash content

(Langmann, 2013). Particles smaller than 30  $\mu\text{m}$  contribute to 30 to 50 % of total ash content of rhyolitic eruptions, but only a few percent of basaltic eruptions (Langmann, 2013). The size of ash particles emitted varies during eruption. For example, during the early hydromagmatic explosive phase of the 2010 eruption of Eyjafjallajökull volcano  $\text{PM}_{10}$  particles accounted for about 20% of all explosive ash, while the later magmatic ash produced less than 2% of the  $\text{PM}_{10}$  particles (Gislason et al., 2011). It is important to emphasize that it is mainly the smaller particles of the diameter of less than 10  $\mu\text{m}$  that can be carried for hundreds of kilometers (Langmann, 2013). Indeed, volcanic particles smaller than 0.3  $\mu\text{m}$  can persist in the atmosphere 3 months after eruption as observed by Vernier et al. after the eruption of Kelud volcano in Indonesia in 2014 (Vernier et al., 2016). Volcanic ash produced during explosive volcanic eruptions forms aggregates of various types that speed up sedimentation rate. Interestingly, it was also suggested that aggregation of particles does not always result in a premature sedimentation of their constitute particles, but that it can also result in a delayed sedimentation due to so-called rafting effect (Rossi, 2020). The decrease in sedimentation rate is explained by the fact that bulk density of ash aggregates can be much lower than that of a solid ash particles of comparable size enabling clusters of 500  $\mu\text{m}$  or more in size to be carried by the wind far greater distances than ash particles of similar size (Sorem, 1982). As an example, rafting can potentially explain the sedimentation of 90  $\mu\text{m}$  particles at about 1300 km from the vent during the 2010 Eyjafjallajökull eruption, which is double the sedimentation distance expected for this particle size (Bagheri et al., 2016). The latitude of the eruption can further influence the lifetime of ash in the air. For example, in the tropics a longer lifetime of volcanic ash is observed due to the upward motion associated with Brewer-Dobson circulation (Vernier et al., 2016). Brewer-Dobson circulation is characterized by tropospheric air rising into the stratosphere in the tropics, moving poleward before descending in the middle and high latitudes (“The Brewer-Dobson circulation - Butchart - 2014 - Reviews of Geophysics - Wiley Online Library,” n.d.).

## **2.2 Impact of volcanic ash on global processes**

The impact of a volcanic eruption depends on its magnitude, intensity, and geographical location.

### **2.2.1 Impact on stratospheric and tropospheric chemistry**

Volcanic ash produced as a result of volcanic eruption, depending on the strength and the type of the eruption, can be released into the troposphere and/or stratosphere (Table 1). With respect to atmospheric chemistry the biggest impact comes from the particles with the diameter smaller than 10  $\mu\text{m}$  as they can be carried over larger distances (Finlayson-Pitts and Jr, 1999).

In the stratosphere, emissions of volcanic ash can be responsible for ozone reduction recorded after major volcanic eruptions (Brasseur et al., 1990). The observation was attested by computer modelling that was able to account for perturbations following El Chichón eruption in Mexico in 1982 and Mount Pinatubo eruption in Philippines in 1991 (Usher et al., 2003). Using data about dispersion of the ash cloud and efficiency of heterogeneous conversions on the surface of the ash particles, the model successfully predicted at the end of the winter following the eruption of Mount Pinatubo a reduction of ozone column abundance much like the one observed over Antarctica in early spring (Granier and Brasseur, 1992). This example demonstrates that heterogeneous processes included in modeling can vastly improve the predictions, even though more work is needed to better define the above mentioned processes.

The effect of the volcanic ash in the troposphere is not yet evaluated. It is very likely though that ash particles can serve as a long-range transporting carrier for many species adsorbed on its surface (Li et al., 2006). While transferring these species it might participate in different heterogeneous reactions that can potentially influence the balance of atmospheric species. As a result of heterogeneous interactions the optical and thermodynamic properties of the particle themselves will change as well (Usher et al., 2003). Therefore, we expect volcanic ash to have a significant impact on the atmospheric processes both on the short-term and long-term range.

### 2.2.2 Impact on climate

Volcanic particles have an ability to affect the climate by scattering solar radiation and thus changing the amount of heat that reaches the Earth's surface (Langmann, 2013). Besides, volcanic ash, having optical and thermal properties similar to those of the black carbon, can also absorb solar radiation (Arnalds et al., 2016). Thus, volcanic ash influences the energy of the atmosphere. Vernier et al. highlighted the significance of the radiative impact of ash, in particular in the tropical latitudes due to the Brewer-Dobson circulation that sustains ash in the stratosphere for longer than was generally assumed (Vernier et al., 2016). Volcanic ash particles can also affect the climate through influencing cloud formation processes and acting as ice-nucleation sites during plume rise (Durant et al., 2008). In addition, volcanic ash fallouts form rich soils for agriculture (McCall, 2004). They also provide a source of nutrients to the oceans in the form of bioavailable iron, which in turn stimulates biological activity (Durant et al., 2010). It happens so that for marine phytoplankton separated from the iron-rich sediment of the ocean floor by a considerable depth, iron supply becomes a limiting factor affecting its growth. Thus, additional influx of iron from volcanic emissions influences its overall productivity. Increase in iron supply allows more efficient use of macronutrients and hence enhances CO<sub>2</sub> uptake by phytoplankton (Jickells et al., 2005). In addition, increased productivity of phytoplankton leads to increased dimethyl sulfide (DMS) emissions. DMS

oxidizes in the atmosphere to form sulfuric acid aerosol, that effectively scatters solar radiation (Jickells et al., 2005).

### 2.2.3 Other impacts

Ash particles from the volcano fallout can present a health hazard to the human population. The concern is especially high for the presence of crystalline silica (cristobalite) that forms nanofibers (Langmann, 2013). Exposure to volcanic ash for a long time is associated with chronic bronchitis and respiratory infections; skin abrasions and eye irritation have also been reported (Thorsteinsson et al., 2012). In the long run ash ingestion and inhalation can lead to silicosis, a chronic and often fatal condition caused by inhalation of particles smaller than 10  $\mu\text{m}$  (Gislason et al., 2011). High  $\text{PM}_{10}$  levels in Iceland were linked to a 4.8 - 7.3 % increase in emergency hospital visits (Arnalds et al., 2016). In Iceland a health limit for particle matter smaller than 10  $\mu\text{m}$  ( $\text{PM}_{10}$ ) is set at 50  $\mu\text{g}/\text{m}^3$  (Thorsteinsson et al., 2012). Additional health risk can be associated with contamination of surface of waters and terrestrial ecosystems by condensed salts and trace elements that are carried by the ash particles and can be released in the surrounding (Gislason et al., 2011). For example, fluoride released during Laki eruption was associated with the most significant loss of life due to fluoride poisoning (Gislason et al., 2011). About 0.5 % of the explosive ash by mass released during the eruption of Eyjafjallajökull volcano in 2010 was found to be soluble, corresponding to a mass of around  $40 \pm 20$  thousand tons of soluble material (Gislason et al., 2011), (Thorsteinsson et al., 2012).

Volcanic eruptions pose particularly severe threat to airplanes as volcanic ash can clog the jet turbines and abrade the outside corpus of the aircraft (Durant et al., 2010). The ash particles are much harder than exposed parts of the airplane and can easily turn pilot window completely opaque due to glass abrasion (Gislason et al., 2011). Melting temperature of the volcanic ash is lower than the operating temperature of the high-performance engines, which is around  $1400^\circ\text{C}$ , so molten ash can get deposited on the cooler parts of the engine and cause flame-outs (Langmann, 2013). The smaller the particles the easier they melt (Gislason et al., 2011). During the eruption of Eyjafjallajökull volcano maximum concentration of 4000  $\mu\text{g}/\text{m}^3$  was reported in the volcanic ash cloud that was spreading over Europe, twice exceeding the threshold for safe aviation (Langmann, 2013). In the last 60 years about 129 flights were affected by volcanic ash (Langmann, 2013).

## 3 Gasses emitted after volcanic eruptions: focus on $\text{SO}_2$

During an eruption, magma releases a diverse range of gases, including water vapor, carbon dioxide, and sulfur dioxide along with smaller amounts of hydrogen sulfide, hydrogen, helium, carbon monoxide, hydrogen chloride, hydrogen fluoride, nitrogen, and argon (Durant et al., 2010). Average volcanic gas

composition of the volcanic gas is reflected in Table 5 (Hoshyaripour et al., 2012). As can be seen from Table 5, the composition of the gas emitted during an explosive eruption varies depending on differences in tectonic settings: converging plates, diverging plates or a hot spot (Hoshyaripour et al., 2012). It happens so that the highest amount of SO<sub>2</sub> (ca. 20 %) is emitted by the volcanoes that are linked to the hot spot (Hoshyaripour et al., 2012). The divergent plates contribute 7.84 % of the SO<sub>2</sub> emissions, followed by 1.44 % by convergent plates (Hoshyaripour et al., 2012). The most significant climate impact from the volcanic emissions comes from SO<sub>2</sub> even though CO<sub>2</sub> and H<sub>2</sub>O are the most abundant gases emitted during a volcanic eruption. It is because their concentrations in the atmosphere are already so high (around 400 ppm for CO<sub>2</sub> and 25,000 ppm for H<sub>2</sub>O) that contributions from volcanic eruptions are more or less negligible (“Atmospheric Composition — OSS Foundation,” n.d.). The background concentration of SO<sub>2</sub>, however, is small, concentrations of SO<sub>2</sub> in remote areas range from 10 to 50 ppt, in rural areas around 1 - 20 ppb, in urban areas – up to several hundred ppb, so additional amounts easily become significant (Finlayson-Pitts and Jr, 1999). Bluth et al. estimate the annual flux of total volcanic SO<sub>2</sub> gas at 13 million tons per year with the contribution from the explosive eruptions at 4 million tons per year (Bluth et al., 1993).

*Table 5: Average High-Temperature Volcanic gas Composition in Mole%. Adapted from “How does the hot core of a volcanic plume control the sulfur speciation in volcanic emission?” (Hoshyaripour et al., 2012).*

	<b>Convergent Plate</b>	<b>Divergent Plate</b>	<b>Hot Spot</b>
<b>H<sub>2</sub>O</b>	91.9	75.1	75.7
<b>CO<sub>2</sub></b>	4.6	13.1	3.2
<b>H<sub>2</sub></b>	0.5	1.59	0.95
<b>SO<sub>2</sub></b>	<b>1.44</b>	<b>7.84</b>	<b>19.4</b>
<b>H<sub>2</sub>S</b>	0.67	1.01	0.16
<b>HCl</b>	0.76	0.42	0.17
<b>HF</b>	0.061	0.42	0.18
<b>CO</b>	0.03	0.6	0.09

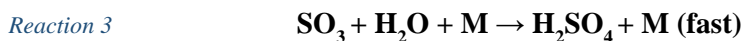
Stevenson et al. estimate that sulfur dioxide (SO<sub>2</sub>) gas emitted in the atmosphere as a result of volcanic activity accounts for 8.8 million tons of sulfur per year, due to anthropogenic activity for 71.2 million tons of sulfur per year, and by biomass burning for 1.4 million tons of sulfur per year (Stevenson et al., 2003). Thus, volcanic emissions are responsible for about 11 % of all the sulfur emitted in the atmosphere.

### 3.1 Impact of volcanic gasses on global processes

#### 3.1.1 Impact of volcanic gasses on stratospheric and tropospheric chemistry

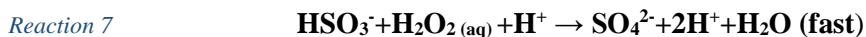
##### Gas phase processes

Sulfur dioxide is a noticeable component in the atmosphere, where release of SO<sub>2</sub> is associated with the decrease in the levels of atmospheric oxidants, such as H<sub>2</sub>O<sub>2</sub>, OH, and O<sub>3</sub> as they are involved in the reactions that convert gaseous and dissolved SO<sub>2</sub> to sulfates (Stevenson et al., 2003). For example, in the troposphere, gas-phase SO<sub>2</sub> reacts to produce sulfur trioxide, which is then converted to sulfuric acid according to Reaction 1- Reaction 3 (Daniel J. Jacob, 1999):



##### Multiphase processes

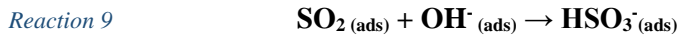
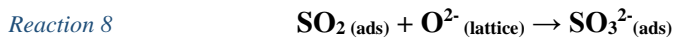
SO<sub>2</sub> is a notorious precursor to acid rain. It was long known that SO<sub>2</sub> gets oxidized by the •OH radical to form H<sub>2</sub>SO<sub>4</sub> (Reaction 1- Reaction 3). In the atmosphere the lifetime of SO<sub>2</sub> against reaction with •OH is 1-2 weeks. While reconciling this relatively long lifetime with the observation that SO<sub>4</sub><sup>2-</sup> concentration in rain is maximum over SO<sub>2</sub> source regions it was realized that there must be an additional pathway to the homogeneous path for the oxidation of SO<sub>2</sub>. Indeed, most of the atmospheric oxidation of SO<sub>2</sub> actually takes place in cloud and rain droplets, where SO<sub>2</sub> is transformed to HSO<sub>3</sub><sup>-</sup> which is then rapidly oxidized in the liquid phase by H<sub>2</sub>O<sub>2</sub> (Reaction 4 - Reaction 7) (Daniel J. Jacob, 1999). This last reaction is now thought to be the dominant pathway for oxidation of SO<sub>2</sub> to H<sub>2</sub>SO<sub>4</sub> (Daniel J. Jacob, 1999).



Besides participating in gas-liquid heterogeneous reactions, SO<sub>2</sub> also participates in heterogeneous reactions with solids. In the marine boundary layer SO<sub>3</sub> is oxidized to sulfate by O<sub>3</sub> and H<sub>2</sub>O<sub>2</sub> on sea salt aerosol (Goodman et al., 2001). It was proposed that SO<sub>2</sub> can also be oxidized to sulfuric acid on the surface of mineral dust by ozone, but the mechanism of this reaction is not completely understood so laboratory studies are under way in order to better understand these interactions (Ullerstam et al., 2002).

SO<sub>2</sub> shows heterogeneous reactivity towards many mineral oxides such as MgO, Al<sub>2</sub>O<sub>3</sub>, Fe<sub>2</sub>O<sub>3</sub>, TiO<sub>2</sub>

(Usher et al., 2002). Gas-phase SO<sub>2</sub> reacts with surface oxygen atoms and/or hydroxyl groups of the metal oxides mentioned above, as shown in Reaction 8 and Reaction 9 (Usher et al., 2002).



SO<sub>2</sub> is a weakly acidic gas. It was recently evidenced by Maters et al. that volcanic ash is reactive to SO<sub>2</sub> uptake with the reactivity that is proportional to the abundance of strongly basic sites (Maters et al., 2017).

### 3.1.2 Impact of volcanic gasses on climate

The quantity of sulfur dioxide released during eruptions is a crucial factor in determining its climate impact. Conversion of SO<sub>2</sub> to H<sub>2</sub>SO<sub>4</sub> and formation of fine sulfur aerosol in the stratosphere, which can persist for 1 or 2 years in the mid-stratosphere, is known to affect the climate by increasing the reflection of radiation from the Sun back into space, thus efficiently cooling the Earth's troposphere (Stevenson et al., 2003), (Highwood and Stevenson, 2003). In case of the release of SO<sub>2</sub> gas in the troposphere the impact of the eruption is not as strong since the formation of sulfur aerosol competes with SO<sub>2</sub> gas deposition and since the sulfur aerosol formed is deposited within days or weeks (Stevenson et al., 2003).

### 3.1.3 Impact of volcanic gasses on health

Significant emissions of SO<sub>2</sub> gas poses considerable health hazard to the population. Analysis of historical records about 1783-1784 Laki eruption clearly links elevated levels of SO<sub>2</sub> to respiratory disorders and increased mortality rates (Schmidt et al., 2011). If a Laki style eruption was to happen today it is estimated that additional 142,000 deaths due to cardiopulmonary failure would occur in Europe (Schmidt et al., 2011).

## 4 Iceland: a study-case?

To study the interactions of volcanic ash with SO<sub>2</sub> gas one would search for a place that is volcanically active, has a favorable composition of volcanic emissions and is geographically relevant, making Iceland a perfect place to study such interactions. Iceland is a volcanic island with an area of 103,000 km<sup>2</sup>, south of the Arctic Circle and about 1000 km from mainland Europe (Arnalds et al., 2016). It is one of the most volcanically active places in the world. There are about 30 active volcanic systems and volcanic eruptions occurring every 3-5 years on average (Thordarson and Larsen, 2007), (Schmidt et al., 2014). Iceland is situated on the Mid-Atlantic ridge, which is a deep rift or crack that marks the actual boundary between adjacent tectonic Eurasian and North-American plates. As the plates are slowly being pulled apart



at the rate of a growing human fingernail magma from the mantle erupts as lava producing new crustal material for the plates. In addition to its position on the ridge, Iceland also lies on top of a hot spot. Iceland's hot plume has been active for the past 65 million years (Thordarson and Larsen, 2007). The presence of the hot spot enhances the volcanism already caused by plate separation (Hoshyaripour et al., 2012). Consequently, Iceland's volcanoes display a wide spectrum of forms, ranging from a crack in the ground to majestic stratovolcanoes (Thordarson and Larsen, 2007).

Iceland's volcanoes are either the result of a hot spot or divergent plates or both. Therefore, explosive eruptions in Iceland are likely to contain high amounts of  $\text{SO}_2$  (Hoshyaripour et al., 2012). Geographical proximity of Iceland to Europe makes the studies especially relevant. Its eruptions in the past have already influenced densely populated European nations. The location of Iceland is the critical factor because it directly affects air travel across Europe (Thordarson and Larsen, 2007).

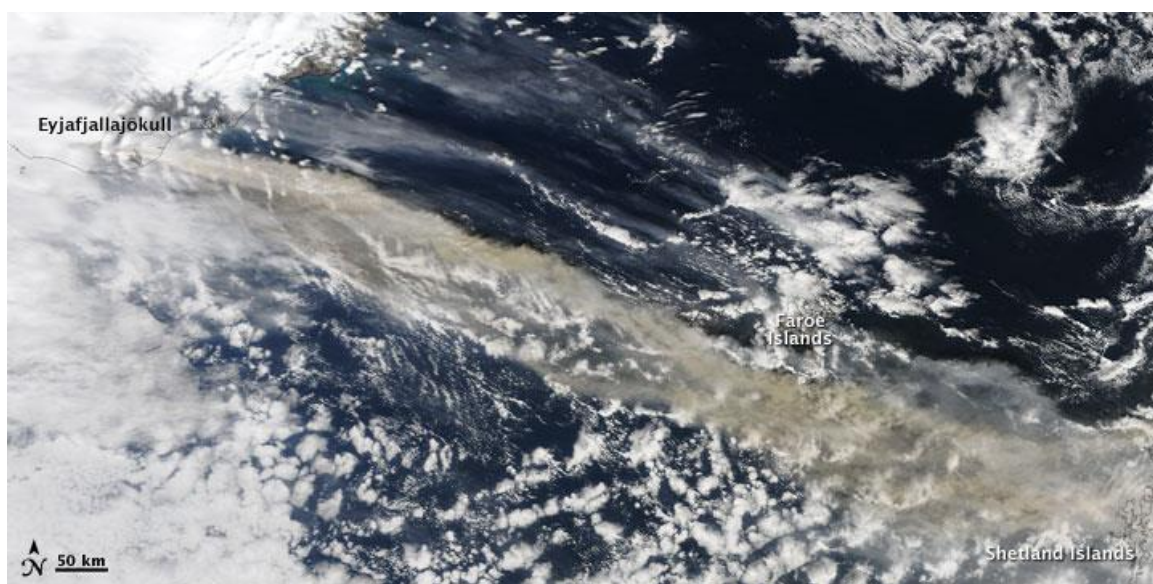


Figure 5: Ash plume from Iceland's Eyjafjallajökull Volcano, April 15 2010 ("Ash Plume across the North Atlantic," 2010). Image Credit: NASA

Figure 5 demonstrates the immensity of the plume of the volcanic ash coming from Iceland's Eyjafjallajökull Volcano as it sends a plume of ash and steam across the North Atlantic Ocean in mid-April 2010, prompting authorities in the United Kingdom, Ireland, France, and Scandinavia to close airspace over their countries ("Ash Plume across the North Atlantic," 2010). During the last eruption of Eyjafjallajökull  $8 \pm 4$  million tons of ash and 0.39 million tons of  $\text{SO}_2$  were emitted in the atmosphere (Thorsteinsson et al., 2012), (Schmidt et al., 2014). Based on the record of eruptions in Iceland in the last 1150 years this eruption is representative of medium size explosive volcanic eruption in Iceland making it a relative model (Schmidt



et al., 2014). Ash from Eyjafjallajökull volcano was shown to be particularly reactive to SO<sub>2</sub> uptake (Maters et al., 2017).

As the global temperatures are increasing, the frequency of volcanic eruptions in Iceland are expected to increase. It happens due to the fact that the glaciers that are covering much of the Iceland's territory are receding at the unprecedented rate exposing the volcanoes that were buried under heavy shields of glaciers. The combination of erosion and melting ice caps decreases the pressure on the Earth's mantle, leading to an increase in both magma production (increase of ~1% for 1 kbar of pressure decrease) and volcanic eruptions (Sternai et al., 2016).

## 5 Fundamentals of heterogeneous reactions

### 5.1 Physical chemistry approach

This section provides a closer look at the interactions between gases and solid surfaces. These interactions can be reversible or irreversible (Crowley et al., 2010). Heterogeneous interactions start with transport of the gas to the surface, its accommodation on it, followed by a number of competitive processes such as desorption back into the gas phase, reaction with the solid substrate or with other trace gases on the surface and photochemistry on the surface. The rate and efficiency of each step is controlled by surface rate coefficients, reactant concentrations, diffusion coefficients in the gas and condensed phase and solubility (Crowley et al., 2010). Each of these factors is further influenced by environmental factors, such as temperature and relative humidity. Besides, a molecule can get adsorbed on the surface with or without subsequent dissociation, thus the nature of the adsorption process can be either dissociative or not (Attard and Barnes, 1998). Atmospheric heterogeneous processes are highly complex and only rarely sufficient information is provided to understand each individual step of the reaction. This section will try to describe some key ideas related to the interactions between gases and solids.

Upon collision with a surface a molecule can undergo elastic or inelastic scattering resulting in its reflection back into the gas phase or it can undergo adsorption. Adsorption is the term that refers to the process in which a molecule interacts with a surface. These interactions are often typified by hydrogen bonds, Van Der Waal interactions, charge transfer, or covalent bonding (Crowley et al., 2010), (Attard and Barnes, 1998). Adsorption of a given species, the adsorbate, can be described in terms of fractional coverage of the solid surface:  $\theta$  as reported in Equation 1.

*Equation 1*

$$\theta = \frac{N_s}{N}$$

In Equation 1, fractional coverage  $\theta$  is the number of surface sites occupied by adsorbate  $N_s$ , divided by the total number of substrate adsorption sites  $N$ . The latter is often estimated through the number of surface atoms of the substrate (Attard and Barnes, 1998), but this approach remains an approximation and more accurate determinations can be retrieved from experimental determinations of adsorption isotherms.

Two types of adsorption can be distinguished:

Physical adsorption, physisorption, is the weak interaction formed via hydrogen bonding, charge transfer or Van Der Waal interactions. Bonding is characterized by redistribution of electron density within the adsorbate and adsorbent separately. There is a negligible exchange of electrons and  $-\Delta H^\circ_{\text{physisorption}} < 35 \text{ kJ/mol}$ . No products are formed as a result of this interaction in that the adsorbate does not react and is not irreversibly modified (Attard and Barnes, 1998).

Chemisorption involves breaking and forming of chemical bonds or significant distortion of electronic structure of adsorbate or substrate (Crowley et al., 2010). Therefore chemisorption is seen as a chemical reaction on the surface. Spectroscopic methods can be used to confirm the nature of the bonding. The magnitude of enthalpy of chemisorption is higher:  $-\Delta H^\circ_{\text{chemisorption}} > 35 \text{ kJ/mol}$  (Attard and Barnes, 1998).

Figure 6 illustrates what happens to the diatomic molecule  $M_2$  as it approaches the surface. Provided that the energy gets released to the surface faster than the molecule can desorb back into the gas phase the molecule gets trapped in a weak physisorbed state. To reach the chemisorbed state, a larger barrier needs to be breached. In the way the sketch is drawn activation energy is required to move from physisorbed to chemisorbed state. However, it is quite possible for the barrier to chemisorption to be below zero, in this case the rate constant towards chemisorption will be faster than separation from the surface. As before, the energy released on chemisorption is taken up by the surface states (Attard and Barnes, 1998).

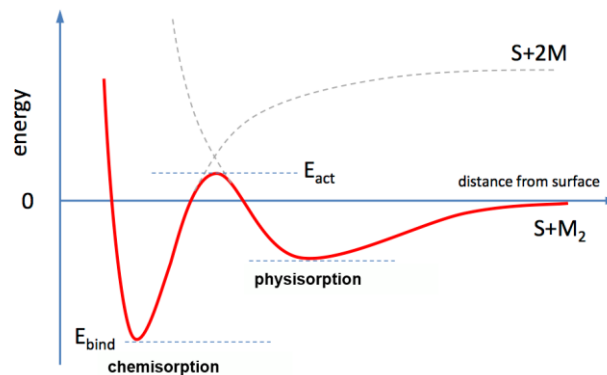


Figure 6: Potential energy of chemisorption and physisorption vs. distance from surface. Adapted from "How does adsorption work?" ("How does adsorption work?," n.d.).

### 5.1.1 Models for adsorption description

Several models were developed to describe the equilibrium between adsorbed and gaseous states. The number of surface sites occupied by adsorbate molecules at equilibrium at a particular pressure depends on the partial pressure  $P$  of the molecule. Adsorption isotherm reflects this dependence of fractional coverage  $\theta$  on partial gas pressure  $P$  of the molecule.

#### The Langmuir adsorption isotherm

One of the simplest and most widely used models is Langmuir adsorption isotherm. To derive this model the following approximations were made.

- (i) The solid surface is uniform and all adsorption sites are equivalent
- (ii) Gas phase molecules and adsorbed layer are in the dynamic equilibrium
- (iii) Only one monolayer of molecules is formed on the solid surface
- (iv) No adsorbate-adsorbate interactions
- (v) Once adsorbed the molecules are localized

The model was derived assuming that molecules in gas phase are in a dynamic equilibrium with the adsorbed layer. For non-dissociative adsorption:



where  $k_a$  (molecules  $\text{s}^{-1} \text{Pa}^{-1}$ ) and  $k_d$  (molecules  $\text{s}^{-1}$ ) are the rate constants for adsorption and desorption respectively.

$$\text{Equation 2} \quad \text{Rate of adsorption} = k_a P (1-\theta)$$

$$\text{Equation 3} \quad \text{Rate of desorption} = k_d \theta$$

where  $\theta$  is the fractional surface coverage,  $(1-\theta)$  is the fractional monolayer coverage not occupied by molecules,  $P$  (Pa) is the partial pressure of M. Equation 2 implies that the rate (molecules  $\text{s}^{-1}$ ) will be fast if the pressure and adsorption constants are high, and surface coverage  $\theta$  is low. Rate of desorption (molecules  $\text{s}^{-1}$ ) is not dependent on pressure (Equation 3). At equilibrium the rate of adsorption is equal to the rate of desorption (Equation 4).

$$\text{Equation 4} \quad k_a P (1-\theta) = k_d \theta$$

Thus, from Equations 1 and 4, Equation 5 is obtained:

$$\text{Equation 5} \quad \theta = \frac{N_s}{N} = \frac{KP}{1+KP} \quad , \text{ where } K = \frac{k(\text{adsorption})}{k(\text{desorption})}$$

$K$  ( $\text{Pa}^{-1}$ ) is the adsorption equilibrium constant. When a gaseous species tends to be massively transferred onto the surface  $K$  is large, in the opposite case  $K$  value is small. Langmuir adsorption isotherm describes how the fractional monolayer coverage  $\theta$  changes with the partial pressure of the compound in the gas phase (Figure 7). When the partial pressure of the gas is very low,  $\theta=KP$ , and as the pressure increases  $\theta$  is approaching saturation, i.e.  $\theta=1$ , corresponding to the formation of a complete monolayer. For dissociative adsorption there are two sites that are required, therefore the reaction rate is a second order process.

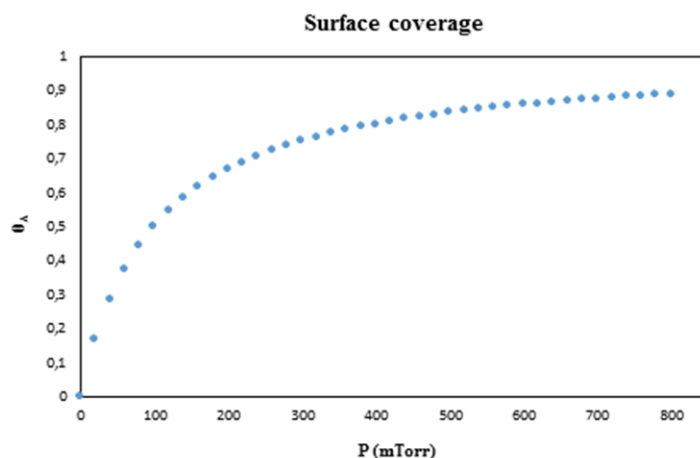


Figure 7: Langmuir adsorption isotherm, adapted from “Langmuir adsorption model” (“Langmuir adsorption model,” 2018)

Multiplying out Equation 5 and rearranging it gives a plot of  $(P/N_s)$  versus  $P$  as a straight line with gradient  $1/N$  and intercept at  $1/NK$  (Equation 6).

$$\text{Equation 6} \quad \left(\frac{P}{N_s}\right) = \frac{1}{NK} + P\left(\frac{1}{N}\right)$$

### The BET isotherm

Langmuir isotherm gives a good general overview of the adsorption process, but fails to account for the adsorbate/adsorbate interactions and for the interactions between monolayers. Brunauer, Emmett and Teller (BET) model attempts to account for multilayer formation. The BET model is based on the following assumptions:

- (i) Adsorption of the first layer takes place on the surface sites of the same energy
- (ii) Multilayer adsorption is possible.
- (iii) At equilibrium the rates of condensation and evaporation are the same for each layer.

Summation of the amount adsorbed in all layers gives the BET equation (Equation 7).

$$\text{Equation 7} \quad \frac{P}{Ns(P_0 - P)} = \frac{1}{NC} + \frac{(C-1)}{NC} \times \frac{P}{P_0}$$

where  $P$  (Pa) is the pressure of gas at equilibrium with adsorbed phase,  $P_0$  (Pa) is the saturated vapor pressure of the adsorbate,  $C \approx e^{(\Delta H_D^\circ - \Delta H_{VAP}^\circ)/RT}$ ,  $\Delta H_D^\circ$  (kJ/mol) is enthalpy of desorption,  $\Delta H_{VAP}^\circ$  (kJ/mol) is enthalpy of vaporization,  $R$  (kJ K<sup>-1</sup> mol<sup>-1</sup>) is the ideal gas constant and  $T$  (K) is temperature.

The BET isotherm model is very often used in surface science for the determination of the specific surface area (m<sup>2</sup>/g) of a solid material. In particular, a plot of  $\frac{P}{Ns(P_0 - P)}$  vs  $\frac{P}{P_0}$  (Equation 7), gives a straight line with the intercept at  $\frac{1}{NC}$  and a slope of  $\frac{(C-1)}{NC}$ . Note that the range of linearity for BET plot is usually restricted  $0.05 < P/P_0 < 0.3$ .

Knowing the total number of adsorbate molecules,  $N$ , and the area (or cross section) of the molecule  $A_m$  (m<sup>2</sup>) it is possible to determine the total surface  $S_A$  (m<sup>2</sup>) (Equation 8).

$$\text{Equation 8} \quad S_A = N \times A_m$$

Total surface  $S_A$  divided by the mass of the substrate allows the determination of the specific surface area (Equation 9), that provides a comparison of the surfaces available for interaction between different solids.

$$\text{Equation 9} \quad \text{specific surface area} = \frac{S_A}{\text{mass of the substrate}}$$

### 5.1.2 Experimentally determined kinetic parameters

The reaction rate constants and uptake coefficients are the variables that can be experimentally determined in the laboratory.

Uptake kinetics to a solid material is normally described in terms of the uptake coefficient  $\gamma$ , which represents the probability that a molecule  $X$  is removed from the gas upon collision with the surface (Equation 10).

$$\text{Equation 10} \quad \gamma = \frac{\text{\#number of collisions leading to removal of the molecule from the gas phase}}{\text{\#number of gas-surface collisions}}$$

Heterogeneous processes/losses are usually treated as first order loss of  $X$  from the gas phase (Equation 11).

$$\text{Equation 11} \quad \frac{d[X]_g}{dt} = -k_{kin}[X]_g = -\gamma \frac{\bar{c}}{4} [SS][X]_g$$

where  $[X]_g$  is the concentration of gas molecule  $X$  (molecules/cm<sup>3</sup>),  $[SS]$  is the surface area of the solid phase per volume of gas (cm<sup>-1</sup>),  $k_{kin}$  (s<sup>-1</sup>) is the first order rate coefficient for loss,  $\bar{c}$  is the mean thermal velocity of  $X$  (cm/s) and  $\gamma$  is the uptake coefficient. It is important to note that the uptake coefficient is not a constant. It may depend on time, due to the limitations imposed by adsorption equilibrium on the surface, by solubility, or by a limited number of reactants on the surface or in the bulk of the substrate. It can also depend on the concentration of gas molecules  $X$ . The rate of change of  $\gamma$  depends on the type of interaction between the solid and the gas. For a reversible process the uptake coefficient depends on surface capacity and concentration of gas phase species. For a reactive process it depends on the number of sites available for the reaction or the rate of delivery of the reactive sites to the surface and the gas phase concentration of the gas. Uptake coefficient may decline rapidly from nearly unity to almost zero in a matter of minutes or the process can take hours, or it can be completely independent of time and equal to the initial uptake, such as in the case of catalytic reactive uptake with no consumption, i.e. regeneration of reactive surface sites (Crowley et al., 2010).

Using Equation 11 one can calculate the uptake coefficient by experimentally obtaining kinetic gas loss rate constant  $k_{kin}$  from the observed change of gas concentration after its exposure to the surface. There are two types of uptake coefficients that are determined in the lab – the initial uptake coefficient  $\gamma_0$  and the steady state uptake coefficient  $\gamma_{SS}$ . The former reflects the interaction between a solid surface and a gas molecule in the first instants after the surface has been exposed, the latter is more concerned with adsorption at equilibrium when a steady state is reached. In atmospheric studies  $\gamma_{SS}$  might bare more significance due to its long term effect.

## 5.2 Laboratory techniques for studying heterogeneous reactions

This section briefly covers the typical laboratory techniques used to determine kinetic parameters that characterize heterogeneous processes in the atmosphere.

### 5.2.1 Coated wall flow-tube reactor

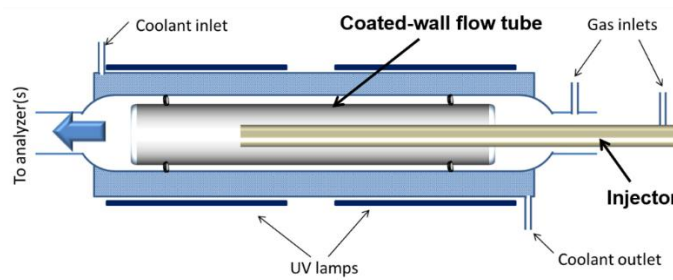


Figure 8: Schematic drawing of a coated wall flow tube reactor.

Coated-wall flow tube (CWFT) reactors have long been used for investigation of uptake and reaction kinetics of gases with solid surfaces. They can be operated either under low pressure (of a few Torr) or under atmospheric pressure. Traditionally low pressure flow tubes are used for the measurement of fast adsorptive/reactive processes related to uptake coefficients in the order of  $10^{-1}$  to  $10^{-6}$ , while atmospheric pressure flow tubes, for slower processes, where uptake coefficients are in the order of  $10^{-5}$  to  $10^{-9}$ . A schematic diagram of a typical CWFT reactor is shown in Figure 8. The flow reactor itself consists of a cylindrical double-wall thermostated tube and a movable sliding injector. The walls of the flow tube are covered with the solid phase (e.g. dust) under investigation and a movable injector supplies the gaseous reactant. At the downstream end, the reactor is connected to a gas analyzer or to a mass spectrometer, for the detection of the gas phase species. Initially, the injector is placed at the downstream end of the reactor to avoid premature exposure of the surface. Subsequently, the injector is moved back to expose the surface to the gas. As the gas interacts with the condensed phase the pseudo-first-order rate constant for the removal of the gas  $k_{obs}$  ( $s^{-1}$ ) is measured from the change of the concentration of the gas that reaches the detector (Equation 12). The evaluation of uptake coefficient is done under several assumptions: that the loss of the gas at the walls occurs through a first-order process (see Equation 12) and that the gas flow is a well-developed laminar flow. Laminar flow can be expected when the dimensionless Reynolds number  $Re$  is less than 2000 (Li et al., 2018).

Equation 12 
$$k_{obs} = \frac{v}{L} \times \ln\left(\frac{I_0}{I_r}\right)$$

where  $I_0$  (molecules/cm<sup>3</sup>) and  $I_r$  (molecules/cm<sup>3</sup>) is the initial and final concentrations of the gas recorded by the analyzer,  $v$  is the flow in the reactor (cm/s),  $L$  is the length of the tube covered with the condensed phase (cm).

The rate of loss of the gas is often limited by diffusion, therefore the measured constant  $k_{obs}$  ( $s^{-1}$ ) obtained in a typical experiment has to be corrected for diffusion. The corrected rate constant is referred to as  $k_{kin}$  ( $s^{-1}$ ) (Equation 13).

Equation 13 
$$\frac{1}{k_{obs}} = \frac{1}{k_{kin}} + \frac{1}{k_{dif}}$$

where  $k_{dif}$  ( $s^{-1}$ ) is the diffusion rate coefficient obtained via Equation 14.

Equation 14 
$$\frac{1}{k_{dif}} = \left(\frac{r^2}{3.66D}\right) \times P$$

where  $r$  is the radius of the tube in cm,  $D$  is diffusion coefficient in Torr $\times$ cm<sup>2</sup>/s, and  $P$  is pressure in Torr.

Diffusion coefficients for different gases have been compiled and can be found in the literature (Massman, 1998), (Tang et al., 2014), (Tang et al., 2015). Diffusion at a temperature other than 296 K can be obtained from Equation 15.

$$\text{Equation 15} \quad D(T) = D(296K) \times \left(\frac{T}{296}\right)^{1.75}$$

Thus, knowing the rate constant  $k_{kin}$  the geometric steady state uptake coefficient can be calculated (Equation 16):

$$\text{Equation 16} \quad \gamma_{ss\ geom} = \frac{4k_{kin}V}{cS_{geom}}$$

where  $V$  (cm<sup>3</sup>) and  $S_{geom}$  (cm<sup>2</sup>) are the volume and geometric surface of the region where the reaction takes place, respectively, and  $c$  (cm/s) is the average molecular speed.

Lastly, if necessary, the geometric uptake coefficient  $\gamma_{ss\ geom}$  can be corrected for BET surface area to obtain  $\gamma_{ss\ BET}$ , which, once again, describes the reactive uptake kinetics (Equation 17).

$$\text{Equation 17} \quad \gamma_{ss\ BET} = \gamma_{ss\ geom} \times \frac{S_{geom}}{S_{BET}}$$

where  $S_{geom}$  (m<sup>2</sup>) is the geometric surface of the exposed solid of interest and  $S_{BET}$  (m<sup>2</sup>) is the total BET surface area (the product of specific surface area and the mass of the sample) as obtained using Equation 7-Equation 9.

A great advantage of flow-tube reactors for investigation of heterogeneous reactivity is the ability to investigate reactions under atmospherically relevant levels of relative humidity and atmospheric pressure (if it is operated under these conditions), which is not the case for other techniques, such as Knudsen Cell reactors, that we introduce in the next section.

### 5.2.2 Knudsen cell

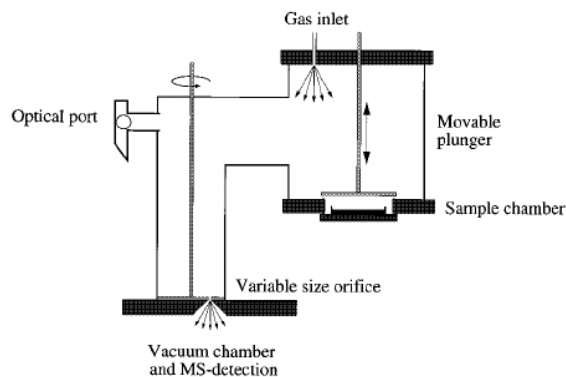


Figure 9: Schematic drawing of a Knudsen Cell.



Knudsen cells have been used as flow reactors for many years to measure kinetic rate constants for heterogeneous gas-solid and gas-liquid reactions (Finlayson-Pitts and Jr, 1999). The Knudsen cell is schematically illustrated in Figure 9. Gas of interest enters the cell through a gas inlet and exits the cell through an escape orifice of a known size. The escaped gas is detected and measured, usually by mass spectrometry. Inside the cell is a sample holder that is initially isolated from the flowing gas by a lid. Knudsen cells are operated under low pressure of less than 10 mTorr to insure that the flow of the gas molecules in the reactor is in the molecular flow regime. Mean free path is defined as the average distance a molecule travels before encountering another molecule. Molecular flow in Knudsen cells is characterized by a long free path (Goodman et al., 2001), (Finlayson-Pitts and Jr, 1999). The long free path insures that the gas molecules collide with the walls of the reactor more than they collide with other gas molecules. This ensures transferability of kinetic results, such as uptake coefficients, to other experimental setups characterized by different surface to volume ratios (Caloz et al., 1997) (Finlayson-Pitts and Jr, 1999). But above all, the long mean free path suppress any limitations related to the gas diffusion of molecules (there are no diffusion corrections in Knudsen cells) and secondary or side reactions that can complicate the chemistry occurring in the reactor.

Quantitative kinetic measurements in Knudsen cells are based on the competition between loss of the gas through the escape orifice and its loss due to heterogeneous interactions with the solid sample. In a typical experiment, initially, the sample of interest is isolated from the gas flow. Under conditions of stable supply of the gas molecules and their constant escape from the Knudsen cell, a steady state flow is established in the reactor. The substrate is then exposed to the gas by lifting the lid. In case there is a net loss of the gas due to its uptake on the reactive surface a decrease in detection signal is observed. From the change in relative concentrations and knowing the area of the escape orifice and the area of the reactive surface, uptake coefficient can be calculated using Equation 18.

*Equation 18* 
$$\gamma = \frac{A_h}{A_s} \times \frac{N_0 - N_r}{N_r}$$

where  $A_h$  ( $\text{m}^2$ ) is the area of the escape orifice,  $A_s$  ( $\text{m}^2$ ) is the geometric area of the reactive surface,  $N_0$  is the number of molecules in the reactor in the absence of reactive surface and  $N_r$  is the number of molecules in the presence of the reactive surface (Finlayson-Pitts and Jr, 1999).

Knudsen cell is an extremely valuable tool extensively used to investigate heterogeneous interactions. The limitations of this technique lay in its inability to mimic relative atmospheric conditions due to the low pressure and dry conditions required for the experiment.

### 5.2.3 Diffuse reflectance infrared Fourier transform spectroscopy

While most of the techniques for studying heterogeneous reactions monitor changes in the gas-phase concentration, some focus on changes on the surface of the solid phase. One of such techniques is diffuse reflectance infrared Fourier transform spectroscopy (DRIFTS). It is used to study the surface of fine particles and powders, and can be used to investigate adsorption of molecules on solid surfaces. Sampling is fast and easy because little or no sample preparation is required. The sample is added to a sample cup and the data is collected on the bulk sample. When the IR beam enters the sample, it can either be reflected off the surface of a particle or be transmitted through a particle. The IR energy reflecting off the surface is typically lost. The IR beam that passes through a particle can either reflect off the next particle or be transmitted through the next particle. The IR radiation interacts with the particles and then reflects off their surfaces, causing the light to diffuse, or scatter, as it moves throughout the sample. This transmission reflectance event can occur many times in the sample, which increases the path length. The detected IR light is partially absorbed by the surface of the particles of the sample, bringing the surface sample information. Shape, compactness, refractive index, reflectivity and absorption of the particles are all characteristics of the material being analyzed. Finally, the diffuse reflection that is produced by the sample surface reflection of the light in all directions is collected by use of an ellipsoid or paraboloid mirror. The output mirror then directs this scattered energy to the detector in the spectrometer. The detector is a semiconductor, usually mercury cadmium telluride (MCT), and the electrons present in it absorb IR light and move from valence band to conduction band. These electrons in the conduction band generate an electrical current proportional to the IR intensity (Subramanian and Rodriguez-Saona, 2009). The detector records the altered IR beam as an interferogram, which can then be used to generate a spectrum. The spectra are plotted in units of log inverse reflectance ( $\log 1/R$ ) versus wavenumber (Finlayson-Pitts and Jr, 1999), (“Volatile Organic Compounds in the Atmosphere,” n.d.), (“FTIR Sample Techniques - Diffuse Reflectance (DRIFTS),” n.d.). The final differential spectra is often calculated by Kubelka-Munk function (“DRIFT Study of the SO<sub>2</sub> Effect on Low-Temperature SCR Reaction over Fe–Mn/TiO<sub>2</sub> - The Journal of Physical Chemistry C (ACS Publications),” n.d.).

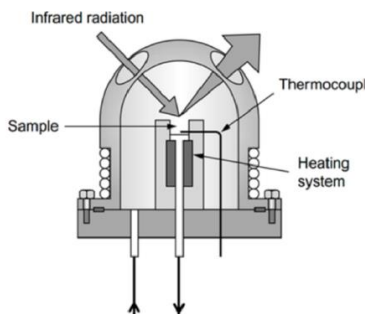


Figure 10: Schematic drawing of a DRIFTS apparatus.

Figure 10 is a schematic diagram of a DRIFTS instrument. DRIFTS can be used to characterize surface reactions. In this case spectra are collected as difference spectra with the unexposed solid as background. The signal is recorded at the regular time intervals in order to observe changes on the surface of the solid phase. If the reaction occurs on the surface, the increase of the products of the reaction can be readily followed and used to describe the reaction kinetics. As the reaction proceeds, growing or decreasing peaks can be attributed to the species formed or consumed on the surface. Infrared spectroscopy provides information about the molecular properties of a sample. In the infrared, bonds that are more active exhibit a large change in dipole moment as they undergo their vibration. The vibrational modes associated with stretching, bending, and rocking motions are analyzed. From this information reaction mechanism can be deduced. Thus, DRIFTS is one of the techniques used to understand heterogeneous processes on the molecular level (Ullerstam et al., 2003) (“Raman + FTIR - A perfect match,” n.d.).

As with other IR spectra DRIFTS peaks reflect quantized adsorptions on the order from 8 to 40 kJ/mol that correspond to the stretching and bending vibrational frequencies of the molecular bonds. In order to be absorbed the radiation frequency should match exactly the natural vibrational frequency of the molecular bond. In addition, a molecule should possess a dipole moment. In general, asymmetric stretching occurs at higher frequencies than symmetric stretching and stretching vibrations occur at higher frequencies than bending vibrations. Another trend is that stronger bonds vibrate at higher frequencies than weaker bonds, and bonds between atoms of higher mass vibrate at lower frequencies than bonds between atoms of lower mass. Since every type of bond has a different frequency of vibration and since the environment of each bond is slightly different for different compounds, the pattern of adsorption is unique for each species. Infrared spectrum provides an important structural information about a molecule (Pavia et al., 2011).

Figure 11 demonstrates a typical DRIFTS spectrum of a mineral dust exposed to SO<sub>2</sub> with assignment of principal bands investigated. A typical peak at 3700 cm<sup>-1</sup> corresponds to the vibration motion of the free surface OH groups. A peak at 3200 cm<sup>-1</sup> is assigned to the stretching of water, while peak at 1650 cm<sup>-1</sup> is due to the bending of water. Peak at 1330 cm<sup>-1</sup> is attributed to the asymmetric stretching vibration of weakly bonded SO<sub>2</sub> species. The expected symmetric stretch vibration of SO<sub>2</sub> at 1140 cm<sup>-1</sup> is not observed. Peaks at 1240 and 2450 cm<sup>-1</sup> are attributed to the formation of SO<sub>4</sub> (Ullerstam et al., 2002). Formation and loss of species as well as the nature of adsorption can be deduced using DRIFTS.

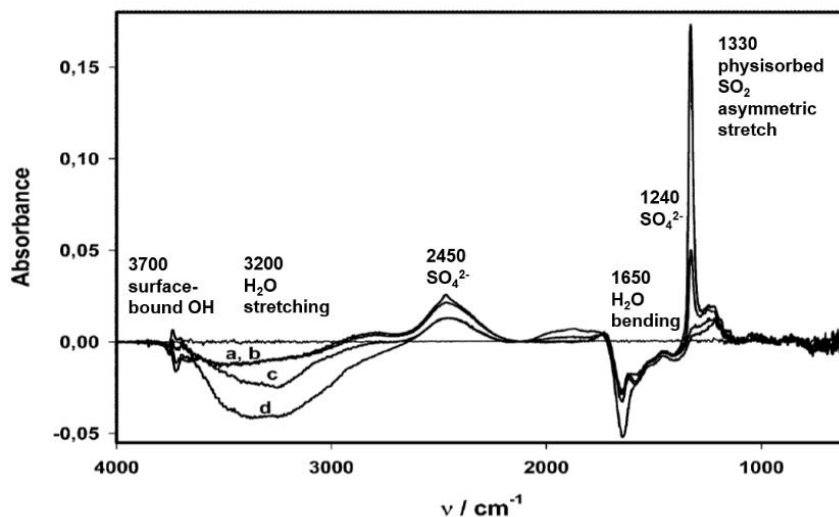


Figure 11: Absorption difference spectra recorded during the reaction of mineral dust with 20 ppm of  $\text{SO}_2$ . Product spectra (a) after addition of  $\text{SO}_2$ , (b) after pumping sample for 10 min without  $\text{SO}_2$ , (c) after pumping sample overnight and (d) after heating of sample to 373 K. Adapted from “The kinetics and mechanism of  $\text{SO}_2$  oxidation by  $\text{O}_3$  on mineral dust” (Ullerstam et al., 2002).

#### 5.2.4 Reactors using suspended aerosol and typical instrumentation

In the past 10 to 15 years, aerosol flow tubes and atmospheric simulation chambers have been widely used to study heterogeneous processes. The objective of these techniques is to provide a more realistic approach to atmospheric particle processing by the gas environment. For that reason, suspended aerosols are introduced using only the finest fraction of particles (in general below 10  $\mu\text{m}$ ,  $< \text{PM}_{10}$ ). In case of aerosol flow tubes, the design and the operational conditions are similar to the atmospheric pressure flow tubes (as described above) with the difference related to the fact that particles are present in suspension (and not deposited) and are continuously introduced in the reactor with the gas mixture. Nevertheless, the volume of aerosol flow tubes is significantly higher than CWFT, ranging in the order of a few liters. As for atmospheric simulation chambers, they are big photochemical reactors (with a volume of a few cubic meters), where a long-lasting aerosol ageing can be carried out under static or dynamic conditions. More information about the simulation chambers can be found on the *EUROCHAMP* community website (“Eurochamp > Eurochamp 2020,” n.d.).

Although the use of suspended aerosol represents a more realistic approach to the processes occurring in the atmosphere, the major disadvantage is that the concentration of the particles introduced in these reactors, i.e. the actual or real surface area of the aerosol particles for reaction, is very low compared to the surface area of the reactor/chamber walls, and thus, the determination of kinetic parameters (such as uptake coefficients) is very challenging. Apart from this, and especially concerning simulation chambers,

the introduction of suspended aerosols, and particularly mineral dust, is not a trivial procedure. The coarse fraction of the dust, being quickly removed through dry deposition, makes the determination of the real surface area of aerosol introduced in the chamber and encountered by gaseous pollutant really problematic. At this point it should be mentioned, that for aerosol flow tubes these limitations are less problematic, since their lower volume allows to achieve higher aerosol concentrations. Besides, dry deposition in aerosol flow tubes can be better controlled, since they are operated under dynamic conditions. **To sum up, both aerosol flow tubes and atmospheric simulation chambers are important tools for the study of heterogeneous processes. Actually, they are ideal tools (especially simulation chambers) to evaluate the impact of long-lasting ageing of aerosols on their physical and chemical properties, but are less adapted to provide kinetic data, such as uptake coefficients.**

To control and monitor the temporal evolution of the physical or chemical properties of the particles, aerosol flow tubes and simulation chambers can be coupled with a wide variety of instrumentation to monitor both the gas and the adsorbed phases. Instruments, such as scanning mobility particle sizer (SMPS) and humidified tandem differential mobility analyzer (HTDMA), are used during a heterogeneous reaction to monitor the evolution of the size fraction and the hygroscopic properties of the aerosol respectively. Other instrumentation such as aerosol mass spectrometry (AMS), is used to evaluate the chemical transformation of the particles during the reaction. Sampling of particles in filters and post analysis can also provide useful information about the chemical transformation of the particles. Common techniques are Ion chromatography (IC), or high performance liquid chromatography (HPLC). Next, we provide a short description of HPLC and AMS techniques that can be used for off-line analysis of aerosol particles and are available and frequently used in our laboratory.

### **High performance liquid chromatography**

High performance liquid chromatography (HPLC) is a technique in analytical chemistry used to separate, identify and quantify components of a mixture. It is the most powerful and applicable separation method. In column chromatography, components of a mixture are carried through stationary phase by the flow of liquid mobile phase causing separation of the components based on differences in migration rates. The stationary phase is held in a narrow tube and mobile phase is forced through the tube under pressure. Stationary phase requires very small particles and thus high pressure of several hundred atmospheres is indispensable for forcing the liquid phase through the column. It wasn't until the late 60-s that technology for producing the sophisticated instrumentation able to use columns with particles of 5 to 10  $\mu\text{m}$  in diameter was developed and commercialized. Mobile phase is usually a combination of solvents, such as a buffered

aqueous solution, acetonitrile, methanol, etc. The interactions between solvent, adsorbent and a sample are physical in nature, such as hydrophobic, dipole-dipole and ionic interactions. Figure 12 shows a diagram of a typical high-pressure chromatographic instrument and includes a solvent reservoir, a degasser, a pump, a sample injector, a column, a detector and data acquisition device. Detectors used in HPLC include UV-VIS, photodiode array, reflective index, fluorescence, inductivity detectors and mass spectrometers (Skoog et al., 1995).

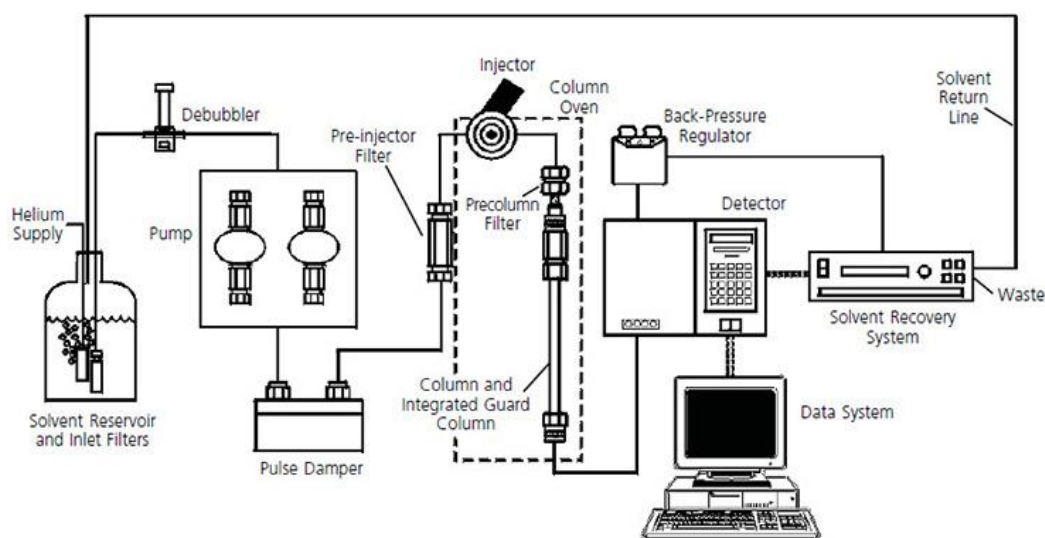


Figure 12: Components of an HPLC system. Adapted from "HPLC Troubleshooting Guide" ("HPLC Troubleshooting Guide," n.d.).

Besides separation, HPLC provides both quantitative and qualitative information for individual components of a mixture whose identities are known. The retention time of an individual component under identical chromatographic conditions is constant. Thus, by comparing the elution time of the unknown to that of the standard, an unknown component can be identified. Besides, the area of the peak is proportional to the amount of the injected compound. Thus, a calibration curve can be derived from peak areas of precisely known concentrations and the peak size of the unknown component can be used to determine its concentration (Meyer, 2004).

Building an HPLC method is a time-consuming and laborious process as it requires testing of many parameters: column type and dimensions, stationary phase, composition and preparation of the mobile phase, temperature, volume, flow rate, and detection and integration parameters of the instrument itself. Once built, the method has to be validated to ensure the consistency of the results and to demonstrate its applicability to the intended use.

## Aerosol mass spectrometry

Aerosol mass spectrometry (AMS) is a valuable method of aerosol characterization applicable to particle sizes in the range of 10 nm to 10  $\mu\text{m}$  in diameter (Nash et al., 2006). A great advantage of using AMS is its compatibility with on-line analysis and consequently the mobility of the instrumentation. AMS is often used on ships, planes other types of mobile laboratory platforms. Instrumental technique can be divided into the methods aiming at bulk characterization and those that focus on single particle characterization (Froyd et al., 2019). In the first case, all aerosol within a defined size range is collected and characterized. This type of mass spectrometry is well adopted to the analysis of non-refractory compounds, which are defined as species that rapidly evaporate at around 600°C under vacuum conditions (e.g. organic molecules, sulfates and nitrates). The most popular AMS instrument that is used for bulk measurements is Aerodyne aerosol mass spectrometer depicted at Figure 13. It consists of three sections: the aerosol inlet, the particle sizing chamber and the particle detection chamber. In the particle detection chamber the particles are flash vaporized and ionized before being analyzed by mass analyzer. Conversely, single-particle aerosol mass spectrometer (SPMS) employs a pulsed laser to desorb particles one at a time (Froyd et al., 2019). The advantage of the second technique is that both refractory and non-refractory particles, such as mineral dust and soot can be analyzed. In general, the limitation of AMS technique lies in the range of sizes and types of particles one instrument can analyze (Nash et al., 2006). In addition, although highly portable, the use of the instrumentation in the immediate vicinity of an active volcano is still very limited, if not entirely impossible.

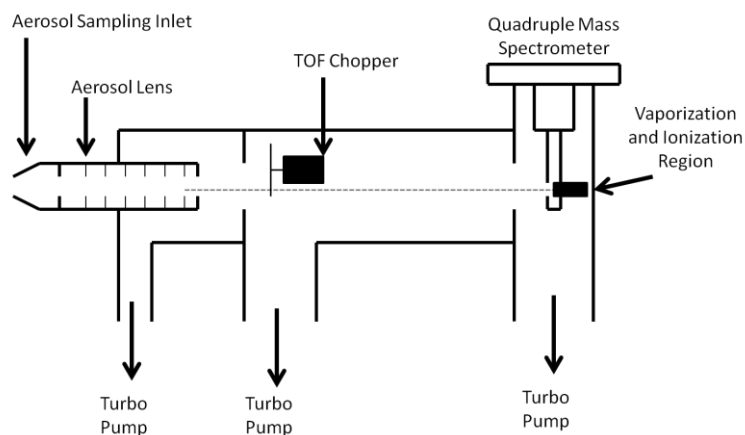


Figure 13: Schematic of the Aerodyne aerosol mass spectrometer (AMS). Adapted from "Aerosol mass spectrometry" ("Aerosol mass spectrometry," 2020).

### 5.3 Laboratory techniques for surface characterization

In order to understand heterogeneous reactivity of solids with a defined gas it is important to investigate the properties of the solid phase in question. Laboratory techniques for bulk and surface

characterizations of solids include scanning electron microscopy, BET analysis, inductively coupled plasma mass spectrometry, X-ray photoelectron spectroscopy, and X-ray powder diffraction spectroscopy. Technically, DRIFTS is also a surface characterization technique, but since in this work it was only used to study adsorbed species and not a solid itself, it was discussed earlier in section 5.2.

### 5.3.1 Scanning electron microscopy (SEM)

SEM is a type of microscopy that uses a focused high-energy beam of electrons to create an image. Electrons from the beam interact with the surface atoms producing secondary electrons, backscatter electrons and characteristic X-rays. Signals obtained due to these interactions are used to obtain surface topography. Typical resolution obtained vary from 1 to 20 nm, but resolution below 1 nm can be achieved by some SEM instruments (“Scanning Electron Microscopy,” n.d.).

### 5.3.2 BET

BET method measures surface area based predominantly on nitrogen gas adsorption. Knowing the size of the probe gas molecule, the amount of the adsorbed gas is correlated to the total surface area of the solid. Measurements are usually done at nitrogen boiling point (-196°C). Principles of Brunauer, Emmett and Teller method for determination of specific surface area were discussed earlier in Section 5.1.1 and the details on the in-house built system is provided in Chapter 2.

### 5.3.3 Inductively coupled plasma mass spectrometry

ICP-MS is a type of mass spectrometry where inductively coupled plasma is used to generate ions from the solid of interest. By definition, a plasma is a conducting gaseous mixture containing a high concentration of cations and anions. ICP-MS uses argon ions as the principle conducting species. Once formed, argon ions can sustain plasma temperatures as high as 10,000 K by absorbing power from an external source. In particular, inductively coupled plasma uses powerful radio-frequency generators as a power source. ICP atomizes the sample and creates atomic ions that are then directed to the mass spectrometer, where they are counted and separated on the basis of their mass-to-charge ratio. The signal received by the detector is proportional to the concentration. ICP-MS is known for its speed, precision and sensitivity. ICP-MS enables detection of elements on levels as low as ppb and ppt (Skoog et al., 1995). It is efficiently used to determine the elemental composition of a solid.

### 5.3.4 X-ray photoelectron spectroscopy

XPS is a technique that studies surface composition and oxidation states of surface atoms. The typical depth of the analyzed sample is about 5 nm. The analysis is done by exciting the sample surface with



mono-energetic Al K $\alpha$  X-rays causing photoelectrons to be emitted from the surface elements. The energy of the emitted photoelectrons is measured by electron energy analyzer. From the binding energy and intensity of a photoelectron peak, the elemental identity, chemical state, and quantity of a detected element can be determined (“X-Ray Photoelectron Spectroscopy (XPS) Surface Analysis Technique,” n.d.).

### 5.3.5 X-ray powder diffraction spectroscopy

XRD is a powerful and rapid technique used for identification of an unknown crystalline material. The basis of the technique is the constructive interference of monochromatic X-rays with the crystalline structure of the sample, which happens when conditions satisfy Bragg's Law:

*Equation 19* 
$$n\lambda = 2d\sin\theta$$

where  $n$  is a positive integer,  $\lambda$  (m) is the wavelength of the incident wave,  $d$  (m) is the interplanar distance between the lattice planes and  $\theta$  is the glancing angle between the incident beam and the surface. Thus, Bragg's Law relates the wavelength of electromagnetic radiation to the diffraction angle and the lattice spacing in a crystalline sample. By scanning the sample through a range of  $2\theta$  angles all possible diffraction directions of the crystalline lattice are obtained. The diffraction peaks are then converted to d-spacings that are unique to each mineral. By comparing the d-spacing of the unknown to that of the reference material the phase is identified. Identification of homogeneous and single-phase material is best for identification of unknown minerals (“X-ray Powder Diffraction (XRD),” n.d.).

Even though multiple techniques are available today to study heterogeneous reactivity, heterogeneous reactions that happen in the atmosphere continue to represent a great challenge to the scientific community (Finlayson-Pitts and Jr, 1999). The main problem comes from limited understanding of how the surface of real atmospheric particles look like on the molecular level. In other words, the environment encountered by a gas molecule in the atmosphere is not well-characterized. In addition, surface changes during reaction, affecting both the reaction mechanism and reactivity. Yet, the consequences of surface “ageing” are also poorly understood. Furthermore, many of the techniques used to describe the surface, such as XPS, are incompatible with atmospheric conditions as they require high vacuum. Nevertheless, great progress has been made in recent years, often using simplified systems, establishing a groundwork for further investigations of heterogeneous interactions. Heterogeneous interactions of SO<sub>2</sub> gas with various solid surfaces are described in the next section (Section 6) laying a groundwork for studying interactions between volcanic SO<sub>2</sub> gas and volcanic ash.

## 6 Groundwork for investigation of the interactions of volcanic dust with SO<sub>2</sub> volcanic gas

Surface chemical and physical properties of the volcanic particles dictate their interactions with atmospheric gases. Being composed of crystals and glass, ash particles display a heterogeneous distribution of sites that can be active in various interactions (Maters et al., 2016). Chemical functional groups that occur on the surface of volcanic ash include weakly acidic silanol groups (Si-OH), siloxanes (Si-O-Si), terminal metal atoms (M), oxo (M-O) and hydroxyl (M-OH) groups. Thus, these sites can provide weakly acidic, basic, reduced or oxidized sites (Table 1) (Maters et al., 2016). The most abundant gases emitted during volcanic eruption are water and carbon dioxide. In comparison with them, sulfur dioxide is a stronger Lewis Acid with a higher affinity for M-O sites and therefore may be preferentially adsorbed on the surface of volcanic ash (Ayris et al., 2013). The elements found in the volcanic ash and reported as oxides include SiO<sub>2</sub>, FeO, TiO<sub>2</sub>, Al<sub>2</sub>O<sub>3</sub>, CaO, MgO, Na<sub>2</sub>O and K<sub>2</sub>O (Dagsson-Waldhauserova et al., 2015). In the following sections heterogeneous reactions of SO<sub>2</sub> gas with various mineral oxides and natural samples are reviewed. In addition, special attention is paid to the influencing factors, such as humidity, UV light and presence of oxidizing species.

Table 6 Active surface sites on the volcanic ash. Adapted from E.C. Maters (Maters et al., 2016)

nature of surface sites	Si-OH	M <sup>+</sup>	M-OH <sup>+</sup>	M-O <sup>-</sup>	M <sup>+</sup> -OH <sup>-</sup>
	Weakly acidic (Brønsted)	Lewis acid	Brønsted acid	Lewis base	Brønsted base

### 6.1 Review of SO<sub>2</sub> interactions with single metal oxides, CaCO<sub>3</sub> and natural dust samples

Using FT-IR Usher et al. investigated formation of sulfite and bisulfite species on the surface of particles representative of mineral dusts found in the atmosphere, such as metal oxides ( $\alpha$ -Al<sub>2</sub>O<sub>3</sub>,  $\alpha$ -Fe<sub>2</sub>O<sub>3</sub>, TiO<sub>2</sub>, SiO<sub>2</sub>, and MgO), calcite (CaCO<sub>3</sub>) and China Loess mineral dust. With the exception of SiO<sub>2</sub>, that showed no adsorption, all other oxides adsorbed SO<sub>2</sub> (Usher et al., 2002).

Reactivity of different mineral oxides comprising earth crust with SO<sub>2</sub> gas was further investigated by Zhang et al. by following the decline in SO<sub>2</sub> concentration in a closed FTIR cell upon contact with various mineral oxides (Zhang et al., 2006). The reactivity of oxides was found to decrease in the following fashion for a fixed mass of sample: FeOOH > Al<sub>2</sub>O<sub>3</sub> > mixture > MgO > TiO<sub>2</sub> > Fe<sub>2</sub>O<sub>3</sub> > SiO<sub>2</sub>. The reactivity normalized by specific area was as follows: Fe<sub>2</sub>O<sub>3</sub> > MgO > TiO<sub>2</sub> > FeOOH > mixture > Al<sub>2</sub>O<sub>3</sub> > SiO<sub>2</sub>. What is more, when

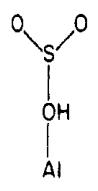
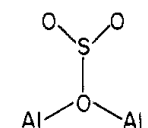
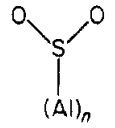
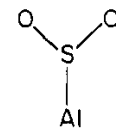
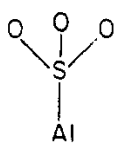
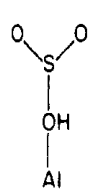
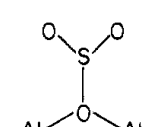
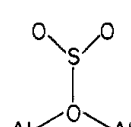
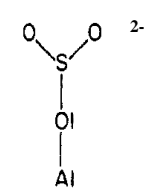
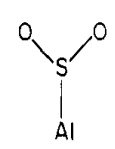
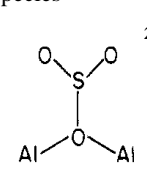
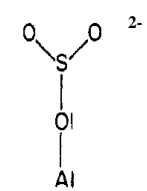
mixed based on the abundance of above oxides in the continental crust ( $\text{SiO}_2:\text{Al}_2\text{O}_3:\text{Fe}_2\text{O}_3:\text{CaO}:\text{MgO}:\text{TiO}_2:\text{MnO}_2 = 61.5:15.1:6.28:5.5:3.7:0.68:0.1$ ), the conversion of  $\text{SO}_2$  was higher than expected due to the synergetic effect of the mixture. Also, more basic type of alumina containing more hydroxyl groups showed higher apparent rate constant for reaction with  $\text{SO}_2$  gas than neutral or acidic aluminum implying that hydroxyls on the surface contribute to the heterogeneous oxidation of  $\text{SO}_2$ . Authors concluded by proposing that metal oxides that have empty or half-empty d atomic orbitals, such as  $\text{Al}_2\text{O}_3$ , show excellent performance in the reactions with  $\text{SO}_2$  while metal oxides with full d orbits, such as  $\text{MgO}$ , show weaker reactivity (Zhang et al., 2006).

Numerous other laboratory studies were undertaken to improve understanding of the interactions of sulfur dioxide with mineral dusts by using various metal oxides as proxies for natural samples. This section of the manuscript covers the literature data on the reactions of various individual mineral oxides and calcite with  $\text{SO}_2$  gas.

#### 6.1.1 $\gamma$ - $\text{Al}_2\text{O}_3$

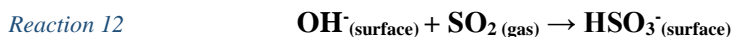
Early studies of Datta et al. in 1985 investigated adsorption of  $\text{SO}_2$  on thermally activated  $\gamma$ -alumina. The authors came to the conclusion that five distinct  $\text{SO}_2$ -like species can be observed by FTIR (Fourier Transform Infrared) spectroscopy (Table 7). The most strongly held one was assigned to the  $\text{SO}_3^{2-}$  bonded in a unidentate mode to the metal atom with characteristic absorption at 1135 and 1065  $\text{cm}^{-1}$ . The most weakly attached species showed absorbance at 1334 and 1148  $\text{cm}^{-1}$  and were labeled as physically adsorbed  $\text{SO}_2$  species weakly bonded to the surface of hydroxyl groups. The other three types of  $\text{SO}_2$ -like species were attached through sulfur atom to either an acidic aluminum metal center or anionic oxygen center and adsorbed at 1140, 1255, 1322, and 1189  $\text{cm}^{-1}$  (Datta et al., 1985). In recent studies Lo et al. performed theoretical calculations for the adsorption of  $\text{SO}_2$  on  $\gamma$ -alumina where they confirmed Datta's assignment of absorption frequencies to type I and II species (see Table 7), but assigned 1255 and 1189  $\text{cm}^{-1}$  bands to  $\text{SO}_2$  that forms strong bonds with surface oxygen atom through sulfur (Lo et al., 2010). As for the  $\text{HSO}_3^-$  bisulfite species the SH stretch vibration was only found in the literature as a theoretical value calculated by Zhang et al. for aqueous solution and reported to be in the range of 2450 to 2620  $\text{cm}^{-1}$  (Zhang and Ewing, 2002).

Table 7: Possible nature of adsorbed species. Adapted from Datta et al., 1985 and Lo et al., 2010 and Goodman et al., 2001

Bands (cm <sup>-1</sup> ) FTIR	1334, 1148	1322, 1140	1255	1189	1135, 1065 (1050)
Type and nature of adsorption on $\gamma$ -Al <sub>2</sub> O <sub>3</sub> as assigned by Datta et al., 1985 using FTIR	<b>type I</b> physisorption, weak 	<b>type II</b> chemisorption on basic O site 	<b>type III</b> chemisorption on acidic Al site 	<b>type VI</b> chemisorption on acidic Al 	<b>type V</b> chemisorption on basic O site (see type II) followed by rearrangement leading to formation of sulfite-like species that gets attached to Al atom in a unidentate fashion 
nature of adsorption on $\gamma$ -Al <sub>2</sub> O <sub>3</sub> as assigned by Lo et al., 2010 by theoretical calculations	physisorption, weak 	chemisorption on basic O site 	SO <sub>2</sub> forms strong bonds with surface oxygen atom through sulfur 	sulfite/bisulfite species in monodentate and bidentate modes 	
nature of adsorption on $\alpha$ -Al <sub>2</sub> O <sub>3</sub> as assigned by Goodman et al., 2001 using FTIR	physisorption, weak 				sulfite/bisulfite species  

### 6.1.2 $\alpha$ -Al<sub>2</sub>O<sub>3</sub> and MgO

Goodman et al. studied formation of sulfate particles on the surface of mineral dust using FTIR (Goodman et al., 2001). In the study they used  $\alpha$ -Al<sub>2</sub>O<sub>3</sub> and MgO, that are characterized as acidic and basic oxides respectively, as models for mineral aerosol found in the atmosphere. They found that SO<sub>2</sub> weakly adsorbs on the surface of  $\alpha$ -Al<sub>2</sub>O<sub>3</sub> and MgO and assigned a band at 1149 cm<sup>-1</sup> as physisorbed v1 symmetric stretch of SO<sub>2</sub> and band at 1330 cm<sup>-1</sup> as physisorbed v3 asymmetric stretch of SO<sub>2</sub>. Both bands disappeared upon evacuation of SO<sub>2</sub> gas. Broad bands between 900 and 1200 cm<sup>-1</sup> on  $\alpha$ -Al<sub>2</sub>O<sub>3</sub> and 800-1125 cm<sup>-1</sup> on MgO surface were assigned to sulfite SO<sub>3</sub><sup>2-</sup> and bisulfite HSO<sub>3</sub><sup>-</sup> species. Upon evacuation of SO<sub>2</sub> gas sulfite/bisulfite bands stayed in the spectra. As for the mechanism of adsorption on  $\alpha$ -Al<sub>2</sub>O<sub>3</sub> surface, contrary to the conclusions of Datta et al. (see Table 7), it was proposed that weakly adsorbed SO<sub>2</sub> forms on acidic sites (coordinately unsaturated aluminum atoms) and surface-coordinated sulfite forms when SO<sub>2</sub> interacts with basic oxide anions (exposed oxygen atoms) or hydroxides on the surface of  $\alpha$ -Al<sub>2</sub>O<sub>3</sub> (Goodman et al., 2001). Moreover, it was suggested that O<sub>2</sub> with low coordination number such as present at kinks and steps of the surface is much more reactive to SO<sub>2</sub> uptake than O<sub>2</sub> found on terrace planes (Goodman et al., 2001). Several reactions leading to the formation of surface coordinated sulfite/bisulfite species were proposed (Goodman et al., 2001).



Growth of peaks around 3524 and 3296 cm<sup>-1</sup> were attributed to the formation of either surface water or OH stretch in the adsorbed bisulfite (Goodman et al., 2001).

A mechanism for the formation of weakly adsorbed SO<sub>2</sub> species and surface coordinated sulfite on MgO surface was very similar to that postulated for  $\alpha$ -Al<sub>2</sub>O<sub>3</sub>: weakly adsorbed SO<sub>2</sub> forms on acidic magnesium sites, while surface coordinated sulfite forms on basic oxide anions (Reaction 14) (Goodman et al., 2001).



Assignment of vibrational peaks of Goodman et al. on  $\alpha$ -Al<sub>2</sub>O<sub>3</sub> and MgO was confirmed by numerous authors on various mineral oxide substrates, such as Wang et al. on Fe<sub>2</sub>O<sub>3</sub> and Nanayakkara on TiO<sub>2</sub> (Wang et al., 2018a), (Nanayakkara et al., 2012). More details on the peak assignments for different individual vibrations on different surfaces can be found in Table 9.

### 6.1.3 Fe<sub>2</sub>O<sub>3</sub>

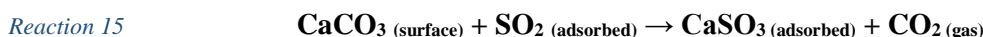
Wang et al. studied heterogeneous reactions of sulfur dioxide on hematite (Fe<sub>2</sub>O<sub>3</sub>) nanoparticles (Wang et al., 2018a). Just as Goodman et al. earlier, he came to the conclusion that when SO<sub>2</sub> gas interacts with the surface it forms weak physical bonds with Lewis acid sites (metal sites) and strong chemical bonds with Lewis base sites (exposed oxygen sites) (Reaction 11). In agreement with Reaction 12 and Reaction 13 they admitted that hydroxyl groups provide additional pathways for the reaction with SO<sub>2</sub>.

### 6.1.4 TiO<sub>2</sub>

Nanayakkara et al. further demonstrated the importance of OH groups by studying adsorption of SO<sub>2</sub> gas on both hydroxylated and dehydroxylated isotopically labeled TiO<sub>2</sub> particles and showed that dehydroxylated particles show less reactivity with little product formation (Nanayakkara et al., 2012). Thus, he concluded that OH groups play a very important role in the conversion of SO<sub>2</sub> gas into surface sulfites and bisulfites (Reaction 12 and Reaction 13). Furthermore he concluded that SO<sub>2</sub> prefers reacting with isolated OH groups followed by bridged hydroxyl groups.

### 6.1.5 CaCO<sub>3</sub>

On the surface of CaCO<sub>3</sub> a slightly different mechanism is observed. Wu et al. suggested that after adsorption to the surface physisorbed SO<sub>2</sub> directly reacts with CaCO<sub>3</sub> surface to yield sulfite ion and CO<sub>2</sub> gas. This reaction is thermodynamically favorable (Reaction 15) (Wu et al., 2011).

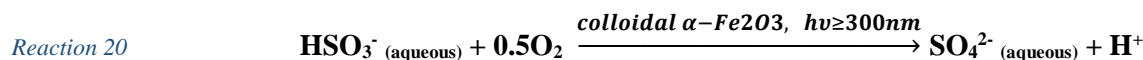
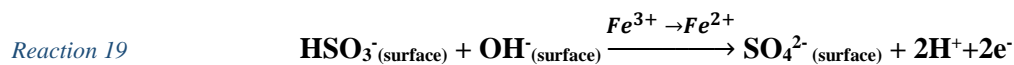
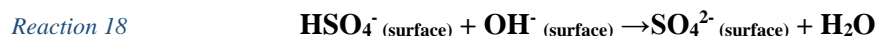
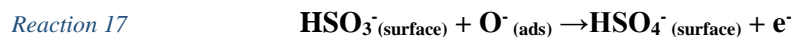
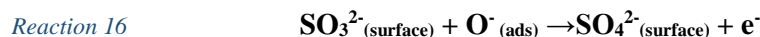


## 6.2 Oxidation of sulfites to sulfates

Conversion of chemisorbed sulfites to sulfates has been reported in the literature for reactions of SO<sub>2</sub> with  $\alpha$ -Al<sub>2</sub>O<sub>3</sub> and MgO oxide surfaces in the presence of molecular oxygen at elevated temperatures (Goodman et al., 2001).

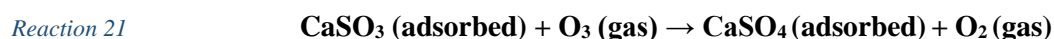
Wang et al. noticed oxidation of sulfites to sulfates on the surface of Fe<sub>2</sub>O<sub>3</sub> in the presence of air and suggested either a one-step process of oxidation of sulfites to sulfates by active oxygen (Reaction 16) or a two-step process of oxidation of bisulfites to bisulfates by active oxygen followed by reaction with hydroxyl group to produce SO<sub>4</sub><sup>2-</sup> ion (Reaction 17, Reaction 18). He suggested that active oxygen O<sup>•</sup> can be derived from molecular oxygen upon reaction with the vacant oxygen sites present on the surface. In addition, it was proposed that iron atoms can contribute to the formation of sulfate species from bisulfites as per Reaction 19 (Wang et al., 2018a). Oxidation of sulfites to sulfates by molecular oxygen catalyzed by

iron-containing species in aqueous medium was first proposed by Faust et al. (Reaction 20) (Faust et al., 1989).



On the surface of TiO<sub>2</sub> mechanism identical to that on Fe<sub>2</sub>O<sub>3</sub> was proposed by Nanayakkara et al. (Reaction 16 - Reaction 18) (Nanayakkara et al., 2012).

Li et al. investigated the oxidation mechanism of sulfur dioxide by ozone on the surface of calcium carbonate. The results demonstrated that SO<sub>2</sub> can be adsorbed on the surface of CaCO<sub>3</sub> to form sulfites that can be rapidly oxidized into sulfates by O<sub>3</sub>. In a step-exposure experiment when SO<sub>2</sub> was introduced a band at 1000-900 cm<sup>-1</sup> was immediately observed, corresponding to the ν<sub>3</sub> stretching vibration of sulfite. Upon introduction of O<sub>3</sub> into the reaction system a band at 980 cm<sup>-1</sup> disappeared within minutes and a band at 1130 cm<sup>-1</sup> appeared, corresponding to the ν<sub>3</sub> stretching vibration of sulfate. In the simultaneous exposure of SO<sub>2</sub> and O<sub>3</sub> experiment the main product detected by DRIFTS was a sulfate band at 1130 cm<sup>-1</sup>. Ion chromatography analysis further confirmed that the main product detected was sulfate species. The reaction rate was calculated to be first order for SO<sub>2</sub> and zero order in respect to O<sub>3</sub> (Li et al., 2006). The reaction of CaSO<sub>3</sub> with O<sub>3</sub> is irreversible and very fast (Reaction 21) (Wu et al., 2011).



Usher et al. investigated oxidation of sulfites in the presence of ozone. Upon reaction with ozone, the conversion of chemisorbed sulfite-bisulfite to sulfate/bisulfate species was observed as new peaks around 1000 and 1100 cm<sup>-1</sup> for MgO and α-Al<sub>2</sub>O<sub>3</sub> respectively (Usher et al., 2002). No conversion was observed in the presence of only air and oxygen (Usher et al., 2002).

Ullerstam et al. further investigated oxidation of sulfites to sulfates by ozone on the surface of Saharah desert dust samples from Cape Verde islands using DRIFTS technique. Formation of sulfate peak was observed at 1240 cm<sup>-1</sup>. In comparison to free sulfate ion that shows a ν<sub>3</sub> vibration at 1105 cm<sup>-1</sup> the peak was shifted to lower frequency due to the lowering the symmetry of the sulfate as it bonds to the surface via the oxygen atom. Addition of water was shown to increase the total amount of sulfate formed on the surface. Authors conclude that the mechanism for oxidation of SO<sub>2</sub> to sulfate ion proceeds via two-step mechanism.

First, SO<sub>2</sub> gets reversibly adsorbed to the surface (Reaction 22). This step is indicated by the formation of an absorption band at 1330 cm<sup>-1</sup> and the loss of free OH<sup>-</sup> around 3700 cm<sup>-1</sup>. Second, adsorbed SO<sub>2</sub> is oxidized to sulfate by ozone (Reaction 23). The permanent loss of OH groups may indicate that sulfuric acid or hydrogen sulfite can be the primary products of this reaction. The reaction order for the first step is close to first order and for the second step to zero order indicating that the first reaction is a rate-determining step. Thus, as soon as SO<sub>2</sub> gets adsorbed on the surface it gets oxidized by ozone (Ullerstam et al., 2002).



where OH are free surface OH groups, M is a metal, and brackets denote surface species.



Similar mechanism was proposed for oxidation of adsorbed SO<sub>2</sub> by NO<sub>2</sub> gas on the surface of Saharah dust (Reaction 24) (Ullerstam et al., 2003). Just as Usher et al., no significant sulfate formation was observed by Ullerstam et al. without presence of the oxidant (Usher et al., 2002) , (Ullerstam et al., 2002), (Ullerstam et al., 2003).



### 6.3 Role of humidity

Grassian et al. studied adsorption of water on alumina powders and identified adsorption at 3420 cm<sup>-1</sup> on α-Al<sub>2</sub>O<sub>3</sub> and 3444 cm<sup>-1</sup> on γ-Al<sub>2</sub>O<sub>3</sub> as OH stretching vibrations of adsorbed water. They also pointed out that the first few layers of water are ordered even at room temperature. Table 8 shows characteristic water IR adsorption wavelengths for different vibrations in gas, liquid and solid phase (Al-Abadleh and Grassian, 2003). In general, distorted molecular environment contributes to broadening of the bands (Al-Abadleh and Grassian, 2003). Formation of water monolayer on the natural dust samples originated from North and West Africa, Saudi Arabia and Gobi desert regions was observed at RH ranging from 15 to 25%, while additional water layers were formed at higher RH levels (Joshi et al., 2017).

*Table 8: IR vibration modes of water using FT-IR. Adapted from “FT-IR Study of Water Adsorption on Aluminum Oxide Surfaces” (Al-Abadleh and Grassian, 2003).*

Vibration Mode	Gas	Water	Solid
<b>Stretching</b>	<i>ν</i> 1 at 3656 cm <sup>-1</sup> <i>ν</i> 3 at 3755 cm <sup>-1</sup>	3319 cm <sup>-1</sup>	3411 cm <sup>-1</sup>
<b>Bending</b>	1594 cm <sup>-1</sup>	1642 cm <sup>-1</sup>	1641 cm <sup>-1</sup>
<b>Association band</b>		2138 cm <sup>-1</sup>	
<b>Overtone band</b>			2243 cm <sup>-1</sup>



In the experiments investigating the role of water on the adsorption of SO<sub>2</sub> gas on the surface of  $\alpha$ -Al<sub>2</sub>O<sub>3</sub> and MgO it was observed that water does not affect strongly adsorbed SO<sub>2</sub> on  $\alpha$ -Al<sub>2</sub>O<sub>3</sub>, but contributes to the creation of sulfate species on the surface of MgO particles (new bands at 957 and 1110 cm<sup>-1</sup> appear in the spectrum) (Goodman et al., 2001). In line with Datta et al. the peak for water adsorption was identified through H<sub>2</sub>O bending mode at 1640 cm<sup>-1</sup> (Goodman et al., 2001), (Al-Abadleh and Grassian, 2003).

While investigating the oxidation mechanism of sulfur dioxide by ozone on the surface of calcium carbonate *Li et al.* showed that the initial rate of sulfate formation is independent of humidity, but the steady-state generation of sulfate is increased with increased humidity. It was concluded that water can regenerate the reactivity of CaCO<sub>3</sub> particles and enhance their capability of sulfate formation (Li et al., 2006). Water on the surface permits more SO<sub>2</sub> into aqueous layer (Li et al., 2006). In its turn, surface containing sulfates adsorbs more water than unprocessed particles (Li et al., 2006). Thus, formation of sulfates on the surface of the particles changes their physical properties and might have important impact on atmospheric chemistry.

In contrast to the above-mentioned results, on the surface of hematite ( $\alpha$ -Fe<sub>2</sub>O<sub>3</sub>) and goethite ( $\alpha$ -FeOOH) particles equivalent saturation coverages and product ratios were observed at RH ranging from 28 to 85% leading to the conclusion that water vapor has no effect on the uptake of SO<sub>2</sub> (Baltrusaitis et al., 2007).

Then again, Shang et al. demonstrated a steady increase in sulfate production on the surface of TiO<sub>2</sub> from dry to 80% followed by a slight decrease at 90% (Shang et al., 2010). The authors suggested that water molecules, besides participating in the reaction as a reactor might also form a film layer that promoted product diffusion and surface refreshment. As for the reduction of sulfate formation at RH higher than 80%, hindering of active sites on the surface by water molecules was offered as a possible cause (Shang et al., 2010).

On the surface of natural samples the role of humidity on SO<sub>2</sub> uptake is rather controversial. Thus, using DRIFTS, the role of water was highlighted in its ability to regenerate the surface of the natural Saharrah desert dust from the Cape Verde Islands located off the coast of west Africa and thus enhance its capacity for sulfate formation (Ullerstam et al., 2002). Meanwhile, no dependency on humidity was found for the initial uptake coefficient of SO<sub>2</sub> gas on the same-origin Saharan dust collected from the Cape Verde Islands using coated wall-tube reactor (Adams et al., 2005). Likewise, no such dependence was observed for Adobe clay soil taken from Los Angeles area (Judeikis and Stewart, 1976). Huang et al. noticed that when three authentic dusts were subjected to SO<sub>2</sub> at RH ranging from 0 to 90% an increase in uptake coefficient was observed for Tengger Desert dust (i.e.  $\gamma_{\text{BET}}(\text{dry}) \approx 3.8 \times 10^{-5}$  and  $\gamma_{\text{BET}}(90\% \text{ RH}) \approx 5.5 \times 10^{-5}$ ) and for

Arizona test dust (i.e.  $\gamma_{\text{BET}}(\text{dry}) \approx 1.3 \times 10^{-5}$  and  $\gamma_{\text{BET}}(90\% \text{ RH}) \approx 2.76 \times 10^{-5}$ ), but a decrease was observed for Asian mineral dust (i.e.  $\gamma_{\text{BET}}(\text{dry}) \approx 3.2 \times 10^{-5}$  and  $\gamma_{\text{BET}}(90\% \text{ RH}) \approx 1.9 \times 10^{-5}$ ) (Huang et al., 2015). Inhibition of the SO<sub>2</sub> uptake by water-soluble inorganic coating present on Asian mineral dust was suggested as a possible cause. Upon removal of the coating by washing, the uptake trend got reversed (i.e.  $\gamma_{\text{BET}}(\text{dry}) \approx 0.85 \times 10^{-5}$  and  $\gamma_{\text{BET}}(90\% \text{ RH}) \approx 1.32 \times 10^{-5}$ ) (Huang et al., 2015). Difference in mineralogy could be responsible for the difference in the observed trends (Zhou et al., 2014).

## 6.4 Role of the UV light

While travelling through the air dust particles are likely to be illuminated by UV light. UV light seems to increase the formation of sulfates on the surface. Two mechanisms were proposed to explain this phenomena: photocatalysis and photochemistry.

### 6.4.1 Photocatalysis

Dupart et al. studied the reactions of SO<sub>2</sub> with two proxies for mineral dust, Arizona Test Dust and Fe<sub>2</sub>O<sub>3</sub>, and suggested that metal oxide groups present on the surface of mineral dust when irradiated with UV light and upon contact with water are able to produce OH radicals, which in turn, initiate conversion of SO<sub>2</sub> to sulfuric acid in the vicinity of the dust particle (Dupart et al., 2012). The authors propose that metal oxides in the dust can act as atmospheric photocatalysts by absorbing UV photons and forming electron-hole (e<sup>-</sup>-h<sup>+</sup>) pairs according to Reaction 25, but this approach needs deeper investigation and confirmation:



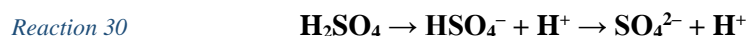
Water molecules could react with holes and split, releasing reactive protons and •OH radicals in the vicinity of the surface (Reaction 26), as shown with SO<sub>2</sub> uptake by Arizona Test Dust (Dupart et al., 2012), (George et al., 2015):



•OH radicals could further react with SO<sub>2</sub> and form HSO<sub>3</sub>• (Reaction 27), which reacts with O<sub>2</sub> to form SO<sub>3</sub> (Reaction 28). Finally, H<sub>2</sub>SO<sub>4</sub> would be formed by reaction of SO<sub>3</sub> with H<sub>2</sub>O (Reaction 29) (Dupart et al., 2012), (Park and Jang, 2016), (Park et al., 2017)



In the presence of water  $\text{H}_2\text{SO}_4$  would readily ionize and successively release two protons, to form  $\text{HSO}_4^-$  and  $\text{SO}_4^{2-}$  as described by Reaction 30 (Wang et al., 2018b).



$\text{H}_2\text{SO}_4$  plays an important role as aerosol precursor as it is implied in nucleation events (Dupart et al., 2012). This reaction network relies mostly on the fact that, in presence of both  $\text{H}_2\text{O}$  and a source of UV radiation,  $\bullet\text{OH}$  radicals are formed. Huang et al. also observed that, in presence of a source of  $\bullet\text{OH}$  radicals ( $\text{H}_2\text{O}_2$  in their study),  $\text{SO}_2$  uptake by mineral dust was largely increased (Huang et al., 2015).

#### 6.4.2 Photochemistry

Alternatively, or in addition to possible surface activation by photons, it was suggested by Martins-Costa et al. that photochemistry could take place at the surface of  $\nu$ -dust covered with a water layer. In the presence of  $\text{H}_2\text{O}$  vapor,  $\text{SO}_2$  photochemistry can lead to the formation of  $\bullet\text{OH}$  and  $\text{HOSO}\bullet$  radicals (Reaction 31) (Martins-Costa et al., 2018):



$\text{HOSO}\bullet$  dissociates spontaneously and completely in water, releasing  $\text{SO}_2^-$  and a proton (Reaction 32).  $\text{SO}_2^-$  finally reacts with  $\bullet\text{OH}$  to form  $\text{HSO}_3^-$  (Reaction 33) (Ruiz-López et al., 2019).



Bisulfite then reacts following Reaction 17, Reaction 18, Reaction 19 to form sulfate ions, or following Reaction 34 to form sulfite ions (Wang et al., 2018a), (Wang et al., 2018b). The reactivity of sulfite ions with radicals has been reviewed by (Neta and Huie, 1985); the reactions involving  $\text{SO}_3^{2-}$  and relevant for atmospheric chemistry are (Reaction 35) with  $\bullet\text{OH}$  radicals, and (Reaction 36) with a photon, both leading to the formation of  $\bullet\text{SO}_3^-$ .



Although the absorption of  $\text{SO}_3^{2-}$  is low in the 350 - 410 nm range, it is not zero (Dogliotti and Hayon, 1968), making Reaction 36 a possible pathway. More reactions can be found in (Neta and Huie, 1985), and show the formation of oxidant species very reactive toward organics, such as  $\bullet\text{SO}_5^-$ ,  $\bullet\text{SO}_4^-$ ,  $\text{HSO}_5^-$ ,  $\text{HSO}_4^-$  and  $\text{S}_2\text{O}_8^-$ . An  $\bullet\text{SO}_3^-$  radical reacts with  $\text{H}_2\text{O}$  and forms  $\text{H}_2\text{SO}_4$  and an electron (Reaction 37).



Finally,  $\text{H}_2\text{SO}_4$  produces bisulfate and sulfate ions following Reaction 30. Overall, photo-activation of the surface and photochemistry of adsorbed species lead to the same final products, but via different pathways, and therefore with different intermediates and kinetics.

## 6.5 Influence of $\text{SO}_2$ -covered particles on other species

An interesting aspect of  $\text{SO}_2$  interaction with the surface is the way it might influence formation of other surface species. Jiang et al. investigated adsorption of  $\text{SO}_2$  on  $\text{Fe}(0.1)\text{-Mn}(0.4)/\text{TiO}_2$  catalytic surface and came to the conclusion that  $\text{SO}_2$  was adsorbed on the surface as the bidentate mononuclear sulfate. This kind of surface could produce new Lewis acid sites on the surface, which upon addition of water would be transferred into Brønsted acid sites. It was also noticed that formation of surface complex of sulfate was in competition with that of nitrate but did not have an effect on the adsorption of  $\text{NH}_3$  (Figure 14) (Jiang et al., 2010).

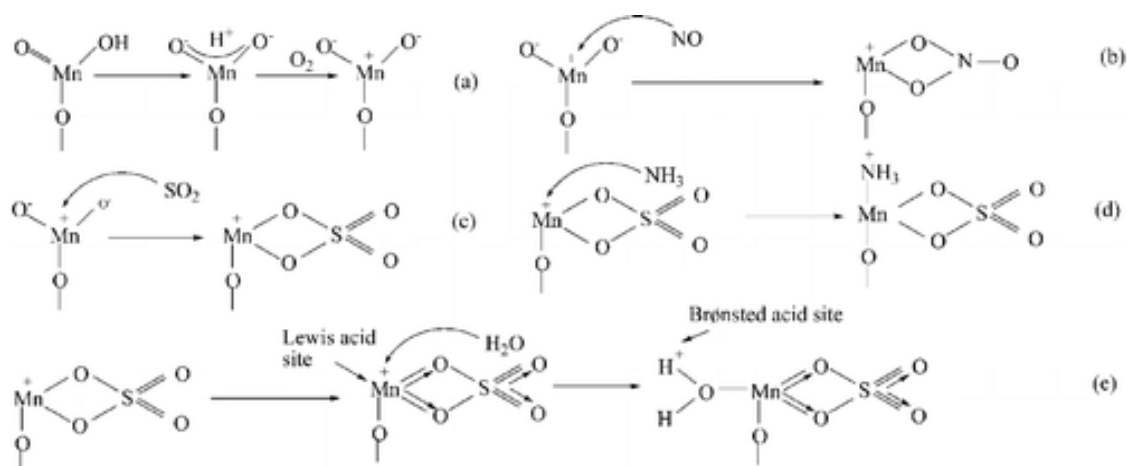


Figure 14: Mechanism of adsorption of  $\text{SO}_2$ ,  $\text{NO}$  and  $\text{NH}_3$  on the surface of  $\text{Fe}(0.1)\text{-Mn}(0.4)/\text{TiO}_2$  catalytic surface. Adapted from “DRIFT Study of the  $\text{SO}_2$  Effect on Low-Temperature SCR Reaction over  $\text{Fe-Mn}/\text{TiO}_2$ ” (Jiang et al., 2010).

## 6.6 Atmospheric implications

The importance of heterogeneous reactions of  $\text{SO}_2$  with different particles can be evaluated against its loss in the gas phase. According to Li et al. the lifetime of  $\text{SO}_2$  reacting on  $\text{CaCO}_3$  is 20-30 hours in dust conditions, 5-10 hours in dust storms, and 3-5 hours in extreme dust storms (Li et al., 2006). Ullerstam et al. calculated the lifetime of  $\text{SO}_2$  reacting on Saharan dust to be 3-6 hours in dust conditions, 1-2 hours in dust storms, and 0.5-1 hours in extreme dust storms (Ullerstam et al., 2002). The average lifetime of  $\text{SO}_2$  in the atmosphere is about 5 days due to cloud processing (Li et al., 2006). Thus, heterogeneous reactions of  $\text{SO}_2$  on the surface of mineral dust and volcanic ash particles might be an important sink for the  $\text{SO}_2$  species.

However, large uncertainties remain due to the lack of detailed information about surface properties (Li et al., 2006).

## **6.7 Limitations of the present research and directions for further work**

The majority of literature sources point out to the adsorption of SO<sub>2</sub> gas on the surface of mineral oxides in the form of sulfites and sulfates, with sulfates being the final and stable product of surface oxidation processes. Hydroxyl groups are suggested to play an important role in the process. Oxidation is reported to be most likely triggered by ozone, NO<sub>2</sub>, or oxygen in the presence of iron-containing species. The role of water in the formation of sulfites and sulfates remains rather controversial, with either increase, decrease or even no effect reported in the literature. UV light seems to increase the formation of sulfates on the surface of mineral dust proxies as well as water-covered particles, but scarce data are available on natural samples. The assignment of vibrational bands corresponding to different sulfur species is still sometimes contradictory (see Table 7). Various mineral oxides are used as models or surrogates for natural mineral dust aerosols found in the troposphere, even though such approach undermines the complexity of their mineralogy and definitively questions the representativeness of proxies. As for the natural mineral dust samples, limited information is available on the components responsible for the uptake and the transformations of SO<sub>2</sub> on natural desert dust. Almost none of the studies deal with complex natural volcanic samples.

**To sum up, after carefully reviewing the extensive published work, the following deficiencies can be established:**

- (i) simplified proxies are often used instead of real natural samples (Goodman et al., 2001), (Usher et al., 2002), (Wang et al., 2018b),**
- (ii) many experiments are performed under atmospherically irrelevant conditions such as 0% RH or/and low pressure (Goodman et al., 2001), (Maters et al., 2016),**
- (iii) high SO<sub>2</sub> concentrations starting from 2.5 ppm (Li et al., 2006), but usually much higher, such as 50 ppm (Shang et al., 2010) are employed for DRIFTS investigations,**
- (iv) initial uptakes, as opposed to steady-state uptakes, are used to describe long-lasting atmospheric processes of interaction of SO<sub>2</sub> gas with atmospheric particles (Maters et al., 2017), (Ullerstam et al., 2003),**
- (v) (iv) very limited information is available on the reactions of SO<sub>2</sub> with natural volcanic dusts.**

**In the following chapters I will attempt to bridge these gaps in knowledge by:**

- (i) using natural volcanic dust samples,**
- (ii) running the experiments under atmospherically relevant conditions of RH and pressure,**
- (iii) measuring steady-state uptake coefficients, and**
- (iv) using whenever possible atmospherically relevant concentrations of SO<sub>2</sub> gas.**

Table 9: Methods and preferred uptake values for reactions of SO<sub>2</sub> with mineral dust and various mineral oxides.

Adsorbent	T	Technique	RH	Concentration of gas	Surface area cm <sup>2</sup> /mg	Results		Uptake coefficients and reaction rate constants	Reference
						wavelength cm <sup>-1</sup>	assigned species		
γ Al <sub>2</sub> O <sub>3</sub>	673 K 973 K	FTIR			A <sub>BET</sub> =2960	1148 1334 1335 1165 1255 1189	v1 symmetric stretch of SO <sub>2</sub> , hydroxyl bonded v3 asymmetric stretch SO <sub>2</sub> , hydroxyl bonded sulfite-like species sulfite-like species SO <sub>2</sub> bonded to aluminum SO <sub>2</sub> bonded to aluminum		Datta et al. 1985
α-Al <sub>2</sub> O <sub>3</sub>	296 K	FT-IR		4 ppm- 468 ppm	A <sub>BET</sub> =140	900-1200  960 1015 1098 1149  1330  3296 3524 3707 3748	broad, chemisorbed, sulfite SO <sub>3</sub> <sup>2-</sup> and bisulfite HSO <sub>3</sub> <sup>2-</sup>  v1 symmetric stretch of weakly, physisorbed SO <sub>2</sub> (disappears upon evacuation of SO <sub>2</sub> ) v3 asymmetric stretch of weakly, physisorbed SO <sub>2</sub> (disappears upon evacuation of SO <sub>2</sub> ) positive, Hydroxyl region positive, Hydroxyl region negative, surface OH loss or OH involved in hydrogen bonding negative, surface OH loss or OH involved in hydrogen bonding		Goodman et al., 2001
	296 K	Knudsen cell						γ <sub>i</sub> Al <sub>2</sub> O <sub>3</sub> = 9.5±0.3×10 <sup>-5</sup>	Goodman et al., 2001
MgO	296 K	FT-IR		4 ppm- 6990 ppm	A <sub>BET</sub> =150	800-1125  896 948 1064 1149  1330	broad, chemisorbed, sulfite SO <sub>3</sub> <sup>2-</sup> and bisulfite HSO <sub>3</sub> <sup>2-</sup>  v1 symmetric stretch of weakly, physisorbed SO <sub>2</sub> (disappears upon evacuation of SO <sub>2</sub> ) v3 asymmetric stretch of weakly, physisorbed SO <sub>2</sub> (disappears upon evacuation of SO <sub>2</sub> )		Goodman et al., 2001
	296 K	Knudsen cell						γ <sub>i</sub> MgO = 2.6±0.2×10 <sup>-4</sup>	Goodman et al., 2001
α-Al <sub>2</sub> O <sub>3</sub>	Room temp.	Knudsen cell	~ 0%		A <sub>BET</sub> =140			γ <sub>i</sub> Al <sub>2</sub> O <sub>3</sub> = 1.6±0.5×10 <sup>-4</sup>	Usher et al., 2002
	Room temp.	FT-IR				1018, broad	stretching motion of adsorbed sulfite SO <sub>3</sub> <sup>2-</sup> and/or bisulfite HSO <sub>3</sub> <sup>2-</sup>		Usher et al., 2002

$\alpha$ -Fe <sub>2</sub> O <sub>3</sub>	Room temp.	Knudsen cell	~ 0%		A <sub>BET</sub> =23			$\gamma_i \alpha$ -Fe <sub>2</sub> O <sub>3</sub> = 7.0±2×10 <sup>-5</sup>	Usher et al., 2002
	Room temp.	FT-IR				850-1100	stretching motion of adsorbed sulfite SO <sub>3</sub> <sup>2-</sup> and/or bisulfite HSO <sub>3</sub> <sup>2-</sup>		Usher et al., 2002
CaCO <sub>3</sub>	Room temp.	Knudsen cell	~ 0%		A <sub>BET</sub> =4.6	CaCO <sub>3</sub>		$\gamma_i$ CaCO <sub>3</sub> = 1.4±0.7×10 <sup>-4</sup>	Usher et al., 2002
	Room temp.	FT-IR				850-1100	stretching motion of adsorbed sulfite SO <sub>3</sub> <sup>2-</sup> and/or bisulfite HSO <sub>3</sub> <sup>2-</sup>		Usher et al., 2002
TiO <sub>2</sub>	Room temp.	Knudsen cell	~ 0%		A <sub>BET</sub> =500	TiO <sub>2</sub>		$\gamma_i$ TiO <sub>2</sub> = 1.0±0.2×10 <sup>-4</sup>	Usher et al., 2002
	Room temp.	FT-IR				850-1100	stretching motion of adsorbed sulfite SO <sub>3</sub> <sup>2-</sup> and/or bisulfite HSO <sub>3</sub> <sup>2-</sup>		Usher et al., 2002
SiO <sub>2</sub>	Room temp.	Knudsen cell	~ 0%		A <sub>BET</sub> =2500			$\gamma_i$ SiO <sub>2</sub> <1×10 <sup>-7</sup>	Usher et al., 2002
	Room temp.	FT-IR					SiO <sub>2</sub> exhibits virtually no reactivity toward SO <sub>2</sub> gas		Usher et al., 2002
MgO	Room temp.	Knudsen cell	~ 0%		A <sub>BET</sub> =150	MgO		$\gamma_i$ MgO = 5.1±0.5×10 <sup>-4</sup>	Usher et al., 2002
	Room temp.	FT-IR				960, broad 923, broad	stretching motion of adsorbed sulfite SO <sub>3</sub> <sup>2-</sup> and/or bisulfite HSO <sub>3</sub> <sup>2-</sup>		Usher et al., 2002
China Loess	Room temp.	Knudsen cell	~ 0%		A <sub>BET</sub> =110			$\gamma_i$ China Loess = 3±1×10 <sup>-5</sup>	Usher et al., 2002
	Room temp.	FT-IR				850-1100	stretching motion of adsorbed sulfite SO <sub>3</sub> <sup>2-</sup> and/or bisulfite HSO <sub>3</sub> <sup>2-</sup>		Usher et al., 2002
Mineral dust from Cape Verde islands	Room temp.	DRIFTS	~ 0%	20 ppm		1330 1240 2450 1650 3200 3700	physisorbed SO <sub>2</sub> , v <sub>3</sub> stretch, sharp, disappears when pumped in the absence of SO <sub>2</sub> sulfate formed upon oxidation with O <sub>3</sub> , weak, stable to pumping and heating broad negative, loss of surface water negative, loss of surface water negative, loss of surface OH groups		Ullerstam et al. 2002
	Room temp.	DRIFTS	~ 0%	0.089 ppm to 0.813 ppm	A <sub>BET</sub> =500			$\gamma$ mineral dust = 5±1×10 <sup>-7</sup> in the presence of 0.227 ppm of O <sub>3</sub>	Ullerstam et al. 2002
Mineral dust from Cape Verde islands	Room temp.	DRIFTS	~ 0%	0.382 ppm	A <sub>BET</sub> =500	1330 1240 1280 2450 3700	physisorbed SO <sub>2</sub> sulfate formed upon oxidation with NO <sub>2</sub> sulfate formed upon oxidation with NO <sub>2</sub> hydrogen sulfite negative, loss of surface OH groups		Ullerstam et al. 2003
	Room temp.	Knudsen cell	~ 0%		A <sub>BET</sub> =500			$\gamma$ mineral dust = 1.6±0.1×10 <sup>-5</sup>	Ullerstam et al. 2003
CaCO <sub>3</sub>	Room temp.	DRIFTS	40%	2.44 ppm -40 ppm	A <sub>BET</sub> =19.5	1000-900 1130	sulfite stretching v <sub>3</sub> vibration sulfate v <sub>3</sub> stretching vibration after explosion to 20 ppm of O <sub>3</sub> , peak remain after heating to 300°C under vacuum		Li et al. 2006



CaCO <sub>3</sub>	296 K	DRIFTS	1% - 90%	19 ppm		923-985 1090-1197	sulfite sulfate		Zhang et al. 2018
Fe(0.1)- Mn(0.4)/TiO <sub>2</sub>	423 K	DRIFTS		500 ppm		976 1050 1149 1278 1344 1428	sulfate or bisulfate stretching, v1 sulfate or bisulfate stretching, v3 sulfate or bisulfate stretching, v3 sulfate or bisulfate stretching, v3 surface sulfate vibration SO <sub>3</sub>		Jiang et al. 2010
Co <sup>II</sup> <sub>3</sub> [Co <sup>III</sup> (C N) <sub>6</sub> ] <sub>2</sub>	298 K	DRIFTS		67585 ppm		1146 1332 2466 1623	v1 symmetric stretch of SO <sub>2</sub> v3 asymmetric stretch SO <sub>2</sub> v1+v3 combination SO <sub>2</sub> band water		Windisch et al. 2010
Al <sub>2</sub> O <sub>3</sub>	Room temp.	DRIFTS			A <sub>BET</sub> =124.6	850-1100  1100-1300	stretching motion of adsorbed sulfite SO <sub>3</sub> <sup>2-</sup> and/or bisulfite HSO <sub>3</sub> <sup>2-</sup> stretching motion of adsorbed sulfate		Zhang et al. 2006
	Room temp.	FTIR		119 ppm				rate constant k=1.35×10 <sup>-2</sup>	Zhang et al. 2006
MgO	Room temp.	DRIFTS			A <sub>BET</sub> =65.52	880-1100  1100-1300	stretching motion of adsorbed sulfite SO <sub>3</sub> <sup>2-</sup> and/or bisulfite HSO <sub>3</sub> <sup>2-</sup> stretching motion of adsorbed sulfate		Zhang et al. 2006
	Room temp.	FTIR		119 ppm				rate constant k=9.4×10 <sup>-3</sup>	Zhang et al. 2006
Fe <sub>2</sub> O <sub>3</sub> (hematite nanoparticles)	298 K	DRIFTS	~ 0%	4.686 ppm	A <sub>BET</sub> =262.3	1045 1153-1223 1260	sulfite sulfate bidentate sulfate	γ <sub>BET</sub> Fe <sub>2</sub> O <sub>3</sub> = (9.00±0.7)×10 <sup>-11</sup>	Wang et al. 2018a
Al <sub>2</sub> O <sub>3</sub>	298 K	DRIFTS	~ 0%	4.686 ppm	A <sub>BET</sub> =469.7	960 1106	sulfite sulfate	γ <sub>BET</sub> Al <sub>2</sub> O <sub>3</sub> = (7.37±2.7)×10 <sup>-13</sup>	Wang et al. 2018a
TiO <sub>2</sub> nanoparticles	296 K	FTIR	0.6% -76%	132 ppm		1139, 1325 1077, 3648 1033, 971, 923 1006, 886 1361, 1297, 1172, 1116, 10150, 1000 1050 1168, 1129 3498, 3211	SO <sub>2</sub> HSO <sub>3</sub> <sup>-</sup> Monodentate SO <sub>3</sub> <sup>2-</sup> Bidentate SO <sub>3</sub> <sup>2-</sup> SO <sub>4</sub> <sup>2-</sup>  Solvated SO <sub>3</sub> <sup>2-</sup> / HSO <sub>3</sub> <sup>-</sup> Solvated SO <sub>4</sub> <sup>2-</sup> OH region of SO <sub>2</sub> ·H <sub>2</sub> O complex		Nanayakkara et al. 2012
TiO <sub>2</sub>	298 K	DRIFTS	0% - 90%	50 ppm		1080 1300-1100 3463-2605 1654 3666, 3628	sulfite and/or bisulfite sulfate surface water water bending vibration hydroxyl groups		Shang et al. 2010

## 7 Thesis objectives and strategy

Very little is known about molecular interactions of natural volcanic dusts with SO<sub>2</sub> gas, especially under relevant atmospheric conditions of RH, pressure and SO<sub>2</sub> concentrations. Most often, natural samples are substituted for mineral oxides to simplify the system of interest. This approach though neglects and undermines the complexity of natural samples and questions their representativeness as models for mineral aerosols found in the troposphere.

This work aims at explaining what happens when SO<sub>2</sub> gas and volcanic dust interact in the real atmospheric conditions. **Thus, the objectives of this thesis are twofold: (i) to provide an accurate description of the fate of SO<sub>2</sub> gas on the surface of natural volcanic particles under atmospheric relevant conditions and (ii) to evaluate the impact of SO<sub>2</sub> interaction on natural volcanic dust on tropospheric chemistry.**

First step on the way to reach these objectives is to characterize in detail the surface of volcanic dust to understand its heterogeneous interactions with volcanic SO<sub>2</sub>. We are going to obtain surface topography using Scanning Electron Spectroscopy (SEM). Specific surface area is determined using Brunauer, Emmett and Teller (BET) technique. Bulk and surface elemental composition is obtained using inductively coupled plasma mass spectrometry (ICP-MS) and X-ray photoelectron spectroscopy (XPS) respectfully.

Second step is to study kinetics and potential mechanisms of formation of different species on the surface of dust. Both processes that occur in the gas phase and in the adsorbed phase need to be investigated.

We start by evaluating the uptake of atmospheric SO<sub>2</sub> on the surface of five selected relevant volcanic dusts. To that end, flow-tube reactors coupled with SO<sub>2</sub> analyzer for the gas phase monitoring of species involved, allow us to determine the temporal profiles of SO<sub>2</sub> uptake and more precisely the steady state uptake coefficients, which are very important kinetic parameters to be implemented in models. These experiments are performed under different atmospheric conditions, such as SO<sub>2</sub> concentrations, RH, and UV light. A great advantage of this approach is its ability to employ atmospherically relevant concentration of SO<sub>2</sub> gas, as well as realistic humidity and atmospheric pressure.

Second, *in-situ* monitoring of adsorbed phase species using DRIFT spectroscopy allows us to identify the surface species formed and to propose a surface reaction pathway. The influence of RH on surface mechanism is also investigated. The concentrations usually employed in DRIFTS studies of adsorption of SO<sub>2</sub> gas on various oxides and natural dusts range from 2.5 to 50 ppm (Li et al., 2006), (Shang et al., 2010), exposing a limitation of the technique to employ atmospherically relevant concentrations of

SO<sub>2</sub>. In case of inability to use atmospherically relevant concentrations, a problem of relevancy of high concentrations needs to be addressed. Particularly, whether the use of high concentrations for a shorter time can mimic longer processes in the atmosphere that employ lower concentrations. This point is questioned and discussed.

Finally, quantification of the species observed using DRIFT spectroscopy is achieved using a new developed and validated HPLC method. Once again, we pay special attention to the role RH plays in surface species formation. Unlike the experimental methods exposed earlier, HPLC investigation requires developing and validating a method to separate and quantify surface species. Besides enabling further investigations of the sulfate species kinetics in laboratory settings, the developed method can also be potentially used to quantify sulfur-containing products on the surface of natural environmental samples, such as recently erupted volcanic ash, or dust passing through polluted areas. In addition, as a result of this investigation a protocol to achieve a controlled aging of volcanic ash with SO<sub>2</sub> gas is proposed.

The possibility of surface species quantification using HPLC allows comparing the behaviors of a large number of natural dust samples, of desert and volcanic origins, as well as mineral proxies. First, this experimental approach provides a relevant overview on the effective representativeness of dust proxies. Second, it allows a better understanding of the impact of the dust surface composition on its surface properties.

## References of Chapter 1

- Adams, J.W., Rodriguez, D., Cox, R.A., 2005. The uptake of SO<sub>2</sub> on Saharan dust: a flow tube study. *Atmospheric Chemistry and Physics* 5, 2679–2689. <https://doi.org/10.5194/acp-5-2679-2005>
- Aerosol mass spectrometry, 2020. . Wikipedia.
- Al-Abadleh, H.A., Grassian, V.H., 2003. FT-IR Study of Water Adsorption on Aluminum Oxide Surfaces. *Langmuir* 19, 341–347. <https://doi.org/10.1021/la026208a>
- Andreae, M., 1995. Climate Effects of Changing Atmospheric Aerosol. *World Survey of Climatology*. Vol. 16: Future Climates of the World, 341–392 (1995).
- Arnalds, O., Dagsson-Waldhauserova, P., Olafsson, H., 2016. The Icelandic volcanic aeolian environment: Processes and impacts — A review. *Aeolian Research* 20, 176–195. <https://doi.org/10.1016/j.aeolia.2016.01.004>
- Arzilli, F., 2020. Highly explosive basaltic eruptions: magma fragmentation induced by rapid crystallisation.
- Ash Plume across the North Atlantic: Image of the Day [WWW Document], 2010. URL <https://earthobservatory.nasa.gov/IOTD/view.php?id=43670&src=eoaiotd> (accessed 5.25.18).
- Atmospheric Composition — OSS Foundation [WWW Document], n.d. URL <http://ossfoundation.us/projects/environment/global-warming/atmospheric-composition> (accessed 6.8.18).
- Attard, G., Barnes, C., 1998. *Surfaces*, Oxford Chemistry Primers. Oxford University Press, Oxford, New York.
- Ayris, P.M., Lee, A.F., Wilson, K., Kueppers, U., Dingwell, D.B., Delmelle, P., 2013. SO<sub>2</sub> sequestration in large volcanic eruptions: High-temperature scavenging by tephra. *Geochimica et Cosmochimica Acta* 110, 58–69. <https://doi.org/10.1016/j.gca.2013.02.018>
- Bagheri, G., Rossi, E., Biass, S., Bonadonna, C., 2016. Timing and nature of volcanic particle clusters based on field and numerical investigations. *Journal of Volcanology and Geothermal Research* 327, 520–530. <https://doi.org/10.1016/j.jvolgeores.2016.09.009>
- Baltrusaitis, J., Cwiertny, D.M., Grassian, V.H., 2007. Adsorption of sulfur dioxide on hematite and goethite particle surfaces. *Phys. Chem. Chem. Phys.* 9, 5542–5554. <https://doi.org/10.1039/B709167B>
- Bluth, G.J.S., SCHNETZLER, C.C., KRUEGER, A.J., WALTER, L.S., 1993. The contribution of explosive volcanism to global atmospheric sulphur dioxide concentrations. *Nature* 327–329.
- Brasseur, G.P., Granier, C., Walters, S., 1990. Future changes in stratospheric ozone and the role of heterogeneous chemistry. *Nature* 348, 626–628. <https://doi.org/10.1038/348626a0>
- Caloz, F., Fenter, F.F., Tabor, K.D., Rossi, M.J., 1997. Paper I: Design and construction of a Knudsen-cell reactor for the study of heterogeneous reactions over the temperature range 130–750 K: Performances and limitations. *Review of Scientific Instruments* 68, 3172–3179. <https://doi.org/10.1063/1.1148263>
- Camprubí, E., de Leeuw, J.W., House, C.H., Raulin, F., Russell, M.J., Spang, A., Tirumalai, M.R., Westall, F., 2019. The Emergence of Life. *Space Sci Rev* 215, 56. <https://doi.org/10.1007/s11214-019-0624-8>
- Crowley, J.N., Ammann, M., Cox, R.A., Hynes, R.G., Jenkin, M.E., Mellouki, A., Rossi, M.J., Troe, J., Wallington, T.J., 2010. Evaluated kinetic and photochemical data for atmospheric chemistry: Volume V – heterogeneous reactions on solid substrates. *Atmos. Chem. Phys.* 10, 9059–9223. <https://doi.org/10.5194/acp-10-9059-2010>
- Dagsson-Waldhauserova, P., Arnalds, O., Olafsson, H., 2014. Long-term variability of dust events in Iceland (1949–2011). *Atmos. Chem. Phys.* 14, 13411–13422. <https://doi.org/10.5194/acp-14-13411-2014>
- Dagsson-Waldhauserova, P., Arnalds, O., Olafsson, H., Hladil, J., Skala, R., Navratil, T., Chadimova, L., Meinander, O., 2015. Snow–Dust Storm: Unique case study from Iceland, March 6–7, 2013. *Aeolian Research* 16, 69–74. <https://doi.org/10.1016/j.aeolia.2014.11.001>

- Daniel J. Jacob, 1999. *Introduction to Atmospheric Chemistry*. Princeton University Press, Princeton, New Jersey.
- Datta, A., Cavell, R.G., Tower, R.W., George, Z.M., 1985. Claus catalysis. 1. Adsorption of SO<sub>2</sub> on the alumina catalyst studied by FTIR and EPR spectroscopy. *J. Phys. Chem.*; (United States) 89:3. <https://doi.org/10.1021/j100249a014>
- Decker, R., Decker, B., 1991. *Mountains of fire: the nature of volcanoes*, First. ed. Cambridge University Press, Cambridge New York.
- Dogliotti, L., Hayon, E., 1968. Flash photolysis study of sulfite, thiocyanate, and thiosulfate ions in solution. *J. Phys. Chem.* 72, 1800–1807. <https://doi.org/10.1021/j100851a073>
- DRIFT Study of the SO<sub>2</sub> Effect on Low-Temperature SCR Reaction over Fe–Mn/TiO<sub>2</sub> - The Journal of Physical Chemistry C (ACS Publications) [WWW Document], n.d. URL <https://pubs.acs.org/doi/abs/10.1021/jp907783g> (accessed 4.24.18).
- Dupart, Y., King, S.M., Nekat, B., Nowak, A., Wiedensohler, A., Herrmann, H., David, G., Thomas, B., Miffre, A., Rairoux, P., D’Anna, B., George, C., 2012. Mineral dust photochemistry induces nucleation events in the presence of SO<sub>2</sub>. *Proc. Natl. Acad. Sci. U.S.A.* 109, 20842–20847. <https://doi.org/10.1073/pnas.1212297109>
- Durant, A.J., Bonadonna, C., Horwell, C.J., 2010. Atmospheric and Environmental Impacts of Volcanic Particulates. *Elements* 6, 235–240.
- Durant, A.J., Shaw, R.A., Rose, W.I., Mi, Y., Ernst, G.G.J., 2008. Ice nucleation and overseeding of ice in volcanic clouds. *Journal of Geophysical Research: Atmospheres* 113. <https://doi.org/10.1029/2007JD009064>
- Eurochamp > Eurochamp 2020 [WWW Document], n.d. URL <https://www.eurochamp.org/> (accessed 10.21.20).
- Faust, B.C., Hoffmann, M.R., Bahnemann, D.W., 1989. Photocatalytic oxidation of sulfur dioxide in aqueous suspensions of .alpha.-iron oxide (Fe<sub>2</sub>O<sub>3</sub>). *J. Phys. Chem.* 93, 6371–6381. <https://doi.org/10.1021/j100354a021>
- Finlayson-Pitts, B.J., Jr, J.N.P., 1999. *Chemistry of the Upper and Lower Atmosphere: Theory, Experiments, and Applications*. Elsevier.
- Froyd, K.D., Murphy, D.M., Brock, C.A., Campuzano-Jost, P., Dibb, J.E., Jimenez, J.-L., Kupc, A., Middlebrook, A.M., Schill, G.P., Thornhill, K.L., Williamson, C.J., Wilson, J.C., Ziemba, L.D., 2019. A new method to quantify mineral dust and other aerosol species from aircraft platforms using single-particle mass spectrometry. *Atmospheric Measurement Techniques* 12, 6209–6239. <https://doi.org/10.5194/amt-12-6209-2019>
- FTIR Sample Techniques - Diffuse Reflectance (DRIFTS) [WWW Document], n.d. URL <https://www.thermofisher.com/fr/en/home/industrial/spectroscopy-elemental-isotope-analysis/spectroscopy-elemental-isotope-analysis-learning-center/molecular-spectroscopy-information/ftir-information/ftir-sample-handling-techniques/ftir-sample-handling-techniques-diffuse-reflectance-drifts.html> (accessed 3.19.18).
- Geishi, N., 2004. Lavas. *Encyclopedia of Geology*.
- George, C., Ammann, M., D’Anna, B., Donaldson, D.J., Nizkorodov, S.A., 2015. Heterogeneous Photochemistry in the Atmosphere. *Chem. Rev.* 115, 4218–4258. <https://doi.org/10.1021/cr500648z>
- Gislason, S.R., Hassenkam, T., Nedel, S., Bovet, N., Eiriksdottir, E.S., Alfredsson, H.A., Hem, C.P., Balogh, Z.I., Dideriksen, K., Oskarsson, N., Sigfusson, B., Larsen, G., Stipp, S.L.S., 2011. Characterization of Eyjafjallajökull volcanic ash particles and a protocol for rapid risk assessment. *PNAS* 108, 7307–7312. <https://doi.org/10.1073/pnas.1015053108>
- Goodman, A.L., Li, P., Usher, C.R., Grassian, V.H., 2001. Heterogeneous Uptake of Sulfur Dioxide On Aluminum and Magnesium Oxide Particles. *J. Phys. Chem. A* 105, 6109–6120. <https://doi.org/10.1021/jp004423z>
- Granier, C., Brasseur, G., 1992. Impact of heterogeneous chemistry on model predictions of ozone changes. *J. Geophys. Res.* 97, 18015–18033. <https://doi.org/10.1029/92JD02021>

- Highwood, E.-J., Stevenson, D.S., 2003. Atmospheric impact of the 1783-1784 Laki Eruption: Part II Climatic effect of sulphate aerosol. *Atmospheric Chemistry and Physics* 3, 1177–1189.
- Hoshyaripour, G., Hort, M., Langmann, B., 2012. How does the hot core of a volcanic plume control the sulfur speciation in volcanic emission? *Geochem. Geophys. Geosyst.* 13, Q07004. <https://doi.org/10.1029/2011GC004020>
- How does adsorption work? [WWW Document], n.d. . Chemistry Stack Exchange. URL <https://chemistry.stackexchange.com/questions/57329/how-does-adsorption-work> (accessed 6.12.18).
- HPLC Troubleshooting Guide [WWW Document], n.d. . Sigma-Aldrich. URL <https://www.sigmaaldrich.com/technical-documents/articles/analytical/hplc-troubleshooting-guide.html> (accessed 5.19.20).
- Huang, L., Zhao, Y., Li, H., Chen, Z., 2015. Kinetics of Heterogeneous Reaction of Sulfur Dioxide on Authentic Mineral Dust: Effects of Relative Humidity and Hydrogen Peroxide. *Environ. Sci. Technol.* 49, 10797–10805. <https://doi.org/10.1021/acs.est.5b03930>
- Jiang, B.Q., Wu, Z.B., Liu, Y., Lee, S.C., Ho, W.K., 2010. DRIFT Study of the SO<sub>2</sub> Effect on Low-Temperature SCR Reaction over Fe–Mn/TiO<sub>2</sub>. *J. Phys. Chem. C* 114, 4961–4965. <https://doi.org/10.1021/jp907783g>
- Jickells, T.D., An, Z.S., Andersen, K.K., Baker, A.R., Bergametti, G., Brooks, N., Cao, J.J., Boyd, P.W., Duce, R.A., Hunter, K.A., Kawahata, H., Kubilay, N., laRoche, J., Liss, P.S., Mahowald, N., Prospero, J.M., Ridgwell, A.J., Tegen, I., Torres, R., 2005. Global Iron Connections Between Desert Dust, Ocean Biogeochemistry, and Climate. *Science* 308, 67–71. <https://doi.org/10.1126/science.1105959>
- Joshi, N., Romanias, M.N., Riffault, V., Thevenet, F., 2017. Investigating water adsorption onto natural mineral dust particles: Linking DRIFTS experiments and BET theory. *Aeolian Research* 27, 35–45. <https://doi.org/10.1016/j.aeolia.2017.06.001>
- Judeikis, H.S., Stewart, T.B., 1976. Laboratory measurement of SO<sub>2</sub> deposition velocities on selected building materials and soils. *Atmospheric Environment* (1967) 10, 769–776. [https://doi.org/10.1016/0004-6981\(76\)90078-0](https://doi.org/10.1016/0004-6981(76)90078-0)
- Kaminski, E., Jaupart, C., 1997. Expansion and quenching of vesicular magma fragments in Plinian eruptions. *JOURNAL OF GEOPHYSICAL RESEARCH* 102, 12187–12203.
- Langmann, B., 2013. Volcanic Ash versus Mineral Dust: Atmospheric Processing and Environmental and Climate Impacts [WWW Document]. *International Scholarly Research Notices*. <https://doi.org/10.1155/2013/245076>
- Langmann, B., Zakšek, K., Hort, M., 2010. Atmospheric distribution and removal of volcanic ash after the eruption of Kasatochi volcano: A regional model study. *Journal of Geophysical Research: Atmospheres* 115. <https://doi.org/10.1029/2009JD013298>
- Langmuir adsorption model, 2018. . Wikipedia.
- Lasne, J., Romanias, M.N., Thevenet, F., 2018. Ozone Uptake by Clay Dusts under Environmental Conditions. *ACS Earth Space Chem.* 2, 904–914. <https://doi.org/10.1021/acsearthspacechem.8b00057>
- Li, G., Su, H., Kuhn, U., Meusel, H., Ammann, M., Shao, M., Pöschl, U., Cheng, Y., 2018. Technical note: Influence of surface roughness and local turbulence on coated-wall flow tube experiments for gas uptake and kinetic studies. *Atmos. Chem. Phys.* 18, 2669–2686. <https://doi.org/10.5194/acp-18-2669-2018>
- Li, L., Chen, Z.M., Zhang, Y.H., Zhu, T., Li, J.L., Ding, J., 2006. Kinetics and mechanism of heterogeneous oxidation of sulfur dioxide by ozone on surface of calcium carbonate. *Atmospheric Chemistry and Physics Discussions* 6, 579–613. <https://doi.org/10.5194/acpd-6-579-2006>
- Lo, J.M.H., Ziegler, T., Clark, P.D., 2010. SO<sub>2</sub> Adsorption and Transformations on  $\gamma$ -Al<sub>2</sub>O<sub>3</sub> Surfaces: A Density Functional Theory Study. *J. Phys. Chem. C* 114, 10444–10454. <https://doi.org/10.1021/jp910895g>

- Ludlow, F., Kostick, C., Rhonda McGovern, Farrelly, L., 2020. Volcanic Impacts on Climate and Society in First Millennium BCE Babylonia.
- Martins-Costa, M.T.C., Anglada, J.M., Francisco, J.S., Ruiz-López, M.F., 2018. Photochemistry of SO<sub>2</sub> at the Air-Water Interface: A Source of OH and HOSO Radicals. *Journal of the American Chemical Society*. <https://doi.org/10.1021/jacs.8b07845>
- Massman, W.J., 1998. A review of the molecular diffusivities of H<sub>2</sub>O, CO<sub>2</sub>, CH<sub>4</sub>, CO, O<sub>3</sub>, SO<sub>2</sub>, NH<sub>3</sub>, N<sub>2</sub>O, NO, and NO<sub>2</sub> in air O<sub>2</sub> and N<sub>2</sub> near STP [WWW Document]. *Atmospheric Environment*. URL <https://eurekamag.com/research/008/072/008072627.php> (accessed 11.5.18).
- Maters, E.C., Delmelle, P., Rossi, M.J., Ayris, P.M., 2017. Reactive Uptake of Sulfur Dioxide and Ozone on Volcanic Glass and Ash at Ambient Temperature. *J. Geophys. Res.-Atmos.* 122, 10077–10088. <https://doi.org/10.1002/2017JD026993>
- Maters, E.C., Delmelle, P., Rossi, M.J., Ayris, P.M., Bernard, A., 2016. Controls on the surface chemical reactivity of volcanic ash investigated with probe gases. *Earth Planet. Sci. Lett.* 450, 254–262. <https://doi.org/10.1016/j.epsl.2016.06.044>
- McCall, G.J.H., 2004. Volcanoes. *Encyclopedia of Geology*.
- Meyer, V.R., 2004. *Practical High-Performance Liquid Chromatography*. John Wiley & Sons.
- Nanayakkara, C.E., Pettibone, J., Grassian, V.H., 2012. Sulfur dioxide adsorption and photooxidation on isotopically-labeled titanium dioxide nanoparticle surfaces: roles of surface hydroxyl groups and adsorbed water in the formation and stability of adsorbed sulfite and sulfate. *Phys. Chem. Chem. Phys.* 14, 6957–6966. <https://doi.org/10.1039/C2CP23684B>
- Nash, D.G., Baer, T., Johnston, M.V., 2006. Aerosol mass spectrometry: An introductory review. *International Journal of Mass Spectrometry, Aerosols/Microparticles Special Issue 258*, 2–12. <https://doi.org/10.1016/j.ijms.2006.09.017>
- Neta, P., Huie, R.E., 1985. Free-radical chemistry of sulfite. *Environ. Health Perspect.* 64, 209–217. <https://doi.org/10.1289/ehp.8564209>
- Palmer, J., n.d. Why ancient myths about volcanoes are often true [WWW Document]. URL <http://www.bbc.com/earth/story/20150318-why-volcano-myths-are-true> (accessed 5.28.20).
- Park, J., Jang, M., Yu, Z., 2017. Heterogeneous Photo-oxidation of SO<sub>2</sub> in the Presence of Two Different Mineral Dust Particles: Gobi and Arizona Dust [WWW Document]. <https://doi.org/10.1021/acs.est.7b00588>
- Park, J.Y., Jang, M., 2016. Heterogeneous photooxidation of sulfur dioxide in the presence of airborne mineral dust particles. *RSC Adv.* 6, 58617–58627. <https://doi.org/10.1039/C6RA09601H>
- Pavia, D., Lampman, G., Kriz, G., 2011. *Introduction to Spectroscopy*, 3rd ed. Thomson learning.
- Raman + FTIR - A perfect match [WWW Document], n.d. URL <http://info1.thermofisher.com/raman-ftir-perfect-match-interest-4206> (accessed 4.24.18).
- Romanías, M.N., Dagaut, P., Bedjanian, Y., Andrade-Eiroa, A., Shahla, R., Emmanouil, K.S., Papadimitriou, V.C., Spyros, A., 2015. Investigation of the Photochemical Reactivity of Soot Particles Derived from Biofuels Toward NO<sub>2</sub>. A Kinetic and Product Study. *J. Phys. Chem. A* 119, 2006–2015. <https://doi.org/10.1021/jp511468t>
- Rossi, E., 2020. The fate of volcanic ash aggregates: premature or delayed sedimentation?
- Ruiz-López, M.F., Martins-Costa, M.T.C., Anglada, J.M., Francisco, J.S., 2019. A New Mechanism of Acid Rain Generation from HOSO at the Air–Water Interface. *J. Am. Chem. Soc.* 141, 16564–16568. <https://doi.org/10.1021/jacs.9b07912>
- Savarino, J., 2020. Where is the Toba eruption in the Vostok ice core? Clues from tephra, O and S isotopes. *Scanning Electron Microscopy*, n.d. *Nanoscience Instruments*. URL <https://www.nanoscience.com/techniques/scanning-electron-microscopy/> (accessed 5.25.20).
- Schmidt, A., Ostro, B., Carslaw, K.S., Wilson, M., Thordarson, T., Mann, G.W., Simmons, A.J., 2011. Excess mortality in Europe following a future Laki-style Icelandic eruption. *PNAS* 108, 15710–15715. <https://doi.org/10.1073/pnas.1108569108>
- Schmidt, A., Witham, C.S., Theys, N., Richards, N.A.D., Thordarson, T., Szpek, K., Feng, W., Hort, M.C., Woolley, A.M., Jones, A.R., Redington, A.L., Johnson, B.T., Hayward, C.L., Carslaw, K.S., 2014.

- Assessing hazards to aviation from sulfur dioxide emitted by explosive Icelandic eruptions. *J. Geophys. Res. Atmos.* 119, 2014JD022070. <https://doi.org/10.1002/2014JD022070>
- Shang, J., Li, J., Zhu, T., 2010. Heterogeneous reaction of SO<sub>2</sub> on TiO<sub>2</sub> particles. *Sci. China Chem.* 53, 2637–2643. <https://doi.org/10.1007/s11426-010-4160-3>
- Sigl, M., Winstrup, M., McConnell, J.R., Welten, K.C., Plunkett, G., Ludlow, F., Büntgen, U., Caffee, M., Chellman, N., Dahl-Jensen, D., Fischer, H., Kipfstuhl, S., Kostick, C., Maselli, O.J., Mekhaldi, F., Mulvaney, R., Muscheler, R., Pasteris, D.R., Pilcher, J.R., Salzer, M., Schüpbach, S., Steffensen, J.P., Vinther, B.M., Woodruff, T.E., 2015. Timing and climate forcing of volcanic eruptions for the past 2,500 years. *Nature* 523, 543–549. <https://doi.org/10.1038/nature14565>
- Skoog, D., Donald West, Holler, J., 1995. *Fundamentals of analytical chemistry*, 7th ed. Harcourt Brace College Publishers, Orlando, Florida.
- Sorem, R.K., 1982. Volcanic ash clusters: Tephra rafts and scavengers. *Journal of Volcanology and Geothermal Research* 13, 63–71. [https://doi.org/10.1016/0377-0273\(82\)90019-1](https://doi.org/10.1016/0377-0273(82)90019-1)
- Springsklee, C., 2020. Prebiotic synthesis in volcanic discharges: lightning, porous ash and volcanic gas atmospheres.
- Sternai, P., Caricchi, L., Castelltort, S., Champagnac, J.-D., 2016. Deglaciation and glacial erosion: A joint control on magma productivity by continental unloading. *Geophysical Research Letters* 43, 1632–1641. <https://doi.org/10.1002/2015GL067285>
- Stevenson, D.S., Johnson, C.E., Highwood, E.J., Gauci, V., Collins, W.J., Derwent, R.G., 2003. Atmospheric impact of the 1783–1784 Laki eruption: Part I Chemistry modelling. *Atmos. Chem. Phys.* 3, 487–507. <https://doi.org/10.5194/acp-3-487-2003>
- Stothers, R.B., 1999. Volcanic Dry Fogs, Climate Cooling, and Plague Pandemics in Europe and the Middle East. *Climatic Change* 42, 713–723. <https://doi.org/10.1023/A:1005480105370>
- Subramanian, A., Rodriguez-Saona, L., 2009. Chapter 7 - Fourier Transform Infrared (FTIR) Spectroscopy, in: Sun, D.-W. (Ed.), *Infrared Spectroscopy for Food Quality Analysis and Control*. Academic Press, San Diego, pp. 145–178. <https://doi.org/10.1016/B978-0-12-374136-3.00007-9>
- Tambora and the “Year Without a Summer” of 1816 [WWW Document], 2016. . Institute of Geography. URL [http://www.geography.unibe.ch/services/geographica\\_bernensia/online/gb2016g9001/index\\_eng.html](http://www.geography.unibe.ch/services/geographica_bernensia/online/gb2016g9001/index_eng.html) (accessed 5.17.18).
- Tang, M.J., Cox, R.A., Kalberer, M., 2014. Compilation and evaluation of gas phase diffusion coefficients of reactive trace gases in the atmosphere: volume 1. Inorganic compounds. *Atmospheric Chemistry and Physics* 14, 9233–9247. <https://doi.org/10.5194/acp-14-9233-2014>
- Tang, M.J., Shiraiwa, M., Pöschl, U., Cox, R.A., Kalberer, M., 2015. Compilation and evaluation of gas phase diffusion coefficients of reactive trace gases in the atmosphere: Volume 2. Diffusivities of organic compounds, pressure-normalised mean free paths, and average Knudsen numbers for gas uptake calculations. *Atmospheric Chemistry and Physics* 15, 5585–5598. <https://doi.org/10.5194/acp-15-5585-2015>
- Textor, C., Graf, H.-F., Herzog, M., Oberhuber, J.M., 2003. Injection of gases into the stratosphere by explosive volcanic eruptions. *Journal of Geophysical Research: Atmospheres* 108. <https://doi.org/10.1029/2002JD002987>
- The Brewer-Dobson circulation - Butchart - 2014 - *Reviews of Geophysics* - Wiley Online Library [WWW Document], n.d. URL <https://agupubs.onlinelibrary.wiley.com/doi/abs/10.1002/2013RG000448> (accessed 6.6.18).
- The volcanic explosivity index (VEI) an estimate of explosive magnitude for historical volcanism, 1982. . *Journal of Geophysical Research: Oceans* 87, 1231–1238. <https://doi.org/10.1029/JC087iC02p01231>
- Thordarson, T., Larsen, G., 2007. Volcanism in Iceland in historical time: Volcano types, eruption styles and eruptive history. *Journal of Geodynamics - J GEODYNAMICS* 43, 118–152. <https://doi.org/10.1016/j.jog.2006.09.005>



- Thorsteinsson, T., Jóhannsson, T., Stohl, A., Kristiansen, N.I., 2012. High levels of particulate matter in Iceland due to direct ash emissions by the Eyjafjallajökull eruption and resuspension of deposited ash. *J. Geophys. Res.* 117, B00C05. <https://doi.org/10.1029/2011JB008756>
- Ullerstam, M., Johnson, M.S., Vogt, R., Ljungstrom, E., 2003. DRIFTS and Knudsen cell study of the heterogeneous reactivity of SO<sub>2</sub> and NO<sub>2</sub> on mineral dust. *Atmos. Chem. Phys.* 3, 2043–2051. <https://doi.org/10.5194/acp-3-2043-2003>
- Ullerstam, M., Vogt, R., Langer, S., Ljungstrom, E., 2002. The kinetics and mechanism of SO<sub>2</sub> oxidation by O<sub>3</sub> on mineral dust. *Phys. Chem. Chem. Phys.* 4, 4694–4699. <https://doi.org/10.1039/b203529b>
- Usher, C.R., Al-Hosney, H., Carlos-Cuellar, S., Grassian, V.H., 2002. A laboratory study of the heterogeneous uptake and oxidation of sulfur dioxide on mineral dust particles. *J.-Geophys.-Res.* 107, 4713. <https://doi.org/10.1029/2002JD002051>
- Usher, C.R., Michel, A.E., Grassian, V.H., 2003. Reactions on Mineral Dust. *Chem. Rev.* 103, 4883–4940. <https://doi.org/10.1021/cr020657y>
- Vernier, J.-P., Fairlie, T.D., Deshler, T., Natarajan, M., Knepp, T., Foster, K., Wienhold, F.G., Bedka, K.M., Thomason, L., Trepte, C., 2016. In situ and space-based observations of the Kelud volcanic plume: The persistence of ash in the lower stratosphere. *Journal of Geophysical Research: Atmospheres* 121, 11,104–11,118. <https://doi.org/10.1002/2016JD025344>
- Volatile Organic Compounds in the Atmosphere [WWW Document], n.d. . Wiley.com. URL <https://www.wiley.com/en-fr/Volatile+Organic+Compounds+in+the+Atmosphere-p-9781405131155> (accessed 4.12.18).
- Volcano Myths and Rituals [WWW Document], 2017. . American Scientist. URL <https://www.americanscientist.org/article/volcano-myths-and-rituals> (accessed 5.28.20).
- Wang, T., Liu, Y., Deng, Y., Fu, H., Zhang, L., Chen, J., 2018a. Emerging investigator series: heterogeneous reactions of sulfur dioxide on mineral dust nanoparticles: from single component to mixed components. *Environ. Sci.: Nano* 5, 1821–1833. <https://doi.org/10.1039/C8EN00376A>
- Wang, T., Liu, Y., Deng, Y., Fu, H., Zhang, L., Chen, J.-M., 2018b. Adsorption of SO<sub>2</sub> on mineral dust particles influenced by atmospheric moisture. *Atmospheric Environment* 191. <https://doi.org/10.1016/j.atmosenv.2018.08.008>
- Wu, L.Y., Tong, S.R., Wang, W.G., Ge, M.F., 2011. Effects of temperature on the heterogeneous oxidation of sulfur dioxide by ozone on calcium carbonate. *Atmospheric Chemistry and Physics* 11, 6593–6605. <https://doi.org/10.5194/acp-11-6593-2011>
- X-Ray Photoelectron Spectroscopy (XPS) Surface Analysis Technique [WWW Document], n.d. URL <https://www.phis.com/surface-analysis-techniques/xps-esca.html> (accessed 5.25.20).
- X-ray Powder Diffraction (XRD) [WWW Document], n.d. . Techniques. URL [https://serc.carleton.edu/research\\_education/geochemsheets/techniques/XRD.html](https://serc.carleton.edu/research_education/geochemsheets/techniques/XRD.html) (accessed 5.25.20).
- Zhang, X., Zhuang, G., Chen, J., Wang, Y., Wang, X., An, Z., Zhang, P., 2006. Heterogeneous Reactions of Sulfur Dioxide on Typical Mineral Particles. *J. Phys. Chem. B* 110, 12588–12596. <https://doi.org/10.1021/jp0617773>
- Zhang, Z., Ewing, G.E., 2002. Infrared spectroscopy of SO<sub>2</sub> aqueous solutions. *Spectrochim Acta A Mol Biomol Spectrosc* 58, 2105–2113.
- Zhou, L., Wang, W., Gai, Y., Ge, M., 2014. Knudsen cell and smog chamber study of the heterogeneous uptake of sulfur dioxide on Chinese mineral dust. *Journal of Environmental Sciences* 26, 2423–2433. <https://doi.org/10.1016/j.jes.2014.04.005>



## **Chapter II. Materials and methods**

## Table of content of Chapter 2

1	Materials .....	78
1.1	Origin of the samples .....	78
1.1.1	Volcanic dusts .....	78
1.1.2	Desert dusts .....	78
1.1.3	Clay samples .....	79
1.1.4	Mineral oxide samples .....	79
1.2	Physical and chemical characterization of the natural volcanic and selected desert dust samples .....	80
1.2.1	Specific surface area measurements of the selected volcanic and desert dust samples, clays and mineral oxides.....	80
1.2.2	Scanning Electron Microscopy of the selected volcanic and desert dusts .....	81
1.2.3	ICP-MS for chemical bulk elemental composition of the selected volcanic and desert dusts .....	83
1.2.4	X-ray photoelectron spectroscopy for surface characterization of the selected v-dust and desert dust samples .....	84
1.3	Gases used for experiments .....	85
1.4	Other chemicals and reagents used for investigations .....	86
2	Experimental strategy and methods.....	86
2.1	Introduction to the experimental strategy .....	86
2.2	Experimental setup of flow-tube experiments .....	87
2.2.1	Typical flow-tube experiment .....	87
2.2.2	Flow-tube experiments involving UV light. Calibration and characterization of the light source.....	89
2.2.3	Sample preparation for flow-tube experiments .....	90
2.2.4	Protocol for a typical flow-tube experiment: dark conditions.....	91
2.2.5	Protocol for a typical flow-tube experiment: UV-light conditions .....	92
2.2.6	Determination of the uptake coefficients from flow-tube experiments.....	93
		74

2.2.7 Determination of the transient number of SO <sub>2</sub> molecules taken up by dust.....	95
2.3 Experimental setup and protocol for DRIFTS experiments.....	95
2.4 Experimental setup and protocol for ageing and HPLC analysis .....	97
3 Conclusions .....	98
References.....	100

## List of Tables of Chapter 2

Table 1: BET specific surface area ( $\text{m}^2 \text{g}^{-1}$ ) of various natural v-dust and desert samples, selected clays and mineral oxides used in the study. SSA of the studied samples was determined using the 2-parameter BET method. At least three nitrogen adsorption experiments were conducted for each sample using a homemade gas sorption analyzer. The values presented are the average of the measurements and the quoted errors correspond to one standard deviation. ....	81
Table 2: % Bulk elemental composition of the v-dust samples used in this study and of mineral dust samples adopted from (Joshi et al., 2017), as determined by ICP-MS experiments. ....	84
Table 3: % Surface elemental composition of the v-dust and desert dust samples used in this study as determined by XPS (surf stands for surface) compared to % bulk composition as determined by ICP-MS (bulk). Both expressed as % by weight. Bulk compositions of mineral dust samples marked with asterisk were adopted from (Joshi et al., 2017). Error on the XPS measurements $< 10\%$ . ....	85
Table 4: The three main techniques used for investigation of interactions of $\text{SO}_2$ gas with Icelandic v-dusts. Parameters investigated. Conditions. Advantages and limitations. ....	87

## List of Figures of Chapter 2

Figure 1: SEM images of eight dusts: (a) Mýrdalssandur, (b) Dyngjusandur, (c) Hagavatn, (d) Maelifellsandur, (e) Eyjafjallajökull, (f) M'Bour, (g) Arizona, (h) Gobi. ....	82
Figure 2: Schematic representation of the coated wall flow-tube (CWFT) reactor used in this study. The space filled with the coolant in between the two walls is shaded in blue. The dust sample coating the inner surface of the Pyrex tube is shown in orange. ....	88
Figure 3: $J_{NO_2}$ as a function of the number of lamps switched on along flow-tube experiments. ....	90
Figure 4: Theoretical $SO_2$ concentration profile during a typical flow-tube experiment with v-dust exposed to $SO_2$ . At the beginning of the experiment where surface is isolated from the gas mixture the initial $SO_2$ concentration is $[SO_2]_0$ , then the dust is exposed to the gas and the concentration of $SO_2$ falls to its minimum, after which it recovers till a steady-state is reached. Note that the steady-state concentration $[SO_2]_{ss}$ is different from the initial state concentration $[SO_2]_0$ . Initial concentration is controlled when the injector is pushed in and the $SO_2$ gas is no longer in contact with the dust. Shaded area corresponds to the integrated area that is used to obtain the number of molecules during the transient initial uptake of $SO_2$ on v-dusts $n_s$ (molecules $cm^{-2}$ ). 300 min was chosen as integration limits for the determination of $N_s$ . ....	92
Figure 5: Theoretical $SO_2$ concentration profile during a typical flow-tube experiment with v-dust under 30% of RH and 296 K. At the beginning of the experiment, the dust is isolated from the gas mixture, in which an initial $SO_2$ concentration, $[SO_2]_0$ , is set. The dust is then exposed to $SO_2$ in the dark (gray area), and $[SO_2]$ decreases initially strongly, before recovering to a steady-state value $[SO_2]_{ss,dark}$ within typically 12 hours. Thereafter, the surface is irradiated with simulated sunlight (yellow area), and a second large consumption of $SO_2$ is observed, before recovering to a steady-state value $[SO_2]_{ss,light}$ within typically 36 hours. Lights are turned off (second gray area) and $[SO_2]$ returns to its steady-state value in the dark. $SO_2$ concentration is then controlled by pushing the injector in, and the dust is no longer exposed to the gas. Black-shaded and red-shaded areas are the integrated areas corresponding to the number of $SO_2$ molecules taken up (in molecules $cm^{-2}$ ) during the initial transient uptake by v-dust, respectively in the dark and under UV, $N_{s,dark}$ and $N_{s,light}$ . The moment at which the steady-state is reached (see text) is chosen as integration limit for the determination of $n_s$ . the $[SO_2]_{ss,dark}$ and $[SO_2]_{ss,light}$ were used to measure the steady state uptake coefficients $\gamma_{ss,dark}$ and $\gamma_{ss,light}$ . ....	93
Figure 8: Scheme of the DRIFT experimental setup. MFC: Mass Flow Controllers are used to supply the optical cell with a defined mixing ratio of dry air, humid air, and $SO_2$ . ....	96
Figure 9: Left: schematic representation of the setup used to age samples of dust with $SO_2$ gas. Right: reactor 1 and 2 with deposited dust, zoomed for clarity. ....	98

This chapter details the materials used during the research and introduces the reader to the methods employed to characterize and analyze the samples. A special attention is given to the methods employed and the experimental protocol followed to investigate the interactions of SO<sub>2</sub> gas with v-dust.

## 1 Materials

### 1.1 Origin of the samples

#### 1.1.1 Volcanic dusts

All five samples of v-dust come from different dust hot spots of Iceland. The geomorphic properties of Hagavatn (64°28'6,12"N 20°16'55,81"W), Mýrdalssandur (63°26'50.1"N 18°48'52.8"W), Maelifellssandur (63°48'48.7"N 19°07'42.5"W) and Dyngjúsandur (64°50'41,885"N 16°59'40,78"W) v-dusts are described by Arnalds et al. (Arnalds et al., 2016). Overall, these areas are subjected to extremely large aeolian erosion due to frequent dust storms, and have extensive areas (from 10 to 140 km<sup>2</sup>), hence providing a large supply (from 30 to 40 million tons annually) of v-dust to the atmosphere (Arnalds et al., 2016). Samples were collected from the top surface layer of each dust hot spot. The samples were dry and did not come in contact with soil or other organics. The fifth sample, the Eyjafjallajökull (63°33'50.4"N 19°27'28.8"W) volcanic ash, was collected and stored dry during the second phase of the explosive-effusive volcanic eruption on April 27, 2010. It is a typical volcanic ash sample as characterized by Gislason et al. (Gislason et al., 2011).

#### 1.1.2 Desert dusts

In order to enrich the discussion and to put the findings about v-dusts in a more global context of aeolian research it was decided to add to the v-dust samples several desert dusts. Three desert mineral dust samples of contrasting elemental compositions come from various regions of the Earth: M'Bour (Senegal), Gobi desert (China), and commercially available Arizona Test Dust (USA). M'Bour natural mineral dust was collected close to the city of M'Bour in Senegal, West Africa (14°25'22.08"N 16°57'55.44"W). It comes from the Sahara and Sahel regions, characterized as the largest sources of atmospheric mineral dust. With annual median emissions of around 1,000 million tons a year, they contribute to about 62 % of the total global dust emissions in the atmosphere (Prospero et al., 2002), (Marticorena et al., 2017). The sample was mechanically sieved after collection and the fraction below 100 μm was used for the investigations. The Gobi mineral desert dust sample comes from Gobi Desert, Ningxia Province, China (36°29'14.39"N 107°28'30.75"E). This area represents another major source of atmospheric mineral dust (Prospero et al., 2002). This is an aeolian sample that was sieved and the fraction below 100 μm was used for further



studies. In addition, the commercially available nominal 0-3  $\mu\text{m}$  Arizona Test Dust (ID 12332M), (ATD, Powder Technology Inc.) collected in October 17, 2014 was used for the research.

### 1.1.3 Clay samples

A number of clays were used for comparison purposes while searching for the origin of specific behaviors observed in desert dusts. Atmospheric loadings of clay dusts are among the largest (i.e., ca. 9 million tons), accounting for more than a half of total dust loading estimated at 19.2 million tons (Tang et al., 2016). The emission fluxes of clay dusts are also the largest, accounting for almost half of the total dust flux (i.e., ca. 800 million tons per year) and providing a large and continuous supply of fresh clay dusts to the atmosphere (Tang et al., 2016). Two commercially available clay samples, Kaolinite (CAS: 1318-74-7, Lot# BCBS7473V) and Montmorillonite K-10 (CAS: 1318-93-0, Lot# 14772-106) natural clays, were purchased from Sigma-Aldrich, St Louis, Mo. The third clay sample illite (85-90% purity) (CAS# 12173-60-3) was obtained from Clay Mineral Society, Aurora, USA and contains 10-15% of quartz. All three minerals are phyllosilicates composed of plate-like structures characterized by varying arrangements of alumina and silica sheets stacked in repeating layers (Hatch et al., 2012). Kaolinite ( $\text{Al}_2\text{Si}_2\text{O}_5(\text{OH})_4$ ) is a 1:1 type clay in which each layer contains one silica and one alumina sheet held together by shared oxygen atoms, while montmorillonite ( $(\text{Na},\text{Ca})_{0.33}(\text{Al},\text{Mg})_2\text{Si}_4\text{O}_{10}(\text{OH})_2 \cdot n\text{H}_2\text{O}$ ) and illite ( $(\text{K},\text{H}_3\text{O})(\text{Al},\text{Mg},\text{Fe})_2(\text{Si},\text{Al})_4\text{O}_{10}[(\text{OH})_2,(\text{H}_2\text{O})]$ ) are 2:1 clays, where alumina sheet is sandwiched between two silica sheets. Kaolinite is unique relative to illite and montmorillonite because the external surface of its alumina sheet contains structural hydroxyl groups (Hatch et al., 2012). Kaolinite and illite have a very low ability to adsorb water, while montmorillonite has a high adsorption capacity (Hatch et al., 2012).

### 1.1.4 Mineral oxide samples

A number of metal oxides were used during research. Pure mineral oxides included silica ( $\text{SiO}_2$ , 98% purity) (Merck, Darmstadt, Germany, Lot# TA565954 912), quartz ( $\text{SiO}_2$ ) (Sigma-Aldrich, St Louis, Mo, CAS 14808-60-7, Lot# BCBZ9191), iron oxide ( $\text{Fe}_3\text{O}_4$ , 99.99% purity) (Sigma-Aldrich, St Louis, Mo, CAS 1317-61-9, Lot# MKBC3159V), goethite ( $\text{FeOOH}$ , 30-63% Fe) (Sigma-Aldrich, St Louis, Mo, CAS 20344-49-4, Lot# BCCB4398), calcium oxide ( $\text{CaO}$ , 99.9% purity) (Merck, Darmstadt, Germany, CAS 1306-78-8, Lot# MKBW2071V), aluminum oxide ( $\text{Al}_2\text{O}_3$ ) (Sigma-Aldrich, St Louis, Mo, CAS 1344-28-1, Lot# STBC4668V), titanium oxide ( $\text{Ti}_2\text{O}_3$ , 99.5% purity) (Evonik industries, Essen, Germany), calcium carbonate ( $\text{CaCO}_3$ , 98% purity) (Sigma-Aldrich, St Louis, Mo, CAS 471-34-1, Lot# MKBV0812V), and magnesium oxide ( $\text{MgO}$ , 98-100.5% purity) (Sigma-Aldrich, St Louis, Mo, CAS 1309-48-4, Lot# SZBF2170V).

## 1.2 Physical and chemical characterization of the natural volcanic and selected desert dust samples

Physical and chemical characterization of the natural volcanic dust samples was undertaken to enable understanding of their interactions with SO<sub>2</sub> gas and to help quantifying these interactions. Desert dust samples were often investigated alongside the v-dusts in order to compare the trends. Specific surface area (SSA) measurements were performed by the author or by the immediate members of the “Reactivity and Air Treatment” research group at IMT Lille Douai, SAGE department. ICP-MS analysis was performed by Dr. L. Alleman at IMT Lille Douai, SAGE department. SEM analysis was done by Dr. V. Thierry, at IMT Lille Douai, GCE department in the presence of the author. XPS measurements were externalized to University of Louvain, Louvain-la-Neuve, Belgium, and were performed by Dr. Elena Maters from the School of Earth and Environment, University of Leeds, UK.

### 1.2.1 Specific surface area measurements of the selected volcanic and desert dust samples, clays and mineral oxides

The SSA is a physical property of solids, which represents the total surface area of a material per mass unit (m<sup>2</sup> g<sup>-1</sup>), and is used for the determination of the kinetic and sorption parameters (Chapter 1, Section 5.1.1). To determine SSA, the Brunauer–Emmett–Teller (BET) method was employed. Nitrogen (N<sub>2</sub>) adsorption measurements were performed with a laboratory gas sorption analysis system (Joshi et al., 2017), (Ibrahim et al., 2018) within 0.05 to 0.3 relative pressure range ( $P/P_0$ ) of N<sub>2</sub>. To determine the range of uncertainty, three adsorption measurements were conducted for each sample. The results of the BET specific surface area ( $SSA_{BET}$ ) of the 5 v-dust samples, 3 mineral dust samples, 2 clays and a number of mineral oxides are displayed in Table 1. Specific surface area is necessary to determine the uptake coefficient and surface coverage of a pollutant (Crowley et al., 2010).

Table 1: BET Specific Surface Area ( $\text{m}^2 \text{g}^{-1}$ ) of various natural v-dust and desert samples, selected clays and mineral oxides used in the study. SSA of the studied samples was determined using the 2-parameter BET method. At least three nitrogen adsorption experiments were conducted for each sample using a homemade gas sorption analyzer. The values presented are the average of the measurements and the quoted errors correspond to one standard deviation. FeOOH data is retrieved from (Xi and Zhang, 2017).

<b>Origin of the Icelandic v-dust sample</b>	<b>BET Specific Surface Area (<math>\text{m}^2 \text{g}^{-1}</math>)</b>
Mýrdalssandur	$1.5 \pm 0.38$
Dyngjusandur	$7.0 \pm 1.8$
Hagavatn	$4.5 \pm 1.1$
Maelifellssandur	$8.2 \pm 2.0$
Eyjafjallajökull	$0.75 \pm 0.19$
<b>Origin of the natural mineral dust sample</b>	
M'Bour	$14.5 \pm 1.0$
Gobi	$10.5 \pm 2.0$
ATD	$67.2 \pm 1.8$
<b>Selected clays</b>	
Kaolinite	$9.2 \pm 2.8$
Montmorillonite	$225 \pm 68$
Illite	$22.2 \pm 6.7$
<b>Selected mineral oxides</b>	
SiO <sub>2</sub> Silica	$402 \pm 40$
SiO <sub>2</sub> Quartz	$1.49 \pm 0.12$
Al <sub>2</sub> O <sub>3</sub>	$118 \pm 22$
CaO	$66.01 \pm 0.54$
CaCO <sub>3</sub>	$0.6 \pm 0.1$
Fe <sub>3</sub> O <sub>4</sub>	$3.4 \pm 0.4$
FeOOH	15.8
TiO <sub>2</sub>	$52 \pm 6.4$
MgO	$49.26 \pm 0.23$

### 1.2.2 Scanning Electron Microscopy of the selected volcanic and desert dusts

Morphology of the v-dust samples was analyzed by Scanning Electron Microscopy (SEM) carried out on a Hitachi S-4300SE/N SEM in high vacuum mode. The images of different v-dust particles together with desert dusts are presented in Figure 1. V-dusts are small particles with rough edges. Dust from Eyjafjallajökull has larger particle size with many particles reaching 500  $\mu\text{m}$  in diameter, while the other four v-dusts have a much finer structure and range from 10 to 50  $\mu\text{m}$  in diameter due to glaciofluvial processes leading to their generation. As for desert dusts, they range from less than 3  $\mu\text{m}$  for Arizona Test Dust to 100  $\mu\text{m}$  for Gobi and M'Bour.

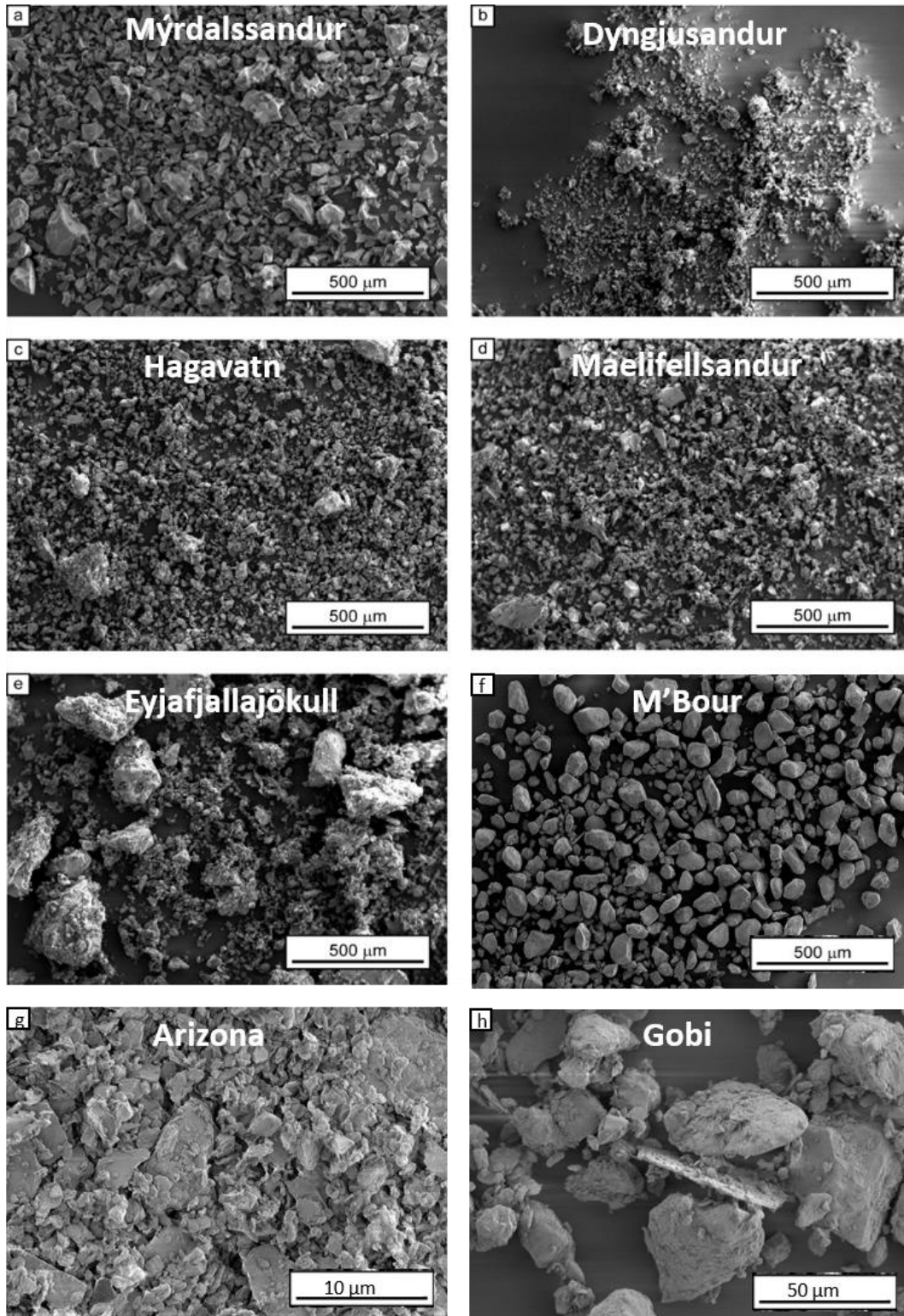


Figure 1: SEM images of eight dusts: (a) Mýrdalssandur, (b) Dyngjusandur, (c) Hagavatn, (d) Maelifellsandur, (e) Eyjafjallajökull, (f) M'Bour, (g) Arizona, (h) Gobi.

### 1.2.3 ICP-MS for chemical bulk elemental composition of the selected volcanic and desert dusts

The bulk elemental composition of the samples of Icelandic v-dust used in this study was determined by ICP-MS using a Perkin Elmer NeXion 300x spectrometer, the results are presented in Table 2. Prior to the analysis, from 2 to 7 mg of each sample were treated in a mixture of acids and peroxide (HF/HNO<sub>3</sub>/H<sub>2</sub>O<sub>2</sub>) in a microwave oven (Milestone Ultrawave) at 500 K and 35 bar for 15 min (Alleman et al., 2010). Six measurements per sample were performed to evaluate their chemical heterogeneity. Repeated measurements were carried out on acid blanks, quality control standard solutions and standard reference material (NIST SRM 1648a and SRM 2584) to evaluate detection limits, accuracy and to validate the whole procedure.

As can be seen from Table 2 silicon is the most abundant element of the v-dusts, followed by iron, calcium, and aluminum. Within the five selected v-dust samples the elemental composition seems to differ only slightly, except for Eyjafjallajökull v-dust which exhibits a higher amount of silicon than other samples and a lower amount of calcium, iron and magnesium. The results of ICP-MS analysis for Eyjafjallajökull v-dust agrees well with the literature (Gislason et al., 2011). The difference in the composition of Eyjafjallajökull v-dust in comparison with other v-dust samples used in this study is most probably due to the difference in the composition of magma that produced it. Indeed, the volcanic systems that supply Dyngjúsandur dust hotspot (Bárðarbunga and Kverkfjöll volcanic systems) and Mýrdalssandur and Maelifellssandur dust hotspots (Katla volcanic system) have magmas of a predominantly basaltic composition, while magma of Eyjafjallajökull is andesitic, meaning that it is higher in silicon (“Icelandic Volcanoes,” n.d.), (Vogel et al., 2017). The decrease of calcium, iron and magnesium with increasing silicon content is in accordance with the expected variation of the composition of magma (Vogel et al., 2017). Other processes that can influence the composition of magma during a particular eruption include crystallization (Clague and Denlinger, 1994), melting of the crustal rocks (Deegan, 2010) and mixing of original magma with another magma that evolved separately (“Icelandic Volcanoes,” n.d.). Since composition of magma can change within the same eruption, one might expect to see different compositions of v-dust both on the time scale and on the location scale. Transported dust can also have a different composition further away from the source. Globally, when compared to other types of mineral dusts, such as Saharan dusts, Gobi dust or Arizona test dust (Joshi et al., 2017), the amount of silicon in all five v-dust samples is considerably lower while the amount of iron, magnesium, and titanium is higher (Romanias et al., 2016), (Langmann, 2013).



Table 2: % bulk elemental composition of the v-dust samples used in this study and of mineral dust samples adopted from (Joshi et al., 2017), as determined by ICP-MS experiments.

Element	Mýrdalssandur	Dyngjusandur	Hagavatn	Maelifellssandur	Eyjafjallajökull	M'Bour Saharan dust (Joshi et al., 2017)	Gobi dust (Joshi et al., 2017)	ATD dust (Joshi et al., 2017)
Si	31.3 ± 2.2	32.7 ± 2.0	27.5 ± 2.8	28.3 ± 2.4	49.5 ± 0.9	94.4	57.6	74.6
Fe	23.0 ± 1.5	19.7 ± 0.2	19.6 ± 0.7	23.8 ± 0.8	13.0 ± 0.5	1.3	5.5	3.1
Ca	13.9 ± 1.3	16.3 ± 0.3	19.5 ± 1.1	14.0 ± 0.3	7.3 ± 0.1	1.0	16.1	4.4
Al	12.3 ± 3.1	15.8 ± 0.2	16.7 ± 3.2	15.5 ± 0.1	13.6 ± 0.9	1.8	11	9.5
Mg	5.1 ± 1.2	7.3 ± 0.1	10.4 ± 1.8	5.7 ± 0.4	3.3 ± 0.2	0.1	2.3	1.0
Ti	7.6 ± 0.7	3.3 ± 0.4	2.4 ± 0.1	6.1 ± 0.4	2.4 ± 0.1	0.7	0.8	0.5
Na	4.8 ± 0.2	3.9 ± 0.1	3.1 ± 0.1	4.6 ± 0.1	7.3 ± 0.3	0.2	2.5	2.5
K	1.3 ± 0.2	0.6 ± 0.1	0.2 ± 0.1	1.5 ± 0.1	3.1 ± 0.1	0.1	3.5	4.0
other	0.7	0.4	0.6	0.5	0.5	0.1	0.7	0.1

#### 1.2.4 X-ray photoelectron spectroscopy for surface characterization of the selected v-dust and desert dust samples

The composition of the samples in the topmost two to ten nanometers of the surface in terms of relative concentrations (in at.%) of O, Si, Fe, Ca, Al, Mg, Ti, Na, K, and Mn, was analyzed by X-ray photoelectron spectroscopy using a Kratos Axis Ultra instrument. High resolution scans at a pass energy of 40 eV were acquired for C1s, O1s, Si2p, Al2p, Fe2p, Mg2p, Ca2p, Na1s, K2p, Ti2p, and Mn2p using a monochromatic Al X-ray beam centered at 1486.6 eV. Data treatment was performed using the CasaXPS software program. The binding energy scale was calibrated by assigning a value of 284.8eV to the C1s peak for adventitious carbon. The obtained results are presented in Table 3.

From Table 3 we can see that, in comparison with bulk composition, surface composition for v-dust samples is considerably lower in Fe, Ca, Mg, Ti, and, with exception of Eyjafjallajökull, in Na and K. A completely opposite trend ( $\%Si_{\text{surface}} > \%Si_{\text{bulk}}$ ,  $\%Al_{\text{surface}} > \%Al_{\text{bulk}}$ ) is observed for Si and, with exception of Eyjafjallajökull, for Al. The fact that a higher amount of Si and Al is observed on the surface v-dust particles could be due to the fact that minerals in ash are overlain by thin glass coating consisting of random three-dimensional network of tetrahedral units made up of  $Si^{4+}$ ,  $Al^{3+}$  and bridging oxygen atoms (Delmelle et al., 2018). As for the desert dusts, they show lower % surface Si and Ti composition and higher % Al composition on the surface than in the bulk ( $\%Si_{\text{surface}} < \%Si_{\text{bulk}}$ ,  $\%Al_{\text{surface}} > \%Al_{\text{bulk}}$ ). The trends for other elements on the surface of desert dusts are less clear. A sharp difference in surface vs bulk composition raises a question of which one would be more important while studying interactions of  $SO_2$  gas with the v-dust. It was highlighted that surface of the ash can be modified during eruption (Maters et al., 2016), (Langmann, 2013). Due to potential modifications of v-dust particles during eruption and to

the fact that SO<sub>2</sub> gas is unlikely to penetrate into the hard dust particle, surface composition is expected to define the interfacial interactions.

*Table 3: % surface elemental composition of the v-dust and desert dust samples used in this study as determined by XPS (surf stands for surface) compared to % bulk composition as determined by ICP-MS (bulk). Both expressed as % by weight. Bulk compositions of mineral dust samples marked with asterisk were adopted from (Joshi et al., 2017). Error on the XPS measurements < 10%.*

Element	Mýrdalssandur		Dyngjusandur		Hagavatn		Maelifelssandur		Eyjafjallajökull		M'Bour Saharan dust		Gobi dust		ATD dust	
	surf	bulk	surf	bulk	surf	bulk	surf	bulk	surf	bulk	surf	bulk*	surf	bulk*	surf	bulk*
Si	47.1	31.3	49.0	32.7	42.8	27.5	43.7	28.3	60.0	49.5	57.0	94.4	54.7	57.6	57.5	74.6
Fe	20.0	23.0	15.9	19.7	10.5	19.6	22.0	23.8	7.7	13.0	6.1	1.3	6.7	5.5	8.2	3.1
Ca	8.1	13.9	9.7	16.3	9.0	19.5	6.3	14.0	5.5	7.3	2.4	1.0	7.7	16.1	5.5	4.4
Al	14.5	12.3	16.8	15.8	31.8	16.7	18.2	15.5	13.4	13.6	32.1	1.8	18.5	11	18.0	9.5
Mg	3.3	5.1	4.8	7.3	2.4	10.4	3.0	5.7	1.5	3.3	0	0.1	6.1	2.3	3.9	1.0
Ti	3.8	7.6	2.0	3.3	1.8	2.4	4.3	6.1	1.0	2.4	0.2	0.7	0	0.8	0.5	0.5
Na	2.3	4.8	1.0	3.9	1.4	3.1	1.3	4.6	7.5	7.3	0.3	0.2	0.8	2.5	1.3	2.5
K	0.9	1.3	0	0.6	0	0.2	0.4	1.5	3.3	3.1	1.9	0.1	4.7	3.5	4.4	4.0
other	0	0.7	0.8	0.4	0.3	0.6	0.8	0.5	0.1	0.5	0	0.1	0	0.7	0.7	0.1

### 1.3 Gases used for experiments

Experiments are carried out using zero air; it is generated by a classical air compressor, and then passed through a catalytic zero air generator (Claind ZeroAir 2020, Lenno, Italy) coupled to a swing adsorption (PSA) device. The remaining impurity levels in the air stream before entering the reactor are lower than the analytical system detection limits: VOCs < 0.1 ppb, CO<sub>2</sub> < 10 ppb, and CO < 80 ppb. Moisture level is ca. 2 ppm. In experiments requiring humid air, a second flow of zero air going through a bubbler of ultrapure water (milli-Q, resistivity 18.2 MΩ cm) is mixed with the dry air flow, in proportions necessary to reach the relative humidity (*RH*) targeted. Certified gas cylinders are used as SO<sub>2</sub> sources. For low concentration experiments aiming to determine uptake coefficients in the flow-tube and for intercomparison studies an SO<sub>2</sub> cylinder of 8.96 ppm in air (20.7 % O<sub>2</sub>, 79.3 % N<sub>2</sub>) provided by “Air Liquide” is used. Regarding the mechanistic investigation employing DRIFT spectroscopy and quantification using HPLC, higher concentrations are used and a certified cylinder of 250 ppm (Messer, France) diluted in synthetic air (nearly 80% N<sub>2</sub> and 20% O<sub>2</sub>) is the SO<sub>2</sub> source.

Throughout the manuscript, gas concentrations are given in ppmv and ppbv (parts per million and parts per billion by volume, respectively). Under usual experimental conditions ( $T = 296$  K,  $P = 1$  atm), the conversion to a concentration is given by 1 ppbv (SO<sub>2</sub>)  $\approx 2.5 \times 10^{10}$  molecules cm<sup>-3</sup>, 1 ppmv (SO<sub>2</sub>)  $\approx 2.5 \times 10^{13}$  molecules cm<sup>-3</sup>. Note that this conversion factor takes a different value when the temperature or total pressure changes.

## 1.4 Other chemicals and reagents used for investigations

HPLC grade acetonitrile (ACN), 99.95% and methanol (MeOH), 99.9% were obtained from Biosolve Chimie, Dieuze, France. Potassium hydrogen phthalate and triethanolamine, 99% of analytical grade were purchased from Acros Organics, Geel, Belgium. Cetylpyridinium chloride, 98% was purchased from Alfa Aesar, Kandel, Germany. Sodium sulfate, 99% purity was purchased from Merck, Darmstadt, Germany. Sodium sulfite, >95 % purity was purchased from Fischer Chemical, Loughborough, UK. Formalin (37% formaldehyde solution by weight containing 10-15 % MeOH as stabilizer) was obtained from Sigma-Aldrich. Other chemicals and solvents of analytical grade were used during research. Deionized water (DI) was used throughout the investigations.

## 2 Experimental strategy and methods

The following experimental setups and protocols constitute the pillar of this thesis, as the author primarily used the following three types of experimental procedures in order to fulfill the scientific objectives: flow-tubes, diffuse reflectance infrared Fourier transform spectroscopy (DRIFTS) and high performance liquid chromatography (HPLC). Parameters investigated by each technique together with experimental conditions, advantages and limitations are summarized in Table 4.

### 2.1 Introduction to the experimental strategy

The decision to start investigations of the interactions of SO<sub>2</sub> with v-dust using flow-tube reactor was motivated by the fact that it is better adapted to study processes under atmospherically relevant conditions of low SO<sub>2</sub> concentration (ppb range), atmospheric pressure, relevant humidity and temperature. By using flow-tubes, such information as uptake coefficients and number of molecules adsorbed on surface can be obtained. Note that the latter is calculated from the number of molecules lost from the gas phase. In this way molecules reaching the detector are serving as messengers for the observed phenomena. Thus, flow-tube experiments are limited to the gas phase and do not provide information on the fate of the molecules taken up on the surface.

To obtain a direct view on the processes that happen on the surface of v-dust when subjected to SO<sub>2</sub> gas DRIFTS was employed. Once again, atmospherically relevant conditions were sought for and relevant pressure, temperature and relative humidity were employed. The concentration of SO<sub>2</sub> gas though was high (ppm range) due to the low sensitivity of the technique. Note that large difference in SO<sub>2</sub> concentrations used for flow-tube versus DRIFTS experiments comes from different technical constrains. DRIFT spectroscopy is used for the in situ characterization of surface adsorbed species but is characterized



by a relatively low sensitivity, depending on the gas-surface interactions. In this work two different reactors serve two different purposes: flow-tube is used to study kinetics by providing uptake coefficients under atmospherically relevant conditions while DRIFTS is used to study surface reaction mechanism. It is important to keep in mind that while the kinetics is changed by the concentration because the surface coverage is changed by the concentration, the reaction mechanism is not likely to be changed as a function of gas phase concentration. Thus, both techniques bring complimentary and valuable information.

Finally, HPLC was considered necessary to quantify the species observed by DRIFTS, as DRIFTS is a qualitative technique and doesn't provide quantitative information. In addition, not constrained by reflectance of samples, all samples could be investigated using HPLC and thus the samples could be easily compared between each other. In the absence of a suitable HPLC method able to separate and quantify surface species encountered in this work, a new method was developed and validated for the intended use (see Chapter 5). The conditions employed were similar to those employed by DRIFTS.

*Table 4: The three main techniques used for investigation of interactions of SO<sub>2</sub> gas with Icelandic v-dusts. Parameters investigated. Conditions. Advantages and limitations.*

<b>Instrumental technique</b>	<b>Purposes</b>	<b>Conditions</b>	<b>Advantages</b>	<b>Limitations</b>
<b>Flow-tube reactor</b>	Determination of the steady state uptake coefficient ( $\gamma_{ss}$ ) Number of molecules transiently adsorbed ( $N_s$ )	[SO <sub>2</sub> ]: 75 ppb RH: 0-70% light: dark and simulated sunlight Temperature: 23°C Pressure: 760 Torr Time: 12hr -80 hr	Atmospherically relevant conditions of SO <sub>2</sub> concentrations, RH, pressure, temperature and light exposure	Only relevant for the investigation of the gas phase, provides no information on the surface fate of the lost gas-phase molecules
<b>DRIFTS</b>	In-situ monitoring of surface species and processes.  Kinetics	[SO <sub>2</sub> ]: 175 ppm RH: 0, 30% light: dark Temperature: 23°C Pressure: 760 Torr Time: 72 hr	Able to distinguish between different species present on the surface, possible to monitor temporal evolutions of surface species	Low reflectance for dark samples generates weak signals Larger than atmospherically relevant concentrations of SO <sub>2</sub> gas Not quantitative Challenging to run continuous and long term experiments
<b>HPLC</b>	Quantifications of sulfates and sulfites present on the surface	[SO <sub>2</sub> ]: 175 ppm RH: 0-82% light: dark Temperature: 23°C Pressure: 760 Torr Time: 5 min-120 hr	Quantification of sulfites and sulfates present on the surface of various samples	Larger than atmospherically relevant concentrations

## 2.2 Experimental setup of flow-tube experiments

### 2.2.1 Typical flow-tube experiment

The heterogeneous interactions of SO<sub>2</sub> with v-dust were investigated in a horizontal double wall flow-tube reactor represented schematically in Figure 2. The experiments were conducted under relevant atmospheric conditions, i.e. SO<sub>2</sub> concentration in the ppb range, atmospheric pressure, room temperature,

various % *RH*, in the dark and under UV light. The objective of this series of experiments was to determine the uptake coefficients of SO<sub>2</sub> on the various Icelandic v-dusts.

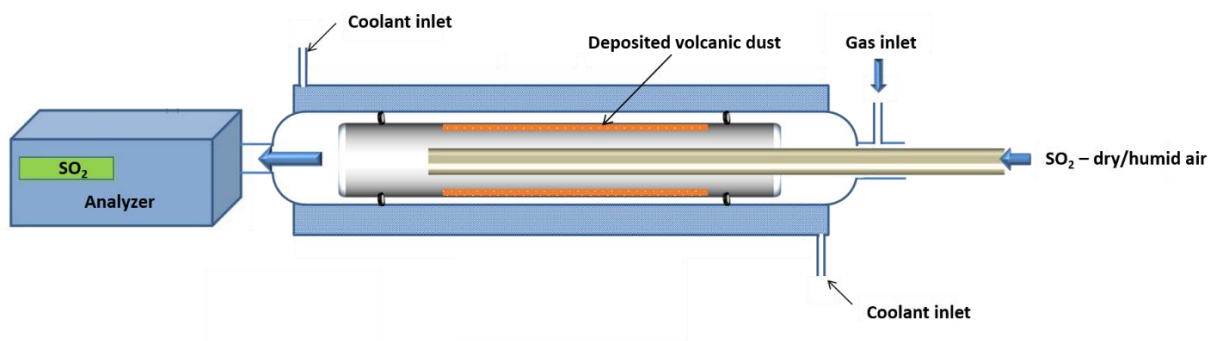


Figure 2: Schematic representation of the Coated Wall Flow Tube (CWFT) reactor used in this study. The space filled with the coolant in between the two walls is shaded in blue. The dust sample coating the inner surface of the Pyrex tube is shown in orange.

Lasne et al described the setup in details in recent publications. It mainly consists of three parts; (i) the gas mixing line, (ii) the reactor and (iii) the analytical device (Romanias et al., 2016), (Lasne et al., 2018). The gas preparation line is used for the mixing of zero dry/humid air with SO<sub>2</sub> resulting in a flow with the desired proportion of *RH* and SO<sub>2</sub> concentration. Dry air, humid air and SO<sub>2</sub> flows are controlled with MKS mass-flow controllers (100 to 1000 sccm) connected to a 4-channel MKS type 247 readout unit; they are mixed at the entrance of the injector. The reactor is made of a double wall Pyrex glass and is thermostated by circulating water in between the double wall surrounding the flow-tube. Inside and along the axis of the reactor, a Pyrex tube covered on its inner wall with the v-dust is introduced. Two Viton O-rings are placed around the Pyrex tube to fix its position inside of the reactor. The gas mixture is flowed through a movable injector (internal diameter of 0.3 cm) with a flow rate ranging between 250 and 500 sccm, ensuring laminar flow conditions with a Reynolds number,  $R_e < 140$ . The role of the moveable injector is to either isolate (placed at the downstream end of the flow tube) or to expose the dust surface to the gas environment (upstream end of the reactor). A thermoregulation unit (Huber, Ministat 230) regulates the reactor temperature by circulating water in between the double-wall of the flow-tube. The outgoing flow is then directed to the SO<sub>2</sub> analyzer (Model 43C, Thermo Environmental Instruments Inc.) for the real time gas phase monitoring of SO<sub>2</sub>, with a time resolution of 10 seconds. SO<sub>2</sub> is detected via its fluorescence signal after absorption of UV photons. The limit of detection is 2.0 ppb. The precision of the measurement given by the supplier is 1.0 ppb or 1% of reading, whichever is greater. Before an experiment is conducted, the setup is flushed with a high concentration of SO<sub>2</sub> to passivate all the surfaces accessible to the gas flow.

### 2.2.2 Flow-tube experiments involving UV light. Calibration and characterization of the light source

For the experiments involving UV light the UVA Philips PL-L 18W lamps were placed evenly around the flow-tube at a distance of 12 cm. The dust samples were irradiated with 3 UVA lamps. The spectrum of the light emitted by the UVA lamps is in the wavelength range 315-400 nm, with maximum emission at 352 nm.

Light source characterization experiments were carried out with high NO<sub>2</sub> concentrations ( $\approx 10^{15}$  molecule cm<sup>-3</sup>, i.e.  $\approx 50$  ppmV) using dry N<sub>2</sub> as bath gas. NO<sub>2</sub> concentrations were recorded with a chemical ionization mass spectrometer (SIFT-MS) (Romanias et al., 2016), (Zeineddine et al., 2017). The total flow rate in the reactor was set at 50 sccm and the kinetics of NO<sub>2</sub> was followed as a function of its residence time (4 - 14 s). Under such experimental conditions, the loss of NO<sub>2</sub> is due to two processes: NO<sub>2</sub> photolysis (Reaction 1) and a secondary reaction with oxygen atoms (Reaction 2):



Therefore, the global rate of NO<sub>2</sub> loss is:

*Equation 1* 
$$d[\text{NO}_2]/dt = -2 J_{\text{NO}_2} [\text{NO}_2]$$

The values of  $J_{\text{NO}_2}$  (s<sup>-1</sup>), determined from the exponential decay of NO<sub>2</sub> concentration for different numbers of lamps switched on, are in the  $1.5 \times 10^{-3} - 4.5 \times 10^{-3}$  s<sup>-1</sup> range (Figure 3). These values are similar to those of  $J_{\text{NO}_2}$  measured in the atmosphere of Earth under cloudy and clear sky conditions (Barnard et al., 2004), (Bohn et al., 2005), (Topaloglou et al., 2005). Since the  $J_{\text{NO}_2}$  values measured in the lab are close to those measured in the real atmosphere, the experiments performed under UV light are referred to as experiments performed under simulated sunlight radiation.

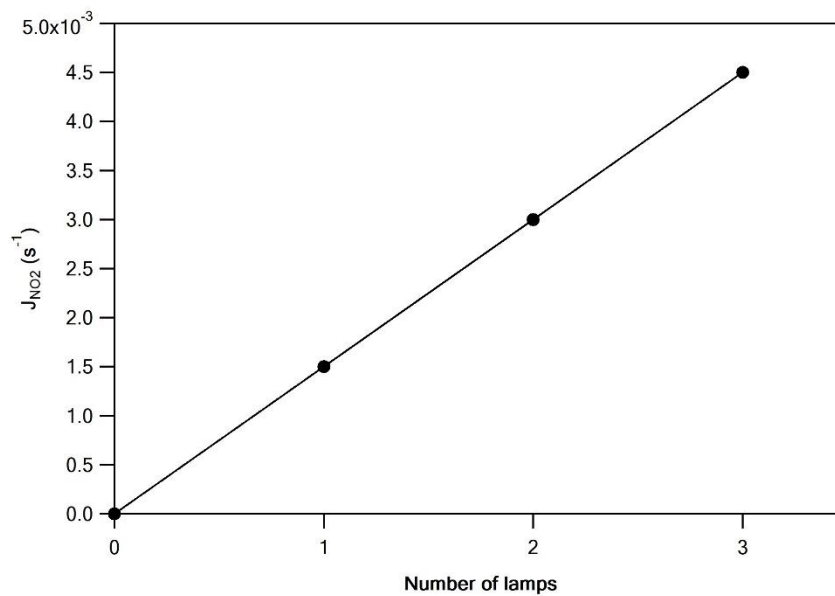


Figure 3:  $J_{NO_2}$  as a function of the number of lamps switched on during flow-tube experiments.

### 2.2.3 Sample preparation for flow-tube experiments

To coat the inner surface of a Pyrex tube with v-dust (orange color in Figure 2), a defined mass of dust is first inserted in a tube. A small amount of water is added to form a slurry and the tube is shaken to deposit an even coating on the Pyrex surface. This way the water/dust suspension is homogeneously spread on the inner wall of the tube, ensuring that no excess suspension has to be removed after the deposition. Then, the tube is heated slightly above 380 K for 10 minutes to evaporate excess water, placed in the reactor and flushed overnight with dry air. Before each experiment, the dust deposited in the tube is left for at least 1 hour under a zero air flow containing the level of relative humidity that will be used during the experiment planned next. This prevents any interplay between  $H_2O$  and  $SO_2$  on the surface of v-dust that may disturb the process of interest, here the interaction of  $SO_2$  with the surface of v-dust.

Potential modifications of the volcanic dust upon its dissolution in water in the process of slurry preparation and subsequent drying process include displacement of soluble salts that might be found on the surface of v-dust particles as well as leaching of alkali and alkaline earth metals from the aluminosilicate network at ash surfaces (Witham et al., 2005). In the case of Hagavatn, Mýrdalssandur, Maelifellssandur and Dyngjusandur natural v-dust samples that were most likely previously exposed to water, the abovementioned phenomena do not seem to effect the results because the soluble salts would be expected to be leached out by the time of the experiment. In the case of fresh Eyjafjallajökull dust,

leaching of the soluble salts formed during ash-gas interaction in the plume presents a valid concern. In order to minimize removal of soluble salts the amount of water added to prepare a slurry was as small as necessary to spread the dust evenly, i.e. 1:3 ash (g) to water (mL) ratio was used, which is much smaller than the 1:25 ash-to-water ratio recommended for preparation of ash leachates (Witham et al., 2005). In addition, contact time with water was minimized to around 10 seconds shaking followed by rapidly drying the slurry, which is also much faster than 90 min agitation procedure recommended by Witham et al. (Witham et al., 2005). One could also expect that drying the slurry would lead to redistribution of the displaced salts, even though some of it could be redeposited on the surface of the glass tube and not the v-particles.

We didn't notice any loss of dust during the uptake experiments. Note that the tubes with the deposited dust are weighed before and after the experiments and the variations noticed were in the range of the mass scale uncertainty ( $< 1\%$ ). In addition, considering that (i) the flow rate during the experiments is relative slow and (ii) the experiments are carried out under atmospheric pressure and no pressure variation takes place between the reactor and the analyzer, it is highly improbable to experience any loss of dust during our measurements. Furthermore, we have not observed (at least visually) any large particles to fail to adhere to the Pyrex tube. However, even if this was the case, in the horizontal flow-tube, these particles would still be subjected to the flow of gas and thus remain accessible to the gas. To conclude, the total mass of the dust inside the reactor is maintained during the entire experiment.

#### 2.2.4 Protocol for a typical flow-tube experiment: dark conditions

Theoretical  $\text{SO}_2$  concentration profile is represented in Figure 4. During a typical flow-tube experiment  $\text{SO}_2$  is flowed through the reactor, the dust being left unexposed initially. After a stable  $\text{SO}_2$  concentration,  $[\text{SO}_2]_0$ , is set, the injector is pulled out and the dust is exposed to  $\text{SO}_2$ ; the change in  $\text{SO}_2$  concentration related to its uptake by dust is recorded by the  $\text{SO}_2$  analyzer. After a steady-state is reached, the injector is pushed back in to control the  $[\text{SO}_2]_0$ . What is obtained as a result of the flow-tube experiment is a time evolution of the trace gas concentration at the tube exit, the so-called breakthrough curve, that is used to determine the steady state uptake coefficient (Huthwelker et al., 2006). In the case of  $\text{SO}_2$  a long-lasting tailing of the breakthrough curve is observed, similar to the one described for the uptake of nitric acid ( $\text{HNO}_3$ ) on ice (Huthwelker et al., 2006). This phenomenon leads to the following question: at which point can we say that a steady state is reached? In the absence of the generally accepted understanding of the nature of tailing and for the practical reasons the following pragmatic approach was adopted. Steady state is considered to be reached when the variation of the signal falls within 1.5% of its value for at least three hours. On average it takes about 12 hours to reach the steady state under 30% humidity. Most studies that use Knudsen cells measure the initial uptakes as opposed to steady state uptakes and thus the time

exposure of the gas to the surface is much shorter, often in the range of several minutes (Ullerstam et al., 2003), (Maters et al., 2017), (Adams et al., 2005), (Zhou et al., 2014). Thus, determination of steady state uptake at 12 hours allows characterization of long-term processes that are rarely studied (Crowley et al., 2010).

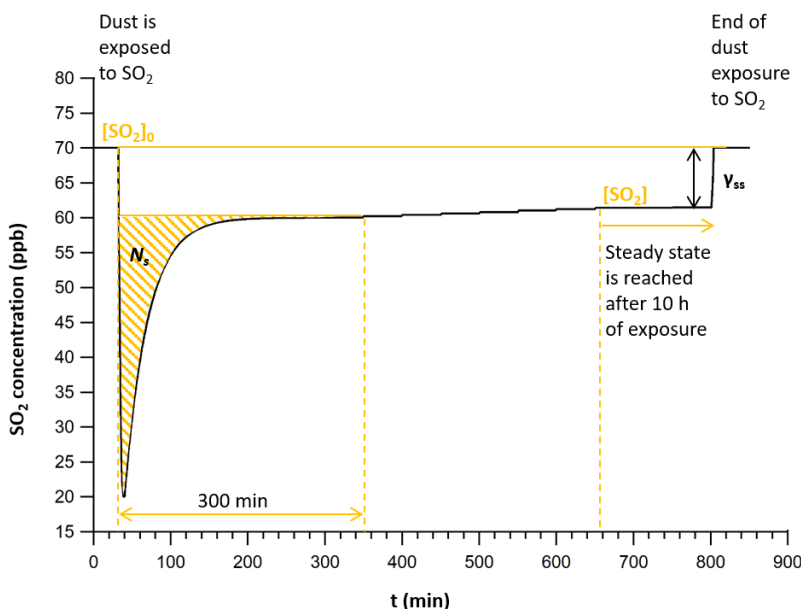


Figure 4: Theoretical  $\text{SO}_2$  concentration profile during a typical flow-tube experiment with  $v$ -dust exposed to  $\text{SO}_2$ . At the beginning of the experiment where surface is isolated from the gas mixture the initial  $\text{SO}_2$  concentration is  $[\text{SO}_2]_0$ , then the dust is exposed to the gas and the concentration of  $\text{SO}_2$  falls to its minimum, after which it recovers till a steady-state is reached. Note that the steady-state concentration  $[\text{SO}_2]_{ss}$  is different from the initial state concentration  $[\text{SO}_2]_0$ . Initial concentration is controlled when the injector is pushed in and the  $\text{SO}_2$  gas in no longer in contact with the dust. Shaded area corresponds to the integrated area that is used to obtain the number of molecules during the transient initial uptake of  $\text{SO}_2$  on  $v$ -dusts  $N_s$  (molecules  $\text{cm}^{-2}$ ). 300 min was chosen as integration limits for the determination of  $N_s$ .

Preliminary experiments were conducted to determine a possible contribution of the Pyrex surfaces to the uptake of  $\text{SO}_2$ . They showed negligible contribution to the parameters determined in the current study. As a consequence, no contribution of the Pyrex glass needs to be subtracted from the steady-state uptake of  $\text{SO}_2$  nor from the transient number of  $\text{SO}_2$  molecules taken up.

### 2.2.5 Protocol for a typical flow-tube experiment: UV-light conditions

Experiments involving UV light are conducted the following fashion.  $\text{SO}_2$  is flowed through the reactor, the dust being left unexposed initially. After a stable initial  $\text{SO}_2$  concentration,  $[\text{SO}_2]_0$ , is set, the injector is pulled and the dust surface is exposed to  $\text{SO}_2$  in the dark; the change in  $\text{SO}_2$  concentration,  $[\text{SO}_2]$ , related to the uptake by dust is recorded by the  $\text{SO}_2$  analyzer downstream of the reactor. After a steady-state is reached in the dark, the UV lamps are turned on, and further modifications of the signal are observed. The UV lamps are turned off after a steady-state under UV is reached and, last, the injector is

pushed back in the reactor to control the level of  $[SO_2]_0$ . A theoretical  $SO_2$  concentration profile is represented in Figure 5.

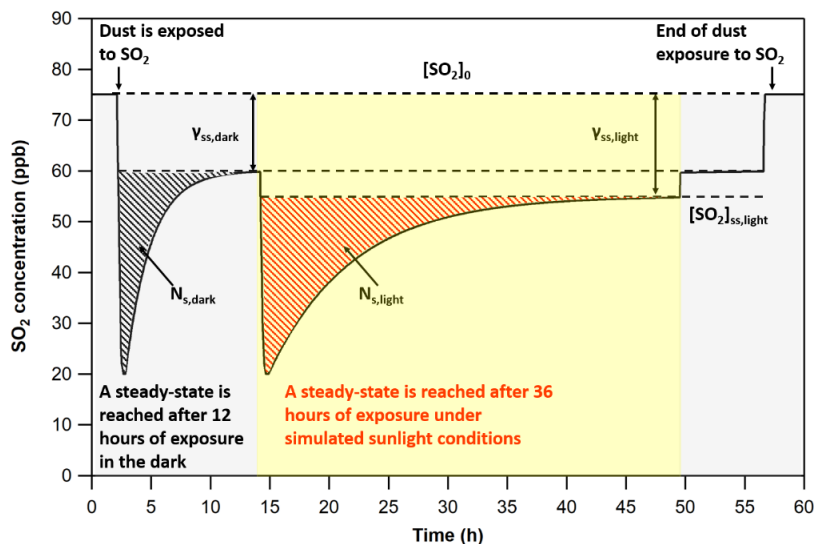


Figure 5: Theoretical  $SO_2$  concentration profile during a typical flow-tube experiment with  $v$ -dust under 30% of RH and 296 K. At the beginning of the experiment, the dust is isolated from the gas mixture, in which an initial  $SO_2$  concentration,  $[SO_2]_0$ , is set. The dust is then exposed to  $SO_2$  in the dark (gray area), and  $[SO_2]$  decreases initially strongly, before recovering to a steady-state value  $[SO_2]_{ss, dark}$  within typically 12 hours. Thereafter, the surface is irradiated with simulated sunlight (yellow area), and a second large consumption of  $SO_2$  is observed, before recovering to a steady-state value  $[SO_2]_{ss, light}$  within typically 36 hours. Lights are turned off (second gray area) and  $[SO_2]$  returns to its steady-state value in the dark.  $SO_2$  concentration is then controlled by pushing the injector in, and the dust is no longer exposed to the gas. Black-shaded and red-shaded areas are the integrated areas corresponding to the number of  $SO_2$  molecules taken up (in molecules  $cm^{-2}$ ) during the initial transient uptake by  $v$ -dust, respectively in the dark and under UV,  $N_{s, dark}$  and  $N_{s, light}$ . The moment at which the steady-state is reached (see text) is chosen as integration limit for the determination of  $N_s$ . The  $[SO_2]_{ss, dark}$  and  $[SO_2]_{ss, light}$  were used to measure the steady state uptake coefficients  $\gamma_{ss, dark}$  and  $\gamma_{ss, light}$ .

### 2.2.6 Determination of the uptake coefficients from flow-tube experiments

The measurements of  $SO_2$  concentration at steady-state,  $[SO_2]_{ss}$ , and at the initial level,  $[SO_2]_0$ , together with the knowledge of the parameters defining our setup are necessary to conduct the analysis leading to the determination of the uptake coefficients under equilibrium conditions,  $\gamma_{ss}$  (Lasne et al., 2018). Assuming first order kinetics for the uptake of  $SO_2$  by  $v$ -dust surfaces, the observed constant of reaction,  $k_{obs}$  (in  $s^{-1}$ ), is determined by Equation 2:

Equation 2

$$k_{obs} = \frac{v}{L} \times \ln\left(\frac{[SO_2]_0}{[SO_2]_{ss}}\right)$$

where  $v$  is the flow in the reactor (in  $cm s^{-1}$ ) and  $L$  is the length of the dust coating (in  $cm$ ). The value of  $k_{obs}$  (in  $s^{-1}$ ) is corrected for diffusion of  $SO_2$  with a constant  $k_{diff}$  (in  $s^{-1}$ ) to give the diffusion-

corrected constant  $k_{kin}$  (in  $s^{-1}$ ). In this work, a diffusion coefficient of  $SO_2$  in the air derived from (Massman, 1998) is used,  $D(296\text{ K}) = 95.28\text{ Torr cm}^2\text{ s}^{-1}$ . This value is in excellent agreement with  $D = 94 \pm 13\text{ Torr cm}^2\text{ s}^{-1}$  suggested by Tang et al. (Tang et al., 2014). The diffusion-corrected constant,  $k_{kin}$ , is then used to determine  $\gamma_{ss}$ , (Equation 3):

Equation 3

$$\gamma_{ss} = \frac{4k_{kin}V}{cS_{geom}}$$

where  $V$  and  $S_{geom}$  are the volume (in  $cm^3$ ) and geometric surface (in  $cm^2$ ) of the region where the reaction takes place, respectively, and  $c$  is the average molecular speed (in  $cm\text{ s}^{-1}$ ). The diffusion-correction accounts for *ca.* 5 % of the measured uptake coefficients.

Determination of the geometric uptake coefficient represents an upper limit to  $\gamma$  since it does not take into account the interaction of the gas with all adsorption sites. Another approach is to use the BET surface area to calculate the uptake coefficient. This approach is especially valid when there is a long processing of the surface and thus there is enough time for the gas to interact with the maximum available surface area (Crowley et al., 2010). A series of experiments were carried out as a function of Mýrdalssandur v-dust mass deposited that showed a linear increase in the 0 - 250 mg range. The linear increase of the uptake with mass and the lack of saturation reflect the fact that the entire surface of the dust is accessible to  $SO_2$  molecules from the gas and thus the specific surface area  $SSA_{BET}$  is used for the calculation of the uptake coefficient,  $\gamma_{ss,BET}$ ,

Equation 4

$$\gamma_{ss,BET} = \gamma_{ss} \times \frac{S_{geom}}{A_s}$$

where  $A_s$ , is the effective surface area of the dust, obtained from multiplying  $SSA_{BET}$  ( $m^2\text{ g}^{-1}$ ) by the mass of the sample (g).

The error on the uptake coefficients is the root-mean-square deviation of the values measured. It was calculated with the precision of the signal (0.5% of the measured concentration) and its propagation to  $k_{obs}$  measurement, the  $SSA$  determination ( $\sim 25\%$ ) and all relevant uncertainties, i.e. on the gas flow measurement, temperature, mass weighing, and length of the exposed dust coating ( $\sim 8\%$ ). The total error calculated for the  $\gamma$  values was estimated to be *ca* 35% in all experiments and a safe limit of 40% is given. Although the quoted uncertainty is significant, it reflects the real error accounted for the measurement of slow uptake processes (uptakes on the order of  $10^{-9}$ ) in the flow-tube.



### 2.2.7 Determination of the transient number of SO<sub>2</sub> molecules taken up by dust

Besides uptake coefficients, the transient initial number of SO<sub>2</sub> molecules taken up per surface area of v-dusts  $N_s$  (molecules cm<sup>-2</sup>) is determined at 0 and 30% of  $RH$ , both in the dark and under UV irradiation (3 UV lamps on,  $J_{NO_2} = 1.5 \times 10^{-2} \text{ s}^{-1}$ ); by integrating the area of the initial uptake process in a typical uptake experiment (Figure 4, Figure 5) divided by the effective surface area of the dust,  $A_s$ , according to Equation 5:

Equation 5

$$N_s = \int_{\tau=0}^{\tau=t} \frac{F_t}{A_s} d\tau$$

where  $F_t$  is the flow rate (molecules min<sup>-1</sup>) of SO<sub>2</sub> molecules through the reactor. The total error in  $N_s$  determination is estimated to be ca. 30% and includes all systematic uncertainties and the error in SSA determination.

It should be noted that since the SO<sub>2</sub> concentration recorded at the steady-state was lower than its pre-exposure concentration, for the determination of  $N_s$  solely the transient initial uptake removal of SO<sub>2</sub> is considered (dashed areas in Figure 4 and Figure 5). The long tailing of the breakthrough curve observed points to additional physico-chemical processes besides the adsorption/desorption. Therefore for the determination of integration parameter a similar to two-third criterion approach was adopted as recommended by Huthwelker et al., where “the surface uptake is considered finished once the breakthrough curve rises to two-thirds of its initial value” (Huthwelker et al., 2006). The integration limits for the determination of the number of molecules  $N_s$  were chosen from the time of the exposure of SO<sub>2</sub> to the dust to 300 min after the exposure to make sure that the change in the breakthrough curve towards steady state has occurred for all the dusts. This criterion was adopted in order to be able to compare the uptake capacity of the v-dusts at the initial stage of the interaction with SO<sub>2</sub>. On longer scale, samples can be compared based on the  $\gamma_{ss,BET}$  values.

## 2.3 Experimental setup and protocol for DRIFTS experiments

The heterogeneous interaction between SO<sub>2</sub> gas and v-dusts was studied *in-situ* inside of the optical DRIFTS cell operated at atmospheric pressure and room temperature under dry and 30%  $RH$  conditions. The objective of this series of experiments was to monitor the adsorbed species formed on the surface of v-dusts, aiming to elucidate the mechanism of the interaction under both dry and humid conditions.

The DRIFT experimental setup consists of three parts: (i) the gas supply line, (ii) the optical reactor, and (iii) the analytical device as described previously by Romanias et al. (Romanías et al., 2016). A representation of the system is given in Figure 6. The heterogeneous reactions between SO<sub>2</sub> and different v-dust samples are monitored *in situ* inside of the optical DRIFTS cell (Praying Mantis Kit, Harrick Scientific Corp.) fitted with zinc selenium (ZnSe) windows. DRIFT spectra are recorded by a Nicolet 6700 FTIR spectrometer equipped with a mercury cadmium telluride (MCT) detector cooled with liquid nitrogen.

The temperature of the sample is measured using a thermocouple placed right below of the sample holder and is monitored/controlled with a Harrick temperature controller (Pleasantville, USA).

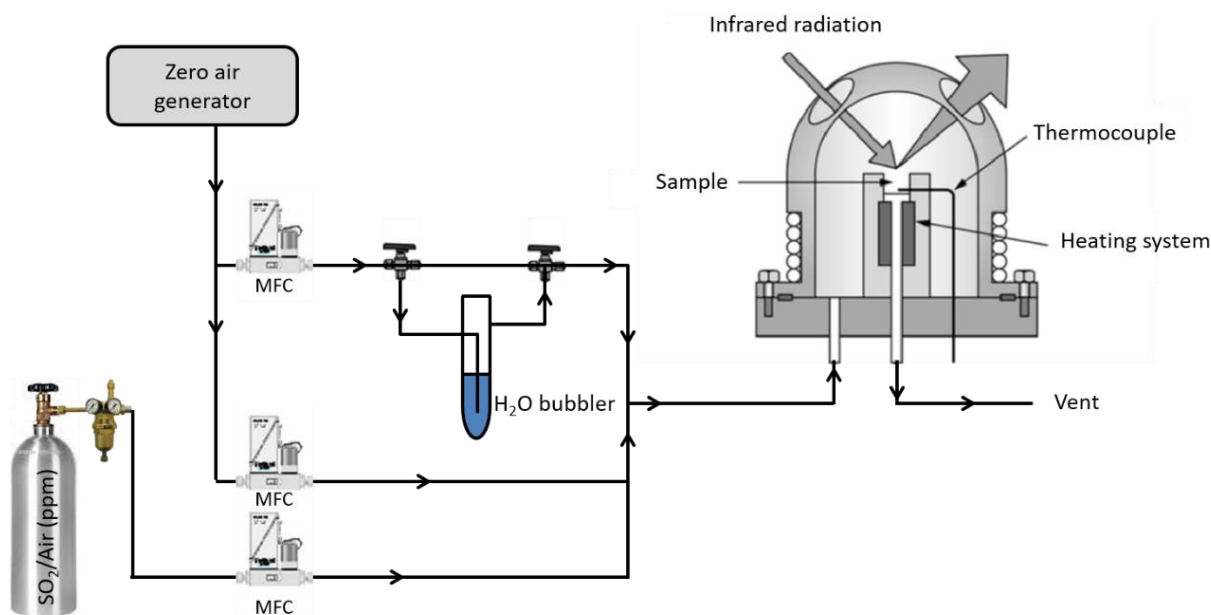


Figure 6: Scheme of the DRIFT experimental setup. MFC: Mass Flow Controllers are used to supply the optical cell with a defined mixing ratio of dry air, humid air, and SO<sub>2</sub>.

At the beginning of the experiment the crucible sample holder inside the DRIFTS cell is filled with about 80-110 mg of v-dust. The cell is then tightly closed and the infrared beam is focused on the surface of the dust. The gas flowed through the DRIFTS cell is made up of different proportions of dry air, humid air and SO<sub>2</sub> gas. Prior to the introduction of the SO<sub>2</sub> gas volcanic samples are heated to 423 K for 1.5 hours to remove any pre-adsorbed species. Samples are then allowed to cool down to room temperature and are purged overnight with either dry or humid air depending on the experimental

conditions in order to equilibrate the system. A background spectrum is recorded right before introduction of SO<sub>2</sub> gas. DRIFT spectra of the v-dust in the presence of SO<sub>2</sub> gas are recorded from 650 to 4000 cm<sup>-1</sup> using Omnic software with 100 scans per spectrum, a spectral resolution of 4 cm<sup>-1</sup>, and a time resolution ranging from 3 minutes to 1 hour depending on the stage of the experiment. The formation and loss of surface species are observed as positive and negative absorption bands respectively. Thus, a typical experiment lasts about 4 days and consists of thermal pre-treatment (1.5 hr), system equilibration (16 hr), SO<sub>2</sub> adsorption phase (72 hr) and desorption upon flushing phase (6 hr). The SO<sub>2</sub> concentration in the mixed gas is 175 ppm. Note that this is over three orders of magnitude higher than the atmospherically relevant SO<sub>2</sub> concentration of ~75 ppb used in the flow-tube reactor experiments.

## 2.4 Experimental setup and protocol for ageing and HPLC analysis

Quantitative analysis of surface species is an important parameter that makes it possible to compare different dusts in their ability to form and store various surface species. In this way the technique is complimentary to DRIFTS as it gives mass values to the peaks observed in the DRIFTS spectra. It is also helpful to deduce reaction kinetics in case of limitations of other instrumental techniques. Such as, heterogeneous nature and low absorbance of dark volcanic samples might prevent using DRIFTS in certain cases due to the low signal obtained from the instrument (Urupina et al., 2019). Unlike the protocols for flow-tube experiments and DRIFTS investigations discussed earlier, employing HPLC for quantification of surface species required developing a novel method. This method had to be validated to demonstrate its suitability for the intended use. An article “*Method development and validation for the determination of sulfites and sulfates on the surface of mineral atmospheric samples using reverse-phase liquid chromatography*” was published in *Talanta* and is presented in Chapter 5. It goes in detail through every step of the method optimization, validation and application. A short summary of the method is provided below.

The setup for ageing samples consists of two parts: (i) the gas mixing line and (ii) the ageing reactor. A schematic representation of the setup is provided in Figure 7. A dust weighing from 100 to 200 mg is spread on a 47 mm Whatman filter paper and is placed in a tightly closed reactor. The gas mixture containing 175 ppm SO<sub>2</sub> entering the reactor is forced through the filter containing the dust at 100 sccm. The ageing of environmental samples is carried out using zero air.

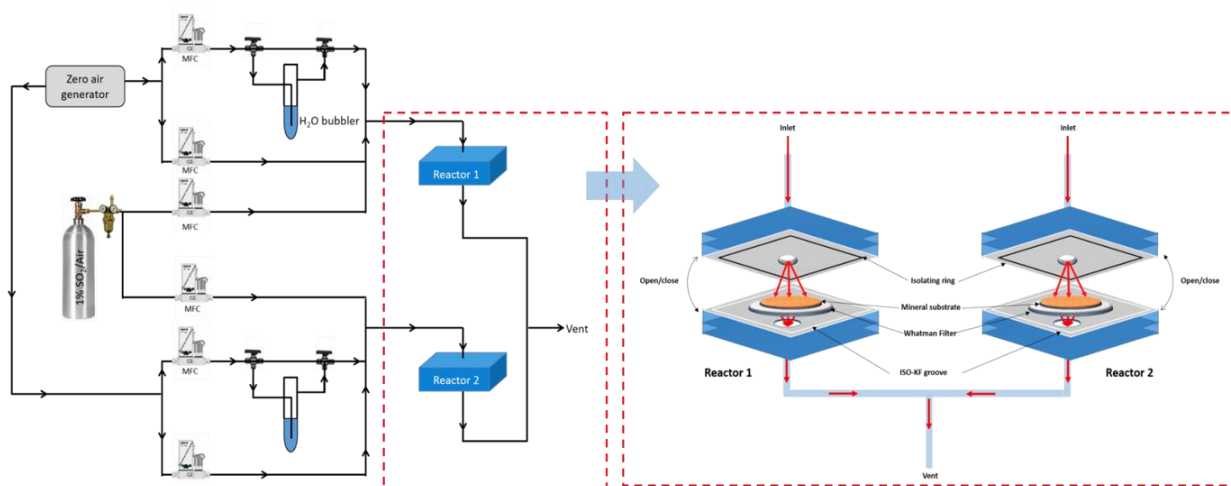


Figure 7: Left: schematic representation of the setup used to age samples of dust with  $\text{SO}_2$  gas. Right: reactor 1 and 2 with deposited dust, zoomed for clarity.

Chromatography equipment consisted of Thermo Scientific Dionex UltiMate 3000 UHPLC System with UV/VIS Detector (Thermo Scientific, Waltham, MA). Chromeleon 7.0 Data Acquisition System for LC (Thermo Scientific, Waltham, MA) was used to analyze the data. Analysis was performed using Restek Ultra Column C18, 5  $\mu\text{m}$ , Length 250 mm, I.D. 4.60 mm dynamically coated with 1.0 mM Cetylpyridinium Chloride in 7% acetonitrile solution to produce a charged surface as recommended by Zuo *et al.* (Zuo and Chen, 2003). The HPLC instrument was operated isocratically at 23  $^\circ\text{C}$  using a solution of Potassium Hydrogen Phthalate 1.0 mM, adjusted to pH 6.5 with a dilute solution of Potassium Hydroxide mobile phase and run at a flow rate of 1.0 mL/min with negative UV-Vis detection at 255 nm for 15 min. The injection volume was 10  $\mu\text{L}$ . Columns were cleaned at 1 mL/min for 30 minutes with ACN/water (50:50, v/v), 30 minutes with ACN/water (75:25, v/v), and 1 hour with 100% ACN before being coated with 1.0 mM cetylpyridinium chloride in ACN/water (7:93, v/v) at 0.5 mL/min for 3 hours. A developed reversed-phase HPLC method was validated for specificity, LOD and LOQ, linearity and range, robustness, injection repeatability and reproducibility for sample preparation and extraction.

### 3 Conclusions

Chapter 2 introduced the samples used for the investigation including their physico-chemical characterization. Following the discussion about the materials used, experimental strategy and methods were detailed. As a result, three main axes of research were defined, each prioritizing a specific instrument: flow-tube reactor to determine the uptake of  $\text{SO}_2$  gas on the v-dust, DRIFTS to monitor surface species and processes, and HPLC to quantify surface species.

Naturally, the following thesis chapters were structured to reflect each of these axes. Chapter 3 describes the SO<sub>2</sub> uptake using flow-tube reactor, and Chapter 4 focuses on surface processes investigation using DRIFTS. Chapter 5 is entirely dedicated to the development and validation of HPLC method for determination of sulfites and sulfates on the surface of mineral atmospheric samples. Chapter 6 and 7 unravel the results of HPLC analysis. Finally, Chapter 8 combines the findings with a purpose of evaluating the results and the instrumental methods used to see them in a more global context.

## References of Chapter 2

- Adams, J.W., Rodriguez, D., Cox, R.A., 2005. The uptake of SO<sub>2</sub> on Saharan dust: a flow tube study. *Atmospheric Chemistry and Physics* 5, 2679–2689. <https://doi.org/10.5194/acp-5-2679-2005>
- Alleman, L.Y., Lamaison, L., Perdrix, E., Robache, A., Galloo, J.-C., 2010. PM10 metal concentrations and source identification using positive matrix factorization and wind sectoring in a French industrial zone. *Atmospheric Research* 96, 612–625. <https://doi.org/10.1016/j.atmosres.2010.02.008>
- Arnalds, O., Dagsson-Waldhauserova, P., Olafsson, H., 2016. The Icelandic volcanic aeolian environment: Processes and impacts — A review. *Aeolian Research* 20, 176–195. <https://doi.org/10.1016/j.aeolia.2016.01.004>
- Barnard, J.C., Chapman, E.G., Fast, J.D., Schmelzer, J.R., Slusser, J.R., Shetter, R.E., 2004. An evaluation of the FAST-J photolysis algorithm for predicting nitrogen dioxide photolysis rates under clear and cloudy sky conditions. *Atmospheric Environment* 38, 3393–3403. <https://doi.org/10.1016/j.atmosenv.2004.03.034>
- Bohn, B., Rohrer, F., Brauers, T., Wahner, A., 2005. Actinometric measurements of NO<sub>2</sub> photolysis frequencies in the atmosphere simulation chamber SAPHIR. *Atmospheric Chemistry and Physics* 5, 493–503. <https://doi.org/10.5194/acp-5-493-2005>
- Clague, D.A., Denlinger, R.P., 1994. Role of olivine cumulates in destabilizing the flanks of Hawaiian volcanoes. *Bull Volcanol* 56, 425–434. <https://doi.org/10.1007/BF00302824>
- Crowley, J.N., Ammann, M., Cox, R.A., Hynes, R.G., Jenkin, M.E., Mellouki, A., Rossi, M.J., Troe, J., Wallington, T.J., 2010. Evaluated kinetic and photochemical data for atmospheric chemistry: Volume V – heterogeneous reactions on solid substrates. *Atmos. Chem. Phys.* 10, 9059–9223. <https://doi.org/10.5194/acp-10-9059-2010>
- Deegan, F.M., 2010. Processes of Magma-crust Interaction Insights from Geochemistry and Experimental Petrology. *Acta Universitatis Upsaliensis*, Uppsala.
- Delmelle, P., Wadsworth, F.B., Maters, E.C., Ayris, P.M., 2018. High Temperature Reactions Between Gases and Ash Particles in Volcanic Eruption Plumes. *Reviews in Mineralogy and Geochemistry* 84, 285–308. <https://doi.org/10.2138/rmg.2018.84.8>
- Gislason, S.R., Hassenkam, T., Nedel, S., Bovet, N., Eiriksdottir, E.S., Alfredsson, H.A., Hem, C.P., Balogh, Z.I., Dideriksen, K., Oskarsson, N., Sigfusson, B., Larsen, G., Stipp, S.L.S., 2011. Characterization of Eyjafjallajökull volcanic ash particles and a protocol for rapid risk assessment. *PNAS* 108, 7307–7312. <https://doi.org/10.1073/pnas.1015053108>
- Hatch, C.D., Wiese, J.S., Crane, C.C., Harris, K.J., Kloss, H.G., Baltrusaitis, J., 2012. Water Adsorption on Clay Minerals As a Function of Relative Humidity: Application of BET and Freundlich Adsorption Models. *Langmuir* 28, 1790–1803. <https://doi.org/10.1021/la2042873>
- Huthwelker, T., Ammann, M., Peter, T., 2006. The Uptake of Acidic Gases on Ice. *Chemical Reviews* 106, 1375–1444. <https://doi.org/10.1021/cr020506v>
- Ibrahim, S., Romanias, M.N., Alleman, L.Y., Zeineddine, M.N., Angeli, G.K., Trikalitis, P.N., Thevenet, F., 2018. Water Interaction with Mineral Dust Aerosol: Particle Size and Hygroscopic Properties of Dust. *ACS Earth Space Chem.* 2, 376–386. <https://doi.org/10.1021/acsearthspacechem.7b00152>
- Icelandic Volcanoes [WWW Document], n.d. URL <http://icelandicvolcanos.is/?volcano=EYJ#> (accessed 2.20.19).
- Joshi, N., Romanias, M.N., Riffault, V., Thevenet, F., 2017. Investigating water adsorption onto natural mineral dust particles: Linking DRIFTS experiments and BET theory. *Aeolian Research* 27, 35–45. <https://doi.org/10.1016/j.aeolia.2017.06.001>
- Langmann, B., 2013. Volcanic Ash versus Mineral Dust: Atmospheric Processing and Environmental and Climate Impacts [WWW Document]. *International Scholarly Research Notices*. <https://doi.org/10.1155/2013/245076>

- Lasne, J., Romanias, M.N., Thevenet, F., 2018. Ozone Uptake by Clay Dusts under Environmental Conditions. *ACS Earth Space Chem.* 2, 904–914. <https://doi.org/10.1021/acsearthspacechem.8b00057>
- Marticorena, B., Chatenet, B., Rajot, J.L., Bergametti, G., Deroubaix, A., Vincent, J., Kouoi, A., Schmechtig, C., Coulibaly, M., Diallo, A., Koné, I., Maman, A., NDiaye, T., Zakou, A., 2017. Mineral dust over west and central Sahel: Seasonal patterns of dry and wet deposition fluxes from a pluriannual sampling (2006–2012). *Journal of Geophysical Research: Atmospheres* 122, 1338–1364. <https://doi.org/10.1002/2016JD025995>
- Massman, W.J., 1998. A review of the molecular diffusivities of H<sub>2</sub>O, CO<sub>2</sub>, CH<sub>4</sub>, CO, O<sub>3</sub>, SO<sub>2</sub>, NH<sub>3</sub>, N<sub>2</sub>O, NO, and NO<sub>2</sub> in air O<sub>2</sub> and N<sub>2</sub> near STP [WWW Document]. *Atmospheric Environment*. URL <https://eurekamag.com/research/008/072/008072627.php> (accessed 11.5.18).
- Maters, E.C., Delmelle, P., Rossi, M.J., Ayriss, P.M., 2017. Reactive Uptake of Sulfur Dioxide and Ozone on Volcanic Glass and Ash at Ambient Temperature. *J. Geophys. Res.-Atmos.* 122, 10077–10088. <https://doi.org/10.1002/2017JD026993>
- Maters, E.C., Delmelle, P., Rossi, M.J., Ayriss, P.M., Bernard, A., 2016. Controls on the surface chemical reactivity of volcanic ash investigated with probe gases. *Earth Planet. Sci. Lett.* 450, 254–262. <https://doi.org/10.1016/j.epsl.2016.06.044>
- Prospero, J.M., Ginoux, P., Torres, O., Nicholson, S.E., Gill, T.E., 2002. Environmental Characterization of Global Sources of Atmospheric Soil Dust Identified with the Nimbus 7 Total Ozone Mapping Spectrometer (toms) Absorbing Aerosol Product. *Reviews of Geophysics* 40, 2-1-2–31. <https://doi.org/10.1029/2000RG000095>
- Romanías, M.N., Ourrad, H., Thévenet, F., Riffault, V., 2016. Investigating the Heterogeneous Interaction of VOCs with Natural Atmospheric Particles: Adsorption of Limonene and Toluene on Saharan Mineral Dusts. *J. Phys. Chem. A* 120, 1197–1212. <https://doi.org/10.1021/acs.jpca.5b10323>
- Romanias, M.N., Zeineddine, M.N., Gaudion, V., Lun, X., Thevenet, F., Riffault, V., 2016. Heterogeneous Interaction of Isopropanol with Natural Gobi Dust. *Environ. Sci. Technol.* 50, 11714–11722. <https://doi.org/10.1021/acs.est.6b03708>
- Tang, M., Cziczo, D.J., Grassian, V.H., 2016. Interactions of Water with Mineral Dust Aerosol: Water Adsorption, Hygroscopicity, Cloud Condensation, and Ice Nucleation. *Chem. Rev.* 116, 4205–4259. <https://doi.org/10.1021/acs.chemrev.5b00529>
- Tang, M.J., Cox, R.A., Kalberer, M., 2014. Compilation and evaluation of gas phase diffusion coefficients of reactive trace gases in the atmosphere: volume 1. Inorganic compounds. *Atmospheric Chemistry and Physics* 14, 9233–9247. <https://doi.org/10.5194/acp-14-9233-2014>
- Topaloglou, C., Kazadzis, S., Bais, A.F., Blumthaler, M., Schallhart, B., Balis, D., 2005. NO<sub>2</sub> and HCHO photolysis frequencies from irradiance measurements in Thessaloniki, Greece. *Atmospheric Chemistry and Physics* 5, 1645–1653. <https://doi.org/10.5194/acp-5-1645-2005>
- Ullerstam, M., Johnson, M.S., Vogt, R., Ljungstrom, E., 2003. DRIFTS and Knudsen cell study of the heterogeneous reactivity of SO<sub>2</sub> and NO<sub>2</sub> on mineral dust. *Atmos. Chem. Phys.* 3, 2043–2051. <https://doi.org/10.5194/acp-3-2043-2003>
- Urupina, D., Lasne, J., Romanias, M.N., Thiery, V., Dagsson-Waldhauserova, P., Thevenet, F., 2019. Uptake and surface chemistry of SO<sub>2</sub> on natural volcanic dusts. *Atmospheric Environment* 217, 116942. <https://doi.org/10.1016/j.atmosenv.2019.116942>
- Vogel, A., Diplas, S., Durant, A.J., Azar, A.S., Sunding, M.F., Rose, W.I., Sytchkova, A., Bonadonna, C., Krüger, K., Stohl, A., 2017. Reference data set of volcanic ash physicochemical and optical properties. *Journal of Geophysical Research: Atmospheres* 122, 9485–9514. <https://doi.org/10.1002/2016JD026328>
- Witham, C.S., Oppenheimer, C., Horwell, C.J., 2005. Volcanic ash-leachates: a review and recommendations for sampling methods. *Journal of Volcanology and Geothermal Research* 141, 299–326. <https://doi.org/10.1016/j.jvolgeores.2004.11.010>
- Xi, J., Zhang, S., 2017. Adsorption and desorption of Sb(III) on goethite. *IOP Conf. Ser.: Earth Environ. Sci.* 100, 012145. <https://doi.org/10.1088/1755-1315/100/1/012145>

- Zeineddine, M.N., Romanias, M.N., Gaudion, V., Riffault, V., Thévenet, F., 2017. Heterogeneous Interaction of Isoprene with Natural Gobi Dust. *ACS Earth Space Chem.* 1, 236–243. <https://doi.org/10.1021/acsearthspacechem.7b00050>
- Zhou, L., Wang, W., Gai, Y., Ge, M., 2014. Knudsen cell and smog chamber study of the heterogeneous uptake of sulfur dioxide on Chinese mineral dust. *Journal of Environmental Sciences* 26, 2423–2433. <https://doi.org/10.1016/j.jes.2014.04.005>
- Zuo, Y., Chen, H., 2003. Simultaneous determination of sulfite, sulfate, and hydroxymethanesulfonate in atmospheric waters by ion-pair HPLC technique. *Talanta* 59, 875–881. [https://doi.org/10.1016/S0039-9140\(02\)00647-1](https://doi.org/10.1016/S0039-9140(02)00647-1)



**Chapter III. Investigation of the uptake of SO<sub>2</sub> on natural v-dust:  
gas-phase approach**

## Table of content of Chapter 3

1	Investigation of the steady state uptake of $\text{SO}_2$ gas on natural v-dusts under ambient conditions .....	109
1.1	First insight on the steady state uptake coefficients of $\text{SO}_2$ on the five selected volcanic dusts ..	109
1.2	Impact of relative humidity on $\text{SO}_2$ steady state uptake on Hagavatn and Myrdalssandur samples .....	112
1.3	Dependence of $\text{SO}_2$ steady state uptake on Myrdalssandur sample on RH.....	114
1.4	Impact of UV radiation on $\text{SO}_2$ steady state uptake on v-dust samples .....	115
1.5	Dependence of steady state uptake of $\text{SO}_2$ on Myrdalssandur under UV on RH.....	117
2	Investigation of the transient uptake of $\text{SO}_2$ gas on natural v-dusts under ambient conditions .....	117
2.1	First insight on the transient uptake of $\text{SO}_2$ on the five selected v-dusts.....	117
2.2	Impact of relative humidity on $\text{SO}_2$ transient uptake on Hagavatn and Myrdalssandur samples .	119
2.3	Dependence of $\text{SO}_2$ transient uptake on Myrdalssandur sample on RH.....	120
2.4	Impact of UV radiation on $\text{SO}_2$ transient uptake on v-dust samples .....	121
2.5	Dependence of transient uptake of $\text{SO}_2$ on Myrdalssandur under UV on RH.....	123
2.6	Dependence of transient uptake of $\text{SO}_2$ on UV photon flux.....	124
3	Atmospheric implications of $\text{SO}_2$ uptake on v-dusts.....	126
3.1	Atmospheric lifetime of $\text{SO}_2$ with respect to v-dust .....	126
3.2	Surface coverage of v-dust by $\text{SO}_2$ molecules.....	127
3.3	Parametrization of $\text{SO}_2$ uptake on v-dusts. ....	127
4	Conclusions .....	129
	References .....	131

### List of Tables of Chapter 3

Table 1: Steady-state BET uptake coefficients of $[\text{SO}_2]_0 = 75$ ppb by the 5 Icelandic v-dust samples at $\text{RH} = 30\%$ and $T = 296$ K under dark conditions and UV-irradiation ( $J_{\text{NO}_2} = 4.5 \times 10^{-3} \text{ s}^{-1}$ ).....	117
Table 2: Steady-state BET uptake coefficients measured as a function of RH after exposure of Mýrdalssandur v-dust to 75 ppb of $\text{SO}_2$ under dark and in presence of light ( $J_{\text{NO}_2} = 4.5 \times 10^{-3} \text{ s}^{-1}$ ). The uncertainties quoted on $\gamma_{\text{SS,BET}}$ correspond to the systematic uncertainties and do not include the errors on the BET surface area determination. ....	117
Table 3: Transient number of $\text{SO}_2$ molecules initially taken up, $N_s$ , at $[\text{SO}_2]_0 = 75$ ppb by the 5 Icelandic v-dust samples at $\text{RH} = 30\%$ and $T = 296$ K under dark conditions and UV-irradiation ( $J_{\text{NO}_2} = 4.5 \times 10^{-3} \text{ s}^{-1}$ ). ....	122

## List of Figures of Chapter 3

- Figure 1: SO<sub>2</sub> concentration recorded by the analyzer during exposure of Mýrdalssandur v-dust at T = 296 K, RH = 30 %. Initial concentration of SO<sub>2</sub> gas: (75 ± 2) ppb. .... 110
- Figure 2: Steady-state uptake coefficients of the Icelandic v-dust samples at [SO<sub>2</sub>]<sub>0</sub> ≈ 75 ppb, RH = 30 %, T = 296 K, under dark conditions. The errors quoted reflects the total error for the steady state uptake coefficient determination. .... 110
- Figure 3: Steady-state uptake coefficients of the Mýrdalssandur and Hagavatn v-dust samples at RH = 30 % (blue bars) and RH=0% (beige bars), [SO<sub>2</sub>]<sub>0</sub> ≈ 75 ppb, T = 296 K, under dark conditions. The errors quoted reflects the total error for the steady state uptake coefficient determination. .... 113
- Figure 4: BET steady-state uptake of 75 ppb of SO<sub>2</sub> by Mýrdalssandur v-dust as a function of RH at T = 296 K under dark conditions. .... 115
- Figure 5: Bar graph showing the BET uptake coefficient at steady-state of [SO<sub>2</sub>]<sub>0</sub> = 75 ppb at RH = 30% and T = 296 K on the 5 types of Icelandic v-dust investigated under dark conditions (grey) and UV-irradiation (J<sub>NO<sub>2</sub></sub> = 4.5 × 10<sup>-3</sup> s<sup>-1</sup>; yellow). .... 116
- Figure 6: Number of SO<sub>2</sub> molecules taken up on the surface of different v-dusts during the transient initial uptake process when exposed to [SO<sub>2</sub>]<sub>0</sub> ≈ 75 ppb, T=296K, RH=30%, dark conditions. The errors quoted reflect the total error for the N<sub>s</sub> determinations. .... 119
- Figure 7: Number of SO<sub>2</sub> molecules taken up on the surface of Mýrdalssandur and Hagavatn v-dust samples at RH = 30 % (blue bars) and RH=0% (yellow bars), [SO<sub>2</sub>]<sub>0</sub> ≈ 75 ppb, T = 296 K, under dark conditions. The errors quoted reflect the total error for the N<sub>s</sub> determinations. .... 120
- Figure 8: Number of SO<sub>2</sub> molecules taken up on the surface of Mýrdalssandur v-dust (N<sub>s,dark</sub>) as a function of RH. Mýrdalssandur v-dust samples exposed to 75 ppb at T = 296 K under dark conditions. The errors quoted reflect the total error for the N<sub>s</sub> determinations. .... 121
- Figure 9: Bar graph showing the transient number of SO<sub>2</sub> molecules initially taken up, N<sub>s</sub>, at [SO<sub>2</sub>]<sub>0</sub> = 75 ppb at RH = 30% and T = 296 K on the 5 types of Icelandic v-dust investigated under dark conditions (grey) and UV-irradiation (J<sub>NO<sub>2</sub></sub> = 4.5 × 10<sup>-3</sup> s<sup>-1</sup>; yellow). .... 122
- Figure 10: Amplification by light of the transient number of SO<sub>2</sub> molecules taken up with respect to dark conditions, N<sub>s,light</sub>/N<sub>s,dark</sub>, as a function of: a) the Ti surface concentration of the v-dust samples and, b) the Ti/Si surface concentration ratio. Experimental conditions: [SO<sub>2</sub>]<sub>0</sub> = 75 ppb, RH = 30% and T = 296 K, under dark and J<sub>NO<sub>2</sub></sub> 4.5×10<sup>-3</sup> s<sup>-1</sup>. The solid lines are the linear fit of experimental results with a correlation coefficient R<sup>2</sup> >0.95 in case of Ti surface concentration and R<sup>2</sup> >0.97 for Ti/Si ratio. .... 123
- Figure 11: A) The transient number of SO<sub>2</sub> molecules taken up in the dark, N<sub>s,dark</sub> (black symbols), and under light (J<sub>NO<sub>2</sub></sub> = 4.5 × 10<sup>-3</sup> s<sup>-1</sup>), N<sub>s,light</sub> (colored symbols), are plotted as a function of RH for Mýrdalssandur v-dust samples exposed to 75 ppb of SO<sub>2</sub> at T = 296 K. The errors quoted on N<sub>s</sub> values reflects the precision of the measurements and the estimated systematic uncertainties related with the N<sub>s</sub> determination, and they do not include the error on the specific surface area measurement. The black line is the fit of experimental results with an empirical function to demonstrate the saturation of N<sub>s</sub> noticed under dark conditions. The yellow

line is the linear fit of results measured under surface irradiation. B) The amplification factors,  $N_{s,\text{light}}/N_{s,\text{dark}}$ , are plotted versus RH. The solid line reflects the linear correlation between the amplification factors and RH. The uncertainties quoted (5%) corresponds to the  $2\sigma$  precision of the fit and does not include other systematic uncertainties..... 124

Figure 12:  $N_s$ , as a function of photon flux ( $J_{\text{NO}_2} = 0-4.5 \times 10^{-3} \text{ s}^{-1}$ ) for Mýrdalssandur v-dust samples exposed to 75 ppb of  $\text{SO}_2$  at RH = 30% and T = 296 K. for comparison, the amplification factors are also plotted as a function of  $J_{\text{NO}_2}$  (right axis). The errors quoted on  $N_s$  values reflects the precision of the measurements and the estimated systematic uncertainties related with the  $N_s$  determination, and they do not include the error on the specific surface area measurement. The solid line is the linear fit of the amplification factors with the corresponding  $J_{\text{NO}_2}$  values. .... 125

During an episode of volcanic eruption volcanic dust reacts with SO<sub>2</sub> gas both in subvolcanic and atmospheric environments (Renggli et al., 2019), (Schmauss and Keppler, 2014). Initially, at near-magmatic high temperatures, over 800 °C, there is a compelling evidence that the adsorption of SO<sub>2</sub> gas is driven by diffusion of Ca<sup>2+</sup> cations from the interior of the glass to its surface followed by precipitation of CaSO<sub>4</sub> (Delmelle et al., 2018). This initial stage is characterized by high concentration of gases and high density of ash particles, but is very short in duration lasting only a couple of minutes, even in the case of Earth's largest explosive eruptions (Delmelle et al., 2018). The pathway is of limited importance in small and medium size eruptions and/or eruptions of volcanoes lacking a deep-seated magma chamber (Ayrís et al., 2013). Subsequent cooling rapidly brings the system to the subzero temperatures (Textor et al., 2003). At ambient and low temperatures, where effective diffusion of cations to the ash surface is no longer possible, the driving force of SO<sub>2</sub> uptake is its physisorption on the surface of ash followed by chemical reaction with active sites that are available on the surface. Previous research under these conditions points out that the rate of sulfate formation is higher at low temperatures compared to room or elevated temperatures of up to 150 °C (Wu et al., 2011), (Schmauss and Keppler, 2014). Interestingly, uptake of SO<sub>2</sub> remains very strong at very low partial pressures, which confirms that adsorption is likely to happen in diluted and cold parts of the plume (Schmauss and Keppler, 2014). Furthermore, an increase in sulfur load on ash surfaces was positively correlated with the distance from the vent during 2010 Eyjafjallajökull eruption (Bagnato et al., 2013). Thus, one can expect that most of the uptake of SO<sub>2</sub> gas during a medium-size volcanic eruption would happen in the horizontal umbrella part of the volcanic ash cloud. In this case it is important to use the steady state uptake coefficient to evaluate the uptake as it should better fit to describe the phenomena of the continuous process.

The impact of v-dust on Earth's atmosphere is governed by the physical and chemical surface properties of the particles. However, the physico-chemical processes that govern the modifications of the particle surface in the plume and in the cloud when ash is in contact with volcanic gases remain poorly investigated. Although some literature studies evaluated the reactivity of SO<sub>2</sub> with different individual mineral oxides, data available on the interactions of the natural volcanic ash and dust particles with SO<sub>2</sub> is rather limited and not descriptive of the processes occurring in the atmosphere. In this chapter, we focus on the kinetics and pathway of the reaction of sulfur dioxide with natural volcanic dust samples under atmospheric conditions using coated wall flow-tube reactor. Important kinetic parameters, such as steady state uptake coefficients,  $\gamma_{ss}$ , and number of molecules taken up,  $N_s$ , for different dusts were obtained and compared. As a reminder,  $\gamma_{ss}$ , reflects the long-term interaction between a solid surface and a gas molecule once the equilibrium between the two has been established; thus, this variable is particularly valuable for atmospheric studies. Initial behavior of the system can be described in terms of the number of molecules per specific area of dust taken up,  $N_s$ . For additional information about physical meaning and determination

these variables see Chapter 1 Section 5.1.2 and Chapter 2, Sections 2.2. In addition to experimentally measuring  $\gamma_{ss}$  and  $N_s$ , the impact of two most important atmospheric variables, (i) relative humidity,  $RH$ , and (ii) simulated solar radiation, on the uptake of  $SO_2$  gas on the surface of v-dust was investigated and analyzed. Atmospheric implications of the experimental results were discussed.

## **1 Investigation of the steady state uptake of $SO_2$ gas on natural v-dusts under ambient conditions**

### **1.1 First insight on the steady state uptake coefficients of $SO_2$ on the five selected volcanic dusts**

The uptake of atmospherically relevant concentration of  $SO_2$  (i.e.  $(75 \pm 2)$  ppb) by the surface of five selected volcanic samples under typical atmospheric conditions of ambient temperature, pressure and 30%  $RH$  was investigated using the flow-tube reactor (Lasne et al., 2018). A typical uptake profile depicted in Figure 1 shows the  $[SO_2]$  uptake of Mýrdalssandur dust in humid ( $RH = 30\%$ ) conditions. It is clearly observed from the profile that after the initial uptake of the gas upon exposure of the v-dust the system reaches a steady-state  $[SO_2]$  that is distinct from the initial state  $[SO_2]_0$ , evidencing continuous consumption of the title molecule for the duration of the experiment. All the samples under investigation demonstrated both an initial uptake and a steady state uptake, alike the profile reported on Figure 1. The latter is worth investigating as it suggests the ability of the v-dusts to exhibit a long-term effect on the atmosphere. The steady state coefficients are in the order of  $10^{-9}$  to  $10^{-8}$  (Figure 2). These values are much lower than the values obtained by Maters et al., who reported initial uptakes of  $SO_2$  on volcanic ash and glass powders in the  $10^{-3}$  to  $10^{-2}$  range (Maters et al., 2017). Large differences in values are not surprising though for a number of reasons. First, the initial uptake describes an uptake on the fresh surface at the first instances of its interaction with gas, while the steady state uptake is an ongoing phenomenon reflecting the ability of the surface to uptake gas continuously. Second, while determining initial uptakes, geometric surface area was used by Maters et al. in order to calculate uptake coefficient (Maters et al., 2017), while the specific surface area was used in this study in order to account for all the surface accessible to the  $SO_2$  molecules on longer time scale. Using geometric vs specific surface area gives an upper value for the uptake coefficient (Crowley et al., 2010). Thus, in this study, depending on the dust, using geometric surface area to determine steady state coefficient gives values 20 to 100 times larger than using BET surface area. Finally, in the study of Maters et al. experiments were performed under low-pressure, 0% humidity of Knudsen cell reactor contrary to atmospherically relevant 760 Torr, 30%  $RH$  used in this study (Maters et al., 2017). Moreover, in the adsorption/desorption experiments on the volcanic glasses performed by Schmauss and Keppler it was

observed that the first layer of  $\text{SO}_2$  molecules was adsorbed on the surface of volcanic glass irreversibly and could not be removed (Schmauss and Keppler, 2014).

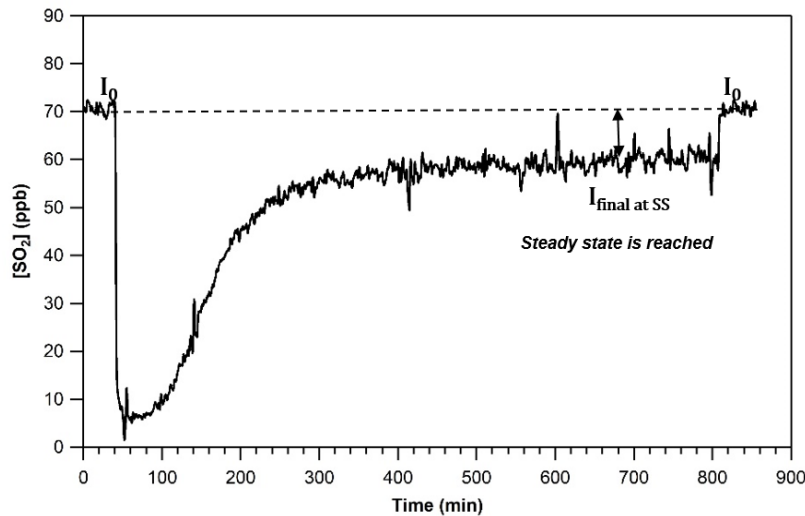


Figure 1:  $\text{SO}_2$  concentration recorded by the analyzer during exposure of Mýrdalssandur v-dust at  $T = 296 \text{ K}$ ,  $\text{RH} = 30 \%$ . Initial concentration of  $\text{SO}_2$  gas:  $(75 \pm 2) \text{ ppb}$ .

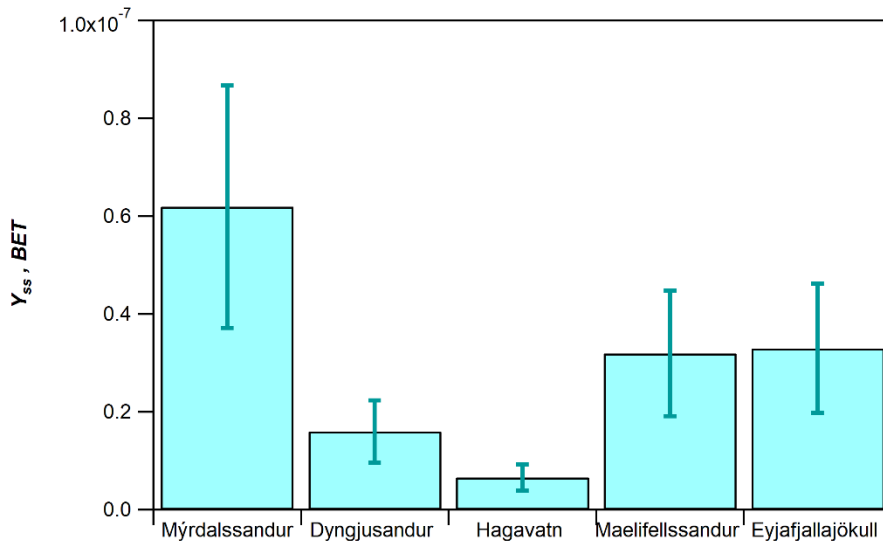


Figure 2: Steady-state uptake coefficients of the Icelandic v-dust samples at  $[\text{SO}_2]_0 \approx 75 \text{ ppb}$ ,  $\text{RH} = 30 \%$ ,  $T = 296 \text{ K}$ , under dark conditions. The errors quoted reflect the total error for the steady state uptake coefficient determination.

Interestingly, the obtained results show somewhat contrasted behaviors from one sample to another. In the literature the differences in the uptake of  $\text{SO}_2$  on solid material are commonly linked to the differences in elemental composition or mineralogy (Maters et al., 2017), (Maters et al., 2016), (Usher et al., 2002), (Zhang et al., 2006), (Harris et al., 2012). Using synthetic and natural silicate glasses as proxies for fresh unweathered volcanic ash is commonly done due to the fact that glass often represents a major component



of v-dust. Besides, a thin layer of glass covering the crystalline components of ash surfaces was observed (Delmelle et al., 2018). Several studies indicate that sulfates are more likely to get adsorbed on the glass fraction of volcanic dust (Schmauss and Keppler, 2014), (Farges et al., 2009). While investigating trends in adsorption of SO<sub>2</sub> on glass, surface and bulk elemental composition is commonly investigated (Maters et al., 2017). This approach though ignores the crystalline phase of the volcanic dust. Maters et al. emphasized that the influence of crystallinity on the adsorption of SO<sub>2</sub> gas is not yet understood (Maters et al., 2017). On the other hand, authors working with natural mineral dust samples, such as desert dusts, often approximate composition of dusts using simple mineral oxides and look for trends in uptake in relationship with the mineral phase composition. In our study v-dusts differ significantly in their crystalline fraction. Volcanic samples used in this study contain from 20% (Hagavatn) to 80-90% (Mýrdalssandur, Maelifellssandur and Dyngjusandur) of amorphous material (Baratoux et al., 2011), (Moroni et al., 2018). The remaining part is crystalline. Eyjafjallajökull is also dominated by glass (Gislason et al., 2011). Plagioclase, pyroxene, and olivine are the mineral phases reported in all five samples, while magnetite was only found in Mýrdalssandur and Maelifellsandur (Moroni et al., 2018), (Baratoux et al., 2011) (Gislason et al., 2011). A very small amount of crystalline silica was found in Eyjafjallajökull and none was reported for other samples (Gislason et al., 2011).

Since amorphous fraction dominates the morphology of v-dusts, an attempt to find trends in the uptake vs elemental composition was undertaken. Among the authors linking the differences in uptake coefficient to the surface elemental composition Maters et al. observed increase of the initial uptake of SO<sub>2</sub> on the surface of synthetic volcanic glasses with decrease of their silica (Si) content and increase of the sum of their sodium (Na), potassium (K), magnesium (Mg) and calcium (Ca) content (Maters et al., 2017). As for the natural volcanic samples the relationship was not as straightforward, even though a dependence of the initial uptake on the total surface content of the sum of Na, K, Mg and Ca was suggested (Maters et al., 2017). In our studies no clear correlation between the bulk elemental composition of a v-dust and its uptake of SO<sub>2</sub> was established (for bulk and surface elemental composition see Chapter 2 Sections 1.2.3-1.2.4). It can be due to the fact that the elemental concentration in the bulk sample may not represent the availability of the elements on the surface. We therefore searched for dependency of uptake coefficient on the surface composition but none was clearly established. One should keep in mind that a given element when incorporated in glass versus crystalline mineral might behave differently. Farges et al. observed that crystalline quartz does not adsorb any sulfur species while amorphous silica does (Farges et al., 2009). The heterogeneous nature of the sample might further complicate finding the trends as elements forming different mineral phases will behave differently depending on the nature of mineral phase. For example, Fe is incorporated in both ilmenite (FeTiO<sub>3</sub>) and fayalite (Fe<sub>2</sub>SiO<sub>4</sub>), yet the SO<sub>2</sub> uptake is significantly higher for the former mineral (Harris et al., 2012).

Earlier studies can be used to understand potential contribution of crystalline fraction of the volcanic ash to the uptake of SO<sub>2</sub>. Both quartz (SiO<sub>2</sub>) and magnetite (Fe<sub>3</sub>O<sub>4</sub>) can be found in volcanic ash. Comparison of the uptakes of SO<sub>2</sub> on individual mineral oxides, such as CaO, Al<sub>2</sub>O<sub>3</sub>, CaCO<sub>3</sub>, Fe<sub>3</sub>O<sub>4</sub> and Fe<sub>2</sub>O<sub>3</sub> showed that the uptake of SO<sub>2</sub> depends on the nature of the mineral oxide with higher uptakes observed when SO<sub>2</sub> interacted with iron-containing compounds (Usher et al., 2002). These observations were further tested by Zhang et al. who compared reactivity of different oxides together with their mixture (based on the abundance of the corresponding elements in continental crust) taking into consideration their specific area and ranked them in the following order: Fe<sub>2</sub>O<sub>3</sub>>MgO>TiO<sub>2</sub>>FeOOH>mixture>Al<sub>2</sub>O<sub>3</sub>>SiO<sub>2</sub> (Zhang et al., 2006). Both studies indicate that conversion of SO<sub>2</sub> per unit surface of Fe<sub>2</sub>O<sub>3</sub> is the highest, suggesting that particles with the highest amount of iron might be the most reactive with SO<sub>2</sub>. Furthermore, the reactivity of the mixture, that was obtained by mixing the different oxides based on their abundance in the continental crust, was measured to be twice its theoretical value, which demonstrates its synergistic effect (Zhang et al., 2006). Even though most studies use simple mineral oxides and synthetic dust as a substitution for natural samples, such approach is questionable, as it undermines the importance of more complex mineralogy in the uptake of SO<sub>2</sub>. While studying the uptake of SO<sub>2</sub> on Saharan dust Harris et al. distinguished ilmenite (FeTiO<sub>3</sub>), rutile (TiO<sub>2</sub>) and iron oxides (Fe<sub>2</sub>O<sub>3</sub>, Fe<sub>3</sub>O<sub>4</sub>, FeOOH) ( $\gamma_{\text{BET(mixture of ilmenite and rutile)}}=3\times 10^{-5}$ ) as major phases of dust responsible for uptake and oxidation of SO<sub>2</sub> (Harris et al., 2012). Uptake on feldspar minerals such as KAlSi<sub>3</sub>O<sub>8</sub>, NaAlSi<sub>3</sub>O<sub>8</sub> or CaAl<sub>2</sub>Si<sub>2</sub>O<sub>8</sub> and quartz (SiO<sub>2</sub>) was found to be slow ( $\gamma_{\text{BET(feldspar)}}=9\times 10^{-7}$ ,  $\gamma_{\text{(quartz with basic components)}}=4\times 10^{-8}$ ) (Harris et al., 2012). To identify the elements associated with adsorption of SO<sub>2</sub> by crystalline material, Harris et al. analyzed individual Saharan dust grains that were relatively rich in S content after their exposure to SO<sub>2</sub> and studied their elemental profile using single-particle SEM–EDX analysis (Harris et al., 2012). Ti, Fe and Ca were identified as the most important reactive elements, while Na, Mg, Al, Si showed no relationship to oxidizing capacity of dust (Harris et al., 2012). While studying the uptake of SO<sub>2</sub> on v-dusts it would be informative to investigate the uptake of SO<sub>2</sub> on other complex mineral phases present in v-dust such as pyroxene, plagioclase, amphibole, biotite, and olivine even though higher uptakes of SO<sub>2</sub> are linked to the presence of minerals lacking silicates, such as ilmenite (FeTiO<sub>3</sub>) and magnetite (Fe<sub>3</sub>O<sub>4</sub>) (Harris et al., 2012).

## 1.2 Impact of relative humidity on SO<sub>2</sub> steady state uptake on Hagavatn and Myrdalssandur samples

Several studies have highlighted the role of *RH* on SO<sub>2</sub> uptake (Li et al., 2006), (Zhou et al., 2014), (Huang et al., 2015). In order to investigate the role that *RH* plays in the steady state uptake of SO<sub>2</sub> on v-dust samples the relationship was investigated for two contrasted samples based on their steady-state uptake values – Myrdalssandur and Hagavatn (Figure 3). For Myrdalssandur we observed that the steady state

uptake coefficient of  $\text{SO}_2$  at 30% of  $RH$  was significantly higher than under dry conditions (i.e.  $\gamma_{ss, BET}(30\% RH) = 6.2 \times 10^{-8}$  and  $\gamma_{ss, BET}(dry) = 2.0 \times 10^{-8}$ ). For the Hagavatn v-dust a similar trend was observed (i.e.  $\gamma_{ss, BET}(30\% RH) = 6.6 \times 10^{-9}$  and  $\gamma_{ss, BET}(dry) = 1.0 \times 10^{-9}$ ). The enhanced uptake trends observed in the presence of water indicate that water plays an important role promoting the partitioning of  $\text{SO}_2$  to the adsorbed phase. There might be various reasons for the observed increased uptake of  $\text{SO}_2$  in the presence of water vapor. Adsorbed water molecules can (i) participate in the reactions as reactants, (ii) serve as a medium for the reaction to take place or (iii) change the physical properties of the particle shifting the equilibrium towards higher  $\text{SO}_2$  uptake. Water molecules can also form water layers that can help the product of the reaction to diffuse along the surface and thus promote the renewal, i.e. the turnover, of surface sites (Shang et al., 2010). The intrinsic ability of metal oxides to adsorb water molecules and form surface hydroxyls was linked to higher reactivity in the heterogeneous interaction with  $\text{SO}_2$  (Zhang et al., 2006).

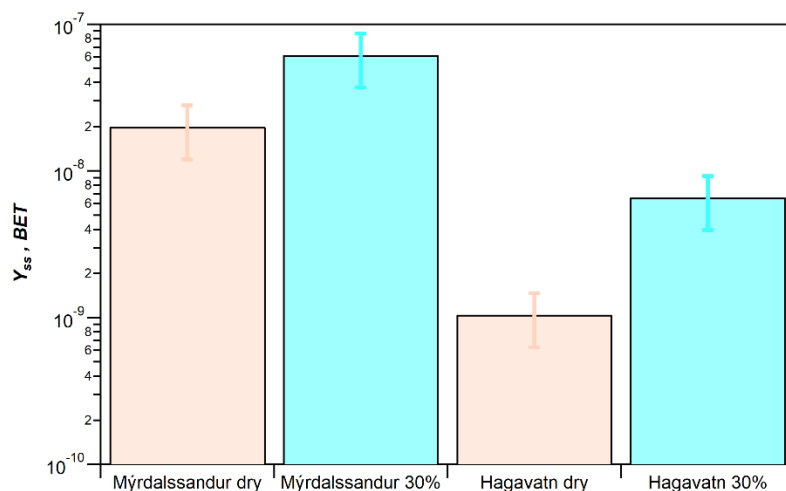


Figure 3: Steady-state uptake coefficients of the Myrdalssandur and Hagavatn v-dust samples at  $RH = 30\%$  (blue bars) and  $RH = 0\%$  (beige bars),  $[\text{SO}_2]_0 \approx 75$  ppb,  $T = 296$  K, under dark conditions. The errors quoted reflect the total error for the steady state uptake coefficient determination.

In the literature the analysis of the influence of  $RH$  on the uptake of  $\text{SO}_2$  on natural mineral dusts shows complex trends. An influence of water vapor on the interaction of  $\text{SO}_2$  with Saharan dust at 258 K showed no effect on initial uptake within statistical error (i.e.  $\gamma_{BET}(27\% RH) = (6.0 \pm 1.0) \times 10^{-5}$  and  $\gamma_{BET}(dry) = (6.4 \pm 0.7) \times 10^{-5}$ ). Likewise, no dependency of the initial uptake coefficient on humidity was found for Adobe clay soil taken from Los Angeles area (Judeikis and Stewart, 1976). Alternatively, when Huang et al. subjected three authentic dusts to  $\text{SO}_2$  at  $RH$  ranging from 0 to 90% an increase in uptake coefficient was observed for Tengger Desert dust (i.e.  $\gamma_{BET}(dry) \approx 3.8 \times 10^{-5}$  and  $\gamma_{BET}(90\% RH) \approx 5.5 \times 10^{-5}$ ) and for Arizona test dust (i.e.  $\gamma_{BET}(dry) \approx 1.3 \times 10^{-5}$  and  $\gamma_{BET}(90\% RH) \approx 2.76 \times 10^{-5}$ ), but a decrease was observed

for Asian mineral dust (i.e.  $\gamma_{BET}(dry) \approx 3.2 \times 10^{-5}$  and  $\gamma_{BET}(90\% RH) \approx 1.9 \times 10^{-5}$ ) (Huang et al., 2015). The negative dependence of humidity on SO<sub>2</sub> uptake in the case of Asian mineral dust was explained by the presence of water-soluble inorganic coating, which made surface more acidic and inhibited uptake of SO<sub>2</sub> (Huang et al., 2015). When the Asian mineral dust was washed and coating was removed, the uptake trend got reversed and showed positive correlation (i.e.  $\gamma_{BET}(dry) \approx 0.85 \times 10^{-5}$  and  $\gamma_{BET}(90\% RH) \approx 1.32 \times 10^{-5}$ ) (Huang et al., 2015). Then again, while the samples from Inner Mongolian desert, characterized by high carbonate contents, demonstrated considerably increased uptakes at higher humidity (i.e.  $\gamma_{ss, BET}(40\% RH) = 1.0 \times 10^{-6}$  and  $\gamma_{ss, BET}(dry) = 1.7 \times 10^{-7}$ ), Xinjiang sierozem natural mineral dust showed only a modest increase in steady-state uptake (i.e.  $\gamma_{ss, BET}(40\% RH) \approx 2.4 \times 10^{-7}$  and  $\gamma_{ss, BET}(dry) \approx 2.2 \times 10^{-7}$ ) (Adams et al., 2005). The authors suggest that difference in the minerology could be responsible for the difference in the observed trends (Zhou et al., 2014). Higher carbonate component of the Inner Mongolian desert dust can promote the SO<sub>2</sub> uptake. Indeed, while investigating carbonate particles Zhang et al. observed that the value of the steady state uptake  $\gamma_{ss, BET}$  drastically increases from  $\gamma_{ss, BET}(1\% RH) = 0.32 \times 10^{-8}$  to  $\gamma_{ss, BET}(85\% RH) = 13.9 \times 10^{-8}$ , at 85% RH reaching 43 times its value at 1% (Zhang et al., 2018). In our study volcanic dusts, void of carbonates, cannot be directly compared to carbonate-rich samples, but the observed trend follows the one of Tengger Desert dust and Arizona test dust discussed earlier. More information about influence of humidity on the steady state uptake of SO<sub>2</sub> on the surface of volcanic glass and ash is necessary to obtain a more comprehensive picture.

While the increase in the SO<sub>2</sub> uptake with the increase of relative humidity is observed for a number of samples, it is not at all the case for the uptakes of other species, such as nonpolar volatile organic compounds (Romanias et al., 2016), hydrogen peroxide (H<sub>2</sub>O<sub>2</sub>) (Romanias et al., 2012a) or ozone (O<sub>3</sub>) (Lasne et al., 2018). In fact, the uptake coefficient can decrease with increased humidity, such as the case for the steady state uptake of O<sub>3</sub> on montmorillonite clay dust reflecting the tendency for the molecules in question and molecules of water to compete with each other for the sorptive sites on the clay surface (Lasne et al., 2018).

### 1.3 Dependence of SO<sub>2</sub> steady state uptake on Myrdalssandur sample on RH

To further investigate the influence of gas-phase water on the uptake of SO<sub>2</sub> a series of experiments were conducted under different relative humidity conditions. Mýrdalssandur v-dust that displayed the highest steady state uptake among the Icelandic v-dusts was chosen as a representative dust.

The experiments were run at 296 K, with  $[SO_2]_0 = 75$  ppb ( $1.88 \times 10^{12}$  molecules cm<sup>-3</sup>). Figure 4 shows the variation of  $\gamma_{ss, BET}$  on Mýrdalssandur v-dust for RH ranging from 0.1 to 70%.

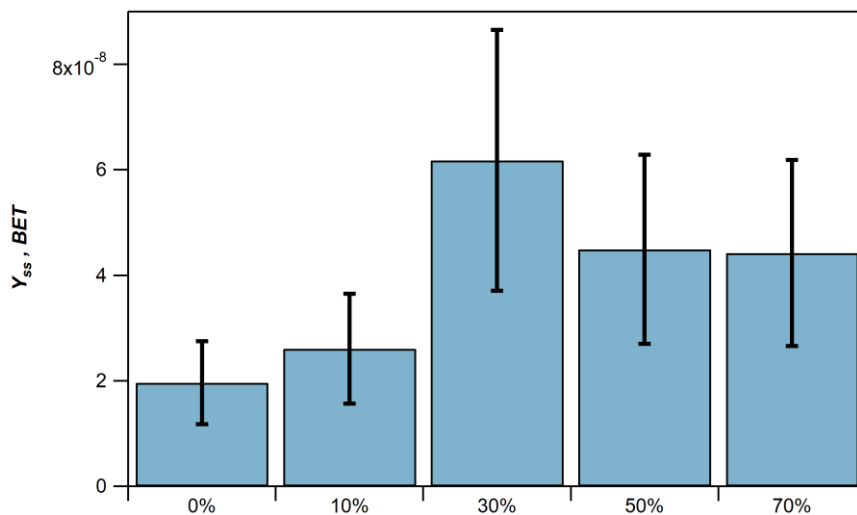


Figure 4: BET steady-state uptake of 75 ppb of  $\text{SO}_2$  by Mýrdalssandur v-dust as a function of RH at  $T = 296 \text{ K}$  under dark conditions.

An increase of  $\text{SO}_2$  uptake by Mýrdalssandur v-dust is observed as RH increases from 0.1 to 30%. Above this value,  $\gamma_{ss, BET}$  remains constant within the uncertainty values. This variation might be related to the formation of an  $\text{H}_2\text{O}$  monolayer at the surface of Mýrdalssandur v-dust at around 30% RH. Thus, from 0 to 30% additional water molecules assist removal of  $\text{SO}_2$  from the gas phase while still keeping surface sites available for interactions with the gas. At values higher than 30% RH, when the monolayer is formed, the surface environment encountered by a gas molecule does not change much and thus steady state uptake remains constant.

Consistently, Joshi et al. observed the formation of the  $\text{H}_2\text{O}$  monolayer at 23% RH on Icelandic volcanic ash, and Lathem et al. at 0.05-20% RH on volcanic ash samples (Joshi et al., 2017), (Lathem et al., 2011). Likewise, formation of the water monolayer is observed at  $28 \pm 2\%$  RH on ATD dust (Ibrahim et al., 2018). The exposure of a surface to water vapor has been shown to generate new reaction sites, and to enhance the formation of sulfate ions (Ullerstam et al., 2002).

#### 1.4 Impact of UV radiation on $\text{SO}_2$ steady state uptake on v-dust samples

The effect of UV radiation was investigated in order to evaluate its impact on the removal of  $\text{SO}_2$  from the gas phase. Sulfur dioxide uptake by five Icelandic v-dusts was studied at  $\text{RH} = 30\%$ ,  $T = 296 \text{ K}$  and  $[\text{SO}_2]_0 = 75 \text{ ppb}$ , in the dark and under light irradiation ( $J_{\text{NO}_2} = 4.5 \times 10^{-3} \text{ s}^{-1}$ ). For the typical profile under simulated sunlight and for more information on experimental setup and protocol involving UV light refer to Chapter 2 Sections 2.2.2, 2.2.5. The experimentally obtained  $\gamma_{ss, BET}$  values fall in the range of  $10^{-8}$

promoted by a factor of 1.1 to 4.6 under light irradiation compared to dark conditions. (Table 1, Figure 5). In particular, the increasing trend is observed for all five v-dust samples, even though for 3 dust (Eyjafjallajökull, Maelifellsandur and Mýrdalssandur) it falls within the relative error bar. For the other two v-dusts, Hagavatn and Dyngjusandur, the steady-state uptake of SO<sub>2</sub> is noticeably higher under UV-irradiation than in the dark. The photo-enhanced removal of SO<sub>2</sub> in the presence of light could be attributed to photo-induced reactions occurring on the surface of v-dust particles. It is well established in literature that reactive species (i.e. hydroxyl radicals, •OH, hydroperoxyl radicals, •O<sub>2</sub>H, or superoxide radicals, O<sub>2</sub>•<sup>-</sup> etc.) can be formed on the surface of mineral samples containing Ti and Fe elements under UV/visible light irradiation (Herrmann, 2005), (Chen et al., 2012), (George et al., 2015). However, at this level of the work, only a photo-enhancement can be pointed out, but we cannot conclude at all on the photocatalytic or surface photochemical nature of the process we observe.

Under dark conditions, the most reactive sample towards SO<sub>2</sub> uptake is Mýrdalssandur v-dust. Indeed, the value of  $\gamma_{ss,BET}$  measured on this sample is the highest among all the v-dusts tested. Under light irradiation, Mýrdalssandur v-dust is again, within the experimental uncertainties, among the most reactive samples. However, the light amplification of its steady state uptake ( $\gamma_{ss,BET,dark}/\gamma_{ss,BET,UV}$ ) is only 1.1, the lowest value registered for dusts (see Table 1, Figure 5). The most intense UV light amplification for  $\gamma_{ss,BET}$  is reported for Dyngjusandur sample (factor of 4.6). We investigated whether the amplification factors (i.e.  $\gamma_{ss,BET,dark}/\gamma_{ss,BET,UV}$ ) are correlated with the surface or bulk elemental composition of the dusts but found no such correlation. Thus, what exactly causes the difference in light amplification is unclear.

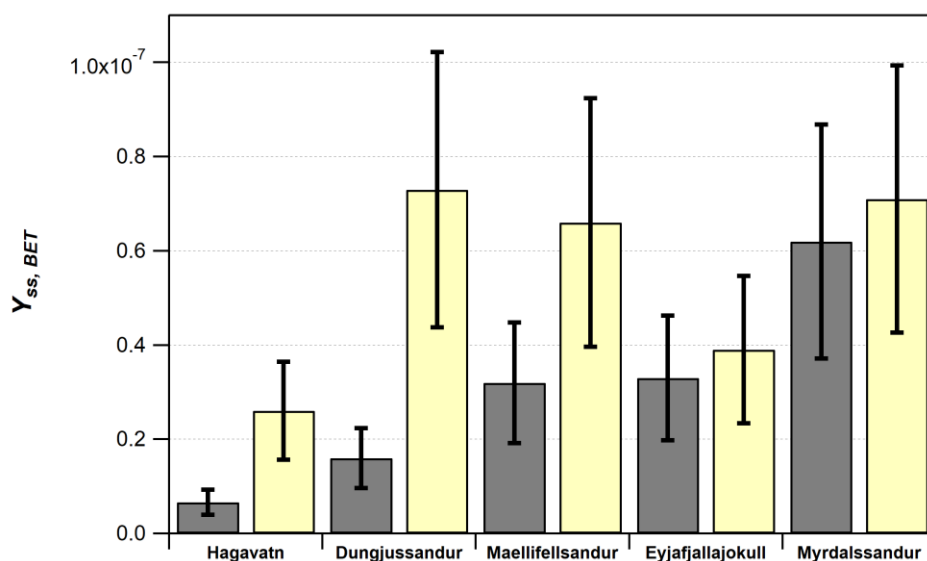


Figure 5: Bar graph showing the BET uptake coefficient at steady-state of [SO<sub>2</sub>]<sub>0</sub> = 75 ppb at RH = 30% and T = 296 K on the 5 types of Icelandic v-dust investigated under dark conditions (grey) and UV-irradiation ( $J_{NO_2} = 4.5 \times 10^{-3} \text{ s}^{-1}$ ; yellow).

Table 1: Steady-state BET uptake coefficients of  $[SO_2]_0 = 75$  ppb by the 5 Icelandic v-dust samples at  $RH = 30\%$  and  $T = 296$  K under dark conditions and UV-irradiation ( $J_{NO_2} = 4.5 \times 10^{-3} s^{-1}$ ).

Dust sample	$\gamma_{ss\text{ BET, dark}}$	$\gamma_{ss\text{ BET, UV}}$	$\gamma_{ss\text{ BET, dark}} / \gamma_{ss\text{ BET, UV}}$
Hagavatn	$(6.6 \pm 2.6) \times 10^{-9}$	$(2.6 \pm 1.0) \times 10^{-8}$	3.9
Dyngjusandur	$(1.6 \pm 0.6) \times 10^{-8}$	$(7.3 \pm 2.3) \times 10^{-8}$	4.6
Maelifellssandur	$(3.2 \pm 1.3) \times 10^{-8}$	$(6.6 \pm 2.6) \times 10^{-8}$	2.0
Eyjafjallajökull	$(3.3 \pm 1.3) \times 10^{-8}$	$(3.9 \pm 1.6) \times 10^{-8}$	1.2
Mýrdalssandur	$(6.2 \pm 2.5) \times 10^{-8}$	$(7.1 \pm 2.8) \times 10^{-8}$	1.1

## 1.5 Dependence of steady state uptake of $SO_2$ on Mýrdalssandur under UV on RH

To investigate the influence of  $RH$  on the steady-state uptake of  $SO_2$  under UV light ( $\gamma_{ss,BET,UV}$ ), controlled experiments were conducted using Mýrdalssandur v-dust at 296 K, with  $[SO_2]_0 = 75$  ppb ( $1.88 \times 10^{12}$  molecules  $cm^{-3}$ ), in the presence of light ( $J_{NO_2} = 4.5 \times 10^{-3} s^{-1}$ ) and varying the  $RH$  in the range of 0.1 to 70%. The results obtained under light irradiation conditions ( $J_{NO_2} = 4.5 \times 10^{-3} s^{-1}$ ) were compared to dark conditions. Table 2 clearly demonstrates that the  $\gamma_{ss,BET}$  of  $SO_2$  by Mýrdalssandur v-dust is, within experimental uncertainty, the same in the dark and under light for all values of  $RH$  investigated (0.1 - 70%).

Table 2: Steady-state BET uptake coefficients measured as a function of  $RH$  after exposure of Mýrdalssandur v-dust to 75 ppb of  $SO_2$  under dark and in presence of light ( $J_{NO_2} = 4.5 \times 10^{-3} s^{-1}$ ). The uncertainties quoted on  $\gamma_{ss,BET}$  correspond to the systematic uncertainties and do not include the errors on the BET surface area determination.

RH (%)	Steady state uptake coefficients, $\gamma_{ss,BET}$	
	$\gamma_{ss\text{ BET, dark}}$	$\gamma_{ss\text{ BET,UV}}$
0.1	$(1.96 \pm 0.3) \times 10^{-8}$	-
11	$(2.6 \pm 0.4) \times 10^{-8}$	$(2.4 \pm 0.4) \times 10^{-8}$
30	$(6.2 \pm 0.9) \times 10^{-8}$	$(7.1 \pm 1.1) \times 10^{-8}$
50	$(4.5 \pm 0.7) \times 10^{-8}$	$(4.4 \pm 0.7) \times 10^{-8}$
70	$(4.4 \pm 0.7) \times 10^{-8}$	$(4.4 \pm 0.7) \times 10^{-8}$

## 2 Investigation of the transient uptake of $SO_2$ gas on natural v-dusts under ambient conditions

### 2.1 First insight on the transient uptake of $SO_2$ on the five selected v-dusts

Apart from the measurement of steady state uptake coefficients that characterizes long-term interactions between v-particles and  $SO_2$  gas, important information can be extracted by characterizing the total transient uptake of  $SO_2$  gas before reaching equilibrium conditions (i.e. steady state). Thus, the number

of SO<sub>2</sub> molecules removed during the transient uptake process per surface area,  $N_s$ , was investigated for the five v-dusts and determined in the order of 10<sup>13</sup> molecules cm<sup>-2</sup> (Figure 6). These values are comparable to the values obtained by Maters et al., who reported the total uptake capacity of SO<sub>2</sub> on volcanic ash and glass powders under dry conditions at 10<sup>11</sup> to 10<sup>13</sup> range (Maters et al., 2017). As with initial uptakes, total uptake capacity of SO<sub>2</sub> on the surface of synthetic volcanic glasses increased with decrease of their Si content and increase of their total Na, K, Mg, Ca content (Maters et al., 2017). As for the natural volcanic ash samples the relationship was less clear and the dependence on total surface Na, K, Mg, Ca content was suggested (Maters et al., 2017). Furthermore, as displayed in Figure 2 and Figure 6, the transient numbers of molecules adsorbed,  $N_s$ , at the initial stage of the exposure, and the steady state uptake coefficients,  $\gamma_{ss,BET}$ , do not follow the same trend. On one hand, Mýrdalssandur seems to adsorb the highest amount of molecules and it has the highest uptake coefficient. On the other hand, Hagavatn that has the smallest uptake coefficient adsorbs almost the same amount of molecules as Eyjafjallajökull and more than Maelifellssandur even though the latter two have an uptake coefficient that is twice as high as uptake coefficient of Hagavatn. Possibly, the absence of correlation between  $N_s$  and  $\gamma_{ss,BET}$  suggest that the surface is modified upon its initial exposure to SO<sub>2</sub>. Indeed, one should keep in mind that uptake behavior of SO<sub>2</sub> on each volcanic dust was characterized by measuring steady state uptake coefficients after 12 hours of exposure, i.e. after long processing. While a transient uptake was observed at the initial stage of the experiment where the number of molecules taken up was measured from 0 to 5 hours of interactions. Differences in the observed trends could indicate that at the initial stage of the experiment the surface of the dust is modified due to SO<sub>2</sub> uptake and the corresponding formation of sulfites and sulfates, and these modifications affect the surface reactivity at longer time scale when the  $\gamma_{ss,BET}$  values are determined. The surface modifications could explain why no correlation was noticed between the  $\gamma_{ss,BET}$  and  $N_s$  with the elemental composition of the v-dusts. Finally, the discrepancies could be due to the fact that the nature of the governing processes behind the initial fast uptake and thus the high amount of molecules adsorbed in the initial stage and those dominating the steady state uptake are fundamentally different (Huthwelker et al., 2006).



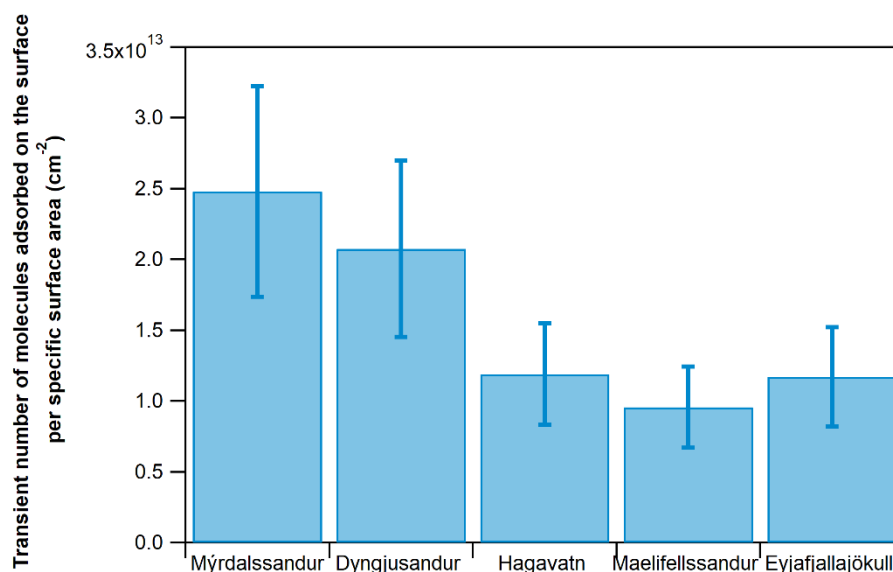


Figure 6: Number of  $\text{SO}_2$  molecules taken up on the surface of different v-dusts during the transient initial uptake process when exposed to  $[\text{SO}_2]_0 \approx 75$  ppb,  $T=296\text{K}$ ,  $\text{RH}=30\%$ , dark conditions. The errors quoted reflect the total error for the  $N_s$  determinations.

## 2.2 Impact of relative humidity on $\text{SO}_2$ transient uptake on Hagavatn and Mýrdalssandur samples

The RH is an important atmospheric parameter that can impact the interactions of pollutants on the surface of mineral dusts and aerosols. Water molecules can (i) block active sites, suppressing the consumption of pollutants (Zeineddine et al., 2017), (Zeineddine et al., 2018); (ii) serve as a medium for the reaction to take place and form water layers on the surface of particles promoting the product of the reaction to diffuse along the surface (Shang et al., 2010); and (iii) act as a source of radical species, especially under light conditions, and enhance the removal of pollutants, etc., (Herrmann, 2005), (Chen et al., 2012), (George et al., 2015), (Tang et al., 2017), (Romanias et al., 2017).

In order to investigate the influence of  $\text{RH}$  on the number of  $\text{SO}_2$  molecules transiently taken up by v-dusts, the relationship was investigated for two specific samples – Mýrdalssandur, that adsorbed the highest number of molecules on its surface, and Hagavatn, that showed average adsorption (Figure 7). For Mýrdalssandur we observed that the number of molecules taken up,  $N_s$ , at 30% of  $\text{RH}$  was significantly higher than under dry conditions (i.e.  $N_s(30\% \text{ RH}) = 2.48 \times 10^{13}$  and  $N_s(\text{dry}) = 3.1 \times 10^{12}$ ). For the Hagavatn v-dust a similar trend was observed (i.e.  $N_s(30\% \text{ RH}) = 1.15 \times 10^{13}$  and  $N_s(\text{dry}) = 7.2 \times 10^{12}$ ). In line with the effect of  $\text{RH}$  on the steady state uptake coefficient, the enhancement in the number of molecules

transiently taken up by the surface of dust in the presence of water once again points out to the important role water plays in promoting adsorption of  $\text{SO}_2$  molecules.

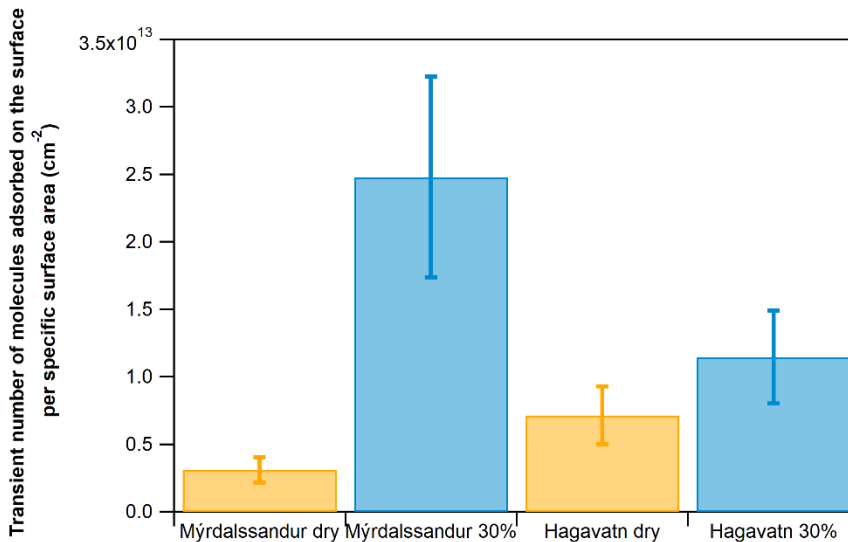


Figure 7: Number of  $\text{SO}_2$  molecules taken up on the surface of Myrdalssandur and Hagavatn v-dust samples at  $\text{RH} = 30\%$  (blue bars) and  $\text{RH} = 0\%$  (yellow bars),  $[\text{SO}_2]_0 \approx 75 \text{ ppb}$ ,  $T = 296 \text{ K}$ , under dark conditions. The errors quoted reflect the total error for the  $N_s$  determinations.

### 2.3 Dependence of $\text{SO}_2$ transient uptake on Myrdalssandur sample on RH

To further investigate the influence of gas-phase water on the ability of dust to take up  $\text{SO}_2$  gas in the initial stage of the experiment, number of molecules taken up by Myrdalssandur v-dust were evaluated under different relative humidity conditions ranging from 0.1 to 70% (Figure 8). The experiments were run at 296 K, with  $[\text{SO}_2]_0 = 75 \text{ ppb}$  ( $1.88 \times 10^{12} \text{ molecules cm}^{-3}$ ). From Figure 8 it can be observed that  $N_{s,\text{dark}}$  increases until  $\text{RH} = 30\%$ , and then saturates. The same threshold value for  $\text{RH}$  was observed for the steady-state uptake, which behavior changes at  $\text{RH} = 30\%$ . As it has been previously discussed, the molecularly adsorbed water monolayer on mineral dust particles is formed above the threshold of 30% of  $\text{RH}$  (Joshi et al., 2017), (Tang et al., 2016). Characteristic change of behavior at 30% points out to the twofold role that water molecules play in the removal of  $\text{SO}_2$ . As  $\text{RH}$  increases from dry to 30% the removal of  $\text{SO}_2$  is enhanced due to the formation of OH groups on the surface of v-dust. The surface OH groups assist in the transformation of  $\text{SO}_2$  to sulfites and sulfates. Above 30% of  $\text{RH}$  there is probably a competition between two processes; the formation of OH groups promoting the removal of  $\text{SO}_2$  and the blocking of active surface sites by molecularly adsorbed water. The competitive nature of these processes probably leads to the saturation of  $N_{s,\text{dark}}$ .

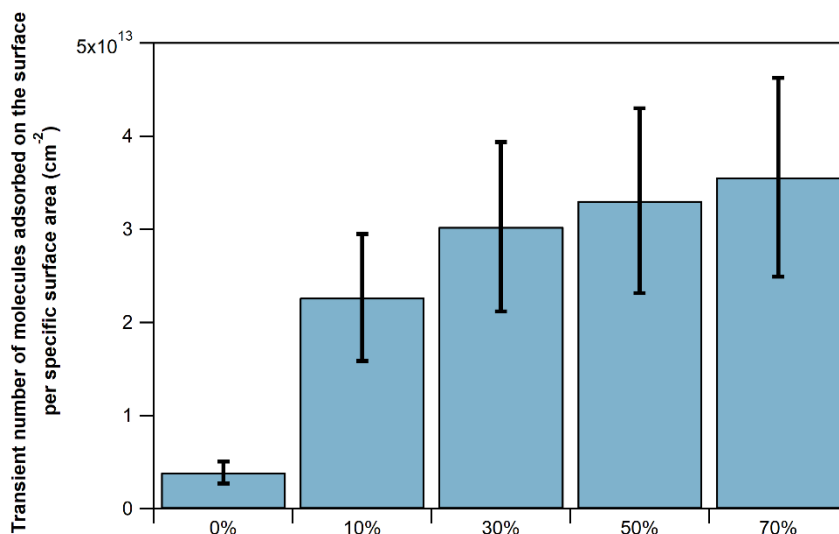


Figure 8: Number of SO<sub>2</sub> molecules taken up on the surface of Mýrdalssandur v-dust ( $N_{s,dark}$ ) as a function of RH. Mýrdalssandur v-dust samples exposed to 75 ppb at  $T = 296$  K under dark conditions. The errors quoted reflect the total error for the  $N_s$  determinations.

## 2.4 Impact of UV radiation on SO<sub>2</sub> transient uptake on v-dust samples

The transient number of molecules taken up by the five v-dusts,  $N_s$ , was measured at  $RH = 30\%$ ,  $T = 296$  K and  $[SO_2]_0 = 75$  ppb, both in the dark and under UV irradiation ( $J_{NO_2} = 4.5 \times 10^{-3} \text{ s}^{-1}$ ).  $N_{s,dark}$  and  $N_{s,UV}$  are given in Table 3 and displayed in Figure 9; they range from roughly  $10^{12}$  to  $10^{14}$  molecules  $\text{cm}^{-2}$ . The number of SO<sub>2</sub> molecules initially taken up by v-dust under UV is markedly larger for Maelifellssandur and Mýrdalssandur v-dusts, falls within relative error bar for Hagavatn and Dyngjusandur v-dusts, and is smaller for Eyjafjallajokull, making it difficult to evaluate. Nevertheless, for four out of five dust samples, Hagavatn, Dyngjusandur, Maelifellssandur and Mýrdalssandur, the  $N_s$  values show an increasing trend between dark and UV irradiation conditions; being larger by a factor of 1.7 to around 3.8 under light irradiation than in the dark. Interestingly, Dyngjusandur sample that exhibited the most intense light amplification for  $\gamma_{SS,BET}$  (factor of 4.6) had the lowest amplification for  $N_s$  (1.7), further suggesting that the processes occurring on the surface of the dust are contrasted on different uptake time scale. As with steady state uptake coefficient, photo-induced reactions occurring on the surface of v-dust particles might be responsible for the enhanced removal of SO<sub>2</sub> in the presence of light. Nevertheless, at this point we cannot state the precise reasons for impact of UV on the number of molecules taken up, it is discussed later based on further experiments.

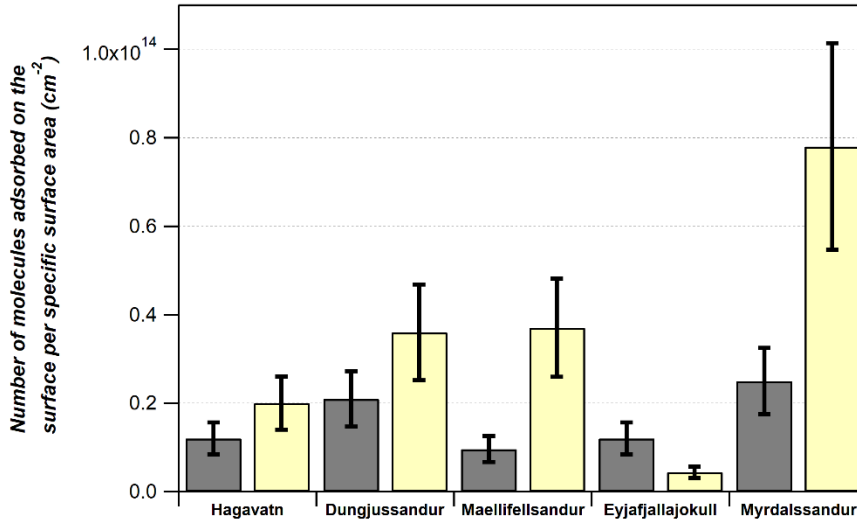


Figure 9: Bar graph showing the transient number of SO<sub>2</sub> molecules initially taken up, N<sub>s</sub>, at [SO<sub>2</sub>]<sub>0</sub> = 75 ppb at RH = 30% and T = 296 K on the 5 types of Icelandic v-dust investigated under dark conditions (grey) and UV-irradiation (J<sub>NO<sub>2</sub></sub> = 4.5 × 10<sup>-3</sup> s<sup>-1</sup>; yellow).

Table 3: Transient number of SO<sub>2</sub> molecules initially taken up, N<sub>s</sub>, at [SO<sub>2</sub>]<sub>0</sub> = 75 ppb by the 5 Icelandic v-dust samples at RH = 30% and T = 296 K under dark conditions and UV-irradiation (J<sub>NO<sub>2</sub></sub> = 4.5 × 10<sup>-3</sup> s<sup>-1</sup>).

Dust sample	N <sub>s,dark</sub> (molecules cm <sup>-2</sup> )	N <sub>s,UV</sub> (molecules cm <sup>-2</sup> )	N <sub>s,UV</sub> /N <sub>s,dark</sub>
Hagavatn	(1.2 ± 0.4) × 10 <sup>13</sup>	(2.0 ± 0.6) × 10 <sup>13</sup>	1.7
Dyngjussandur	(2.1 ± 0.6) × 10 <sup>13</sup>	(3.6 ± 1.0) × 10 <sup>13</sup>	1.7
Maelifellssandur	(9.6 ± 2.9) × 10 <sup>12</sup>	(3.7 ± 1.1) × 10 <sup>13</sup>	3.8
Eyjafjallajökull	(1.2 ± 0.4) × 10 <sup>13</sup>	(4.4 ± 1.3) × 10 <sup>12</sup>	0.2
Mýrdalssandur	(2.5 ± 0.8) × 10 <sup>13</sup>	(7.8 ± 2.5) × 10 <sup>13</sup>	3.1

Next step was to investigate whether the amplification factors (i.e. N<sub>s,light</sub>/N<sub>s,dark</sub>) are correlated with the surface elemental composition of the dusts in respect to these elements. Interestingly, as presented in Figure 10 there is a linear increase of the N<sub>s,light</sub>/N<sub>s,dark</sub> as a function of the Ti surface concentration (Figure 10a), and the Ti/Si ratio (Figure 10b) as determined by XPS. Trends with elemental Fe were not straightforward and thus they are not further discussed. The photo-enhanced removal of SO<sub>2</sub> on the surface of v-dusts is related to the presence of elemental surface Ti. To parametrize the results of the current study (see also Section 2.3) we consider the Ti/Si ratio as more representative since it indicates the relative abundance of the element of interest versus the most abundant element of the v-dusts. Therefore, according to the linear fit of results in Figure 10b and under the defined experimental conditions the amplification factor is given by the following expression (Equation 1):

Equation 1

$$N_{s,light}/N_{s,dark} = 39.4 \times (Ti/Si)$$

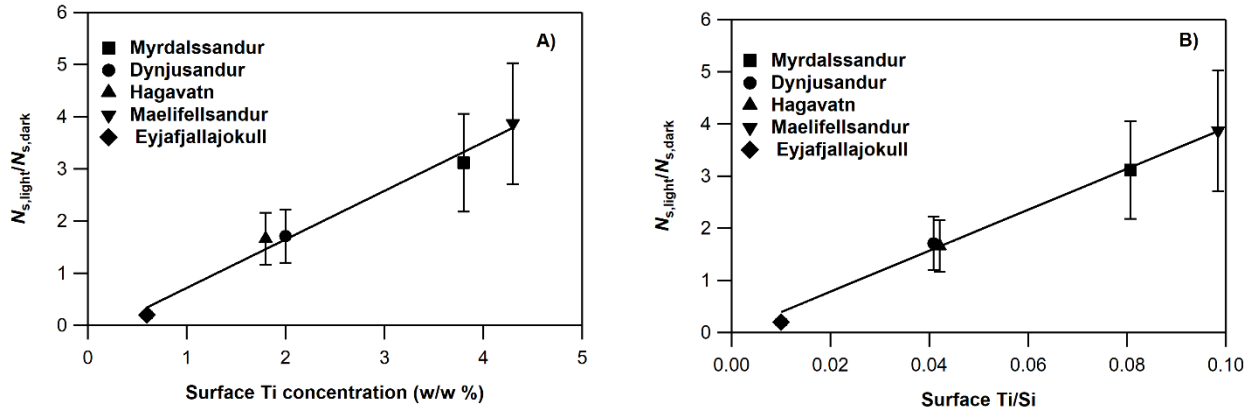


Figure 10: Amplification by light of the transient number of SO<sub>2</sub> molecules taken up with respect to dark conditions,  $N_{s,light}/N_{s,dark}$ , as a function of: a) the Ti surface concentration of the v-dust samples and, b) the Ti/Si surface concentration ratio. Experimental conditions:  $[SO_2]_0 = 75$  ppb,  $RH = 30\%$  and  $T = 296$  K, under dark and  $J_{NO_2} 4.5 \times 10^{-3} s^{-1}$ . The solid lines are the linear fit of experimental results with a correlation coefficient  $R^2 > 0.95$  in case of Ti surface concentration and  $R^2 > 0.97$  for Ti/Si ratio.

In the following of the chapter, aiming to evaluate the impact of atmospheric relevant parameters (i.e. photon flux, and RH) to the photo-induced removal of SO<sub>2</sub>, Mýrdalssandur v-dust was chosen as a model sample. Two basic criteria were set for this selection. The first one was the precision of the measurements and the second one the photo-enhanced removal of SO<sub>2</sub>. Mýrdalssandur v-dust showed the highest  $N_s$  values both under dark and light conditions which ensures a higher accuracy of measurements and a significant photo-induced uptake of SO<sub>2</sub>.

## 2.5 Dependence of transient uptake of SO<sub>2</sub> on Myrdalssandur under UV on RH

To evaluate the dependence of  $N_{s,UV}$  on  $RH$  a series of controlled experiments were carried out exposing Mýrdalssandur v-dust to a fixed concentration of SO<sub>2</sub>, at 296 K under light conditions ( $J_{NO_2} 4.5 \times 10^{-3} s^{-1}$ ) and varying the  $RH$  in the range of 0.1% - 70%. The results were compared to the dark conditions and are displayed in Figure 11. When the surface is irradiated with simulated sunlight, a linear increase of  $N_s$  was noticed as a function of  $RH$ , without showing any saturation (from  $4 \times 10^{13}$  molecules cm<sup>-2</sup> at  $RH = 11\%$  to  $2.3 \times 10^{14}$  molecules cm<sup>-2</sup> at  $RH = 70\%$ ). The trends observed are consistent with Park et al. and Jang et al. who studied SO<sub>2</sub> uptake by ATD in a photo-irradiation chamber (Park and Jang, 2016), (Yu et al., 2017). In the dark, they observed an almost constant uptake with  $RH$ , whereas under UV, it increased exponentially. Remember, that  $N_{s,dark}$  determined earlier for Mýrdalssandur dust was found to increase from dry to 30% of  $RH$ , and then reach a saturation regime remaining constant. Clearly, as opposed to dark conditions, the photo-induced processes that occur on the surface of v-dust are promoted as  $RH$  increases. The latter could be either attributed to induced photochemical processes, supposedly on Ti-surface sites,

leading to the formation of reactive species on the surface of the dust  $\bullet\text{OH}$ ,  $\bullet\text{O}_2\text{H}$ ,  $\text{O}_2\bullet^-$ , etc., or to the photolysis of some reactive surface species (Herrmann, 2005), (Chen et al., 2012). Both processes would accelerate the transformation of  $\text{SO}_2$  to reaction products (e.g. sulfites and/or sulfates) (George et al., 2015), (Park et al., 2017), (Dupart et al., 2012). To quantify the enhancement of  $N_s$  in presence of light, the amplification factors were plotted as a function of RH (Figure 11). The results were linearly fitted according the following Equation 2:

Equation 2 
$$N_{s,\text{light}}/N_{s,\text{dark}} = 1 + (7.76 \times 10^{-2}) \times (\%RH)$$

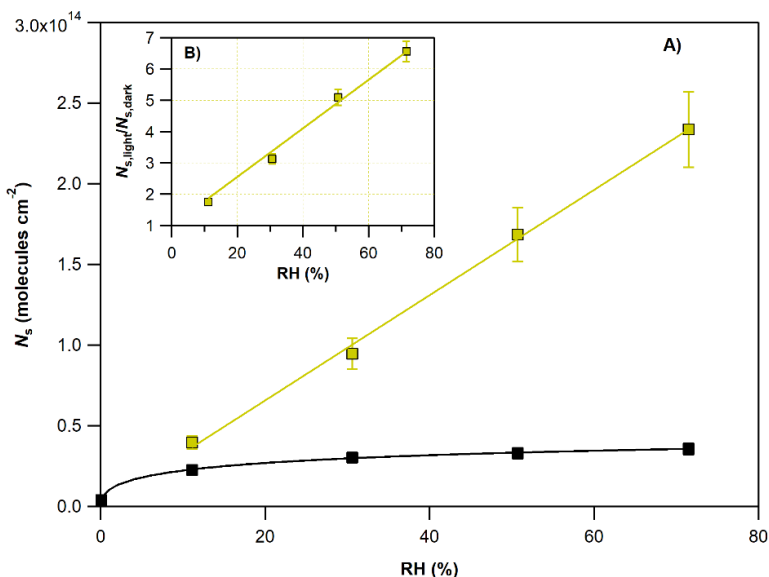


Figure 11: A) The transient number of  $\text{SO}_2$  molecules taken up in the dark,  $N_{s,\text{dark}}$  (black symbols), and under light ( $J_{\text{NO}_2} = 4.5 \times 10^{-3} \text{ s}^{-1}$ ),  $N_{s,\text{light}}$  (colored symbols), are plotted as a function of RH for Mýrdalssandur v-dust samples exposed to 75 ppb of  $\text{SO}_2$  at  $T = 296 \text{ K}$ . The errors quoted on  $N_s$  values reflect the precision of the measurements and the estimated systematic uncertainties related with the  $N_s$  determination, and they do not include the error on the specific surface area measurement. The black line is the fit of experimental results with an empirical function to demonstrate the saturation of  $N_s$  noticed under dark conditions. The yellow line is the linear fit of results measured under surface irradiation. B) The amplification factors,  $N_{s,\text{light}}/N_{s,\text{dark}}$ , are plotted versus RH. The solid line reflects the linear correlation between the amplification factors and RH. The uncertainties quoted (5%) correspond to the  $2\sigma$  precision of the fit and do not include other systematic uncertainties.

Further experiments are needed to elucidate the processes at play in the heterogeneous interaction of  $\text{SO}_2$  with the surface of v-dust.

## 2.6 Dependence of transient uptake of $\text{SO}_2$ on UV photon flux

To evaluate the impact of irradiance intensity on the transient uptake of  $\text{SO}_2$  ( $N_{s,\text{UV}}$ ), a series of experiments was performed under controlled experimental conditions, i.e. 30% RH, 296 K and 75 ppb of  $\text{SO}_2$ , and varying photon flux, i.e. the  $J_{\text{NO}_2}$  inside the reactor using Mýrdalssandur v-dust. The results are presented in Figure 12 where the values of  $N_s$  are plotted as a function of  $J_{\text{NO}_2}$  together with the amplification factor calculated as a ratio of the  $N_s$  values measured under the corresponding intensity of light and in dark

conditions.  $N_s$  increases linearly with the photon flux indicating that the removal of  $\text{SO}_2$  molecules from the gas phase is proportional to the photons absorbed by the surface (Herrmann, 2005). An amplification by a factor of three was noticed for the highest irradiance intensity ( $J_{\text{NO}_2} = 4.5 \times 10^{-3} \text{ s}^{-1}$ ) compared to dark conditions. Similar trends have been also noticed in literature for the degradation of pollutants on the surface of mineral dust proxies (Romanias et al., 2012a), (Zein et al., 2014), (Romanias et al., 2012b), and on volcanic dusts (Romanias et al., 2020). The following expression (Equation 3) is proposed to describe the photo-enhanced uptake of  $\text{SO}_2$  under the current experimental conditions:

Equation 3 
$$N_{s,\text{light}}/N_{s,\text{dark}} = 1 + 480.5 \times J_{\text{NO}_2}$$

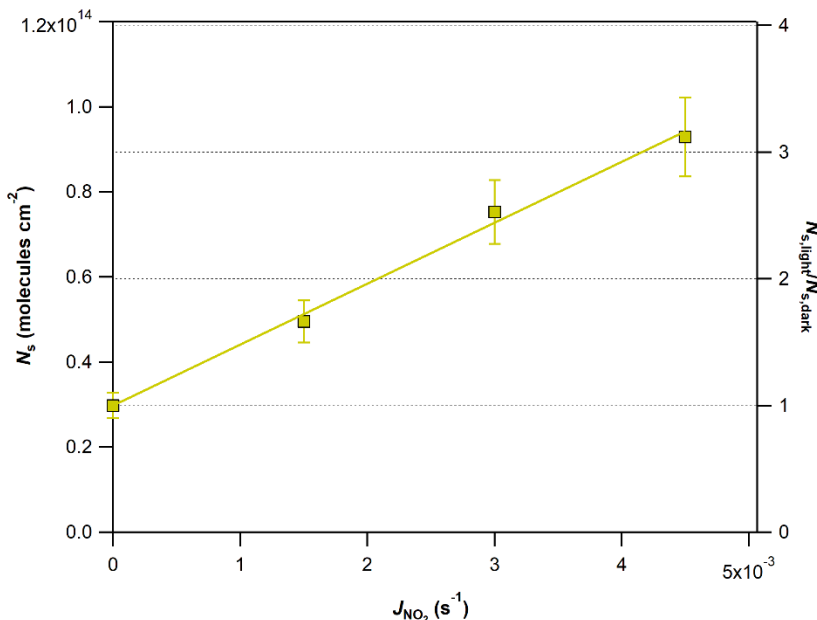


Figure 12:  $N_s$  as a function of photon flux ( $J_{\text{NO}_2} = 0\text{-}4.5 \times 10^{-3} \text{ s}^{-1}$ ) for Mýrdalssandur v-dust samples exposed to 75 ppb of  $\text{SO}_2$  at  $\text{RH} = 30\%$  and  $T = 296 \text{ K}$ . For comparison, the amplification factors are also plotted as a function of  $J_{\text{NO}_2}$  (right axis). The errors quoted on  $N_s$  values reflect the precision of the measurements and the estimated systematic uncertainties related with the  $N_s$  determination, and they do not include the error on the specific surface area measurement. The solid line is the linear fit of the amplification factors with the corresponding  $J_{\text{NO}_2}$  values.

**This series of experiments lead to the conclusion that the number of  $\text{SO}_2$  molecules transiently taken up by the selected v-dust per surface area unit,  $N_{s,UV}$ , is linearly and positively influenced by both (i) the UV photon flux and (ii)  $\text{RH}$ , *i.e.* the number (or density) of  $\text{H}_2\text{O}$  molecules in the air flow when the dust is irradiated with UV light, but not in the dark. In contrast, the  $\gamma_{ss,BET}$  of  $\text{SO}_2$  by Mýrdalssandur v-dust was demonstrated to be the same in the dark and under light for all values of  $\text{RH}$  investigated (0.1 - 70%). This observation once again points to the existence of one or several transient surface reaction mechanisms increasing the uptake of  $\text{SO}_2$  at the early times of the experiment (measured as  $N_{s,UV}$ ); these mechanisms are quenched at later stages of the exposure, leading to similar steady-state uptake observed in the dark and under light. The observed**

phenomenon may be due to the surface of dust being modified during the light irradiation process (light-induced ageing effect). Initially, the modification or activation of the surface increases transiently the uptake of SO<sub>2</sub>; then, surface species that do not absorb or weakly absorb light radiation form, leading to a smaller consumption of SO<sub>2</sub> at steady-state.

### 3 Atmospheric implications of SO<sub>2</sub> uptake on v-dusts

#### 3.1 Atmospheric lifetime of SO<sub>2</sub> with respect to v-dust

In order to evaluate potential impact of SO<sub>2</sub> uptake on v-dust on the atmosphere, its atmospheric lifetime was calculated using Equation 4.

Equation 4 
$$\tau_{het} = \frac{4}{\gamma c D}$$

where  $\gamma$  is the uptake coefficient,  $c$  is the mean molecular velocity (m s<sup>-1</sup>), and  $D$  is the volcanic dust surface area density (m<sup>2</sup> m<sup>-3</sup>). Considering (i) concentrations of volcanic ash in a vertical column of the volcanic cloud passing over Faroe Islands located about 650 km from the Eyjafjallajökull volcano measured during its eruption on April 15 2010 ranging from 200 to 6000 µg m<sup>-3</sup> (Gudmundsson et al., 2012) and (ii) the SSA of Eyjafjallajökull dust sample of 0.75 m<sup>2</sup> g<sup>-1</sup>,  $D$  can be calculated by direct multiplication of the dust concentration and the SSA of the v-dust and was found to be in the range from 1.5×10<sup>-4</sup> m<sup>2</sup> m<sup>-3</sup> to 4.5×10<sup>-3</sup> m<sup>2</sup> m<sup>-3</sup> for the lower and higher ash load respectively. This leads to the calculation of lifetime of SO<sub>2</sub> molecule as a result of its heterogeneous loss on Eyjafjallajökull v-dust particle to 81 to 2.7 years. If we consider a higher 7.5 m<sup>2</sup> g<sup>-1</sup> SSA values for Eyjafjallajökull dust obtained by Maters et al. the atmospheric lifetime falls to 8.1 years to 99 days (Maters et al., 2016). For comparison, the lifetime of SO<sub>2</sub> in the atmosphere as measured over the Eastern United States in the absence of volcanic activity ranges from 15 h in summer to 65 hours in winter (Lee et al., 2011). On the base of these calculations it may appear that the lifetime of SO<sub>2</sub> molecule in the atmosphere is mainly determined by the gas phase oxidation by aqueous (i.e., H<sub>2</sub>O<sub>2</sub>) and gas-phase (i.e., OH) processes.

However, in case of higher volcanic ash concentrations in the plume, for example 2.0×10<sup>6</sup> µg m<sup>-3</sup> estimated during 1991 Pinatubo eruption (SSA 1.5 m<sup>2</sup> g<sup>-1</sup> (Maters et al., 2016)) at the direct proximity to the vent (Witham et al., 2012), and considering the same uptake coefficient measured in this study for Eyjafjallajökull, calculations lead to a radically shorter lifetime of 36 hr and make heterogeneous uptake of SO<sub>2</sub> on volcanic dust particles equally important. Furthermore, the lifetime of SO<sub>2</sub> could be further decreased for volcanic particles with higher specific surface area. These calculations point out that



adsorption of SO<sub>2</sub> on the surface of volcanic ash is most likely to happen in the part of volcanic cloud closest to the vent where ash concentration is the highest. The process of SO<sub>2</sub> loss due to heterogeneous reactions with v-dust particles could be further enhanced in the presence of oxidizing species (i.e., O<sub>3</sub>, OH) and needs to be quantitatively evaluated.

### 3.2 Surface coverage of v-dust by SO<sub>2</sub> molecules

Following the calculation of Romanias et al. the fully-stacked SO<sub>2</sub> monolayer is composed of  $N_{\text{SO}_2} = 4.3 \times 10^{14}$  molecules cm<sup>-2</sup> (Romanias et al., 2016). In the literature, the surface coverage of reversibly adsorbed SO<sub>2</sub> has been determined as  $(1.5 \pm 0.3) \times 10^{14}$  molecules cm<sup>-2</sup> on  $\alpha$ -Al<sub>2</sub>O<sub>3</sub> and  $(3.5 \pm 0.6) \times 10^{14}$  molecules cm<sup>-2</sup> on MgO (Goodman et al., 2001), (Usher et al., 2002). They represent 1/3 and 2/3 of the calculated monolayer, respectively. During SO<sub>2</sub> uptake by Saharan dust, flow-tube experiments suggest a maximum surface coverage of  $(2 \pm 1) \times 10^{13}$  molecules cm<sup>-2</sup>, an order of magnitude lower than the coverage on  $\alpha$ -Al<sub>2</sub>O<sub>3</sub> and MgO and the theoretical monolayer (Adams et al., 2005). Addition of H<sub>2</sub>O to the carrier gas did not affect the measured SO<sub>2</sub> surface coverage, in agreement with our observation of a constant value of  $N_{s,\text{dark}}$  for  $RH > 30\%$  (Adams et al., 2005).

Assuming that all of the molecules lost from the gas phase are adsorbed by the surface, number of molecules transiently taken up,  $N_s$ , is roughly equivalent to the surface coverage. In the dark, our experiments show a saturation of  $N_{s,\text{dark}}$  at roughly  $3 \times 10^{13}$  molecules cm<sup>-2</sup> for  $RH = 30\%$ , a value consistent with that found on Saharan dust by Adams et al., representing almost 1/10 of the full surface coverage (Adams et al., 2005). This value is also consistent with Maters et al., who reported values of  $N_{s,\text{dark}}$  in the  $10^{11} - 10^{13}$  molecules cm<sup>-2</sup> range for SO<sub>2</sub> uptake by volcanic ash and glass powder (Maters et al., 2017). Under UV, however, a strong transient process takes place on a number of dusts, which can be further enhanced by increase in  $RH$ . Thus, on the surface of Mýrdalssandur v-dust  $N_{s,\text{UV}}$  increases linearly both with  $RH$  and with the flux of UV photons.  $N_{s,\text{UV}}$  increases from  $4 \times 10^{13}$  molecules cm<sup>-2</sup> at  $RH = 11\%$  to  $2.3 \times 10^{14}$  molecules cm<sup>-2</sup> at  $RH = 70\%$ . The latter value represents 1/2 of a fully-compact monolayer, suggesting that some sites may still remain available for SO<sub>2</sub> uptake.

### 3.3 Parametrization of SO<sub>2</sub> uptake on v-dusts.

Based on the experimental strategy followed, which includes (i) the screening of v-dusts towards their capacity to uptake SO<sub>2</sub> (ii) the control set of experiments carried out by tuning only one atmospheric parameter and evaluating its impact on the removal of SO<sub>2</sub> under dark and light conditions, it was feasible to parametrize the experimental results applying linear expressions (expressions 1 to 3). The objective of fitting the results was to elucidate the impact of the experimental conditions on the photo-enhanced removal

of SO<sub>2</sub>. Using Mýrdalssandur v-dust as a model sample, we propose a general equation that describes the correlation between the amplification factor with the chemical composition of the sample, the photon flux and relative humidity according to the following Equation 5:

*Equation 5*       $N_{s,light}/N_{s,dark} = 3.68 \times [(1 + 7.76 \times 10^{-2} \times (\%RH))] \times (1 + 480 \times J_{NO_2}) \times (Ti/Si)$

Despite the fact that we did not performed a detailed RH study for all the v-dusts, Equation 5 seems to describe (within 10%) the expected amplification factors for all the other volcanic dusts and to overestimate by 50 % the amplification on Eyjafjallajökull volcanic ash. It should be noted that this type of expressions can be useful in modelling, since different atmospheric parameters are combined to describe the photo-enhanced removal of SO<sub>2</sub>.

## 4 Conclusions

In this chapter the uptake of SO<sub>2</sub> gas by Icelandic v-dust has been investigated inside a coated wall flow-tube reactor. These values are of interest as they can be used for the modelling of atmospheric processes to better evaluate the effect of SO<sub>2</sub> volcanic emissions. Uptake of SO<sub>2</sub> by v-dusts was observed even though all of them have already been exposed to SO<sub>2</sub> in the volcanic conduit and plume owing to their production/emission mode. Upon exposure of the v-dust to SO<sub>2</sub> the system reaches a steady state clearly distinct from the initial state indicating continuous consumption of SO<sub>2</sub> molecules. The steady state uptake coefficients for v-dusts at 30% *RH* range from  $(6.6 \pm 2.6) \times 10^{-9}$  for Hagavatn to  $(6.2 \pm 2.5) \times 10^{-8}$  for Mýrdalssandur. Moreover, increased uptake of the SO<sub>2</sub> gas at 30% *RH* as compared to dry conditions suggests that water plays an important role in the above-mentioned processes (for Mýrdalssandur  $\gamma_{ss, BET}(30\% RH) = 6.2 \times 10^{-8}$  and  $\gamma_{ss, BET}(dry) = 2.0 \times 10^{-8}$ ); for Hagavatn  $\gamma_{ss, BET}(30\% RH) = 6.6 \times 10^{-9}$  and  $\gamma_{ss, BET}(dry) = 1.0 \times 10^{-9}$ ). After 30% *RH* steady state uptake coefficient stabilizes and no further increase is noted. It can be suggested that increase in concentration of water molecules enhances steady state uptake coefficient up till the formation of water monolayer at 30% *RH*, after which the molecule can encounter the same water-covered surface and thus the  $\gamma_{ss}$  does not change. As for the effect of UV on the steady state uptake coefficient, an increase was observed for two out of five dusts (Dyngjusandur and Hagavatn) while no effect within the uncertainty could be noted for the other three samples (Eyjafjallajökull, Maelifellsandur and Mýrdalssandur). In addition, the uptake coefficient for Mýrdalssandur v-dust in the dark and under simulated sunlight was the same for levels of humidity up to 70%. However, more extensive sampling is necessary to verify the latter trend under simulated sunlight, as a Mýrdalssandur sample, used for this study, exhibited the lowest light amplification factor.

The initial capacity of the selected dusts to uptake SO<sub>2</sub> molecules was also investigated by calculating the transient number of molecules initially taken up. The transient number of molecules initially taken up for v-dusts at 30% *RH* range from  $(9.6 \pm 2.9) \times 10^{12}$  for Maelifellsandur to  $(2.5 \pm 0.8) \times 10^{13}$  for Mýrdalssandur. Just as steady state uptake, the number of molecules transiently taken up in the dark increases as *RH* is increased from 0% to 30% and then remains stable at higher values (for Mýrdalssandur:  $N_s(30\% RH) = 2.48 \times 10^{13}$  and  $N_s(dry) = 3.1 \times 10^{12}$ ; for Hagavatn:  $N_s(30\% RH) = 1.15 \times 10^{13}$  and  $N_s(dry) = 7.2 \times 10^{12}$ ). For four out of five dust samples, Hagavatn, Dyngjusandur, Maelifellssandur and Mýrdalssandur, the  $N_s$  values show an increasing trend between dark and UV irradiation conditions, even though for the first two dusts the increase is within the relative error. On Mýrdalssandur  $N_s$  scales linearly both with the photon flux and with *RH*. Thus, for the dusts that exhibit light amplification effect on  $N_s$ , such as Mýrdalssandur, the initial number of uptaken molecules  $N_s$  is greatly affected by a combination of humidity and simulated sunlight.

Processes leading to the uptake of  $\text{SO}_2$  on the surface of dust under simulated sunlight at the initial period of exposure versus steady state are rather different. Thus, Maelifellsandur and Mýrdalssandur exhibit the highest amplification factor for  $\text{SO}_2$  uptake at the beginning, but some of the lowest amplification factors for steady state, while Dyngjusandur and Hagavatn show the opposite trend. Surface ageing might be a reasonable explanation for this behavior. To further explain the trends in uptake on dust one would need to take a closer look at the formation of surface species.

In the framework of the current study, we have investigated the uptake of  $\text{SO}_2$  by natural samples of Icelandic v-dusts under atmospherically relevant conditions of humidity, in the absence and in presence of simulated solar irradiation. We found that the uptake of  $\text{SO}_2$  gas on the surface of v-dust with respect to reactions occurring in the atmosphere could be important, especially in the denser part of the plume/cloud and when the emitted particles have a high specific surface area. After passing through the plume rich in  $\text{SO}_2$  gas, v-particles are expected to be only partially covered with sulfur species. If the interactions are happening in the part of the plume/cloud exposed to sunlight and in high levels of  $RH$  up to 50% of the particle surface could be covered with sulfur species. The photo-enhanced removal of  $\text{SO}_2$ ,  $N_{s,\text{light}}/N_{s,\text{dark}}$  was found to be correlated with the Ti surface elemental composition and the Ti/Si ratio of the dusts. In addition, performing experiments under controlled experimental conditions we managed to correlate the photo-induced removal of  $\text{SO}_2$  with each of the atmospheric parameter tuned and to propose a generic expression of the photo-enhanced removal of  $\text{SO}_2$  on v-dusts. This type of expressions could be useful for the implementation of the results in models. Above all, we showed a strategy that needs to be followed to investigate the heterogeneous reaction of a gas species with a surface and to provide kinetic data that can be parametrized.

## References of Chapter 3

- Adams, J.W., Rodriguez, D., Cox, R.A., 2005. The uptake of SO<sub>2</sub> on Saharan dust: a flow tube study. *Atmospheric Chemistry and Physics* 5, 2679–2689. <https://doi.org/10.5194/acp-5-2679-2005>
- Ayris, P.M., Lee, A.F., Wilson, K., Kueppers, U., Dingwell, D.B., Delmelle, P., 2013. SO<sub>2</sub> sequestration in large volcanic eruptions: High-temperature scavenging by tephra. *Geochimica et Cosmochimica Acta* 110, 58–69. <https://doi.org/10.1016/j.gca.2013.02.018>
- Bagnato, E., Aiuppa, A., Bertagnini, A., Bonadonna, C., Cioni, R., Pistolesi, M., Pedone, M., Hoskuldsson, A., 2013. Scavenging of sulphur, halogens and trace metals by volcanic ash: The 2010 Eyjafjallajökull eruption. *Geochimica et Cosmochimica Acta* 103, 138–160. <https://doi.org/10.1016/j.gca.2012.10.048>
- Baratoux, D., Mangold, N., Arnalds, O., Bardintzeff, J.-M., Platevoet, B., Grégoire, M., Pinet, P., 2011. Volcanic Sand in Iceland: Diverse origins of aeolian sand deposits revealed at Dyngjúsandur and Lambahraun, Iceland. *Earth Surface Processes and Landforms* 36, 1789–1808. <https://doi.org/10.1002/esp.2201>
- Chen, H., Nanayakkara, C.E., Grassian, V.H., 2012. Titanium Dioxide Photocatalysis in Atmospheric Chemistry. *Chem. Rev.* 112, 5919–5948. <https://doi.org/10.1021/cr3002092>
- Crowley, J.N., Ammann, M., Cox, R.A., Hynes, R.G., Jenkin, M.E., Mellouki, A., Rossi, M.J., Troe, J., Wallington, T.J., 2010. Evaluated kinetic and photochemical data for atmospheric chemistry: Volume V – heterogeneous reactions on solid substrates. *Atmos. Chem. Phys.* 10, 9059–9223. <https://doi.org/10.5194/acp-10-9059-2010>
- Delmelle, P., Wadsworth, F.B., Maters, E.C., Ayris, P.M., 2018. High Temperature Reactions Between Gases and Ash Particles in Volcanic Eruption Plumes. *Reviews in Mineralogy and Geochemistry* 84, 285–308. <https://doi.org/10.2138/rmg.2018.84.8>
- Dupart, Y., King, S.M., Nekat, B., Nowak, A., Wiedensohler, A., Herrmann, H., David, G., Thomas, B., Miffre, A., Rairoux, P., D’Anna, B., George, C., 2012. Mineral dust photochemistry induces nucleation events in the presence of SO<sub>2</sub>. *Proc. Natl. Acad. Sci. U.S.A.* 109, 20842–20847. <https://doi.org/10.1073/pnas.1212297109>
- Farges, F., Keppler, H., Flank, A.M., Lagarde, P., 2009. Sulfur K-edge XANES study of S sorbed onto volcanic ashes. *Journal of Physics: Conference Series* 190, 012177. <https://doi.org/10.1088/1742-6596/190/1/012177>
- George, C., Ammann, M., D’Anna, B., Donaldson, D.J., Nizkorodov, S.A., 2015. Heterogeneous Photochemistry in the Atmosphere. *Chem. Rev.* 115, 4218–4258. <https://doi.org/10.1021/cr500648z>
- Gislason, S.R., Hassenkam, T., Nedel, S., Bovet, N., Eiríksdóttir, E.S., Alfredsson, H.A., Hem, C.P., Balogh, Z.I., Dideriksen, K., Oskarsson, N., Sigfusson, B., Larsen, G., Stipp, S.L.S., 2011. Characterization of Eyjafjallajökull volcanic ash particles and a protocol for rapid risk assessment. *PNAS* 108, 7307–7312. <https://doi.org/10.1073/pnas.1015053108>
- Goodman, A.L., Li, P., Usher, C.R., Grassian, V.H., 2001. Heterogeneous Uptake of Sulfur Dioxide On Aluminum and Magnesium Oxide Particles. *J. Phys. Chem. A* 105, 6109–6120. <https://doi.org/10.1021/jp004423z>
- Gudmundsson, M.T., Thordarson, T., Höskuldsson, Á., Larsen, G., Björnsson, H., Prata, F.J., Oddsson, B., Magnússon, E., Högnadóttir, T., Petersen, G.N., Hayward, C.L., Stevenson, J.A., Jónsdóttir, I., 2012. Ash generation and distribution from the April-May 2010 eruption of Eyjafjallajökull, Iceland. *Scientific Reports* 2, 572. <https://doi.org/10.1038/srep00572>
- Harris, E., Sinha, B., Foley, S., Crowley, J.N., Borrmann, S., Hoppe, P., 2012. Sulfur isotope fractionation during heterogeneous oxidation of SO<sub>2</sub> on mineral dust. *Atmospheric Chemistry and Physics* 12, 4867–4884. <https://doi.org/10.5194/acp-12-4867-2012>

- Herrmann, J.-M., 2005. Heterogeneous photocatalysis: state of the art and present applications In honor of Pr. R.L. Burwell Jr. (1912–2003), Former Head of Ipatieff Laboratories, Northwestern University, Evanston (Ill). *Top Catal* 34, 49–65. <https://doi.org/10.1007/s11244-005-3788-2>
- Huang, L., Zhao, Y., Li, H., Chen, Z., 2015. Kinetics of Heterogeneous Reaction of Sulfur Dioxide on Authentic Mineral Dust: Effects of Relative Humidity and Hydrogen Peroxide. *Environ. Sci. Technol.* 49, 10797–10805. <https://doi.org/10.1021/acs.est.5b03930>
- Huthwelker, T., Ammann, M., Peter, T., 2006. The Uptake of Acidic Gases on Ice. *Chemical Reviews* 106, 1375–1444. <https://doi.org/10.1021/cr020506v>
- Ibrahim, S., Romanias, M.N., Alleman, L.Y., Zeineddine, M.N., Angeli, G.K., Trikalitis, P.N., Thevenet, F., 2018. Water Interaction with Mineral Dust Aerosol: Particle Size and Hygroscopic Properties of Dust. *ACS Earth Space Chem.* 2, 376–386. <https://doi.org/10.1021/acsearthspacechem.7b00152>
- Joshi, N., Romanias, M.N., Riffault, V., Thevenet, F., 2017. Investigating water adsorption onto natural mineral dust particles: Linking DRIFTS experiments and BET theory. *Aeolian Research* 27, 35–45. <https://doi.org/10.1016/j.aeolia.2017.06.001>
- Judeikis, H.S., Stewart, T.B., 1976. Laboratory measurement of SO<sub>2</sub> deposition velocities on selected building materials and soils. *Atmospheric Environment* (1967) 10, 769–776. [https://doi.org/10.1016/0004-6981\(76\)90078-0](https://doi.org/10.1016/0004-6981(76)90078-0)
- Lasne, J., Romanias, M.N., Thevenet, F., 2018. Ozone Uptake by Clay Dusts under Environmental Conditions. *ACS Earth Space Chem.* 2, 904–914. <https://doi.org/10.1021/acsearthspacechem.8b00057>
- Latham, T.L., Kumar, P., Nenes, A., Dufek, J., Sokolik, I.N., Trail, M., Russell, A., 2011. Hygroscopic properties of volcanic ash. *Geophysical Research Letters* 38. <https://doi.org/10.1029/2011GL047298>
- Lee, C., Martin, R.V., Donkelaar, A. van, Lee, H., Dickerson, R.R., Hains, J.C., Krotkov, N., Richter, A., Vinnikov, K., Schwab, J.J., 2011. SO<sub>2</sub> emissions and lifetimes: Estimates from inverse modeling using in situ and global, space-based (SCIAMACHY and OMI) observations. *Journal of Geophysical Research: Atmospheres* 116. <https://doi.org/10.1029/2010JD014758>
- Li, L., Chen, Z.M., Zhang, Y.H., Zhu, T., Li, J.L., Ding, J., 2006. Kinetics and mechanism of heterogeneous oxidation of sulfur dioxide by ozone on surface of calcium carbonate. *Atmospheric Chemistry and Physics Discussions* 6, 579–613. <https://doi.org/10.5194/acpd-6-579-2006>
- Maters, E.C., Delmelle, P., Rossi, M.J., Ayris, P.M., 2017. Reactive Uptake of Sulfur Dioxide and Ozone on Volcanic Glass and Ash at Ambient Temperature. *J. Geophys. Res.-Atmos.* 122, 10077–10088. <https://doi.org/10.1002/2017JD026993>
- Maters, E.C., Delmelle, P., Rossi, M.J., Ayris, P.M., Bernard, A., 2016. Controls on the surface chemical reactivity of volcanic ash investigated with probe gases. *Earth Planet. Sci. Lett.* 450, 254–262. <https://doi.org/10.1016/j.epsl.2016.06.044>
- Moroni, B., Arnalds, O., Dagsson-Waldhauserová, P., Crocchianti, S., Vivani, R., Cappelletti, D., 2018. Mineralogical and Chemical Records of Icelandic Dust Sources Upon Ny-Ålesund (Svalbard Islands). *Front. Earth Sci.* 6. <https://doi.org/10.3389/feart.2018.00187>
- Park, J., Jang, M., Yu, Z., 2017. Heterogeneous Photo-oxidation of SO<sub>2</sub> in the Presence of Two Different Mineral Dust Particles: Gobi and Arizona Dust [WWW Document]. <https://doi.org/10.1021/acs.est.7b00588>
- Park, J.Y., Jang, M., 2016. Heterogeneous photooxidation of sulfur dioxide in the presence of airborne mineral dust particles. *RSC Adv.* 6, 58617–58627. <https://doi.org/10.1039/C6RA09601H>
- Renggli, C., King, P., W. Henley, R., Guagliardo, P., McMorrow, L., Middleton, J., Turner, M., 2019. An experimental study of SO<sub>2</sub> reactions with silicate glasses and supercooled melts in the system anorthite–diopside–albite at high temperature. *Contributions to Mineralogy and Petrology* 174. <https://doi.org/10.1007/s00410-018-1538-2>
- Romanias, M.N., El Zein, A., Bedjanian, Y., 2012a. Heterogeneous Interaction of H<sub>2</sub>O<sub>2</sub> with TiO<sub>2</sub> Surface under Dark and UV Light Irradiation Conditions. *J. Phys. Chem. A* 116, 8191–8200. <https://doi.org/10.1021/jp305366v>

- Romanias, M.N., El Zein, A., Bedjanian, Y., 2012b. Reactive uptake of HONO on aluminium oxide surface. *Journal of Photochemistry and Photobiology A: Chemistry* 250, 50–57. <https://doi.org/10.1016/j.jphotochem.2012.09.018>
- Romanias, M.N., Ren, Y., Grosselin, B., Daële, V., Mellouki, A., Dagsson-Waldhauserova, P., Thevenet, F., 2020. Reactive uptake of NO<sub>2</sub> on volcanic particles: A possible source of HONO in the atmosphere. *Journal of Environmental Sciences*. <https://doi.org/10.1016/j.jes.2020.03.042>
- Romanias, M.N., Zeineddine, M.N., Gaudion, V., Lun, X., Thevenet, F., Riffault, V., 2016. Heterogeneous Interaction of Isopropanol with Natural Gobi Dust. *Environ. Sci. Technol.* 50, 11714–11722. <https://doi.org/10.1021/acs.est.6b03708>
- Romanias, M.N., Zeineddine, M.N., Riffault, V., Thevenet, F., 2017. Isoprene Heterogeneous Uptake and Reactivity on TiO<sub>2</sub>: A Kinetic and Product Study. *International Journal of Chemical Kinetics* 49, 773–788. <https://doi.org/10.1002/kin.21114>
- Schmauss, D., Keppler, H., 2014. Adsorption of sulfur dioxide on volcanic ashes. *American Mineralogist* 99, 1085–1094. <https://doi.org/10.2138/am.2014.4656>
- Shang, J., Li, J., Zhu, T., 2010. Heterogeneous reaction of SO<sub>2</sub> on TiO<sub>2</sub> particles. *Sci. China Chem.* 53, 2637–2643. <https://doi.org/10.1007/s11426-010-4160-3>
- Tang, M., Cziczo, D.J., Grassian, V.H., 2016. Interactions of Water with Mineral Dust Aerosol: Water Adsorption, Hygroscopicity, Cloud Condensation, and Ice Nucleation. *Chem. Rev.* 116, 4205–4259. <https://doi.org/10.1021/acs.chemrev.5b00529>
- Tang, M., Huang, X., Lu, K., Ge, M., Li, Y., Cheng, P., Zhu, T., Ding, A., Zhang, Y., Gligorovski, S., Song, W., Ding, X., Bi, X., Wang, X., 2017. Heterogeneous reactions of mineral dust aerosol: implications for tropospheric oxidation capacity. *Atmos. Chem. Phys.* 17, 11727–11777. <https://doi.org/10.5194/acp-17-11727-2017>
- Textor, C., Graf, H.-F., Herzog, M., Oberhuber, J.M., 2003. Injection of gases into the stratosphere by explosive volcanic eruptions. *Journal of Geophysical Research: Atmospheres* 108. <https://doi.org/10.1029/2002JD002987>
- Ullerstam, M., Vogt, R., Langer, S., Ljungstrom, E., 2002. The kinetics and mechanism of SO<sub>2</sub> oxidation by O<sub>3</sub> on mineral dust. *Phys. Chem. Chem. Phys.* 4, 4694–4699. <https://doi.org/10.1039/b203529b>
- Usher, C.R., Al-Hosney, H., Carlos-Cuellar, S., Grassian, V.H., 2002. A laboratory study of the heterogeneous uptake and oxidation of sulfur dioxide on mineral dust particles. *J.-Geophys.-Res.* 107, 4713. <https://doi.org/10.1029/2002JD002051>
- Witham, C., Webster, H., Hort, M., Jones, A., Thomson, D., 2012. Modelling concentrations of volcanic ash encountered by aircraft in past eruptions. *Atmospheric Environment, Volcanic ash over Europe during the eruption of Eyjafjallajökull on Iceland, April-May 2010* 48, 219–229. <https://doi.org/10.1016/j.atmosenv.2011.06.073>
- Wu, L.Y., Tong, S.R., Wang, W.G., Ge, M.F., 2011. Effects of temperature on the heterogeneous oxidation of sulfur dioxide by ozone on calcium carbonate. *Atmospheric Chemistry and Physics* 11, 6593–6605. <https://doi.org/10.5194/acp-11-6593-2011>
- Yu, Z., Jang, M., Park, J., 2017. Modeling atmospheric mineral aerosol chemistry to predict heterogeneous photooxidation of SO<sub>2</sub>. *Atmospheric Chemistry and Physics* 17, 10001–10017. <https://doi.org/10.5194/acp-17-10001-2017>
- Zein, A.E., Romanias, M.N., Bedjanian, Y., 2014. Heterogeneous Interaction of H<sub>2</sub>O<sub>2</sub> with Arizona Test Dust. *J. Phys. Chem. A* 118, 441–448. <https://doi.org/10.1021/jp409946j>
- Zeineddine, M.N., Romanias, M.N., Gaudion, V., Riffault, V., Thévenet, F., 2017. Heterogeneous Interaction of Isoprene with Natural Gobi Dust. *ACS Earth Space Chem.* 1, 236–243. <https://doi.org/10.1021/acsearthspacechem.7b00050>
- Zeineddine, M.N., Romanias, M.N., Riffault, V., Thévenet, F., 2018. Heterogeneous Interaction of Various Natural Dust Samples with Isopropyl Alcohol as a Probe VOC. *The Journal of Physical Chemistry A*. <https://doi.org/10.1021/acs.jpca.8b02034>

- Zhang, X., Zhuang, G., Chen, J., Wang, Y., Wang, X., An, Z., Zhang, P., 2006. Heterogeneous Reactions of Sulfur Dioxide on Typical Mineral Particles. *J. Phys. Chem. B* 110, 12588–12596. <https://doi.org/10.1021/jp0617773>
- Zhang, Y., Tong, S., Ge, M., Jing, B., Hou, S., Tan, F., Chen, Y., Guo, Y., Wu, L., 2018. The influence of relative humidity on the heterogeneous oxidation of sulfur dioxide by ozone on calcium carbonate particles. *Sci. Total Environ.* 633, 1253–1262. <https://doi.org/10.1016/j.scitotenv.2018.03.288>
- Zhou, L., Wang, W., Gai, Y., Ge, M., 2014. Knudsen cell and smog chamber study of the heterogeneous uptake of sulfur dioxide on Chinese mineral dust. *Journal of Environmental Sciences* 26, 2423–2433. <https://doi.org/10.1016/j.jes.2014.04.005>



**Chapter IV. *In-situ* monitoring of SO<sub>2</sub> uptake on natural v-dust by  
DRIFT spectroscopy: toward surface reaction pathways**

## Table of content of Chapter 4

1	Exploration of DRIFT spectra during SO <sub>2</sub> interaction with v-dust .....	139
2	From DRIFT spectra to surface reaction pathways .....	145
2.1	Uptake and reaction of SO <sub>2</sub> on Hagavatn under DRY conditions using DRIFT .....	145
2.2	Uptake and reaction of SO <sub>2</sub> on Hagavatn under WET conditions using DRIFT .....	148
2.3	Comparison of surface processes between dry and humid conditions.....	150
3	Conclusions and atmospheric implications based on DRIFT approach .....	152
	References.....	153

## List of Tables of Chapter 4

Table 1: Vibrational wavenumbers ( $\text{cm}^{-1}$ ) of sulfur-containing species adsorbed on v-dust and metal oxide ..... 144

## List of Figures of Chapter 4

- Figure 1: DRIFTS spectra of SO<sub>2</sub> uptake by Hagavattn v-dust at 0% RH and 296 K depicting evolution of bands for free surface OH groups (4000-3500 cm<sup>-1</sup>), adsorbed water (3500-2600 cm<sup>-1</sup>), physisorbed SO<sub>2</sub> (1385-1320 cm<sup>-1</sup>), sulfates/bisulfates (1320-975 cm<sup>-1</sup>), sulfites/bisulfites (975-716 cm<sup>-1</sup>) as a function of time: black line – before introduction of SO<sub>2</sub>, red line- after 1.5 h of exposure to SO<sub>2</sub>, blue line- after 2.5 h of exposure to SO<sub>2</sub>, green line- after 22 h of exposure to SO<sub>2</sub>, yellow line- after 71 h of exposure to SO<sub>2</sub>..... 140
- Figure 2: DRIFTS spectra of SO<sub>2</sub> uptake on Hagavattn v-dust at 30% RH and 296 K depicting evolution of bands for free surface OH groups (4000-3500 cm<sup>-1</sup>), adsorbed water (3500-2600 cm<sup>-1</sup>), SH groups (2600-2400 cm<sup>-1</sup>), physisorbed SO<sub>2</sub> (1367-1320), sulfates/bisulfates (1302-1050 cm<sup>-1</sup>), sulfites/bisulfites (1053-700 cm<sup>-1</sup>) as a function of time: black line – before introduction of SO<sub>2</sub>, red line- after 1.5 h of exposure to SO<sub>2</sub>, blue line- after 2.5 h of exposure to SO<sub>2</sub>, green line- after 22 h of exposure to SO<sub>2</sub>, yellow line- after 71 h of exposure to SO<sub>2</sub>. ..... 141
- Figure 3: Integrated absorbance for (a) sulfites/bisulfites, (b) sulfates/bisulfates as a function of time under 0% RH and 296K. Upper graph: sulfites/bisulfites are stabilized after 22 hours of exposure. The solid line is an exponential fitting of experimental results to better display the observed trends. Lower graph: A linear growth of sulfates/bisulfates with time is noticed; note that the peak is stable for the first couple of hours and then keeps increasing in a linear fashion. The solid line is the linear fit of experimental results. ... 148
- Figure 4: Integrated absorbance for (a) free hydroxyl groups, (b) physisorbed SO<sub>2</sub>, (c) sulfites/bisulfites, (d) sulfates/bisulfates as a function of time under 30% RH and 296 K. a) The free OH groups get consumed very fast at the beginning of the experiment and reach a minimum at 1.5 hours, then the consumption of OH groups decreases and reaches a stable level at 2.5 hr. The solid line is an empirical fitting of experimental results to better display the observed trends. b) The peak for physisorbed SO<sub>2</sub> is quite noisy but increases slowly and remains weak for the duration of the experiment. c) Sulfites/bisulfites grow rapidly and almost linearly for the first 1.5 hr and then stabilize. The solid line is an exponential fitting of experimental results to better display the observed trends. d) The peak for sulfates/bisulfates is stable at low values for the first 2.5 hr, increases in the linear fashion from 2.5 to about 40 hr, and then starts fluctuating. The solid line is the linear fit of experimental results. .... 150
- Figure 5: Schematic representation of SO<sub>2</sub> reaction pathways at the surface of v-dust. Reactions occurring under dark and dry conditions are shown in black; reactions promoted under humid conditions are shown in blue. .... 152

While flow-tube reactor monitors changes in the gas-phase concentration, DRIFTS focuses on changes on the solid phase. It is commonly used to study fine particles and powders, and can be used to investigate adsorption of molecules on solid surfaces. In this case spectra are collected as difference spectra with the unexposed solid as background. As the reaction proceeds, growing or decreasing infrared absorption peaks can be attributed to the species formed or consumed on the surface. Infrared spectroscopy based on light diffuse reflectance offers information about the vibrational modes associated with stretching, bending, and rocking motions of the adsorbed molecules. However, in order to monitor these vibrations the sample has to have high enough reflectance to insure an adequate signal in response to changes in the adsorbed phase. Moreover, the surface concentration needs to be high enough due to the moderate sensitivity of the technique. If the sample highly absorbs incident light, which is the case of v-dust samples, it is usually diluted in a non-absorbent matrix, such as KBr. In our case, however, this type of matrix could not be used because of the interactions of KBr with SO<sub>2</sub> and thus the use of pure v-dust was required. The background obtained for each v-dust under dry conditions showed that all of them absorb light strongly and, as a result, a weak diffused IR signal was recorded in response to changes in the adsorbed phase. To study the adsorption of SO<sub>2</sub> on v-dust, backgrounds of five samples were taken to choose the least absorbent varieties. In comparison with other v-dusts the backgrounds for Hagavatn and Eyjafjallajökull show higher reflectances in the wavenumber range from 800 to 1350 cm<sup>-1</sup> where sulfite and sulfate species usually absorb. Because of its higher reflectance and higher specific surface area, Hagavatn v-dust was selected as the most appropriate sample for DRIFTS experiments. Besides, results obtained from the flow-tube studies showed similar trends in SO<sub>2</sub> adsorption by the selected v-dusts based on gas-phase monitoring of SO<sub>2</sub>, i.e. rapid consumption of SO<sub>2</sub> gas at the initial stage of surface exposure followed by a steady state removal of the probe molecule. Furthermore, in the flow-tube experiments both steady state uptake coefficients ( $\gamma_{ss}$ ) and initial amounts of molecules taken up ( $N_s$ ) were demonstrated to increase as a function of *RH* and, with the exception of Eyjafjallajökull, UV light. Therefore, it appeared justified to choose one dust as a representative sample to study the mechanism of product formation on the surface of aerosols. **Aiming to further investigate the results obtained from the flow-tube study and to deeper assess the role of humidity on the uptake process, the DRIFTS experiments were performed under dry conditions and 30% *RH* using Hagavatn as a representative v-dust sample.**

## 1 Exploration of DRIFT spectra during SO<sub>2</sub> interaction with v-dust

Figure 1 and Figure 2 show DRIFT typical spectra of Hagavatn v-dust at increasing SO<sub>2</sub> exposure time intervals at room temperature under 0% and 30% *RH* respectively. In order to provide a detailed

understanding of the spectra recorded during SO<sub>2</sub> interaction with Hagavath sample, Table 1 introduces the assignment of peaks of different adsorbed sulfur-containing species as well as water and hydroxyl groups on the surface of v-dust investigated, and different metal oxides found in the literature. The construction of this table results from a detailed literature survey of the IR signature of the species of interest.

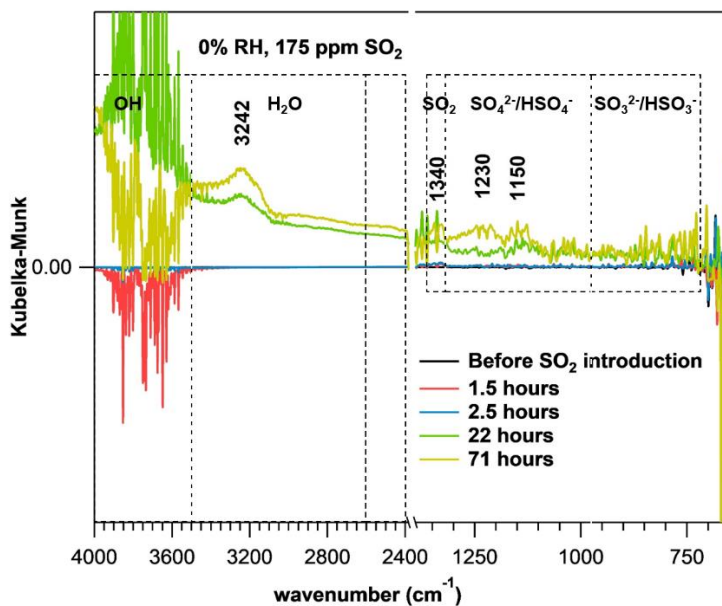


Figure 1: DRIFTS spectra of SO<sub>2</sub> uptake by Hagavath v-dust at 0% RH and 296 K depicting evolution of bands for free surface OH groups (4000-3500 cm<sup>-1</sup>), adsorbed water (3500-2600 cm<sup>-1</sup>), physisorbed SO<sub>2</sub> (1385-1320 cm<sup>-1</sup>), sulfates/bisulfates (1320-975 cm<sup>-1</sup>), sulfites/bisulfites (975-716 cm<sup>-1</sup>) as a function of time: black line – before introduction of SO<sub>2</sub>, red line- after 1.5 h of exposure to SO<sub>2</sub>, blue line- after 2.5 h of exposure to SO<sub>2</sub>, green line- after 22 h of exposure to SO<sub>2</sub>, yellow line- after 71 h of exposure to SO<sub>2</sub>.

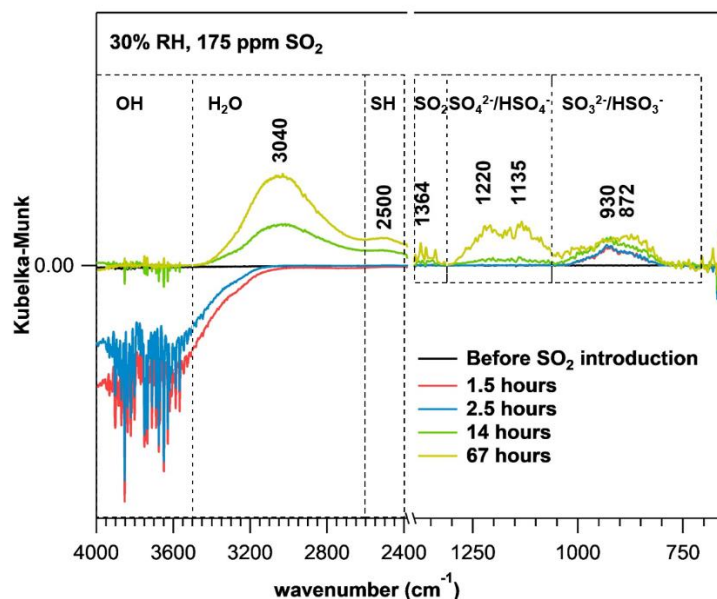


Figure 2: DRIFTS spectra of  $\text{SO}_2$  uptake on Hagavath v-dust at 30% RH and 296 K depicting evolution of bands for free surface OH groups ( $4000\text{-}3500\text{ cm}^{-1}$ ), adsorbed water ( $3500\text{-}2600\text{ cm}^{-1}$ ), SH groups ( $2600\text{-}2400\text{ cm}^{-1}$ ), physisorbed  $\text{SO}_2$  ( $1367\text{-}1320$ ), sulfates/bisulfates ( $1302\text{-}1050\text{ cm}^{-1}$ ), sulfites/bisulfites ( $1053\text{-}700\text{ cm}^{-1}$ ) as a function of time: black line – before introduction of  $\text{SO}_2$ , red line- after 1.5 h of exposure to  $\text{SO}_2$ , blue line- after 2.5 h of exposure to  $\text{SO}_2$ , green line- after 22 h of exposure to  $\text{SO}_2$ , yellow line- after 71 h of exposure to  $\text{SO}_2$ .

Negative and positive absorption peaks in the area from  $4000$  to  $3500\text{ cm}^{-1}$  are visible in both Figure 1 and Figure 2, i.e. irrespectively of the RH level. They correspond to the free OH groups that are naturally present on the surface of v-dust (Hair, 1975). These groups are attached to the surface atoms, such as Si for example, and can be either completely isolated or hydrogen-bonded to each other (Hair, 1975). Adsorption of molecules containing a lone-pair of electrons is often associated with isolated surface OH groups, while neighboring hydrogen-bonded surface OH groups are involved in the adsorption of water (Hair, 1975), (Nanayakkara et al., 2012). The exact assignment of each individual peak is not possible due to the complex response reflecting slightly different vibrational energies of OH groups bonded to different minerals composing the v-dust. A peak from  $3500$  to  $2600\text{ cm}^{-1}$  and another peak from  $1800$  to  $1400\text{ cm}^{-1}$  centered at  $1620\text{ cm}^{-1}$  (not displayed) are attributed to vibration modes in molecular water (Hair, 1975).

A weak broad peak from  $2600$  to  $2400\text{ cm}^{-1}$ , visible under humid conditions, could be assigned to the S-H stretch vibration of the  $\text{HSO}_3^-$  bisulfite species that is only found in the literature as a theoretical value calculated by Zhang et al. for aqueous solution and reported to be in the range of  $2620$  to  $2450\text{ cm}^{-1}$  (Zhang and Ewing, 2002). This peak is not visible under dry condition. Sulfur-containing products appear in the area from  $1385$  to  $700\text{ cm}^{-1}$  under humid conditions and from  $1367$  to  $716\text{ cm}^{-1}$  under dry conditions.

Spectra under humid conditions are better resolved and several peaks can be distinguished: 3040, 2500, 1364, 1220, 1135, 930 and 872  $\text{cm}^{-1}$ . Peaks under dry conditions are much noisier, nevertheless the following peaks are observed: 3242, 1340, 1230 and 1150  $\text{cm}^{-1}$ . A double peak centered at 1364  $\text{cm}^{-1}$  under humid conditions and at 1340  $\text{cm}^{-1}$  under dry conditions appears rapidly upon exposure of the surface to  $\text{SO}_2$  gas and disappears right away from the spectra after ceasing the  $\text{SO}_2$  flow. It was therefore assigned to the weakly, reversibly physisorbed  $\text{SO}_2$  species. The peak corresponds well to the literature values for  $\text{SO}_2$  adsorption under dry conditions on the surfaces of aluminum, magnesium or titanium oxides identified in previous studies at 1330  $\text{cm}^{-1}$  and its gas-phase value of 1362  $\text{cm}^{-1}$  (Nanayakkara et al., 2012), (Goodman et al., 2001). Another band appears rapidly upon exposure of  $\text{SO}_2$  to the surface between 1053 and 700  $\text{cm}^{-1}$  under humid conditions. A corresponding band between 975 and 716  $\text{cm}^{-1}$  under dry conditions takes more time to develop and is hard to interpret since its intensity is almost at the limit of detection of the DRIFTS instrument. The attribution of this band is based on the previous assignments of  $\text{SO}_2$  adsorption on the surface of different metal oxides found in the literature and corresponds to the stretching motion of sulfite and bisulfite species that are bonded to the surface in a monodentate or bidentate mode. Different coordination environments as well as heterogeneous nature of  $\nu$ -dust contribute to the broadening of the band (Usher et al., 2002). In particular, Goodman et al (Goodman et al., 2001), Usher et al. (Usher et al., 2002) and Zhang et al. (Zhang et al., 2006) assigned the band between 1100 to 850  $\text{cm}^{-1}$  to adsorbed sulfite and bisulfite on  $\alpha\text{-Al}_2\text{O}_3$  and MgO. Li et al. (Li et al., 2006) and Wu et al. (Wu et al., 2011) assigned a 1000-900  $\text{cm}^{-1}$  band on  $\text{CaCO}_3$  to a stretching vibration of sulfite.

A peak from 1200 to 800  $\text{cm}^{-1}$  on  $\text{TiO}_2$  was assigned to sulfite and bisulfite species by Nanayakkara et al. (Wu et al., 2011). On hematite particles Wang et al. assigned to sulfites a peak between 950 and 800  $\text{cm}^{-1}$  under dry conditions and a series of peaks from 1050 to 900  $\text{cm}^{-1}$  under humid conditions (Wang et al., 2018b).

Finally, a band from 1320 to 975  $\text{cm}^{-1}$  with features at 1230 and 1150  $\text{cm}^{-1}$  in dry conditions and from 1302 to 1055  $\text{cm}^{-1}$  with features at 1220 and 1135  $\text{cm}^{-1}$  under humid conditions was attributed to sulfate and bisulfate species. The assignment agrees well with the results published previously, where sulfates/bisulfates were found around 1300-1100  $\text{cm}^{-1}$  on  $\alpha\text{-Al}_2\text{O}_3$  and MgO (Usher et al., 2002), (Zhang et al., 2006); between 1240 and 1012  $\text{cm}^{-1}$  on  $\text{CaCO}_3$  with features at 1198, 1127, and 1090  $\text{cm}^{-1}$  (Wu et al., 2011), (Li et al., 2006). Sulfates were reported between 1300 and 1100  $\text{cm}^{-1}$  on  $\text{TiO}_2$  (Nanayakkara et al., 2012), (Shang et al., 2010); and at 1220  $\text{cm}^{-1}$  on  $\text{Fe}_2\text{O}_3$  (Wang et al., 2018b).

Just as sulfites, sulfates can be bonded to the surface in bidentate or monodentate modes (Jiang et al., 2010). A peak centered at 1220  $\text{cm}^{-1}$  under humid conditions and at 1230  $\text{cm}^{-1}$  under dry conditions



could be attributed to the formation of bisulfate species (Wang et al., 2018a). The process of sulfate/sulfite formation is explained later in the reaction mechanism section.

Molecular species (wavenumbers are expressed in $\text{cm}^{-1}$ )	V-dust (this work)	$\text{Si}_2\text{O}_3$	$\text{Al}_2\text{O}_3$	MgO	$\text{TiO}_2$	$\text{CaCO}_3$	$\text{Fe}_2\text{O}_3$	Theoretical calculations
SH stretch of $\text{HSO}_3^-$	2600-2400	2600-2400 (Hair, 1975)						2620 to 2450 (Zhang and Ewing, 2002)
$\text{SO}_2$	1364, 1340		1330, 1149 (Goodman et al., 2001)	1330, 1149 (Goodman et al., 2001)	1139, 1325 (Nanayakkara et al., 2012)		1400 (Nanayakkara et al., 2012)	
$\text{HSO}_3^-/\text{SO}_3^{2-}$	1053-700 975-716		1200-900 (Goodman et al., 2001) 1100-850 (Zhang et al., 2006)		1200-800 (Nanayakkara et al., 2012) 1080 (Shang et al., 2010)		Dry: 950-800 Humid: 1050-900 (Wang et al., 2018b)	
$\text{SO}_3^{2-}$				1125-800 (Goodman et al., 2001)	Monodentate: 1033, 971, 923 (Nanayakkara et al., 2012) Bidentate: 1006, 886 (Nanayakkara et al., 2012)	1000-900 (Li et al., 2006) 1000-885 (Wu et al., 2011)	Dry: 891 (Wang et al., 2018b) Humid: 981 (Wang et al., 2018b)	
$\text{HSO}_3^-$					1077 (Nanayakkara et al., 2012)			1054, 1154, 1219 (Zhang and Ewing, 2002)
$\text{HSO}_4^-/\text{SO}_4^{2-}$	1320-975 1302-1055		1245, 1170 (Usher et al., 2002)	1150, 1050 (Usher et al., 2002)		1240-1012 (Wu et al., 2011)		
$\text{HSO}_4^-$	1220, 1230						1219 (Wang et al., 2018a)	
$\text{SO}_4^{2-}$			1300-1100 (Zhang et al., 2006)	1300-1100 (Zhang et al., 2006)	1361, 1297, 1172, 1116, 1050, 1000 (Nanayakkara et al., 2012) 1300-1100 (Shang et al., 2010)	1130 (Li et al., 2006)	Dry: 1339-1014 Humid: 1208-1222 (Wang et al., 2018b)	
free OH groups	4000-3500	4000-3500 (Hair, 1975)	3748, 3707 (Goodman et al., 2001)		3800-3600 (Nanayakkara et al., 2012) 1666, 3628 (Shang et al., 2010)		3704 (Wang et al., 2018b)	
OH groups of acids							3447, 3548 (Wang et al., 2018b)	3622 (Zhang and Ewing, 2002)
molecular water	3500-2600 1400-1800	3450, 1630 (Hair, 1975)	3524, 3296 (Goodman et al., 2001)		3160, 1654 (Shang et al., 2010)		3208, 1642 (Wang et al., 2018b)	

Table 1: Vibrational wavenumbers ( $\text{cm}^{-1}$ ) of sulfur-containing species adsorbed on v-dust and metal oxide

## 2 From DRIFT spectra to surface reaction pathways

Changes in the DRIFT spectra of the surface of Hagavattn v-dust are clearly seen upon introduction of SO<sub>2</sub> (Figure 1 and 2). In comparison with the studies of the interaction of SO<sub>2</sub> with high reflectance pure metal oxides reported earlier by different authors, it appears that DRIFT peaks are weaker, most probably due to low sensitivity when dealing with dark natural v-dusts where the reflectance of the infrared light is limited (Zhang et al., 2006), (Usher et al., 2002), (Goodman et al., 2001), (Li et al., 2006), (Wu et al., 2011), (Nanayakkara et al., 2012), (Shang et al., 2010), (Wang et al., 2018b). Nonetheless, the time evolution of five selected peaks corresponding to different key species, such as free OH groups, molecular water, physisorbed SO<sub>2</sub>, sulfites/bisulfites and sulfates/bisulfates are followed.

### 2.1 Uptake and reaction of SO<sub>2</sub> on Hagavattn under DRY conditions using DRIFT

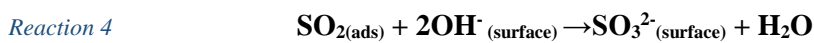
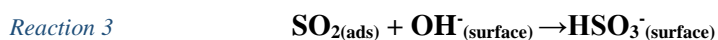
From our flow-tube experiments presented in Chapter 3 it is evidenced that SO<sub>2</sub> gas is massively lost from the gas phase upon its exposure to the v-dust surface. Interestingly, the first peaks that appear in the DRIFT spectra after introduction of SO<sub>2</sub> gas are positive peaks for physisorbed SO<sub>2</sub> gas and negative peaks for free OH groups (Figure 1). Note that although the sample has been thermally pretreated and the experiment is performed under dry conditions, surface OH groups are present on the surface of the sample. The complete dehydroxylation of the surface would have required stronger thermal pretreatment. The loss of surface free OH groups reaches its local minimum at around 1.5 hr of exposure to SO<sub>2</sub> before returning to its initial pre-exposed level where it starts fluctuating around zero. The peak for SO<sub>2</sub> gas is stable, but hard to interpret due to its small size and overlap with a much more pronounced peak for bulk water. Bulk water peak is highly unstable. The disappearance of free OH groups and appearance of physisorbed SO<sub>2</sub> suggest that in the first instants of the reaction, SO<sub>2</sub> gas gets weakly bonded to hydroxyl groups of the surface as first proposed by Datta et al. and later proved by theoretical calculations by Lo et al. for  $\gamma$ -alumina (Datta et al., 1985), (Lo et al., 2010). Maters et al. suggested that due to the weakly acidic nature of SO<sub>2</sub> gas, its uptake is likely to happen on strongly basic sites affiliated with alkaline and alkaline earth metals on the surface of the volcanic glass (-K-OH, -Mg-OH, -Ca-OH, Mg-OH) (Maters et al., 2017). At the same time it is also possible for the SO<sub>2</sub> gas to get adsorbed on metallic Lewis acid sites of mineral phase as proposed by Wang et al. (Wang et al., 2018a). Hence, the first interaction of SO<sub>2</sub> gas with the surface under dry conditions is its distribution on different sites of the v-dust leading to a reversible physisorption of SO<sub>2</sub>, as indicated by subscript (*ads*) (Reaction 1). Throughout the manuscript the chemisorbed species or chemical groups that form a chemical bond with the surface are indicated as (*surface*).



Physisorbed SO<sub>2</sub> can then participate in reactions leading to chemisorbed species. Sulfites and sulfates, under dry conditions first appear after several hours of exposure probably due to a lack of sensitivity of our DRIFT setup to address the dark system of interest. Sulfites can be formed on the lattice oxygen sites that can be viewed as Lewis basic sites (Wang et al., 2018a) as in Reaction 2.

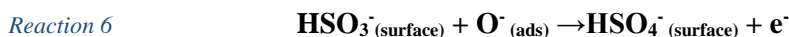
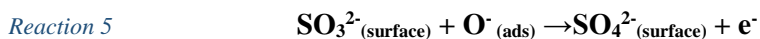


Alternatively, sulfites can be formed in the presence of hydroxyl groups as SO<sub>2</sub> can react with either one hydroxyl group to form bisulfite (Reaction 3) or two neighboring hydroxyl groups to form sulfite and water (Reaction 4) (Wang et al., 2018a). Surface hydroxyl groups themselves can be bonded to a single metal atom or bridge two, creating different environments for interactions with SO<sub>2</sub> (Ullerstam et al., 2002).



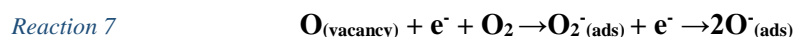
Chemisorption of SO<sub>2</sub> gas on oxide anions (O<sup>2-</sup>) and hydroxyl groups of volcanic ash and glass leading to the formation of sulfites and bisulfites was suggested earlier by Maters et al. and detection of sulfites in the leachates confirmed the conversion (Maters et al., 2017).

From Figure 3, that shows time evolutions of sulfites and sulfates, it can be observed that, under dry conditions, sulfites (SO<sub>3</sub><sup>2-</sup>) get completely stabilized after 22 hours of exposure, but sulfates (SO<sub>4</sub><sup>2-</sup>) keep growing linearly, suggesting that sulfites are the intermediate species in the oxidation of SO<sub>2</sub> to sulfates. Oxidation of sulfites to sulfates on the surface of volcanic glass was observed by Farges et al. (Farges et al., 2009). Sulfites can be oxidized to sulfates via several pathways. Active oxygen derived from molecular oxygen adsorbed on the active sites (Reaction 7) can oxidize sulfites to sulfates and bisulfites to bisulfates as in Reaction 5 and Reaction 6 (Wang et al., 2018a).



Contrary to our observations and to results reported by Shang et al. (Shang et al., 2010), who also noticed a stable rate of sulfate production on the surface of titanium dioxide particles in the presence of oxygen, Usher et al. (Usher et al., 2002) noted complete saturation of mineral oxide surfaces with SO<sub>2</sub> gas and observed no sulfate formation even upon exposure of SO<sub>2</sub>-treated surface to air and oxygen. It could be due to the fact that the minerals under investigation were not able to convert molecular oxygen into active oxygen under the specific experimental conditions of these measurements.

Reaction 7 was reported to enable the conversion of sulfites to sulfates on the surface of mineral phase by converting molecular oxygen into active oxygen, but a similar process can be expected to happen on the amorphous fraction of the volcanic ash due to the high defect population on silicate glasses (A Leed and Pantano, 2003), (Farges et al., 2009). Noticeably, reaction proceeds in the absence of light (Baltrusaitis et al., 2007).

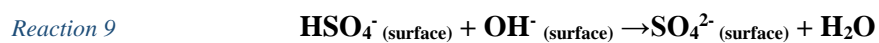


where  $e^-$  is a conductive electron trapped in the vacant oxygen site on the surface of some oxides that are prone to having defect sites, such as on the surface of  $Fe_2O_3$ , for example (Wang et al., 2018b), (Baltrusaitis et al., 2007).

Additionally, certain metal centers that can be readily reduced, such as  $Fe^{3+}$  to  $Fe^{2+}$ , contribute to the formation of sulfates from bisulfites as per Reaction 8 (Wang et al., 2018a).



Finally, bisulfates can be oxidized to sulfates by hydroxyl groups as per Reaction 9 (Wang et al., 2018a).



On ceasing the gas flow and flushing the system for 6 hours, the peak for sulfites decreases due to its oxidation as per Reaction 5, Reaction 6 and Reaction 8, while the peak for sulfates increases for a couple of hours before getting stable, at the same time slightly changing its shape. The peak centered at  $1230\text{ cm}^{-1}$  gets smaller in comparison with the peak at  $1135\text{ cm}^{-1}$  suggesting indeed further conversion of bisulfates to sulfates. A decrease in sulfite peak with simultaneous increase in the sulfate peak upon cutting off  $SO_2$  supply and addition of  $O_3$  was observed by Li et al. (Li et al., 2006). Thus, sulfates appear to be the final product of oxidation of  $SO_2$  gas and they keep being formed on the surface as long as there are sulfites available for oxidation. Sulfates were also reported as a final irreversible product of the interaction of  $SO_2$  gas with volcanic glass by Farges et al. and by Maters et al. (Farges et al., 2009), (Maters et al., 2017).

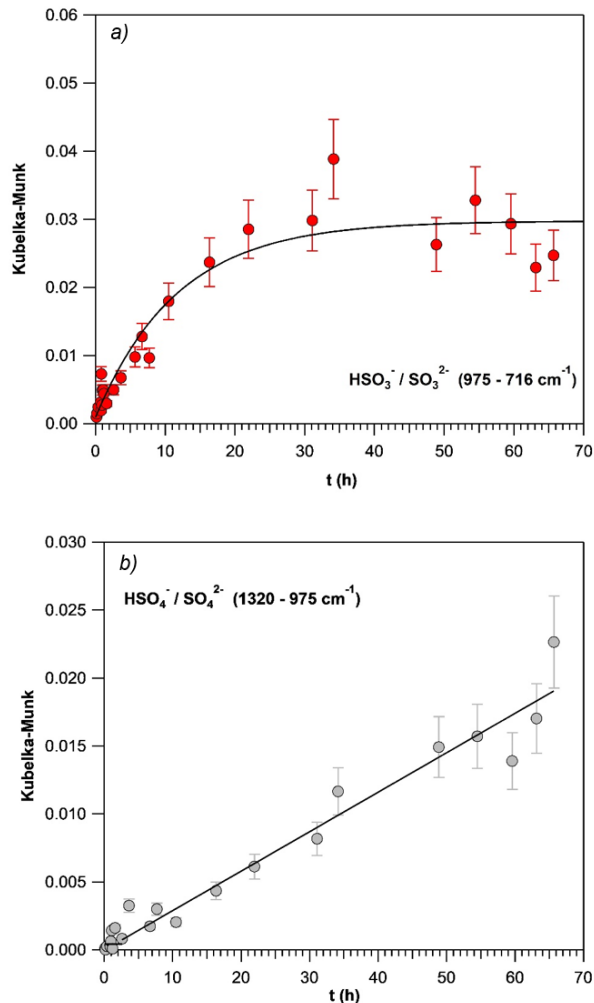
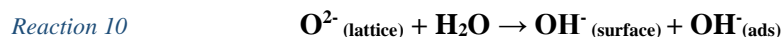


Figure 3: Integrated absorbance for (a) sulfites/bisulfites, (b) sulfates/bisulfates as a function of time under 0% RH and 296K. Upper graph: sulfites/bisulfites are stabilized after 22 hours of exposure. The solid line is an exponential fitting of experimental results to better display the observed trends. Lower graph: A linear growth of sulfates/bisulfates with time is noticed; note that the peak is stable for the first couple of hours and then keeps increasing in a linear fashion. The solid line is the linear fit of experimental results.

## 2.2 Uptake and reaction of $\text{SO}_2$ on Hagavatn under WET conditions using DRIFT

After exposure of v-dust to  $\text{SO}_2$  gas under humid conditions the following changes are observed in the analysis of DRIFT spectra as seen in Figure 2 and Figure 4. At the very beginning of the experiment, the free OH groups get consumed and reach a minimum after 1.5 hours exposure to  $\text{SO}_2$ , at the same time sulfites form rapidly and at an almost linear rate. The peak for physisorbed  $\text{SO}_2$  increases much slower and the peak remains small for the duration of the experiment. The initial time period corresponds well with the reaction mechanism proposed by Wang et al. in Reaction 3 and Reaction 4 both of which require consumption of free OH groups to produce sulfites and bisulfites. From 1.5 to 2.5 hours consumption of OH groups slows down and finally reaches a stable level. It is important to stress out that, when working under

humid conditions, surface OH groups are continuously regenerated. The mechanism for metal oxide surface hydroxylation proposed by Tamura et al. assumes that an exposed oxygen center of the metal oxide lattice acts as Lewis base with water to form a surface terminal hydroxyl group and a hydroxide ion as shown in Reaction 10 (Tamura et al., 2001). In other words, a surface oxide ion gets neutralized by water to become  $\text{OH}^-_{(\text{surface})}$ , while water itself loses a proton to become hydroxide ion  $\text{OH}^-_{(\text{ads})}$ .



Sulfates/bisulfates are first observed in the DRIFT spectra at 2.5 hours exposure to  $\text{SO}_2$ . Sulfites/bisulfites are transformed to sulfates/bisulfates by three different pathways shown in Reaction 5, Reaction 6, and Reaction 8 (Wang et al., 2018a). In addition, bisulfates react with hydroxyl groups to form sulfates (Reaction 9). Unlike sulfites that reach a stable level within 2.5 hours, a peak for sulfates linearly increases for about 40 hours and then starts fluctuating, making it difficult to evaluate whether the amount of sulfates on the surface keeps growing or reaches a stable level. A peak for molecular water is hard to evaluate at 30% RH as water is being constantly supplied in large excess. Initially, the peak for water seems to decrease, which could be due to the competition with  $\text{SO}_2$  gas molecules for active sites on the surface (Figure 4). At 14 hours the water peak stabilizes at a positive value, indicating that the surface is now storing more  $\text{H}_2\text{O}$  molecules than before introduction of  $\text{SO}_2$  gas (Figure 4). Formation of sulfite and sulfate species could have changed equilibrium for adsorption of water on the dust surface (*e.g.* due to chemical changes of the mineral structure that increase the hygroscopicity of the samples). Particularly, it was argued that adsorption of bidentate sulfate on the surface of Fe-Mn/ $\text{TiO}_2$  catalyst increases the Lewis acid character of the metal ion to which it is attached, thus potentially favoring the adsorption of water on the metal center (Jiang et al., 2010). Finally, when the flow of  $\text{SO}_2$  is stopped, the peak for sulfite gradually decreases while the peak for sulfate increases for a couple of hours, stabilizes and stays in the spectra for at least six hours. Like under dry conditions the peak for bisulfates/sulfates changes its shape by decreasing the peak associated with bisulfates (at  $1220 \text{ cm}^{-1}$ ) suggesting its conversion to sulfates.

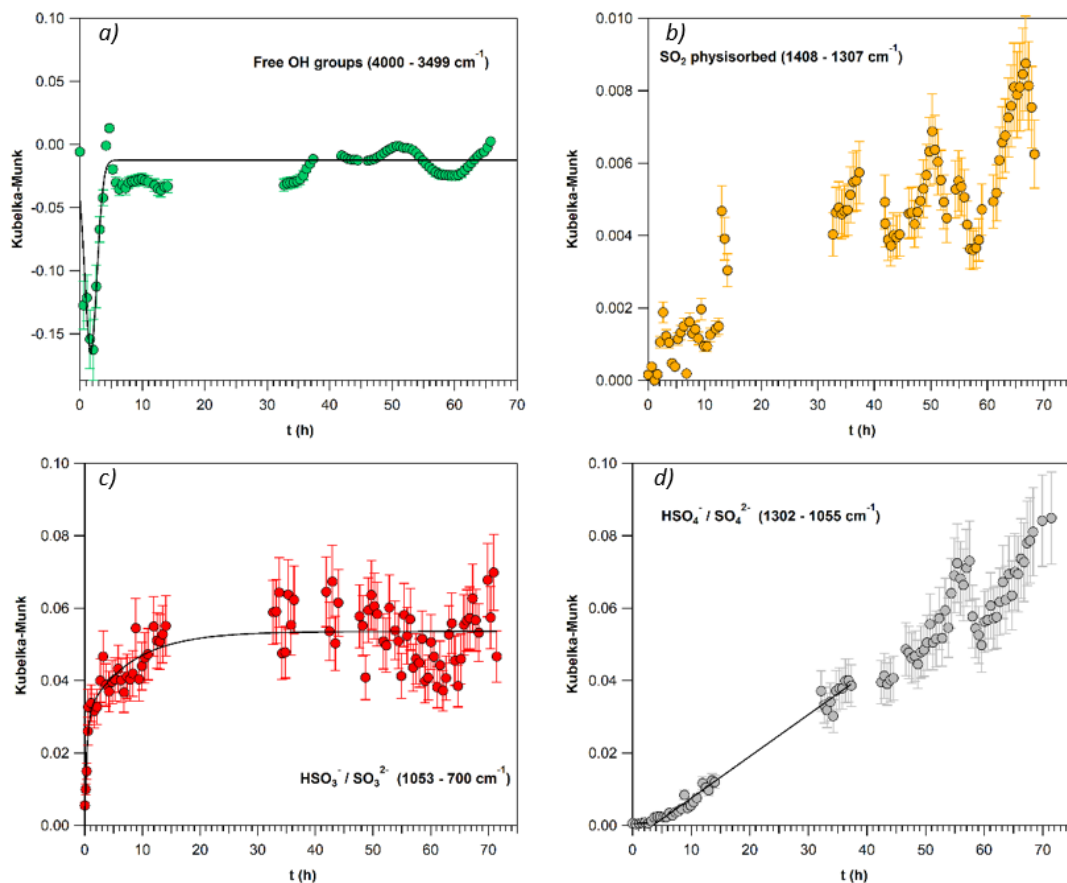


Figure 4: Integrated absorbance for (a) free hydroxyl groups, (b) physisorbed  $\text{SO}_2$ , (c) sulfites/bisulfites, (d) sulfates/bisulfates as a function of time under 30% RH and 296 K. a) The free OH groups get consumed very fast at the beginning of the experiment and reach a minimum at 1.5 hours, then the consumption of OH groups decreases and reaches a stable level at 2.5 hr. The solid line is an empirical fitting of experimental results to better display the observed trends. b) The peak for physisorbed  $\text{SO}_2$  is quite noisy but increases slowly and remains weak for the duration of the experiment. c) Sulfites/bisulfites grow rapidly and almost linearly for the first 1.5 hr and then stabilize. The solid line is an exponential fitting of experimental results to better display the observed trends. d) The peak for sulfates/bisulfates is stable at low values for the first 2.5 hr, increases in the linear fashion from 2.5 to about 40 hr, and then starts fluctuating. The solid line is the linear fit of experimental results.

### 2.3 Comparison of surface processes between dry and humid conditions

Although DRIFTS is a semi-quantitative technique, it is feasible to compare the results obtained under dry and humid conditions. Thus, in comparison with the reaction under dry conditions, the reaction under humid conditions is much more pronounced, resulting in both faster reaction rates and higher integration values obtained for all sulfur containing species involved. This observation is in line with the results obtained from the flow-tube experiments, where significantly higher steady state uptakes and initial number of molecules taken up were determined for  $\text{SO}_2$  under humid compared to dry conditions.

Faster sulfite formation is most likely related to the dramatic increase in the amount of hydroxyl groups covering the surface under humid conditions, driving the sulfite and bisulfite formation through



Reaction 3 and Reaction 4. Indeed, under humid conditions the amount of hydroxyl groups lost in the first minutes is much larger than under dry conditions, thus adsorbed SO<sub>2</sub> molecules convert rapidly to form sulfites (Figure 1 and Figure 2). Huang et al. reported that the rate of sulfate formation on the surface of Arizona test dust increased with *RH* and reached its maximum at 70% *RH* (Huang et al., 2015). The importance of surface OH groups in the heterogeneous oxidation of SO<sub>2</sub> gas was discussed by Zhang et al. who compared basic, neutral and acidic Al<sub>2</sub>O<sub>3</sub> in their ability to oxidize SO<sub>2</sub> and noted that basic Al<sub>2</sub>O<sub>3</sub> was much more efficient due to its higher concentration of hydroxyl groups on the surface (Zhang et al., 2006). It was also suggested that reactivity of different oxides to SO<sub>2</sub> uptake could be predicted by evaluating their intrinsic ability to form surface hydroxyl groups. Thus, metal oxides that have empty or half-empty d atomic orbitals, such as Al<sub>2</sub>O<sub>3</sub>, easily adsorb molecular oxygen and gaseous water and show excellent performance in the reactions with SO<sub>2</sub> while metals with full d orbitals, such as MnO<sub>2</sub>, show weak reactivity (Zhang et al., 2006). Reaction of SO<sub>2</sub> gas with the lattice oxygen as in Reaction 2 seems to proceed much slower. The observation is in line with the results of experiments on dehydroxylated surfaces that show very little reactivity towards product formation, suggesting low reactivity of lattice oxygen groups (Nanayakkara et al., 2012). Absence of S-H stretch from the spectra of the v-dust under dry conditions could be due to the fact that bisulfites and bisulfates are formed in much lower quantities than in humid conditions.

### 3 Conclusions and atmospheric implications based on DRIFT approach

DRIFTS analysis enabled us to propose a mechanistic scheme of  $\text{SO}_2$  uptake on the volcanic dust. The DRIFTS data indicate the presence of sulfite and sulfate ions on the surface and addresses their temporal dynamics. Hydroxyl groups play a major role in the uptake and conversion of  $\text{SO}_2$  gas to sulfites, while oxidizing agents in the form of active oxygen, metal centers and/or hydroxyl groups are involved in their conversion to sulfates. Furthermore, sulfates formed on the surface of v-dust are stable chemisorbed species, not desorbed even after flushing for several hours in the absence of  $\text{SO}_2$  gas. Figure 5 overviews the reactional pathways proposed under dry and humid conditions.

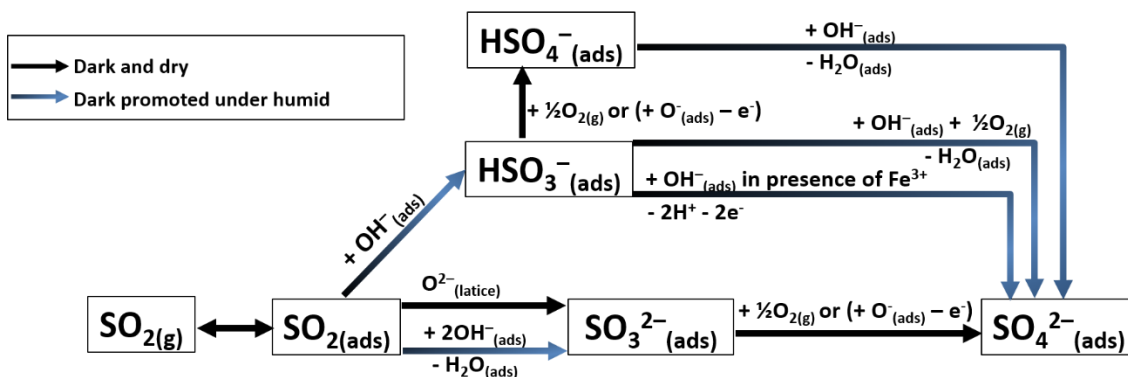


Figure 5: Schematic representation of  $\text{SO}_2$  reaction pathways at the surface of v-dust. Reactions occurring under dark and dry conditions are shown in black; reactions promoted under humid conditions are shown in blue.

Having identified the species formed on the surface and the important role RH plays in the transformation of  $\text{SO}_2$  gas to sulfites and sulfates it was imperative to (i) quantify the amount of sulfites and sulfates formed on the surface and (ii) clarify the trend of sulfate formation under humid conditions in order to find out when sulfates reach a stable level and if they actually reach it. In order to reach these objectives it was decided to investigate the potentialities of HPLC method. In the light of the fact that no suitable method was identified in the literature to accomplish this goal, a new method was developed and validated. Development and validation of an HPLC method for determination of sulfites and sulfates on the surface of mineral atmospheric samples is described in Chapter 5 together with its application to natural samples.

## References of Chapter 4

- A Leed, E., Pantano, C., 2003. Computer Modeling of Water Adsorption on Silica and Silicate Glass Fracture Surfaces. *Journal of Non-Crystalline Solids* 325, 48–60. [https://doi.org/10.1016/S0022-3093\(03\)00361-2](https://doi.org/10.1016/S0022-3093(03)00361-2)
- Baltrusaitis, J., Cwiertny, D.M., Grassian, V.H., 2007. Adsorption of sulfur dioxide on hematite and goethite particle surfaces. *Phys. Chem. Chem. Phys.* 9, 5542–5554. <https://doi.org/10.1039/B709167B>
- Datta, A., Cavell, R.G., Tower, R.W., George, Z.M., 1985. Claus catalysis. 1. Adsorption of SO<sub>2</sub> on the alumina catalyst studied by FTIR and EPR spectroscopy. *J. Phys. Chem.*; (United States) 89:3. <https://doi.org/10.1021/j100249a014>
- Farges, F., Keppler, H., Flank, A.M., Lagarde, P., 2009. Sulfur K-edge XANES study of S sorbed onto volcanic ashes. *Journal of Physics: Conference Series* 190, 012177. <https://doi.org/10.1088/1742-6596/190/1/012177>
- Goodman, A.L., Li, P., Usher, C.R., Grassian, V.H., 2001. Heterogeneous Uptake of Sulfur Dioxide On Aluminum and Magnesium Oxide Particles. *J. Phys. Chem. A* 105, 6109–6120. <https://doi.org/10.1021/jp004423z>
- Hair, M.L., 1975. Hydroxyl groups on silica surface. *Journal of Non-Crystalline Solids, Glass Surfaces* 19, 299–309. [https://doi.org/10.1016/0022-3093\(75\)90095-2](https://doi.org/10.1016/0022-3093(75)90095-2)
- Huang, L., Zhao, Y., Li, H., Chen, Z., 2015. Kinetics of Heterogeneous Reaction of Sulfur Dioxide on Authentic Mineral Dust: Effects of Relative Humidity and Hydrogen Peroxide. *Environ. Sci. Technol.* 49, 10797–10805. <https://doi.org/10.1021/acs.est.5b03930>
- Jiang, B.Q., Wu, Z.B., Liu, Y., Lee, S.C., Ho, W.K., 2010. DRIFT Study of the SO<sub>2</sub> Effect on Low-Temperature SCR Reaction over Fe–Mn/TiO<sub>2</sub>. *J. Phys. Chem. C* 114, 4961–4965. <https://doi.org/10.1021/jp907783g>
- Li, L., Chen, Z.M., Zhang, Y.H., Zhu, T., Li, J.L., Ding, J., 2006. Kinetics and mechanism of heterogeneous oxidation of sulfur dioxide by ozone on surface of calcium carbonate. *Atmospheric Chemistry and Physics Discussions* 6, 579–613. <https://doi.org/10.5194/acpd-6-579-2006>
- Lo, J.M.H., Ziegler, T., Clark, P.D., 2010. SO<sub>2</sub> Adsorption and Transformations on  $\gamma$ -Al<sub>2</sub>O<sub>3</sub> Surfaces: A Density Functional Theory Study. *J. Phys. Chem. C* 114, 10444–10454. <https://doi.org/10.1021/jp910895g>
- Maters, E.C., Delmelle, P., Rossi, M.J., Ayriss, P.M., 2017. Reactive Uptake of Sulfur Dioxide and Ozone on Volcanic Glass and Ash at Ambient Temperature. *J. Geophys. Res.-Atmos.* 122, 10077–10088. <https://doi.org/10.1002/2017JD026993>
- Nanayakkara, C.E., Pettibone, J., Grassian, V.H., 2012. Sulfur dioxide adsorption and photooxidation on isotopically-labeled titanium dioxide nanoparticle surfaces: roles of surface hydroxyl groups and adsorbed water in the formation and stability of adsorbed sulfite and sulfate. *Phys. Chem. Chem. Phys.* 14, 6957–6966. <https://doi.org/10.1039/C2CP23684B>
- Shang, J., Li, J., Zhu, T., 2010. Heterogeneous reaction of SO<sub>2</sub> on TiO<sub>2</sub> particles. *Sci. China Chem.* 53, 2637–2643. <https://doi.org/10.1007/s11426-010-4160-3>
- Tamura, H., Mita, K., Tanaka, A., Ito, M., 2001. Mechanism of Hydroxylation of Metal Oxide Surfaces. *Journal of Colloid and Interface Science* 243, 202–207. <https://doi.org/10.1006/jcis.2001.7864>
- Ullerstam, M., Vogt, R., Langer, S., Ljungstrom, E., 2002. The kinetics and mechanism of SO<sub>2</sub> oxidation by O<sub>3</sub> on mineral dust. *Phys. Chem. Chem. Phys.* 4, 4694–4699. <https://doi.org/10.1039/b203529b>
- Usher, C.R., Al-Hosney, H., Carlos-Cuellar, S., Grassian, V.H., 2002. A laboratory study of the heterogeneous uptake and oxidation of sulfur dioxide on mineral dust particles. *J.-Geophys.-Res.* 107, 4713. <https://doi.org/10.1029/2002JD002051>
- Wang, T., Liu, Y., Deng, Y., Fu, H., Zhang, L., Chen, J., 2018a. Emerging investigator series: heterogeneous reactions of sulfur dioxide on mineral dust nanoparticles: from single component to mixed components. *Environ. Sci.: Nano* 5, 1821–1833. <https://doi.org/10.1039/C8EN00376A>

- Wang, T., Liu, Y., Deng, Y., Fu, H., Zhang, L., Chen, J.-M., 2018b. Adsorption of SO<sub>2</sub> on mineral dust particles influenced by atmospheric moisture. *Atmospheric Environment* 191. <https://doi.org/10.1016/j.atmosenv.2018.08.008>
- Wu, L.Y., Tong, S.R., Wang, W.G., Ge, M.F., 2011. Effects of temperature on the heterogeneous oxidation of sulfur dioxide by ozone on calcium carbonate. *Atmospheric Chemistry and Physics* 11, 6593–6605. <https://doi.org/10.5194/acp-11-6593-2011>
- Zhang, X., Zhuang, G., Chen, J., Wang, Y., Wang, X., An, Z., Zhang, P., 2006. Heterogeneous Reactions of Sulfur Dioxide on Typical Mineral Particles. *J. Phys. Chem. B* 110, 12588–12596. <https://doi.org/10.1021/jp0617773>
- Zhang, Z., Ewing, G.E., 2002. Infrared spectroscopy of SO<sub>2</sub> aqueous solutions. *Spectrochim Acta A Mol Biomol Spectrosc* 58, 2105–2113.

**Chapter V. HPLC method development and validation for the quantification of sulfites and sulfates on the surface of natural dusts**

## Table of content of Chapter 5

1	Introduction.....	160
2	Specific experimental consideration for HPLC method development.....	161
2.1	Samples and Standards for HPLC method development .....	161
2.1.1	Dust samples.....	161
2.1.2	Chemicals and reagents .....	161
2.1.3	Standards .....	162
2.2	Experimental Set-Up and Procedure for HPLC method development.....	162
2.2.1	General Outline .....	162
2.2.2	Dust ageing by SO <sub>2</sub> gas .....	163
2.2.3	Extraction and stabilization of surface sulfites and sulfates.....	163
2.2.4	HPLC analysis. Instrumentation and chromatographic conditions .....	163
3	Results and discussion of the HPLC method development .....	164
3.1	Optimization of the HPLC Analytical Method .....	164
3.2	Optimization of sulfite and sulfate extraction from dust surface .....	167
3.2.1	Dissolution.....	167
3.2.2	Recovery.....	168
3.2.3	Solution stability.....	169
3.3	Validation of Analytical Performance of the HPLC Method.....	170
3.3.1	Specificity.....	170
3.3.2	Limit of detection (LOD) and limit of quantitation (LOQ).....	171
3.3.3	Linearity and range.....	171
3.3.4	Injection repeatability.....	173
3.3.5	Robustness.....	173
3.4	Evaluation of Method Reproducibility: Sample Preparation and Extraction Performance. ....	174
3.5	Summary of the HPLC Method Developed.....	176
3.6	Application of the HPLC Method developed.....	177

3.6.1 Application of the method to natural samples .....	177
3.6.2 Application of the method to aged samples.....	179
4 Conclusions on HPLC method development and validation .....	182
References.....	184

## List of Tables of Chapter 5

Table 1: Parameters investigated and changed in order to adapt a method for “Simultaneous determination of sulfite, sulfate, and hydroxymethanesulfonate in atmospheric waters by ion-pair HPLC technique” by Zuo et al. to determination of sulfites and sulfates on the surface of environmental samples investigated in this work (Zuo and Chen, 2003).....	166
Table 2: Recovery results for 3 consecutive extracts of the sample of Hagavatn aged in 175 ppm SO <sub>2</sub> for various time periods. Extraction with 1mL of 1% Formalin. ....	169
Table 3: Analytical Performance: Range, Linearity (calibration curve equation, coefficient of determination, root mean square error) and Injection Repeatability (expressed as %RSD for 6 consecutive injections of a solution of 20 ppm K <sub>2</sub> SO <sub>3</sub> and 10 ppm K <sub>2</sub> SO <sub>4</sub> ). ....	172
Table 4: Method robustness results. Small changes in method parameters were introduced and evaluated as percent change for the amounts of SO <sub>3</sub> <sup>2-</sup> and SO <sub>4</sub> <sup>2-</sup> ions in samples of Hagavatn dust as compared to their determination under original conditions (marked by asterisk). ....	174
Table 5: Sample preparation and extraction reproducibility study for samples of Hagavatn aged in 175 ppm SO <sub>2</sub> for 1 hr. Extraction with 1mL of 1% Formalin. ....	175
Table 6: Summary of the validated conditions used to age, extract and quantify sulfites and sulfates from a sample of dust aged with SO <sub>2</sub> gas. ....	176
Table 7: Results of method reproducibility study for determination of SO <sub>3</sub> <sup>2-</sup> and SO <sub>4</sub> <sup>2-</sup> ions in Hagavatn and Gobi natural samples. Note, that samples were not subjected to laboratory ageing. LOD and LOQ for sulfites and sulfates for each sample mass expressed in µg/m <sup>2</sup> were calculated from corresponding sample’s mass, specific surface area, extraction volume (2ml) and the values for LOQ and LOD expressed in µg/mL measured earlier (LOD for SO <sub>3</sub> <sup>2-</sup> =0.32 µg/mL, LOQ for SO <sub>3</sub> <sup>2-</sup> =0.64 µg/mL; LOD for SO <sub>4</sub> <sup>2-</sup> =0.68 µg/mL, LOQ for SO <sub>4</sub> <sup>2-</sup> =3.38 µg/mL). Determination of the absolute amounts of SO <sub>3</sub> <sup>2-</sup> and SO <sub>4</sub> <sup>2-</sup> requires the observed concentrations of corresponding ions to be equal or more than LOQ. ....	178
Table 8: Sulfite and sulfate coverage on the surface of Hagavatn and Gobi dusts expressed in terms of (i)micrograms of SO <sub>3</sub> <sup>2-</sup> / SO <sub>4</sub> <sup>2-</sup> per meter squared of dust (µg/m <sup>2</sup> ), (ii) number of SO <sub>3</sub> <sup>2-</sup> SO <sub>4</sub> <sup>2-</sup> ions per centimeter squared of dust (N <sub>molecules</sub> /cm <sup>2</sup> ), and (iii) percent monolayer sulfates and sulfites occupy. The number of molecules needed to form a monolayer were calculated to be 5.75 × 10 <sup>14</sup> molecule cm <sup>-2</sup> and 4.22 × 10 <sup>14</sup> molecule cm <sup>-2</sup> for sulfites and sulfates respectively. ....	181



## List of Figures of Chapter 5

- Figure 1: Diagram representing two protocols: (A) “environmental sampling” that includes (i) sample collection, (ii) extraction and stabilization of sulfites and sulfates and (iii) HPLC analysis and (B) “kinetics study” that includes (i) sample collection, (ii) dust ageing, (iii) extraction and stabilization of sulfites and sulfates and (iv) HPLC analysis. Dark blue arrows lead through “environmental sampling” protocol, while orange arrows lead through “kinetics study” protocol. .... 163
- Figure 2: Representative chromatograms of: green) Formalin, offset 45 units for clarity; red) 10 ppm  $K_2SO_4$  in 1% Formalin, offset 30 units for clarity; blue) 20 ppm  $K_2SO_3$  in 1% Formalin, offset 15 units for clarity ; black) Hagavtn dust aged in 175 ppm  $SO_2$  for 1 hr and extracted in 1% Formalin. .... 167
- Figure 3: Dissolution studies for Hagavtn dust aged in 175 ppm  $SO_2$  for 1 hr and extracted in 1% Formalin. % RSD for sulfites and sulfates is equal to 12.1 % and 23.6 % respectfully (see section 3.4). .... 168
- Figure 4: Stability study results for 158.2 mg sample of Hagavtn aged in 175 ppm  $SO_2$  for 10 min. Extraction with 1ml of 1% Formalin. Samples are stored at 4°C. % RSD for sulfites and sulfates is equal to 4.7% and 8.7% respectfully (see 3.3.4)..... 170
- Figure 5: The typical plot of peak area versus concentration for a) sulfite (blue solid line) and b) sulfate (red dashed line) ions. The linearity plot was created daily before conducting experiments and each time the mobile phase solution was changed..... 172
- Figure 6: Amount of sulfites and sulfates quantified on the surfaces of Hagavtn volcanic dust and Gobi desert dust formed after 1 hr ageing with 175 ppm  $SO_2$  gas..... 180

# 1 Introduction

Chemical characterization plays a vital role in scientific representation of any process. Defined as a set of techniques that allows an analyst to know qualitatively and/or quantitatively the composition of the material, a method is created to reach this goal. The following Chapter V guides the reader through the development of the method for quantitative determination of sulfites and sulfates on the surface of mineral dust. As such, we have started by building an analytical HPLC method for analysis of a mixture of sulfites and sulfates. We then optimized extraction procedure to ensure optimal extraction of sulfites and sulfates from a dust sample. Finally, we assessed the validity of the method by going through validation studies using, when possible, SO<sub>2</sub>-laboratory-aged dust samples in order to have a sufficient amount of sulfites on the surface, indeed as evidenced in Chapter IV, unless immediately stabilized, adsorbed sulfites get oxidized to adsorbed sulfates.

The global objective of validation of the method is to demonstrate its suitability for the intended use (“ICH Official web site : ICH,” n.d.). In the case of this study the method is expected to be used for research purposes. More specifically, method validation is a process that uses a defined set of experiments to establish the performance criteria that should be achieved by an analyst using the method and that provides a means to assess the reliability of results obtained. Method validation is commonly used to check compliance with certain established criteria. In the case of this study though, method validation is primarily used to establish performance criteria, as, to the best of our knowledge, no regulatory body is concerned with determination of sulfites and sulfates on the surface of natural mineral samples and no reference method exists for extraction, stabilization, and determination of both sulfites and sulfates on the surface of mineral dusts.

The ion-chromatography methods available in the literature and employed to quantify the amount of SO<sub>2</sub> adsorbed on the surface of volcanic ash are almost solely concerned with quantification of sulfates as the final oxidation product completely ignoring sulfite quantification (Witham et al., 2005). Indeed, it is widely accepted that SO<sub>2</sub> gas reacts at the surface of the volcanic dust and forms sulfites or bisulfites, which are then converted to sulfates (T. Wang et al., 2018). However, quantification of sulfites along with the sulfates could provide a more comprehensive description of the SO<sub>2</sub> uptake processes. Simultaneous determination of sulfites and sulfates by reversed-phase ion-pair HPLC technique in atmospheric waters was proposed by Zuo et al. (Zuo and Chen, 2003). When applied to environmental samples though, the method failed to determine sulfites due to their fast conversion to sulfates (Zuo and Chen, 2003). Nevertheless, ion-pairing technique is a good tool to separate polar compounds by means of user-friendly widely-used HPLC technique.

**The goal of this study is to develop a method that would (i) extract both sulfites and sulfates from the surface of minerals, (ii) stop the conversion of sulfites to sulfates and (iii) successfully quantify both species individually.** The method can then be used for two distinctive purposes: to quantify sulfites and sulfates on the surface of natural environmental samples, such as recently erupted volcanic ash or dust passing through polluted areas, and to study the kinetics of the sulfite to sulfate transformation in laboratory settings. The challenge in separating sulfites from sulfates in the solution containing mineral dust comes from the nature of these dust particles, as they contain various oxidizing elements, such as iron, that contribute to the oxidation of sulfites into sulfates (Zuo and Hoigné, 1993), (Zuo et al., 2005), (Michigami and Ueda, 1994). This method proposes (i) a controlled ageing of mineral samples by SO<sub>2</sub> gas in laboratory settings, (ii) extraction and stabilization of sulfites and sulfates with a subsequent use of (iii) HPLC for quantitative analysis as a technique that can be used to study the conversion of sulfites to sulfates on the surface of natural samples. While in the case of taking field measurements artificial ageing is not required, it is important to be able to age samples in reproducible fashion in order to study kinetics of the sulfite to sulfate transformation as a part of laboratory experimental work.

## **2 Specific experimental consideration for HPLC method development**

### **2.1 Samples and Standards for HPLC method development**

#### **2.1.1 Dust samples**

Two representative natural samples, Hagavattn v-dust and Gobi desert dusts, were chosen for this study. Details on these samples, including their physical and chemical characterization can be found in Chapter 2 Sections 1 and 2. Hagavattn sample was chosen over other v-dust samples due to the fact that it was extensively studied with DRIFTS technique (Chapter 4). Gobi dust was chosen as a representative desert dust due to its major contribution to the global dust loading (Prospero et al., 2002). It was also highlighted as a reactive natural sample (X. Wang et al., 2018).

#### **2.1.2 Chemicals and reagents**

HPLC grade acetonitrile (ACN), 99.95% and methanol (MeOH), 99.9% were obtained from Biosolve Chimie, Dieuze, France. Potassium hydrogen phthalate and triethanolamine, 99% of analytical grade were purchased from Acros Organics, Geel, Belgium. Cetylpyridinium chloride, 98% was purchased from Alfa Aesar, Kander, Germany. Sodium sulfate was purchased from Merck, Darmstadt, Germany. Sodium sulfite was purchased from Fischer Chemical, Loughborough, UK. Formalin (37% formaldehyde solution by weight containing 10-15 % MeOH as stabilizer) was obtained from Sigma-Aldrich. Other

chemicals and solvents of analytical grade were used during research. Deionized water (DI) was used throughout the investigation. A certified SO<sub>2</sub> cylinder, 250 ppm diluted in synthetic air (nearly 80% N<sub>2</sub> and 20% O<sub>2</sub>) was purchased from Messer, France.

### 2.1.3 Standards

The solution of 1% Formalin was used to prepare a 1000 ppm stock solution of potassium sulfite (K<sub>2</sub>SO<sub>3</sub>) and a 1000 ppm stock solution of potassium sulfate (K<sub>2</sub>SO<sub>4</sub>). Other concentrations of K<sub>2</sub>SO<sub>3</sub> and K<sub>2</sub>SO<sub>4</sub> standards were prepared from their stock solutions through serial dilution with 1% Formalin. Stock solution of 1% Formalin was prepared by adding 10 ml of Formalin in a 1000 mL volumetric flask and diluting to the volume with 10% methanol/water to prevent polymerization.

## 2.2 Experimental Set-Up and Procedure for HPLC method development

### 2.2.1 General Outline

*This work serves two distinctive purposes: (i) to analyze sulfites and sulfates on the surface of environmental dust samples during field campaign measurements (referred to as “environmental sampling”) and (ii) to study kinetics of sulfite and sulfate formation on the surface of different dusts in the laboratory environment by subjecting them to SO<sub>2</sub> ageing and analyzing the product formation (referred to as “kinetics study”).*

The developed method for “environmental sampling” protocol consists of three parts: (i) sample collection, (ii) extraction and stabilization of sulfites and sulfates and (iii) HPLC analysis (Figure 1); the developed method for “kinetics study” protocol includes four steps: (i) sample collection, (ii) dust ageing, (iii) extraction and stabilization of sulfites and sulfates and (iv) HPLC analysis (Figure 1). Thus, the difference between the two protocols is an additional step of controlled SO<sub>2</sub> ageing required for the “kinetics study”. Sample analysis step that includes extraction and HPLC analysis is exactly the same in both cases.

Method for HPLC analysis was validated for specificity, limit of detection and quantitation, linearity and range, injection repeatability, and robustness. Sample preparation and extraction reproducibility was validated for the entire “kinetics study” protocol. Note that reproducibility for “environmental sampling” is expected to be superior to reproducibility for “kinetics study” due to the lack of ageing that introduces additional uncertainties.

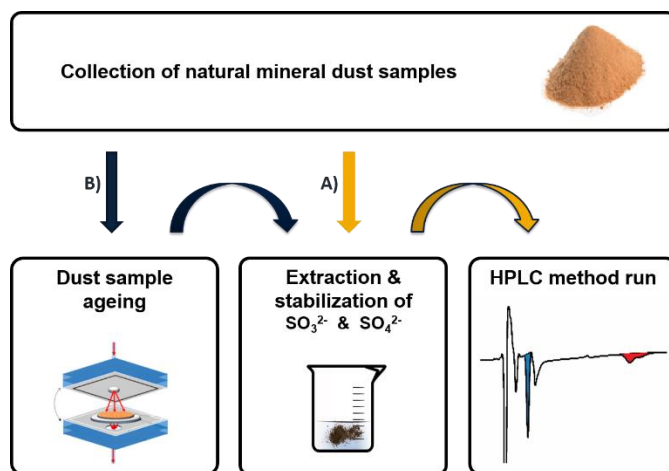


Figure 1: Diagram representing two protocols: (A) “environmental sampling” that includes (i) sample collection, (ii) extraction and stabilization of sulfites and sulfates and (iii) HPLC analysis and (B) “kinetics study” that includes (i) sample collection, (ii) dust ageing, (iii) extraction and stabilization of sulfites and sulfates and (iv) HPLC analysis. Dark blue arrows lead through “environmental sampling” protocol, while orange arrows lead through “kinetics study” protocol.

### 2.2.2 Dust ageing by SO<sub>2</sub> gas

The setup and protocol for ageing samples was described in detail in Chapter 2 Section 2.4.

### 2.2.3 Extraction and stabilization of surface sulfites and sulfates

After a defined period of ageing in the laboratory or in the absence of controlled ageing, such as in the case of samples collected in the environment, a sample weighing from 100 to 200 mg was transferred to a 10 mL glass container and stabilized with 1 mL of 1% Formalin. This step was followed by 10 min sonication in the ultrasound bath. The solution was then filtered through a 0.45 μm pore size 30 mm diameter filter using a syringe. The remaining dust was washed with 1 mL of 1% Formalin and filtered through the same filter that was used to filter the first solution. The combined final solution was analyzed by HPLC system.

### 2.2.4 HPLC analysis. Instrumentation and chromatographic conditions

Chromatography equipment used to develop an HPLC method consisted of Thermo Scientific Dionex UltiMate 3000 UHPLC System with UV/VIS Detector (Thermo Scientific, Waltham, MA). Chromeleon 7.0 Data Acquisition System for LC (Thermo Scientific, Waltham, MA) was used to analyze the data. Analysis was performed using Restek Ultra Column C18, 5 μm, Length 250 mm, I.D. 4.60 mm dynamically coated with cetylpyridinium chloride to produce a charged surface as recommended by Zuo et al. (Zuo and Chen, 2003). More specifically, columns were cleaned at 1 mL/min for 1.5 hour with 100% ACN before being coated with 1.0 mM cetylpyridinium chloride in ACN/water (7:93, v/v) at 0.5 mL/min

for 3 hours (Zuo and Chen, 2003). The HPLC instrument was operated isocratically at 23 C° at a flow rate of 1 mL/min for 15 min. Potassium hydrogen phthalate solution, 1.0 mM was adjusted to pH 6.5 with a dilute solution of potassium hydroxide (KOH), vacuum filtered and used as a mobile phase. The injection volume was 10 µL. An indirect photometric detection was used for quantification of sulfates and sulfites. Detector was set at 255 nm as the mobile phase showed the highest absorbance at this wavelength. A 6-point linear calibration curve was established daily for SO<sub>3</sub><sup>2-</sup> and SO<sub>4</sub><sup>2-</sup> ions in the range of 6 µg/mL to 191 µg/mL and 3 µg/mL to 101 µg/mL respectively. Concentration of sulfites and sulfates in the extracts of natural samples was determined using the slope of the calibration curve and converted to micrograms per gram (µg/g) of dust using the mass of the sample.

### **3 Results and discussion of the HPLC method development**

#### **3.1 Optimization of the HPLC Analytical Method**

The method for determination of sulfites, sulfates and hydroxymethanesulfonate (HMS) in natural and atmospheric water samples developed by Zuo et al. was used as a base for development of the method for determination of sulfites and sulfates on the surface of natural mineral samples discussed in this paper (Zuo and Chen, 2003). The main drawback of the method was the lack of sulfite-stabilizing agent during sample preparation and, as a consequence, inability to detect sulfites in environmental samples. The authors acknowledged the problem in the “quantitative analysis” part of their study and recommended to use methanol in order to stabilize sulfites. Following the suggestion, a 50/50 ppm solution of K<sub>2</sub>SO<sub>3</sub>/ K<sub>2</sub>SO<sub>4</sub> was dissolved in 10% methanol used as stabilizing agent. Unfortunately, in our experiments, methanol solution either did not stabilize sulfites and they were converted into sulfates, or sulfites co-eluted with sulfates, as only one peak was observed. Besides, methanol would be a poor choice for the extraction of sulfites in the presence of reactive ions, such as Mn or Fe, which are both known to be present in volcanic dust (Michigami and Ueda, 1994). Formalin was reported to prevent the conversion of sulfites to sulfates by converting it to hydroxymethanesulfonate (HMS) and was tested as an extracting solvent (Michigami and Ueda, 1994). A number of reactions and reaction rate constants were proposed by Kovacs et al. to demonstrate interactions of sulfites/bisulfates with formaldehyde and its hydrate (Kovacs et al., 2005). Reaction rate constants suggest that formation of HMS is a favorable process and it is expected that in access of formaldehyde all of the sulfite/bisulfite will be converted to HMS.

Two concentrations of a mixture of sulfites and sulfates of 50/50 ppm and 5/5 ppm were prepared using Formalin of the following concentrations: 0.5%, 1% and 5%. A solvent peak for 5% Formalin overlapped with a sulfite peak, and 5% Formalin concentration was rejected for further studies. Solvent peaks of both 0.5 and 1% Formalin were well separated from sulfite peak. Besides, less than 5% change

was observed for sulfites and sulfates in the corresponding solutions when left at ambient temperature for 2 days. Between 0.5% and 1% concentrations of Formalin, a solution of 1% Formalin was chosen as an extracting solvent for further studies.

A second concern about the method of Zuo et al. was the high pH value of the mobile phase. The diluted 1.0 mM phthalate mobile phase suggested by the author could not be adjusted to pH 7.9 as pH became unstable and decreased with time. Addition of triethanolamine drastically increased the pH of the mobile phase. Taking into consideration that pH higher than 8.0 is detrimental for the column and can easily dissolve the stationary phase, it was decided to work at pH 6.5, which was stable and easy to maintain. Addition of methanol to mobile phase did not make any difference on formaldehyde/sulfite pair, but broadened and pushed the sulfate peak further. It was therefore decided to work with 1.0 mM Potassium phthalate solution pH 6.5 as a mobile phase. Several other parameters, such as column type, injection volume and detection wavelength were varied to find the optimum conditions for getting a sharp peak and a good separation of sulfites and sulfates from formaldehyde peak present in the solvent. Parameters investigated are listed in Table 1.

Table 1: Parameters investigated and changed in order to adapt a method for “Simultaneous determination of sulfite, sulfate, and hydroxymethanesulfonate in atmospheric waters by ion-pair HPLC technique” by Zuo et al. to determination of sulfites and sulfates on the surface of environmental samples investigated in this work (Zuo and Chen, 2003).

	Method by Zuo et al.	Parameters investigated	Parameters chosen
<b>Column</b>	150 mm C18 Column, Particle size: 5 $\mu\text{m}$ , I.D. 4.60 mm	250 mm Restek Ultra Column C18, Particle size: 5 $\mu\text{m}$ , I.D. 4.60 mm  250 mm Acclaim 120 Column C18, Particle size: 3 $\mu\text{m}$ , I.D. 3 mm	250 mm Restek Ultra Column C18, Particle size: 5 $\mu\text{m}$ , I.D. 4.60 mm
<b>Column coating</b>	1.0 mM cetylpyridinium chloride in 7% ACN solution		1.0 mM cetylpyridinium chloride in 7% ACN solution
<b>Mobile phase</b>	potassium hydrogen phthalate 0.5 mM-0.015% triethanolamine-3% methanol	triethanolamine: 0%, 0.015%  potassium hydrogen phthalate: 0.5 mM, 1mM, 10 mM  % Methanol: 0%, 1%, 3% 5%	1 mM potassium hydrogen phthalate
<b>pH</b>	7.9	6.0, 6.5, 7.0, 7.5, 8.0, 8.5	6.5
<b>Flow rate</b>	1.0 ml/min	0.5 ml/min, 1 ml/min	1.0 ml/min
<b>Detection</b>	negative UV-Vis detection at 265 nm	negative UV-Vis detection at 265nm, 255 nm	negative UV-Vis detection at 255 nm
<b>Time</b>	15 min	10 min, 15 min	15 min
<b>HPLC mode</b>	isocratic elution		isocratic elution
<b>Temperature</b>	23 $^{\circ}\text{C}$	20 $^{\circ}\text{C}$ , 23 $^{\circ}\text{C}$ , 26 $^{\circ}\text{C}$ , 30 $^{\circ}\text{C}$ , 35 $^{\circ}\text{C}$	23 $^{\circ}\text{C}$
<b>Injection volume</b>	10 $\mu\text{L}$	10, 15, 20 $\mu\text{L}$	10 $\mu\text{L}$
<b>Sulfite-stabilizing reagent</b>	none	methanol 10 %  Formalin: 0.5%, 1%, 5%	1% Formalin

Finally, the following chromatographic conditions were determined as optimum: 25 mm Restek Ultra Column C18, Particle size: 5  $\mu\text{m}$ , I.D. 4.60 mm column which was dynamically coated with 1.0 mM cetylpyridinium chloride in 7% acetonitrile solution to produce a charged surface as recommended by Zuo et al. (Zuo and Chen, 2003). Mobile phase used: 1 mM potassium hydrogen phthalate at pH 6.5 at a flow rate of 1.0 ml/min with negative UV-Vis detection at 255 nm in 15 min.

Figure 2 displays four chromatograms offset for clarity: 1% Formalin, 20 ppm  $\text{K}_2\text{SO}_3$ , 10 ppm  $\text{K}_2\text{SO}_4$ , and Hagavatn extract obtained after ageing the dust for 1 hr in 175 ppm  $\text{SO}_2$ . The peak for  $\text{SO}_3^{2-}$  is observed at 2.7 minutes and  $\text{SO}_4^{2-}$  peak is observed at 7.2 min. Both peaks demonstrate a high number of theoretical plates: for Hagavatn extract they are equal to 2235 for  $\text{SO}_3^{2-}$  and 884 for  $\text{SO}_4^{2-}$ . Two small peaks



around 2.2 and 3.0 min belong to formaldehyde and are separated from the peak for  $\text{SO}_3^{2-}$  at 2.7 min. The sulfite peak present in the form of HMS eluted rather closely to the formaldehyde peak. Therefore, in order to preserve separation, it was decided to stay with a 250 mm long column.

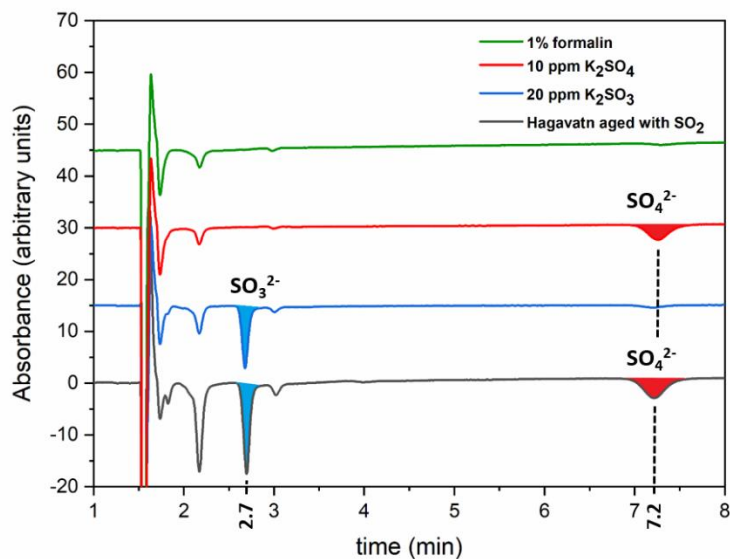


Figure 2: Representative chromatograms of: green) Formalin, offset 45 units for clarity; red) 10 ppm  $\text{K}_2\text{SO}_4$  in 1% Formalin, offset 30 units for clarity; blue) 20 ppm  $\text{K}_2\text{SO}_3$  in 1% Formalin, offset 15 units for clarity; black) Hagavatn dust aged in 175 ppm  $\text{SO}_2$  for 1 hr and extracted in 1% Formalin.

### 3.2 Optimization of sulfite and sulfate extraction from dust surface

Different parameters, such as extraction time and extraction techniques (shaking vs sonication), as well as volume of the extracting solution, were studied to insure maximum extraction of sulfites and sulfates. Solution stability was investigated to assess the time window during which the analysis can be performed.

#### 3.2.1 Dissolution

The dissolution time of up to 40 min of Hagavatn extract was investigated using sonication. Sulfites and sulfates immediately dissolved as shown in Figure 3. Similar results were obtained with

mechanical shaking, and 10 minutes sonication was found to be an appropriate dissolution technique.

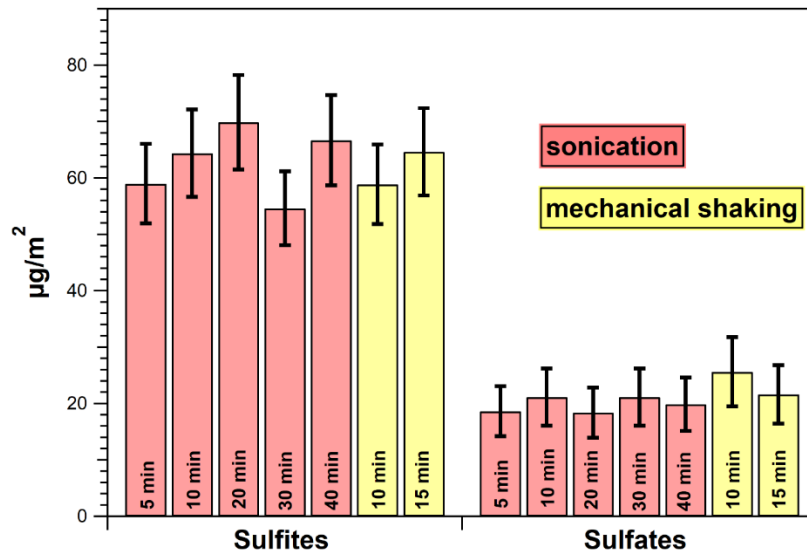


Figure 3: Dissolution studies for Hagavtn dust aged in 175 ppm SO<sub>2</sub> for 1 hr and extracted in 1% Formalin. % RSD for sulfites and sulfates is equal to 12.1 % and 23.6 % respectively (see section 3.4).

### 3.2.2 Recovery

Recovery studies were intended to prove that maximum amount of the sulfites and sulfates are extracted. Three consecutive extractions with 1 mL of 1 % Formalin were evaluated for the amount of sulfites and sulfates after the sample was aged by 175 ppm SO<sub>2</sub> for 10 min, 30 min, 1 hr, and 2hr. The criteria is less than 5 % of the product can be left unaccounted. As can be observed from Table 2, all of the sulfates are extracted from the surface of Hagavtn dust after the first extraction with 1 mL of 1% Formalin. As for the sulfites, two extractions with 1ml of 1% Formalin are necessary. The third extraction represents from 0 to 3.9 % of the total amount of SO<sub>3</sub><sup>2-</sup> extracted and therefore is not required based on the established criteria. Method demonstrates efficient recovery after only two extractions. As a result, it was decided to extract sulfites and sulfates with 1 mL of 1% Formalin, wash the remaining dust with another 1 mL of 1% Formalin and, using the same syringe, filter and combine the solution.

Table 2: Recovery results for 3 consecutive extracts of the sample of Hagavatn aged in 175 ppm SO<sub>2</sub> for various time periods. Extraction with 1mL of 1% Formalin.

Sample	Hagavatn aged with 175 ppm SO <sub>2</sub>			
	10 min	30 min	1hr	2hr
<b>Extract 1</b> SO <sub>3</sub> <sup>2-</sup> (ppm)	64.1	69.3	71.7	78.4
<b>Extract 2</b> SO <sub>3</sub> <sup>2-</sup> (ppm)	14.9	11.9	19.9	16.6
<b>Extract 3</b> SO <sub>3</sub> <sup>2-</sup> (ppm)	0.1	3.3	0	1.6
<b>% SO<sub>3</sub><sup>2-</sup> in the 3<sup>rd</sup> extract</b>	0.1	3.9	0.00	1.2
<b>% recovery after 3 extract</b>	<b>99.9</b>	<b>96.1</b>	<b>100.00</b>	<b>98.0</b>
<b>Extract 1</b> SO <sub>4</sub> <sup>2-</sup> (ppm)	3.4	3.7	3.7	8.5
<b>Extract 2</b> SO <sub>4</sub> <sup>2-</sup> (ppm)	0	0	0	0
<b>% recovery</b>	<b>100.00</b>	<b>100.00</b>	<b>100.00</b>	<b>100.00</b>

### 3.2.3 Solution stability

In order to observe how analytes of interest change over time, Hagavatn extract was prepared and injected into the HPLC system. The same solution was injected after 3, 5, 7, and 10 days. Solution stability results obtained from injecting a sample of 158.2 mg of Hagavatn aged for 10 min are shown in Figure 4. Solution stability studies indicate that both sulfites and sulfates remain stable up to 10 days, which means that a sample can be easily collected and extracted to be kept for later analysis, which is indispensable during geological sampling when the analyzing facility might be far away from the sampling location. Moreover, in separate experiments a 165 mg sample of Hagavatn aged with SO<sub>2</sub> for 1hr was checked for stability after 10 days and 3 months. Percent change in ppm concentration for sulfites was established at 4.5% after 10 days and 3.2% in 3 months; as for sulfates 5.4 % change was observed after both 10 days and 3 months. Thus, the results indicate that dust samples aged with SO<sub>2</sub> and stabilized with 1% Formalin are stable for long periods (at least up to 3 months). Exceptional stability of solutions is very important in field campaigns as it makes it possible to collect and stabilize a sample on the go, but analyze it later in the laboratory.

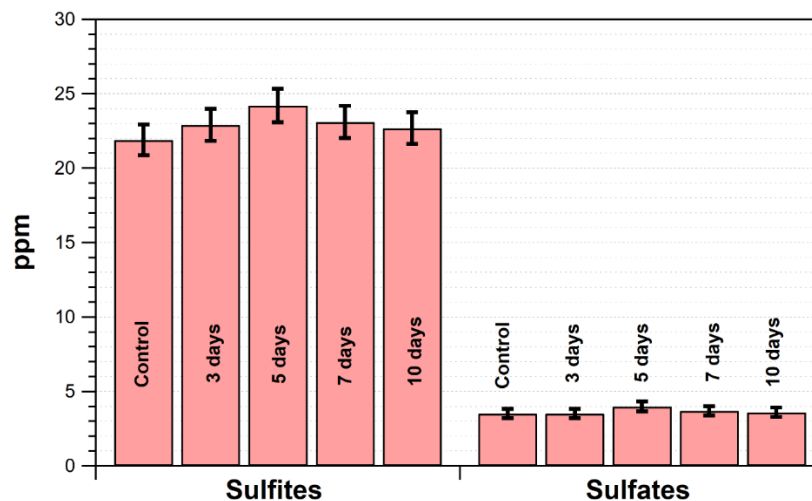


Figure 4: Stability study results for 158.2 mg sample of Hagavatn aged in 175 ppm SO<sub>2</sub> for 10 min. Extraction with 1ml of 1% Formalin. Samples are stored at 4°C. % RSD for sulfites and sulfates is equal to 4.7% and 8.7% respectively (see 3.3.4).

### 3.3 Validation of Analytical Performance of the HPLC Method

The developed method was validated for specificity, limit of detection and limit of quantitation, linearity and range, injection repeatability, and robustness.

#### 3.3.1 Specificity

To ensure that the peak response is due to only one component and no co-elution occurs, a solution of Hagavatn dust aged in 175 ppm SO<sub>2</sub> for 10 min and extracted in 1% Formalin was analyzed by Waters 2695 HPLC system equipped with Diode Array Detector using Empower software. Thus, specificity was evaluated as spectral purity. In peak purity testing the software compares the spectrum from each data point within the peak against the peak apex spectrum. Two parameters are evaluated: purity threshold, which accounts for the presence of non-ideal and solvent-induced spectral changes, and purity angle. When the purity angle exceeds purity threshold, a detectable impurity is present within a single chromatographic peak.

A solution of 165 mg of Hagavatn dust aged in 175 ppm SO<sub>2</sub> for 10 min and extracted in 1% Formalin showed no interfering peaks. All peaks were well separated from the analyte peaks. Peak purity was proved by purity threshold exceeding the purity angle for both sulfite and sulfate peaks.

### 3.3.2 Limit of detection (LOD) and limit of quantitation (LOQ)

Limits of detection for sulfites and sulfates were investigated to determine the lowest concentration of sulfites and sulfates that can be detected but not quantified. It was based on a signal-to-noise ratio  $S/N \geq 3$ . Limits of quantitation were studied to determine the lowest levels of the analyte concentrations that can be quantified and were determined by the concentrations corresponding to signal-to-noise ratio  $S/N \geq 10$ .

The LOD for determination of sulfites was found to be 0.5  $\mu\text{g/mL}$  of  $\text{K}_2\text{SO}_3$  (0.32  $\mu\text{g/mL}$  of  $\text{SO}_3^{2-}$  ion). This value is 5 times lower than the 1.52  $\mu\text{g/mL}$  of  $\text{SO}_3^{2-}$  ion reported as LOD by Zuo et al. (corresponding to 19  $\mu\text{M}$  of  $\text{SO}_3^{2-}$  ion), but in a good agreement with the limit of detection of hydroxymethylsulfonate (HMS) reported at 0.42  $\mu\text{g/mL}$  (corresponding to 3.8  $\mu\text{M}$  of HMS ion). This is to be expected, as the  $\text{SO}_3^{2-}$  in our case elutes as a HMS complex. The reason for improved detection limit is earlier elution of  $\text{SO}_3^{2-}$  in the form of HMS at around 3 min instead of 7.5 min as a free sulfite ion using the original method (Zuo and Chen, 2003). Earlier elution prevents peak broadening and improves LOD and LOQ. LOQ for determination of  $\text{SO}_3^{2-}$  ion was found to be 1  $\mu\text{g/mL}$  of  $\text{K}_2\text{SO}_3$  (0.64  $\mu\text{g/mL}$  of  $\text{SO}_3^{2-}$  ion).

LOD for determination of sulfates was found to be 1  $\mu\text{g/mL}$  of  $\text{K}_2\text{SO}_4$  (0.68  $\mu\text{g/mL}$  of  $\text{SO}_4^{2-}$  ion). This value is in excellent agreement with the limit of detection for  $\text{SO}_4$  ion reported by Zuo et al. and established at 6.7  $\mu\text{M}$   $\text{SO}_4^{2-}$  ion which is 0.64  $\mu\text{g/mL}$  of  $\text{SO}_4^{2-}$ . LOQ for determination of sulfates was found to be 5  $\mu\text{g/mL}$  of  $\text{K}_2\text{SO}_4$  (3.38  $\mu\text{g/mL}$  of  $\text{SO}_4^{2-}$  ion).

### 3.3.3 Linearity and range

Linearity proves that the detector response is directly proportional to the concentrations of the analyte in the sample, and range provides an interval for which the procedure is linear. Calibration ranges were defined as to include possible concentrations of sulfites and sulfates that can be found on the surface of mineral dust. This approach was based on preliminary results used to frame the order of magnitude of typical  $\text{SO}_3^{2-}$  and  $\text{SO}_4^{2-}$  surface concentrations. To investigate linearity for extracted sulfites, six different concentrations of  $\text{K}_2\text{SO}_3$  were prepared from 1000  $\mu\text{g/mL}$  stock solution of  $\text{K}_2\text{SO}_3$  in the range 10 – 300  $\mu\text{g/mL}$  (corresponding to 6  $\mu\text{g/mL}$  to 191  $\mu\text{g/mL}$  of  $\text{SO}_3^{2-}$  ion). To explore linearity for sulfates, six different concentrations of  $\text{K}_2\text{SO}_4$  were prepared from 1000  $\mu\text{g/mL}$  stock solution of  $\text{K}_2\text{SO}_4$  in the range 5-150  $\mu\text{g/mL}$  and injected into the HPLC system (corresponding to 3  $\mu\text{g/mL}$  to 101  $\mu\text{g/mL}$  of  $\text{SO}_4^{2-}$  ion).

Calibration plots were constructed every day in order to insure accurate identification of sulfates and sulfites in dust. Moreover, since the detection is achieved in negative mode (i.e. the mobile phase absorbs UV light and the peaks are “observed” when a compound lacking chromophore is passing through the column) the absorbance of the mobile phase depends on the concentration of the UV absorbing solution.

Even slightest variations in phthalate concentration can change the slope of the calibration plot. Therefore, it is crucial to construct a new calibration curve every time a freshly-made mobile phase is introduced into the system. Nevertheless, it is important to keep in mind that even though the slope of the calibration curve may change the curve remains linear within the range. Therefore, the daily-constructed curve can be used for quantitation purposes as long as the same batch of phthalate solution is used. Calibration curves from a typical experimental day are represented in Figure 5; calibration curve equations, coefficients of determination ( $R^2$ ) and root mean square errors are provided in Table 3. While  $R^2$  shows how close the data are to the fitted regression line, root mean square error can be interpreted as the average distance of a data point from the fitted line, measured along a vertical line.

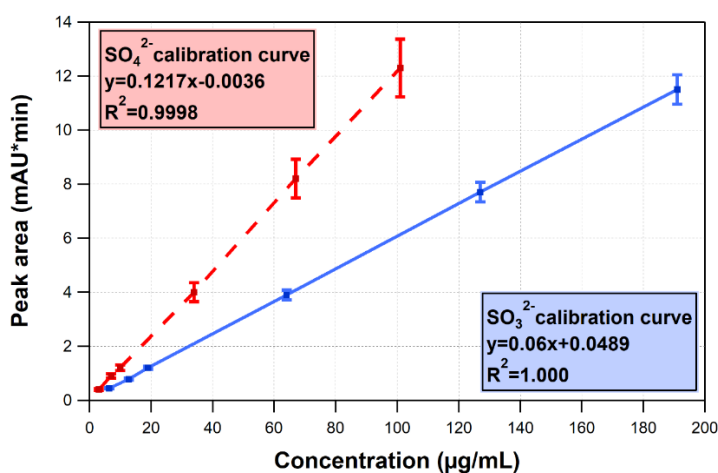


Figure 5: The typical plot of peak area versus concentration for a) sulfite (blue solid line) and b) sulfate (red dashed line) ions. The linearity plot was created daily before conducting experiments and each time the mobile phase solution was changed.

Table 3: Analytical Performance: Range, Linearity (calibration curve equation, coefficient of determination, root mean square error) and Injection Repeatability (expressed as %RSD for 6 consecutive injections of a solution of 20 ppm  $K_2SO_3$  and 10 ppm  $K_2SO_4$ ).

	Test range (µg/mL)	Calibration curve	$R^2$	Root Mean Square Error	% RSD n=6
<b>Sulfites</b>	6-191	$y = 0,06x + 0,0489$	1.0000	0.024	4.7
<b>Sulfates</b>	3-101	$y = 0,1217x - 0,0036$	0.9998	0.079	8.7

### 3.3.4 Injection repeatability

Injection repeatability was tested to measure the sensitivity of the method towards errors coming from the instrument itself: the column, the detector, the injector, the integration device. To evaluate injection repeatability a solution of a mixture of 20 ppm  $K_2SO_3$  and 10 ppm  $K_2SO_4$  were injected into the HPLC system 6 times and evaluated for area % relative standard deviation (%RSD). Injection repeatability for a solution of 20 ppm  $K_2SO_3$  and 10 ppm  $K_2SO_4$  was calculated to be 4.7 % for sulfites and 8.7% for sulfates (Table 3).

### 3.3.5 Robustness

Robustness of an analytical procedure is a measure of its capacity to remain unaffected by small but deliberate variations in parameters listed in the procedure. In this study “remain unaffected” was defined as no change of the detected amount of the analyte in a sample in spite of the variation of the method parameter. Stability of the method was evaluated with respect to variations of the internal factors of the method such as pH of the mobile phase pH ( $6.5\pm 0.5$ ), column temperature ( $23\pm 3$ ), different column lots (Lot #160210E and Lot #130505R) and 1 month old vs 4 months column. Changes in temperature, pH, column age (up to 4 months) and lot number (Lot #160210E and Lot #130505R) did not affect the amounts of  $SO_3^{2-}$  and  $SO_4^{2-}$  ions determined in the solutions, as they fell within injection variations, where 4.7 % RSD and 8.7 % RSD were reported for sulfites and sulfates respectively (Table 4). This is important, as it means that small fluctuations in pH that can come from mobile phase preparation will not affect quantification. Stability towards temperature changes suggests that method could be used in instruments not equipped with temperature control function. Stability of the column for at least 4 months and robustness towards change of column (different batches) assures normal use of the method.

Table 4: Method robustness results. Small changes in method parameters were introduced and evaluated as percent change for the amounts of  $SO_3^{2-}$  and  $SO_4^{2-}$  ions in samples of Hagavattn dust as compared to their determination under original conditions (marked by asterisk).

Sample	T (C°)	pH	Column Lot#	Column age (months)	Amount for $SO_3^{2-}$ (ppm)	% Change	Amount for $SO_4^{2-}$ (ppm)	% Change
Hagavattn 194 mg aged for 1hr*	<b>23</b>	6.5	160210E	1	27.5		10.45	
Hagavattn 194 mg aged for 1hr	<b>20</b>	6.5	160210E	1	26.7	<b>-2.9</b>	10.82	<b>3.5</b>
Hagavattn 194 mg aged for 1hr	<b>26</b>	6.5	160210E	1	27.2	<b>-1.1</b>	10.45	<b>0.0</b>
Hagavattn 158 mg aged for 10 min*	23	<b>6.5</b>	160210E	1	22.7		3.6	
Hagavattn 158 mg aged for 10 min	23	<b>7.0</b>	160210E	1	23.09	<b>1.7</b>	3.7	<b>2.8</b>
Hagavattn 158 mg aged for 10 min	23	<b>6.0</b>	160210E	1	21.7	<b>-4.4</b>	3.4	<b>-5.6</b>
Hagavattn 165 mg aged for 1hr*	23	6.5	<b>160210E</b>	1	27.8		8.2	
Hagavattn 165 mg aged for 1hr	23	6.5	<b>130505R</b>	1	26.6	<b>-4.5</b>	8.6	<b>5.4</b>
Hagavattn 165 mg aged for 1hr*	23	6.5	160210E	<b>1</b>	27.8		8.2	
Hagavattn 165 mg aged for 1hr	23	6.5	160210E	<b>4</b>	26.9	<b>-3.2</b>	8.6	<b>5.4</b>

### 3.4 Evaluation of Method Reproducibility: Sample Preparation and Extraction Performance.

The developed method was further validated for sample preparation and extraction reproducibility. It was decided to use the protocol for “kinetics study” to evaluate reproducibility because, in comparison with “environmental sampling” protocol, it has a supplementary step of dust ageing that can introduce additional errors.

Sample preparation and extraction reproducibility studies were conducted to evaluate the sensitivity of the method towards errors that may result from the combination of steps starting from ageing, extraction and preparation of the samples to their subsequent analysis by HPLC instrument. To evaluate sample preparation and extraction reproducibility for the “kinetics study” protocol, seven samples of Hagavattn volcanic dust were aged with 175 ppm  $SO_2$  for 1 hr and extracted in 1% Formalin. The solutions were injected into HPLC system and %RSD for mass of sulfites/sulfates per square meter of dust was calculated.



The %RSD for reproducibility (that includes ageing and extraction of sulfites/sulfates) as reported in Table 5 was found to be 12.1% for sulfites and 23.6% for sulfates. It is important to stress that reproducibility for ageing and extraction of sulfites/sulfates in a dust sample depends on heterogeneity of the sample. Like most of the natural mineral dusts, Hagavattn volcanic dust represents a highly heterogeneous sample and variations in adsorption/transformation of SO<sub>2</sub> gas by its different components are expected. Many studies use a combination of different oxides as proxies for natural samples. In this case %RSD for reproducibility would be expected to be lower as the sample composition is well-defined and ageing process more reproducible. Nevertheless, the importance of using natural samples cannot be overstated, as they often demonstrate different adsorption patterns when compared to the mixture of mineral oxides used as proxies (Zeineddine et al., 2018), (Lasne et al., 2018), (X. Wang et al., 2018). For example, when studying adsorption of SO<sub>2</sub> on individual oxides and comparing them to their mixture Zhang et al. observed that the reactivity of the mixture is twice as high as the reactivity of individual components (Zhang et al., 2006). In addition, substituting natural samples characterized by complex mineralogy by simple mineral oxides risks oversimplification of the observed trends.

*Table 5: Sample preparation and extraction reproducibility study for samples of Hagavattn aged in 175 ppm SO<sub>2</sub> for 1 hr. Extraction with 1mL of 1% Formalin.*

Preparation	Date of sample preparation	Sample mass (mg)	Concentration	Concentration
			SO <sub>3</sub> <sup>2-</sup> (µg/m <sup>2</sup> )	SO <sub>4</sub> <sup>2-</sup> (µg/m <sup>2</sup> )
1	April 8	134.0	59.3	25.2
2	April 12	89.0	66.4	28.7
3	April 12	194.0	67.1	20.5
4	April 15	137.3	69.6	22.7
5	April 15	138.6	56.2	39.1
6	April 16	158.0	75.7	26.1
7	April 16	165.4	79.3	22.5
<b>Average</b>			<b>67.7</b>	<b>26.5</b>
<b>Standard Deviation</b>			<b>8.2</b>	<b>6.2</b>
<b>%RSD</b>			<b>12.1</b>	<b>23.6</b>

### 3.5 Summary of the HPLC Method Developed

The validated method is summarized in Table 6. If “environmental sampling” is the desired purpose of the method, ageing is not required and one can start the protocol from the extraction section. For “kinetics study”, ageing is followed by extraction and HPLC analysis. Mass of the sample introduced into the reactor will depend on the specific surface area of the dust. In case of high specific surface area a higher SO<sub>2</sub> adsorption might be expected and therefore a smaller sample mass can be used for extraction. Likewise, if the specific surface area of the dust is low an increased mass might be necessary in order to detect sulfites/sulfates on the surface. Thus, the method can be easily adapted to different dust samples.

Table 6: Summary of the validated conditions used to age, extract and quantify sulfites and sulfates from a sample of dust aged with SO<sub>2</sub> gas.

Ageing		Extraction		Chromatographic conditions	
Dust sample mass	100.0-200.0 mg	Extracting solution	1% Formalin in 10% MeOH/water	Column	250 mm Restek Ultra Column C18, Particle size: 5 µm, I.D. 4.60 mm
SO <sub>2</sub> concentration	175 ppm	Mode of dissolution	sonication	Column modification	coated with 1.0 mM cetylpyridinium chloride in 7% ACN solution
SO <sub>2</sub> flow	100 cm <sup>3</sup> /min	Time of dissolution	10 min	Mobile phase	1 mM potassium hydrogen phthalate at pH 6.5
RH	30%	Filter	0.45 µm pore size 30 mm diameter Whatman filter	Flow rate	1.0 ml/min
Time	10 min - 1 hr	Total volume of extracting solution	2 mL	Detection	negative UV-Vis detection at 255 nm
				Time	15 min

## 3.6 Application of the HPLC Method developed

### 3.6.1 Application of the method to natural samples

Natural samples of Hagavattn volcanic dust and Gobi desert dust were tested for sulfites and sulfates using the “environmental sampling” method for extraction and quantification described above. Samples were not aged in the laboratory, but could have been previously subjected to SO<sub>2</sub> gas. In case of Hagavattn, the samples were certainly exposed to SO<sub>2</sub> gas during volcanic eruption. As for aeolian samples of Gobi dust, it is also likely that during its long-range transfer the dust encountered industrially polluted areas of China known to contain high levels of SO<sub>2</sub> (Zhang et al., 2006). Six samples of natural desert dust ranging from 124.2 to 144.5 mg and seven Hagavattn volcanic dust samples ranging from 110.6 to 505.4 mg were tested to determine their intrinsic SO<sub>3</sub><sup>2-</sup> and SO<sub>4</sub><sup>2-</sup> ion surface concentrations.

As can be seen from Table 7, the extraction of both Gobi and Hagavattn surface dust did not reveal sulfites above the limit of detection of 0.32 µg/mL for SO<sub>3</sub><sup>2-</sup> ion. Note, that the absolute amount of sulfites and sulfates are directly dependent on the sample mass since this parameter drives the effective surface area of the considered sample.

As for the sulfates, although the amounts on the surface of Hagavattn samples were above the LOD level of 0.68 µg/mL of SO<sub>4</sub><sup>2-</sup> for five out of seven samples, they remained under the LOQ level of 3.38 µg/mL of SO<sub>4</sub><sup>2-</sup> ion even when the mass of the sample was increased to 505.4 mg. Furthermore, in terms of absolute amounts of sulfates detected on Hagavattn dust, increasing the mass of the dust sample to 505.4 mg increases its total surface area and therefore decreases the minimum amount of SO<sub>4</sub><sup>2-</sup> ion per meter square that could be detected on the surface. The fact that the amount of sulfates in µg/mL recorded after extraction of 113.5 mg sample (1.95 µg/mL) is the same as on the 505.4 mg sample (1.86 µg/mL) suggests that sulfates are not coming from Hagavattn sample. A small amount of sulfates determined in Hagavattn and Gobi dust samples could have also come from 1% Formalin extracting solution that contains traces of sulfate impurities. The amount of sulfates in 1% Formalin solution was measured at 1 µg/mL, which is under LOQ limit.

The low density of sulfates on the surface of Hagavattn volcanic dust might be explained by the fact that sulfates were dissolved from the surface of the natural sample by rain or surface water, as the sample is coming from the lava field formed about 4,000 years ago and is subjected to fluctuating water levels (Baratoux et al., 2011), (Arnalds et al., 2016). As for Gobi dust, it displayed a considerable amount of sulfates averaging at 15.4±1.3 µg/m<sup>2</sup>. Interestingly, method reproducibility for extraction and quantification of sulfates on the surface of Gobi dust was evaluated at 8.4 %RSD for 6 samples, which is three times lower than 23.6% RSD for sample preparation and extraction reproducibility determined earlier for seven

Hagavatn samples used for validation of “kinetics study” protocol (see section 3.4, Table 5). In addition, one should keep in mind that 8.4% RSD for Gobi samples was calculated based on average amount of  $\text{SO}_4^{2-}$  of  $15.4 \mu\text{g}/\text{m}^2$ , while higher average of  $29.0 \mu\text{g}/\text{m}^2$  was used for calculation of 23.6% RSD for Hagavatn samples. Thus, the developed method for environmental sampling demonstrates good reproducibility and can be used in field measurements to evaluate the amount of sulfites and sulfates on the surface of natural dusts.

Table 7: Results of method reproducibility study for determination of  $\text{SO}_3^{2-}$  and  $\text{SO}_4^{2-}$  ions in Hagavatn and Gobi natural samples. Note, that samples were not subjected to laboratory ageing. LOD and LOQ for sulfites and sulfates for each sample mass expressed in  $\mu\text{g}/\text{m}^2$  were calculated from corresponding sample's mass, specific surface area, extraction volume (2ml) and the values for LOQ and LOD expressed in  $\mu\text{g}/\text{mL}$  measured earlier (LOD for  $\text{SO}_3^{2-}=0.32 \mu\text{g}/\text{mL}$ , LOQ for  $\text{SO}_3^{2-}=0.64 \mu\text{g}/\text{mL}$ ; LOD for  $\text{SO}_4^{2-}=0.68 \mu\text{g}/\text{mL}$ , LOQ for  $\text{SO}_4^{2-}=3.38 \mu\text{g}/\text{mL}$ ). Determination of the absolute amounts of  $\text{SO}_3^{2-}$  and  $\text{SO}_4^{2-}$  requires the observed concentrations of corresponding ions to be equal or more than LOQ.

Sample	mass (mg)	$\text{SSA}_{\text{BET}}$ ( $\text{m}^2/\text{g}$ )	LOD for $\text{SO}_3^{2-}$ ( $\mu\text{g}/\text{m}^2$ )	LOQ for $\text{SO}_3^{2-}$ ( $\mu\text{g}/\text{m}^2$ )	Amount of $\text{SO}_3^{2-}$ ( $\mu\text{g}/\text{m}^2$ )	LOD for $\text{SO}_4^{2-}$ ( $\mu\text{g}/\text{m}^2$ )	LOQ for $\text{SO}_4^{2-}$ ( $\mu\text{g}/\text{m}^2$ )	Amount of $\text{SO}_4^{2-}$ ( $\mu\text{g}/\text{m}^2$ )
Gobi	136.2	$10.5 \pm 2.0$	0.45	0.90	< LOD	0.95	4.73	<b>14.1</b>
Gobi	138.5	$10.5 \pm 2.0$	0.44	0.88	< LOD	0.94	4.65	<b>14.8</b>
Gobi	139.5	$10.5 \pm 2.0$	0.44	0.87	< LOD	0.93	4.62	<b>16.5</b>
Gobi	126.2	$10.5 \pm 2.0$	0.48	0.97	< LOD	1.03	5.10	<b>14.4</b>
Gobi	144.5	$10.5 \pm 2.0$	0.42	0.84	< LOD	0.90	4.46	<b>15.5</b>
Gobi	124.2	$10.5 \pm 2.0$	0.49	0.98	< LOD	1.04	5.18	<b>17.2</b>
<b>Average</b>								<b>15.4</b>
<b>STD</b>								<b>1.3</b>
<b>%RSD</b>								<b>8.4</b>
Hagavatn	116.8	$4.5 \pm 1.1$	1.22	2.44	< LOD	2.59	12.86	< LOD
Hagavatn	113.0	$4.5 \pm 1.1$	1.26	2.52	< LOD	2.67	13.26	<b>6.1 &lt; LOQ</b>
Hagavatn	125.4	$4.5 \pm 1.1$	1.13	2.27	< LOD	2.41	11.98	<b>4.6 &lt; LOQ</b>
Hagavatn	113.5	$4.5 \pm 1.1$	1.25	2.51	< LOD	2.66	13.24	<b>7.6 &lt; LOQ</b>
Hagavatn	190.0	$4.5 \pm 1.1$	0.75	1.50	< LOD	1.59	7.91	< LOD
Hagavatn	110.6	$4.5 \pm 1.1$	1.29	2.57	< LOD	2.73	13.58	<b>5.9 &lt; LOQ</b>
Hagavatn	505.4	$4.5 \pm 1.1$	0.28	0.56	< LOD	0.60	2.97	<b>1.6 &lt; LOQ</b>
<b>Average</b>								<b>NA</b>
<b>STD</b>								<b>NA</b>
<b>%RSD</b>								<b>NA</b>

### 3.6.2 Application of the method to aged samples

Following “kinetics study” protocol, samples of 134.0 mg of Hagavatn and 115.0 mg of Gobi dusts were exposed to 175 ppm of gaseous SO<sub>2</sub> for 1 hour at room temperature and under 30 % RH. After extraction, the amount of sulfites formed on the surface was calculated at 54.4±6.5 μg/m<sup>2</sup> (μg of sulfites per m<sup>2</sup> specific surface area) for Hagavatn and 27.0±3.2 μg/m<sup>2</sup> for Gobi desert dust (Figure 6). In the study of Maters et al. the amount of sulfites measured by ion-chromatography on the surface of laboratory-generated volcanic glass samples exposed to 60 ppb SO<sub>2</sub> for a couple of minutes varied from 10 μg/m<sup>2</sup> for the glass of rhyolitic composition to 63 μg/m<sup>2</sup> on the surface of glass of trachybasaltic composition (Maters et al., 2017). In this respect the amount of sulfites on the surface of Hagavatn basaltic volcanic dust agrees well with that measured on the surface of laboratory-generated glass samples of trachybasaltic composition. However, the direct comparison of the results is difficult due to fact that the above-mentioned studies were performed under low-pressure, 0% humidity, in Knudsen cell reactor (Maters et al., 2017).

The amount of sulfates formed after 1 hr ageing was estimated at 25.2±6.1 μg/m<sup>2</sup> (μg of sulfate per m<sup>2</sup> specific surface area) for Hagavatn and 53.4±12.8 μg/m<sup>2</sup> for Gobi desert dust. Note, that blank subtraction of 15.4±1.3 μg/m<sup>2</sup> (μg of sulfates per m<sup>2</sup> specific surface area) was applied to quantify the amount of sulfates formed on Gobi dust during laboratory ageing. From this experiment, it appears that after 1 hr of SO<sub>2</sub> exposure volcanic dust accumulates a higher amount of sulfites than desert dust and a lower amount of sulfates. From earlier studies it was proposed that SO<sub>2</sub> gas reacts on the surface of the volcanic dust and forms sulfites or bisulfites, which are then converted to sulfates (T. Wang et al., 2018), (Urupina et al., 2019). It is possible that certain mineralogical compounds on the surface of Gobi desert dust are contributing to a more efficient conversion of sulfites to sulfates. Sulfite conversion to sulfates on Hagavatn is suggested to be a more limiting kinetic step than on Gobi sample. A larger sample distribution would be required to confirm the trend and elucidate how the surface chemical composition may influence the respective kinetics of sulfites and sulfates.

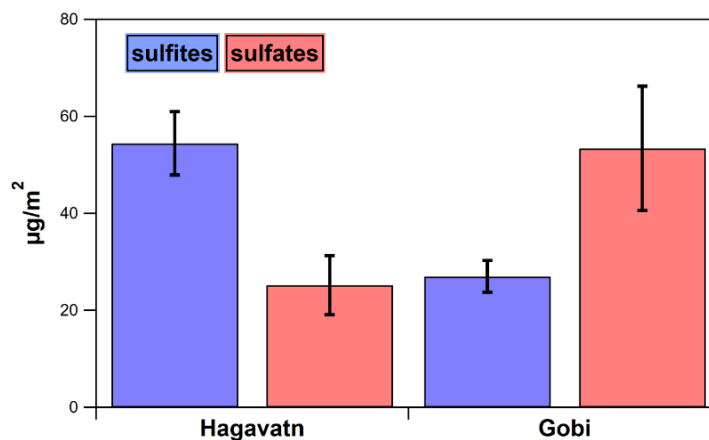


Figure 6: Amount of sulfites and sulfates quantified on the surfaces of Hagavathn volcanic dust and Gobi desert dust formed after 1 hr ageing with 175 ppm SO<sub>2</sub> gas.

The amounts of SO<sub>3</sub><sup>2-</sup> and SO<sub>4</sub><sup>2-</sup> ions expressed in (µg/m<sup>2</sup>) were also expressed in terms of the number of SO<sub>3</sub><sup>2-</sup> and SO<sub>4</sub><sup>2-</sup> ions per centimeter squared of dust and percent monolayer they form (see Table 8). The number of molecules needed to form a monolayer were calculated to be  $5.75 \times 10^{14}$  molecule cm<sup>-2</sup> for sulfites and  $4.22 \times 10^{14}$  molecule cm<sup>-2</sup> for sulfates. These values are consistent with the values reported for surface density of sorptive sites on mineral oxides, ca.  $3 \times 10^{13}$  -  $5 \times 10^{14}$  sites cm<sup>-2</sup> (Kulkarni and Wachs, 2002). It should be noted that the experimental monolayer coverage should be assumed to be lower than the theoretical because the molecules are not expected to pack together perfectly and because the degree of their interactions with various surface sites is not the same (Hudson et al., 2002), (Diaz et al., 2005). The shape of the molecules and hindering interactions would render some of the active sites on the surface inaccessible. Knowing the number of molecules needed to form a monolayer and the amount present on the surface, percent monolayer coverage was calculated. Accordingly, in terms of a molecular coverage the sulfites occupy about 7% of the available area on the surface of Hagavathn and 3.8% on the surface of Gobi dust, while sulfates occupy 3.5% of the calculated monolayer on Hagavathn and 7.8% on the Gobi dust. Based on this approximation, we can thus calculate that ca. 90% of surface sites are still free and available for the formation of sulfites/sulfates and the reactive uptake process can continue. Considering that not all surface sites are available for interactions with SO<sub>2</sub> the available surface fraction most probably represents less than 90%.

Table 8: Sulfite and sulfate coverage on the surface of Hagavtn and Gobi dusts expressed in terms of (i) micrograms of  $SO_3^{2-}/SO_4^{2-}$  per meter squared of dust ( $\mu\text{g}/\text{m}^2$ ), (ii) number of  $SO_3^{2-}/SO_4^{2-}$  ions per centimeter squared of dust ( $N_{\text{molecules}}/\text{cm}^2$ ), and (iii) percent monolayer sulfates and sulfites occupy. The number of molecules needed to form a monolayer were calculated to be  $5.75 \times 10^{14}$  molecule  $\text{cm}^{-2}$  and  $4.22 \times 10^{14}$  molecule  $\text{cm}^{-2}$  for sulfites and sulfates respectively.

Dust	$SO_3^{2-}$ ( $\mu\text{g}/\text{m}^2$ )	$SO_3^{2-}$ ( $N_{\text{molecules}}/\text{cm}^2$ )	% monolayer Sulfite Surface Coverage (lower limit)	$SO_4^{2-}$ ( $\mu\text{g}/\text{m}^2$ )	$SO_4^{2-}$ ( $N_{\text{molecules}}/\text{cm}^2$ )	% monolayer Sulfate Surface Coverage (lower limit)
Hagavtn	54.4±6.5	(4.1±0.5)×10 <sup>13</sup>	7%	25.2±6.1	(1.6±0.4)×10 <sup>13</sup>	3.8%
Gobi	27.0±3.2	(2.0±0.2)×10 <sup>13</sup>	3.5%	53.4±12.8	(3.3±0.8)×10 <sup>13</sup>	7.8%

To evaluate how relevant the artificial ageing is to the processes encountered in real atmosphere, results obtained after a one-hour laboratory ageing of Gobi dust with 175 ppm  $SO_2$  were compared to the field measurements of sulfates performed during a severe dust storm in China. Similarly, results from Hagavtn ageing were compared to leachate measurements of ashes coming from Stromboli volcano in Italy and Soufriere Hills Volcano, Montserrat.

In spring of 2002 a dust storm originating from Gobi desert in Mongolia and Taklimakan desert in western China spread over China, Korea and Japan (Sun et al., 2005). On March 20 2002, the dust peak concentrations over Beijing reached  $10.9 \text{ mg}/\text{m}^3$  (mg of dust per  $\text{m}^3$  of air) (Sun et al., 2005). Using the same particle matter concentrations as the ones reported over Beijing and the specific surface area of Gobi dust determined in the current study ( $10.5 \text{ m}^2/\text{g}$ ), our results of  $53.4 \pm 12.8 \mu\text{g}/\text{m}^2$  of sulfates on the surface of Gobi dust correspond to  $6.07 \pm 1.43 \mu\text{g}/\text{m}^3$  ( $\mu\text{g}$  of sulfates present in  $1 \text{ m}^3$  of gas), considering a dust density of  $10.9 \text{ mg}/\text{m}^3$  as reported by Sun et al. (Sun et al., 2005). This result is on the same order of magnitude than the volume concentration of sulfates determined from Ion Chromatography analysis of airborne samples: from 18 to  $19 \mu\text{g}/\text{m}^3$  (Sun et al., 2005). As for the samples of volcanic origin, Bagnato et al. measured the amount of sulfates on the surface of ash coming from Stromboli volcano, Italy. The results showed a vast variability from 7 to  $55,000 \mu\text{g}/\text{g}$  ( $\mu\text{g}$  of sulfates per g of volcanic sample) (Bagnato et al., 2011). High variability in the amount of sulfates in ash leachates was noted by Edmonds et al. (from 34 to  $9,280 \mu\text{g}/\text{g}$ ) at Soufriere Hills Volcano, Montserrat (Edmonds et al., 2003). The amount of sulfate per specific surface determined on Hagavtn volcanic dust ( $25.2 \pm 6.1 \mu\text{g}/\text{m}^2$ ), after 1 hr ageing, corresponds to  $115 \pm 27 \mu\text{g}/\text{g}$  ( $\mu\text{g}$  of sulfates per g of dust). Results retrieved from our study fall within the range of concentrations determined by Bagnato et al. and Edmonds et al (Bagnato et al., 2011), (Edmonds et al., 2003). Note that for elevated concentrations of sulfates on the surface of volcanic dust, samples can be easily diluted in higher volumes of extraction solution, in our case 1% Formalin.

## 4 Conclusions on HPLC method development and validation

A reversed-phase HPLC method was successfully developed for the assay of sulfites and sulfates on the surface of dust. This method was developed on a 25 mm Restek Ultra Column C18, Particle size: 5  $\mu\text{m}$ , I.D. 4.60 mm column which was dynamically coated with 1.0 mM cetylpyridinium chloride in 7% acetonitrile solution to produce a charged surface as recommended by Zuo et al (Zuo and Chen, 2003). Mobile phase used: 1 mM potassium hydrogen phthalate at pH 6.5 at a flow rate of 1.0 ml/min with negative UV-Vis detection at 255 nm in 15 min.

The developed method was validated for the specificity, LOD and LOQ, linearity and range, robustness, injection repeatability and reproducibility for sample preparation and extraction. In addition, the sampling method is easy and fast, and does not require expensive or particularly dangerous solvents. Besides, the extracted solution displays excellent stability, which is very important in remote sampling during geological expeditions. Samples can be extracted on site and analyzed days after sampling, provided they are kept in cool temperature conditions.

We would like to stress out that in case of “environmental sampling” the method should only be applied if the sample is believed to be recently subjected to  $\text{SO}_2$  gas and if quantification of sulfites is desired. Due to the conversion of sulfites to sulfates, the former are not expected to stay on the surface of dust for a long time (Michigami and Ueda, 1994). Examples of missions that could use the method developed could be: identification of sulfites and sulfates on fresh volcanic ash samples following an eruption, identification of sulfites and sulfates in desert dust samples that pass through industrially polluted areas, as well as laboratory investigation of sulfite and sulfate formation on the surface of natural dusts of different origins.

Validity of ageing procedure in the reference to natural gas-particle interactions was discussed. The developed method was successfully applied to assay the amount of sulfites and sulfates formed on the surface of Hagavath and Gobi dusts both in natural environmental settings and after artificial ageing. Sulfates in the amount of  $15.4 \pm 1.3 \mu\text{g}/\text{m}^2$  were detected on the surface of unexposed Gobi dust. As for the laboratory-aged samples, both sulfites and sulfates were detected on the surface of the two dusts. Sulfites were found to be formed in higher quantities on the surface of Hagavath volcanic dust in comparison with Gobi desert dust sample ( $54.4 \pm 6.5 \mu\text{g}/\text{m}^2$  of  $\text{SO}_3^{2-}$  ion for Hagavath versus  $27.0 \pm 3.2 \mu\text{g}/\text{m}^2$  of  $\text{SO}_3^{2-}$  ion for Gobi desert dust), while the opposite trend was observed for sulfates ( $25.2 \pm 6.1 \mu\text{g}/\text{m}^2$  of  $\text{SO}_4^{2-}$  for Hagavath and  $53.4 \pm 12.8 \mu\text{g}/\text{m}^2$  of  $\text{SO}_4^{2-}$  for Gobi desert dust).

Having a method to quantify sulfites and sulfates on the surface of dust paves a pathway to in-depth investigation of the sulfite/sulfate formation on the surface. In Chapter 6 we will study five volcanic dusts,



three desert dusts, 3 clays and a number of mineral oxides in their ability to form sulfites and sulfates on their surfaces. In this way we will be able to (i) compare different samples between each other and (ii) test the validity of using simple oxide proxies to study complex natural dusts.

## References of Chapter 5

- Arnalds, O., Dagsson-Waldhauserova, P., Olafsson, H., 2016. The Icelandic volcanic aeolian environment: Processes and impacts — A review. *Aeolian Research* 20, 176–195. <https://doi.org/10.1016/j.aeolia.2016.01.004>
- Bagnato, E., Aiuppa, A., Andronico, D., Cristaldi, A., Liotta, M., Brusca, L., Miraglia, L., 2011. Leachate analyses of volcanic ashes from Stromboli volcano: A proxy for the volcanic gas plume composition? *Journal of Geophysical Research: Atmospheres* 116. <https://doi.org/10.1029/2010JD015512>
- Baratoux, D., Mangold, N., Arnalds, O., Bardintzeff, J.-M., Platevoet, B., Grégoire, M., Pinet, P., 2011. Volcanic Sand in Iceland: Diverse origins of aeolian sand deposits revealed at Dyngjúsandur and Lambahraun, Iceland. *Earth Surface Processes and Landforms* 36, 1789–1808. <https://doi.org/10.1002/esp.2201>
- Diaz, L., Liauw, C.M., Edge, M., Allen, N.S., McMahon, A., Rhodes, N., 2005. Investigation of factors affecting the adsorption of functional molecules onto gel silicas. 1. Flow microcalorimetry and infrared spectroscopy. *J Colloid Interface Sci* 287, 379–387. <https://doi.org/10.1016/j.jcis.2004.09.039>
- Edmonds, M., Oppenheimer, C., Pyle, D., Herd, R., 2003. Rainwater and ash leachate analysis as proxies for plume chemistry at Soufriere Hills Volcano, Montserrat. *Geological Society Special Publication* 213, 203–218. <https://doi.org/10.1144/GSL.SP.2003.213.01.12>
- Hudson, P.K., Zondlo, M.A., Tolbert, M.A., 2002. The Interaction of Methanol, Acetone, and Acetaldehyde with Ice and Nitric Acid-Doped Ice: Implications for Cirrus Clouds. *J. Phys. Chem. A* 106, 2882–2888. <https://doi.org/10.1021/jp012718m>
- ICH Official web site : ICH [WWW Document], n.d. URL <https://www.ich.org/page/quality-guidelines> (accessed 3.6.20).
- Kovacs, K., McIlwaine, R., Gannon, K., Taylor, A.F., Scott, S.K., 2005. Complex Behavior in the Formaldehyde–Sulfite Reaction. *J. Phys. Chem. A* 109, 283–288. <https://doi.org/10.1021/jp0464324>
- Kulkarni, D., Wachs, I.E., 2002. Isopropanol oxidation by pure metal oxide catalysts: number of active surface sites and turnover frequencies. *Applied Catalysis A: General* 237, 121–137. [https://doi.org/10.1016/S0926-860X\(02\)00325-3](https://doi.org/10.1016/S0926-860X(02)00325-3)
- Lasne, J., Romanias, M.N., Thevenet, F., 2018. Ozone Uptake by Clay Dusts under Environmental Conditions. *ACS Earth Space Chem.* 2, 904–914. <https://doi.org/10.1021/acsearthspacechem.8b00057>
- Maters, E.C., Delmelle, P., Rossi, M.J., Ayris, P.M., 2017. Reactive Uptake of Sulfur Dioxide and Ozone on Volcanic Glass and Ash at Ambient Temperature. *J. Geophys. Res.-Atmos.* 122, 10077–10088. <https://doi.org/10.1002/2017JD026993>
- Michigami, Y., Ueda, K., 1994. Sulphite stabilizer in ion chromatography. *Journal of Chromatography A* 663, 255–258. [https://doi.org/10.1016/0021-9673\(94\)85252-9](https://doi.org/10.1016/0021-9673(94)85252-9)
- Prospero, J.M., Ginoux, P., Torres, O., Nicholson, S.E., Gill, T.E., 2002. Environmental Characterization of Global Sources of Atmospheric Soil Dust Identified with the Nimbus 7 Total Ozone Mapping Spectrometer (toms) Absorbing Aerosol Product. *Reviews of Geophysics* 40, 2-1-2–31. <https://doi.org/10.1029/2000RG000095>
- Sun, Y., Zhuang, G., Wang, Y., Zhao, X., Li, J., Wang, Z., An, Z., 2005. Chemical composition of dust storms in Beijing and implications for the mixing of mineral aerosol with pollution aerosol on the pathway. *Journal of Geophysical Research: Atmospheres* 110. <https://doi.org/10.1029/2005JD006054>
- Urupina, D., Lasne, J., Romanias, M.N., Thiery, V., Dagsson-Waldhauserova, P., Thevenet, F., 2019. Uptake and surface chemistry of SO<sub>2</sub> on natural volcanic dusts. *Atmospheric Environment* 217, 116942. <https://doi.org/10.1016/j.atmosenv.2019.116942>

- Wang, T., Liu, Y., Deng, Y., Fu, H., Zhang, L., Chen, J., 2018. Emerging investigator series: heterogeneous reactions of sulfur dioxide on mineral dust nanoparticles: from single component to mixed components. *Environ. Sci.: Nano* 5, 1821–1833. <https://doi.org/10.1039/C8EN00376A>
- Wang, X., Romanias, M.N., Thévenet, F., Rousseau, A., 2018. Geocatalytic Uptake of Ozone onto Natural Mineral Dust. *Catalysts* 8, 263. <https://doi.org/10.3390/catal8070263>
- Witham, C.S., Oppenheimer, C., Horwell, C.J., 2005. Volcanic ash-leachates: a review and recommendations for sampling methods. *Journal of Volcanology and Geothermal Research* 141, 299–326. <https://doi.org/10.1016/j.jvolgeores.2004.11.010>
- Zeineddine, M.N., Romanias, M.N., Riffault, V., Thévenet, F., 2018. Heterogeneous Interaction of Various Natural Dust Samples with Isopropyl Alcohol as a Probe VOC. *The Journal of Physical Chemistry A*. <https://doi.org/10.1021/acs.jpca.8b02034>
- Zhang, X., Zhuang, G., Chen, J., Wang, Y., Wang, X., An, Z., Zhang, P., 2006. Heterogeneous Reactions of Sulfur Dioxide on Typical Mineral Particles. *J. Phys. Chem. B* 110, 12588–12596. <https://doi.org/10.1021/jp0617773>
- Zuo, Y., Chen, H., 2003. Simultaneous determination of sulfite, sulfate, and hydroxymethanesulfonate in atmospheric waters by ion-pair HPLC technique. *Talanta* 59, 875–881. [https://doi.org/10.1016/S0039-9140\(02\)00647-1](https://doi.org/10.1016/S0039-9140(02)00647-1)
- Zuo, Y., Hoigné, J., 1993. Evidence for Photochemical Formation of H<sub>2</sub>O<sub>2</sub> and Oxidation of SO<sub>2</sub> in Authentic Fog Water. *Science* 260, 71–73. <https://doi.org/10.1126/science.260.5104.71>
- Zuo, Y., Zhan, J., Wu, T., 2005. Effects of Monochromatic UV-Visible Light and Sunlight on Fe(III)-Catalyzed Oxidation of Dissolved Sulfur Dioxide. *J Atmos Chem* 50, 195–210. <https://doi.org/10.1007/s10874-005-2813-y>



**Chapter VI. How atmospherically relevant is to use mineral proxies  
to mimic the reactivity of natural dust samples? A reactivity study  
using SO<sub>2</sub> as probe molecule**

## Table of content of Chapter 6

1	Introduction .....	191
2	Specific experimental considerations to address mineral dusts and their surrogates regarding SO <sub>2</sub> uptake. .....	192
3	Results and discussion.....	194
3.1	First insights on SO <sub>2</sub> uptake on mineral samples .....	194
3.2	Classification of mineral samples based on their efficiency to form sulfites and/or sulfates. Can a natural dust be represented by one chosen individual component? .....	195
3.3	Can a natural dust be characterized by a sum of “representative” simple mineral proxies? .....	196
4	Conclusions .....	200
	References .....	201

## List of Tables of Chapter 6

Table 1: % surface elemental composition of the v-dust and desert dust samples used in this study as determined by XPS (surf stands for surface) compared to % bulk composition as determined by ICP-MS (bulk). Both expressed as % by weight. Bulk compositions of mineral dust samples marked with asterisk were adopted from (Joshi et al., 2017). Error on the XPS measurements < 10% and for ICP-MS < 10% for major elements. .....	193
Table 2: Classification of mineral samples based on their ability to form sulfites and/or sulfates on their surfaces.	196
Table 3: Quantitative comparison for the amount of sulfites and sulfates on the surface of natural dusts (i) calculated from the addition of the contributions of individual pure oxides and (ii) experimentally measured on the surface of dust. Elemental composition for dusts expressed as % oxide (by weight) was calculated from % elemental composition (by weight) measured with XPS and discussed earlier (see Section 2.2, Table 1)..	198

## List of Figures of Chapter 6

Figure 1: Amounts of sulfites and sulfates quantified on the surface of desert and volcanic dust samples as compared to the amounts of sulfites and sulfates formed on various pure metal oxides, calcium carbonate, goethite and clays. All samples were exposed to 175 ppm SO<sub>2</sub> for 1 hr at 30% RH. Sulfites and sulfates were extracted with 2 mL of 1% Formalin, sonicated for 10 min and analyzed by HPLC. .... 194



# 1 Introduction

Since mineral dust originates from the soil it has a similar elemental composition. The major components of mineral dust are relatively uniform and, expressed as oxides, consist of around 60% SiO<sub>2</sub> and 10-15 % of Al<sub>2</sub>O<sub>3</sub> followed by Fe<sub>2</sub>O<sub>3</sub> (6%), MgO (6%) and CaO (3%) (Usher et al., 2003). Note that the convention of reporting elemental composition in the percent oxide form dates back to when minerals and rocks were analyzed using wet-chemical methods to precipitate an element. The precipitate was oxidized under high temperature and the results were weighed as the oxide. However, it should be noted that, although customary, representation of soil composition in the form of oxides is largely artificial and contrary to the actual mineralogy of soils (Vodyanitskii, 2018).

Airborne desert dust has a complex composition and consists of quartz, feldspars, micas, chlorite, kaolinite, illite, smectite, palygorskyte, calcite, dolomite, gypsum, halite, opal, and mixed-layer clays (Usher et al., 2003). The mineral composition of the volcanic dust reflects the composition of magma from which it was generated and consists mostly of aluminosilicate glass (Langmann, 2013), (Delmelle et al., 2018). The individual mineral grains and crystals of volcanic dust are imbedded in the glass (Dagsson-Waldhauserova et al., 2015). From the crystalline phases, silicates are the main components found in volcanic ash, such as feldspar, olivine, pyroxene, hornblende, and biotite (Langmann, 2013).

Low abundance of crystalline mineral phases makes their determination and quantification difficult. Thus, two major differences can be highlighted between desert and volcanic dusts. First, v-dust contains high share of amorphous material (40-100%), while desert dust is mostly crystalline (Delmelle et al., 2018). Second, the composition of desert dust, as opposed to volcanic dust, results from chemical weathering of desert dust on geological timescales (Langmann, 2013). As an example, feldspars present in desert dusts weather to clays, while iron-bearing materials, such as amphiboles and pyroxenes, weather to hematite and goethite (Earle, 2015), (Langmann, 2013). Primary iron-bearing phases of v-dust, such as amphiboles and pyroxenes, are not identified in desert dust (Langmann, 2013).

Due to the crystalline nature of desert dusts authors investigating their behavior often substitute natural samples for simple metal oxides in order to mimic the behavior of complex minerals. In the most recent IUPAC review of kinetic data on heterogeneous reactions on dust surfaces, only 30% of the studies were carried out using natural desert dusts and none dealt with volcanic samples (Crowley et al., 2010). Thus, kinetic and mechanistic data on natural mineral samples are very limited and their reactivity is often studied by using mainly “reactive components”, typically hydroxides, and carbonates: Fe<sub>2</sub>O<sub>3</sub>, FeOOH, Al<sub>2</sub>O<sub>3</sub>, MgO, CaO, TiO<sub>2</sub>, MnO<sub>2</sub>, SiO<sub>2</sub>, CaCO<sub>3</sub> (Crowley et al., 2010), (Goodman et al., 2001), (Zhang et al.,

2006), (Wang et al., 2018a), (Wang et al., 2018b), (Nanayakkara et al., 2012), (Wu et al., 2011), (Usher et al., 2002), (Zhang et al., 2018), (Huang et al., 2016), (Li et al., 2006). The investigations of volcanic dust are more commonly carried out using aluminosilicate amorphous material (Delmelle et al., 2018). Oftentimes a single component or a mixture of several components are used to approximate behavior of dusts. The kinetic or mechanistic results of the studies using surrogates are then used to estimate the atmospheric implication of the reactions studied and to elucidate their atmospheric impact. However, is it really appropriate to use simplified surrogates in order to mimic the behavior of a complex mineral mixtures? And do the values obtained by using proxies correctly describe atmospheric processes?

To respond to the above questions in the framework of the current study, SO<sub>2</sub> was used as a probe molecule to investigate its interactions with a wide variety of mineral samples (including surrogates, clays, and natural samples). The choice of using SO<sub>2</sub> is twofold. First, it is an important widely-studied atmospheric molecule (Bluth et al., 1993), (Highwood and Stevenson, 2003), (Daniel J. Jacob, 1999), (Finlayson-Pitts and Jr, 1999), (Schmidt et al., 2011), (US EPA, 2016), (Stevenson et al., 2003), (Li et al., 2006). Second, multiple, sometimes conflicting trends in uptake of SO<sub>2</sub> and evaluation of influence of difference variables, such as RH, have been reported in the literature while using different proxies for atmospheric dust (Crowley et al., 2010), (Baltrusaitis et al., 2007), (Goodman et al., 2001), (Zhang et al., 2006), (Wang et al., 2018a), (Wang et al., 2018b), (Nanayakkara et al., 2012), (Wu et al., 2011), (Usher et al., 2002), (Zhang et al., 2018), (Huang et al., 2016), (Li et al., 2006). For instance, for a mixture of two pure metal oxides, alumina and hematite, two opposite effects on sulfate yields in respect to each individual component are observed: synergistic effect for hematite (higher sulfate yields for hematite-rich mixtures compared to theoretical calculation based on its contribution) and antagonistic effect for alumina (lower sulfate yields for alumina-rich mixtures compared to theoretical calculation based on its contribution) (Wang et al., 2018a). In order to further examine relevance of using proxies, heterogeneous interactions of SO<sub>2</sub> gas with 20 different mineral samples, such as commonly used proxies, clays, and a number of natural desert and volcanic dusts were investigated. In particular, the mineral samples were aged for 1 hour with 175 ppm of SO<sub>2</sub>, 30% of RH. The sulfites and sulfates formed on the surface were identified and quantified using a recently developed method based on HPLC analysis (Urupina et al., 2020).

## **2 Specific experimental considerations to address mineral dusts and their surrogates regarding SO<sub>2</sub> uptake.**

To compare the behavior of natural samples when subjected to SO<sub>2</sub> gas to the behavior of common proxies, the following samples were investigated. Natural samples include five v-dusts: (i) Hagavatn, Mýrdalssandur, Maelifellssandur, Dyngjusandur and Eyjafjallajökull, (ii) three desert dusts: Gobi, M'Bour

and Arizona Test Dust (ATD), (iii) three clays: kaolinite, montmorillonite, illite. The metal oxides include silica ( $\text{SiO}_2$ ), quartz ( $\text{SiO}_2$ ), iron oxide ( $\text{Fe}_3\text{O}_4$ ), goethite ( $\text{FeOOH}$ ), calcium oxide ( $\text{CaO}$ , 99.9% purity), aluminum oxide ( $\text{Al}_2\text{O}_3$ ), titanium oxide ( $\text{Ti}_2\text{O}_3$ ), calcium carbonate ( $\text{CaCO}_3$ ), and magnesium oxide ( $\text{MgO}$ ).

Details on the origins of the samples are provided in Chapter 2, Section 1.1. Physical and chemical characterization of volcanic and desert dusts, ICP-MS bulk elemental composition and XRD surface elemental composition analysis, was discussed in Chapter 2 Section 1.2 and is once more provided below in Table 1 to ease the comprehension of the current chapter. **As one can see, bulk and surface compositions are rather different. For further investigations surface composition (expressed in % element by weight) was preferred to bulk composition as it is considered to be more relevant in representation of the physical and chemical properties of dust surfaces (Chapter 2 Section 1.2.4).**

*Table 1: % surface elemental composition of the v-dust and desert dust samples used in this study as determined by XPS (surf stands for surface) compared to % bulk composition as determined by ICP-MS (bulk). Both expressed as % by weight. Bulk compositions of mineral dust samples marked with asterisk were adopted from (Joshi et al., 2017). Error on the XPS measurements < 10% and for ICP-MS < 10% for major elements.*

Element	Mýrdalssandur		Dyngjusandur		Hagavatn		Maelifellssandur		Eyjafjallajökull		M'Bour Saharan dust		Gobi dust		ATD dust	
	surf	bulk	surf	bulk	surf	bulk	surf	bulk	surf	bulk	surf	bulk*	surf	bulk*	surf	bulk*
Si	47.1	31.3	49.0	32.7	42.8	27.5	43.7	28.3	60.0	49.5	57.0	94.4	54.7	57.6	57.5	74.6
Fe	20.0	23.0	15.9	19.7	10.5	19.6	22.0	23.8	7.7	13.0	6.1	1.3	6.7	5.5	8.2	3.1
Ca	8.1	13.9	9.7	16.3	9.0	19.5	6.3	14.0	5.5	7.3	2.4	1.0	7.7	16.1	5.5	4.4
Al	14.5	12.3	16.8	15.8	31.8	16.7	18.2	15.5	13.4	13.6	32.1	1.8	18.5	11	18.0	9.5
Mg	3.3	5.1	4.8	7.3	2.4	10.4	3.0	5.7	1.5	3.3	0	0.1	6.1	2.3	3.9	1.0
Ti	3.8	7.6	2.0	3.3	1.8	2.4	4.3	6.1	1.0	2.4	0.2	0.7	0	0.8	0.5	0.5
Na	2.3	4.8	1.0	3.9	1.4	3.1	1.3	4.6	7.5	7.3	0.3	0.2	0.8	2.5	1.3	2.5
K	0.9	1.3	0	0.6	0	0.2	0.4	1.5	3.3	3.1	1.9	0.1	4.7	3.5	4.4	4.0
other	0	0.7	0.8	0.4	0.3	0.6	0.8	0.5	0.1	0.5	0	0.1	0	0.7	0.7	0.1

As can be seen from Table 1, surface composition of desert and volcanic dusts is dominated by silicon (Si), aluminum (Al) and, in the case of volcanic dusts, iron (Fe), followed by other elements, such as calcium (Ca), magnesium (Mg) and Ti (titanium). With exception of Si that demonstrated low reactivity, oxides of Fe, Ca, Al, Mg and Ti and relatively simple minerals, such as calcite ( $\text{CaCO}_3$ ) and goethite ( $\text{FeOOH}$ ) were used in the literature as proxies to study behavior of natural dusts based on the fact that they are seen as “reactive components” (Usher et al., 2002).

In this study all samples were aged for 1 hr using 175 ppm  $\text{SO}_2$ , at 30% RH, ambient temperature and atmospheric pressure using the system described in Chapter 2 Section 2.4. They were analyzed for surface sulfites and sulfates using the method and chromatographic equipment developed in Chapter 5. Additional details on chemicals and reagents and are available in Chapter 2 Section 1.3-1.4.

### 3 Results and discussion

Several authors investigating desert dust samples use mineral oxides and so-called “reactive components” as proxies for natural samples. In the following study it was decided to directly compare the amount of sulfites/sulfates present on the surface of natural volcanic and desert dusts after 1 hr ageing with 175 ppm of SO<sub>2</sub> gas versus sulfites/sulfates present on commonly used surrogates in order to evaluate this approach.

#### 3.1 First insights on SO<sub>2</sub> uptake on mineral samples

Figure 1 shows the amounts of sulfites and sulfates quantified on: (i) different metal oxides based on Al, Fe, Ti, Mg, Ca and Si content identified on the surface of desert and volcanic dusts (Table 1), (ii) volcanic dusts, (iii) desert dusts, (iv) clays, (v) goethite and (vi) calcium carbonate. Note, that clays, calcium carbonate and goethite are not observed in volcanic ash but they are found in desert dusts and discussed in the literature, thus they were also included to better explain the behavior of natural samples (Ayris and Delmelle, 2012). All sample were aged for 1hr under the same experimental conditions using 175 ppm SO<sub>2</sub>.

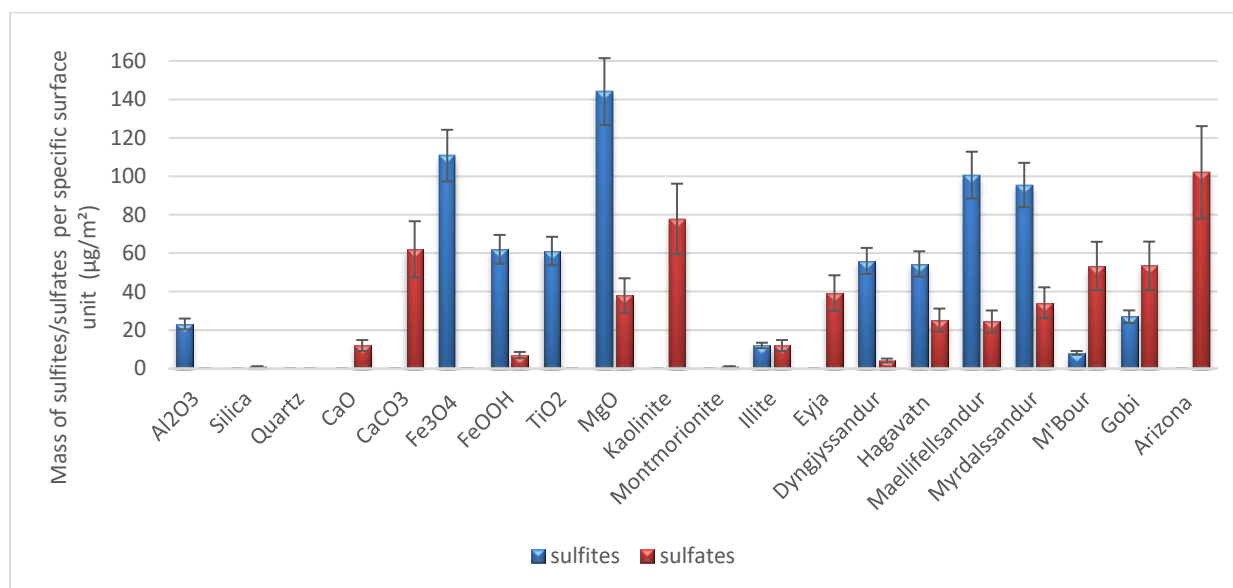


Figure 1: Amounts of sulfites and sulfates quantified on the surface of desert and volcanic dust samples as compared to the amounts of sulfites and sulfates formed on various pure metal oxides, calcium carbonate, goethite and clays. All samples were exposed to 175 ppm SO<sub>2</sub> for 1 hr at 30% RH. Sulfites and sulfates were extracted with 2 mL of 1% Formalin, sonicated for 10 min and analyzed by HPLC.

From Figure 1 we can see that on the surface of pure single mineral oxides, with the exception of MgO (contains both sulfites and sulfates) and SiO<sub>2</sub> (sulfites/sulfates are below the detection limits), only one type of sulfur species is observed: either sulfites or sulfates. In particular, on the surface of Al<sub>2</sub>O<sub>3</sub>, Fe<sub>2</sub>O<sub>3</sub>, TiO<sub>2</sub>, sulfites are solely formed, while on the surface of CaO, CaCO<sub>3</sub>, only sulfates are observed.

Meanwhile, both sulfites and sulfates are detected on the surface of most desert and volcanic dusts, except for Eyjafjallajökull and Arizona dusts that exhibit only sulfates. As a general trend, on the surface of v-dusts, with exception of Eyjafjallajökull, we observe a higher amount of sulfites and a lower amount of sulfates than on the surface of desert dusts. In addition, goethite contains both sulfites and sulfates. Three clays show contrasting behavior: sulfites are only observed on the surface of illite, while sulfates are observed for kaolinite and illite, but not for montmorillonite. Apparently, different minerals have different behaviors towards SO<sub>2</sub> gas and its further conversion from sulfites to sulfates.

Different distribution of sulfites and sulfates on the surface can be investigated from the “rate of conversion” point of view. Since sulfite formation necessarily precedes sulfate formation, the fact that we observe different sulfite to sulfate ratios on different dusts means that conversion of sulfites to sulfates follows different timeframe (Wang et al., 2018a). Apparently, the rate of sulfate formation is higher for desert dusts in comparison with volcanic dusts. It suggests that at least a part of the surface of desert dusts has a high sulfite-to-sulfate conversion rate and that at least a part of the surface of v-dusts has a lower reaction rate. The fact that no sulfites are observed on the surface of certain mineral oxides and natural samples by no means implies that they are not formed. If the sulfates are observed it follows that sulfites are formed as well but that their rate of consumption is too fast to be observed by our method (Urupina et al., 2019). On the other hand, absence of sulfates on the surface means that they were not formed (or they are formed in concentrations below the detection limit) due to extremely slow rate of sulfite to sulfate conversion on the corresponding surface.

### **3.2 Classification of mineral samples based on their efficiency to form sulfites and/or sulfates. Can a natural dust be represented by one chosen individual component?**

Based on Figure 1 mineral dusts and metal oxides can be grouped in the following way (Table 2). Group 1 forms neither sulfites nor sulfates on the surface: silica (SiO<sub>2</sub>), quartz (SiO<sub>2</sub>) and Montmorillonite. Group 2 has only sulfites and fails to convert them to sulfates: Al<sub>2</sub>O<sub>3</sub>, Fe<sub>3</sub>O<sub>4</sub>, and TiO<sub>2</sub>. Group 3 exhibits both sulfites and sulfates: FeOOH, MgO, Illite, Dyngjúsandur, Hagavatn, Mýrdalssandur, Maelifellssandur, Gobi and M’Bour. Finally, Group 4 converts sulfites to sulfates so fast, that no sulfites are observed: CaO, CaCO<sub>3</sub>, Eyjafjallajökull, and Arizona Test Dust.

Table 2: Classification of mineral samples based on their ability to form sulfites and/or sulfates on their surfaces.

Group	Samples	Comments
1	silica (SiO <sub>2</sub> ) quartz (SiO <sub>2</sub> ), Montmorionite	Neither formation nor detection of sulfites and sulfates.
2	Al <sub>2</sub> O <sub>3</sub> , Fe <sub>3</sub> O <sub>4</sub> , and TiO <sub>2</sub>	Formation and detection of sulfites only.
3	FeOOH, MgO, Illite, Dyngjusandur, Hagavatn, Mýrdalssandur, Maelifellssandur, Gobi and M'Bour	Formation and detection of sulfites and sulfates.
4	CaO, CaCO <sub>3</sub> , Eyjafjallajökull, and Arizona Test Dust	Detection of sulfates only. Fast conversion of sulfites to sulfates prevents their detection.

As we can see, not one surrogate is able to completely represent formation of sulfites and sulfates on the surface of all the dusts, as dusts themselves differ in the amount and distribution of sulfur species. Especially bad candidates for proxies would be Group 1 and 2 oxides, as they either form no sulfur species or demonstrate an extremely low rate of sulfite to sulfate conversion. Moreover, we can clearly see that Al<sub>2</sub>O<sub>3</sub> and CaCO<sub>3</sub> that are often chosen as proxies based on the assumption that each represents “the most important reactive component of mineral dust” show highly contrasted behaviors: only sulfites are formed on Al<sub>2</sub>O<sub>3</sub> while only sulfates are observed on CaCO<sub>3</sub> (Zhang et al., 2018), (Huang et al., 2016). Likewise, Huang et al. saw a 10 times decrease in the total amount of sulfur species formed on the surface of alumina vs Asian Mineral Dust particles collected in Beijing (Huang et al., 2016). Those discrepancies could be at least in part be explained by using alumina as a proxy. In addition, with exception of SiO<sub>2</sub>, all other proxy candidates exhibit significant reactivity towards formation of sulfites/sulfates, and thus choosing only one component while ignoring all the others does not seem justified (Figure 1). A conclusion can be made that no individual oxide can relevantly represent the reactivity of a complex heterogeneous mixture. But can reactivity of a mixture be investigated as a sum of reactivities of individual contributors, keeping in mind that these individual contributors are not necessarily present in the natural mixture in the assigned oxide form? Next, we will try to deduce individual contribution of pure oxides, goethite and calcium carbonate surrogates in the formation of sulfites/sulfates on natural samples.

### 3.3 Can a natural dust be characterized by a sum of “representative” simple mineral proxies?

Zhang et al. compared the reactivities of different oxides together with their mixture (based on the abundance of the corresponding elements in continental crust) taking into consideration their specific area and placed them in the following order: Fe<sub>2</sub>O<sub>3</sub>>MgO>TiO<sub>2</sub>>FeOOH>mixture>Al<sub>2</sub>O<sub>3</sub>>SiO<sub>2</sub> (Zhang et al., 2006). These authors came to the conclusion that the reactivity of the mixture, that was obtained by mixing the different oxides based on their abundances in the continental crust, was measured to be twice its theoretical value, which demonstrates a synergistic effect (Zhang et al., 2006). Contrary to the results obtained by Zhang et al., reactivity of China Loess was successfully predicted from the reactivity of its single component oxides and carbonates (Usher et al., 2002). Following the same logic we decided to test

whether the amount of sulfites and sulfates formed on the surface of a natural dust can be predicted from the sum of relative contributions of its individual oxides without accounting for K and Na component. **Note that, to take into account the well-known discrepancies between bulk and surface composition, the surface composition for dusts expressed as % oxide (by weight) was calculated from % surface elemental composition (by weight) measured with XPS.** This approach was tested by calculating the theoretical amount of sulfites/sulfates expected on the surface of dust  $S_{\text{dust}}^{\text{theoretical}}$  ( $\mu\text{g}/\text{m}^2$ ) based on our experimental results for simple oxides using Equation 1. The calculated amount of sulfites and sulfates was then compared to the experimentally measured results on natural volcanic/desert dusts.

*Equation 1* 
$$S_{\text{dust}}^{\text{theoretical}} = \sum_i f_i S_i$$

Where  $f_i$  is the fraction of  $i^{\text{th}}$  component and  $S_i$  ( $\mu\text{g}/\text{m}^2$ ) is the amount of sulfur species measured on the surface of  $i^{\text{th}}$  component.

Table 3: Quantitative comparison for the amount of sulfites and sulfates on the surface of natural dusts (i) calculated from the addition of the contributions of individual pure oxides and (ii) experimentally measured on the surface of dust. Elemental composition for dusts expressed as % oxide (by weight) was calculated from % elemental composition (by weight) measured with XPS and discussed earlier (see Section 2.2, Table 1).

Dust sample		SiO <sub>2</sub>	Al <sub>2</sub> O <sub>3</sub>	CaO	Na <sub>2</sub> O	MgO	TiO <sub>2</sub>	K <sub>2</sub> O	Fe <sub>2</sub> O <sub>3</sub>	MnO	Calculated from individual contributions of pure oxides ( $S_{dust}^{theoretical}$ )	Experimentally measured ( $S_{dust}^{experimental}$ )
Myrdalssandur	%	59,96	17,61	4,89	2,36	3,86	2,27	0,47	8,59	0		
	Sulfites ( $\mu\text{g}/\text{m}^2$ )	0	23	0		144	61		111		20,5	95
	Sulfates ( $\mu\text{g}/\text{m}^2$ )	1	0	12		38	0		0		2,7	34
Dyngjusandur	%	60,14	19,67	5,68	0,95	5,56	1,18	0,00	6,59	0,23		
	Sulfites ( $\mu\text{g}/\text{m}^2$ )	0	23	0		144	61		111		20,6	56
	Sulfates ( $\mu\text{g}/\text{m}^2$ )	1	0	12		38	0		0		3,4	4
Hagavatn	%	50,24	35,50	5,03	1,35	2,65	1,00	0,00	4,14	0,08		
	Sulfites ( $\mu\text{g}/\text{m}^2$ )	0	23	0		144	61		111		17,2	54
	Sulfates ( $\mu\text{g}/\text{m}^2$ )	1	0	12		38	0		0		2,1	25
Maelifellsandur	%	56,23	22,34	3,86	1,33	3,59	2,63	0,24	9,53	0,25		
	Sulfites ( $\mu\text{g}/\text{m}^2$ )	0	23	0		144	61		111		22,5	101
	Sulfates ( $\mu\text{g}/\text{m}^2$ )	1	0	12		38	0		0		2,4	24
Eyjafjallajökull	%	68,76	14,63	3,00	6,88	1,64	0,55	1,59	2,96	0,00		
	Sulfites ( $\mu\text{g}/\text{m}^2$ )	0	23	0		144	61		111		9,3	0
	Sulfates ( $\mu\text{g}/\text{m}^2$ )	1	0	12		38	0		0		1,7	39
Gobi	%	63,03	20,30	4,22	0,76	6,56	0,00	2,27	2,60	0,24		
	Sulfites ( $\mu\text{g}/\text{m}^2$ )	0	23	0		144	61		111		17,0	27
	Sulfates ( $\mu\text{g}/\text{m}^2$ )	1	0	12		38	0		0		3,6	53
M'Bour	%	62,01	33,27	1,26	0,24	0,00	0,12	0,87	2,24	0,00		
	Sulfites ( $\mu\text{g}/\text{m}^2$ )	0	23	0		144	61		111		10,2	8
	Sulfates ( $\mu\text{g}/\text{m}^2$ )	1	0	12		38	0		0		0,8	53
ATD	%	66,10	19,77	2,98	1,20	4,12	0,30	2,14	3,19	0,23		
	Sulfites ( $\mu\text{g}/\text{m}^2$ )	0	23	0		144	61		111		14,2	0
	Sulfates ( $\mu\text{g}/\text{m}^2$ )	1	0	12		38	0		0		2,6	102



From Table 3 it can be observed that the calculated and measured values are very different. Theoretical amounts of sulfates are up to 50 times lower than the experimentally measured ones. Indeed, for sulfates, theoretical values range from 1 to 4  $\mu\text{g}/\text{m}^2$  while the experimental values range from 4 to 100  $\mu\text{g}/\text{m}^2$ . As for sulfites, the theoretical values range from 2 to 20  $\mu\text{g}/\text{m}^2$  while the experimental values range from 0 to 100  $\mu\text{g}/\text{m}^2$ . The reason of the mismatch is most probably related to the fact that : (i) mineralogical surface composition of proxies is not the same as the one of real natural samples and (ii) there is a synergetic effect of the mixture of components of natural samples on the transformation of  $\text{SO}_2$  to sulfites/sulfates, which cannot be reproduced by using proxies. Thus, substituting a complex mineral for a collection of simple oxides does not seem to be appropriate for  $\text{SO}_2$  transformation. For example, silicate enstatite with molecular formula  $\text{MgSiO}_3$ , reported as 60%  $\text{SiO}_2$  and 40%  $\text{MgO}$  cannot be investigated as a mixture of these two simple oxides. If that is the case it explains why kaolinite clay which formula in terms of oxides is sometimes represented as  $\text{Al}_2\text{O}_3 \cdot 2\text{SiO}_2 \cdot 2\text{H}_2\text{O}$  does not at all behaves as  $\text{Al}_2\text{O}_3$  (no sulfites observed on kaolinite, while only sulfites are observed on  $\text{Al}_2\text{O}_3$ ) nor as quartz (a negligible amount of sulfate is observed on quartz, while a high amount is present on kaolinite) (Figure 1).

A better approach to approximate the behavior of a complex mixture is to identify and quantify the amount of minerals present in a selected dust and directly compare individual mineral phases to the behavior of the heterogeneous mixture. Thus, sulfites on the surface of desert dusts can be compared to those detected on pure hematite ( $\text{Fe}_2\text{O}_3$ ), goethite ( $\text{FeOOH}$ ), magnesium oxide ( $\text{MgO}$ ), rutile ( $\text{TiO}_2$ ), aluminum oxide ( $\text{Al}_2\text{O}_3$ ), carbonates ( $\text{CaCO}_3$ ), plagioclase ( $\text{NaAlSi}_3\text{O}_8$ ), muscovite ( $\text{KAl}_3\text{Si}_3\text{O}_{10}(\text{OH})_2$ ), kaolinite ( $\text{Al}_2\text{Si}_2\text{O}_5(\text{OH})_4$ ), pyrope ( $\text{Mg}_3\text{Al}_2(\text{SiO}_4)_3$ ), talc ( $\text{Mg}_3\text{Si}_4\text{O}_{10}(\text{OH})_2$ ), etc., while plagioclase ( $\text{NaAlSi}_3\text{O}_8$  -  $\text{CaAl}_2\text{Si}_2\text{O}_8$ ), pyroxene ( $(\text{Ca},\text{Na})(\text{Mg},\text{Fe},\text{Al},\text{Ti})(\text{Si},\text{Al})_2\text{O}_6$ ), olivine ( $(\text{Mg},\text{Fe})_2[\text{SiO}_4]$ ), magnetite ( $\text{Fe}_3\text{O}_4$ ), ilmenite ( $\text{FeTiO}_3$ ) and aluminosilicate glasses would be more appropriate minerals to consider in the case of v-dust. As for sulfates, presence of kaolinite ( $\text{Al}_2\text{Si}_2\text{O}_5(\text{OH})_4$ ) and calcium carbonate ( $\text{CaCO}_3$ ) can explain higher amount of sulfates on the surface of Gobi and M'Bour dusts. The exact quantities of minerals are necessary in order to evaluate trends in formation. But mineralogical analysis of dusts and its accurate quantification is laborious and expensive. In addition, certain mineral phases are present in dusts in very small amounts and are not readily obtained in their pure form. Thus, an optimum approach would be to use natural samples of dusts to study their heterogeneous interactions with gases to provide the most accurate description of heterogeneous processes on their surfaces.

## 4 Conclusions

In this study, three desert and five volcanic dusts were compared to a number of commonly used mineral surrogates in their ability to form sulfites and sulfates in order to see if metal oxides, calcium carbonates and goethite could be used as proxies to investigate reactivity of natural samples. **We can conclude that no proxy mimics the behavior of natural dust. Due to the complex crystalline structure of different mineral phases, approximation of natural samples using a mixture of simple proxies also does not satisfyingly reflect the behavior of natural samples.**

The fact that oxides do not depict the behaviors of natural samples definitely questions the representativeness of proxies to predict the behavior of natural samples in the atmosphere. For example, the degradation of  $\text{SO}_2$  on the surface of  $\text{Al}_2\text{O}_3$ ,  $\text{Fe}_3\text{O}_4$  or  $\text{TiO}_2$  is not the same as on the surface of desert dusts while metals of these oxides are present in the dusts. Desert dusts effectively convert  $\text{SO}_2$  into sulfates, while  $\text{Al}_2\text{O}_3$ ,  $\text{Fe}_3\text{O}_4$  and  $\text{TiO}_2$  have an extremely slow rate of conversion. In the complex atmospheric reaction pathways, stabilizing a molecule in sulfite form could offer reactivity towards compounds in respect to which sulfates are immune. Since the dusts behave differently in respect to the pollutants, approximations done on the lifetime of pollutants using proxies might be questionable. To sum up, trying to evaluate the impact of natural dusts on the climate using surrogates is problematic as this approach assumes that a proxy and a real heterogeneous mixture have similar properties, such as particle size, chemical composition, morphology, hygroscopicity, photo activity, electrical conductivity and other characteristics when they clearly don't. Therefore, we propose that the best approach to evaluate the influence of natural dust on atmospheric processes is to work directly with the natural samples to address the real effects of desert and volcanic dusts.

## References of Chapter 6

- Alleman, L.Y., Lamaison, L., Perdrix, E., Robache, A., Galloo, J.-C., 2010. PM10 metal concentrations and source identification using positive matrix factorization and wind sectoring in a French industrial zone. *Atmospheric Research* 96, 612–625. <https://doi.org/10.1016/j.atmosres.2010.02.008>
- Andreae, M., 1995. Climate Effects of Changing Atmospheric Aerosol. *World Survey of Climatology*. Vol. 16: Future Climates of the World, 341–392 (1995).
- Arnalds, O., Dagsson-Waldhauserova, P., Olafsson, H., 2016. The Icelandic volcanic aeolian environment: Processes and impacts — A review. *Aeolian Research* 20, 176–195. <https://doi.org/10.1016/j.aeolia.2016.01.004>
- Ayris, P., Delmelle, P., 2012. Volcanic and atmospheric controls on ash iron solubility: A review. *Physics and Chemistry of the Earth* 45, 103–112. <https://doi.org/10.1016/j.pce.2011.04.013>
- Bagheri, G., Rossi, E., Biass, S., Bonadonna, C., 2016. Timing and nature of volcanic particle clusters based on field and numerical investigations. *Journal of Volcanology and Geothermal Research* 327, 520–530. <https://doi.org/10.1016/j.jvolgeores.2016.09.009>
- Baltrusaitis, J., Cwiertny, D.M., Grassian, V.H., 2007. Adsorption of sulfur dioxide on hematite and goethite particle surfaces. *Phys. Chem. Chem. Phys.* 9, 5542–5554. <https://doi.org/10.1039/B709167B>
- Baratoux, D., Mangold, N., Arnalds, O., Bardintzeff, J.-M., Platevoet, B., Grégoire, M., Pinet, P., 2011. Volcanic Sand in Iceland: Diverse origins of aeolian sand deposits revealed at Dyngjúsandur and Lambahraun, Iceland. *Earth Surface Processes and Landforms* 36, 1789–1808. <https://doi.org/10.1002/esp.2201>
- Bluth, G.J.S., Schnetzler, C.C., Krueger, A.J., Walter, L.S., 1993. The contribution of explosive volcanism to global atmospheric sulphur dioxide concentrations. *Nature* 327–329.
- Bristow, C.S., Hudson-Edwards, K.A., Chappell, A., 2010. Fertilizing the Amazon and equatorial Atlantic with West African dust. *Geophysical Research Letters* 37. <https://doi.org/10.1029/2010GL043486>
- Crowley, J.N., Ammann, M., Cox, R.A., Hynes, R.G., Jenkin, M.E., Mellouki, A., Rossi, M.J., Troe, J., Wallington, T.J., 2010. Evaluated kinetic and photochemical data for atmospheric chemistry: Volume V – heterogeneous reactions on solid substrates. *Atmos. Chem. Phys.* 10, 9059–9223. <https://doi.org/10.5194/acp-10-9059-2010>
- Dagsson-Waldhauserova, P., Arnalds, O., Olafsson, H., Hladil, J., Skala, R., Navratil, T., Chadimova, L., Meinander, O., 2015. Snow–Dust Storm: Unique case study from Iceland, March 6–7, 2013. *Aeolian Research* 16, 69–74. <https://doi.org/10.1016/j.aeolia.2014.11.001>
- Daniel J. Jacob, 1999. *Introduction to Atmospheric Chemistry*. Princeton University Press, Princeton, New Jersey.
- Delmelle, P., Wadsworth, F.B., Maters, E.C., Ayris, P.M., 2018. High Temperature Reactions Between Gases and Ash Particles in Volcanic Eruption Plumes. *Reviews in Mineralogy and Geochemistry* 84, 285–308. <https://doi.org/10.2138/rmg.2018.84.8>
- Durant, A.J., Bonadonna, C., Horwell, C.J., 2010. Atmospheric and Environmental Impacts of Volcanic Particulates. *Elements* 6, 235–240.
- Earle, S., 2015. 5.2 Chemical Weathering, in: *Physical Geology*. BCcampus.
- Finlayson-Pitts, B.J., Jr, J.N.P., 1999. *Chemistry of the Upper and Lower Atmosphere: Theory, Experiments, and Applications*. Elsevier.
- Gislason, S.R., Hassenkam, T., Nedel, S., Bovet, N., Eiríksdóttir, E.S., Alfredsson, H.A., Hem, C.P., Balogh, Z.I., Dideriksen, K., Oskarsson, N., Sigfusson, B., Larsen, G., Stipp, S.L.S., 2011. Characterization of Eyjafjallajökull volcanic ash particles and a protocol for rapid risk assessment. *PNAS* 108, 7307–7312. <https://doi.org/10.1073/pnas.1015053108>
- Goodman, A.L., Li, P., Usher, C.R., Grassian, V.H., 2001. Heterogeneous Uptake of Sulfur Dioxide On Aluminum and Magnesium Oxide Particles. *J. Phys. Chem. A* 105, 6109–6120. <https://doi.org/10.1021/jp004423z>

- Hatch, C.D., Wiese, J.S., Crane, C.C., Harris, K.J., Kloss, H.G., Baltrusaitis, J., 2012. Water Adsorption on Clay Minerals As a Function of Relative Humidity: Application of BET and Freundlich Adsorption Models. *Langmuir* 28, 1790–1803. <https://doi.org/10.1021/la2042873>
- Highwood, E.-J., Stevenson, D.S., 2003. Atmospheric impact of the 1783-1784 Laki Eruption: Part II Climatic effect of sulphate aerosol. *Atmospheric Chemistry and Physics* 3, 1177–1189.
- Huang, L., Zhao, Y., Li, H., Chen, Z., 2016. Hydrogen peroxide maintains the heterogeneous reaction of sulfur dioxide on mineral dust proxy particles. *Atmospheric Environment* 141, 552–559. <https://doi.org/10.1016/j.atmosenv.2016.07.035>
- Ibrahim, S., Romanias, M.N., Alleman, L.Y., Zeineddine, M.N., Angeli, G.K., Trikalitis, P.N., Thevenet, F., 2018. Water Interaction with Mineral Dust Aerosol: Particle Size and Hygroscopic Properties of Dust. *ACS Earth Space Chem.* 2, 376–386. <https://doi.org/10.1021/acsearthspacechem.7b00152>
- Joshi, N., Romanias, M.N., Riffault, V., Thevenet, F., 2017. Investigating water adsorption onto natural mineral dust particles: Linking DRIFTS experiments and BET theory. *Aeolian Research* 27, 35–45. <https://doi.org/10.1016/j.aeolia.2017.06.001>
- Langmann, B., 2013. Volcanic Ash versus Mineral Dust: Atmospheric Processing and Environmental and Climate Impacts [WWW Document]. *International Scholarly Research Notices*. <https://doi.org/10.1155/2013/245076>
- Li, L., Chen, Z.M., Zhang, Y.H., Zhu, T., Li, J.L., Ding, J., 2006. Kinetics and mechanism of heterogeneous oxidation of sulfur dioxide by ozone on surface of calcium carbonate. *Atmospheric Chemistry and Physics Discussions* 6, 579–613. <https://doi.org/10.5194/acpd-6-579-2006>
- Marticorena, B., Chatenet, B., Rajot, J.L., Bergametti, G., Deroubaix, A., Vincent, J., Kouoi, A., Schmechtig, C., Coulibaly, M., Diallo, A., Koné, I., Maman, A., NDiaye, T., Zakou, A., 2017. Mineral dust over west and central Sahel: Seasonal patterns of dry and wet deposition fluxes from a pluriannual sampling (2006–2012). *Journal of Geophysical Research: Atmospheres* 122, 1338–1364. <https://doi.org/10.1002/2016JD025995>
- Maters, E.C., Delmelle, P., Rossi, M.J., Ayris, P.M., Bernard, A., 2016. Controls on the surface chemical reactivity of volcanic ash investigated with probe gases. *Earth Planet. Sci. Lett.* 450, 254–262. <https://doi.org/10.1016/j.epsl.2016.06.044>
- Moroni, B., Arnalds, O., Dagsson-Waldhauserová, P., Crocchianti, S., Vivani, R., Cappelletti, D., 2018. Mineralogical and Chemical Records of Icelandic Dust Sources Upon Ny-Ålesund (Svalbard Islands). *Front. Earth Sci.* 6. <https://doi.org/10.3389/feart.2018.00187>
- Nanayakkara, C.E., Pettibone, J., Grassian, V.H., 2012. Sulfur dioxide adsorption and photooxidation on isotopically-labeled titanium dioxide nanoparticle surfaces: roles of surface hydroxyl groups and adsorbed water in the formation and stability of adsorbed sulfite and sulfate. *Phys. Chem. Chem. Phys.* 14, 6957–6966. <https://doi.org/10.1039/C2CP23684B>
- Prospero, J.M., Ginoux, P., Torres, O., Nicholson, S.E., Gill, T.E., 2002. Environmental Characterization of Global Sources of Atmospheric Soil Dust Identified with the Nimbus 7 Total Ozone Mapping Spectrometer (toms) Absorbing Aerosol Product. *Reviews of Geophysics* 40, 2-1-2–31. <https://doi.org/10.1029/2000RG000095>
- Schepanski, K., 2018. Transport of Mineral Dust and Its Impact on Climate. *Geosciences* 8, 151. <https://doi.org/10.3390/geosciences8050151>
- Schmidt, A., Ostro, B., Carslaw, K.S., Wilson, M., Thordarson, T., Mann, G.W., Simmons, A.J., 2011. Excess mortality in Europe following a future Laki-style Icelandic eruption. *PNAS* 108, 15710–15715. <https://doi.org/10.1073/pnas.1108569108>
- Stevenson, D.S., Johnson, C.E., Highwood, E.J., Gauci, V., Collins, W.J., Derwent, R.G., 2003. Atmospheric impact of the 1783–1784 Laki eruption: Part I Chemistry modelling. *Atmos. Chem. Phys.* 3, 487–507. <https://doi.org/10.5194/acp-3-487-2003>
- Tang, M., Cziczo, D.J., Grassian, V.H., 2016. Interactions of Water with Mineral Dust Aerosol: Water Adsorption, Hygroscopicity, Cloud Condensation, and Ice Nucleation. *Chem. Rev.* 116, 4205–4259. <https://doi.org/10.1021/acs.chemrev.5b00529>

- Urupina, D., Gaudion, V., Romanias, M.N., Verrielle, M., Thevenet, F., 2020. Method development and validation for the determination of sulfites and sulfates on the surface of mineral atmospheric samples using reverse-phase liquid chromatography. *Talanta* 219, 121318. <https://doi.org/10.1016/j.talanta.2020.121318>
- Urupina, D., Lasne, J., Romanias, M.N., Thiery, V., Dagsson-Waldhauserova, P., Thevenet, F., 2019. Uptake and surface chemistry of SO<sub>2</sub> on natural volcanic dusts. *Atmospheric Environment* 217, 116942. <https://doi.org/10.1016/j.atmosenv.2019.116942>
- US EPA, O., 2016. Sulfur Dioxide Basics [WWW Document]. US EPA. URL <https://www.epa.gov/so2-pollution/sulfur-dioxide-basics> (accessed 8.14.20).
- Usher, C.R., Al-Hosney, H., Carlos-Cuellar, S., Grassian, V.H., 2002. A laboratory study of the heterogeneous uptake and oxidation of sulfur dioxide on mineral dust particles. *J.-Geophys.-Res.* 107, 4713. <https://doi.org/10.1029/2002JD002051>
- Usher, C.R., Michel, A.E., Grassian, V.H., 2003. Reactions on Mineral Dust. *Chem. Rev.* 103, 4883–4940. <https://doi.org/10.1021/cr020657y>
- Vodyanitskii, Yu.N., 2018. Elements oxides as a source of errors in the gross chemical composition of soil and ways to eliminate the errors. *Annals of Agrarian Science* 16, 90–93. <https://doi.org/10.1016/j.aasci.2017.09.003>
- Wang, T., Liu, Y., Deng, Y., Fu, H., Zhang, L., Chen, J., 2018a. Emerging investigator series: heterogeneous reactions of sulfur dioxide on mineral dust nanoparticles: from single component to mixed components. *Environ. Sci.: Nano* 5, 1821–1833. <https://doi.org/10.1039/C8EN00376A>
- Wang, T., Liu, Y., Deng, Y., Fu, H., Zhang, L., Chen, J.-M., 2018b. Adsorption of SO<sub>2</sub> on mineral dust particles influenced by atmospheric moisture. *Atmospheric Environment* 191. <https://doi.org/10.1016/j.atmosenv.2018.08.008>
- Wang, X., Romanias, M.N., Pei, Z., Rousseau, A., Thévenet, F., 2020. Uptake Mechanism of Acetic Acid onto Natural Gobi Dust. *ACS Earth Space Chem.* 4, 1650–1662. <https://doi.org/10.1021/acsearthspacechem.0c00168>
- Wu, L.Y., Tong, S.R., Wang, W.G., Ge, M.F., 2011. Effects of temperature on the heterogeneous oxidation of sulfur dioxide by ozone on calcium carbonate. *Atmospheric Chemistry and Physics* 11, 6593–6605. <https://doi.org/10.5194/acp-11-6593-2011>
- Zhang, X., Zhuang, G., Chen, J., Wang, Y., Wang, X., An, Z., Zhang, P., 2006. Heterogeneous Reactions of Sulfur Dioxide on Typical Mineral Particles. *J. Phys. Chem. B* 110, 12588–12596. <https://doi.org/10.1021/jp0617773>
- Zhang, Y., Tong, S., Ge, M., Jing, B., Hou, S., Tan, F., Chen, Y., Guo, Y., Wu, L., 2018. The influence of relative humidity on the heterogeneous oxidation of sulfur dioxide by ozone on calcium carbonate particles. *Sci. Total Environ.* 633, 1253–1262. <https://doi.org/10.1016/j.scitotenv.2018.03.288>
- Zuo, Y., Chen, H., 2003. Simultaneous determination of sulfite, sulfate, and hydroxymethanesulfonate in atmospheric waters by ion-pair HPLC technique. *Talanta* 59, 875–881. [https://doi.org/10.1016/S0039-9140\(02\)00647-1](https://doi.org/10.1016/S0039-9140(02)00647-1)



**Chapter VII. Investigating the distributions of sulfites and sulfates  
on the surface of natural volcanic dusts**

## Table of content of Chapter 7

1	Introduction.....	210
2	Specific experimental considerations for the investigation of sulfite and sulfate distribution .....	211
3	Results and discussion .....	211
3.1	Investigating the influence of RH on the formation of sulfites and sulfates on the surface of natural dusts .....	211
3.2	Investigating the influence of the surface elemental composition on the formation of sulfites and sulfates at different values of RH .....	217
3.3	Sulfite and sulfate formation as a function of time. Stability of surface species. ....	220
3.3.1	What happens on the surface of a natural dust particle subjected to SO <sub>2</sub> ? .....	220
3.3.2	What happens on the surface of a natural dust particle previously subjected to SO <sub>2</sub> when the gas is no longer available? .....	225
3.3.3	What happens on the surface of a natural dust particle when ageing with SO <sub>2</sub> on ppb level? 227	
4	Conclusions.....	228
	References.....	230



## List of Tables of Chapter 7

Table 1: Relationship between elemental surface composition and the amount of sulfites and sulfates formed on the surface. ....	218
---	-----

## List of Figures of Chapter 7

- Figure 1: HPLC analysis of mineral and volcanic dust samples 30 mg-180 mg, 175 ppm of SO<sub>2</sub>, extracted with 2 ml of 1% Formalin, sonicated for 10 min. (a) Amount of sulfites and sulfates formed on the surface of volcanic and desert dusts while aging with 175 ppm SO<sub>2</sub> for 1 hr at different values of relative humidity: 0, 30, and 60 and 83 % RH. (b) Total amount sulfur formed on the surface of volcanic and desert dusts while aging with 175 ppm SO<sub>2</sub> for 1 hr at different values of relative humidity: 0, 30, and 60 and 83 % RH. ....213
- Figure 2: Various scenarios leading to the formation of sulfites and sulfates as observed on the Hagavatt v-dust when detected with HPLC. Remember that only sulfites (blue circles) and sulfates (red circles) are detected by HPLC technique. SO<sub>2</sub> gas (yellow circles) is not detected by HPLC. The total sulfur content of the adsorbed sulfites and sulfates as a function of RH is kept constant as was evidenced for Hagavatt dust earlier....215
- Figure 3: Various scenarios leading to the formation of sulfites and sulfates as observed on the Gobi dust when detected with HPLC. Remember that only sulfites (blue circles) and sulfates (red circles) are detected by HPLC technique. SO<sub>2</sub> gas (yellow circles) is not detected by HPLC. The total sulfur content of the adsorbed sulfites and sulfates is increasing as a function of RH.....216
- Figure 4: Dependence of the amount of sulfites quantified on the surface of eight natural dusts on the samples' surface ratio of (Ti+Fe) over Si. Surface elemental composition expressed in % element by weight was obtained from XRD measurements (See Chapter 2 Section 1.2.4). Ageing conditions: 1 hr, 175 ppm SO<sub>2</sub>, 30% RH. ....219
- Figure 5: Dependence of the amount of sulfates quantified on the surface of eight natural dusts on the samples' surface ratio of Na over Si. Surface elemental composition expressed in % element by weight was obtained from XRD measurements (See Chapter 2 Section 1.2.4). Ageing conditions: 1 hr, 175 ppm SO<sub>2</sub>, 0% RH.....219
- Figure 6: HPLC analysis of desert and volcanic dust samples 0,089-0,194 g, aged for up to 1400 min, 175 ppm of SO<sub>2</sub>, 30 % RH extracted with 2 ml of 1% Formalin, sonicated for 10 min (a) Formation of sulfites on the surface of volcanic and desert dusts as a function time, (b) Formation of sulfates on the surface on the surface of volcanic and desert dusts as a function time, (c) Total sulfur content of various volcanic and desert dusts at 1 hr and 24 hr. ....223
- Figure 7: Ageing profiles of Hagavatt volcanic dust sample exposed to 175 ppm SO<sub>2</sub> for up to 4320 min (72 hours) HPLC analysis 0,086-0,192 g, 30 % RH extracted with 2 ml of 1% Formalin, sonicated for 10 min. (a) Profiles of sulfites and sulfates formed on the surface of Hagavatt v-dust as a function of time while ageing with 175 ppm SO<sub>2</sub>, (b) Total amount of sulfur formed of the surface of Hagavatt v-dust as a function of time while ageing with 175 ppm SO<sub>2</sub>. ....224
- Figure 8: HPLC analysis of the volcanic and mineral dusts aged with 175 ppm SO<sub>2</sub> for 1 hr and then kept for 20 or 30 hr in a closed container. 30 % RH was maintained during experiments. HPLC analysis 0,082-0,189 g, extracted with 2 ml of 1% Formalin, sonicated for 10 min. (a) Amount of sulfites and sulfates formed on the surface of dusts while aging with 175 ppm SO<sub>2</sub> for 1 hr and then keeping them in a closed container,

(b) Total amount of sulfur formed on the surface of dusts while aging with 175 ppm SO <sub>2</sub> for 1hr and then keeping them for in a closed container. ....	226
Figure 9: Ageing profiles of Mýrdalssandur volcanic dust sample exposed to 175 ppm SO <sub>2</sub> for up to 24 and 75 ppb for up to 120 hr. ....	228

# 1 Introduction

In this chapter, the influence of humidity and elemental composition on the formation of sulfites and sulfates on the surface of  $\nu$ -dust was investigated using the HPLC method introduced and developed in Chapter 5. Desert dusts were likewise studied to put the findings in a more global context. In Chapter 3 we already evidenced an increase of the uptake of  $\text{SO}_2$  molecules on the surface of two natural  $\nu$ -dusts, Hagavatn and Myrdalssandur, as a function of RH, using flow-tube reactor. This trend was confirmed in Chapter 4 by following the formation of surface sulfate species on Hagavatn  $\nu$ -dust using DRIFTS optical cell (Urupina et al., 2019). In the literature, various studies report an increase of sulfate formation with the increase of RH. For instance, Huang et al. observed the phenomena on the surface of Arizona Test Dust and Tengger Desert Dust and explained it by an accelerated hydration of  $\text{SO}_2$  in the presence of adsorbed water (Huang et al., 2015). Most of the studies, though, limit themselves to the investigation of sulfates as the final oxidation product and ignore the sulfite intermediate while this compounds can be meaningful regarding the surface reactivity of the dust sample (Wang et al., 2018). Indeed, quantification of sulfites along with sulfates could provide a more comprehensive description of the  $\text{SO}_2$  adsorption and transformation. To the best of our knowledge this is the first study aiming to simultaneously quantitatively evaluate both sulfites and sulfates formed on the surface of natural dusts at different levels of humidity. The method developed earlier enabled the individual investigation of both surface species, providing a full picture of the conversion of  $\text{SO}_2$  gas to sulfates (Urupina et al., 2020).

Due to the wide range of temperatures (1100 to 230K) and levels of RH (few percent to 100%) in the volcanic plumes, no fixed experimental conditions are able to fully represent heterogeneous interactions during volcanic eruptions (Textor et al., 2003). This chapter is more relevant to the investigations of the processes that happen in the plume as opposed to the processes at high temperatures that happen in the volcanic vent. Experiments were run at atmospherically relevant conditions: various RH values, atmospheric pressure of 760 Torr, room temperature, 293 K. The concentration of  $\text{SO}_2$  is kept at elevated level of 175 ppm in order to speed up a relatively long ageing process. The validity of this approximation is addressed at the end of this chapter (Section 3.3.3) in order to estimate how atmospherically relevant is the one-hour ageing performed at 175 ppm  $\text{SO}_2$  to processes that happen on the scale of days or weeks, but with much lower concentrations. Additionally, a search for the elements that might influence the formation of sulfites and sulfates on the surface of dust was undertaken. Next, long-time ageing profiles (for at least 24 hours) for sulfites and sulfates were conducted to quantitatively evaluate the capacity of dusts to store sulfur species. Stability of the adsorbed species was likewise addressed. This information will hopefully enable us to better evaluate the impact of dust on atmospheric processes, such as ability of dusts to remove

SO<sub>2</sub>, potential change of reactivity of the dusts followed by the formation of surface sulfur species, and the hygroscopic and optical properties of the dust aged with SO<sub>2</sub>.

Finally, we evaluated whether ageing the dusts with high SO<sub>2</sub> concentration of 175 ppm is justified for atmospheric investigations. For this matter we performed long term ageing of dusts for up to 5 days with atmospherically relevant concentration of 75 ppb SO<sub>2</sub>. We then compared the results obtained employing one-hour ageing with 175 ppm SO<sub>2</sub> to the results obtained using 75 ppb SO<sub>2</sub> in order to find how the concentration of SO<sub>2</sub> influences the formation of sulfur surface species.

## **2 Specific experimental considerations for the investigation of sulfite and sulfate distribution**

To evaluate the influence of humidity on sulfite and sulfate formation on the surface, five volcanic dusts and three desert dusts described and characterized earlier (Chapter II Section 1.1 and Section 1.2 ) were investigated under various conditions of humidity: 0%, 30%, 60%, and 83 %. A detailed description of the setup, as well as the method for dust ageing and sulfite/sulfate quantification is provided in Chapter 2 and Chapter 5. Ageing profiles for up to 24 hr using 175 ppm SO<sub>2</sub> were obtained for all the samples at 30% RH. The Hagavatn sample was additionally aged at 175 ppm SO<sub>2</sub> for 38 hr, 45 hr, 54 hr and 72 hr. Further transformation of the surface species in the absence of SO<sub>2</sub> was investigated by (i) ageing the samples for 1 hr with 175 ppm SO<sub>2</sub> followed by flushing with air (ii) ageing a dust for 1hr with 175 ppm SO<sub>2</sub>, transferring it in a 7 ml vial and keeping it closed for a 20 to 30 hr before HPLC analysis. To evaluate whether ageing the dusts with high SO<sub>2</sub> concentrations of 175 ppm is justified for atmospheric investigations a Mýrdalssandur dust was aged at atmospherically relevant 75 ppb SO<sub>2</sub> for 5 hr, 20 hr and 120 hr (5 days). This dust was chosen due to the fact that it demonstrated a particularly high amount of sulfites and sulfates on the surface (Chapter 6).

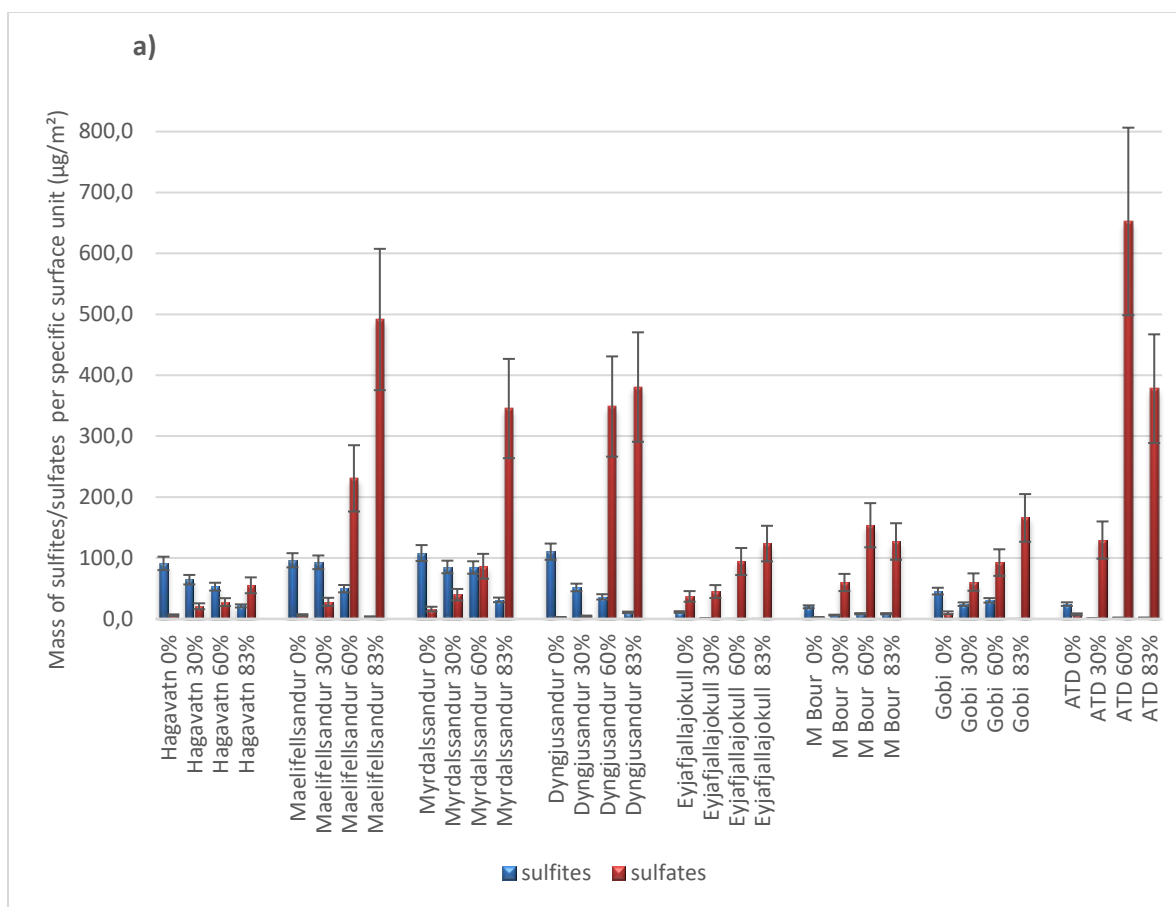
## **3 Results and discussion**

### **3.1 Investigating the influence of RH on the formation of sulfites and sulfates on the surface of natural dusts**

The first step in the investigation of the behavior of dusts of volcanic and desert origin was to subject them to 1 hr ageing with SO<sub>2</sub> gas, 175 ppm, at different levels of relative humidity, such as 0%, 30%, 60%, and 83%. One hour ageing was selected based on the fact that within this time period sulfites already reach a stable level, while sulfates are formed in detectable amounts and keep increasing. Formation of both species is necessary to study the reaction mechanism. Longer ageing would be beneficial for the

detection of sulfates. At the same time the longer is the experiment the more the surface is modified. It is probable that intensive surface modifications at long ageing times could obscure information of the “pristine” chemical composition with the sulfites/sulfates formation. Thus, one hour ageing is a compromise between relevant shorter time of ageing and ability to observe sulfites and sulfates.

From Figure 1A it can be observed that with increase of humidity from 0 to 83 % the amount of sulfites on the surface is decreasing for all samples. Meanwhile, the amount of sulfates is increasing from 0 to 60% RH, after which level the amount of sulfates formed either stabilizes within the relative error or keeps increasing to a lower extent. Arizona test dust seems to be an exception to the rule as its sulfate content is slightly decreasing from 60 to 83 % RH. For the majority of samples the increase in the sulfate formation is visibly higher than the decrease in sulfite formation. In addition, most of v-dusts form higher amount of sulfites than desert dusts. This difference could be related to the surface composition of the dusts and is addressed later in Section 3.2. Figure 1B evaluates the total amount of sulfur-based species formed on the surface as a function of humidity. As a general rule, with exception of Hagavatn, the total amount of sulfur-based species increases as a function of RH.



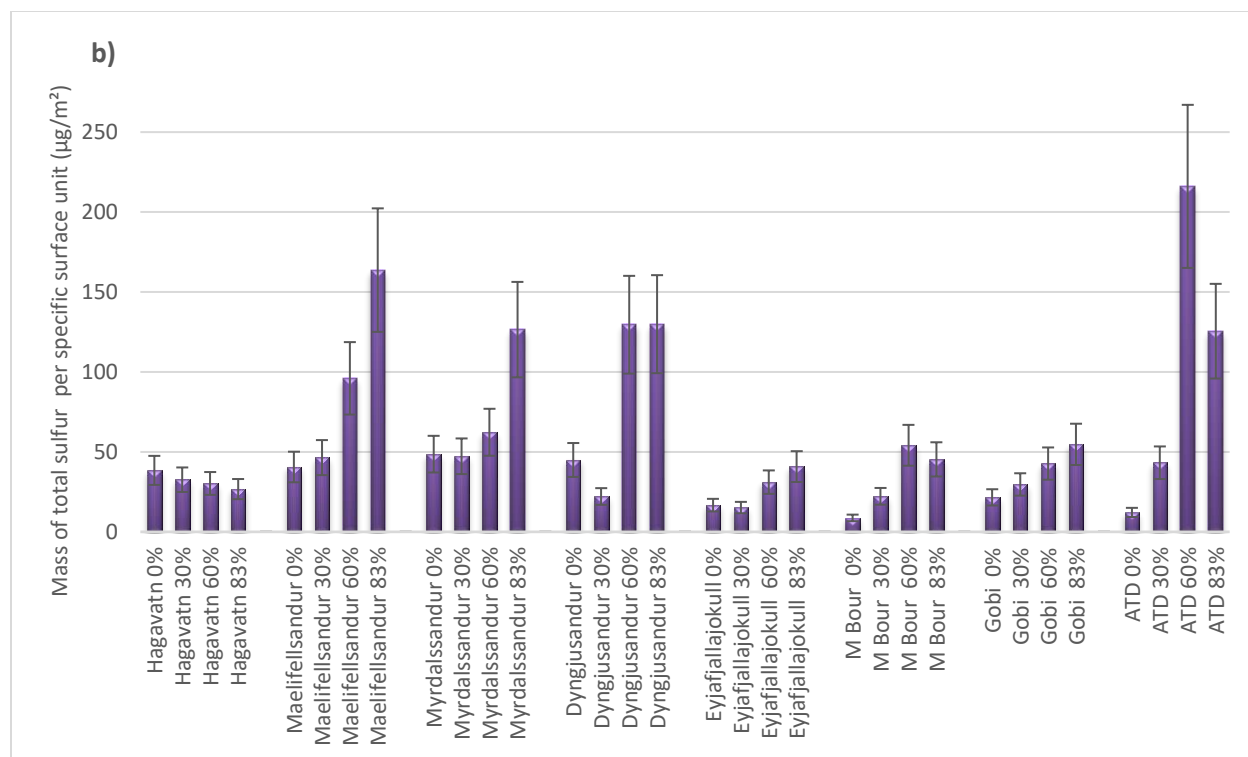
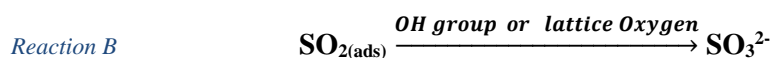
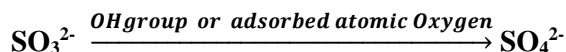


Figure 1: HPLC analysis of mineral and volcanic dust samples 30 mg-180 mg, 175 ppm of SO<sub>2</sub>, extracted with 2 mL of 1% Formalin, sonicated for 10 min. (a) Amount of sulfites and sulfates formed on the surface of volcanic and desert dusts while aging with 175 ppm SO<sub>2</sub> for 1 hr at different values of relative humidity: 0, 30, and 60 and 83 % RH. (b) Total amount sulfur formed on the surface of volcanic and desert dusts while aging with 175 ppm SO<sub>2</sub> for 1 hr at different values of relative humidity: 0, 30, and 60 and 83 % RH.

Based on Figure 1A and Figure 1 B the influence of humidity on the uptake and transformation of SO<sub>2</sub> can be interpreted and evaluated. Figure 1 provides information about (i) the influence of RH on the transformation of adsorbed SO<sub>2</sub> to sulfites, and sulfites to sulfates and (ii) the influence of RH on total sulfur uptake. Note that the influence of humidity on the transformation of gas phase SO<sub>2</sub> to adsorbed phase SO<sub>2</sub> cannot be deduced from Figure 1, as we are unable to monitor and quantify molecularly adsorbed SO<sub>2</sub> on the surface with HPLC technique. Nevertheless, as discussed in chapter 4, DRIFTS experiments evidenced the presence of physisorbed SO<sub>2</sub> on the surface of v-dusts. Furthermore, as a reminder, flow-tube experiments revealed an increase in the total number of molecules of SO<sub>2</sub> lost from the gas phase as a function of RH (Chapter 3), which, while not directly related to the increase of physisorbed SO<sub>2</sub>, signifies that the transformation of SO<sub>2</sub> to surface species seems to be enhanced in presence of water.

The reactions of SO<sub>2</sub> with the surface can be simplified in the following way based on the reactions discussed earlier (Chapter 4):





Simply by looking at the reactions A, B and C it is possible that increasing the amount OH groups can theoretically increase the rates of all 3 reactions. The decrease in sulfites with concomitant increase of sulfates that we observe as a function of RH (Figure 1) is particularly in accordance with mechanism discussed in Chapter 4 and depicted in Reaction C, and is based on the fact that OH groups were demonstrated to contribute to sulfite to sulfate conversion (Wang et al., 2018). Next we try to provide possible scenarios for the formation of sulfites and sulfates and the role of RH.

Based on the influence of RH on the total amount of sulfur species formed, samples can be grouped in the following way: (i) increase in the total amount of sulfur as a function of RH, (ii) no effect, and (iii) decrease. The dusts investigated in this work exhibited two types of behavior: no effect for Hagavattn and increase in total amount of sulfur surface species as a function of RH for all the other samples. Thus, various reaction scenarios were considered for a representative of each group: (i) *Hagavattn* that exhibits a steady amount of total surface sulfur on the surface and (ii) *Gobi* that demonstrates an increase in the total amount of sulfur with increased humidity.

Hagavattn v-dust has a stable amount of total sulfur as a function of %RH, while displaying a decrease of sulfites accompanied by a growth of sulfates. Two possible scenarios that fit this pattern were developed (Figure 2). In both scenarios sulfite-to-sulfate conversion rate (Reaction C) is increased as function of RH.

In scenario #1, the RH has an influence on reaction A and C, but not on reaction B. In other words, the initial adsorption of SO<sub>2</sub> gas molecules increases with increased humidity as well as sulfite-to-sulfate conversion rate, but the reaction of adsorbed SO<sub>2</sub> that leads to the formation of sulfites is independent of RH.

In scenario #2 the adsorption of SO<sub>2</sub> (Reaction A) and conversion of SO<sub>2</sub> to sulfites (Reaction B) are both independent of RH. From what we have observed earlier in flow-tube experiments the total amount of SO<sub>2</sub> lost from the gas phase increases as a function of RH. Thus, scenario #1 seems to be more probable.

Gobi dust, on the other hand, has a different behavior from Hagavattn in the way that its total sulfur content increases as a function of RH (Figure 3). As for the conversion of sulfites to sulfates, just as Hagavattn v-dust, we observe a decrease of sulfites accompanied by an increase of sulfates. Three possible scenarios fit this pattern.



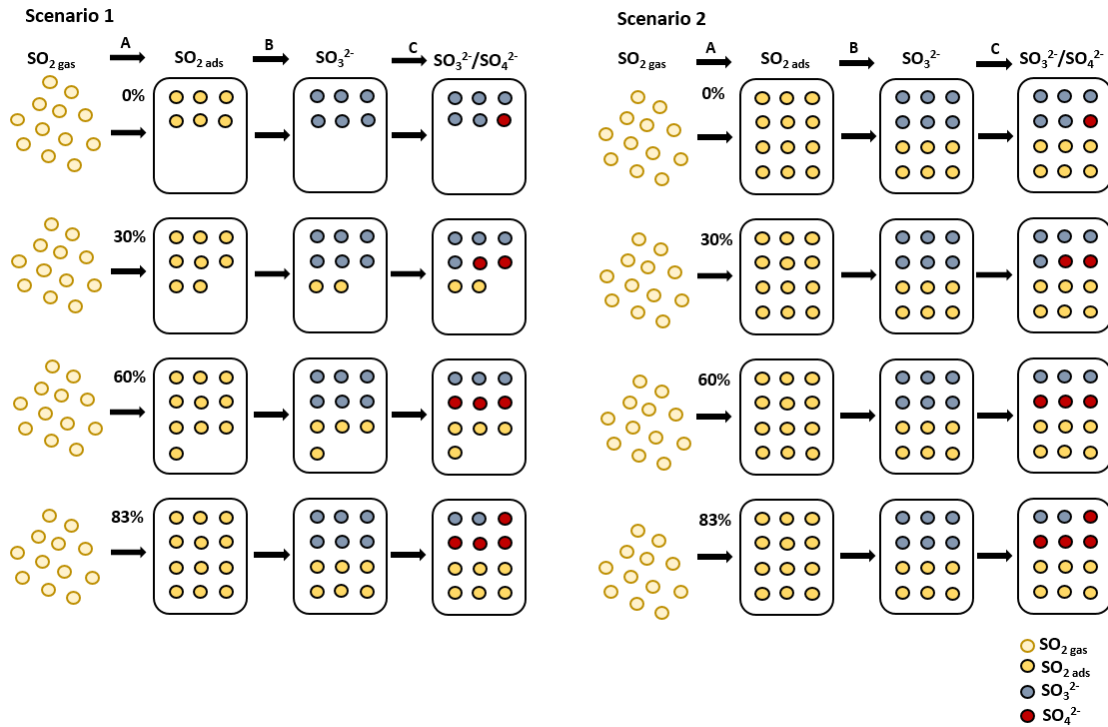


Figure 2: Various scenarios leading to the formation of sulfites and sulfates as observed on the Hagavatt v-dust when detected with HPLC. Remember that only sulfites (blue circles) and sulfates (red circles) are detected by HPLC technique. SO<sub>2</sub> gas (yellow circles) is not detected by HPLC. The total sulfur content of the adsorbed sulfites and sulfates as a function of RH is kept constant as was evidenced for Hagavatt dust earlier.

In scenario #1 all three steps are increased as a function of RH: adsorption of SO<sub>2</sub> molecules on the surface (Reaction A), conversion of SO<sub>2 ads</sub> to SO<sub>3</sub><sup>2-</sup> (Reaction B), and, finally SO<sub>3</sub><sup>2-</sup> to SO<sub>4</sub><sup>2-</sup> (Reaction C). This scenario reflects well the increase of the total number of SO<sub>2</sub> lost from the gas phase as a function of RH observed in reactions with flow-tubes using v-dusts.

In scenario #2 Reaction A and C are dependent on RH, while Reaction B is not. This scenario reflects the possibility that conversion of SO<sub>2 ads</sub> to SO<sub>3</sub><sup>2-</sup> is not reliant on RH. In this case all SO<sub>2</sub> molecules adsorbed on the surface are converted to sulfites.

In scenario #3 the number of SO<sub>2</sub> molecules physisorbed on the surface does not depend on RH (Reaction A), but both the conversion of SO<sub>2 ads</sub> to SO<sub>3</sub><sup>2-</sup> (Reaction B) and SO<sub>3</sub><sup>2-</sup> to SO<sub>4</sub><sup>2-</sup> do (Reaction C). This scenario though does not explain increased amount of SO<sub>2</sub> lost from the gas phase as a function of RH.

Thus, scenarios #1 and #2 are more likely, as both fit the increase in the total SO<sub>2</sub> lost from the gas phase observed in flow-tube experiments. Note, that effectively scenario #2 for Gobi is the same as scenario #1 for Hagavatt: in both cases Reaction A and Reaction C depend on RH while Reaction B does not.

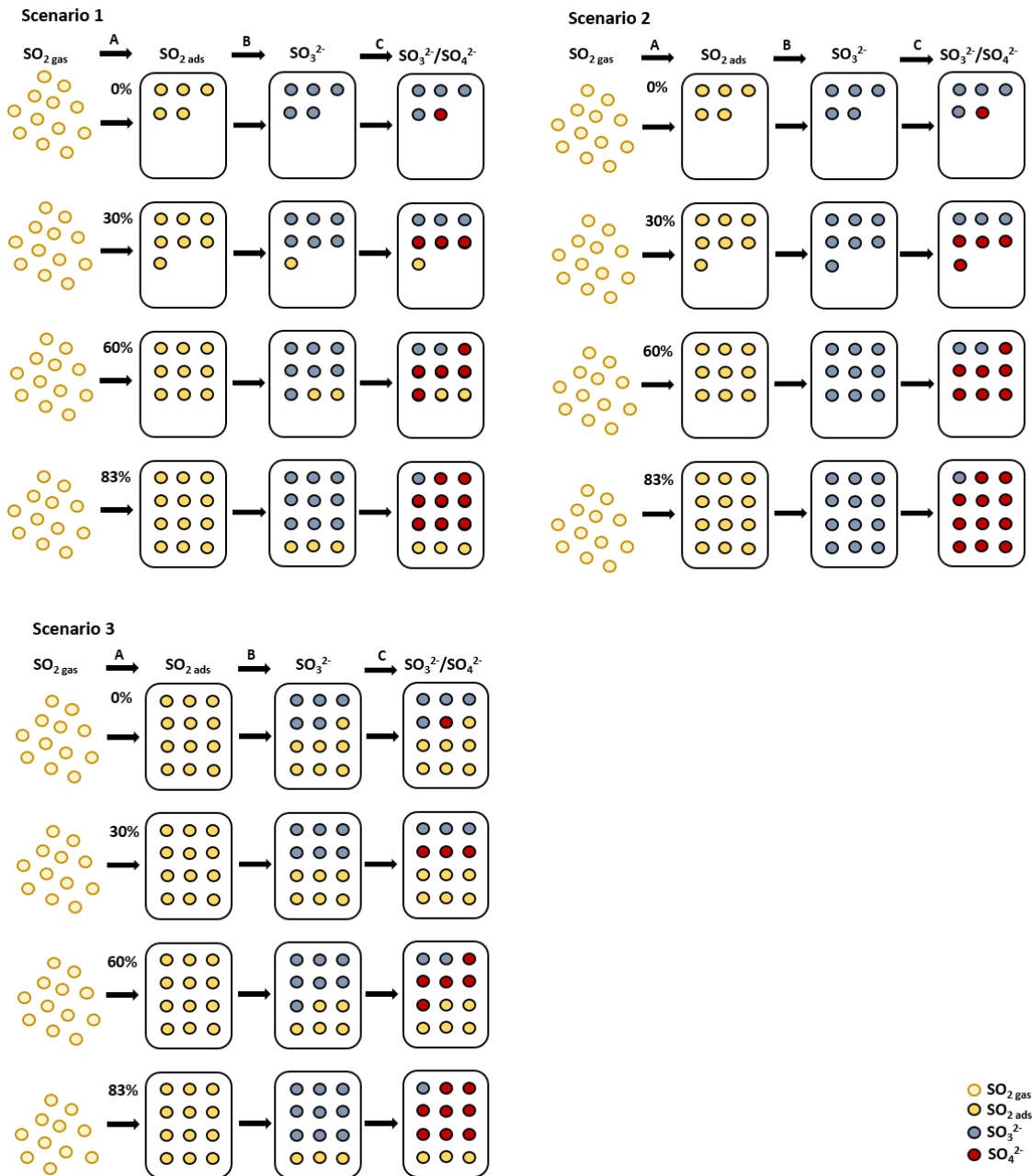


Figure 3: Various scenarios leading to the formation of sulfites and sulfates as observed on the Gobi dust when detected with HPLC. Remember that only sulfites (blue circles) and sulfates (red circles) are detected by HPLC technique. SO<sub>2</sub> gas (yellow circles) is not detected by HPLC. The total sulfur content of the adsorbed sulfites and sulfates is increasing as a function of RH.

To sum up, the most likely scenarios in case of both Hagavtn and Gobi dusts include dependence of the Reaction A and Reaction C on relative humidity. The presence of water molecules creates new active sites where SO<sub>2</sub> can be taken up more efficiently (Reaction A) as well as supplies OH groups for sulfite to sulfate conversion (Reaction C).

Nevertheless, these theoretical scenarios aim to demonstrate the impact of RH on the distribution of sulfites and sulfates. Dusts can potentially exhibit a range of behaviors: it is possible to observe a very low amount of sulfates at high RH levels and a very low amount of sulfites at low levels RH. The latter seems to be the case for Eyjafjallajökull v-dust and Arizona desert dusts that convert sulfites to sulfates so fast that we are only able to witness sulfites at 0% RH.

Another way of evaluating the influence of RH on the formation of surface sulfur species is evaluating % coverage of the species in question. Formation of total sulfur species on the surface of v-dust increases as a function of humidity for 7 out of 8 samples, the exception being Hagavatn v-dust, where the total amount of sulfur species remains relatively stable. Following the calculations of Romanias et al. a fully-stacked monolayer for sulfurous or sulfuric acid is composed of  $N_{H_2SO_3} = 5.75 \times 10^{14}$  molecules  $cm^{-2}$  and  $N_{H_2SO_4} = 4.22 \times 10^{14}$  molecules  $cm^{-2}$  respectively (Romanias et al., 2016). Thus, the amount of sulfur species measured on the surface of dust at different RH levels was converted in molecules  $cm^{-2}$  and using a total number of molecules necessary to form a monolayer, %coverage of sulfites and sulfates was calculated. It ranges from 5% total sulfur species coverage at 0% RH to about 60% total sulfur species coverage at 83% RH. Considering the fact that not all surface sites are involved in adsorption of  $SO_2$  molecules, as was demonstrated in case of quartz and silica in Chapter 6 (neither sulfites, nor sulfates observed), it is possible that the dusts in question reach a monolayer of sulfur species at elevated levels of RH.

### **3.2 Investigating the influence of the surface elemental composition on the formation of sulfites and sulfates at different values of RH**

To investigate the influence of the surface composition on the formation of sulfites and sulfates five mineral dusts and three desert dusts were aged for 1 hr under 4 levels of relative humidity: 0%, 30%, 60% and 83%. Percent surface composition of Si, Al, Fe, Ti, K, Ca, Na, Mg and Mn for five mineral dusts and three desert dusts was plotted as a function of the amount of sulfites and sulfates measured on the surface. The selected results that suggested a correlation are displayed in Table 1.

Interactions of  $SO_2$  gas with volcanic dust can be studied from two different angles. At 0% RH information on interactions with pure mineral surfaces is revealed, while at higher % humidity the importance of the presence of water on these processes can be evaluated. In the former case we can elucidate which element is associated with the formation of which surface species. In the latter case information about complex influence of water on the adsorption processes is highlighted.

An increase in sulfite surface concentration was observed as a function of Ti and Fe content. Formation of sulfites on the surface of pure oxides of titanium and iron was observed earlier (Chapter 6). While studying natural samples it is logical to try to look for the trends including the highest amount of elements as they are a better fit to represent a complex mixture. The best correlation trends were found for (Fe+Ti)/Si (Table 1, Figure 4). Elemental Si was included based on the fact that it represents the most abundant element on the surface of dust. When moving from 0 to 30% RH the slope of the fit doesn't change which means that the dependence of the amount of the sulfites formed on the % composition stays the same. The intercept of the graph decreases due to the decreased amount of sulfites quantified on the surface at 30 % as opposed to 0% due to their increased transformation to sulfates. At 60 and 83 % the trends are completely lost (the correlation coefficient is below 0.6) most probably due to the fact that water dominates transformation of SO<sub>2</sub>. Hence, elemental composition seems to play an important role in the range from 0 to 30% humidity. It can be hypothesized that the formation of a water monolayer observed around 30% RH minimizes the direct influence of surface elements on the formation sulfites (Joshi et al., 2017), (Lathem et al., 2011), (Ibrahim et al., 2018).

As for sulfates, the only trend found is the increase in the amount of sulfates as a function % Na observed under dry conditions (Figure 5). The lack of the correlation at higher %RH is most probably due to the fact that OH groups play a dominant role in sulfate formation and therefore in the presence of humidity a direct correlation of surface sulfates with Na or any other element is not observed.

*Table 1: Relationship between elemental surface composition and the amount of sulfites and sulfates formed on the surface.*

Ion	RH (%)	Element	Linear regression equation	R <sup>2</sup>	Slope
Sulfite (SO <sub>3</sub> <sup>2-</sup> )	0	(Ti+Fe)/Si	$y = 188,83x + 9,2685$	R <sup>2</sup> = 0,7108	188,8
	30	(Ti+Fe)/Si	$y = 187,5x - 12,954$	R <sup>2</sup> = 0,8796	187,5
Sulfate (SO <sub>4</sub> <sup>2-</sup> )	0	Na	$y = 4,8263x + 1,1151$	R <sup>2</sup> = 0,9369	4,8

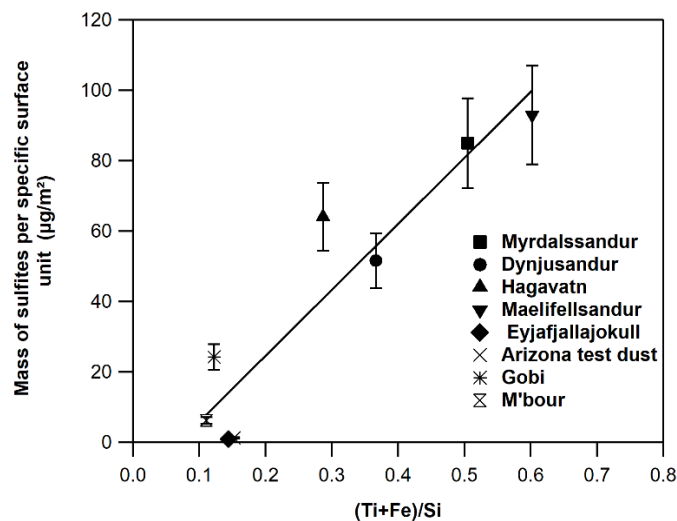


Figure 4: Dependence of the amount of sulfites quantified on the surface of eight natural dusts on the samples' surface ratio of (Ti+Fe) over Si. Surface elemental composition expressed in % element by weight was obtained from XRD measurements (See Chapter 2 Section 1.2.4). Ageing conditions: 1 hr, 175 ppm SO<sub>2</sub>, 30% RH.

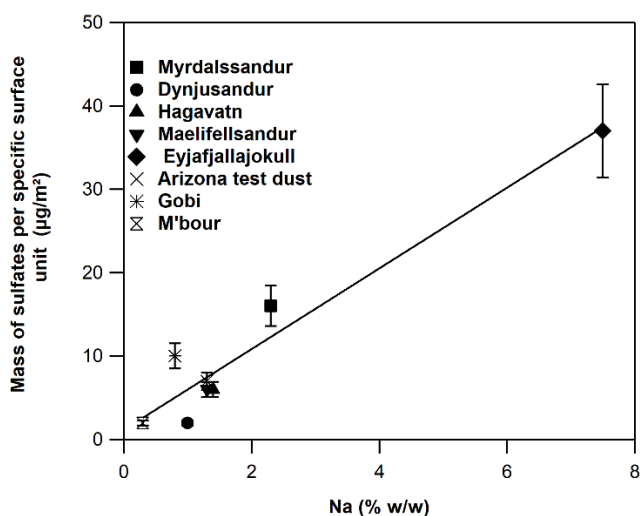


Figure 5: Dependence of the amount of sulfates quantified on the surface of eight natural dusts on the samples' surface ratio of Na over Si. Surface elemental composition expressed in % element by weight was obtained from XRD measurements (See Chapter 2 Section 1.2.4). Ageing conditions: 1 hr, 175 ppm SO<sub>2</sub>, 0% RH.

Surface composition plays an important role in sulfite/sulfate formation. Else, we would not observe a vast variety of trends in their formation on the surface of mineral dusts. Finding the trends though is complicated by the heterogeneous nature of samples, where the same element can be found as a constituent of different mineral phases. In addition, surface composition could influence the uptake of water, which plays a key role by participating in the formation of sulfites and sulfates, further complicating finding the trends with elemental composition. Nevertheless, higher amounts of sulfites are observed as a

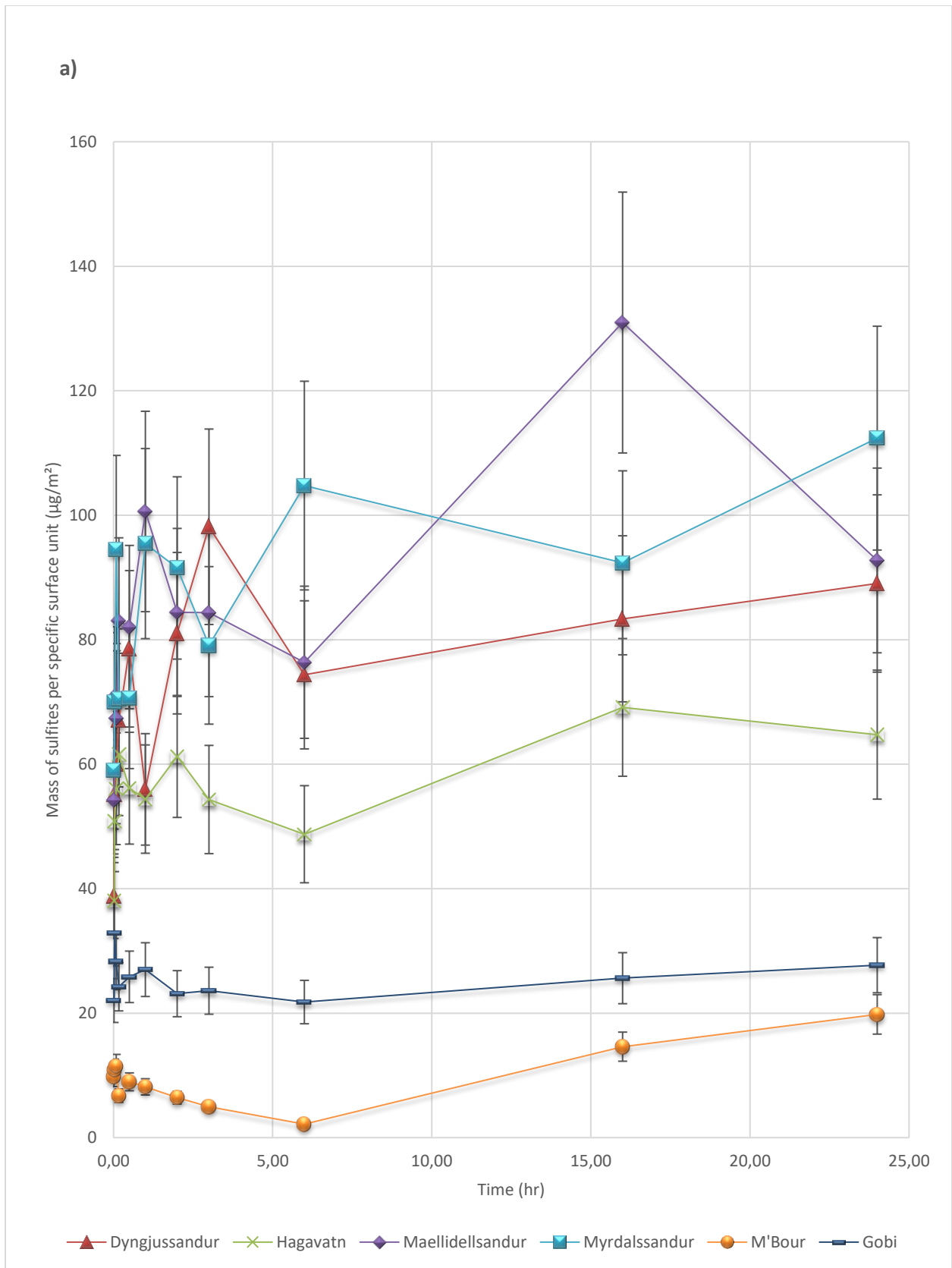
function of Ti and Fe surface composition at 0 and 30% RH, while Na is positively associated with the amount of sulfates formed on the surface at 0% RH. A great approach would be to evaluate the influence of surface water uptake as a function of elemental composition, as it actually might be the water that controls the amount of sulfites and sulfates formed.

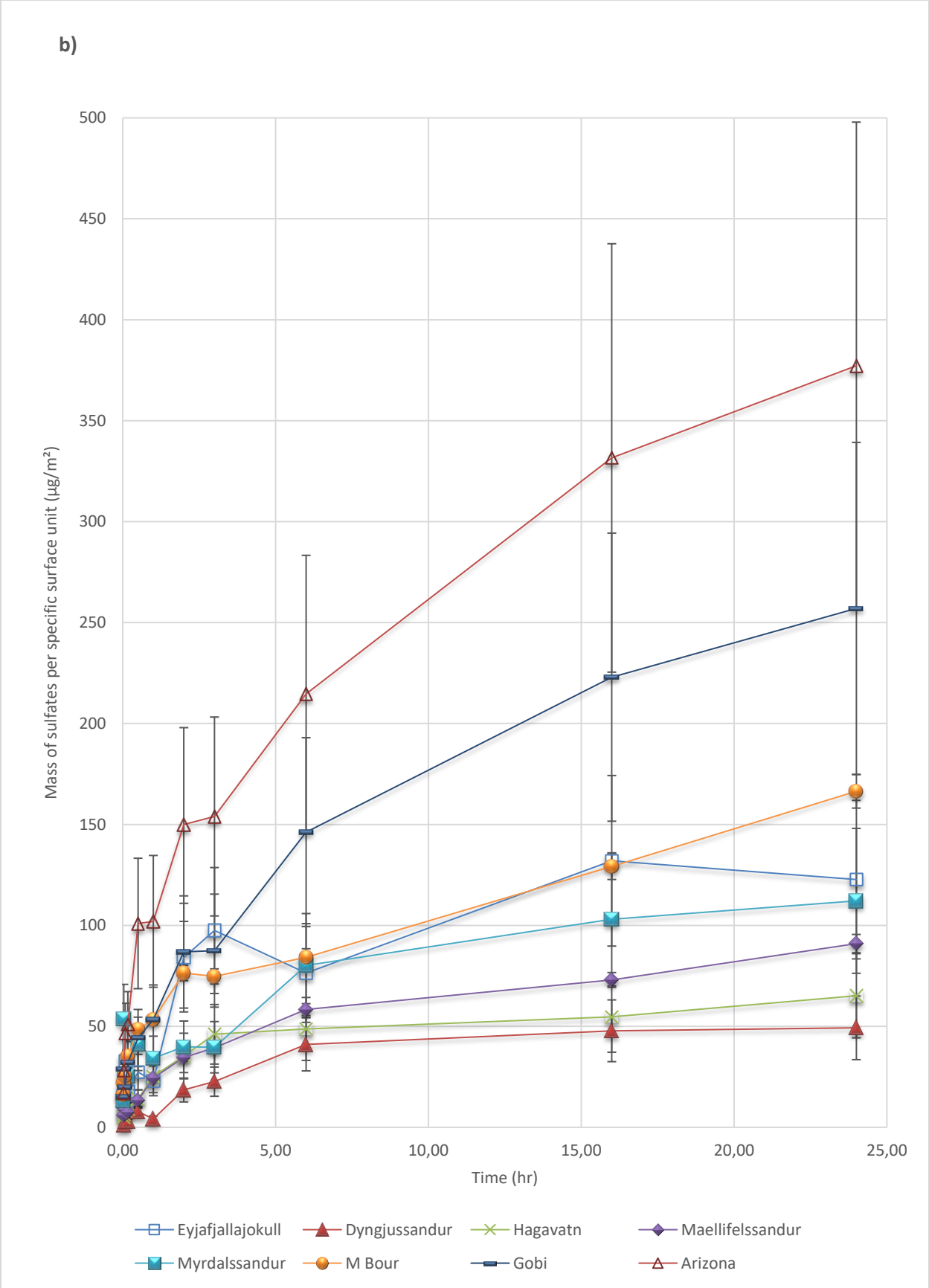
### **3.3 Sulfite and sulfate formation as a function of time. Stability of surface species.**

#### **3.3.1 What happens on the surface of a natural dust particle subjected to SO<sub>2</sub>?**

In order to study the temporal evolution of sulfur species on the surface, volcanic and desert dust samples were exposed to 175 ppm SO<sub>2</sub> at room temperature at 30 % RH for increasing time intervals (from a few minutes up to 24 hr). The choice of 30% RH was based on two criteria: (i) both sulfites and sulfates were observed for most samples (as opposed to mostly sulfites at 0% RH and mostly sulfates at 83% RH), (ii) both surface sites and water molecules influence adsorption at this RH, as was demonstrated in previous section. Blanks of each dust were run and subtracted from the investigated samples. Figure 6 shows the ageing profiles of sulfites and sulfates on the surface of five volcanic dusts and three desert mineral dusts.

Mineral desert dusts showed a lower amount of sulfites but a higher amount of sulfates per specific surface unit of dust in comparison with v-dusts. Another trend for both desert and volcanic dusts is that sulfite formation reaches a plateau fast, around 30 min, while sulfates keep increasing for most of the samples. Sulfate formation rate gradually decreases for all samples. For v-dust it slows down considerably at around 6 hours, for desert mineral dust - after 16 hr. In the case of Arizona dust and Eyjafjallajokull v-dust no sulfites were observed at 30% RH, indicating an ability of the surface to convert sulfites to sulfates very quickly. It was suggested in the literature that the fact that fresh v-ash has been recently exposed to acids in the plume would make it less likely to adsorb SO<sub>2</sub> gas due to pH-dependent solubility of acid dissolution (Ayris and Delmelle, 2012). In the case of Eyjafjallajokull it is definitely not the case. Even though it is a fresh dust that has a much higher amount of sulfates determined in the blanks (167 µg/m<sup>2</sup> for Eyjafjallajokull vs 0-36 µg/m<sup>2</sup> for other samples), it is still active in accumulation of sulfates. At 24 hours, the total sulfur species coverage roughly ranges from 20% to 60% of the total surface coverage. As it was noted earlier, lower limit of 60% could indicate formation of sulfur species monolayer, as some parts of the particles, notably quartz, are not expected to form sulfur species.







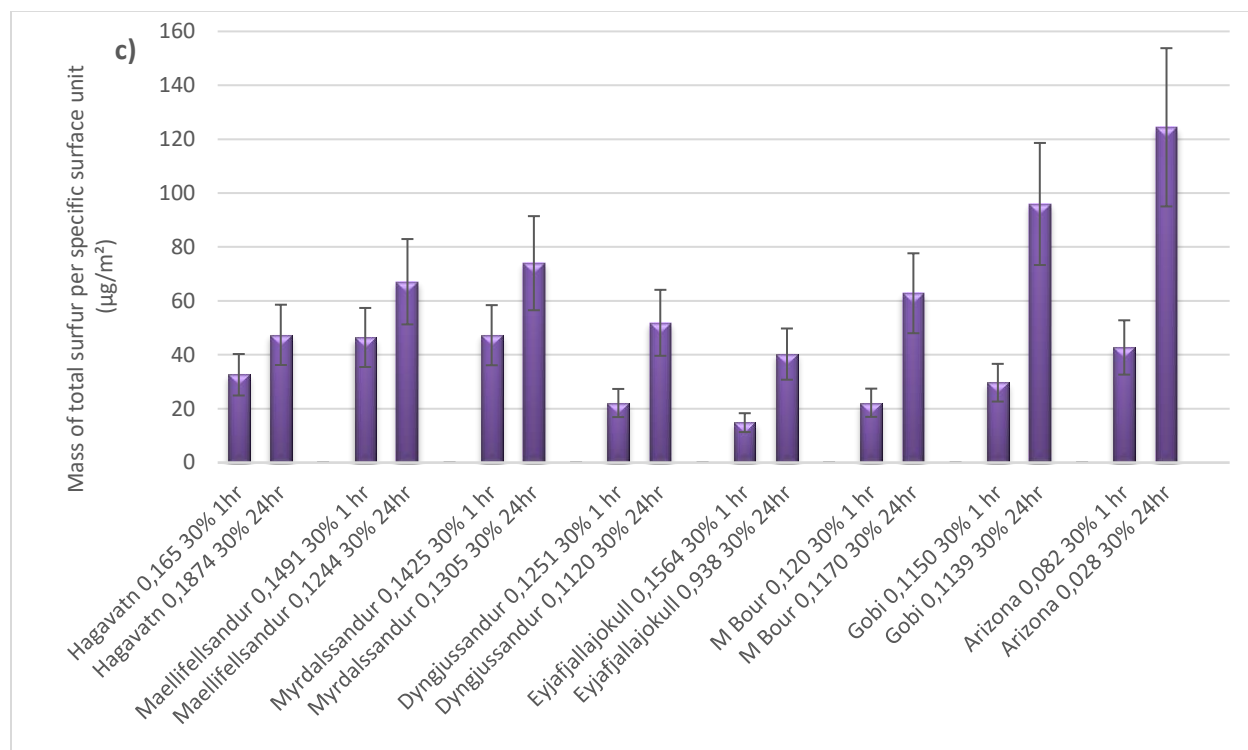


Figure 6: HPLC analysis of desert and volcanic dust samples 0,089-0,194 g, aged for up to 1400 min, 175 ppm of SO<sub>2</sub>, 30 % RH extracted with 2 mL of 1% Formalin, sonicated for 10 min (a) Formation of sulfites on the surface of volcanic and desert dusts as a function time, (b) Formation of sulfates on the surface on the surface of volcanic and desert dusts as a function time, (c) Total sulfur content of various volcanic and desert dusts at 1 hr and 24 hr.

To further investigate the formation of sulfites and sulfates at longer time scales, a sample of Hagavatn dust was aged for 72 hours. Figure 7 shows the profile sulfur based surface species of this dust with time.

An increase in the amount of sulfates is observed till 38 hours after which a stable amount of sulfates is monitored from 38 to 72 hours. Remember that previously, in Chapter 4, while interpreting the results of ageing of Hagavatn dust under similar experimental conditions (SO<sub>2</sub> concentration, RH, temperature) but using DRIFTS technique, we were not able to interpret the sulfate trend after 40 hours of ageing due to high signal fluctuation. Further comparison of sulfite and sulfate trends by using HPLC and DRIFTS techniques is provided in Chapter 8.

As for the sulfites, a slight decrease is observed at 38 hours and the amount is constant from 38 to 72 hours. In addition, if we look at the total number of sulfur adsorbed on the surface it stabilizes even earlier at around 16 hours. It could mean that at 16 hours the surface approached its saturation limit. The fact that finally not all sulfites are converted to sulfates at this RH level (30%) could be due to the fact that a certain phase of the surface (most probably an Fe or Ti bearing mineral phase associated with the detection

of sulfites on the surface) is responsible for a very slow oxidation of sulfites to sulfates, thus effectively hindering the conversion.

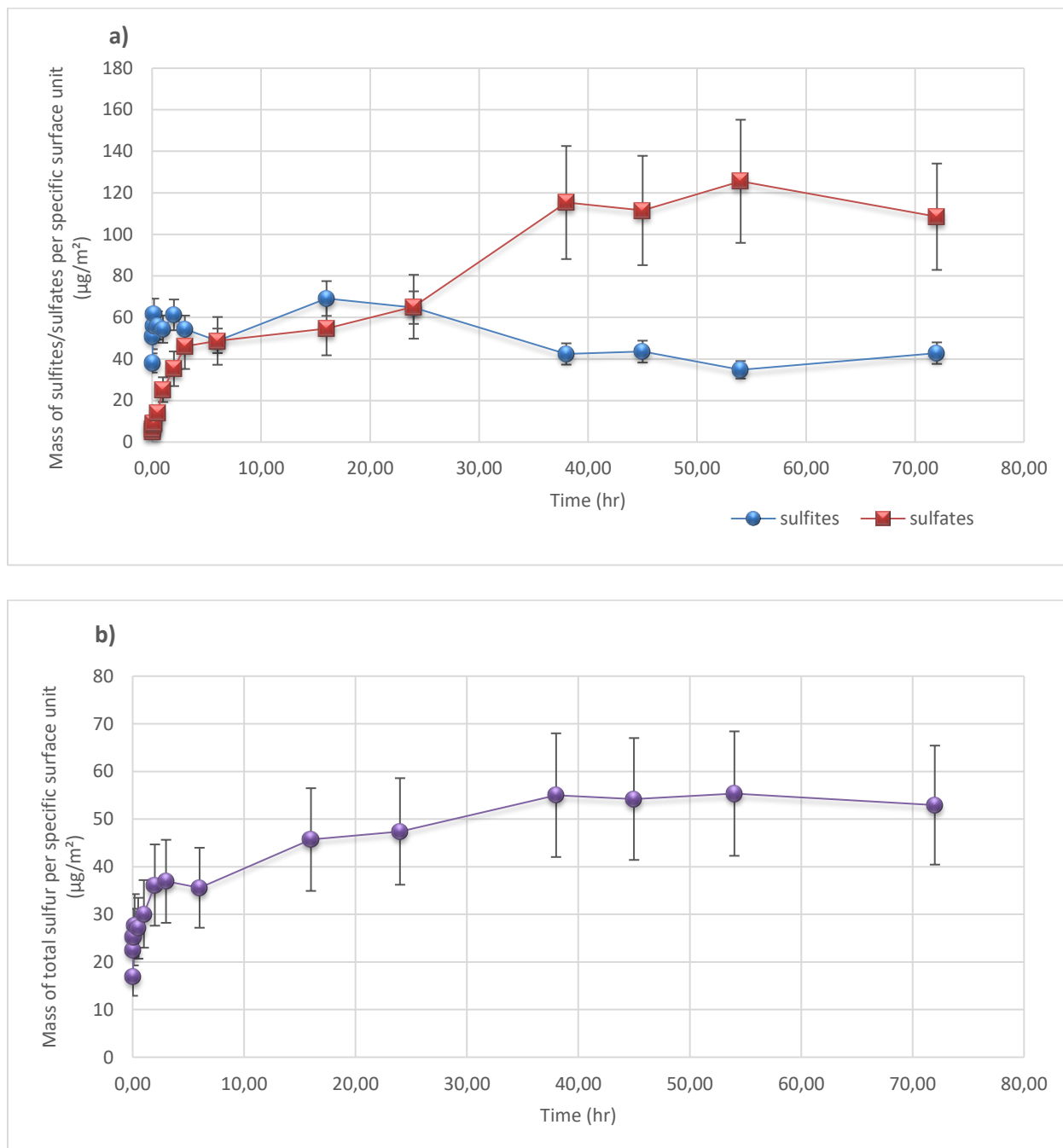


Figure 7: Ageing profiles of Hagavati volcanic dust sample exposed to 175 ppm SO<sub>2</sub> for up to 4320 min (72 hours) HPLC analysis 0,086-0,192 g, 30 % RH extracted with 2 mL of 1% Formalin, sonicated for 10 min. (a) Profiles of sulfites and sulfates formed on the surface of Hagavati v-dust as a function of time while ageing with 175 ppm SO<sub>2</sub>, (b) Total amount of sulfur formed of the surface of Hagavati v-dust as a function of time while ageing with 175 ppm SO<sub>2</sub>.

### 3.3.2 What happens on the surface of a natural dust particle previously subjected to SO<sub>2</sub> when the gas is no longer available?

To evaluate what happens on the surface of v-dust that was previously exposed to volcanic SO<sub>2</sub> gas when the gas is no longer present in the volcanic plume or its concentration falls dramatically, it was decided to age different v-dust and desert dust samples in the presence of 175 ppm SO<sub>2</sub> for one hour and then flush the samples with pure air. For comparison, desert mineral dust samples were subjected to the same procedure. Under this protocol, we observed a slight decreasing trend for sulfites and a slight increasing trend for sulfates.

Two different processes could explain the decreasing trend for sulfites: (i) desorption of sulfites from the surface or (ii) their conversion to sulfates. In order to check whether sulfites can be easily detached from the surface and partition to the gas phase, it was decided to bubble the airflow exiting the reactor through two consecutive beakers containing 4 mL of 1% formalin each after turning off SO<sub>2</sub> supply. One and six hour ageing of Mýrdalssandur and M'Bour dusts with 175 SO<sub>2</sub> was followed by one hour flushing. In the blanks (after flowing SO<sub>2</sub> gas through the system for 1 hr in the absence of dust and then passing pure air through the setup including the beaker filled with 1% formalin for 1 hour) sulfites were identified only in the first beaker suggesting effective reaction. Sulfites in excess of the blanks were not found in 1% formalin upon bubbling the gas exiting the reactor containing aged dust. Therefore, the drop for sulfites can only be explained as the conversion into sulfates. Note that sulfates do not react with 1% formalin, so absence of sulfates in excess of the blanks in the exit beakers does not prove that they are not found in the flow exiting the reactor.

The sulfite to sulfate conversion was further investigated in a closed system; where after exposure of a v-dust or desert mineral dust sample to 175 ppm of SO<sub>2</sub> gas for 1 hr, the dust was transferred to a closed 7 mL clear vial, where it remained for 20 or 30 hours before being analyzed. The conversion of sulfites to sulfates in a closed system is illustrated in Figure 8. It is clearly observed that the amount of sulfites decrease while the amount of sulfates increase for all dust samples which exhibited sulfites on the surface after 1 hr exposure to SO<sub>2</sub> gas. The dusts that exhibited the smallest amount of sulfites, such as M'Bour, and no sulfites, such as Arizona desert dust, demonstrated a negligible increase in sulfates (that can be interpreted as no increase in sulfates within statistical error). Sulfur balance is maintained within the error when cutting the SO<sub>2</sub> supply. Interestingly, even Eyjafjallajökull, for which determination of sulfites was not possible (below detection limit), exhibited increase in sulfates. The reason could be related to the ability of this particular dust to store high amounts of physisorbed SO<sub>2</sub> on the surface. As the supply of SO<sub>2</sub> is stopped the stock of SO<sub>2</sub> on the surface continues to feed the reaction (Reaction A). In this case transformation of physisorbed SO<sub>2</sub> to sulfites is a rate-limiting step (Reaction B). The conversion of sulfites to sulfates

(Reaction C) is fast, as was noted earlier, and explains reasonably well, why we observe no sulfites on the surface of dust.

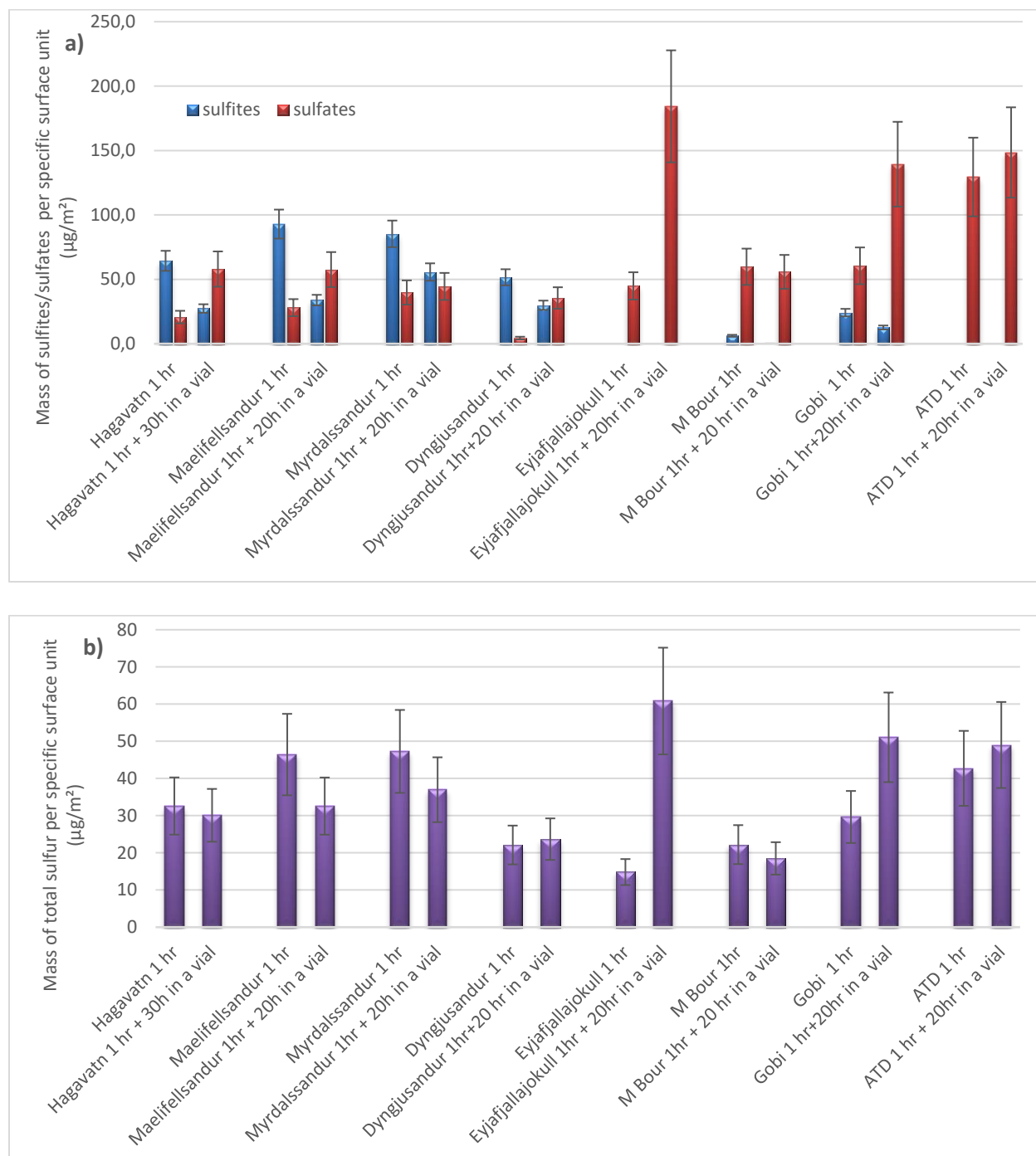


Figure 8: HPLC analysis of the volcanic and mineral dusts aged with 175 ppm SO<sub>2</sub> for 1 hr and then kept for 20 or 30 hr in a closed container. 30 %RH was maintained during experiments. HPLC analysis 0,082-0,189 g, extracted with 2 mL of 1% Formalin, sonicated for 10 min. (a) Amount of sulfites and sulfates formed on the surface of dusts while aging with 175 ppm SO<sub>2</sub> for 1 hr and then keeping them in a closed container, (b) Total amount of sulfur formed on the surface of dusts while aging with 175 ppm SO<sub>2</sub> for 1hr and then keeping them in a closed container.

To conclude, a v-dust particle in the presence of 175 ppm of SO<sub>2</sub> gas exhibits both sulfite and sulfate species on the surface for at least 24 hours (with the exception of Eyjafjallajökull and Arizona dusts that at 30% RH display only sulfates). The surface of desert dust is able to convert sulfites to sulfates faster than volcanic dusts. Upon cutting SO<sub>2</sub> supply sulfite share will gradually go down and the amount of sulfates on the surface will increase. Eventually, with time and in the absence of SO<sub>2</sub> supply, all sulfites are expected to be converted to sulfates.

### **3.3.3 What happens on the surface of a natural dust particle when ageing with SO<sub>2</sub> on ppb level?**

It is important to estimate how atmospherically relevant is the one hour ageing performed at 175 ppm to processes that happen on the scale of days or weeks, but with much lower concentrations.

To justify employing elevated concentrations of SO<sub>2</sub> gas for ageing experiments that are meant to describe atmospheric phenomena, we compared the amount of total sulfur species measured on the surface of Mýrdalssandur v-dust while using high concentration of SO<sub>2</sub> equal to 175 ppm to those obtained at low atmospherically relevant concentration of 75 ppb. Note that only sulfate species are observed on the surface of Mýrdalssandur v-dust when using 75 ppb SO<sub>2</sub>, while both sulfites and sulfates are observed when using 175 ppm SO<sub>2</sub>. This is most probably due the fact that more active sites for sulfite-to-sulfate conversion are available per SO<sub>2</sub> molecule thus leaving no sulfites behind. To compare the amounts of the sulfur species formed on the surface of Mýrdalssandur v-dust while using two different concentration, the obtained sulfites and sulfates at each concentration were expressed as total sulfur.

From Figure 9 we can see that for Mýrdalssandur dust 1 hour ageing with 175 ppm SO<sub>2</sub> corresponds roughly to 3 days ageing with 75 ppb. Thus, ageing with higher concentrations to speed up the formation of surface species seems valid and justified. Note, that increasing SO<sub>2</sub> concentration by 2333 times leads to 72 times shorter ageing to obtain the same amount of surface product. It follows that at lower concentrations the uptake of SO<sub>2</sub> is higher, which is expected.

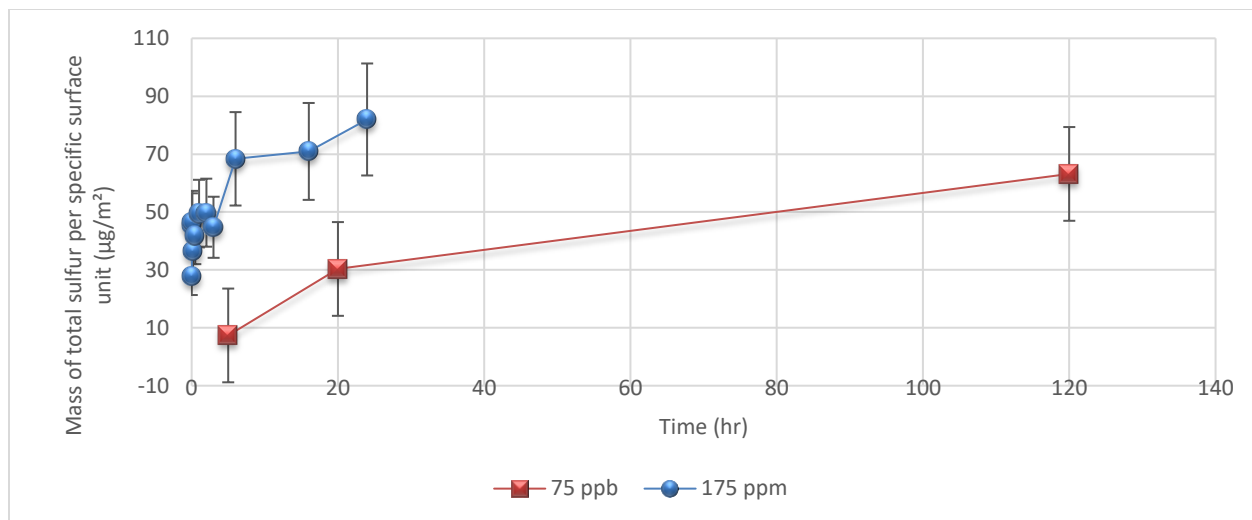


Figure 9: Ageing profiles of Mýrdalssandur volcanic dust sample exposed to 175 ppm SO<sub>2</sub> for up to 24 and 75 ppb for up to 120 hr.

## 4 Conclusions

The reversed-phase HPLC method, developed in that work, was successfully applied to assay the amount of sulfites and sulfates formed on the surface of dust at different levels of RH: 0%, 30%, 60%, and 83%. For the majority of samples it was clearly observed that the amount of sulfites on the surface of dust decreases as a function of RH while a sharp increase is observed for sulfates. **Water therefore exhibits the highest level of control on the distribution of sulfites and sulfates on the surface of dusts by changing the rate on their transformation. The surface elemental composition also plays a direct role on sulfite formation, especially at levels of humidity ranging from 0 to 30%.** Thus, higher amounts of sulfites are correlated with (Fe+Ti)/Si parameter. As for sulfates, the amount of Na on the surface of dust was positively correlated to the ability of samples to form sulfates at 0%. At higher RH, water plays a dominant role and no such correlation is observed. The role of elemental composition on the water uptake could provide us with additional information on the formation of sulfites and sulfates on the surface of natural dusts.

As for the time profiles, the ageing of dust is a long term process. Sulfites reach a steady level rather fast, but sulfates increase continuously on the dust surface. At high 175 ppm concentration of SO<sub>2</sub> it takes about 38 hours for Hagavatn v-dust to saturate, at which point total surface coverage by sulfites and sulfates corresponds roughly to the lower limit of 6% and 17% of the available surface respectively. The amount of sulfates on the surface of other dusts keeps increasing for as long as the experiment is run, i.e. up to 24 hr. At lower atmospherically relevant concentrations of SO<sub>2</sub> the time to achieve saturation is

expected to be even longer. Thus, ageing a Mýrdalssandur sample at 175 ppm SO<sub>2</sub> for 1 hr roughly corresponds to ageing at atmospherically relevant 75 ppb for 3 days. When the dust particle is no longer in contact with the SO<sub>2</sub> gas the amount of sulfites detected on the surface goes down while the transformation to sulfates continues. **Thus, a particle travelling through the air contains two types of species: sulfites and sulfates, but their distribution is a function of time, humidity and SO<sub>2</sub> concentration.** This information can be used in atmospheric modelling to better evaluate the impact of dust on various atmospheric processes such as the ability of dusts to remove SO<sub>2</sub> gas and thus better evaluate air quality. The results suggest that it is imperative to evaluate hygroscopic and optical properties of the dust aged with SO<sub>2</sub> because sulfates form a stable layer. This work opens perspective toward the investigation of the potential reactivity of the surface sulfur compounds with reactive species, such as O<sub>3</sub>, H<sub>2</sub>O<sub>2</sub> and NO<sub>x</sub>.

In the next chapter we objectively evaluate the trends that we have obtained using different instruments and approaches.

## References of Chapter 7

- Ayris, P., Delmelle, P., 2012. Volcanic and atmospheric controls on ash iron solubility: A review. *Physics and Chemistry of the Earth* 45, 103–112. <https://doi.org/10.1016/j.pce.2011.04.013>
- Huang, L., Zhao, Y., Li, H., Chen, Z., 2015. Kinetics of Heterogeneous Reaction of Sulfur Dioxide on Authentic Mineral Dust: Effects of Relative Humidity and Hydrogen Peroxide. *Environ. Sci. Technol.* 49, 10797–10805. <https://doi.org/10.1021/acs.est.5b03930>
- Ibrahim, S., Romanias, M.N., Alleman, L.Y., Zeineddine, M.N., Angeli, G.K., Trikalitis, P.N., Thevenet, F., 2018. Water Interaction with Mineral Dust Aerosol: Particle Size and Hygroscopic Properties of Dust. *ACS Earth Space Chem.* 2, 376–386. <https://doi.org/10.1021/acsearthspacechem.7b00152>
- Joshi, N., Romanias, M.N., Riffault, V., Thevenet, F., 2017. Investigating water adsorption onto natural mineral dust particles: Linking DRIFTS experiments and BET theory. *Aeolian Research* 27, 35–45. <https://doi.org/10.1016/j.aeolia.2017.06.001>
- Latham, T.L., Kumar, P., Nenes, A., Dufek, J., Sokolik, I.N., Trail, M., Russell, A., 2011. Hygroscopic properties of volcanic ash. *Geophysical Research Letters* 38. <https://doi.org/10.1029/2011GL047298>
- Romanias, M.N., Zeineddine, M.N., Gaudion, V., Lun, X., Thevenet, F., Riffault, V., 2016. Heterogeneous Interaction of Isopropanol with Natural Gobi Dust. *Environ. Sci. Technol.* 50, 11714–11722. <https://doi.org/10.1021/acs.est.6b03708>
- Textor, C., Graf, H.-F., Herzog, M., Oberhuber, J.M., 2003. Injection of gases into the stratosphere by explosive volcanic eruptions. *Journal of Geophysical Research: Atmospheres* 108. <https://doi.org/10.1029/2002JD002987>
- Urupina, D., Gaudion, V., Romanias, M.N., Verrielle, M., Thevenet, F., 2020. Method development and validation for the determination of sulfites and sulfates on the surface of mineral atmospheric samples using reverse-phase liquid chromatography. *Talanta* 219, 121318. <https://doi.org/10.1016/j.talanta.2020.121318>
- Urupina, D., Lasne, J., Romanias, M.N., Thiery, V., Dagsson-Waldhauserova, P., Thevenet, F., 2019. Uptake and surface chemistry of SO<sub>2</sub> on natural volcanic dusts. *Atmospheric Environment* 217, 116942. <https://doi.org/10.1016/j.atmosenv.2019.116942>
- Wang, T., Liu, Y., Deng, Y., Fu, H., Zhang, L., Chen, J., 2018. Emerging investigator series: heterogeneous reactions of sulfur dioxide on mineral dust nanoparticles: from single component to mixed components. *Environ. Sci.: Nano* 5, 1821–1833. <https://doi.org/10.1039/C8EN00376A>



**Chapter VIII. Connections between the three experimental approaches: coated wall flow-tube, DRIFT optical cell, and HPLC**

## Table of content of Chapter 8

1	Introduction .....	235
2	Connecting results of flow-tube experiments with results obtained from HPLC: a sulfur balance determination.....	236
3	Connecting results of DRIFTS with results obtained from HPLC.....	238
4	Conclusions .....	240
	References.....	241

## List of Tables of Chapter 8

Table 1: Uptake coefficients for Mýrdalssandur and Maelifellsandur dusts at different times. Time values marked with asterisk are extrapolated from the fitting of the breakthrough curve obtained in a typical flow-tube experiment (see Chapter 2 Section 2.2.4). .....	236
---	-----

## List of Figures of Chapter 8

- Figure 1: The amount of sulfur on the surface of (a) Mýrdalssandur and (b) Maelifellsandur dusts after ageing with 75 ppb of SO<sub>2</sub> as measured with HPLC (blue line, circles) and the amount of sulfur lost from the gas phase as calculated from flow-tube experiments (green line, squares)..... 237
- Figure 2: Overlaid results of two studies: (i) in blue triangles is the amount of sulfites (µg/m<sup>2</sup>) from HPLC studies and (ii) in black squares is an integrated area for sulfite peak obtained from DRIFTS experiment. .... 239
- Figure 3: Overlaid results of two studies: (i) in blue triangles is the amount of sulfates (µg/m<sup>2</sup>) from HPLC studies and (ii) in black squares is an integrated area for sulfate peak obtained from DRIFTS experiment. Purple squares refer to the part of the DRIFTS experiment that exhibited high signal fluctuation. .... 240

# 1 Introduction

Studying heterogeneous reactivity is challenging because of the lack of sufficient understanding of how the surface appears on the molecular level. Indeed, it is unclear, what is the exact environment a gas molecule encounters, when it interacts with the surface. In addition, in case of surface chemical reactions, surface modifications might occur, and the comprehensive understanding of how these changes affect mechanism or reactivity remains to be explored. Adding to the challenge the fact that techniques commonly used to study the structure of surfaces require high vacuum conditions while atmospherically relevant reactions require a significant level of moisture and pressures, up to 1 atm, it becomes clear that evaluating heterogeneous processes is not a trivial experimental task (Finlayson-Pitts and Jr, 1999).

The biggest challenge comes from the fact that the different techniques used to obtain kinetic measurements require highly contrasted experimental conditions. For instance, results obtained using a Knudsen cell that requires low pressure and dry conditions with a time resolution in the millisecond range, are different from the results obtained under atmospherically relevant conditions of a flow-tube reactor (Chapter 1), where time resolution is in the range of seconds, while the system addressed can be the same. In addition, sample preparation and introduction may contribute to the poor agreement of the results. Considering mineral dust as an example, it is well known in literature that the chemical composition is dependent on the size fraction. Therefore, the reactivity of an aerosolized dust sample studied in a simulation chamber could be different from the reactivity of a sample of the same origin studied in a coated wall flow-tube where much bigger particles are left to react (Ibrahim et al., 2018). As a result, the agreement between measurements of heterogeneous reactions is often poor. In the recent IUPAC evaluation the errors associated with measuring uptake coefficients on the surface of dust are commonly well over a factor of 10 (Crowley et al., 2010). In comparison, gas phase reactions nowadays demonstrate solid agreement within only ca 15% (“JPL Data Evaluation,” n.d.). In this Chapter, in order to face the experimental difficulty in the frame of this work, we compare the measurements obtained by the various techniques used and evaluate their consistency.

**The objective of this chapter is to attempt to make a comparison and a connection between the results obtained during the course of this thesis with the three distinct experimental techniques used: the coated wall flow-tube, the DRIFT optical cell, and the HPLC.** First, using different selected dust samples, the quantitative losses of gaseous SO<sub>2</sub> measured during flow-tube experiments are compared to the amounts of sulfur species determined with HPLC. Thereafter, we attempt to correlate the trends observed for the formation of sulfites and sulfates using (i) DRIFTS and (ii) HPLC. This approach is

especially useful to evaluate the performance of the DRIFTS instrument that tends to exhibit considerable signal fluctuations after 45 hours of continuous use.

## 2 Connecting results of flow-tube experiments with results obtained from HPLC: a sulfur balance determination.

Two volcanic dusts Mýrdalssandur and Maelifellsandur were chosen for sulfur balance investigations as they formed the highest number of sulfur species on the surface, as was demonstrated by long-time ageing experiments with HPLC (Chapter 7). To calculate the amount of sulfites and sulfates formed on the surface of v-dusts, Mýrdalssandur and Maelifellsandur v-dust samples ranging from 0.120 to 0.250 g were aged for 5 hr, 20 hr and 120 hr with 75 ppb SO<sub>2</sub>, 30% RH, at ambient temperature and analyzed by the HPLC method described in Chapter 5. The long-term ageing was necessary in order to largely exceed the limit of detection of the HPLC method and permit a precise quantification of sulfur species on the surface of dust. Interestingly, only sulfate species were observed on the surface when using 75 ppb concentration. This is most probably due to the fast conversion of sulfites to sulfates. The mass of sulfur in SO<sub>4</sub><sup>2-</sup> ion was calculated from the mass of sulfates experimentally obtained with HPLC. To evaluate gas-phase loss of SO<sub>2</sub> at 5 hours, the uptake coefficient was extracted using the breakthrough curve from the corresponding uptake experiment (Chapter 3). To obtain the uptake coefficients at 20 and 120 hours the results obtained during the 10 hr flow-tube experiments (see Chapter 3) were extrapolated from the fitting of the breakthrough curve. The results are displayed in Table 1.

Table 1: Uptake coefficients for Mýrdalssandur and Maelifellsandur dusts at different times. Time values marked with asterisk are extrapolated from the fitting of the breakthrough curve obtained in a typical flow-tube experiment (Chapter 2 Section 2.2.4).

	$\gamma$ at 5 hr	$\gamma$ 20 hr*	$\gamma$ 120 hr*
Mýrdalssandur	$9.32 \times 10^{-8}$	$6.20 \times 10^{-8}$	$1.94 \times 10^{-8}$
Maelifellsandur	$3.71 \times 10^{-8}$	$2.76 \times 10^{-8}$	$1.62 \times 10^{-8}$

As can be seen from Table 1, the uptake coefficients diminish with time. This behavior could be explained by the fact that the surface gets gradually saturated with sulfur species and, since sulfates are unlikely to leave the surface, the surface is permanently modified and its capacity to accommodate SO<sub>2</sub> molecules changes. Uptake coefficients were then used to calculate the total amount of sulfur lost from the gas phase expressed in grams by using Equation 1.

$$\text{Equation 1: } \quad \text{Total mass of S removed} = \frac{\gamma v(SO_2) C(SO_2) M(s) t}{4A}$$

where  $\gamma$  is the uptake coefficient at time  $t$ ,  $t$  is time in s,  $v(SO_2)$  is the molecular speed of  $SO_2$  molecule, i.e. 312 m/s,  $C(SO_2)$  is the concentration of  $SO_2$  molecules in the reactor (in our case  $1.18 \times 10^{18}$  molecules/ $m^3$ ),  $M(S)$  is the molar mass of sulfur in g/mole and  $A$  is Avagadro's number ( $6.43 \times 10^{23}$  molecules/mole). The amount of sulfur lost from the gas phase was calculated and compared to the amounts obtained with HPLC. The results are displayed in Figure 1.

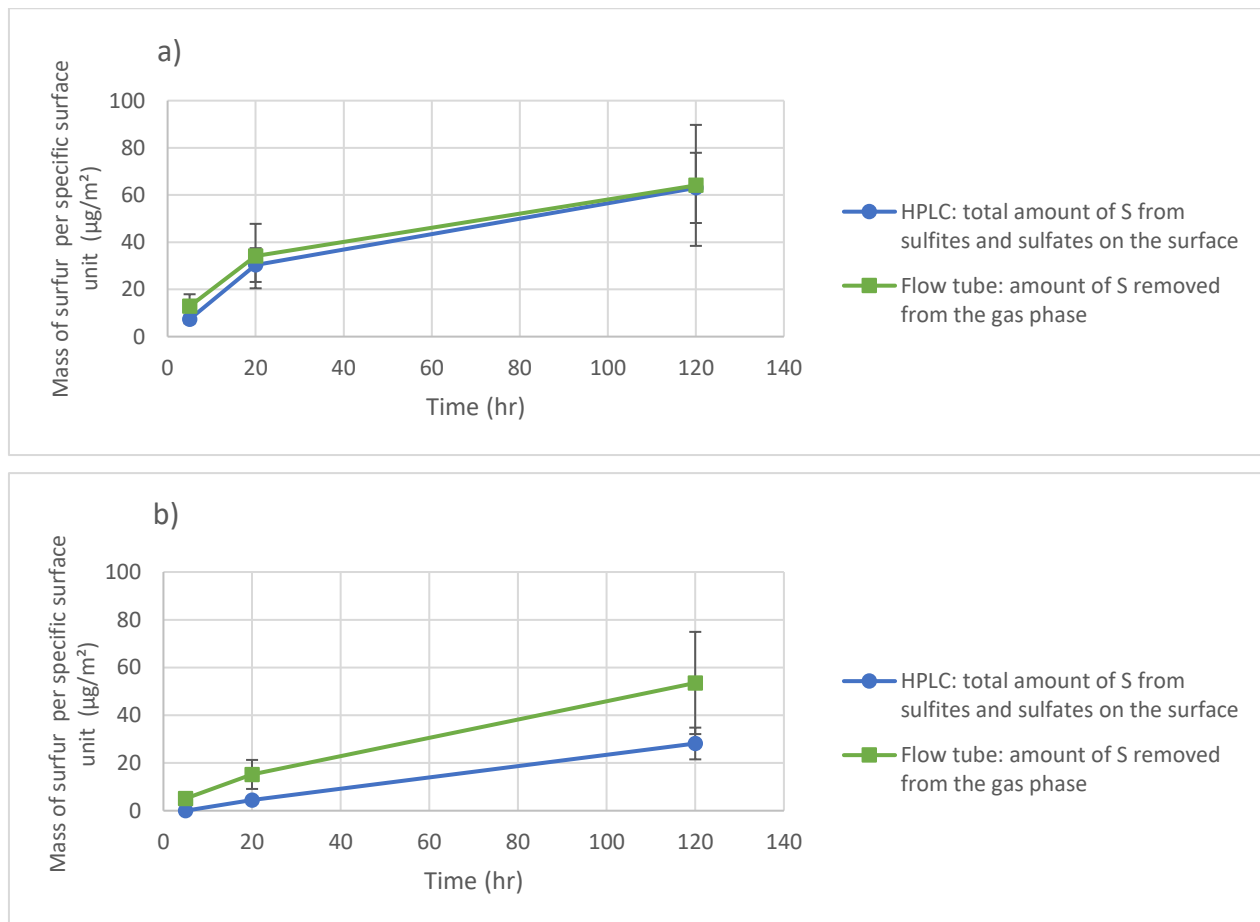


Figure 1: The amount of sulfur on the surface of (a) Mýrdalssandur and (b) Maelifellsandur dusts after ageing with 75 ppb of  $SO_2$  as measured with HPLC (blue line, circles) and the amount of sulfur lost from the gas phase as calculated from flow-tube experiments (green line, squares).

From the graphs displayed in Figure 1, it is clear that the amounts of sulfur lost from the gas phase (flow-tube) and formed on the surface (HPLC) at 5, 20 and 120 hours are in excellent agreement for Mýrdalssandur dust. The latter implies that it is possible to make a direct and quantitative correlation of the two different experimental approaches when experiments are carried out under the same experimental conditions. In addition, it also signifies that the  $SO_2$  removed from the gas phase is entirely transformed to sulfates, leading to a complete sulfur balance.

As for Maelifellsandur, the results show that the sulfur detected on the surface of the sample is lower than that lost from the gas phase. This observation does not necessarily imply that the experimental approaches are not consistent. Indeed, two different scenarios could explain this discrepancy. Either Maelifellsandur dust stores a lot of sulfur on the surface in the form of physisorbed SO<sub>2</sub>, preventing its quantification with HPLC and/or the uptake coefficient extrapolated from flow-tube experiments is overestimated from the fitting of the flow-tube uptake experiment at longer timescales.

To conclude, the flow tube and the HPLC experimental approaches seem to be consistent when compared from the sulfur mass balance point of view. Moreover, coupling flow-tube experiments with HPLC method for sulfite and sulfate determination provides a complementary quantitative information on the process of SO<sub>2</sub> adsorption on the surface of volcanic dusts.

### **3 Connecting results of DRIFTS with results obtained from HPLC.**

To compare the trends obtained in Chapter 4 with DRIFTS instrument using Hagavatn volcanic dust to the profiles of the same dust obtained with HPLC in Chapter 7, the DRIFTS profiles were overlaid with those obtained with HPLC. This comparison does not intend to provide a calibration of the DRIFTS instrument, but aims to address the consistency of the temporal dynamics provided by two experimental approaches. First, the surface concentrations of sulfites as a function of time measured on Hagavatn volcanic dust using HPLC are compared to the DRIFTS sulfite profile for the same dust. Second, a profile of Hagavatn surface sulfates determined with HPLC is compared to that determined with DRIFTS.

Looking at the HPLC profile (Figure 2), one can see that the amount of sulfites goes sharply up and reaches a level of  $(61 \pm 7) \mu\text{g}/\text{m}^2$  in just 10 minutes. It stays around this maximum level for 24 hours before decreasing and establishing, beyond 38 hours, a new level of  $(42 \pm 5) \mu\text{g}/\text{m}^2$ . With DRIFTS, the first sulfite measurement, of  $(0.03 \pm 0.004)$  AU, is done only after 30 min.; at around 3 hours the system seems to reach a plateau at  $(0.04 \pm 0.006)$ , but due to the fluctuations of the signal we are unable to make clear conclusions about the trends. Figure 2 shows a noticeable correlation of sulfite profiles using DRIFTS and HPLC techniques. The main difference in trends comes from the fact that with HPLC two stable periods in the sulfite concentrations can be noted: from 10 minutes to 24 hours and from 38 to 72 hours, while with DRIFTS only one global stable period can be observed: from 3 hours up to 72 hours. Globally, the behavior of sulfites determined by two techniques is consistent. The reason for this mismatch is probably due to lower detection limit and higher instrumental uncertainty of DRIFTS technique when applied to dark volcanic dusts.



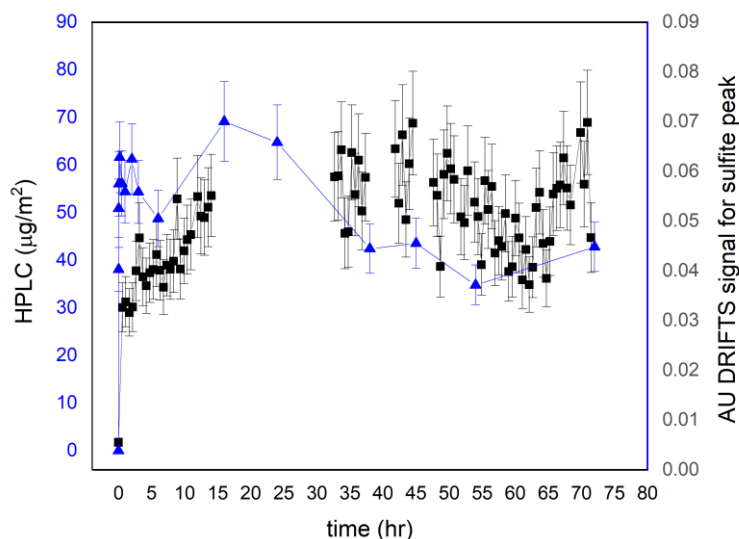


Figure 2: Overlaid results of two studies: (i) in blue triangles is the amount of sulfites ( $\mu\text{g}/\text{m}^2$ ) from HPLC studies and (ii) in black squares is an integrated area for sulfite peak obtained from DRIFTS experiment.

As for the sulfates, examining the HPLC profile in Figure 3 we observe a fast increase in sulfates during the first 3 hours, reaching  $(46\pm 6) \mu\text{g}/\text{m}^2$ . Then, a slower increase, from 3 hours to 38 hours, reaching  $(115\pm 14) \mu\text{g}/\text{m}^2$ , is noticed, after which level the attained surface concentration of sulfates remains stable for the duration of the experiment, i.e. 72 hours. When DRIFTS profile is examined, sulfates remain below the detection limits of the instrument along the first 3 hours. Then, the signal of sulfates increase linearly up to 14 hours reaching 0.01 AU. From 14 to 32 hours the data on the DRIFTS signal is not available. From 35 to 54 hours DRIFTS signal for sulfates reaches a relatively stable level of around  $(0.04\pm 0.005)$  AU. After 54 hours due to high fluctuations of the DRIFTS signal, the determination of the trend is not possible. The common trend observed from HPLC and DRIFTS techniques is the increase in the amount of surface sulfates from 3 to about 35 hours followed by a rather stable amount recorded from 35 to 54 hours. The discrepancies are observed at the very beginning and at the end of the experiment. At the beginning of the experiment the amount of sulfates recorded on the surface with DRIFTS is much smaller than that registered with HPLC. It has to do with the low sensitivity of the DRIFTS instrument towards detection of sulfates on dark  $\nu$ -dust surfaces as discussed earlier in Chapter 4. Thus, at this point we are operating at the limit of detection of sulfates by DRIFTS. After 54 hours we have to rely solely on HPLC results because of the high fluctuation in the DRIFTS signal that is related to instabilities of the MCT detector of the instrument after long utilization and consecutive refilling of the liquid nitrogen chamber. For that reason, DRIFTS data points beyond 54 hr are reported in purple to display the sulfate trend provided by DRIFTS experiment, and to underline the fact that it should not be exploited with the same level of reliability as the HPLC measurements.

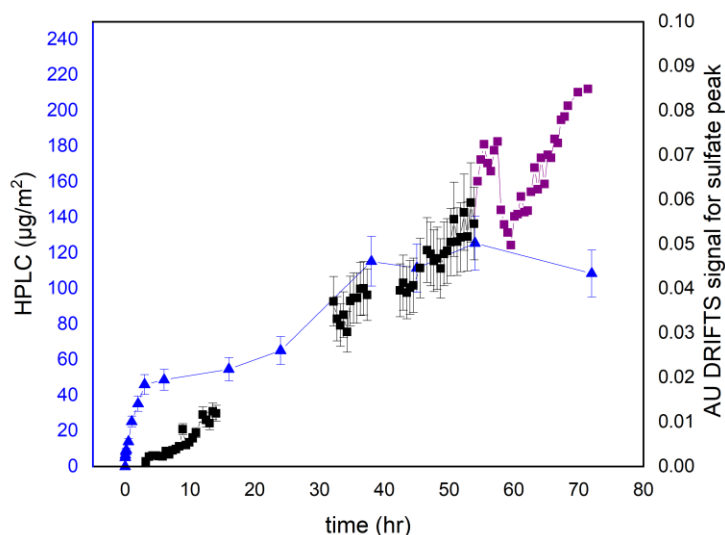


Figure 3: Overlaid results of two studies: (i) in blue triangles is the amount of sulfates ( $\mu\text{g}/\text{m}^2$ ) from HPLC studies and (ii) in black squares is an integrated area for sulfate peak obtained from DRIFTS experiment. Purple squares refer to the part of the DRIFTS experiment that exhibited high signal fluctuation.

In conclusion, a global agreement in trends can be established for DRIFTS and HPLC measurements for the determination of sulfites for the duration of the 72 hour experiment. As for sulfates, once the amount detected by DRIFTS is above 0.001 AU, i.e. around 3 hours, the trends for DRIFTS and HPLC can correlate till 54 hours. If DRIFTS provides specific signals for surface species with high temporal resolution, it is limited by its limit of detection and by long term operation of the system, which may induce signal fluctuations hindering any accurate interpretation. The HPLC approach, is far more compliant with extra long-term ageing experiments as well as for early sulfate determination on mineral surfaces regardless of their reflectance.

## 4 Conclusions

In this chapter we evaluated the experimental consistency of the measurements obtained with different techniques: flow-tube, DRIFTS, and HPLC. Flow-tubes and HPLC were proven to be consistent and complementary quantitative techniques that enriched the understanding of the transformation of  $\text{SO}_2$  gas on the surface of volcanic dust. As for DRIFTS and HPLC techniques, they showed a noticeable correlation as long as DRIFTS measurements are above 0.001 AU. In addition, using DRIFTS for monitoring longer than 54 hours is not recommended based on the instrumental constrains. Thus, the added value of HPLC technique is unquestionable as it helps to clarify the trends observed on the surface of v-dust with DRIFTS and enriches the discussion provided by the flow-tube experiments by enabling determination of the sulfur balance.

## References of Chapter 8

- Crowley, J.N., Ammann, M., Cox, R.A., Hynes, R.G., Jenkin, M.E., Mellouki, A., Rossi, M.J., Troe, J., Wallington, T.J., 2010. Evaluated kinetic and photochemical data for atmospheric chemistry: Volume V – heterogeneous reactions on solid substrates. *Atmos. Chem. Phys.* 10, 9059–9223. <https://doi.org/10.5194/acp-10-9059-2010>
- Finlayson-Pitts, B.J., Jr, J.N.P., 1999. *Chemistry of the Upper and Lower Atmosphere: Theory, Experiments, and Applications*. Elsevier.
- Ibrahim, S., Romanias, M.N., Alleman, L.Y., Zeineddine, M.N., Angeli, G.K., Trikalitis, P.N., Thevenet, F., 2018. Water Interaction with Mineral Dust Aerosol: Particle Size and Hygroscopic Properties of Dust. *ACS Earth Space Chem.* 2, 376–386. <https://doi.org/10.1021/acsearthspacechem.7b00152>
- JPL Data Evaluation [WWW Document], n.d. URL <https://jpldataeval.jpl.nasa.gov/> (accessed 10.15.20).



## **General conclusions and perspectives**

This PhD thesis is driven by a multifaceted approach to investigate the uptake of SO<sub>2</sub> on Icelandic volcanic dusts. This experimental work has been based on existing protocols and it allowed new methodological developments to provide an accurate insight into an atmospheric heterogeneous system of interest under realistic environmental conditions. The main outcomes of this work can be categorized in three complementary sections.

### **Outcomes regarding experimental protocols and methods**

Three distinct techniques have been combined, confronted and questioned: flow tube reactor, DRIFTS and HPLC. Considering their advantages and limitations, these techniques have been proved consistent and complementary. When relevantly associated, they can shed light on the fate of volcanic SO<sub>2</sub> in relation to the volcanic dust surface. Combining these approaches allowed us to examine various heterogeneous interactions of the SO<sub>2</sub> molecule with the surface from two different angles (i) by quantitatively examining the loss of the SO<sub>2</sub> molecules from the gas phase using flow-tube reactor and (ii) by qualitatively and quantitatively following the formation of surface species using respectively DRIFTS and HPLC. When possible, we worked under real atmospheric conditions of relevant SO<sub>2</sub> concentrations, RH, temperature and pressure. For DRIFTS and HPLC studies, we had to increase SO<sub>2</sub> concentration in order to obtain sufficient amounts of surface species, but the validity of this experimental approach has been questioned and assessed.

To increase the scope of our experimental instrumentation, a new HPLC method has been fully developed and validated. The new method includes a detailed protocol for controlled SO<sub>2</sub> ageing of volcanic dusts that enabled us to obtain time profiles and to examine the influence of humidity and composition on the formation of surface species on various dust samples. This method is unique in the sense that it simultaneously quantifies both sulfites and sulfates while preventing conversion of sulfites to sulfates. The method can be used on other environmental samples, such as desert dusts, and can be applied to field studies due to the ease of the sampling technique and stability of the final solution.

In addition, during this work we addressed a question of validity of using surrogates to substitute for natural samples. This work highlighted the importance of using natural samples in the investigations of atmospheric heterogeneous systems. Meanwhile, it also pointed at the necessity of innovative experimental developments to face the diversity and the complexity of natural samples.

New possibilities that stem from the developed methodology include the production of control-aged natural dust samples for the exploration of their surface properties. The capacity of preparing control-aged natural samples opens new perspective to address the behavior of mineral aerosols at various steps of their atmospheric transport. As such, a research project can be envisioned in collaboration with colleagues from

aerosol physics. Another interesting area for further research is the investigation of iron solubility of volcanic particles aged with SO<sub>2</sub> that could provide a new understanding of cycling of this important micronutrient.

### Outcomes regarding surface processes on mineral aerosols

Likewise, new insights were brought by this PhD regarding heterogeneous processes on mineral aerosols. The reaction scheme for the formation of surface species was proposed in detail. It includes (i) physisorption of SO<sub>2</sub> molecules on the surface of v-dust, followed by (ii) reaction with the surface to form sulfites and (iii) oxidation of sulfites to sulfates.

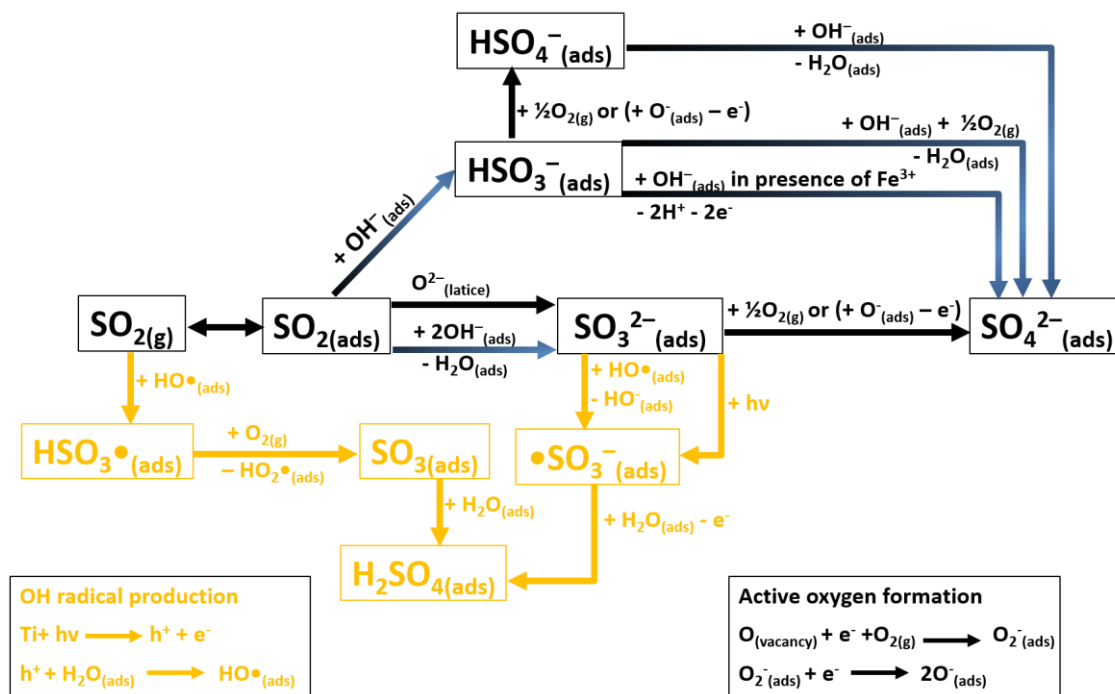


Figure 1: Schematic representation of SO<sub>2</sub> reaction pathways at the surface of v-dust. Reactions occurring under dark and dry conditions are shown using black arrows; reactions occurring in the dark and are promoted under humid conditions are shown in black-blue colored arrows; reactions occurring in presence of light are shown in orange.

The influential parameters on v-dust surface processes have been identified and explored. They include: RH, elemental composition and UV light. We have demonstrated that UV light enhances the uptake of SO<sub>2</sub> molecules by the volcanic dust. Elemental composition influences sulfite and sulfate formation, especially under dry conditions. Above all, it is clear that water plays a major role both in the adsorption of SO<sub>2</sub> and in the distribution of sulfites and sulfates on the surface of dusts. At high levels of humidity a monolayer of sulfates might be formed, confirming that the surface properties of the aged aerosol are modified. Besides, sulfates formed on the surface of v-dust are stable chemisorbed species, not desorbed

even after flushing for several hours in the absence of SO<sub>2</sub> gas. This extensive stable sulfate coverage of a v-dust particle changes the way we see the volcanic particles travelling through the air as it changes the way their surface looks and reacts.

An interesting direction in the area of heterogeneous atmospheric chemistry would be to explore the stability of the sulfate coverage on dust, including possible further transformations, such as potential to form sulfuric acid. Investigating the role of elemental composition of the volcanic dusts on the water uptake is another area that might be especially important to understanding how the surface composition influences SO<sub>2</sub> uptake at high humidity.

### **Outcomes regarding atmospheric chemistry**

With respect to atmospheric chemistry, we can state that the uptake of SO<sub>2</sub> gas on the surface of v-dust with respect to reactions occurring in the atmosphere is significant, especially in the denser part of the plume/cloud and when the emitted particles have a high specific surface area. Moreover, the kinetic data on the uptake of SO<sub>2</sub> obtained by our group has already enabled scientific inquiries in climate simulations. Thus, the data on saturation coverage of SO<sub>2</sub> contributed to the re-estimation of SO<sub>2</sub> lifetime following 2014 Mt. Kelut eruption that agrees better with real-life observations, as reported in recent “*Nature Communications*” (Zhu et al., 2020). In particular, about 43% more volcanic sulfur is removed in 3 months following the eruption when considering SO<sub>2</sub> heterogeneous chemistry (Zhu et al., 2020).

In addition, we demonstrated that ageing a v-dust particle in the presence of SO<sub>2</sub> gas is a long-term process, and we now better understand how it changes its surface. Interestingly, in comparison with desert dust, the surface of volcanic dusts converts sulfites to sulfates slower, most probably due to the difference in surface composition. Contrary to former estimations based on other heterogeneous atmospheric systems, in the presence of SO<sub>2</sub> gas, the uptake on the v-dust surface continues for days and weeks. Upon cutting SO<sub>2</sub> supply sulfite share gradually goes down because of the continuous surface reaction process and the amount of sulfates on the surface increases. Eventually, with time and in the absence of SO<sub>2</sub> supply, all sulfites are expected to be converted to sulfates. Thus, a particle exposed to high levels of humidity and SO<sub>2</sub> gas in the volcanic plume clearly acts as an SO<sub>2</sub> sink and can be expected to be covered with a sulfate layer which can definitely alter the particle hygroscopic and optical properties. The quantitative experimental data gained through this work can be used in atmospheric modelling to better evaluate the impact of dust on various atmospheric processes such as ability of dusts to remove SO<sub>2</sub> gas and thus better evaluate air quality. The perspectives for future atmospheric studies include investigations of how modifications of dust reactivity due to ageing changes its behavior towards important atmospheric oxidants, such as O<sub>3</sub> and NO<sub>x</sub>. Beyond the evaluation of optical and hygroscopic properties of dust at various SO<sub>2</sub> ageing levels, it is also imperative



to see how ageing the dust affects its ice nucleation and cloud nucleation properties. Besides, incorporating the long-term steady state uptake coefficients of SO<sub>2</sub> on v-dust in climate simulations provides a way to correct the current models, especially if the effect of UV radiation is included.

## References

Zhu, Y., Toon, O.B., Jensen, E.J., Bardeen, C.G., Mills, M.J., Tolbert, M.A., Yu, P., Woods, S., 2020. Persisting volcanic ash particles impact stratospheric SO<sub>2</sub> lifetime and aerosol optical properties. *Nature Communications* 11, 4526. <https://doi.org/10.1038/s41467-020-18352-5>



## **Valorization**

### **List of journal publications related to this thesis**

- 1) D. URUPINA, J. LASNE, M. ROMANIAS, V. THIERY, P. DAGSSON-WALDHAUSEROVA, F. THEVENET, Uptake and surface chemistry of SO<sub>2</sub> on natural volcanic dusts, *Atmospheric Environment*, Vol 217, pp 116942, 2019. DOI: 10.1016/j.atmosenv.2019.116942
- 2) D. URUPINA, V. GAUDION, M. ROMANIAS, M. VERRIELE, F. THEVENET, Method development and validation for the determination of sulfites and sulfates on the surface of mineral atmospheric samples using reverse-phase liquid chromatography, *Talanta*, Vol 219, 2020. DOI: 10.1016/j.talanta.2020.121318

### **List of international communications related to this thesis**

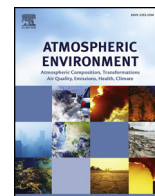
- 1) J. LASNE, M. ROMANIAS, D. URUPINA, F. THEVENET, Influence of humidity and UV-irradiation on SO<sub>2</sub> uptake by volcanic dust, *3rd International Conference on Atmospheric Dust*, Villa Romanazzi Carducci, Bari, Italy, May 29-31, 2018
- 2) D. URUPINA, F. THEVENET, M. ROMANIAS, J. LASNE Uptake and surface chemistry of SO<sub>2</sub> on natural Icelandic volcanic dusts under simulated atmospheric conditions, *EGU General Assembly 2020*, Online, 4-8 May, 2020

### **List of national communications related to this thesis**

- 1) D. URUPINA, J. LASNE, M. ROMANIAS, F. THEVENET, Impact of SO<sub>2</sub> uptake by Icelandic volcanic dust on tropospheric chemistry, *Conseil Scientifique du Labex CaPPA*, Villeneuve d'Ascq, 1 juillet 2019
- 2) D. URUPINA, J. LASNE, M. ROMANIAS, F. THEVENET, Impact of SO<sub>2</sub> uptake by Icelandic volcanic dust on tropospheric chemistry, *5ème Journée Scientifique Labex Cappa*, Villeneuve d'Ascq, 6 mars 2019

## **Annex 1**





## Uptake and surface chemistry of SO<sub>2</sub> on natural volcanic dusts

D. Urupina<sup>a,\*</sup>, J. Lasne<sup>a</sup>, M.N. Romanias<sup>a</sup>, V. Thiery<sup>b</sup>, P. Dagsson-Waldhauserova<sup>c,d</sup>, F. Thevenet<sup>a</sup>

<sup>a</sup> IMT Lille Douai, Univ. Lille, SAGE, 59000, Lille, France

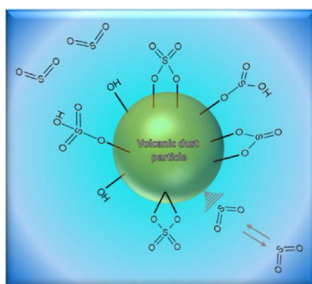
<sup>b</sup> IMT Lille Douai, Univ. Lille, GCE, 59000, Lille, France

<sup>c</sup> Agricultural University of Iceland, Keldnaholt, Reykjavik, 112, Iceland

<sup>d</sup> Faculty of Environmental Sciences, Czech University of Life Sciences, Prague, 165 21, Czech Republic



### GRAPHICAL ABSTRACT



### ARTICLE INFO

#### Keywords:

V-dust  
Heterogeneous reactions  
Sulfur dioxide  
Sulfate formation  
Uptake coefficient  
DRIFTS

### ABSTRACT

V-dust (v-dust) is a highly variable source of natural particles in the atmosphere, and during the period of high volcanic activity it can provide a large surface for heterogeneous interactions with other atmospheric compounds. Icelandic v-dust was chosen as a case study due to frequency of volcanic eruptions and high aeolian activity in the area. In this study, we focus on the kinetics and mechanism of the reaction of sulfur dioxide (SO<sub>2</sub>) with natural v-dust samples under atmospheric conditions using coated wall flow tube reactor and diffuse reflectance infrared Fourier transform spectroscopy (DRIFTS). Steady state uptake coefficients determined are in the range of 10<sup>-9</sup> to 10<sup>-8</sup> depending on the considered v-dust. Concomitantly with SO<sub>2</sub> uptake, both sulfites and sulfates are monitored on the surface of v-dust, with sulfates being the final oxidation product, attesting of SO<sub>2</sub> surface reaction. Surface hydroxyl groups play a crucial role in the conversion of SO<sub>2</sub> to sulfites as evidenced from both flow tube and DRIFTS experiments. Based on these experimental results, a mechanism for SO<sub>2</sub> interaction with different surface sites of v-dust is proposed and discussed. This study provides original insights in the kinetics of SO<sub>2</sub> uptake under simulated atmospheric conditions and its mechanism and transformation on volcanic material. To that regards, it brings an accurate perspective on SO<sub>2</sub> heterogeneous sinks in the atmosphere.

### 1. Introduction

Volcanic eruptions comprise one of the most significant natural hazards directly threatening people living in the proximity, and, in the

extreme case, can affect livelihoods of the humankind on the global scale. Large volcanic eruptions of the past have significantly influenced Earth's climate by injecting vast amounts of volcanic gases and aerosols into the atmosphere (Stevenson et al., 2003). Volcanic emissions can

\* Corresponding author.

E-mail address: [darya.urupina@imt-lille-douai.fr](mailto:darya.urupina@imt-lille-douai.fr) (D. Urupina).

<https://doi.org/10.1016/j.atmosenv.2019.116942>

Received 23 April 2019; Received in revised form 26 August 2019; Accepted 28 August 2019

Available online 03 September 2019

1352-2310/ © 2019 Elsevier Ltd. All rights reserved.

cause both regional and global changes to climate by affecting monsoon circulation, causing either excessive or limited rainfall thus leading to floods and droughts (Stevenson et al., 2003), (Highwood and Stevenson, 2003), (“Tambora and the ‘Year Without a Summer’ of 1816,” 2016). Volcanic particles have an ability to affect the climate by scattering solar radiation and thus changing the Earth radiation budget (Langmann, 2013). Besides, volcanic ash, having optical and thermal properties similar to those of the black carbon, can absorb solar radiation (Arnalds et al., 2016). Vernier et al. highlighted the significance of the radiative impact of ash, in particular in the tropical latitudes due to the Brewer-Dobson circulation that sustains ash in the stratosphere for longer than was generally assumed (Vernier et al., n.d.). Finally, volcanic ash particles can affect the climate through influencing cloud formation processes and acting as ice nucleation sites during plume rise (Durant et al., 2008). The impact of v-dust on Earth's atmosphere is governed by the physical and chemical surface properties of the particles. However, the physico-chemical processes that govern the modifications of the particle surface in the plume and in the cloud when ash is in contact with volcanic gases remain poorly investigated.

Volcanic eruptions are a highly variable sources of solid particles ranging from 33 million tons (Mt) on an average year to over 100,000 Mt of ash after a major volcanic eruption, as was the case for the eruption of Mount Tambora in 1815 (Andreae, 1995). With respect to atmospheric chemistry the most significant impact would be expected to come from the particles that are in the 0.002–10  $\mu\text{m}$  range as they can be carried over thousands of kilometers before eventually being deposited onto land or into the ocean by gravitational settling and wet deposition (Finlayson-Pitts and Jr, 1999), (Langmann et al., 2010), (Dagsson-Waldhauserova et al., 2014). When settled on land, v-dust (v-dust) can then be once again remobilized by the wind and entrained into the atmosphere. Some places on Earth are particularly prone to high aeolian activity. Such is, for example, the case for Iceland, that experiences on average about 135 dust days per year, partly due to frequent volcanic eruptions and re-suspension of volcanic materials (Dagsson-Waldhauserova et al., 2014). In fact, this volcanic island of North Atlantic with an area of 103,000  $\text{km}^2$  lying south of the Arctic Circle is one of the dustiest areas of the world as well as the largest desert in Europe and the Arctic (Dagsson-Waldhauserova et al., 2014). It is also one of the most volcanically active areas. There are about 30 active volcanic systems and volcanic eruptions occurring every 3–5 years on average (Thordarson and Larsen, 2007), (Schmidt et al., 2014). Frequent dust events in Iceland transport dust over long distances, often exceeding 2500 km, towards High Arctic (> 80° N) and Europe (Ovadnevaite et al., 2009), (Groot Zwaaftink et al., 2017), (Moroni et al., 2018), (Dordevic et al., 2019). Located only 1000 km from mainland Europe, it makes a particularly interesting case study due to its proximity to densely populated European countries.

In the stratosphere, emissions of volcanic ash were linked to ozone reduction recorded after major volcanic eruptions, such as El Chichón eruption in Mexico in 1982 and Mount Pinatubo eruption in Philippines in 1991 (Brasseur et al., 1990), (“Reactions on Mineral Dust - Chemical Reviews (ACS Publications),” n.d.). Even if the effect of volcanic ash in the chemistry of the troposphere has not yet been evaluated, it is suggested that ash particles act as a long-range transporting carrier for various species adsorbed on their surface and as a solid support for their reactions with atmospheric trace gases (Li et al., 2006), (Maters et al., 2017). Some of these species are formed during eruption, when a variety of gases are released along with volcanic ash. Sulfur dioxide ( $\text{SO}_2$ ) is typically the third most emitted volcanic gas after water and carbon dioxide (Durant et al., 2010).  $\text{SO}_2$  is known to contribute to the formation of sulfuric acid aerosol, which, when injected in the stratosphere, stays there for up to 2 years effectively cooling the troposphere below (Stevenson et al., 2003), (Highwood and Stevenson, 2003).

Volcanic ash and  $\text{SO}_2$  are likely to participate in a variety of heterogeneous reactions that could potentially influence the balance of other atmospheric species.  $\text{SO}_2$  has already been shown to exhibit

heterogeneous reactivity towards many mineral oxides such as  $\text{MgO}$ ,  $\text{Al}_2\text{O}_3$ ,  $\text{Fe}_2\text{O}_3$  and  $\text{TiO}_2$  (Usher et al., 2002). Along  $\text{SO}_2$  uptake on these materials, sulfite and sulfate formation was detected on the surface of most mineral oxides and synthetic mineral dust and it was proposed that hydroxyl groups and surface-active oxygen are responsible for oxidation of sulfites to sulfates (Zhang et al., 2006). Nevertheless, limited data exist on the mechanism of the interaction of  $\text{SO}_2$  gas with natural multi-component samples, such as volcanic ash as well as on the stability of the surface species formed during reaction.

It was recently evidenced by Maters et al. that volcanic ash is reactive to the uptake of weakly acidic  $\text{SO}_2$  gas with a reactivity that is proportional to the abundance of strongly basic sites, such as those affiliated with alkaline and alkaline earth metals (Maters et al., 2017). Although very informative of the processes occurring on the short scale, the initial uptake and the total uptake capacity measured by the authors have limited ability to explain the interactions on the longer time scale. Besides, the above-mentioned experiments were performed in a Knudsen cell under very low pressure and dry conditions that are not compliant with the atmospheric processes (Maters et al., 2017). It was therefore decided to undertake a comprehensive study of the interactions of  $\text{SO}_2$  with v-dust under atmospheric conditions. Iceland was chosen as a location of interest for sample collection required to study heterogeneous reactivity of volcanic ash and  $\text{SO}_2$  gas. The scope of this study is threefold. First, different natural volcanic and Icelandic samples were collected and characterized using various techniques, such as SEM (Scanning Electron Microscopy) and ICP-MS (Inductively Coupled Plasma-Mass Spectrometry). Second, the uptake of atmospheric  $\text{SO}_2$  by the surface of selected v-dusts was investigated using a flow tube reactor. Finally, Diffuse Reflectance Fourier Transformed Spectroscopy (DRIFTS) employed for the *in-situ* monitoring of adsorbed phase was used to identify the surface species formed and to clarify the surface reaction mechanisms. The *in-situ* spectroscopic approach has been complemented by HPLC (High-Performance Liquid Chromatography) technique employed for quantification of the surface products.

## 2. Experimental section

### 2.1. Materials

#### 2.1.1. Origin of the dust samples

All five samples of v-dust come from different dust hot spots of Iceland. The properties of Hagavatn (64°28'6,12"N 20°16'55,81"W), Mýrdalssandur (63°26'50.1"N 18°48'52.8"W), Maelifellssandur (63°48'48.7"N 19°07'42.5"W) and Dyngjúsandur (64°50'41,885"N 16°59'40,78"W) v-dusts are described by Arnalds et al. (2016). Overall, these areas are subjected to extremely large aeolian erosion due to frequent dust storms, and have extensive areas (10–140  $\text{km}^2$ ), hence providing a large supply (31–40 million tons annually) of v-dust to the atmosphere. Samples were collected from the top surface layer of each dust hot spot. The samples were dry and did not come in contact with soil or other organics. The fifth sample of Eyjafjallajökull (63°33'50.4"N 19°27'28.8"W) volcanic ash was collected and stored dry during the second phase of the explosive-effusive volcanic eruption on April 27. It is a typical volcanic ash sample as characterized by Gíslason et al. (2011).

#### 2.1.2. Characterization of the samples

**Scanning Electron Microscopy/Morphology** of the samples was analyzed by SEM carried out on a Hitachi S-4300SE/N SEM in high vacuum mode. The images of different v-dust particles are presented in Fig. 1. These are small particles with rough edges. Dust from Eyjafjallajökull (Fig. 1e) has larger particle size with many particles reaching 500  $\mu\text{m}$  in diameter, while the other four dusts (Fig. 1a–d) have a much finer structure and range from 10 to 50  $\mu\text{m}$  in diameter due to glaciofluvial processes leading to their generation.

**Specific surface area measurements/**To avoid any overestimation



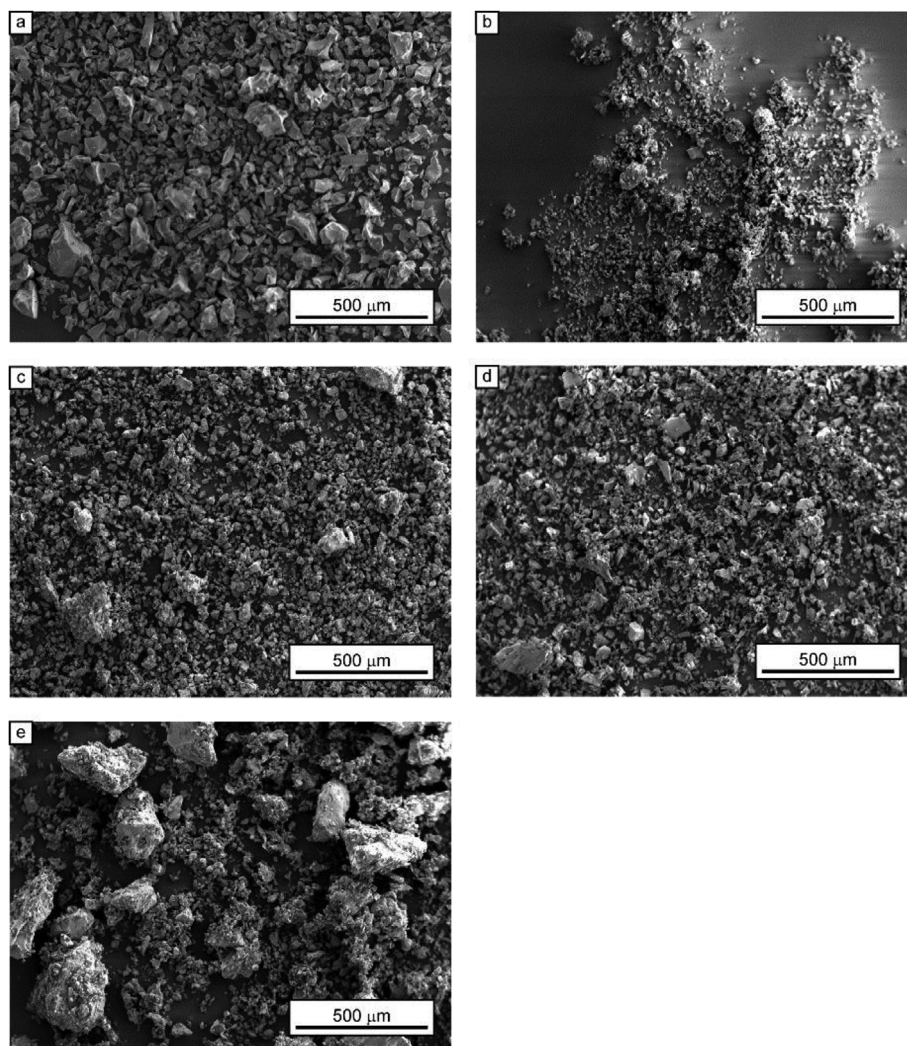


Fig. 1. SEM images of five v-dusts: (a) Mýrdalssandur, (b) Dyngjusandur, (c) Hagavatn, (d) Maelifellsandur, (e) Eyjafjallajökull.

of the uptake coefficients by the use of the geometric surface of the sample bed, it was decided to use the specific surface area (SSA) in the uptake calculations as discussed in the latest IUPAC evaluation (Crowley et al., 2010). In brief, the determination of the uptake coefficient using the geometric surface - i.e. the geometric area of the tube covered with the volcanic dust as noted in equation (2) (see section 2.2.1) of the manuscript-overestimates the uptake since it does not consider all the surface of the dust as accessible to gaseous  $\text{SO}_2$ . However, in a series of experiments it was evidenced that the entire surface area of the sample is accessible to the gas environment and thus the total surface area of the dust deposited in the tube should be used to determine the real uptake coefficient. The SSA is a physical property of solids, which represents the total surface area of a material per mass unit ( $\text{m}^2 \text{g}^{-1}$ ), and is used for the determination of the kinetic and sorption parameters (see section 2.2.1). To determine SSA, the Brunauer–Emmett–Teller (BET) method was employed. Nitrogen ( $\text{N}_2$ ) adsorption measurements were performed with a laboratory gas sorption analysis system (Joshi et al., 2017), (Ibrahim et al., 2018) within 0.05–0.3 relative pressure range ( $P/P_0$ ) of  $\text{N}_2$ . To determine the range of uncertainty, three adsorption measurements were conducted for each sample. The results of the BET specific surface area ( $SSA_{\text{BET}}$ ) of the 5 samples are displayed in Table 1.

**Chemical composition**/The bulk elemental composition of the samples of Icelandic v-dust used in this study was determined by ICP-MS using a Perkin Elmer NeXion 300x spectrometer, the results are

Table 1

BET Specific Surface Area of the v-dust samples used in this study.

Origin of the Icelandic v-dust sample	BET Specific Surface Area ( $\text{m}^2 \text{g}^{-1}$ )
Mýrdalssandur	$1.5 \pm 0.38$
Dyngjusandur	$7.0 \pm 1.8$
Hagavatn	$4.5 \pm 1.1$
Maelifellsandur	$8.2 \pm 2.0$
Eyjafjallajökull	$0.75 \pm 0.19$

presented in Table 2. Prior to the analysis, from 2 to 7 mg of each sample were treated in a mixture of acids ( $\text{HF}/\text{HNO}_3/\text{H}_2\text{O}_2$ ) in a microwave oven (Milestone Ultrawave) at 500 K and 35 bar for 15 min (Alleman et al., 2010). Six measurements per sample were performed to evaluate their chemical heterogeneity. Repeated measurements were carried out on acid blanks, quality control standard solutions and standard reference material (NIST SRM 1648a and SRM 2584) to evaluate detection limits, accuracy and to validate the whole procedure. As can be seen from Table 2 silicon is the most abundant element of the v-dust, followed by iron, calcium, and aluminum. Within the five selected v-dust samples the elemental composition seems to differ only slightly, except for Eyjafjallajökull v-dust which exhibits a higher amount of silicon than other samples and a lower amount of calcium, iron and magnesium. The results of ICP-MS analysis for Eyjafjallajökull v-dust agrees well with the literature (Gislason et al., 2011). The

**Table 2**

% Elemental composition of the v-dust samples used in this study and of mineral dust samples adopted from (Joshi et al., 2017), as determined by ICP-MS experiments.

Element	Mýrdalssandur	Dyngjusandur	Hagavatn	Maelifellssandur	Eyjafjallajökull	Bordj Saharan dust (Joshi et al., 2017)	Gobi dust (Joshi et al., 2017)
Si	31.3 ± 2.2	32.7 ± 2.0	27.5 ± 2.8	28.3 ± 2.4	49.5 ± 0.9	94.4	57.6
Fe	23.0 ± 1.5	19.7 ± 0.2	19.6 ± 0.7	23.8 ± 0.8	13.0 ± 0.5	1.3	5.5
Ca	13.9 ± 1.3	16.3 ± 0.3	19.5 ± 1.1	14.0 ± 0.3	7.3 ± 0.1	1.0	16.1
Al	12.3 ± 3.1	15.8 ± 0.2	16.7 ± 3.2	15.5 ± 0.1	13.6 ± 0.9	1.8	11
Mg	5.1 ± 1.2	7.3 ± 0.1	10.4 ± 1.8	5.7 ± 0.4	3.3 ± 0.2	0.1	2.3
Ti	7.6 ± 0.7	3.3 ± 0.4	2.4 ± 0.1	6.1 ± 0.4	2.4 ± 0.1	0.7	0.8
Na	4.8 ± 0.2	3.9 ± 0.1	3.1 ± 0.1	4.6 ± 0.1	7.3 ± 0.3	0.2	2.5
K	1.3 ± 0.2	0.6 ± 0.1	0.2 ± 0.1	1.5 ± 0.1	3.1 ± 0.1	0.1	3.5
other	0.7	0.4	0.6	0.5	0.5	0.1	0.7

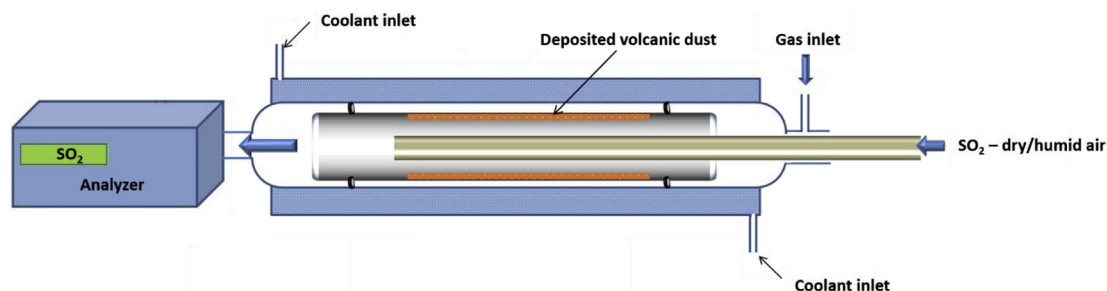


**Fig. 2.** Schematic representation of the Coated wall Flow Tube (CWFT) reactor used in this study. The space filled with the coolant in between the two walls is shaded in blue. The dust sample coating the inner surface of the Pyrex tube is shown in orange. (For interpretation of the references to color in this figure legend, the reader is referred to the Web version of this article.)

difference in the composition of Eyjafjallajökull v-dust in comparison with other samples is most probably due to the difference in the composition of magma that produced it. Indeed, the volcanic systems that supply Dyngjusandur dust hotspot (Bárðarbunga and Kverkfjöll volcanic systems) and Mýrdalssandur and Maelifellssandur dust hotspots (Katla volcanic system) have magmas of a predominantly basaltic composition, while magma of Eyjafjallajökull is andesitic, meaning that it is higher in silicon (“Icelandic Volcanoes,” n.d.), (Vogel et al., 2017). The decrease of calcium, iron and magnesium with increasing silicon content is in accordance with the expected variation of the composition of magma (Vogel et al., 2017). Other processes that can influence the composition of magma during a particular eruption include crystallization (Clague and Denlinger, 1994), melting of the crustal rocks (Deegan, 2010) and mixing of original magma with another magma that evolved separately (“Icelandic Volcanoes,” n.d.). Since composition of magma can change within the same eruption, one might expect to see different compositions of v-dust both on the time scale and on the location scale. Transported dust can also have a different composition further away from the source. Globally, when compared to other types of mineral dusts, such as Saharan dusts or Gobi dust (Joshi et al., 2017), the amount of silicon in all five v-dust samples is considerably lower while the amount of iron, magnesium, and titanium is higher (Romanias et al., 2016), (Langmann, 2013).

### 2.1.3. Gases

Experiments are carried out using zero air; it is generated by a classical air compressor, and then passed through a catalytic zero air generator (Claind ZeroAir, 2020, Lenno, Italy) coupled to a swing adsorption (PSA) device. The remaining impurity levels in the air stream before entering the reactor are lower than the analytical system detection limits: VOCs < 0.1 ppb, CO<sub>2</sub> < 10 ppb, and CO < 80 ppb. Moisture level is ca. 2 ppm. In experiments requiring humid air, a second flow of zero air going through a bubbler of ultrapure water (milli-Q, resistivity 18.2 MΩ cm) is mixed with the dry air flow, in proportions necessary to reach the relative humidity (RH) targeted. Certified gas cylinders are used as SO<sub>2</sub> source. For low concentration

experiments aiming to determine uptake coefficients in the flow tube, an SO<sub>2</sub> cylinder of 8.96 ppm in air (20.7% O<sub>2</sub>, 79.3% N<sub>2</sub>) provided by “Air Liquide” is used. Regarding the mechanistic investigation employing DRIFT spectroscopy, higher concentrations are used and a certified cylinder of 250 ppm (Messer, France) diluted in synthetic air (nearly 80% N<sub>2</sub> and 20% O<sub>2</sub>) is the SO<sub>2</sub> source.

Throughout the manuscript, gas concentrations are given in ppmv and ppbv (parts per million and parts per billion by volume, respectively). Under usual experimental conditions ( $T = 296\text{ K}$ ,  $P = 1\text{ atm}$ ), the conversion to a concentration is given by 1 ppbv (SO<sub>2</sub>)  $\approx 2.5 \times 10^{10}$  molecules cm<sup>-3</sup>. Note that this conversion factor takes a different value when the temperature or total pressure changes.

## 2.2. Experimental set ups

### 2.2.1. Coated wall flow tube reactor

The heterogeneous interaction of SO<sub>2</sub> with v-dust was investigated in a horizontal double wall flow tube reactor represented schematically in Fig. 2. The experiments were conducted under relevant atmospheric conditions, i.e. SO<sub>2</sub> concentration in the ppb range, atmospheric pressure, room temperature, under dry conditions and 30% RH. The objective of this series of experiments was to determine the uptake coefficients of SO<sub>2</sub> on the various Icelandic v-dusts.

The setup was described in detail in a previous paper (Lasne et al., 2018) it mainly consists of three parts; (i) the gas mixing line, (ii) the reactor and (iii) the analytical device. The gas preparation line is used for the mixing of zero dry/humid air with SO<sub>2</sub> resulting in a flow with the desired proportion of RH and SO<sub>2</sub> concentration. The reactor is made of a double wall Pyrex glass and is thermostated by circulating water in between the double wall surrounding the flow tube. Inside and along the axis of the reactor, a Pyrex tube covered on its inner wall with the v-dust is introduced. To coat the inner surface of a Pyrex tube with v-dust (orange color in Fig. 2), a defined mass of dust is first inserted in a tube. A small amount of water is added to form a slurry and the tube is shaken to deposit an even coating on the Pyrex surface. Then, the tube is heated slightly above 380 K for 10 min to evaporate excess water,

placed in the reactor and flushed overnight with dry air. Potential modifications of the volcanic dust upon its dissolution in water in the process of slurry preparation and subsequent drying process include displacement of soluble salts that might be found on the surface of v-dust particles as well as leaching of alkali and alkaline earth metals from the aluminosilicate network at ash surfaces (Witham et al., 2005). In the case of Hagavatn, Mýrdalssandur, Maelifellssandur and Dyngju-sandur natural v-dust samples, that were likely previously exposed to water the above mentioned phenomena does not seem to effect the results because the soluble salts would be expected to leach out by the time of the experiment. In the case of fresh Eyjafjallajökull dust leaching of the soluble salts formed during ash-gas interaction in the plume presents a valid concern. In order to minimize removal of soluble salts the amount of water added to prepare a slurry was as small as necessary to spread the dust evenly, i.e. in the case of Eyjafjallajökull 1:3 ash (g) to water (mL) ratio was used, which is much smaller than the 1:25 ash-to-water ratio recommended for preparation of ash leachates (Witham et al., 2005). In addition, contact time with water was minimized to around 10 s shaking followed by rapidly drying the slurry, which is also much faster than 90 min agitation procedure recommended by Witham et al. (2005). One could also expect that drying the slurry would lead to redistribution of the displaced salts, even though some of it could be redeposited on the surface of the glass tube and not the v-particles. Two Viton O-rings are placed around the Pyrex tube to fix its position inside of the reactor. The gas mixture is flowed through a movable injector (internal diameter of 0.3 cm) with a flow rate ranging between 250 and 500 sccm, ensuring laminar flow conditions with a Reynolds number,  $Re < 50$ . The role of the moveable injector is to either isolate (placed at the downstream end of the flow tube) or to expose the dust surface to the gas environment (upstream end of the reactor). The outgoing flow is then directed to the SO<sub>2</sub> analyzer (Model 43C, Thermo Environmental Instruments Inc.) for the real time gas phase monitoring of SO<sub>2</sub>, with a time resolution of 10 s. We didn't noticed any loss of dust during the uptake experiments. Note that the tubes with the deposited dust are weighted before and after the experiments and the variations noticed were in the range of the mass scale uncertainty (< 1%). In addition, considering that the flow rate during the experiments is relative slow, the experiments are carried out under atmospheric pressure and no pressure variation takes place between the reactor and the analyzer, it is highly improbable to experience any loss of dust during our measurements. Furthermore, we have not observed (at least visually) any large particles to fail to adhere to the Pyrex tube. However, even if this was the case, in the horizontal flow tube, these particles would still be subjected to the flow of gas and thus remain accessible to the gas. To conclude, the total mass of the dust inside the reactor is maintained during the entire experiment and is accessible to the gas environment and hence the total surface area does not change and no correction is required to determine the uptake coefficients. The uptake of SO<sub>2</sub> by v-dust is studied under dark conditions at  $T = 296$  K,  $[SO_2] \approx 75$  ppb ( $1.88 \times 10^{12}$  molecules cm<sup>-3</sup>) in air, and a relative humidity of either 30% or under dry conditions (i.e.  $RH < 0.1\%$ ). Regarding  $RH$ , studying the uptake under dry conditions provides an evaluation of the interaction of the probe gas with the direct surface of volcanic material, while increasing  $RH$  to 30% contributes to the understanding of the impact of the water coverage on the mineral aerosol (Joshi et al., 2017).

Theoretical SO<sub>2</sub> concentration profile is represented in Fig. 3. During a typical flow tube experiment SO<sub>2</sub> is flowed through the reactor, the dust being left unexposed initially. After a stable SO<sub>2</sub> concentration,  $[SO_2]_0$ , is set, the injector is pulled out and the dust is exposed to SO<sub>2</sub>; the change in SO<sub>2</sub> concentration related to its uptake by dust is recorded by the SO<sub>2</sub> analyzer. After a steady-state is reached, the injector is pushed back in to control the  $[SO_2]_0$ . What is obtained as a result of the flow tube experiment is a time evolution of the trace gas concentration at the tube exit, the so-called breakthrough curve, that is used to calculate the steady state uptake coefficient (Huthwelker et al.,

2006). In the case of SO<sub>2</sub> a long-lasting tailing of the breakthrough curve is observed, similar to the one described for the uptake of nitric acid (HNO<sub>3</sub>) on ice (Huthwelker et al., 2006). This phenomena leads to the following question: at which point can we say that a steady state is reached? In the absence of the generally accepted understanding of the nature of tailing and for the practical reasons the following pragmatic approach was adopted. Steady state is considered to be reached when the variation of the signal falls within 1.5% of its value for at least 3 h. On average it takes about 12 h to reach the steady state under 30% humidity, which is much longer than 1 h needed to achieve a steady-state for the uptake of ozone by clay dust (Lasne et al., 2018).

Preliminary experiments were conducted to determine a possible contribution of the Pyrex surfaces to the uptake of SO<sub>2</sub>. They showed negligible contribution to the parameters determined in the current study.

The measurements of  $[SO_2]$  at steady-state and at the initial level,  $[SO_2]_0$ , together with the knowledge of the parameters defining our setup are necessary to conduct the analysis leading to the determination of the uptake coefficients under equilibrium conditions,  $\gamma_{ss}$  (Lasne et al., 2018). Assuming first order kinetics for the uptake of SO<sub>2</sub> by v-dust surfaces, the observed constant of reaction,  $k_{obs}$  (in s<sup>-1</sup>), is determined by (1):

$$k_{obs} = \frac{v}{L} \times \ln\left(\frac{[SO_2]_0}{[SO_2]}\right) \quad (1)$$

where  $v$  is the flow in the reactor (in cm s<sup>-1</sup>) and  $L$  is the length of the dust coating (in cm). The value of  $k_{obs}$  (in s<sup>-1</sup>) is corrected for diffusion of SO<sub>2</sub> with a constant  $k_{diff}$  (in s<sup>-1</sup>) to give the diffusion-corrected constant  $k_{kin}$  (in s<sup>-1</sup>). In this work, a diffusion coefficient of SO<sub>2</sub> in the air derived from (Massman, 1998) is used,  $D(296$  K) = 95.28 Torr cm<sup>2</sup> s<sup>-1</sup>. This value is in excellent agreement with  $D = 94 \pm 13$  Torr cm<sup>2</sup> s<sup>-1</sup> suggested by Tang et al. (2014). The diffusion-corrected constant,  $k_{kin}$ , is then used to determine  $\gamma_{ss}$ , (2):

$$\gamma_{ss} = \frac{4k_{kin}V}{cS_{geom}} \quad (2)$$

where  $V$  and  $S_{geom}$  are the volume (in cm<sup>3</sup>) and geometric surface (in cm<sup>2</sup>) of the region where the reaction takes place, respectively, and  $c$  is the average molecular speed (in cm s<sup>-1</sup>). The diffusion-correction accounts for ca. 5% of the measured uptake coefficients.

A series of experiments were carried out as a function of Mýrdalssandur v-dust mass deposited that showed a linear increase in the 0–250 mg range. The linear increase of the uptake with mass and the lack of saturation reflect the fact that the entire surface of the dust is accessible to SO<sub>2</sub> molecules from the gas and thus the specific surface area  $SSA_{BET}$  is used for the calculation of the uptake coefficient,  $\gamma_{ss,BET}$ , (3):

$$\gamma_{ss,BET} = \gamma_{ss} \times \frac{S_{geom}}{A_s} \quad (3)$$

where  $A_s$  is the effective surface area of the dust, obtained from multiplying  $SSA_{BET}$  (m<sup>2</sup> g<sup>-1</sup>) by the mass of the sample (g).

The error on the uptake coefficients is the root-mean-square deviation of the values measured. It was calculated with the precision of the signal (0.5% of the measured concentration) and its propagation to  $k_{obs}$  measurement, the  $SSA$  determination (~25%) and all relevant uncertainties, i.e. on the gas flow measurement, temperature, mass weighting, and length of the exposed dust coating (~8%). The total error calculated for the  $\gamma$  values was estimated to be ca 35% in all experiments and a safe limit of 40% is given. Although the quoted uncertainty is significant, it reflects the real error accounted for the measurement of slow uptake processes (uptakes on the order of 10<sup>-9</sup>) in the flow tube.

Besides uptake coefficients, the transient initial number of SO<sub>2</sub> molecules taken up per surface area of v-dusts  $N_t$  (molecules cm<sup>-2</sup>) is determined at 30% of  $RH$ ; by integrating the area of the initial uptake



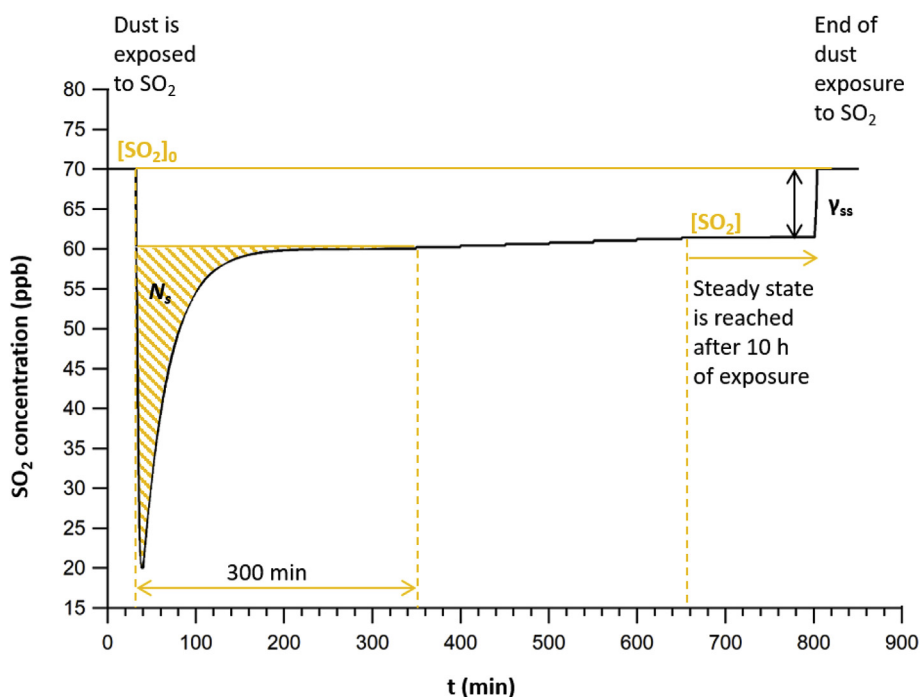


Fig. 3. Theoretical  $\text{SO}_2$  concentration profile during a typical flow tube experiment with v-dust exposed to  $\text{SO}_2$ . At the beginning of the experiment where surface is isolated from the gas mixture the initial  $\text{SO}_2$  concentration is  $[\text{SO}_2]_0$ , then the dust is exposed to the gas and the concentration of  $\text{SO}_2$  falls to its minimum, after which it recovers till a steady-state is reached. Note that the steady-state concentration  $[\text{SO}_2]$  is different from the initial state concentration  $[\text{SO}_2]_0$ . Initial concentration is controlled when the injector is pushed in and the  $\text{SO}_2$  gas is no longer in contact with the dust. Shaded area corresponds to the integrated area that is used to obtain the number of molecules during the transient initial uptake of  $\text{SO}_2$  on v-dusts  $N_s$  (molecules  $\text{cm}^{-2}$ ). 300 min was chosen as integration limits for the determination of  $N_s$ .

process in a typical uptake experiment (Fig. 3) divided by the effective surface area of the dust,  $A_s$ , according to (4):

$$N_s = \int_{\tau=0}^{\tau=t} \frac{F_t}{A_s} d\tau \quad (4)$$

where  $F_t$  is the flow rate (molecules  $\text{min}^{-1}$ ) of  $\text{SO}_2$  molecules through the reactor. The total error in  $N_s$  determination is estimated to be ca. 30% and includes all systematic uncertainties and the error in  $SSA$  determination.

It should be noted that since the  $\text{SO}_2$  concentration recorded at the steady-state was lower than its pre-exposure concentration, for the determination of  $N_s$  solely the transient initial uptake removal of  $\text{SO}_2$  is considered (dashed area in Fig. 3). The long tailing of the breakthrough curve observed points to additional physico-chemical processes besides the absorption/desorption. Therefore for the determination of integration parameter a similar to two-third criterion approach was adopted as recommended by Huthwelker et al., where “the surface uptake is considered finished once the breakthrough curve rises to two-thirds of its initial value” (Huthwelker et al., 2006). The integration limits for the determination of the number of molecules  $N_s$  were chosen from the time of the exposure of  $\text{SO}_2$  to the dust to 300 min after the exposure to make sure that the change in the breakthrough curve towards steady state has occurred for all the dusts. This criterion was adopted in order to be able to compare the uptake capacity of the v-dusts at the initial stage of the interaction with  $\text{SO}_2$ . On longer scale, samples can be compared based on the  $\gamma_{ss,BET}$  values.

### 2.2.2. DRIFTS experiments

The heterogeneous interaction between  $\text{SO}_2$  gas and v-dusts was studied *in-situ* inside of the optical DRIFTS cell operated at atmospheric pressure and room temperature under dry and 30% RH conditions. The objective of this series of experiments was to monitor the adsorbed species formed on the surface of v-dusts, aiming to elucidate the mechanism of the interaction under both dry and humid conditions.

The DRIFT experimental setup consists of three parts: (i) the gas supply line, (ii) the optical reactor, and (iii) the analytical device as described previously by Romanias et al. (Romanias et al., 2016). A representation of the system is given in Fig. 4. The heterogeneous reactions between  $\text{SO}_2$  and different v-dust samples are monitored *in situ*

inside of the optical DRIFTS cell (Praying Mantis Kit, Harrick Scientific Corp.) fitted with zinc selenide (ZnSe) windows. DRIFT spectra are recorded by a Nicolet 6700 FTIR spectrometer equipped with a mercury cadmium telluride (MCT) detector cooled with liquid nitrogen.

The temperature of the sample is measured using a thermocouple placed right below of the sample holder and is monitored/controlled with a Harrick temperature controller (Pleasantville, USA).

At the beginning of the experiment the crucible sample holder inside the DRIFTS cell is filled with about 80–110 mg of v-dust. The cell is then tightly closed and the infrared beam is focused on the surface of the dust. The gas flowed through the DRIFTS cell is made up of different proportions of dry air, humid air and  $\text{SO}_2$  gas. Prior to the introduction of the  $\text{SO}_2$  gas volcanic samples are heated to 423 K for 1.5 h to remove any pre-adsorbed species. Samples are then allowed to cool down to room temperature and are purged overnight with either dry or humid air depending on the experimental conditions in order to equilibrate system. A background spectrum is recorded right before introduction of  $\text{SO}_2$  gas. DRIFT spectra of the v-dust in the presence of  $\text{SO}_2$  gas are recorded from 650 to 4000  $\text{cm}^{-1}$  using Omnic software with 100 scans per spectrum, a spectral resolution of 4  $\text{cm}^{-1}$ , and a time resolution ranging from 3 min to 1 h depending on the stage of the experiment. The formation and loss of surface species are observed as positive and negative absorption bands respectively. Thus, a typical experiment lasts about 4 days and consists of thermal pre-treatment (1.5 h), system equilibration (16 h),  $\text{SO}_2$  adsorption phase (72 h) and desorption upon flushing phase (6 h). The  $\text{SO}_2$  concentration in the mixed gas is 175 ppm. Note that this is over three orders of magnitude higher than the atmospherically relevant  $\text{SO}_2$  concentration of  $\sim 75$  ppb used in the flow-tube reactor experiments. Large difference in  $\text{SO}_2$  concentrations used for flow tube versus DRIFTS experiments comes from different technical constrains. For instance, DRIFT spectroscopy is used for the *in situ* characterization of surface adsorbed species but is characterized by a relatively low sensitivity, depending on the gas-surface interactions. Likewise, the observation of the steady state in flow tubes, when the flowing gas is in ppm level, is not possible. In this work two different reactors serve two different purposes: flow tube is used to study kinetics by providing uptake coefficients under atmospherically relevant conditions while DRIFTS is used to study surface reaction mechanism. It is important to keep in mind that while the kinetics is changed by the

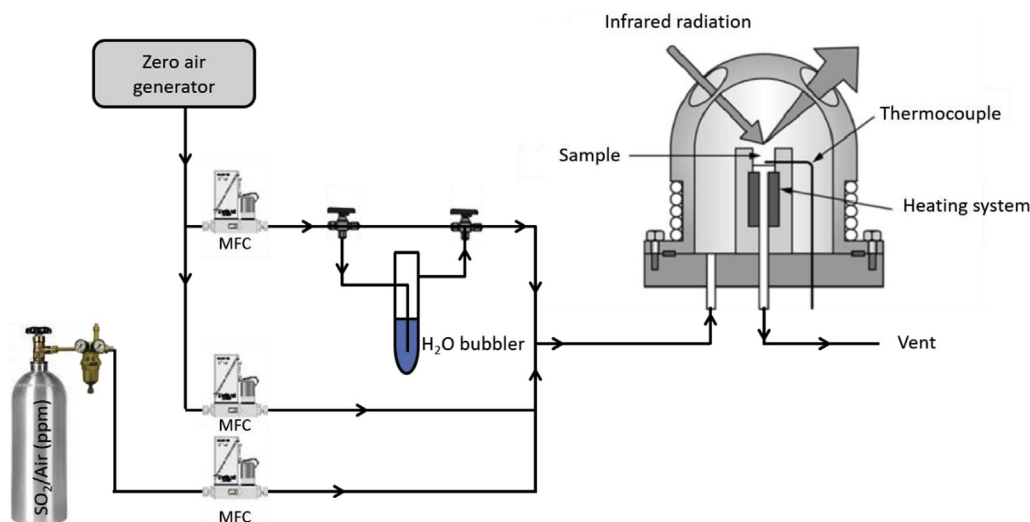


Fig. 4. Scheme of the DRIFT experimental setup. MFC: Mass Flow Controllers are used to supply the optical cell with a defined mixing ratio of dry air, humid air, and  $\text{SO}_2$ .

concentration because the surface coverage is changed by the concentration, the reaction mechanism is not likely to be changed as a function of gas phase concentration. Thus, both techniques bring complimentary and valuable information.

### 2.2.3. Ion analysis

A reverse-phase HPLC method with indirect photometric detection for the simultaneous determination of sulfates and sulfites was used for quantification of sulfates and sulfites formed following experiments with DRIFTS. To prevent oxidation of sulfites to sulfates, 1.0 mL of 1% formalin in pure water is used as an extracting solvent as recommended by Michigami (Michigami and Ueda, 1994). After 20 min of mechanical shaking the extracted solution is passed through a  $0.2\ \mu\text{m}$  PTFE membrane and a filtered leaching solution is analyzed by Waters HPLC system. Chromatography equipment consists of Waters 2695 Series HPLC System equipped with 2487 UV/VIS Dual wavelength absorbance detector, (Waters Corporation, Milford, MA). Empower 2 Data Acquisition System for LC (Copyright, 2005, Waters Corporation, Milford, MA) is used to analyze the data. Analysis is performed using Restek Ultra Column C18,  $5\ \mu\text{m}$ , Length 250 mm, I.D. 4.60 mm column dynamically coated with 1.0 mM cetylpyridinium chloride in 7% acetonitrile solution to produce a charged surface as recommended by Zuo et al. (Zuo and Chen, 2003) The HPLC instrument is operated isocratically at ambient temperature using Methanol-Potassium Hydrogen Phthalate Buffer 1.0 mM, adjusted to pH 6.5 with dilute potassium hydroxide (1:99, v/v) mobile phase and run at a flow rate of 1 mL/min for 15 min. The injection volume is  $10\ \mu\text{L}$ . Detector is set at 255 nm. All chemicals and solvents used for HPLC analysis are of analytical grade.

## 3. Results and discussion

### 3.1. Exploring $\text{SO}_2$ uptake on v-dust from the gas phase: flow tube study

#### 3.1.1. First insight on $\text{SO}_2$ uptake on various natural v-dusts under ambient conditions

The uptake of atmospheric relevant concentration of  $\text{SO}_2$  (i.e.  $\approx 75\ \text{ppb}$ ) by the surface of five selected v-dusts under typical atmospheric conditions of ambient temperature, pressure and 30% RH was investigated using the flow tube reactor (Lasne et al., 2018). A typical uptake profile depicted in Fig. 5 shows the  $[\text{SO}_2]$  uptake of Mýrdalssandur dust in humid ( $\text{RH} = 30\%$ ) conditions. It is clearly observed from the profile that after the initial uptake of the gas upon exposure of the v-dust the system reaches a steady-state  $[\text{SO}_2]$  that is

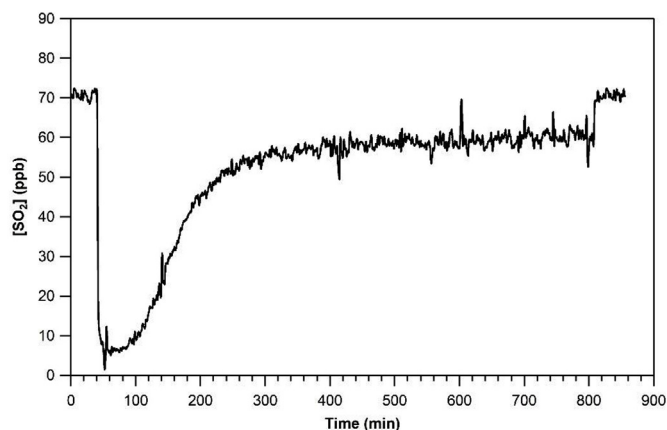


Fig. 5.  $\text{SO}_2$  concentration recorded by the analyzer during exposure of Mýrdalssandur v-dust at  $T = 296\ \text{K}$ ,  $\text{RH} = 30\%$ .

distinct from the initial state  $[\text{SO}_2]_0$ , evidencing continuous consumption of the title molecule at least for the duration of the experiment. All the samples under investigation demonstrated both an initial uptake and a steady state uptake (similar to Fig. 5). The latter is worth investigating as it suggests the ability of the v-dusts to exhibit a long-term effect on the equilibrium composition of the atmosphere. The steady state coefficients are in the order of  $10^{-9}$  to  $10^{-8}$  (Fig. 6, Table 3). These values are much lower than the values obtained by Maters et al., who reported the initial uptakes of  $\text{SO}_2$  on volcanic ash and glass powders at  $10^{-3}$  to  $10^{-2}$  range (Maters et al., 2017). Large difference in values is not surprising though for a number of reasons. First, the initial uptake describes an uptake on the fresh surface at the first instances of its interaction with gas, while the steady state uptake is an ongoing phenomenon reflecting the ability of the surface to adsorb gas continuously. Second, while determining initial uptakes geometric surface area was used by Maters et al. in order to calculate uptake coefficient (Maters et al., 2017), while specific surface area was used in this study in order to account for all the surface accessible to the  $\text{SO}_2$  molecules on longer time scales. Using geometric vs specific surface area gives an upper value for the uptake coefficient (Crowley et al., 2010). Finally, in the study of Maters et al. experiments were performed under dry conditions contrary to 30% RH used in this study. Moreover, in the adsorption/desorption experiments on the volcanic glasses performed by Schmauss and Keppler it was observed that the first layer of

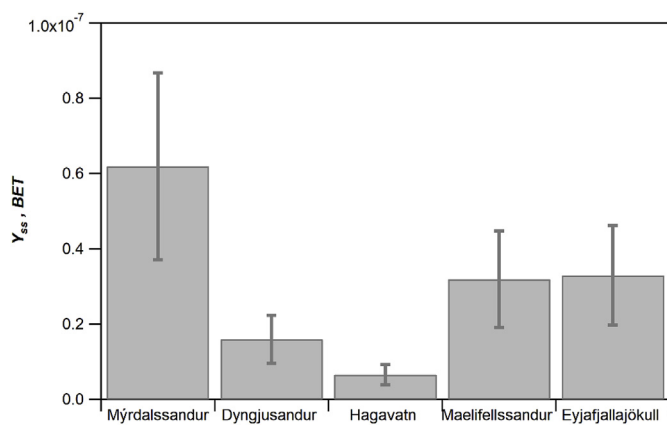


Fig. 6. Steady-state uptake coefficients of the Icelandic v-dust samples at  $[\text{SO}_2]_0 \approx 75$  ppb,  $\text{RH} = 30\%$ ,  $T = 296$  K, under dark conditions. The errors quoted reflects the total error for the steady state uptake coefficient determination.

Table 3

$\text{SO}_2$  steady-state uptake coefficients ( $\gamma_{\text{ss,BET}}$ ) and transient initial number of molecules adsorbed ( $N_s$ ) on the surface of v-dusts. Experimental conditions:  $[\text{SO}_2]_0 \approx 75$  ppb,  $\text{RH} = 30\%$ ,  $T = 296$  K, under dark conditions.

Origin of the Icelandic v-dust	$\gamma_{\text{ss,BET}}$	$N_s$ (molecules $\text{cm}^{-2}$ )
Mýrdalssandur	$(6.2 \pm 2.5) \times 10^{-8}$	$(2.5 \pm 0.8) \times 10^{13}$
Dyngjusandur	$(1.6 \pm 0.6) \times 10^{-8}$	$(2.1 \pm 0.6) \times 10^{13}$
Hagavatn	$(6.6 \pm 2.6) \times 10^{-9}$	$(1.2 \pm 0.4) \times 10^{13}$
Maelifellssandur	$(3.2 \pm 1.3) \times 10^{-8}$	$(9.6 \pm 2.9) \times 10^{12}$
Eyjafjallajökull	$(3.3 \pm 1.3) \times 10^{-8}$	$(1.2 \pm 0.4) \times 10^{13}$

$\text{SO}_2$  molecules was adsorbed on the surface of volcanic glass irreversibly and could not be removed (Schmauss and Keppler, 2014).

Interestingly, the obtained results show somewhat contrasted behaviors from one sample to another. In the literature the differences in the uptake of  $\text{SO}_2$  on solid material are commonly linked to the differences in elemental composition or mineralogy (Maters et al., 2017), (Maters et al., 2016), (Usher et al., 2002), (Zhang et al., 2006), (Harris et al., 2012). Using synthetic and natural silicate glasses as proxies for fresh unweathered volcanic ash is commonly done due to the fact that glass often represents a major component of v-dust. Besides, a thin layer of glass covering the crystalline components of ash surfaces was observed (Delmelle et al., 2018). Several studies indicated that sulfates are more likely to get adsorbed on the glass fraction of volcanic dust (Schmauss and Keppler, 2014), (Farges et al., 2009). While investigating trends in adsorption of  $\text{SO}_2$  on glass, elemental composition is commonly investigated (Maters et al., 2017). This approach though ignores the crystalline phase of the volcanic dust. Maters et al. emphasized that the influence of crystallinity on the adsorption of  $\text{SO}_2$  gas is not yet understood (Maters et al., 2017). On the other hand author working with natural mineral dust samples, such as desert dusts often approximate composition of dusts using simple mineral oxides and look for trends in adsorption in relationship with the mineral phase composition. In our study v-dusts differ significantly in their crystalline fraction. Volcanic samples used in this study contain from 20% (Hagavatn) to 80–90% (Mýrdalssandur, Maelifellssandur and Dyngjusandur) of amorphous material (Baratoux et al., 2011), (Moroni et al., 2018). The remaining part is crystalline. Eyjafjallajökull is also dominated by glass (Gislason et al., 2011). Plagioclase, pyroxene, and olivine are the mineral phases reported in all five samples, while magnetite was only found in Mýrdalssandur and Maelifellssandur (Moroni et al., 2018), (Baratoux et al., 2011) (Gislason et al., 2011). A very small amount of crystalline silica was found in Eyjafjallajökull and none was reported for other samples (Gislason et al., 2011).

Since amorphous fraction dominates composition of v-dusts, an attempt to find trends in the uptake vs elemental composition was undertaken. Among the authors linking the differences in uptake coefficient to the elemental composition Maters et al. observed increase of the initial uptake of  $\text{SO}_2$  on the surface of synthetic volcanic glasses with decrease of their silica (Si) content and increase of the sum of their sodium (Na), potassium (K), magnesium (Mg) and calcium (Ca) content (Maters et al., 2017). As for the natural volcanic samples the relationship was not as straightforward, even though a dependence of the initial uptake on the total surface content of the sum of Na, K, Mg and Ca was suggested (Maters et al., 2017). In our studies no clear correlation between the bulk elemental composition of a v-dust and its uptake of  $\text{SO}_2$  was established. It can be due to the fact that the elemental concentration in the bulk sample may not represent the availability of the elements on the surface. Therefore, one might expect the information derived from elemental surface composition to be more accurate, yet care must be taken in interpreting such results. One should keep in mind that a given element when incorporated in glass versus crystalline mineral might behave differently. Farges et al. observed that crystalline quartz does not adsorb any sulfur species while amorphous silica does (Farges et al., 2009). The heterogeneous nature of the sample might further complicate finding the trends as elements forming different mineral phases will behave differently depending on the nature of mineral phase. For example, Fe is incorporated in both ilmenite ( $\text{FeTiO}_3$ ) and fayalite ( $\text{Fe}_2\text{SiO}_4$ ), yet the  $\text{SO}_2$  uptake is significantly higher for the former mineral (Harris et al., 2012).

Earlier studies can be used to understand potential contribution of crystalline fraction of the volcanic ash to the uptake of  $\text{SO}_2$ . Both quartz ( $\text{SiO}_2$ ) and magnetite ( $\text{Fe}_3\text{O}_4$ ) can be found in volcanic ash. Comparison of the uptakes of  $\text{SO}_2$  on individual mineral oxides, such as  $\text{CaO}$ ,  $\text{Al}_2\text{O}_3$ ,  $\text{CaCO}_3$ ,  $\text{Fe}_3\text{O}_4$  and  $\text{Fe}_2\text{O}_3$  showed that the uptake of  $\text{SO}_2$  depends on the nature of the mineral oxide with higher uptakes observed when  $\text{SO}_2$  interacted with iron-containing compounds (Usher et al., 2002). These observations were further tested by Zhang et al. who compared reactivity of different oxides taking into consideration their specific area and placed them in the following order:  $\text{Fe}_2\text{O}_3 > \text{MgO} > \text{TiO}_2 > \text{FeOOH} > \text{mixture} > \text{Al}_2\text{O}_3 > \text{SiO}_2$  (Zhang et al., 2006). Both studies indicate that conversion of  $\text{SO}_2$  per unit surface of  $\text{Fe}_2\text{O}_3$  is the highest, suggesting that particles with the highest amount of iron might be the most reactive in reactions with  $\text{SO}_2$ . Furthermore, the reactivity of the mixture, that was obtained by mixing the different oxides based on their abundance in the continental crust, was measured to be twice its theoretical value, which demonstrates its synergistic effect (Zhang et al., 2006). Even though most studies use simple mineral oxides and synthetic dust as a substitution for natural samples, such approach is problematic, as it undermines the importance of more complex mineralogy in the uptake of  $\text{SO}_2$ . While studying the uptake of  $\text{SO}_2$  on Saharan dust Harris et al. distinguished ilmenite ( $\text{FeTiO}_3$ ), rutile ( $\text{TiO}_2$ ) and iron oxides ( $\text{Fe}_2\text{O}_3$ ,  $\text{Fe}_3\text{O}_4$ ,  $\text{FeOOH}$ ) ( $\gamma_{\text{BET}}(\text{mixture of ilmenite and rutile}) = 3 \times 10^{-5}$ ) as major phases of dust responsible for uptake and oxidation of  $\text{SO}_2$  (Harris et al., 2012). Uptake on feldspar minerals such as  $\text{KAlSi}_3\text{O}_8$ ,  $\text{NaAlSi}_3\text{O}_8$  or  $\text{CaAl}_2\text{Si}_2\text{O}_8$  and quartz ( $\text{SiO}_2$ ) was found to be slow ( $\gamma_{\text{BET}}(\text{feldspar}) = 9 \times 10^{-7}$ ,  $\gamma_{\text{BET}}(\text{quartz with basic components}) = 4 \times 10^{-8}$ ) (Harris et al., 2012). To identify the elements associated with adsorption of  $\text{SO}_2$  by crystalline material Harris et al. analyzed individual Saharan dust grains that were relatively rich in S content after their exposure to  $\text{SO}_2$  and studied their elemental profile using single-particle SEM-EDX analysis (Harris et al., 2012). Ti, Fe and Ca were identified as the most important reactive elements, while Na, Mg, Al, Si showed no relationship to oxidizing capacity of dust (Harris et al., 2012). While studying the uptake of  $\text{SO}_2$  on v-dusts it would be informative to investigate the uptake of  $\text{SO}_2$  on other complex mineral phases present in v-dust such as pyroxene, plagioclase, amphibole, biotite, and olivine even though higher uptakes of  $\text{SO}_2$  are linked to the presence of minerals lacking silicates, such as ilmenite ( $\text{FeTiO}_3$ ) and magnetite ( $\text{Fe}_3\text{O}_4$ ) (Harris et al., 2012).

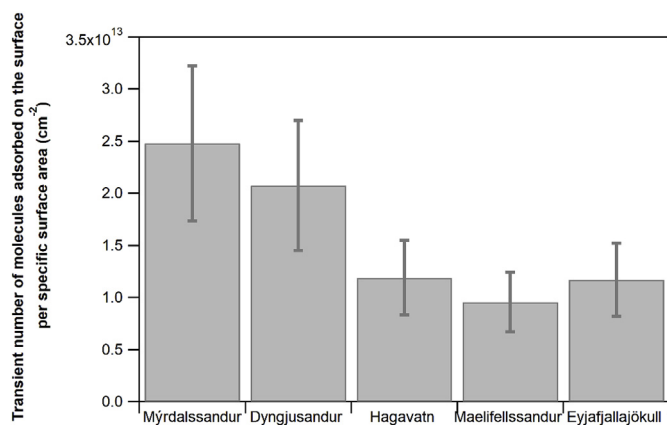


Fig. 7. Number of SO<sub>2</sub> molecules taken up on the surface of different v-dusts during the transient initial uptake process when exposed to [SO<sub>2</sub>]<sub>0</sub> ≈ 75 ppb, T = 296K, RH = 30%, dark conditions. The errors quoted reflect the total error for the N<sub>s</sub> determinations.

The number of SO<sub>2</sub> (N<sub>s</sub>) molecules removed during the transient initial uptake process per surface area was also investigated and was calculated to be in the order of 10<sup>13</sup> molecules cm<sup>-2</sup> (Table 3). These values are comparable to the values obtained by Maters et al., who reported the total uptake capacity of SO<sub>2</sub> on volcanic ash and glass powders under dry conditions at 10<sup>11</sup> to 10<sup>13</sup> range (Maters et al., 2017). As with initial uptakes, total uptake capacity of SO<sub>2</sub> on the surface of synthetic volcanic glasses increased with decrease of their Si content and increase of their total Na, K, Mg, Ca content (Maters et al., 2017). As for the natural volcanic ash samples the relationship was less clear and the dependence on total surface Na, K, Mg, Ca content was suggested (Maters et al., 2017). Furthermore, as displayed in Fig. 7, the transient number of molecules adsorbed N<sub>s</sub> at the initial stage of the exposure, and the steady state uptake coefficients do not follow the same trend. On one hand, Mýrdalssandur seems to adsorb the highest amount of molecules and it has the highest uptake coefficient. On the other hand, Hagavatn that has the smallest uptake coefficient adsorbs almost the same amount of molecules as Eyjafjallajökull and more than Maelifellssandur even though the latter two have an uptake coefficient that is twice as high as uptake coefficient of Hagavatn. The discrepancies between N<sub>s</sub> and γ<sub>ss,BET</sub> suggest that the surface is modified upon its initial exposure to SO<sub>2</sub>. Indeed, one should keep in mind that

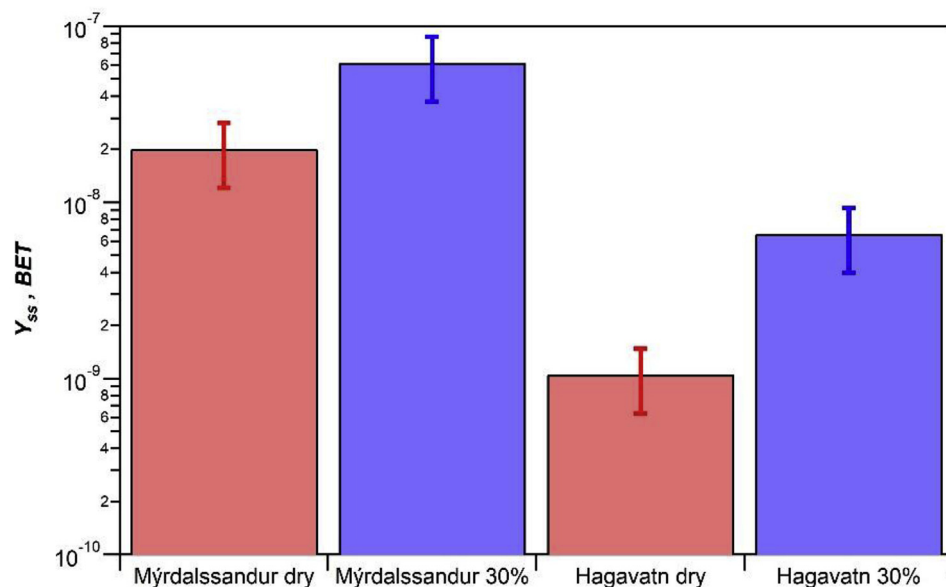


Fig. 8. Steady-state uptake coefficients of the Mýrdalssandur and Hagavatn v-dust samples at RH = 30% (blue bars) and RH = 0% (red bars), [SO<sub>2</sub>]<sub>0</sub> ≈ 75 ppb, T = 296 K, under dark conditions. The errors quoted reflects the total error for the steady state uptake coefficient determination. (For interpretation of the references to color in this figure legend, the reader is referred to the Web version of this article.)

adsorption behavior of SO<sub>2</sub> on each volcanic dust was characterized by measuring the steady state uptake coefficients after 12 h of exposure, i.e. after long processing, while the number of molecules taken up was measured after the first 5 h of the interaction where a transient uptake was observed at the initial stage of the experiment. Differences in the observed trends could indicate that at the initial stage of the experiment the surface of the dusts is modified due to SO<sub>2</sub> uptake and the corresponding formation of sulfites and sulfates, and these modifications affect the surface reactivity at longer time scale when the γ<sub>ss,BET</sub> values are determined. The modifications could explain why no correlation was noticed between the γ<sub>ss,BET</sub> and N<sub>s</sub> with the elemental composition of the v-dusts. Finally, the discrepancies could be due to the fact that the nature of the governing processes behind the initial fast uptake and thus the high amount of molecules adsorbed in the initial stage and those dominating the steady state uptake are fundamentally different (Huthwelker et al., 2006).

### 3.1.2. The role of relative humidity on the uptake of SO<sub>2</sub> on v-dusts

Several studies have highlighted the role of RH on SO<sub>2</sub> uptake (Li et al., 2006), (Zhou et al., 2014), (Huang et al., 2015). In order to investigate the role that RH plays in the steady state uptake of SO<sub>2</sub> on v-dust samples the relationship was investigated for two contrasted samples based on their steady-state uptakes – Mýrdalssandur and Hagavatn (Fig. 8). For Mýrdalssandur we observed that the steady state uptake coefficient of SO<sub>2</sub> at 30% of RH was significantly higher than under dry conditions (i.e. γ<sub>ss, BET</sub> (30% RH) = 6.2 × 10<sup>-8</sup> and γ<sub>ss, BET</sub> (dry) = 2.0 × 10<sup>-8</sup>). For the Hagavatn v-dust a similar trend was observed (i.e. γ<sub>ss, BET</sub> (30% RH) = 6.6 × 10<sup>-9</sup> and γ<sub>ss, BET</sub> (dry) = 1.0 × 10<sup>-9</sup>). The enhanced uptake trends observed in the presence of water indicate that water plays an important role promoting the partitioning of SO<sub>2</sub> to the adsorbed phase. There might be numerous reasons for the observed increased uptake of SO<sub>2</sub> in the presence of water vapor. Adsorbed water molecules can (i) participate in the reactions as reactants, (ii) serve as a medium for the reaction to take place or (iii) change the physical properties of the particle shifting the equilibrium towards higher SO<sub>2</sub> uptake. Water molecules can also form water layers that can help the product of the reaction to diffuse along the surface and thus promote the renewal, i.e. the turnover, of surface sites (Shang et al., 2010). The intrinsic ability of metal oxides to adsorb water molecules and form surface hydroxyls was linked to higher reactivity in the heterogeneous reaction with SO<sub>2</sub> (Zhang et al., 2006).

In the literature the analysis of the influence of RH on the uptake of



SO<sub>2</sub> on natural mineral dusts shows complex trends. An influence of water vapor on the interaction of SO<sub>2</sub> with Saharrah dust at 258 K showed no effect on initial uptake within statistical error (i.e.  $\gamma_{\text{BET}}$  (27% RH) =  $(6.0 \pm 1.0) \times 10^{-5}$  and  $\gamma_{\text{BET}}$  (dry) =  $(6.4 \pm 0.7) \times 10^{-5}$ ). Likewise, no dependency of the initial uptake coefficient on humidity was found for Adobe clay soil taken from Los Angeles area (Judeikis and Stewart, 1976). Alternatively, when Huang et al. subjected three authentic dusts to SO<sub>2</sub> at RH ranging from 0 to 90% an increase in uptake coefficient was observed for Tengger Desert dust (i.e.  $\gamma_{\text{BET}}$  (dry)  $\approx 3.8 \times 10^{-5}$  and  $\gamma_{\text{BET}}$  (90% RH)  $\approx 5.5 \times 10^{-5}$ ) and for Arizona test dust (i.e.  $\gamma_{\text{BET}}$  (dry)  $\approx 1.3 \times 10^{-5}$  and  $\gamma_{\text{BET}}$  (90% RH)  $\approx 2.76 \times 10^{-5}$ ), but a decrease was observed for Asian mineral dust (i.e.  $\gamma_{\text{BET}}$  (dry)  $\approx 3.2 \times 10^{-5}$  and  $\gamma_{\text{BET}}$  (90% RH)  $\approx 1.9 \times 10^{-5}$ ) (Huang et al., 2015). The negative dependence of humidity on SO<sub>2</sub> uptake in the case of Asian mineral dust was explained by the presence of water-soluble inorganic coating, which made surface more acidic and inhibited uptake of SO<sub>2</sub> (Huang et al., 2015). When the Asian mineral dust was washed and coating was removed, the uptake trend got reversed and showed positive correlation (i.e.  $\gamma_{\text{BET}}$  (dry)  $\approx 0.85 \times 10^{-5}$  and  $\gamma_{\text{BET}}$  (90% RH)  $\approx 1.32 \times 10^{-5}$ ) (Huang et al., 2015). Then again, while the samples from Inner Mongolian desert, characterized by high carbonate contents, demonstrated considerably increased uptakes at higher humidity (i.e.  $\gamma_{\text{ss, BET}}$  (40% RH) =  $1.0 \times 10^{-6}$  and  $\gamma_{\text{ss, BET}}$  (dry) =  $1.7 \times 10^{-7}$ ), Xinjiang sierozem natural mineral dust showed only a modest increase in steady-state uptake (i.e.  $\gamma_{\text{ss, BET}}$  (40% RH)  $\approx 2.4 \times 10^{-7}$  and  $\gamma_{\text{ss, BET}}$  (dry)  $\approx 2.2 \times 10^{-7}$ ) (Adams et al., 2005). The authors suggest that difference in the mineralogy could be responsible for the difference in the observed trends (Zhou et al., 2014). Higher carbonate component of the Inner Mongolian desert dust can promote the SO<sub>2</sub> uptake. Indeed, while investigating carbonate particles Zhang et al. observed that the value of the steady state uptake  $\gamma_{\text{ss, BET}}$  drastically increases from  $\gamma_{\text{ss, BET}}$  (1%) =  $0.32 \times 10^{-8}$  to  $\gamma_{\text{ss, BET}}$  (85% RH) =  $13.9 \times 10^{-8}$ , at 85% RH reaching 43 times its value at 1% (Zhang et al., 2018). In our study volcanic dusts, void of carbonates, cannot be directly compared to carbonate-rich samples, but the observed trend follows the one of Tengger Desert dust and Arizona test dust discussed earlier. More information about influence of humidity on the steady state uptake of SO<sub>2</sub> on the surface of volcanic glass and ash is necessary to obtain a more comprehensive picture.

While the increase in the SO<sub>2</sub> uptake with the increase of relative humidity is observed for a number of samples, it is not at all the case for the uptakes of other species, such as nonpolar volatile organic compounds (Romanias et al., 2016), hydrogen peroxide (H<sub>2</sub>O<sub>2</sub>) (Romanias et al., 2012) or ozone (O<sub>3</sub>) (Lasne et al., 2018). In fact, the uptake coefficient can decrease with increased humidity, such as the case for the steady state uptake of O<sub>3</sub> on montmorillonite clay dust reflecting the tendency for the molecules in question and molecules of water to compete with each other for the sorptive sites on the clay surface (Lasne et al., 2018).

The observation of the steady state nature of the uptakes points out that there are important and maybe cyclic processes occurring on the surface of the v-dust. The gas phase monitoring limits us to the determination of kinetic parameters; in order to investigate the mechanism of the SO<sub>2</sub> uptake surface monitoring is necessary. Increased SO<sub>2</sub> uptake at higher RH suggests that humidity plays a particularly important role in the adsorption of SO<sub>2</sub> to the surface. To monitor the adsorbed phase, determine the functional groups that are involved in the adsorption of SO<sub>2</sub> and to further evaluate the role of water to the reaction system, a series of experiments were carried out employing DRIFT spectroscopy.

### 3.2. Exploring SO<sub>2</sub> uptake on v-dust from the adsorbed phase: DRIFTS study

While flow tube reactor monitors changes in the gas-phase concentration, DRIFTS focuses on changes on the solid phase. It is

commonly used to study fine particles and powders, and can be used to investigate adsorption of molecules on solid surfaces. In this case spectra are collected as difference spectra with the unexposed solid as background. As the reaction proceeds, growing or decreasing peaks can be attributed to the species formed or consumed on the surface. Infrared spectroscopy based on light diffuse reflectance offers information about the vibrational modes associated with stretching, bending, and rocking motions of the adsorbed molecules. However, in order to monitor these vibrations the sample has to have high enough reflectance to insure an adequate signal in response to changes in the adsorbed phase, and the surface concentration needs to be high enough due to the low sensitivity of the technique. If the sample is highly absorbent, which is the case of v-dust samples, it is usually diluted in a non-absorbent matrix, such as KBr. In our case, however, this type of matrix could not be used because of the interactions of KBr with SO<sub>2</sub> and thus the use of pure v-dust was required. The background obtained for each v-dust under dry conditions showed that all of them absorb light strongly and, as a result, a weak IR signal was recorded in response to changes in the adsorbed phase. To study the adsorption of SO<sub>2</sub> on v-dust, backgrounds of five samples were taken to choose the least absorbent varieties. In comparison with other v-dusts the background for Hagavatn and Eyjafjallajökull shows higher reflectance in the area from 800 to 1350 cm<sup>-1</sup> where sulfite and sulfate species usually absorb. Because of its higher reflectance and higher specific surface area, Hagavatn v-dust was selected as the most appropriate sample for DRIFTS experiments. Besides, results obtained from the flow tube studies showed similar trends in SO<sub>2</sub> adsorption by the v-dusts based on gas-phase monitoring of SO<sub>2</sub>, i.e. rapid consumption of SO<sub>2</sub> gas at the initial stage of surface exposure followed by a steady state removal of the probe molecule. Therefore, it appeared justified to choose one dust as a representative sample to study the mechanism of product formation on the surface of aerosols. Aiming to further investigate the observations from the flow tube study and to further assess the role of humidity on the reaction mechanism, the DRIFTS experiments were performed under dry conditions and 30% RH using Hagavatn as a sample material.

#### 3.2.1. Typical DRIFT spectra of SO<sub>2</sub> interaction on v-dust

Fig. 9 and Fig. 10 show DRIFT spectra of Hagavatn v-dust at increasing SO<sub>2</sub> exposure time intervals at room temperature under 0% and 30% RH respectively. Table 4 introduces the assignment of peaks of different adsorbed sulfur-containing species as well as water and hydroxyl groups on the surface of v-dust investigated and different metal oxides found in the literature.

In Particular, the negative and positive absorption peaks in the area from 4000 to 3500 cm<sup>-1</sup> correspond to the free OH groups that are naturally present on the surface of v-dust (Hair, 1975). These groups are attached to the surface atoms, such as Si for example, and can be either completely isolated or hydrogen-bonded to each other (Hair, 1975). Adsorption of molecules containing a lone-pair of electrons is often associated with isolated surface OH groups, while neighboring hydrogen-bonded surface OH groups are involved in the adsorption of water (Hair, 1975), (Nanayakkara et al., 2012). The exact assignment of each individual peak is not possible due to the complex response reflecting slightly different vibrational energies of OH groups bonded to different minerals composing the v-dust. A peak from 3500 to 2600 cm<sup>-1</sup> and another peak from 1800 to 1400 cm<sup>-1</sup> centered at 1620 cm<sup>-1</sup> (not displayed) are attributed to vibration modes in molecular water (Hair, 1975).

A weak broad peak from 2600 to 2400 cm<sup>-1</sup>, visible under humid conditions, could be assigned to the S–H stretch vibration of the HSO<sub>3</sub><sup>-</sup> bisulfite species that is only found in the literature as a theoretical value calculated by Zhang et al. for aqueous solution and reported to be in the range of 2620 to 2450 cm<sup>-1</sup> (Zhang and Ewing, 2002). This peak is not visible under dry condition. Sulfur-containing products appear in the area from 1385 to 700 cm<sup>-1</sup> under humid conditions and from 1367 to 716 cm<sup>-1</sup> under dry conditions. Spectra under humid conditions are



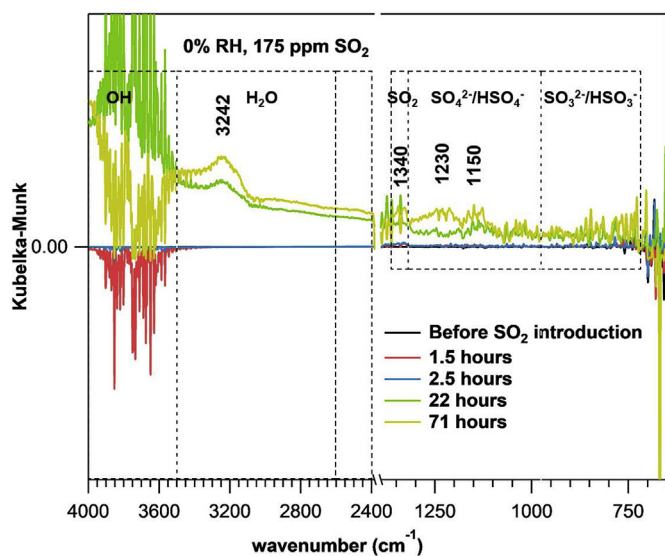


Fig. 9. DRIFTS spectra of  $\text{SO}_2$  uptake by Hagavatt v-dust at 0% RH and 296 K depicting evolution of bands for free surface OH groups ( $4000\text{--}3500\text{ cm}^{-1}$ ), adsorbed water ( $3500\text{--}2600\text{ cm}^{-1}$ ), physisorbed  $\text{SO}_2$  ( $1385\text{--}1320\text{ cm}^{-1}$ ), sulfates/bisulfates ( $1320\text{--}975\text{ cm}^{-1}$ ), sulfites/bisulfites ( $975\text{--}716\text{ cm}^{-1}$ ) as a function of time: black line – before introduction of  $\text{SO}_2$ , red line–after 1.5 h of exposure to  $\text{SO}_2$ , blue line–after 2.5 h of exposure to  $\text{SO}_2$ , green line–after 22 h of exposure to  $\text{SO}_2$ , yellow line–after 71 h of exposure to  $\text{SO}_2$ . (For interpretation of the references to color in this figure legend, the reader is referred to the Web version of this article.)

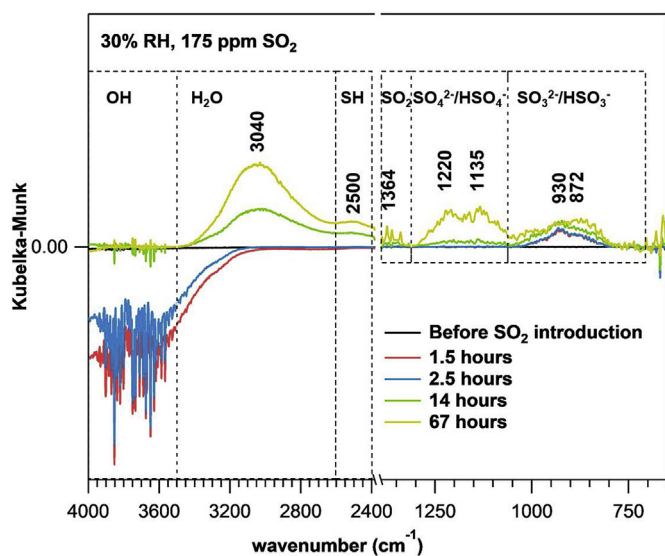


Fig. 10. DRIFTS spectra of  $\text{SO}_2$  uptake on Hagavatt v-dust at 30% RH and 296 K depicting evolution of bands for free surface OH groups ( $4000\text{--}3500\text{ cm}^{-1}$ ), adsorbed water ( $3500\text{--}2600\text{ cm}^{-1}$ ), SH groups ( $2600\text{--}2400\text{ cm}^{-1}$ ), physisorbed  $\text{SO}_2$  ( $1367\text{--}1320$ ), sulfates/bisulfates ( $1302\text{--}1050\text{ cm}^{-1}$ ), sulfites/bisulfites ( $1053\text{--}700\text{ cm}^{-1}$ ) as a function of time: black line – before introduction of  $\text{SO}_2$ , red line–after 1.5 h of exposure to  $\text{SO}_2$ , blue line–after 2.5 h of exposure to  $\text{SO}_2$ , green line–after 22 h of exposure to  $\text{SO}_2$ , yellow line–after 71 h of exposure to  $\text{SO}_2$ . (For interpretation of the references to color in this figure legend, the reader is referred to the Web version of this article.)

better resolved and several peaks can be distinguished:  $3040$ ,  $2500$ ,  $1364$ ,  $1220$ ,  $1135$ ,  $930$  and  $872\text{ cm}^{-1}$ . Peaks under dry conditions are much noisier, nevertheless the following peaks are observed:  $3242$ ,  $1340$ ,  $1230$  and  $1150\text{ cm}^{-1}$ . A double peak centered at  $1364\text{ cm}^{-1}$  under humid conditions and at  $1340\text{ cm}^{-1}$  under dry conditions appears rapidly upon exposure of the surface to  $\text{SO}_2$  gas and disappears

right away from the spectra after ceasing the  $\text{SO}_2$  flow. It was therefore assigned to the weakly, reversibly physisorbed  $\text{SO}_2$  species. The peak corresponds well to the literature values for  $\text{SO}_2$  adsorption under dry conditions on the surfaces of aluminum, magnesium or titanium oxides identified in the previous studies at  $1330\text{ cm}^{-1}$  and its gas-phase value of  $1362\text{ cm}^{-1}$  (Nanayakkara et al., 2012), (Goodman et al., 2001). Another band appears rapidly upon exposure of  $\text{SO}_2$  to the surface between  $1053$  and  $700\text{ cm}^{-1}$  under humid conditions. A corresponding band between  $975$  and  $716\text{ cm}^{-1}$  under dry conditions takes more time to develop and is hard to interpret since its intensity is almost at the limit of detection of the DRIFTS instrument. The assignment of this band is based on the previous assignments of  $\text{SO}_2$  adsorption on the surface of different metal oxides found in the literature and corresponds to the stretching motion of sulfite and bisulfite species that are bonded to the surface in a monodentate or bidentate mode. Different coordination environments as well as heterogeneous nature of v-dust contribute to the broadening of the band (Usher et al., 2002). In particular, Goodman et al. (2001), Usher et al. (2002) and Zhang et al. (2006) assigned the band between  $1100$  and  $850\text{ cm}^{-1}$  to adsorbed sulfite and bisulfite on  $\alpha\text{-Al}_2\text{O}_3$  and MgO. Li et al. (2006) and Wu et al. (2011) assigned a  $1000\text{--}900\text{ cm}^{-1}$  band on  $\text{CaCO}_3$  to a stretching vibration of sulfite. A peak from  $1200$  to  $800\text{ cm}^{-1}$  on  $\text{TiO}_2$  was assigned to sulfite and bisulfite species by Nanayakkara et al. (2012). On hematite particles Wang et al. assigned to sulfites a peak between  $950$  and  $800\text{ cm}^{-1}$  under dry conditions and a series of peaks from  $1050$  to  $900\text{ cm}^{-1}$  under humid conditions (Wang et al., 2018b). Finally, a band from  $1320$  to  $975\text{ cm}^{-1}$  with features at  $1230$  and  $1150\text{ cm}^{-1}$  in dry conditions and from  $1302$  to  $1055\text{ cm}^{-1}$  with features at  $1220$  and  $1135\text{ cm}^{-1}$  under humid conditions was attributed to sulfate and bisulfate species. The assignment agrees well with the results published previously, where sulfates/bisulfates were found around  $1300\text{--}1100\text{ cm}^{-1}$  on  $\alpha\text{-Al}_2\text{O}_3$  and MgO (Usher et al., 2002), (Zhang et al., 2006); between  $1240$  and  $1012\text{ cm}^{-1}$  on  $\text{CaCO}_3$  with features at  $1198$ ,  $1127$ , and  $1090\text{ cm}^{-1}$  (Wu et al., 2011), (Li et al., 2006). Sulfates were reported between  $1300$  and  $1100\text{ cm}^{-1}$  on  $\text{TiO}_2$  (Nanayakkara et al., 2012), (Shang et al., 2010); and at  $1220\text{ cm}^{-1}$  on  $\text{Fe}_2\text{O}_3$  (Wang et al., 2018b). Just as sulfites, sulfates can be bonded to the surface in bidentate or monodentate modes (Jiang et al., 2010). A peak centered at  $1220\text{ cm}^{-1}$  under humid conditions and at  $1230\text{ cm}^{-1}$  under dry conditions could be attributed to the formation of bisulfate species (Wang et al., 2018a). The process of sulfate/sulfite formation is explained later in the reaction mechanism section.

### 3.2.2. Surface reaction mechanism

Changes in the DRIFT spectra of the surface of Hagavatt v-dust are clearly seen upon introduction of  $\text{SO}_2$  (Figs. 9 and 10). In comparison with the studies of the interaction of  $\text{SO}_2$  with pure metal oxides reported earlier by different researchers, it is evident that the peaks for sulfur-containing species appear much slower, most probably due to low sensitivity when dealing with dark v-dusts where the reflectance of the infrared light is limited (Zhang et al., 2006), (Usher et al., 2002), (Goodman et al., 2001), (Li et al., 2006), (Wu et al., 2011), (Nanayakkara et al., 2012), (Shang et al., 2010), (Wang et al., 2018b). The time evolution of five peaks corresponding to different species, such as free OH groups, molecular water, physisorbed  $\text{SO}_2$ , sulfites/bisulfites and sulfates/bisulfates is followed.

**3.2.2.1. Dry conditions.** From our flow tube experiments presented earlier it is apparent that  $\text{SO}_2$  gas is massively lost from the gas phase upon its exposure to the v-dust surface. Interestingly, the first peaks that appear in the DRIFT spectra after introduction of  $\text{SO}_2$  gas are positive peaks for physisorbed  $\text{SO}_2$  gas and negative peaks for free OH groups (Fig. 9). Note that although the sample has been thermally pretreated and the experiment is performed under dry conditions, surface OH groups are present on the surface of the sample. The complete dehydroxylation of the surface would have required stronger thermal

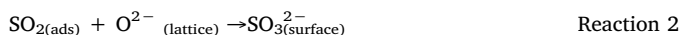
**Table 4**  
Vibrational wavenumbers ( $\text{cm}^{-1}$ ) of sulfur-containing species adsorbed on v-dust and metal oxides.

Molecular species (wavenumbers are expressed in $\text{cm}^{-1}$ )	V-dust (this work)	$\text{Si}_2\text{O}_3$	$\text{Al}_2\text{O}_3$	$\text{MgO}$	$\text{TiO}_2$	$\text{CaCO}_3$	$\text{Fe}_2\text{O}_3$	Theoretical calculations
SH stretch of $\text{HSO}_3^-$	2600–2400	2600-2400 (Hair, 1975)						
$\text{SO}_2$	1364, 1340	1330, 1149 (Goodman et al., 2001)	1330, 1149 (Goodman et al., 2001)	1330, 1149 (Goodman et al., 2001)	1139, 1325 (Nanayakkara et al., 2012)		1400 (Nanayakkara et al., 2012)	2620 to 2450 (Zhang and Ewing, 2002)
$\text{HSO}_3^- / \text{SO}_3^{2-}$	1053–700 975–716	1200-900 (Goodman et al., 2001)	1200-900 (Goodman et al., 2001)	1100-850 (Zhang et al., 2006)	1200-800 (Nanayakkara et al., 2012) 1080 (Shang et al., 2010)		Dry: 950–800 Humid: 1050-900 (Wang et al., 2018b)	
$\text{SO}_3^{2-}$				1125-800 (Goodman et al., 2001)	Monodentate: 1033, 971, 923 (Nanayakkara et al., 2012) Bidentate: 1006, 886 (Nanayakkara et al., 2012) 1077 (Nanayakkara et al., 2012)	1000-900 (Li et al., 2006) 1000-885 (Wu et al., 2011)	Dry:891 (Wang et al., 2018b) Humid: 981 (Wang et al., 2018b)	
$\text{HSO}_3^-$								
$\text{HSO}_4^- / \text{SO}_4^{2-}$	1320–975 1302–1055 1220, 1230	1245, 1170 (Usher et al., 2002)		1150, 1050 (Usher et al., 2002)		1240-1012 (Wu et al., 2011)		1054, 1154, 1219 (Zhang and Ewing, 2002)
$\text{HSO}_4^-$							1219 (Wang et al., 2018b)	
$\text{SO}_4^{2-}$							Dry: 1339–1014 Humid: 1208-1222 (Wang et al., 2018b)	
free OH groups	4000–3500	1300-1100 (Zhang et al., 2006)	3748, 3707 (Goodman et al., 2001)	1300-1100 (Zhang et al., 2006)	1361, 1297, 1172, 1116, 1050, 1000 (Nanayakkara et al., 2012) 1300-1100 (Shang et al., 2010)	1130 (Li et al., 2006)	3704 (Wang et al., 2018b)	
OH groups of acids								
molecular water	3500–2600 1400–1800	3450, 1630 (Hair, 1975)	4000-3500 (Hair, 1975)	3800-3600 (Nanayakkara et al., 2012) 1666, 3628 (Shang et al., 2010)	3800-3600 (Nanayakkara et al., 2012) 1666, 3628 (Shang et al., 2010)		3447, 3548 (Wang et al., 2018b) 3208, 1642 (Wang et al., 2018b)	3622 (Zhang and Ewing, 2002)

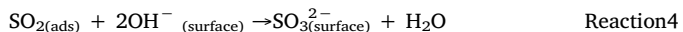
pretreatment. The loss of surface free OH groups reaches its local minimum at around 1.5 h exposure to SO<sub>2</sub> before returning to its initial pre-exposed level where it starts fluctuating around zero. The peak for SO<sub>2</sub> gas is stable, but hard to integrate due to its small size and overlap with a much more pronounced peak for bulk water. Bulk water peak is highly unstable. The disappearance of free OH groups and appearance of physisorbed SO<sub>2</sub> suggest that in the first instants of the reaction, SO<sub>2</sub> gas gets weakly bonded to hydroxyl groups of the surface as first proposed by Datta et al. and later proved by theoretical calculations by Lo et al. for  $\gamma$ -alumina (Datta et al., 1985), (Lo et al., 2010). Maters et al. suggested that due to the weakly acidic nature of SO<sub>2</sub> gas its uptake is likely to happen on strongly basic sites affiliated with alkaline and alkaline earth metals on the surface of the volcanic glass (-K-OH, -Mg-OH, -Ca-OH, Mg-OH) (Maters et al., 2017). At the same time it is also possible for the SO<sub>2</sub> gas to get adsorbed on metallic Lewis acid sites of mineral phase as proposed by Wang et al. (2018a). Hence, the first interaction of SO<sub>2</sub> gas with the surface under dry conditions is its distribution on different sites of the v-dust leading to a reversible physisorption of SO<sub>2</sub>, as indicated by subscript (*ads*) (Reaction 1). Throughout the manuscript the chemisorbed species or chemical groups that form a chemical bond with the surface are indicated as (*surface*).



Physisorbed SO<sub>2</sub> can then participate in reactions leading to chemisorbed species. Sulfites and sulfates, under dry conditions first appear after several hours of exposure probably due to the low sensitivity of our DRIFT setup, as abovementioned. Sulfites can be formed on the lattice oxygen sites that can be viewed as Lewis basic sites (Wang et al., 2018a) as in Reaction 2.

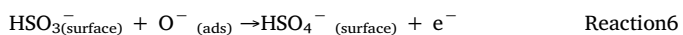
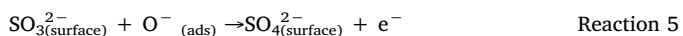


Alternatively, sulfites can be formed in the presence of hydroxyl groups as SO<sub>2</sub> can react with either one hydroxyl group to form bisulfite (Reaction 3) or two neighboring hydroxyl groups to form sulfite and water (Reaction 4) (Wang et al., 2018a). Surface hydroxyl groups themselves can be bonded to a single metal atom or bridge two, creating different environments for interactions with SO<sub>2</sub> (Ullerstam et al., 2002).



Chemisorption of SO<sub>2</sub> gas on oxide anions (O<sup>2-</sup>) and hydroxyl groups of volcanic ash and glass leading to the formation of sulfites and bisulfites was suggested earlier by Maters et al. and detection of sulfites in the leachates confirmed the conversion (Maters et al., 2017).

From Fig. 11 that shows time evolutions of sulfites and sulfates, it can be observed that, under dry conditions, sulfites (SO<sub>3</sub><sup>2-</sup>) get completely stabilized after 22 h of exposure, but sulfates (SO<sub>4</sub><sup>2-</sup>) keep growing linearly, suggesting that sulfites are the intermediate species in the oxidation of SO<sub>2</sub> to sulfates. Oxidation of sulfites to sulfates on the surface of volcanic glass was observed by Farges et al. (2009). Sulfites can be oxidized to sulfates via several pathways. Active oxygen derived from molecular oxygen adsorbed on the active sites (Reaction 7) can oxidize sulfites to sulfates and bisulfites to bisulfates as in Reaction 5 and Reaction 6 (Wang et al., 2018a).



Contrary to our observations and to results reported by Shang et al. (2010), who also noticed a stable rate of sulfate production on the surface of titanium dioxide particles in the presence of oxygen, Usher et al. (2002) noted complete saturation of mineral oxide surfaces with SO<sub>2</sub> gas and observed no sulfate formation even upon exposure of SO<sub>2</sub>-treated surface to air and oxygen. It could be due to the fact that the

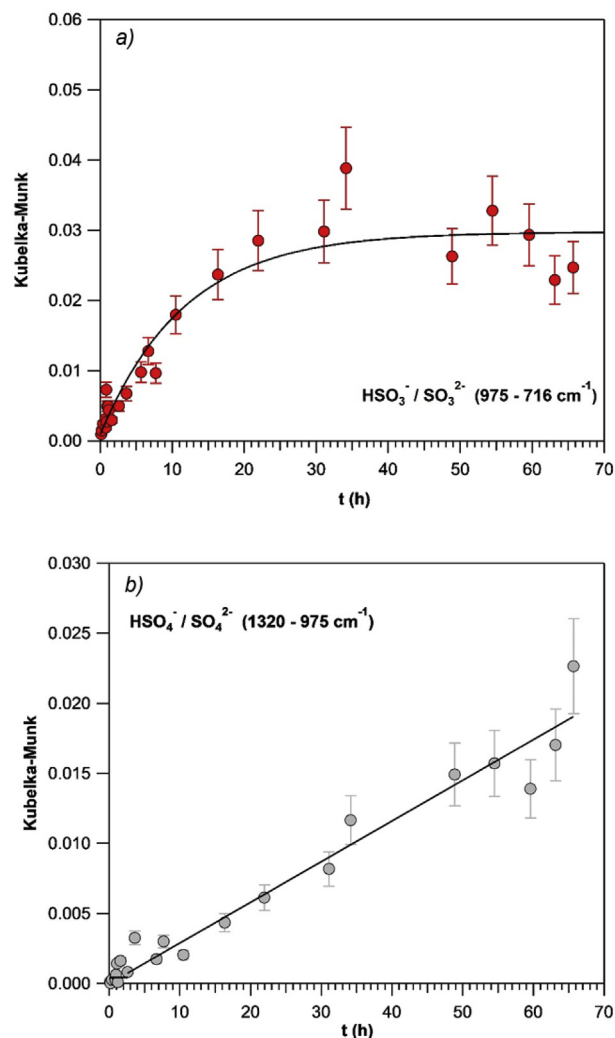
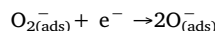


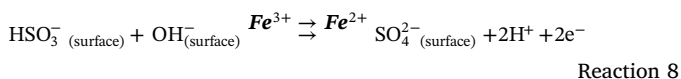
Fig. 11. Integrated absorbance for (a) sulfites/bisulfites, (b) sulfates/bisulfates as a function of time under 0% RH and 296K. Upper graph: sulfites/bisulfites are stabilized after 22 h of exposure. The solid line is an exponential fitting of experimental results to better display the observed trends. Lower graph: A linear growth of sulfates/bisulfates with time is noticed; note that the peak is stable for the first couple of hours and then keeps increasing in a linear fashion. The solid line is the linear fit of experimental results.

minerals under investigation were not able to convert molecular oxygen into active oxygen under the specific experimental conditions of these measurements.

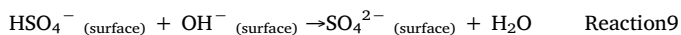


where  $e^{-}$  is a conductive electron trapped in the vacant oxygen site on the surface of some oxides that are prone to having defect sites, such as on the surface of Fe<sub>2</sub>O<sub>3</sub>, for example (Wang et al., 2018b), (Baltrusaitis et al., 2007). Noticeably, reaction proceeds in the absence of light (Baltrusaitis et al., 2007). Reaction 7 was reported to enable the conversion of sulfites to sulfates on the surface of mineral phase, but a similar process can be expected to happen on the amorphous fraction of the volcanic ash due to the high defect population on silicate glasses (A Leed and Pantano, 2003), (Farges et al., 2009).

Additionally, certain metal centers that can be readily reduced, such as Fe<sup>3+</sup> to Fe<sup>2+</sup>, contribute to the formation of sulfates from bisulfites as per Reaction 8 (Wang et al., 2018a).



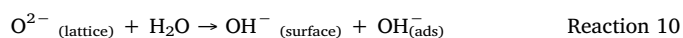
Finally, bisulfates can be oxidized to sulfates by hydroxyl groups as per [Reaction 9](#) ([Wang et al., 2018a](#)).



On ceasing the gas flow and flushing the system for 6 h, the peak for sulfites decreases due to its oxidation as per [Reaction 5](#), [Reaction 6](#) and [Reaction 8](#), while the peak for sulfates increases for a couple of hours before getting stable, at the same time slightly changing its shape. The peak centered at  $1230 \text{ cm}^{-1}$  gets smaller in comparison with the peak at  $1135 \text{ cm}^{-1}$  suggesting indeed further conversion of bisulfates to sulfates. A decrease in sulfite peak with simultaneous increase in the sulfate peak upon cutting off  $\text{SO}_2$  supply and addition of  $\text{O}_3$  was observed by [Li et al. \(2006\)](#). Thus, sulfates appear to be the final product of oxidation of  $\text{SO}_2$  gas and they keep being formed on the surface as long as there are sulfites available for oxidation. Sulfates were also reported as a final irreversible product of the interaction of  $\text{SO}_2$  gas with volcanic glass by [Farges et al.](#) and by [Maters et al. \(Farges et al., 2009\)](#), ([Maters et al., 2017](#)).

**3.2.2.2. Humid conditions.** After exposure of v-dust to  $\text{SO}_2$  gas under humid conditions the following changes are observed in the analysis of

DRIFT spectra as seen in [Figs. 10](#) and [12](#). At the very beginning of the experiment, the free OH groups get consumed and reach a minimum after 1.5 h exposure to  $\text{SO}_2$ , at the same time sulfites form rapidly and at an almost linear rate. The peak for physisorbed  $\text{SO}_2$  increases much slower and the peak remains small for the duration of the experiment. The initial time period corresponds well with the reaction mechanism proposed by [Wang et al.](#) in [Reaction 3](#) and [Reaction 4](#) both of which require consumption of free OH groups to produce sulfites and bisulfites. From 1.5 to 2.5 h consumption of OH groups slows down and finally reaches a stable level. It is important to stress out that, when working under humid conditions, surface OH groups are continuously regenerated. The mechanism for metal oxide surface hydroxylation proposed by [Tamura et al.](#) assumes that an exposed oxygen center of the metal oxide lattice acts as Lewis base with water to form a surface terminal hydroxyl group and a hydroxide ion as shown in [Reaction 10](#) ([Tamura et al., 2001](#)). In other words, a surface oxide ion gets neutralized by water to become  $\text{OH}^- (\text{surface})$ , while water itself loses a proton to become hydroxide ion  $\text{OH}^- (\text{ads})$ .



Sulfates are first observed in the DRIFT spectra at 2.5 h exposure to  $\text{SO}_2$ . Sulfates can be formed by three different pathways shown in [Reaction 5](#), [Reaction 6](#), and [Reaction 8](#) ([Wang et al., 2018a](#)). Unlike sulfites, the peak for sulfates keeps growing linearly with time once

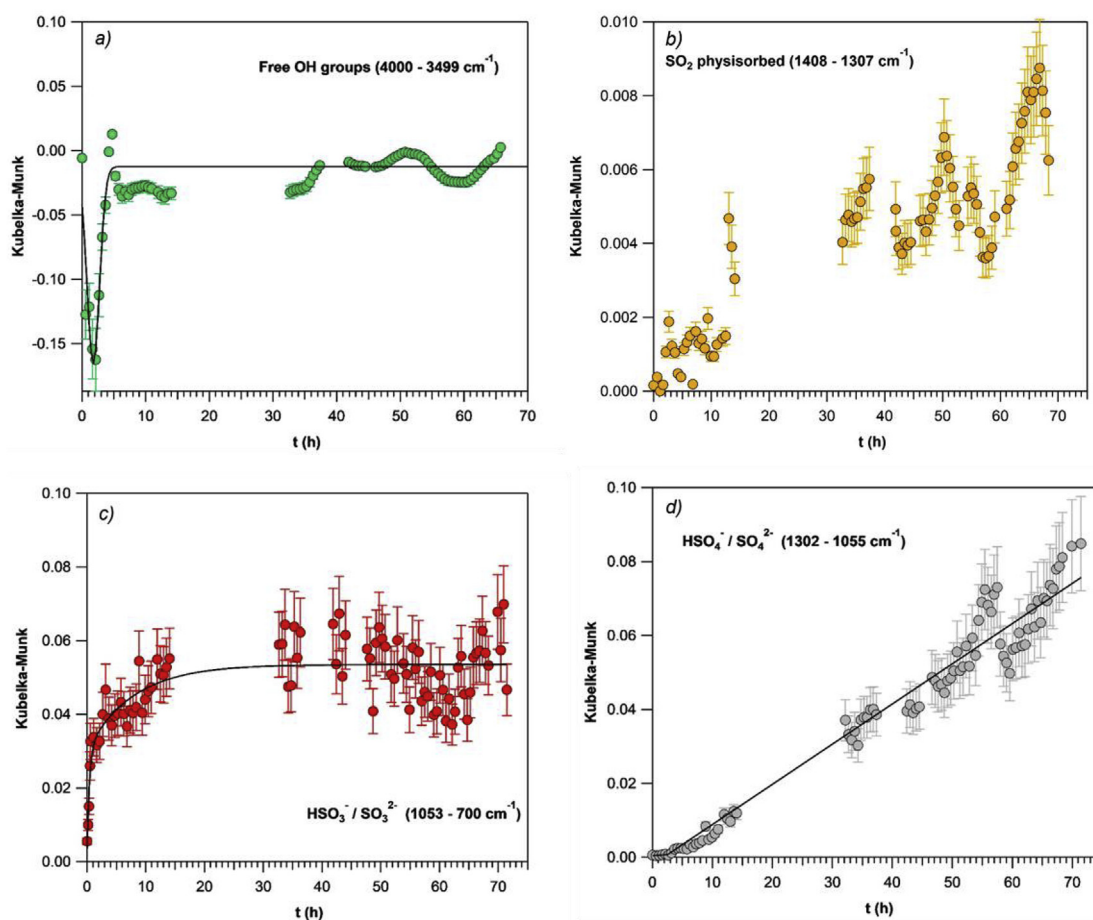


**Fig. 12.** Integrated absorbance for (a) free hydroxyl groups, (b) physisorbed  $\text{SO}_2$ , (c) sulfites/bisulfites, (d) sulfates/bisulfates as a function of time under 30% RH and 296 K. The free OH groups get consumed very fast at the beginning of the experiment and reach a minimum at 1.5 h, then the consumption of OH groups decreases and reaches a stable level at 2.5 h. The solid line is an empirical fitting of experimental results to better display the observed trends. The peak for physisorbed  $\text{SO}_2$  is quite noisy but increases slowly and remains weak for the duration of the experiment. The solid line is an empirical fitting of experimental data points. Sulfites/bisulfites grow rapidly and almost linearly for the first 1.5 h and then stabilize. The solid line is an exponential fitting of experimental results to better display the observed trends. The peak for sulfates/bisulfates is stable at low values for the first 2.5 h and then increases in the linear fashion. The solid line is the linear fit of experimental results.



again suggesting that sulfate is the final product of SO<sub>2</sub> oxidation and that the surface does not get saturated within the duration of the experiment. A peak for molecular water is hard to evaluate at 30% RH as water is being constantly supplied in large excess. Initially, the peak for water seems to decrease, which could be due to the competition with SO<sub>2</sub> gas molecules for active sites on the surface (Fig. 10). At 14 h the water peak stabilizes at a positive value, indicating that the surface is now storing more H<sub>2</sub>O molecules than before introduction of SO<sub>2</sub> gas (Fig. 10). Formation of sulfite and sulfate species could have changed equilibrium for adsorption of water on the dust surface (e.g. due to chemical changes of the mineral structure that increase the hygroscopicity of the samples). Particularly, it was argued that adsorption of bidentate sulfate on the surface of Fe–Mn/TiO<sub>2</sub> catalyst increases the Lewis acid character of the metal ion to which it is attached, thus potentially favoring the adsorption of water on the metal center (Jiang et al., 2010). Finally, when the flow of SO<sub>2</sub> is stopped, the peak for sulfite gradually decreases while the peak for sulfate increases for a couple of hours, stabilizes and stays in the spectra for at least 6 h. Like under dry conditions the peak for bisulfates/sulfates changes its shape by decreasing the peak associated with bisulfates (at 1220 cm<sup>-1</sup>) suggesting its conversion to sulfates.

**3.2.2.3. Comparison between dry and humid conditions.** Although DRIFTS is a semi-quantitative technique, it is feasible to compare the results obtained under dry and humid conditions. Thus, in comparison with the reaction under dry conditions the reaction under humid conditions is much more pronounced, resulting in both faster reaction rates and higher integration values obtained for all sulfur containing species involved. This observation is in line with the results obtained from the flow tube experiments, where significantly higher steady state uptakes were determined for SO<sub>2</sub> under humid compared to dry conditions. Faster sulfite formation is most likely related to the dramatic increase in the amount of hydroxyl groups covering the surface under humid conditions, driving the sulfite and bisulfite formation through Reaction 3 and Reaction 4. Indeed, under humid conditions the amount of hydroxyl groups lost in the first minutes is much larger than under dry conditions, thus adsorbed SO<sub>2</sub> molecules convert rapidly to form sulfites (Figs. 9 and 10). Huang et al. reported that the rate of sulfate formation on the surface of Arizona test dust increased with RH and reached its maximum at 70% RH (Huang et al., 2015). Importance of surface OH groups in the heterogeneous oxidation of SO<sub>2</sub> gas was discussed by Zhang et al. who compared basic, neutral and acidic Al<sub>2</sub>O<sub>3</sub> in their ability to oxidize SO<sub>2</sub> and noted that basic Al<sub>2</sub>O<sub>3</sub> was much more efficient due to its higher concentration of hydroxyl groups on the surface (Zhang et al., 2006). It was also suggested that reactivity of different oxides to SO<sub>2</sub> uptake could be predicted by evaluating their intrinsic ability to form surface hydroxyl groups. Thus, metal oxides that have empty or half-empty d atomic orbitals, such as Al<sub>2</sub>O<sub>3</sub>, easily adsorb molecular oxygen and gaseous water and show excellent performance in the reactions with SO<sub>2</sub> while metal with full d orbitals, such as MnO<sub>2</sub>, show weak reactivity (Zhang et al., 2006). Reaction of SO<sub>2</sub> gas with the lattice oxygen as in Reaction 2 seems to proceed much slower. The observation is in line with the results of experiments on dehydroxylated surfaces that show very little reactivity towards product formation, suggesting low reactivity of lattice oxygen groups (Nanayakkara et al., 2012). Absence of S–H stretch from the spectra of the v-dust under dry conditions could be due to the fact that bisulfites and bisulfates are formed in much lower quantities than in humid conditions.

**3.2.2.4. Surface coverage of v-dust with SO<sub>4</sub><sup>2-</sup> ions.** The uptake of SO<sub>2</sub> gas on the surface of the v-dust proved to be very long and the process of conversion to H<sub>2</sub>SO<sub>4</sub> was not declining for as long as the SO<sub>2</sub> gas was supplied, at least for the duration of the experiments. At the same time no product leaving the surface was identified. This is puzzling since there seems to be no reason for continuous uptake in the absence of

some kind of catalytic process leading to regeneration of active sites. In this case it only makes sense that sooner or later the process should come to an end. In order to evaluate a potential for further uptake and conversion of SO<sub>2</sub> to H<sub>2</sub>SO<sub>4</sub> it was decided to evaluate the surface coverage of SO<sub>4</sub><sup>2-</sup> at the end of the experiment. The amount of the product formed on the surface was quantified using HPLC. A 109 mg sample of Hagavatt dust was exposed to 175 ppm of SO<sub>2</sub> gas for 24 h at 23 °C and 30% RH and then flushed for 6 h to allow complete oxidation of sulfites into sulfates. The dust was then extracted in 1 mL of 1% formalin. A calibration curve was constructed using Na<sub>2</sub>SO<sub>4</sub> as a standard solution. The amount of SO<sub>4</sub><sup>2-</sup> recovered was calculated at 62.79 µg corresponding to 0.57 mg of SO<sub>4</sub><sup>2-</sup> ion per 1g of Hagavatt dust. The number of molecules formed after 24 h of continuous exposure was calculated as  $7.95 \times 10^{13}$  molecules cm<sup>-2</sup>. Considering the linear trend that we observed in DRIFTS experiments, the coverage of SO<sub>4</sub><sup>2-</sup> ions after 72 h of exposure was estimated at ca.  $2.3 \times 10^{14}$  molecules cm<sup>-2</sup>. To approximate whether the monolayer coverage was reached it was decided to compare the amount of molecules formed on the surface to its theoretical monolayer coverage.

The calculated value for the amount of sulfuric acid molecules necessary to form a monolayer was calculated to be  $4.22 \times 10^{14}$  molecule cm<sup>-2</sup>. This value is consistent with the usually reported surface density of sorptive sites on mineral oxides, ca.  $3 \times 10^{13}$ – $5 \times 10^{14}$  sites cm<sup>-2</sup> (Kulkarni and Wachs, 2002). The coverage of SO<sub>4</sub><sup>2-</sup> ions after 72 h of exposure was estimated to be almost by a factor of 2 lower than the theoretical monolayer coverage of the sample by H<sub>2</sub>SO<sub>4</sub> molecules. At this point it should be noted that experimentally, the molecules are not expected to pack together perfectly since the shape of the molecules and hindering interactions would render some of the active sites on the surface inaccessible. Thus, the experimental monolayer coverage would be assumed to be lower than the theoretical one (Hudson et al., 2002), (Diaz et al., 2005).

The rough approximation points to the fact that the surface coverage  $\theta$  after 72 h of exposure is approximately  $\theta = 0.5$ . Therefore, it can be concluded that there are still available sites on the surface of v-dust for the conversion of SO<sub>2</sub> to occur and the subsequent sorption of sulfates. Moreover, the process does not seem to slow down. Longer exposure times are necessary to determine how the sulfate formation will behave at  $\theta = 1$  when a monolayer of sulfate ions forms. Further on, what happens after the formation of monolayer? Will the process stop, and if it continues what are the driving forces behind it?

#### 4. Conclusions and atmospheric implications

In this study the uptake of SO<sub>2</sub> gas by Icelandic v-dust was investigated. Uptake of SO<sub>2</sub> by v-dusts was observed even though all of them have already been exposed to SO<sub>2</sub> in the volcanic conduit and plume owing to their production/emission mode. Upon exposure of the v-dust to SO<sub>2</sub> the system reaches a steady state clearly distinct from the initial state indicating continuous consumption of SO<sub>2</sub> molecules. The steady state uptake coefficients for v-dusts at 30% RH range from  $(6.6 \pm 2.6) \times 10^{-9}$  for Hagavatt to  $(6.2 \pm 2.5) \times 10^{-8}$  for Mýrdalssandur. Moreover, increased uptake of the SO<sub>2</sub> gas in humid conditions suggests that water plays an important role in the above-mentioned processes. The DRIFTS data indicate the presence of sulfite and sulfate ions on the surface. Presence of sulfates was further detected by HPLC analysis and it was also noted that after 3 days of exposure of v-dust to 175 ppm SO<sub>2</sub> the surface coverage by SO<sub>4</sub><sup>2-</sup> ions is ca.  $\theta = 0.5$ , i.e. lower than the monolayer coverage suggesting that the surface of the v-dust is still active in uptake processes that are occurring on the surface. It is most likely that SO<sub>2</sub> gas reacts at the surface of the v-dust and forms sulfites or bisulfites, which are then converted to sulfates. Hydroxyl groups play a major role in the conversion of SO<sub>2</sub> gas to sulfites, while oxidizing agents in the form of active oxygen or metal centers are necessary to their conversion to sulfates. Furthermore, sulfates formed on the surface of v-dust are a stable chemisorbed species

not easily desorbed even after flushing for hours in the absence of SO<sub>2</sub> gas.

During an episode of volcanic eruption volcanic dust will react with SO<sub>2</sub> gas both in subvolcanic and atmospheric environments (Renggli et al., 2019), (Schmauss and Keppler, 2014). Initially, at near-magmatic high temperatures of over 800 °C there is a compelling evidence that the adsorption of SO<sub>2</sub> gas is driven by diffusion of Ca<sup>2+</sup> cations from the interior of the glass to its surface followed by precipitation of CaSO<sub>4</sub> (Delmelle et al., 2018). This initial stage is characterized by high concentration of gases and high density of ash particles, but is very short in duration lasting only a couple of minutes even in the case of Earth's largest explosive eruptions (Delmelle et al., 2018). The pathway is of limited importance in small and medium size eruptions and/or eruptions of volcanoes lacking a deep-seated magma chamber (Ayris et al., 2013). Subsequent cooling rapidly brings the system to the subzero temperatures (Textor et al., n.d.). At ambient and low temperatures where effective diffusion of cations to the ash surface is no longer possible the driving force of SO<sub>2</sub> adsorption is its physisorption on the surface of ash followed by chemical reaction with active sites that are available on the surface. Previous research under these conditions points out that the rate of sulfate formation is higher at low temperatures compared to room or elevated temperatures of up to 150 °C (Wu et al., 2011) (Schmauss and Keppler, 2014). Interestingly, adsorption of SO<sub>2</sub> remains very strong at very low partial pressures, which confirms that adsorption is likely to happen in diluted cold parts of the plume (Schmauss and Keppler, 2014). Furthermore, an increase in sulfur load on ash surfaces was observed to increase with increase of distance from the vent during 2010 Eyjafjallajökull eruption (Bagnato et al., 2013). Thus, one can expect that most of the adsorption of SO<sub>2</sub> gas during a medium-size volcanic eruption would happen in the horizontal umbrella part of the volcanic ash cloud. In this case it is important to use the steady state uptake coefficient to evaluate the uptake as it is better fit to describe the phenomena of the continuous process. In this research it was demonstrated that even after 3 days of exposure of natural v-dust to the SO<sub>2</sub> gas there are still active sites available for the reaction to take place. Therefore one can expect a v-dust particle travelling through the air to remain active to the adsorption of SO<sub>2</sub> gas.

In order to evaluate potential impact of SO<sub>2</sub> adsorption on v-dust on atmosphere its atmospheric lifetime was calculated using equation (5).

$$\tau_{net} = \frac{4}{\gamma c D} \quad (5)$$

where  $\gamma$  is the uptake coefficient,  $c$  is the mean molecular velocity (m s<sup>-1</sup>), and  $D$  is the volcanic dust surface area density (m<sup>2</sup> m<sup>-3</sup>). Considering (i) concentrations of volcanic ash in a vertical column of the volcanic cloud passing over Faroe Islands located about 650 km from the Eyjafjallajökull volcano measured during its eruption on April 15 2010 ranging from 200 to 6000 µg m<sup>-3</sup> (Gudmundsson et al., 2012) and (ii) the SSA of Eyjafjallajökull dust sample of 0.75 m<sup>2</sup> g<sup>-1</sup>,  $D$  can be calculated by direct multiplication of the dust concentration and the SSA of the v-dust and was found to be in the range from 1.5 × 10<sup>-4</sup> m<sup>2</sup> m<sup>-3</sup> to 4.5 × 10<sup>-3</sup> m<sup>2</sup> m<sup>-3</sup> for the lower and higher ash load respectively. This leads to the calculation of lifetime of SO<sub>2</sub> molecule as a result of its heterogeneous loss on Eyjafjallajökull v-dust particle to 81 to 2.7 years. If we consider a higher 7.5 m<sup>2</sup> g<sup>-1</sup> SSA values for Eyjafjallajökull dust obtained by Maters et al. the atmospheric lifetime falls to 8.1 years to 99 days (Maters et al., 2016). For comparison, the lifetime of SO<sub>2</sub> in the atmosphere as measured over the Eastern United States in the absence of volcanic activity ranges from 15 h in summer to 65 h in winter (Lee et al., 2011). On the base of these calculations it appears that the heterogeneous uptake of SO<sub>2</sub> molecule on the surface of v-dust particle is a negligible process in comparison with the gas phase oxidation by aqueous (i.e., H<sub>2</sub>O<sub>2</sub>) and gas-phase (i.e., OH) processes. However, in case of higher volcanic ash concentrations in the plume, for example 2.0 × 10<sup>6</sup> µg m<sup>-3</sup> estimated during 1991 Pinatubo eruption (SSA 1.5 m<sup>2</sup> g<sup>-1</sup> (Maters et al., 2016)) at the direct

proximity to the vent (Witham et al., 2012), and considering the same uptake coefficient measured in this study for Eyjafjallajökull, calculations lead to a radically shorter lifetime of 36 h and make heterogeneous uptake of SO<sub>2</sub> on volcanic dust particles equally important. Furthermore, the lifetime of SO<sub>2</sub> could be further decreased for volcanic particles with higher specific surface area. These calculations point out that adsorption of SO<sub>2</sub> on the surface of volcanic ash is most likely to happen in the part of volcanic cloud closest to the vent where ash concentration is the highest. The process of SO<sub>2</sub> loss due to heterogeneous reactions with v-dust particles could be further enhanced in the presence of oxidizing species (i.e., O<sub>3</sub>, OH) and sunlight, and needs to be quantitatively evaluated.

## Declaration of competing interest

The authors declare that they have no known competing financial interests or personal relationships that could have appeared to influence the work reported in this paper.

## Acknowledgments

The authors acknowledge Mr Vincent Gaudion and Dr Mohamad Zeineddine (SAGE, IMT Lille Douai) for their assistance in the lab. We are grateful to Mr Bruno Malet and Dr Laurent Alleman (SAGE, IMT Lille Douai) for conducting the ICP-MS experiments. This work was achieved in the frame of Labex CaPPA, funded by ANR through the PIA under contract ANR-11-LABX-0005-01, and CPER CLIMIBIO project, both funded by the Hauts-de-France Regional Council and the European Regional Development Fund (ERDF). J. Lasne acknowledges support from the Labex CaPPA and CPER CLIMIBIO projects and the Hauts-de-France Regional Council for his post-doctoral fellowship.

## Appendix A. Supplementary data

Supplementary data to this article can be found online at <https://doi.org/10.1016/j.atmosenv.2019.116942>.

## References

- Harris, E., Sinha, B., Foley, S., Crowley, J.N., Borrmann, S., Hoppe, P., 2012. Sulfur isotope fractionation during heterogeneous oxidation of SO<sub>2</sub> on mineral dust. *Atmos. Chem. Phys.* 12, 4867–4884. <https://doi.org/10.5194/acp-12-4867-2012>.
- A Leed, E., Pantano, C., 2003. Computer modeling of water adsorption on silica and silicate glass fracture surfaces. *J. Non-Cryst. Solids* 325, 48–60. [https://doi.org/10.1016/S0022-3093\(03\)00361-2](https://doi.org/10.1016/S0022-3093(03)00361-2).
- Adams, J.W., Rodriguez, D., Cox, R.A., 2005. The uptake of SO<sub>2</sub> on Saharan dust: a flow tube study. *Atmos. Chem. Phys.* 5, 2679–2689. <https://doi.org/10.5194/acp-5-2679-2005>.
- Alleman, L.Y., Lamaison, L., Perdrix, E., Robache, A., Galloo, J.-C., 2010. PM10 metal concentrations and source identification using positive matrix factorization and wind sectoring in a French industrial zone. *Atmos. Res.* 96, 612–625. <https://doi.org/10.1016/j.atmosres.2010.02.008>.
- Andreae, M., 1995. *Climate Effects of Changing Atmospheric Aerosol. World Survey of Climatology, vol. 16. Future Climates of the World*, pp. 341–392 1995.
- Arnalds, O., Dagsson-Waldhauserova, P., Olafsson, H., 2016. The Icelandic volcanic aeolian environment: processes and impacts — a review. *Aeolian Res.* 20, 176–195. <https://doi.org/10.1016/j.aeolia.2016.01.004>.
- Ayris, P.M., Lee, A.F., Wilson, K., Kueppers, U., Dingwell, D.B., Delmelle, P., 2013. SO<sub>2</sub> sequestration in large volcanic eruptions: high-temperature scavenging by tephra. *Geochem. Cosmochim. Acta* 110, 58–69. <https://doi.org/10.1016/j.gca.2013.02.018>.
- Bagnato, E., Aiuppa, A., Bertagnini, A., Bonadonna, C., Cioni, R., Pistolesi, M., Pedone, M., Hoskuldsson, A., 2013. Scavenging of sulphur, halogens and trace metals by volcanic ash: the 2010 Eyjafjallajökull eruption. *Geochem. Cosmochim. Acta* 103, 138–160. <https://doi.org/10.1016/j.gca.2012.10.048>.
- Baltrusaitis, J., Cwiertny, D.M., Grassian, V.H., 2007. Adsorption of sulfur dioxide on hematite and goethite particle surfaces. *Phys. Chem. Chem. Phys.* 9, 5542–5554. <https://doi.org/10.1039/B709167B>.
- Baratoux, D., Mangold, N., Arnalds, O., Bardintzeff, J.-M., Platevoet, B., Grégoire, M., Pinet, P., 2011. Volcanic Sand in Iceland: diverse origins of aeolian sand deposits revealed at Dyngjúsandur and Lambahraun, Iceland. *Earth Surf. Process. Landforms* 36, 1789–1808. <https://doi.org/10.1002/esp.2201>.
- Brasseur, G.P., Granier, C., Walters, S., 1990. Future changes in stratospheric ozone and the role of heterogeneous chemistry. *Nature* 348, 626–628. <https://doi.org/10.1038/348626a0>.

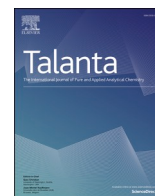
- Clague, D.A., Denlinger, R.P., 1994. Role of olivine cumulates in destabilizing the flanks of Hawaiian volcanoes. *Bull. Volcanol.* 56, 425–434. <https://doi.org/10.1007/BF00302824>.
- Crowley, J.N., Ammann, M., Cox, R.A., Hynes, R.G., Jenkin, M.E., Melloouki, A., Rossi, M.J., Troe, J., Wallington, T.J., 2010. Evaluated kinetic and thermochemical data for atmospheric chemistry: volume V – heterogeneous reactions on solid substrates. *Atmos. Chem. Phys.* 10, 9059–9223. <https://doi.org/10.5194/acp-10-9059-2010>.
- Dagsson-Waldhauserova, P., Arnalds, O., Olafsson, H., 2014. Long-term variability of dust events in Iceland (1949–2011). *Atmos. Chem. Phys.* 14, 13411–13422. <https://doi.org/10.5194/acp-14-13411-2014>.
- Datta, A., Cavell, R.G., Tower, R.W., George, Z.M., 1985. Claus catalysis. 1. Adsorption of SO<sub>2</sub> on the alumina catalyst studied by FTIR and EPR spectroscopy. *J. Phys. Chem.* 89, 3. <https://doi.org/10.1021/j100249a014>.
- Deegan, F.M., 2010. *Processes of Magma-Crust Interaction Insights from Geochemistry and Experimental Petrology*. Acta Universitatis Upsaliensis, Uppsala.
- Delmelle, P., Wadsworth, F.B., Maters, E.C., Ayris, P.M., 2018. High temperature reactions between gases and ash particles in volcanic eruption plumes. *Rev. Mineral. Geochem.* 84, 285–308. <https://doi.org/10.2138/rmg.2018.84.8>.
- Diaz, L., Liauw, C.M., Edge, M., Allen, N.S., McMahon, A., Rhodes, N., 2005. Investigation of factors affecting the adsorption of functional molecules onto gel silicas. 1. Flow microcalorimetry and infrared spectroscopy. *J. Colloid Interface Sci.* 287, 379–387. <https://doi.org/10.1016/j.jcis.2004.09.039>.
- Dordevic, D., Tošić, I., Sakan, S., Petrović, S., Đuričić-Milanković, J., Finger, D., Waldhauserova, P., 2019. Can volcanic dust suspended from surface soil and deserts of Iceland be transferred to central Balkan similarly to African dust (Sahara)? *Front. Earth Sci.* 7, 142. <https://doi.org/10.3389/feart.2019.00142>.
- Durant, A.J., Shaw, R.A., Rose, W.I., Mi, Y., Ernst, G.G.J., 2008. Ice nucleation and over seeding of ice in volcanic clouds. *J. Geophys. Res.: Atmosphere* 113. <https://doi.org/10.1029/2007JD009064>.
- Durant, A.J., Bonadonna, C., Horwell, C.J., 2010. Atmospheric and environmental impacts of volcanic particulates. *Elements* 6, 235–240.
- Farges, F., Keppler, H., Flank, A.M., Lagarde, P., 2009. Sulfur K-edge XANES study of S sorbed onto volcanic ashes. *J. Phys. Conf. Ser.* 190, 012177. <https://doi.org/10.1088/1742-6596/190/1/012177>.
- Finlayson-Pitts Jr., B.J., J.N.P., 1999. *Chemistry of the Upper and Lower Atmosphere: Theory, Experiments, and Applications*. Elsevier.
- Gislason, S.R., Hassenkam, T., Nedel, S., Bovet, N., Eiríksdóttir, E.S., Alfredsson, H.A., Hem, C.P., Balogh, Z.I., Dideriksen, K., Oskarsson, N., Sigfusson, B., Larsen, G., Stipp, S.L.S., 2011. Characterization of Eyjafjallajökull volcanic ash particles and a protocol for rapid risk assessment. *Proc. Natl. Acad. Sci.* 108, 7307–7312. <https://doi.org/10.1073/pnas.1015053108>.
- Goodman, A.L., Li, P., Usher, C.R., Grassian, V.H., 2001. Heterogeneous uptake of sulfur dioxide on aluminum and magnesium oxide particles. *J. Phys. Chem. A* 105, 6109–6120. <https://doi.org/10.1021/jp004423z>.
- Groot Zwaartfink, C.D., Arnalds, Ó., Dagsson-Waldhauserova, P., Eckhardt, S., Prospero, J.M., Stohl, A., 2017. Temporal and spatial variability of Icelandic dust emissions and atmospheric transport. *Atmos. Chem. Phys.* 17, 10865–10878. <https://doi.org/10.5194/acp-17-10865-2017>.
- Gudmundsson, M.T., Thordarson, T., Höskuldsson, Á., Larsen, G., Björnsson, H., Prata, F.J., Oddsson, B., Magnússon, E., Högnadóttir, T., Petersen, G.N., Hayward, C.L., Stevenson, J.A., Jónsdóttir, I., 2012. Ash generation and distribution from the April–May 2010 eruption of Eyjafjallajökull, Iceland. *Sci. Rep.* 2, 572. <https://doi.org/10.1038/srep00572>.
- Hair, M.L., 1975. Hydroxyl groups on silica surface. *J. Non-Cryst. Solids Glass Surf.* 19, 299–309. [https://doi.org/10.1016/0022-3093\(75\)90095-2](https://doi.org/10.1016/0022-3093(75)90095-2).
- Highwood, E.-J., Stevenson, D.S., 2003. Atmospheric impact of the 1783–1784 Laki Eruption: Part II Climatic effect of sulphate aerosol. *Atmos. Chem. Phys.* 3, 1177–1189.
- Huang, L., Zhao, Y., Li, H., Chen, Z., 2015. Kinetics of heterogeneous reaction of sulfur dioxide on authentic mineral dust: effects of relative humidity and hydrogen peroxide. *Environ. Sci. Technol.* 49, 10797–10805. <https://doi.org/10.1021/acs.est.5b03930>.
- Hudson, P.K., Zondlo, M.A., Tolbert, M.A., 2002. The interaction of Methanol, acetone, and acetaldehyde with ice and nitric acid-doped ice: implications for cirrus clouds. *J. Phys. Chem. A* 106, 2882–2888. <https://doi.org/10.1021/jp012718m>.
- Huthwelker, T., Ammann, M., Peter, T., 2006. The uptake of acidic gases on ice. *Chem. Rev.* 106, 1375–1444. <https://doi.org/10.1021/cr02506v>.
- Ibrahim, S., Romanias, M.N., Alleman, L.Y., Zeineddine, M.N., Angeli, G.K., Trikalitis, P.N., Thevenet, F., 2018. Water interaction with mineral dust aerosol: particle size and hygroscopic properties of dust. *ACS Earth Space Chem.* 2, 376–386. <https://doi.org/10.1021/acsearthspacechem.7b00152>.
- Icelandic volcanoes [WWW Document], n.d. URL <http://icelandicvolcanoes.is/?volcano=EYJ#> (accessed 2.20.2019).
- Jiang, B.Q., Wu, Z.B., Liu, Y., Lee, S.C., Ho, W.K., 2010. DRIFT study of the SO<sub>2</sub> effect on low-temperature SCR reaction over Fe–Mn/TiO<sub>2</sub>. *J. Phys. Chem. C* 114, 4961–4965. <https://doi.org/10.1021/jp907783g>.
- Joshi, N., Romanias, M.N., Riffault, V., Thevenet, F., 2017. Investigating water adsorption onto natural mineral dust particles: linking DRIFTS experiments and BET theory. *Aeolian Res.* 27, 35–45. <https://doi.org/10.1016/j.aeolia.2017.06.001>.
- Judeikis, H.S., Stewart, T.B., 1976. Laboratory measurement of SO<sub>2</sub> deposition velocities on selected building materials and soils. *Atmos. Environ.* 10, 769–776. 1967. [https://doi.org/10.1016/0004-6981\(76\)90078-0](https://doi.org/10.1016/0004-6981(76)90078-0).
- Kulkarni, D., Wachs, I.E., 2002. Isopropanol oxidation by pure metal oxide catalysts: number of active surface sites and turnover frequencies. *Appl. Catal. Gen.* 237, 121–137. [https://doi.org/10.1016/S0926-860X\(02\)00325-3](https://doi.org/10.1016/S0926-860X(02)00325-3).
- Langmann, B., 2013. Volcanic ash versus mineral dust: atmospheric processing and environmental and climate impacts. [WWW Document]. International Scholarly Research Notices. <https://doi.org/10.1155/2013/245076>.
- Langmann, B., Zakšek, K., Hort, M., 2010. Atmospheric distribution and removal of volcanic ash after the eruption of Kasatochi volcano: a regional model study. *J. Geophys. Res.: Atmosphere* 115. <https://doi.org/10.1029/2009JD013298>.
- Lasne, J., Romanias, M.N., Thevenet, F., 2018. Ozone uptake by clay dusts under environmental conditions. *ACS Earth Space Chem.* 2, 904–914. <https://doi.org/10.1021/acsearthspacechem.8b00057>.
- Lee, C., Martin, R.V., Donkelaar, A. van, Lee, H., Dickerson, R.R., Hains, J.C., Krotkov, N., Richter, A., Vinnikov, K., Schwab, J.J., 2011. SO<sub>2</sub> emissions and lifetimes: estimates from inverse modeling using in situ and global, space-based (SCIAMACHY and OMI) observations. *J. Geophys. Res.: Atmosphere* 116. <https://doi.org/10.1029/2010JD014758>.
- Li, L., Chen, Z.M., Zhang, Y.H., Zhu, T., Li, J.L., Ding, J., 2006. Kinetics and mechanism of heterogeneous oxidation of sulfur dioxide by ozone on surface of calcium carbonate. *Atmos. Chem. Phys. Discuss.* 6, 579–613. <https://doi.org/10.5194/acpd-6-579-2006>.
- Lo, J.M.H., Ziegler, T., Clark, P.D., 2010. SO<sub>2</sub> adsorption and transformations on  $\gamma$ -Al<sub>2</sub>O<sub>3</sub> surfaces: a density functional theory study. *J. Phys. Chem. C* 114, 10444–10454. <https://doi.org/10.1021/jp910895g>.
- Massman, W.J., 1998. A review of the molecular diffusivities of H<sub>2</sub>O, CO<sub>2</sub>, CH<sub>4</sub>, CO, O<sub>3</sub>, SO<sub>2</sub>, NH<sub>3</sub>, N<sub>2</sub>O, NO, and NO<sub>2</sub> in air O<sub>2</sub> and N<sub>2</sub> near STP. [WWW Document]. Atmospheric Environment. URL <https://eurekamag.com/research/008/072/008072627.php>, Accessed date: 11 May 2018.
- Maters, E.C., Delmelle, P., Rossi, M.J., Ayris, P.M., Bernard, A., 2016. Controls on the surface chemical reactivity of volcanic ash investigated with probe gases. *Earth Planet. Sci. Lett.* 450, 254–262. <https://doi.org/10.1016/j.epsl.2016.06.044>.
- Maters, E.C., Delmelle, P., Rossi, M.J., Ayris, P.M., 2017. Reactive uptake of sulfur dioxide and ozone on volcanic glass and ash at ambient temperature. *J. Geophys. Res. Atmos.* 122, 10077–10088. <https://doi.org/10.1002/2017JD026993>.
- Michigami, Y., Ueda, K., 1994. Sulphite stabilizer in ion chromatography. *J. Chromatogr. A* 663, 255–258. [https://doi.org/10.1016/0021-9673\(94\)85252-9](https://doi.org/10.1016/0021-9673(94)85252-9).
- Moroni, B., Arnalds, O., Dagsson-Waldhauserova, P., Crocchianti, S., Viviani, R., Cappelletti, D., 2018. Mineralogical and chemical records of Icelandic dust sources upon Ny-Ålesund (Svalbard islands). *Front. Earth Sci.* 6. <https://doi.org/10.3389/feart.2018.00187>.
- Nanayakkara, C.E., Pettibone, J., Grassian, V.H., 2012. Sulfur dioxide adsorption and photooxidation on isotopically-labeled titanium dioxide nanoparticle surfaces: roles of surface hydroxyl groups and adsorbed water in the formation and stability of adsorbed sulfate and sulfite. *Phys. Chem. Chem. Phys.* 14, 6957–6966. <https://doi.org/10.1039/C2CP23684B>.
- Ovadnevaite, J., Ceburnis, D., Plauskaite-Sukiene, K., Modini, R., Dupuy, R., Rimselyte, I., Ramonet, M., Kvietkus, K., Ristovski, Z., Berresheim, H., O'Dowd, C.D., 2009. Volcanic sulphate and arctic dust plumes over the North Atlantic Ocean. *Atmos. Environ.* 43, 4968–4974. <https://doi.org/10.1016/j.atmosenv.2009.07.007>.
- Reactions on Mineral Dust - Chemical Reviews [ACS Publications] [WWW Document], n.d. URL <https://pubs.acs.org/doi/abs/10.1021/cr020657y> (accessed 2.8.2018).
- Renggli, C., King, P., Henley, W.R., Guagliardo, P., McMorrow, L., Middleton, J., Turner, M., 2019. An experimental study of SO<sub>2</sub> reactions with silicate glasses and super-cooled melts in the system anorthite–diopside–albite at high temperature. *Contrib. Mineral. Petrol.* 174. <https://doi.org/10.1007/s00410-018-1538-2>.
- Romanias, M.N., El Zein, A., Bedjanian, Y., 2012. Heterogeneous interaction of H<sub>2</sub>O<sub>2</sub> with TiO<sub>2</sub> surface under dark and UV light irradiation conditions. *J. Phys. Chem. A* 116, 8191–8200. <https://doi.org/10.1021/jp305366v>.
- Romanias, M.N., Ourrad, H., Thevenet, F., Riffault, V., 2016. Investigating the heterogeneous interaction of VOCs with natural atmospheric particles: adsorption of limonene and toluene on saharan mineral dusts. *J. Phys. Chem. A* 120, 1197–1212. <https://doi.org/10.1021/acs.jpca.5b10323>.
- Romanias, M.N., Zeineddine, M.N., Gaudion, V., Lun, X., Thevenet, F., Riffault, V., 2016. Heterogeneous interaction of isopropanol with natural Gobi dust. *Environ. Sci. Technol.* 50, 11714–11722. <https://doi.org/10.1021/acs.est.6b03708>.
- Schmaus, D., Keppler, H., 2014. Adsorption of sulfur dioxide on volcanic ashes. *Am. Mineral.* 99, 1085–1094. <https://doi.org/10.2138/am.2014.4656>.
- Schmidt, A., Witham, C.S., Theys, N., Richards, N.A.D., Thordarson, T., Szpek, K., Feng, W., Hort, M.C., Woolley, A.M., Jones, A.R., Redington, A.L., Johnson, B.T., Hayward, C.L., Carslaw, K.S., 2014. Assessing hazards to aviation from sulfur dioxide emitted by explosive Icelandic eruptions. *J. Geophys. Res. Atmos.* 119, 2014JD022070. <https://doi.org/10.1002/2014JD022070>.
- Shang, J., Li, J., Zhu, T., 2010. Heterogeneous reaction of SO<sub>2</sub> on TiO<sub>2</sub> particles. *Sci. China Chem.* 53, 2637–2643. <https://doi.org/10.1007/s11426-010-4160-3>.
- Stevenson, D.S., Johnson, C.E., Highwood, E.J., Gauci, V., Collins, W.J., Derwent, R.G., 2003. Atmospheric impact of the 1783–1784 Laki eruption: Part I Chemistry modelling. *Atmos. Chem. Phys.* 3, 487–507. <https://doi.org/10.5194/acp-3-487-2003>.
- Tambora and the “Year Without a Summer” of 1816, 2016. Institute of geography. WWW Document, URL [http://www.geography.unibe.ch/services/geographica\\_bernenisia/online/gb2016g9001/index\\_eng.html](http://www.geography.unibe.ch/services/geographica_bernenisia/online/gb2016g9001/index_eng.html), Accessed date: 17 May 2018.
- Tamura, H., Mita, K., Tanaka, A., Ito, M., 2001. Mechanism of hydroxylation of metal oxide surfaces. *J. Colloid Interface Sci.* 243, 202–207. <https://doi.org/10.1006/jcis.2001.7864>.
- Tang, M.J., Cox, R.A., Kalberer, M., 2014. Compilation and evaluation of gas phase diffusion coefficients of reactive trace gases in the atmosphere: volume 1. Inorganic compounds. *Atmos. Chem. Phys.* 14, 9233–9247. <https://doi.org/10.5194/acp-14-9233-2014>.
- Textor, C., Graf, H.-F., Herzog, M., Oberhuber, J.M., n.d. Injection of gases into the stratosphere by explosive volcanic eruptions. *Journal of Geophysical Research: Atmospheres* 108. <https://doi.org/10.1029/2002JD002987>.
- Thordarson, T., Larsen, G., 2007. Volcanism in Iceland in historical time: volcano types,

- eruption styles and eruptive history. *J. Geodyn.* 43, 118–152. <https://doi.org/10.1016/j.jog.2006.09.005>.
- Ullerstam, M., Vogt, R., Langer, S., Ljungstrom, E., 2002. The kinetics and mechanism of SO<sub>2</sub> oxidation by O<sub>3</sub> on mineral dust. *Phys. Chem. Chem. Phys.* 4, 4694–4699. <https://doi.org/10.1039/b203529b>.
- Usher, C.R., Al-Hosney, H., Carlos-Cuellar, S., Grassian, V.H., 2002. A laboratory study of the heterogeneous uptake and oxidation of sulfur dioxide on mineral dust particles. *J. Geophys. Res.* 107, 4713. <https://doi.org/10.1029/2002JD002051>.
- Vernier, J.-P., Fairlie, T.D., Deshler, T., Natarajan, M., Knepp, T., Foster, K., Wienhold, F. G., Bedka, K.M., Thomason, L., Trepte, C., n.d. In situ and space-based observations of the Kelud volcanic plume: The persistence of ash in the lower stratosphere. *J. Geophys. Res.: Atmosphere* 121, 11,104–11,118. <https://doi.org/10.1002/2016JD025344>.
- Vogel, A., Diplas, S., Durant, A.J., Azar, A.S., Sunding, M.F., Rose, W.I., Sytchkova, A., Bonadonna, C., Krüger, K., Stohl, A., 2017. Reference data set of volcanic ash physicochemical and optical properties. *J. Geophys. Res.: Atmosphere* 122, 9485–9514. <https://doi.org/10.1002/2016JD026328>.
- Wang, T., Liu, Y., Deng, Y., Fu, H., Zhang, L., Chen, J., 2018a. Emerging investigator series: heterogeneous reactions of sulfur dioxide on mineral dust nanoparticles: from single component to mixed components. *Environ. Sci.: Nano* 5, 1821–1833. <https://doi.org/10.1039/C8EN00376A>.
- Wang, T., Liu, Y., Deng, Y., Fu, H., Zhang, L., Chen, J.-M., 2018b. Adsorption of SO<sub>2</sub> on mineral dust particles influenced by atmospheric moisture. *Atmos. Environ.* 191. <https://doi.org/10.1016/j.atmosenv.2018.08.008>.
- Witham, C.S., Oppenheimer, C., Horwell, C.J., 2005. Volcanic ash-leachates: a review and recommendations for sampling methods. *J. Volcanol. Geotherm. Res.* 141, 299–326. <https://doi.org/10.1016/j.jvolgeores.2004.11.010>.
- Witham, C., Webster, H., Hort, M., Jones, A., Thomson, D., 2012. Modelling concentrations of volcanic ash encountered by aircraft in past eruptions. *Atmospheric Environment, Volcanic ash over Europe during the eruption of Eyjafjallajökull on Iceland. April-May 2010* 48, 219–229. <https://doi.org/10.1016/j.atmosenv.2011.06.073>.
- Wu, L.Y., Tong, S.R., Wang, W.G., Ge, M.F., 2011. Effects of temperature on the heterogeneous oxidation of sulfur dioxide by ozone on calcium carbonate. *Atmos. Chem. Phys.* 11, 6593–6605. <https://doi.org/10.5194/acp-11-6593-2011>.
- Zhang, Z., Ewing, G.E., 2002. Infrared spectroscopy of SO<sub>2</sub> aqueous solutions. *Spectrochim. Acta A Mol. Biomol. Spectrosc.* 58, 2105–2113.
- Zhang, X., Zhuang, G., Chen, J., Wang, Y., Wang, X., An, Z., Zhang, P., 2006. Heterogeneous reactions of sulfur dioxide on typical mineral particles. *J. Phys. Chem. B* 110, 12588–12596. <https://doi.org/10.1021/jp0617773>.
- Zhang, Y., Tong, S., Ge, M., Jing, B., Hou, S., Tan, F., Chen, Y., Guo, Y., Wu, L., 2018. The influence of relative humidity on the heterogeneous oxidation of sulfur dioxide by ozone on calcium carbonate particles. *Sci. Total Environ.* 633, 1253–1262. <https://doi.org/10.1016/j.scitotenv.2018.03.288>.
- Zhou, L., Wang, W., Gai, Y., Ge, M., 2014. Knudsen cell and smog chamber study of the heterogeneous uptake of sulfur dioxide on Chinese mineral dust. *J. Environ. Sci.* 26, 2423–2433. <https://doi.org/10.1016/j.jes.2014.04.005>.
- Zuo, Y., Chen, H., 2003. Simultaneous determination of sulfite, sulfate, and hydroxymethanesulfonate in atmospheric waters by ion-pair HPLC technique. *Talanta* 59, 875–881. [https://doi.org/10.1016/S0039-9140\(02\)00647-1](https://doi.org/10.1016/S0039-9140(02)00647-1).



## **Annex 2**





# Method development and validation for the determination of sulfites and sulfates on the surface of mineral atmospheric samples using reverse-phase liquid chromatography

Darya Urupina<sup>\*</sup>, Vincent Gaudion, Manolis N. Romanias, Marie Verrielle<sup>\*\*</sup>, Frederic Thevenet

IMT Lille Douai, Univ. Lille, SAGE, 59000, Lille, France

## ARTICLE INFO

### Keywords:

Sulfite  
Sulfate  
Mineral dust  
Surface analysis  
HPLC

## ABSTRACT

Earlier studies suggest that SO<sub>2</sub> gas reacts at the surface of mineral dust and forms sulfites or bisulfites, which are then converted to sulfates. In order to monitor and quantify the amounts of both sulfites and sulfates formed on the surface of mineral dusts of volcanic and desert origins an accurate and precise reversed-phase liquid chromatography method was developed and validated to extract, stabilize and individually analyze sulfites and sulfates initially present on the surface of dusts exposed to SO<sub>2</sub>. The method was developed on a 25 mm Restek Ultra Column C18, Particle size: 5 μm, I.D. 4.60 mm column which was dynamically coated with 1.0 mM cetylpyridinium chloride in 7% acetonitrile solution to produce a charged surface as recommended in the literature. Mobile phase used: 1 mM Potassium Hydrogen Phthalate at pH 6.5 at a flow rate of 1.0 ml/min with negative UV-Vis detection at 255 nm in 15 min. The method was validated for specificity, linearity and range, injection repeatability, stability, robustness, limit of detection and limit of quantitation, and sample preparation and extraction reproducibility. The method was adapted for straight sulfite and sulfate quantification: (i) of environmental samples, and (ii) natural samples additionally exposed to SO<sub>2</sub> gas in a dedicated laboratory setup. The method was then successfully applied to quantify sulfites and sulfates on natural volcanic and a desert dust samples both collected in the environment and additionally exposed to SO<sub>2</sub> gas in the laboratory. The method can be efficiently used to identify sulfites and sulfates on fresh volcanic ash following an eruption, on aeolian desert dust exposed to industrial pollutants, as well as for laboratory investigations of sulfite and sulfate formation on the surface of minerals and natural dusts of different origins.

## 1. Introduction

Sulfur dioxide (SO<sub>2</sub>) is a noticeable component in the atmosphere, where release of SO<sub>2</sub> is associated with the decrease in the levels of atmospheric oxidants, such as H<sub>2</sub>O<sub>2</sub>, OH, and O<sub>3</sub> as they are involved in the reactions that convert gaseous and dissolved SO<sub>2</sub> to sulfates [1,2]. Stevenson et al. estimate that, on average, emissions of SO<sub>2</sub> gas in the atmosphere due to anthropogenic activity account for the 71.2 Tg/yr, while volcanic eruptions contribute 8.8 Tg/yr, and 1.4 Tg/yr is due to the biomass burning [2]. Needless to say, volcanic eruptions are a highly variable source of SO<sub>2</sub> gas. The 2014–2015 Holuhraun eruption in Iceland, emitted ca. 11 Tg of SO<sub>2</sub> into the troposphere over a 6 month period, and caused one of the most intense and widespread volcanogenic air pollution events in centuries [3]. It was an effusive eruption with

very little volcanic ash produced, yet with the amount of SO<sub>2</sub> that exceeded all of the anthropological flux in Europe for the year 2011 [3]. That is not to undermine the significance of the anthropogenic contribution. The “Great smog” of 1952 in London was caused by SO<sub>2</sub> emitted from coal burning and reached levels as high as 1.34 ppm [4]. From the industrial point of view removal of SO<sub>2</sub> gas from the exhaust fumes is an area of ongoing active research [5–7].

Explosive volcanic eruptions have a potential to inject vast amounts of SO<sub>2</sub> gas into the stratosphere, where conversion of SO<sub>2</sub> to H<sub>2</sub>SO<sub>4</sub> leads to the formation of fine sulfur aerosol that can persist in the mid-stratosphere for up to 2 years [2]. Sulfate aerosols are known to affect the climate by increasing the reflection of radiation from the Sun back into space, thus efficiently cooling the Earth’s troposphere [2]. In the troposphere itself, formation of sulfur aerosols due to anthropogenic and

<sup>\*</sup> Corresponding author.

<sup>\*\*</sup> Corresponding author.

E-mail addresses: [darya.urupina@imt-lille-douai.fr](mailto:darya.urupina@imt-lille-douai.fr) (D. Urupina), [marie.verrielle@imt-lille-douai.fr](mailto:marie.verrielle@imt-lille-douai.fr) (M. Verrielle).

natural emissions competes with SO<sub>2</sub> gas deposition, and therefore sulfur aerosols formed are deposited within days or weeks [2]. Important reactions of SO<sub>2</sub> gas in the troposphere include oxidation of SO<sub>2</sub> in cloud and rain droplets, leading to the formation of acid rain, and oxidation to sulfate on the surface of atmospheric particles [1,6,8–11]. Adsorption of sulfur dioxide SO<sub>2</sub> gas on the surface of atmospheric samples leads to the formation of sulfate coating that can affect both the dust properties and the sulfur cycle [12]. Volcanic dusts acquire the sulfate coating while passing through the volcanic conduit [13], as well as further away from the crater, in the colder parts of the plume, higher in the atmosphere [14,15]. Desert dusts as well are known to accumulate hygroscopic sulfate coating during their long-range transport [16]. Thus, a negative correlation was observed between atmospheric concentrations of SO<sub>2</sub> and both Saharan and Chinese desert dust loadings [17]. Once coated, these particles can act as large cloud condensation nuclei (CCN) and affect cloud formation [18]. They may also affect climate forcing by forming cirrus ice clouds, ice nuclei (IN), at relatively warm temperatures and low supersaturation [18].

The physico-chemical processes that govern transformation of SO<sub>2</sub> gas on the surface of dusts are poorly understood and need further investigation. SO<sub>2</sub> shows heterogeneous reactivity towards many mineral oxides such as MgO, Al<sub>2</sub>O<sub>3</sub>, Fe<sub>2</sub>O<sub>3</sub>, TiO<sub>2</sub>, as well as volcanic ash and mineral dust [9,10,19,20]. Reactivity of the dusts towards the uptake of SO<sub>2</sub> as well as influence of different atmospheric conditions and various oxidants is often evaluated in terms of uptake coefficient using Knudsen cell and flow-tube reactors [10,19,20]. Quantifications of the amounts of products formed on the surface of dust could provide additional information and might clarify reaction pathways.

While summarizing previous work on volcanic ash analysis, Witham et al. cited about 55 articles reporting original volcanic ash-leaching data [21]. The ion-chromatography methods available in the literature and employed to quantify the amount of SO<sub>2</sub> adsorbed on the surface of volcanic ash are almost solely concerned with quantification of sulfates as the final oxidation product completely ignoring sulfite quantification [21]. Indeed, it is widely accepted that SO<sub>2</sub> gas reacts at the surface of the volcanic dust and forms sulfites or bisulfites, which are then converted to sulfates [22]. However, quantification of sulfites along with the sulfates could provide a more comprehensive description of the SO<sub>2</sub> adsorption processes. The ability of transitional metal such as iron ions to catalytically oxidize SO<sub>2</sub> in fog was first suggested by Zuo et al. [1]. The reaction order of Fe (III)-catalyzed thermal chemical and photochemical oxidation of dissolved sulfur dioxide in atmospheric liquids was found to be first order in respect to sulfite ion concentration [23]. Sulfite to sulfate conversion on synthetic mineral dust aerosol (using  $\alpha$ -Al<sub>2</sub>O<sub>3</sub>, CaO, ZnO, TiO<sub>2</sub>, MgO, and Fe<sub>2</sub>O<sub>3</sub> oxides) was recently studied by He et al. using DRIFTS in order to better explain haze formation mechanism in China [4]. The need to explore the effect of mineralogy on SO<sub>2</sub> adsorption using authentic dust samples of various compositions in laboratory studies was expressed by Sullivan et al. [24]. However, employment of DRIFTS is limited on natural heterogeneous samples that are dark in color, such as volcanic dust or ash. In addition, DRIFTS is a qualitative technique and does not provide quantitative data. Simultaneous determination of sulfites and sulfates by reversed-phase ion-pair HPLC technique in atmospheric waters was proposed by Zuo et al. [25]. When applied to environmental samples though, the method failed to determine sulfites due to their fast conversion to sulfates [25]. Nevertheless, ion-pairing technique is a good tool to separate polar compounds by means of user-friendly widely-used HPLC technique.

The goal of this study is to develop a method that would (i) extract both sulfites and sulfates, (ii) stop the conversion of sulfites to sulfates and (iii) successfully quantify both species. The method can then be used for two distinctive purposes: to quantify sulfites and sulfates on the surface of natural environmental samples, such as recently erupted volcanic ash or dust passing through polluted areas, and to study the kinetics of the sulfite to sulfate transformation in laboratory settings. The challenge in separating sulfites from sulfates in the solution

containing mineral dust comes from the nature of these dust particles, as they contain various oxidizing elements, such as iron, that contribute to the oxidation of sulfites into sulfates [1,23,26]. This article proposes (i) a controlled ageing of mineral samples by SO<sub>2</sub> gas in laboratory settings, (ii) extraction and stabilization of sulfites and sulfates with a subsequent use of (iii) HPLC for quantitative analysis as a technique that can be used to study the conversion of sulfites to sulfates on the surface of natural samples. While in the case of taking field measurements artificial ageing is not required, it is important to be able to age samples in reproducible fashion in order to study kinetics of the sulfite to sulfate transformation as a part of laboratory experimental work.

## 2. Experimental

### 2.1. Samples and standards

#### 2.1.1. Dust samples

A sample of volcanic dust of basaltic origin, used for method development and method application, comes from Hagavatn - an active desert area of Iceland. It was collected dry from the top surface layer. Particles are small, ranging from 10 to 50  $\mu$ m in diameter due to glaciofluvial processes leading to their generation. Modal composition of Hagavatn dust (referred as Lambahraun sand by Baratoux et al.) and, in particular, the amount of crystalline material versus glassy material, was determined by Baratoux et al. using optical and scanning mode microscope [27]. Hagavatn sample contains about 80% of minerals and 20% of glassy material [27]. Mineral phases typical of basaltic rocks include olivine, pyroxene and plagioclase [27].

The mineral desert dust sample, used for method application only, comes from Gobi Desert, Ningxia Province, China. This area represents the second most important source of atmospheric mineral dusts after Sahara desert [28]. This is an aeolian sample that was sieved and only the fraction below 100  $\mu$ m was used for further studies. The morphology of the sieved fraction of the natural Gobi dust sample was evaluated using scanning electron microscopy (SEM) carried out on a Hitachi S-4300SE/N SEM in high vacuum mode. Gobi dust particles are chunky, irregular in shape, with mean diameter ranging from a few to 50  $\mu$ m. Flat particles are also observed, suggesting the presence of distinct crystalline phase structures. The relative abundance of mineral phases for Gobi dust was determined using X-ray diffraction (XRD; Bruker D2 phaser 2 theta analyzer). Gobi dust shows a low silica content typical for Asian desert dusts (33.0%). Other minerals include calcite (8.7%), albite (8.6%), muscovite (25.8%), kaolinite (8.9%), rutile (4.4%), hedenbergite (6.2%), chromian pyrope (4.1%) and beaconite (0.3%).

Elemental compositions of Hagavatn and Gobi dusts as determined by ICP-MS are presented in Table 1 [20,29].

Specific surface area (SSA) for Hagavatn and Gobi dusts was determined in previous studies using the Brunauer–Emmett–Teller (BET) method, and the values obtained are as follows:  $4.5 \pm 1.1$  m<sup>2</sup>/g for Hagavatn and  $10.5 \pm 2.0$  m<sup>2</sup>/g for Gobi dust [20,30].

#### 2.1.2. Chemicals and reagents

HPLC grade acetonitrile (ACN), 99.95% and methanol (MeOH), 99.9% were obtained from Biosolve Chimie, Dieuze, France. Potassium hydrogen phthalate and triethanolamine, 99% of analytical grade were purchased from Acros Organics, Geel, Belgium. Cetylpyridinium chloride, 98% was purchased from Alfa Aesar, Kander, Germany. Sodium sulfate was purchased from Merck, Darmstadt, Germany. Sodium sulfite was purchased from Fischer Chemical, Loughborough, UK. Formalin (37% formaldehyde solution by weight containing 10–15% MeOH as stabilizer) was obtained from Sigma-Aldrich. Other chemicals and solvents of analytical grade were used during research. Deionized water (DI) was used throughout the investigation. A certified SO<sub>2</sub> cylinder, 250 ppm diluted in synthetic air (nearly 80% N<sub>2</sub> and 20% O<sub>2</sub>) was purchased from Messer, France.

**Table 1**

% elemental composition of mineral dust samples used in this study adapted from Ref. [20,29] as determined by ICP-MS experiments.

	Si	Al	Ca	Na	Mg	Ti	K	Fe	other
Hagavatn	27.5	16.7	19.5	3.1	10.4	2.4	0.2	19.6	0.6
Gobi	57.6	11.0	16.1	2.5	2.3	0.8	3.5	5.5	0.7

### 2.1.3. Standards

The solution of 1% Formalin was used to prepare a 1000 ppm stock solution of potassium sulfite ( $K_2SO_3$ ) and a 1000 ppm stock solution of potassium sulfate ( $K_2SO_4$ ). Other concentrations of  $K_2SO_3$  and  $K_2SO_4$  standards were prepared from their stock solutions through serial dilution with 1% Formalin. Stock solution of 1% Formalin was prepared by adding 10 ml of Formalin in a 1000 mL volumetric flask and diluting to the volume with 10% methanol/water to prevent polymerization.

## 2.2. Experimental set-up and procedure

### 2.2.1. General outline

This work serves two distinctive purposes: (i) analyze sulfites and sulfates on the surface of environmental dust samples during field campaign measurements (referred to as “environmental sampling”) and (ii) study kinetics of sulfite and sulfate formation on the surface of different dusts in the laboratory environment by subjecting them to  $SO_2$  ageing and analyzing the product formation (referred to as “kinetics study”).

The developed method for “environmental sampling” protocol consists of three parts: (i) sample collection, (ii) extraction and stabilization of sulfites and sulfates and (iii) HPLC analysis (Fig. 1); the developed method for “kinetics study” protocol includes four steps: (i) sample collection, (ii) dust ageing, (iii) extraction and stabilization of sulfites and sulfates and (iv) HPLC analysis (Fig. 1). Thus, the difference between the two protocols is an additional step of controlled  $SO_2$  ageing required for the “kinetics study”. Sample analysis step that includes extraction and HPLC analysis is exactly the same in both cases.

Method for HPLC analysis was validated for specificity, limit of detection and quantitation, linearity and range, injection repeatability, and robustness. Sample preparation and extraction reproducibility was validated for the entire “kinetics study” protocol. Note that reproducibility for “environmental sampling” is expected to be superior to

reproducibility for “kinetics study” due to the lack of ageing that introduces additional uncertainties.

### 2.2.2. Dust ageing by $SO_2$ gas

The setup for ageing samples consists of two parts: (i) the gas mixing line and (ii) the ageing reactor. A schematic representation of the setup is provided in Fig. 2. A dust weighing from 100 to 200 mg is spread on a 47 mm Whatman filter paper and is placed in a tightly closed reactor. The gas mixture containing 175 ppm  $SO_2$  entering the reactor is forced through the filter containing the dust at  $100\text{ cm}^3/\text{min}$ . The ageing of environmental samples is carried out using zero air; it is generated by a classical air compressor, and then passed through a catalytic zero air generator (Claind ZeroAir 2020, Lenno, Italy) coupled to a pressure swing adsorption (PSA) device. The remaining impurity levels in the air stream before entering the reactor are lower than the analytical system detection limits: VOCs  $<0.1$  ppb,  $CO_2 < 10$  ppb, and  $CO < 80$  ppb. Moisture level is ca. 2 ppm. In experiments requiring humid air, a second flow of zero air going through a bubbler of ultrapure water (Milli-Q, resistivity  $18.2\text{ M}\Omega\text{ cm}$ ) is mixed with the dry air flow, in proportions necessary to reach the relative humidity (RH) targeted.

### 2.2.3. Extraction and stabilization of surface sulfites and sulfates

After a defined period of ageing in the laboratory or in the absence of controlled ageing, such as in the case of samples collected in the environment, a sample weighing from 100 to 200 mg was transferred to a 10 mL glass container and stabilized with 1 mL of 1% Formalin. This step was followed by 10 min sonication in the ultrasound bath. The solution was then filtered through a  $0.45\text{ }\mu\text{m}$  pore size 30 mm diameter filter using a syringe. The remaining dust was washed with 1 mL of 1% Formalin and filtered through the same filter that was used to filter the first solution. The combined final solution was analyzed by HPLC system.

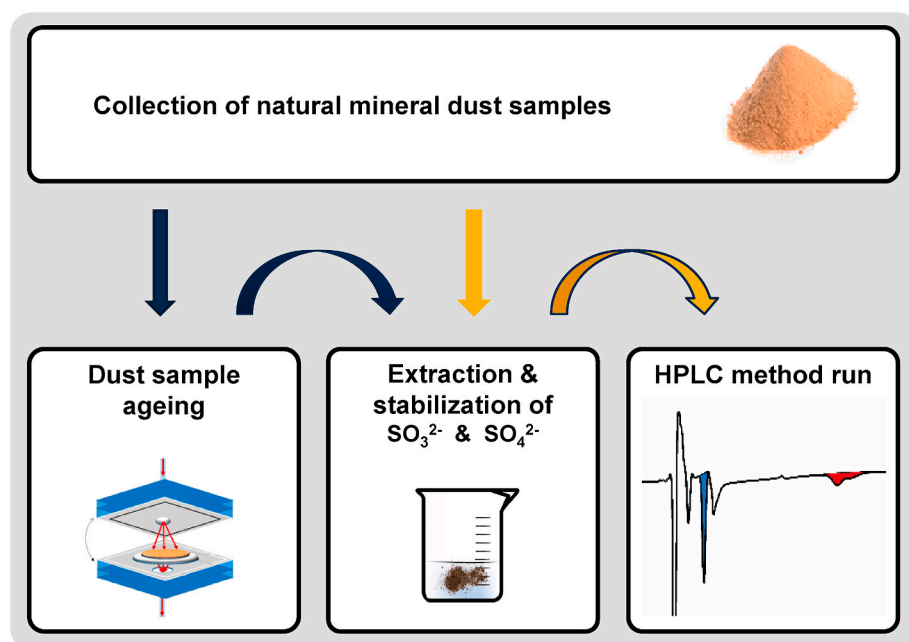


**Fig. 1.** Diagram representing two protocols: (A) “environmental sampling” that includes (i) sample collection, (ii) extraction and stabilization of sulfites and sulfates and (iii) HPLC analysis and (B) “kinetics study” that includes (i) sample collection, (ii) dust ageing, (iii) extraction and stabilization of sulfites and sulfates and (iv) HPLC analysis. Dark blue arrows lead through “environmental sampling” protocol, while orange arrows lead through “kinetics study” protocol. (For interpretation of the references to color in this figure legend, the reader is referred to the Web version of this article.)

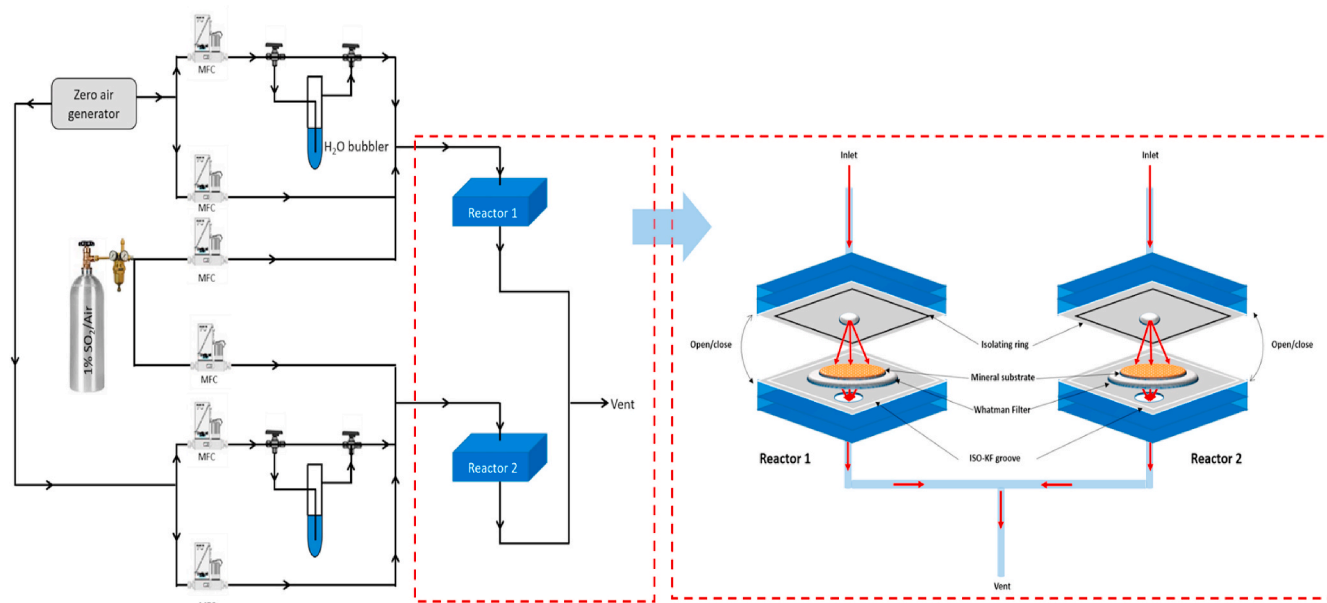


Fig. 2. Left: schematic representation of the setup used to age samples of dust with  $\text{SO}_2$  gas. Right: reactor 1 and 2 with deposited dust, zoomed for clarity.

#### 2.2.4. HPLC analysis. Instrumentation and chromatographic conditions

Chromatography equipment used to develop an HPLC method consisted of Thermo Scientific Dionex UltiMate 3000 UHPLC System with UV/VIS Detector (Thermo Scientific, Waltham, MA). Chromeleon 7.0 Data Acquisition System for LC (Thermo Scientific, Waltham, MA) was used to analyze the data. Analysis was performed using Restek Ultra Column C18, 5  $\mu\text{m}$ , Length 250 mm, I.D. 4.60 mm dynamically coated with cetylpyridinium chloride to produce a charged surface as recommended by Zuo et al. [25]. More specifically, columns were cleaned at 1 mL/min for 1.5 h with 100% ACN before being coated with 1.0 mM cetylpyridinium chloride in ACN/water (7:93, v/v) at 0.5 mL/min for 3 h [25]. The HPLC instrument was operated isocratically at 23  $^\circ\text{C}$  at a flow rate of 1 mL/min for 15 min. Potassium hydrogen phthalate solution, 1.0 mM was adjusted to pH 6.5 with a dilute solution of potassium hydroxide (KOH), vacuum filtered and used as a mobile phase. The injection volume was 10  $\mu\text{L}$ . An indirect photometric detection was used for quantification of sulfates and sulfites. Detector was set at 255 nm as the mobile phase showed the highest absorbance at this wavelength. A 6-point linear calibration curve was established daily for  $\text{SO}_3^{2-}$  and  $\text{SO}_4^{2-}$  ions in the range of 6  $\mu\text{g}/\text{mL}$  to 191  $\mu\text{g}/\text{mL}$  and 3  $\mu\text{g}/\text{mL}$  to 101  $\mu\text{g}/\text{mL}$  respectively. Concentration of sulfites and sulfates in the extracts of natural samples was determined using the slope of the calibration curve and converted to micrograms per gram ( $\mu\text{g}/\text{g}$ ) of dust using the mass of the sample.

### 3. Results and discussion

#### 3.1. HPLC analytical method optimization

The method for determination of sulfites, sulfates and hydroxymethanesulfonate (HMS) in natural and atmospheric water samples developed by Zuo et al. was used as a base for development of the method for determination of sulfites and sulfates on the surface of natural mineral samples discussed in this paper [25]. The main drawback of the method was the lack of sulfite-stabilizing agent during sample preparation and, as a consequence, inability to detect sulfites in environmental samples. The authors acknowledged the problem in the “quantitative analysis” part of their study and recommended to use methanol in order to stabilize sulfites. Following the suggestion, a 50/50 ppm solution of  $\text{K}_2\text{SO}_3/\text{K}_2\text{SO}_4$  was dissolved in 10% methanol used as stabilizing agent. Unfortunately, in our experiments, methanol

solution either did not stabilize sulfites and they were converted into sulfates, or sulfites co-eluted with sulfates, as only one peak was observed. Besides, methanol would be a poor choice for the extraction of sulfites in the presence of reactive ions, such as Mn or Fe, which are both known to be present in volcanic dust [26]. Formalin was reported to prevent the conversion of sulfites to sulfates by converting it to hydroxymethanesulfonate (HMS) and was tested as an extracting solvent [26]. A number of reactions and reaction rate constants were proposed by Kovacs et al. to demonstrate interactions of sulfites/bisulfates with formaldehyde and its hydrate [31]. Reaction rate constants suggest that formation of HMS is a favorable process and it is expected that in access of formaldehyde all of the sulfite/bisulfite will be converted to HMS.

Two concentrations of a mixture of sulfites and sulfates of 50/50 ppm and 5/5 ppm were prepared using Formalin of the following concentrations: 0.5%, 1% and 5%. A solvent peak for 5% Formalin overlapped with a sulfite peak, and 5% Formalin concentration was rejected for further studies. Solvent peaks of both 0.5 and 1% Formalin were well separated from sulfite peak. Besides, less than 5% change was observed for sulfites and sulfates in the corresponding solutions when left at ambient temperature for 2 days. Between 0.5% and 1% concentrations of Formalin, a solution of 1% Formalin was chosen as an extracting solvent for further studies.

A second concern about the method of Zuo et al. was the high pH value of the mobile phase. The diluted 1.0 mM phthalate mobile phase suggested by the author could not be adjusted to pH 7.9 as pH became unstable and decreased with time. Addition of triethanolamine drastically increased the pH of the mobile phase. Taking into consideration that pH higher than 8.0 is detrimental for the column and can easily dissolve the stationary phase, it was decided to work at pH 6.5, which was stable and easy to maintain. Addition of methanol to mobile phase didn't make any difference on formaldehyde/sulfite pair, but broadened and pushed the sulfate peak further. It was therefore decided to work with 1.0 mM Potassium phthalate solution pH 6.5 as a mobile phase. Several other parameters, such as column type, injection volume and detection wavelength were varied to find the optimum conditions for getting a sharp peak and a good separation of sulfites and sulfates from formaldehyde peak present in the solvent. Parameters investigated are listed in Table 2.

Finally, the following chromatographic conditions were determined as optimum: 25 mm Restek Ultra Column C18, Particle size: 5  $\mu\text{m}$ , I.D.



**Table 2**

Parameters investigated and changed in order to adapt a method for “Simultaneous determination of sulfite, sulfate, and hydroxymethanesulfonate in atmospheric waters by ion-pair HPLC technique” by Zuo et al. to determination of sulfites and sulfates on the surface of environmental samples investigated in this work [25].

	Method by Zuo et al.	Parameters investigated	Parameters chosen
Column	150 mm C18 Column, Particle size: 5 $\mu$ m, I.D. 4.60 mm	250 mm Restek Ultra Column C18, Particle size: 5 $\mu$ m, I.D. 4.60 mm 250 mm Acclaim 120 Column C18, Particle size: 3 $\mu$ m, I.D. 3 mm	250 mm Restek Ultra Column C18, Particle size: 5 $\mu$ m, I.D. 4.60 mm
Column coating	1.0 mM cetylpyridinium chloride in 7% ACN solution		1.0 mM cetylpyridinium chloride in 7% ACN solution
Mobile phase	potassium hydrogen phthalate 0.5 mM-0.015% triethanolamine-3% methanol	triethanolamine: 0%, 0.015% potassium hydrogen phthalate: 0.5 mM, 1 mM, 10 mM % Methanol: 0%, 1%, 3%, 5%	1 mM potassium hydrogen phthalate
pH	7.9	6.0, 6.5, 7.0, 7.5, 8.0, 8.5	6.5
Flow rate	1.0 ml/min	0.5 ml/min, 1 ml/min	1.0 ml/min
Detection	negative UV-Vis detection at 265 nm	negative UV-Vis detection at 265 nm, 255 nm	negative UV-Vis detection at 255 nm
Time	15 min	10 min, 15 min	15 min
HPLC mode	isocratic elution		isocratic elution
Temperature	23 °C	20 °C, 23 °C, 26 °C, 30 °C, 35 °C	23 °C
Injection volume	10 $\mu$ L	10, 15, 20 $\mu$ L	10 $\mu$ L
Sulfite-stabilizing reagent	None	methanol 10% Formalin: 0.5%, 1%, 5%	1% Formalin

4.60 mm column which was dynamically coated with 1.0 mM cetylpyridinium chloride in 7% acetonitrile solution to produce a charged surface as recommended by Zuo et al. [25]. Mobile phase used: 1 mM potassium hydrogen phthalate at pH 6.5 at a flow rate of 1.0 ml/min with negative UV-Vis detection at 255 nm in 15 min.

Fig. 3 displays four chromatograms offset for clarity: 1% Formalin, 20 ppm  $K_2SO_3$ , 10 ppm  $K_2SO_4$ , and Hagavatn extract obtained after ageing the dust for 1 h in 175 ppm  $SO_2$ . The peak for  $SO_3^{2-}$  is observed at 2.7 min and  $SO_4^{2-}$  peak is observed at 7.2 min. Both peaks demonstrate a high number of theoretical plates: for Hagavatn extract they are equal to 2235 for  $SO_3^{2-}$  and 884 for  $SO_4^{2-}$ . Two small peaks around 2.2 and 3.0 min belong to formaldehyde and are separated from the peak for  $SO_3^{2-}$  at 2.7 min. The sulfite peak present in the form of HMS eluted rather closely to the formaldehyde peak. Therefore, in order to preserve separation, it was decided to stay with a 250 mm long column.

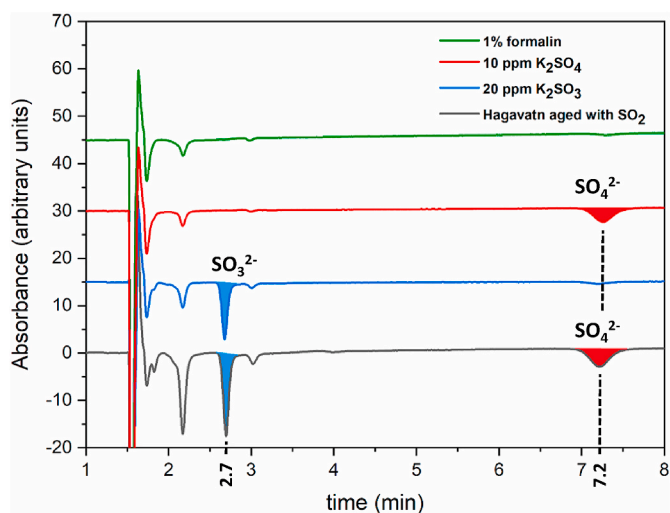


**Fig. 3.** Representative chromatograms of: green) Formalin, offset 45 units for clarity; red) 10 ppm  $K_2SO_4$  in 1% Formalin, offset 30 units for clarity; blue) 20 ppm  $K_2SO_3$  in 1% Formalin, offset 15 units for clarity; black) Hagavatn dust aged in 175 ppm  $SO_2$  for 1 h and extracted in 1% Formalin. (For interpretation of the references to color in this figure legend, the reader is referred to the Web version of this article.)

### 3.2. Extraction optimization

Different parameters, such as extraction time and extraction techniques (shaking vs sonication), as well as volume of the extracting solution, were studied to insure maximum extraction of sulfites and sulfates. Solution stability was investigated to assess the time window during which the analysis can be performed.

#### 3.2.1. Dissolution

The dissolution time of up to 40 min of Hagavatn extract was investigated using sonication. Sulfites and sulfates immediately dissolved as shown in Fig. 4. Similar results were obtained with mechanical shaking, and 10 min sonication was found to be an appropriate dissolution technique.

#### 3.2.2. Recovery

Recovery studies were intended to prove that maximum amount of the sulfites and sulfates are extracted. Three consecutive extractions with 1 mL of 1% Formalin were evaluated for the amount of sulfites and sulfates after the sample was aged by 175 ppm  $SO_2$  for 10 min, 30 min, 1 h, and 2hr. The criteria is less than 5% of the product can be left

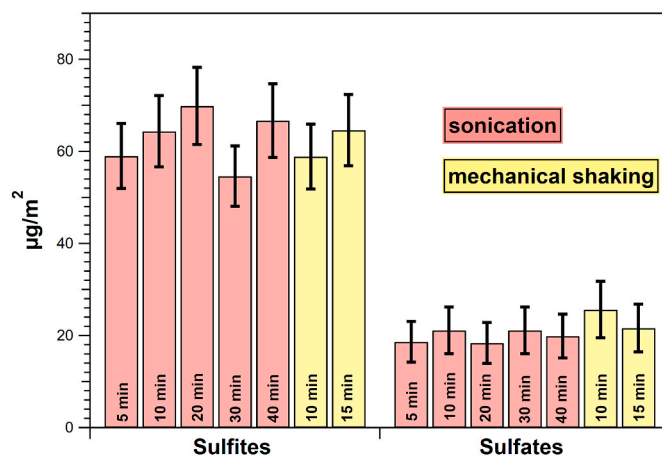


**Fig. 4.** Dissolution studies for Hagavatn dust aged in 175 ppm  $SO_2$  for 1 h and extracted in 1% Formalin. % RSD for sulfites and sulfates is equal to 12.1% and 23.6% respectively (see section 3.4).

**Table 3**

Recovery results for 3 consecutive extracts of the sample of Hagavattn aged in 175 ppm SO<sub>2</sub> for various time periods. Extraction with 1 mL of 1% Formalin.

Sample	Hagavattn aged with 175 ppm SO <sub>2</sub>			
	10 min	30 min	1hr	2hr
Extract 1 SO <sub>3</sub> <sup>2-</sup> (ppm)	64.1	69.3	71.7	78.4
Extract 2 SO <sub>3</sub> <sup>2-</sup> (ppm)	14.9	11.9	19.9	16.6
Extract 3 SO <sub>3</sub> <sup>2-</sup> (ppm)	0.1	3.3	0	1.6
% SO <sub>3</sub> <sup>2-</sup> in the 3rd extract	0.1	3.9	0.00	1.2
% recovery after 3 extract	99.9	96.1	100.00	98.0
Extract 1 SO <sub>4</sub> <sup>2-</sup> (ppm)	3.4	3.7	3.7	8.5
Extract 2 SO <sub>4</sub> <sup>2-</sup> (ppm)	0	0	0	0
% recovery	100.00	100.00	100.00	100.00

unaccounted. As can be observed from Table 3, all of the sulfates are extracted from the surface of Hagavattn dust after the first extraction with 1 mL of 1% Formalin. As for the sulfites, two extractions with 1 mL of 1% Formalin are necessary. The third extraction represents from 0 to 3.9% of the total amount of SO<sub>3</sub><sup>2-</sup> extracted and therefore is not required based on the established criteria. Method demonstrates efficient recovery after only two extractions. As a result, it was decided to extract sulfites and sulfates with 1 mL of 1% Formalin, wash the remaining dust with another 1 mL of 1% Formalin and, using the same syringe, filter and combine the solution.

### 3.2.3. Solution stability

In order to observe how analytes of interest change over time, Hagavattn extract was prepared and injected into the HPLC system. The same solution was injected after 3, 5, 7, and 10 days. Solution stability results obtained from injecting a sample of 158.2 mg of Hagavattn aged for 10 min are shown in Fig. 5. Solution stability studies indicate that both sulfites and sulfates remain stable up to 10 days, which means that a sample can be easily collected and extracted to be kept for later analysis, which is indispensable during geological sampling when the analyzing facility might be far away from the sampling location. Moreover, in separate experiments a 165 mg sample of Hagavattn aged with SO<sub>2</sub> for 1hr was checked for stability after 10 days and 3 months. Percent change in ppm concentration for sulfites was established at 4.5% after 10 days and 3.2% in 3 months; as for sulfates 5.4% change was observed after both 10 days and 3 months. Thus, the results indicate that dust samples aged with SO<sub>2</sub> and stabilized with 1% Formalin are stable

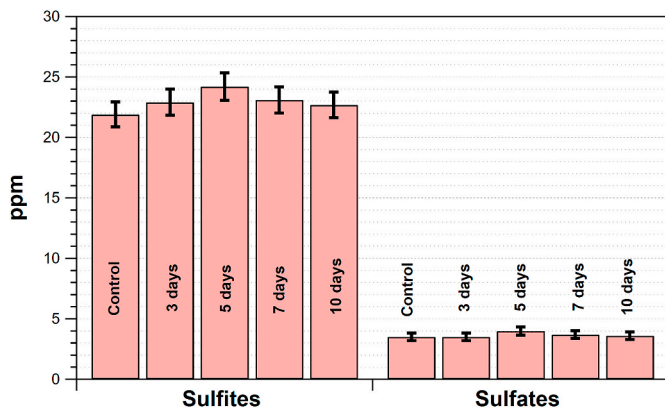


Fig. 5. Stability study results for 158.2 mg sample of Hagavattn aged in 175 ppm SO<sub>2</sub> for 10 min. Extraction with 1 ml of 1% Formalin. Samples are stored at 4 °C. % RSD for sulfites and sulfates is equal to 4.7% and 8.7% respectively (see 3.3.4).

for long periods (at least up to 3 months). Exceptional stability of solutions is very important in field campaigns as it makes it possible to collect and stabilize a sample on the go, but analyze it later in the laboratory.

### 3.3. Validation of analytical performance

The developed method was validated for specificity, limit of detection and limit of quantitation, linearity and range, injection repeatability, and robustness.

#### 3.3.1. Specificity

To ensure that the peak response is due to only one component and no co-elution occurs, a solution of Hagavattn dust aged in 175 ppm SO<sub>2</sub> for 10 min and extracted in 1% Formalin was analyzed by Waters 2695 HPLC system equipped with Diode Array Detector using Empower software. Thus, specificity was evaluated as spectral purity. In peak purity testing the software compares the spectrum from each data point within the peak against the peak apex spectrum. Two parameters are evaluated: purity threshold, which accounts for the presence of non-ideal and solvent-induced spectral changes, and purity angle. When the purity angle exceeds purity threshold, a detectable impurity is present within a single chromatographic peak.

A solution of 165 mg of Hagavattn dust aged in 175 ppm SO<sub>2</sub> for 10 min and extracted in 1% Formalin showed no interfering peaks. All peaks were well separated from the analyte peaks. Peak purity was proved by purity threshold exceeding the purity angle for both sulfite and sulfate peaks.

#### 3.3.2. Limit of detection (LOD) and limit of quantitation (LOQ)

Limits of detection for sulfites and sulfates were investigated to determine the lowest concentration of sulfites and sulfates that can be detected but not quantified. It was based on a signal-to-noise ratio S/N ≥ 3. Limits of quantitation were studied to determine the lowest levels of the analyte concentrations that can be quantified and were determined by the concentrations corresponding to signal-to-noise ratio S/N ≥ 10.

The LOD for determination of sulfites was found to be 0.5 µg/mL of K<sub>2</sub>SO<sub>3</sub> (0.32 µg/mL of SO<sub>3</sub><sup>2-</sup> ion). This value is 5 times lower than the 1.52 µg/mL of SO<sub>3</sub><sup>2-</sup> ion reported as LOD by Zuo et al. (corresponding to 19 µM of SO<sub>3</sub><sup>2-</sup> ion), but in a good agreement with the limit of detection of hydroxymethylsulfonate (HMS) reported at 0.42 µg/mL (corresponding to 3.8 µM of HMS ion). This is to be expected, as the SO<sub>3</sub><sup>2-</sup> in our case elutes as a HMS complex. The reason for improved detection limit is earlier elution of SO<sub>3</sub><sup>2-</sup> in the form of HMS at around 3 min instead of 7.5 min as a free sulfite ion using the original method [25]. Earlier elution prevents peak broadening and improves LOD and LOQ. LOQ for determination of SO<sub>3</sub><sup>2-</sup> ion was found to be 1 µg/mL of K<sub>2</sub>SO<sub>3</sub> (0.64 µg/mL of SO<sub>3</sub><sup>2-</sup> ion).

LOD for determination of sulfates was found to be 1 µg/mL of K<sub>2</sub>SO<sub>4</sub> (0.68 µg/mL of SO<sub>4</sub><sup>2-</sup> ion). This value is in excellent agreement with the limit of detection for SO<sub>4</sub> ion reported by Zuo et al. and established at 6.7 µM SO<sub>4</sub><sup>2-</sup> ion which is 0.64 µg/mL of SO<sub>4</sub><sup>2-</sup>. LOQ for determination of sulfates was found to be 5 µg/mL of K<sub>2</sub>SO<sub>4</sub> (3.38 µg/mL of SO<sub>4</sub><sup>2-</sup> ion).

#### 3.3.3. Linearity and range

Linearity proves that the detector response is directly proportional to the concentrations of the analyte in the sample, and range provides an interval for which the procedure is linear. Calibration ranges were defined as to include possible concentrations of sulfites and sulfates that can be found on the surface of mineral dust. This approach was based on preliminary results used to frame the order of magnitude of typical SO<sub>3</sub><sup>2-</sup> and SO<sub>4</sub><sup>2-</sup> surface concentrations. To investigate linearity for extracted sulfites, six different concentrations of K<sub>2</sub>SO<sub>3</sub> were prepared from 1000 µg/mL stock solution of K<sub>2</sub>SO<sub>3</sub> in the range 10–300 µg/mL (corresponding to 6 µg/mL to 191 µg/mL of SO<sub>3</sub><sup>2-</sup> ion). To explore linearity for sulfates, six different concentrations of K<sub>2</sub>SO<sub>4</sub> were prepared from 1000



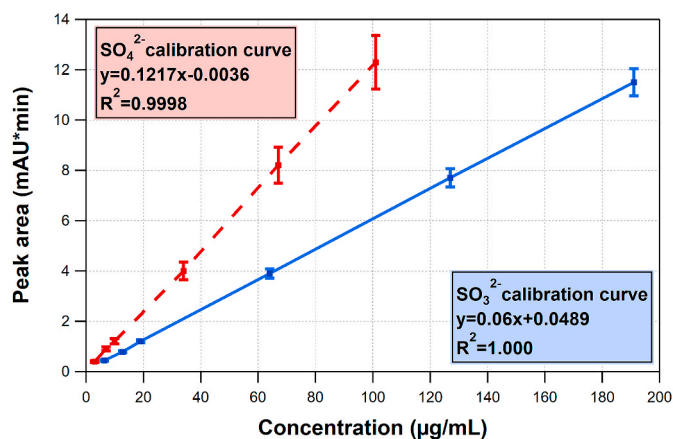


**Fig. 6.** The typical plot of peak area versus concentration for a) sulfite (blue solid line) and b) sulfate (red dashed line) ions. The linearity plot was created daily before conducting experiments and each time the mobile phase solution was changed. (For interpretation of the references to color in this figure legend, the reader is referred to the Web version of this article.)

$\mu\text{g/mL}$  stock solution of  $\text{K}_2\text{SO}_4$  in the range 5–150  $\mu\text{g/mL}$  and injected into the HPLC system (corresponding to 3  $\mu\text{g/mL}$  to 101  $\mu\text{g/mL}$  of  $\text{SO}_4^{2-}$  ion).

Calibration plots were constructed every day in order to insure accurate identification of sulfates and sulfites in dust. Moreover, since the detection is achieved in negative mode (i.e. the mobile phase absorbs UV light and the peaks are “observed” when a compound lacking chromophore is passing through the column) the absorbance of the mobile phase depends on the concentration of the UV absorbing solution. Even slightest variations in phthalate concentration can change the slope of the calibration plot. Therefore, it is crucial to construct a new calibration curve every time a freshly-made mobile phase is introduced into the system. Nevertheless, it is important to keep in mind that even though the slope of the calibration curve may change the curve remains linear within the range. Therefore, the daily-constructed curve can be used for quantitation purposes as long as the same batch of phthalate solution is used. Calibration curves from a typical experimental day are represented in Fig. 6; calibration curve equations, coefficients of determination ( $R^2$ ) and root mean square errors are provided in Table 4. While  $R^2$  shows how close the data are to the fitted regression line, root mean square error can be interpreted as the average distance of a data point from the fitted line, measured along a vertical line.

### 3.3.4. Injection repeatability

Injection repeatability was tested to measure the sensitivity of the method towards errors coming from the instrument itself: the column, the detector, the injector, the integration device. To evaluate injection repeatability a solution of a mixture of 20 ppm  $\text{K}_2\text{SO}_3$  and 10 ppm  $\text{K}_2\text{SO}_4$  were injected into the HPLC system 6 times and evaluated for area % relative standard deviation (%RSD). Injection repeatability for a solution of 20 ppm  $\text{K}_2\text{SO}_3$  and 10 ppm  $\text{K}_2\text{SO}_4$  was calculated to be 4.7% for sulfites and 8.7% for sulfates (Table 4).

**Table 4**

Analytical Performance: Range, Linearity (calibration curve equation, coefficient of determination, root mean square error) and Injection Repeatability (expressed as %RSD for 6 consecutive injections of a solution of 20 ppm  $\text{K}_2\text{SO}_3$  and 10 ppm  $\text{K}_2\text{SO}_4$ ).

	Test range ( $\mu\text{g/mL}$ )	Calibration curve	$R^2$	Root Mean Square Error	% RSD n = 6
Sulfites	6–191	$y = 0,06x + 0,0489$	1.0000	0.024	4.7
Sulfates	3–101	$y = 0,1217x - 0,0036$	0.9998	0.079	8.7

### 3.3.5. Robustness

Robustness of an analytical procedure is a measure of its capacity to remain unaffected by small but deliberate variations in parameters listed in the procedure. In this study “remain unaffected” was defined as no change of the detected amount of the analyte in a sample in spite of the variation of the method parameter. Stability of the method was evaluated with respect to variations of the internal factors of the method such as pH of the mobile phase pH ( $6.5 \pm 0.5$ ), column temperature ( $23 \pm 3$ ), different column lots (Lot #160210E and Lot #130505R) and 1 month old vs 4 months column. Changes in temperature, pH, column age (up to 4 months) and lot number (Lot #160210E and Lot #130505R) did not affect the amounts of  $\text{SO}_3^{2-}$  and  $\text{SO}_4^{2-}$  ions determined in the solutions, as they fell within injection variations, where 4.7% RSD and 8.7% RSD were reported for sulfites and sulfates respectively (Table 5). This is important, as it means that small fluctuations in pH that can come from mobile phase preparation will not affect quantification. Stability towards temperature changes suggests that method could be used in instruments not equipped with temperature control function. Stability of the column for at least 4 months and robustness towards change of column (different batches) assures normal use of the method.

### 3.4. Validation of the sample preparation and extraction performance.

#### Method reproducibility

The developed method was further validated for sample preparation and extraction reproducibility. It was decided to use the protocol for “kinetics study” to evaluate reproducibility because in comparison with “environmental sampling” protocol it has a supplementary step of dust ageing that can introduce additional errors.

Sample preparation and extraction reproducibility studies were conducted to evaluate the sensitivity of the method towards errors that may result from the combination of steps starting from ageing, extraction and preparation of the samples to their subsequent analysis by HPLC instrument. To evaluate sample preparation and extraction reproducibility for the “kinetics study” protocol, seven samples of Hagavtn volcanic dust were aged with 175 ppm  $\text{SO}_2$  for 1 h and extracted in 1% Formalin. The solutions were injected into HPLC system and %RSD for mass of sulfites/sulfates per square meter of dust was calculated. The %RSD for reproducibility (that includes ageing and extraction of sulfites/sulfates) as reported in Table 6 was found to be 12.1% for sulfites and 23.6% for sulfates. It is important to stress that reproducibility for ageing and extraction of sulfites/sulfates in a dust sample depends on heterogeneity of the sample. Like most of the natural mineral dusts, Hagavtn volcanic dust represents a highly heterogeneous sample and variations in adsorption/transformation of  $\text{SO}_2$  gas by its different components are expected. Many studies use a combination of different oxides as proxies for natural samples. In this case %RSD for reproducibility would be expected to be lower as the sample composition is well-defined and ageing process more reproducible. Nevertheless, the importance of using natural samples cannot be overstated, as they often demonstrate different adsorption patterns when compared to the mixture of mineral oxides used as proxies [28,32,33]. For example, when studying adsorption of  $\text{SO}_2$  on individual oxides and comparing them to their mixture Zhang et al. observed that the reactivity of the mixture is twice as high as the reactivity of individual components [3]. In addition, substituting natural samples characterized by complex

**Table 5**

Method robustness results. Small changes in method parameters were introduced and evaluated as percent change for the amounts of  $\text{SO}_3^{2-}$  and  $\text{SO}_4^{2-}$  ions in samples of Hagavattn dust as compared to their determination under original conditions (marked by asterisk).

Sample	T (C°)	pH	Column Lot#	Column age (months)	Amount for $\text{SO}_3^{2-}$ (ppm)	% Change	Amount for $\text{SO}_4^{2-}$ (ppm)	% Change
Hagavattn 194 mg aged for 1hr*	23	6.5	160210E	1	27.5		10.45	
Hagavattn 194 mg aged for 1hr	20	6.5	160210E	1	26.7	-2.9	10.82	3.5
Hagavattn 194 mg aged for 1hr	26	6.5	160210E	1	27.2	-1.1	10.45	0.0
Hagavattn 158 mg aged for 10 min*	23	6.5	160210E	1	22.7		3.6	
Hagavattn 158 mg aged for 10 min	23	7.0	160210E	1	23.09	1.7	3.7	2.8
Hagavattn 158 mg aged for 10 min	23	6.0	160210E	1	21.7	-4.4	3.4	-5.6
Hagavattn 165 mg aged for 1hr*	23	6.5	160210E	1	27.8		8.2	
Hagavattn 165 mg aged for 1hr	23	6.5	130505R	1	26.6	-4.5	8.6	5.4
Hagavattn 165 mg aged for 1hr*	23	6.5	160210E	1	27.8		8.2	
Hagavattn 165 mg aged for 1hr	23	6.5	160210E	4	26.9	-3.2	8.6	5.4

**Table 6**

Sample preparation and extraction reproducibility study for samples of Hagavattn aged in 175 ppm  $\text{SO}_2$  for 1 h. Extraction with 1 mL of 1% Formalin.

Preparation	Date of sample preparation	Sample mass (mg)	Concentration $\text{SO}_3^{2-}$ ( $\mu\text{g}/\text{m}^2$ )	Concentration $\text{SO}_4^{2-}$ ( $\mu\text{g}/\text{m}^2$ )
1	April 8	134.0	59.3	25.2
2	April 12	89.0	66.4	28.7
3	April 12	194.0	67.1	20.5
4	April 15	137.3	69.6	22.7
5	April 15	138.6	56.2	39.1
6	April 16	158.0	75.7	26.1
7	April 16	165.4	79.3	22.5
Average			67.7	26.5
Standard Deviation			8.2	6.2
%RSD			12.1	23.6

mineralogy by simple mineral oxides risks oversimplification of the observed trends.

### 3.5. Method summary

The validated method is summarized in Table 7. If “environmental sampling” is the desired purpose of the method, ageing is not required and one can start the protocol from the extraction section. For “kinetics study”, ageing is followed by extraction and HPLC analysis. Mass of the sample introduced into the reactor will depend on the specific surface area of the dust. In case of high specific surface area a higher  $\text{SO}_2$  adsorption might be expected and therefore a smaller sample mass can be used for extraction. Likewise, if the specific surface area of the dust is low an increased mass might be necessary in order to detect sulfites/

**Table 7**

Summary of the validated conditions used to age, extract and quantify sulfites and sulfates in the sample of dust aged with  $\text{SO}_2$  gas.

Ageing		Extraction		Chromatographic conditions	
Dust sample mass	100.0–200.0 mg	Extracting solution	1% Formalin in 10% MeOH/water	Column	250 mm Restek Ultra Column C18, Particle size: 5 $\mu\text{m}$ , I.D. 4.60 mm
$\text{SO}_2$ concentration	175 ppm	Mode of dissolution	sonication	Column modification	coated with 1.0 mM cetylpyridinium chloride in 7% ACN solution
$\text{SO}_2$ flow	100 cm <sup>3</sup> /min	Time of dissolution	10 min	Mobile phase	1 mM potassium hydrogen phthalate at pH 6.5
RH	30%	Filter	0.45 $\mu\text{m}$ pore size 30 mm diameter Whatman filter	Flow rate	1.0 ml/min
Time	10 min - 1 h	Total volume of extracting solution	2 mL	Detection	negative UV-Vis detection at 255 nm
				Time	15 min

sulfates on the surface. Thus, the method can be easily adapted to different dust samples.

### 3.6. Method application

#### 3.6.1. Application of the method to natural samples

Samples of Hagavattn volcanic dust and Gobi desert dust were tested for sulfites and sulfates using the “environmental sampling” method for extraction and quantification described above. Samples were not aged in the laboratory, but could have been previously subjected to  $\text{SO}_2$  gas. In case of Hagavattn, the samples were certainly exposed to  $\text{SO}_2$  gas during volcanic eruption. As for aeolian samples of Gobi dust, it is also likely that during its long-range transfer the dust encountered industrially polluted areas of China known to contain high levels of  $\text{SO}_2$  [16]. Six samples of natural desert dust ranging from 124.2 to 144.5 mg and seven Hagavattn volcanic dusts ranging from 110.6 to 505.4 mg were tested to determine their  $\text{SO}_3^{2-}$  and  $\text{SO}_4^{2-}$  ion surface concentrations. As can be seen from Table 8, the extraction of both Gobi and Hagavattn surface dust did not reveal sulfites above the limit of detection of 0.32  $\mu\text{g}/\text{mL}$  for  $\text{SO}_3^{2-}$  ion. Note, that the absolute amounts of sulfites and sulfates are directly dependent on the sample mass since this parameter drives the effective surface area of the considered sample. As for the sulfates, although the amounts on the surface of Hagavattn samples were above the LOD level of 0.68  $\mu\text{g}/\text{mL}$  of  $\text{SO}_4^{2-}$  for five out of seven samples, they remained under the LOQ level of 3.38  $\mu\text{g}/\text{mL}$  of  $\text{SO}_4^{2-}$  ion even when the mass of the sample was increased to 505.4 mg. Furthermore, in terms of absolute amounts of sulfates detected on Hagavattn dust, increasing the mass of the dust sample to 505.4 mg increases its total surface area and therefore decreases the minimum amount of  $\text{SO}_4^{2-}$  ion per meter square that could be detected on the surface. The fact that the amount of

**Table 8**

Results of method reproducibility study for determination of  $\text{SO}_3^{2-}$  and  $\text{SO}_4^{2-}$  ions in Hagavavn and Gobi natural samples. Note, that samples were not subjected to laboratory ageing. LOD and LOQ for sulfites and sulfates for each sample mass expressed in  $\mu\text{g}/\text{m}^2$  were calculated from corresponding sample's mass, specific surface area, extraction volume (2 ml) and the values for LOQ and LOD expressed in  $\mu\text{g}/\text{mL}$  measured earlier (LOD for  $\text{SO}_3^{2-} = 0.32 \mu\text{g}/\text{mL}$ , LOQ for  $\text{SO}_3^{2-} = 0.64 \mu\text{g}/\text{mL}$ ; LOD for  $\text{SO}_4^{2-} = 0.68 \mu\text{g}/\text{mL}$ , LOQ for  $\text{SO}_4^{2-} = 3.38 \mu\text{g}/\text{mL}$ ). Determination of the absolute amounts of  $\text{SO}_3^{2-}$  and  $\text{SO}_4^{2-}$  requires the observed concentrations of corresponding ions to be equal or more than LOQ.

Sample	mass (mg)	$\text{SSA}_{\text{BET}}$ ( $\text{m}^2/\text{g}$ )	LOD for $\text{SO}_3^{2-}$ ( $\mu\text{g}/\text{m}^2$ )	LOQ for $\text{SO}_3^{2-}$ ( $\mu\text{g}/\text{m}^2$ )	Amount of $\text{SO}_3^{2-}$ ( $\mu\text{g}/\text{m}^2$ )	LOD for $\text{SO}_4^{2-}$ ( $\mu\text{g}/\text{m}^2$ )	LOQ for $\text{SO}_4^{2-}$ ( $\mu\text{g}/\text{m}^2$ )	Amount of $\text{SO}_4^{2-}$ ( $\mu\text{g}/\text{m}^2$ )
Gobi	136.2	$10.5 \pm 2.0$	0.45	0.90	< LOD	0.95	4.73	14.1
Gobi	138.5	$10.5 \pm 2.0$	0.44	0.88	< LOD	0.94	4.65	14.8
Gobi	139.5	$10.5 \pm 2.0$	0.44	0.87	< LOD	0.93	4.62	16.5
Gobi	126.2	$10.5 \pm 2.0$	0.48	0.97	< LOD	1.03	5.10	14.4
Gobi	144.5	$10.5 \pm 2.0$	0.42	0.84	< LOD	0.90	4.46	15.5
Gobi	124.2	$10.5 \pm 2.0$	0.49	0.98	< LOD	1.04	5.18	17.2
Average								15.4
STD								1.3
%RSD								8.4
Hagavavn	116.8	$4.5 \pm 1.1$	1.22	2.44	< LOD	2.59	12.86	< LOD
Hagavavn	113.0	$4.5 \pm 1.1$	1.26	2.52	< LOD	2.67	13.26	6.1 < LOQ
Hagavavn	125.4	$4.5 \pm 1.1$	1.13	2.27	< LOD	2.41	11.98	4.6 < LOQ
Hagavavn	113.5	$4.5 \pm 1.1$	1.25	2.51	< LOD	2.66	13.24	7.6 < LOQ
Hagavavn	190.0	$4.5 \pm 1.1$	0.75	1.50	< LOD	1.59	7.91	< LOD
Hagavavn	110.6	$4.5 \pm 1.1$	1.29	2.57	< LOD	2.73	13.58	5.9 < LOQ
Hagavavn	505.4	$4.5 \pm 1.1$	0.28	0.56	< LOD	0.60	2.97	1.6 < LOQ
Average								NA
STD								NA
%RSD								NA

sulfates in  $\mu\text{g}/\text{mL}$  recorded after extraction of 113.5 mg sample (1.95  $\mu\text{g}/\text{mL}$ ) is the same as on the 505.4 mg sample (1.86  $\mu\text{g}/\text{mL}$ ) suggests that sulfates are not coming from Hagavavn sample. A small amount of sulfates determined in Hagavavn and Gobi dust samples could have also come from 1% Formalin extracting solution that contains traces of sulfate impurities. The amount of sulfates in 1% Formalin solution was measured at 1  $\mu\text{g}/\text{mL}$ , which is under LOQ limit. The lack of sulfates on the surface of Hagavavn volcanic dust might be explained by the fact that sulfates were dissolved from the surface of the natural sample by rain or surface water, as the sample is coming from the lava field formed about 4000 years ago and is subjected to fluctuating water levels [27,34]. As for Gobi dust, it displayed a considerable amount of sulfates averaging at  $15.4 \pm 1.3 \mu\text{g}/\text{m}^2$ . Interestingly, method reproducibility for extraction and quantification of sulfates on the surface of Gobi dust was evaluated at 8.4 %RSD for 6 samples, which is three times lower than 23.6% RSD for sample preparation and extraction reproducibility determined earlier for seven Hagavavn samples used for validation of “kinetics study” protocol (see section 3.4, Table 6). In addition, one should keep in mind that 8.4% RSD for Gobi samples was calculated based on average amount of  $\text{SO}_4^{2-}$  of  $15.4 \mu\text{g}/\text{m}^2$ , while higher average of  $29.0 \mu\text{g}/\text{m}^2$  was used for calculation of 23.6% RSD for Hagavavn samples. The improvement in method reproducibility for “environmental sampling”

most certainly comes from the fact that no artificial ageing was performed.

### 3.6.2. Application of the method to aged samples

In the next step, following “kinetics study” protocol samples of 134.0 mg of Hagavavn and 115.0 mg of Gobi dusts were exposed to 175 ppm of gaseous  $\text{SO}_2$  for 1 h at room temperature and under 30% RH. After extraction, the amount of sulfites formed on the surface was calculated at  $54.4 \pm 6.5 \mu\text{g}/\text{m}^2$  ( $\mu\text{g}$  of sulfites per  $\text{m}^2$  specific surface area) for Hagavavn and  $27.0 \pm 3.2 \mu\text{g}/\text{m}^2$  for Gobi desert dust (Fig. 7). In the study of Maters et al. the amount of sulfites measured by ion-chromatography on the surface of laboratory-generated volcanic glass samples exposed to 60 ppb  $\text{SO}_2$  for a couple of minutes varied from  $10 \mu\text{g}/\text{m}^2$  for the glass of rhyolitic composition to  $63 \mu\text{g}/\text{m}^2$  on the surface of glass of trachybasaltic composition [9]. In this respect the amount of sulfites on the surface of Hagavavn basaltic volcanic dust agrees well with that measured on the surface of laboratory-generated glass samples of trachybasaltic composition. However, the direct comparison of the results is difficult due to fact that the above-mentioned studies were performed under low-pressure, 0% humidity of Knudsen cell reactor [9].

The amount of sulfates formed after 1 h ageing was estimated at  $25.2 \pm 6.1 \mu\text{g}/\text{m}^2$  ( $\mu\text{g}$  of sulfate per  $\text{m}^2$  specific surface area) for Hagavavn and  $53.4 \pm 12.8 \mu\text{g}/\text{m}^2$  for Gobi desert dust. Note, that blank subtraction of  $15.4 \pm 1.3 \mu\text{g}/\text{m}^2$  ( $\mu\text{g}$  of sulfates per  $\text{m}^2$  specific surface area) was applied to quantify the amount of sulfates formed on Gobi dust during laboratory ageing. From this experiment it is evident that after 1 h of  $\text{SO}_2$  exposure volcanic dust accumulates a higher amount of sulfites than desert dust and a lower amount of sulfates. From earlier studies it was proposed that  $\text{SO}_2$  gas reacts on the surface of the volcanic dust and forms sulfites or bisulfites, which are then converted to sulfates [20,22]. It is possible that certain mineralogical compounds on the surface of Gobi desert dust are contributing to a more efficient conversion of sulfites to sulfates. A larger sample distribution would be required to confirm the trend and elucidate how the surface chemical composition may influence the respective kinetics of sulfites and sulfates.

The amounts of  $\text{SO}_3^{2-}$  and  $\text{SO}_4^{2-}$  ions expressed in ( $\mu\text{g}/\text{m}^2$ ) were also expressed in terms of the number of  $\text{SO}_3^{2-}$  and  $\text{SO}_4^{2-}$  ions per centimeter squared of dust and percent monolayer they form (see Table 9). The number of molecules needed to form a monolayer were calculated to be  $5.75 \times 10^{14}$  molecule  $\text{cm}^{-2}$  for sulfites and  $4.22 \times 10^{14}$  molecule  $\text{cm}^{-2}$

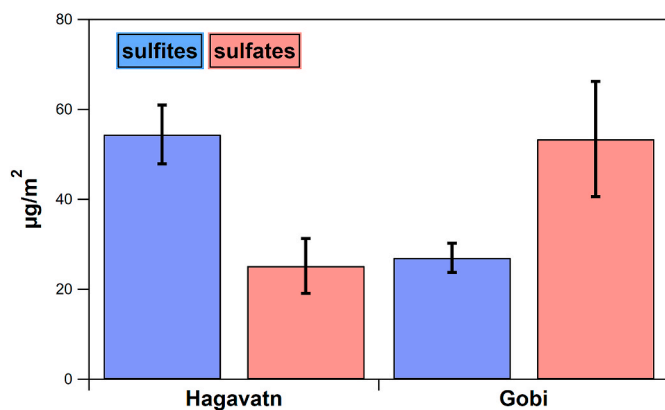


**Fig. 7.** Amount of sulfites and sulfates on the surface of Hagavavn volcanic dust and Gobi desert dust formed after ageing with 175 ppm  $\text{SO}_2$  gas.

**Table 9**

Sulfite and sulfate coverage on the surface of Hagavtn and Gobi dusts expressed in terms of (i) micrograms of  $\text{SO}_3^{2-}/\text{SO}_4^{2-}$  per meter squared of dust ( $\mu\text{g}/\text{m}^2$ ), (ii) number of  $\text{SO}_3^{2-}/\text{SO}_4^{2-}$  ions per centimeter squared of dust ( $N_{\text{molecules}}/\text{cm}^2$ ), and (iii) percent monolayer sulfates and sulfites occupy. The number of molecules needed to form a monolayer were calculated to be  $5.75 \times 10^{14}$  molecule  $\text{cm}^{-2}$  and  $4.22 \times 10^{14}$  molecule  $\text{cm}^{-2}$  for sulfites and sulfates respectively.

Dust	$\text{SO}_3^{2-}$ ( $\mu\text{g}/\text{m}^2$ )	$\text{SO}_3^{2-}$ ( $N_{\text{molecules}}/\text{cm}^2$ )	% monolayer Sulfite Surface Coverage (lower limit)	$\text{SO}_4^{2-}$ ( $\mu\text{g}/\text{m}^2$ )	$\text{SO}_4^{2-}$ ( $N_{\text{molecules}}/\text{cm}^2$ )	% monolayer Sulfate Surface Coverage (lower limit)
Hagavtn	$54.4 \pm 6.5$	$(4.1 \pm 0.5) \times 10^{13}$	7%	$25.2 \pm 6.1$	$(1.6 \pm 0.4) \times 10^{13}$	2.8%
Gobi	$27.0 \pm 3.2$	$(2.0 \pm 0.2) \times 10^{13}$	3.5%	$53.4 \pm 12.8$	$(3.3 \pm 0.8) \times 10^{13}$	7.8%

for sulfates. These values are consistent with the values reported for surface density of sorptive sites on mineral oxides, ca.  $3 \times 10^{13}$ – $5 \times 10^{14}$  sites  $\text{cm}^{-2}$  [35]. It should be noted that the experimental monolayer coverage should be assumed to be lower than the theoretical because the molecules are not expected to pack together perfectly and because the degree of their interactions with various surface sites is not the same [36, 37]. The shape of the molecules and hindering interactions would render some of the active sites on the surface inaccessible. Knowing the number of molecules needed to form a monolayer and the amount present on the surface, percent monolayer coverage was calculated. Accordingly, in terms of a molecular coverage the sulfites occupy about 7% of the available area on the surface of Hagavtn and 2.8% on the surface of Gobi dust, while sulfates occupy 3.5% of the calculated monolayer on Hagavtn and 7.8% on the Gobi dust. We can thus calculate that about 90% of space is still free and available for the formation of sulfites/sulfates and the reaction can continue. Note that this is a very rough approximation. Considering that not all surface sites are available for interactions with  $\text{SO}_2$  the percent space available most probably represents less than 90%.

To evaluate how relevant the artificial ageing is to the processes encountered in real atmosphere, results obtained after a 1-h laboratory ageing of Gobi dust with 175 ppm  $\text{SO}_2$  were compared to the field measurements of sulfates performed during a severe dust storm in China. Similarly, results from Hagavtn ageing were compared to leachate measurements of ashes coming from Stromboli volcano in Italy and Soufriere Hills Volcano, Montserrat.

In spring of 2002 a dust storm originating from Gobi desert in Mongolia and Taklimakan desert in western China spread over China, Korea and Japan [38]. On March 20 2002, the dust peak concentrations over Beijing reached  $10.9 \text{ mg}/\text{m}^3$  (mg of dust per  $\text{m}^3$  of air) [38]. Using the same particle matter concentrations as the ones reported over Beijing and the specific surface area of Gobi dust determined in the current study ( $10.5 \text{ m}^2/\text{g}$ ), our results of  $53.4 \pm 12.8 \mu\text{g}/\text{m}^2$  of sulfates on the surface of Gobi dust correspond to  $6.07 \pm 1.43 \mu\text{g}/\text{m}^3$  ( $\mu\text{g}$  of sulfates present in  $1 \text{ m}^3$  of gas), considering a dust density of  $10.9 \text{ mg}/\text{m}^3$  as reported by Sun et al. [38]. This result is on the same order of magnitude than the volume concentration of sulfates determined from Ion Chromatography analysis of airborne samples: from 18 to  $19 \mu\text{g}/\text{m}^3$  [38]. As for the samples of volcanic origin, Bagnato et al. measured the amount of sulfates on the surface of ash coming from Stromboli volcano, Italy. The results showed a vast variability from 7 to  $55,000 \mu\text{g}/\text{g}$  ( $\mu\text{g}$  of sulfates per g of volcanic sample) [39]. High variability in the amount of sulfates in ash leachates was noted by Edmonds et al. (from 34 to  $9280 \mu\text{g}/\text{g}$ ) at Soufriere Hills Volcano, Montserrat [40]. The amount of sulfate per specific surface determined on Hagavtn volcanic dust ( $25.2 \pm 6.1 \mu\text{g}/\text{m}^2$ ), after 1 h ageing, corresponds to  $115 \pm 27 \mu\text{g}/\text{g}$ . ( $\mu\text{g}$  of sulfates per g of dust). Results retrieved from our study fall within the range of concentrations determined by Bagnato et al. and Edmonds et al. [39,40]. Note that for elevated concentrations of sulfates on the surface of volcanic dust, samples can be easily diluted in higher volumes of extraction solution, in our case 1% Formalin.

#### 4. Conclusions

A reversed-phase HPLC method was successfully developed for the assay of sulfites and sulfates on the surface of dust. A method was developed on a 25 mm Restek Ultra Column C18, Particle size:  $5 \mu\text{m}$ , I.D. 4.60 mm column which was dynamically coated with 1.0 mM cetylpyridinium chloride in 7% acetonitrile solution to produce a charged surface as recommended by Zuo et al. [25]. Mobile phase used: 1 mM potassium hydrogen phthalate at pH 6.5 at a flow rate of 1.0 ml/min with negative UV–Vis detection at 255 nm in 15 min. The developed method was validated for the specificity, LOD and LOQ, linearity and range, robustness, injection repeatability and reproducibility for sample preparation and extraction. In addition, the sampling method is easy and fast, and does not require expensive or particularly dangerous solvents. Besides, the extracted solution displays excellent stability, which is very important in remote sampling during geological expeditions. Samples can be extracted on site and analyzed days after sampling, provided they are kept in cool temperature conditions. We would like to stress out that in case of “environmental sampling” the method should only be applied if the sample is believed to be recently subjected to  $\text{SO}_2$  gas and if quantification of sulfites is desired. Due to the conversion of sulfites to sulfates, the former are not expected to stay on the surface of dust for a long time [26]. Examples of missions that could use the method developed could be: identification of sulfites and sulfates on fresh volcanic ash samples following an eruption, identification of sulfites and sulfates in desert dust samples that pass through industrially polluted areas, as well as laboratory investigation of sulfite and sulfate formation on the surface of natural dusts of different origins. Validity of ageing procedure in the reference to natural gas-particle interactions was discussed. The developed method was successfully applied to assay the amount of sulfites and sulfates formed on the surface of Hagavtn and Gobi dusts both in natural environmental settings and after artificial ageing. Sulfates in the amount of  $15.4 \pm 1.3 \mu\text{g}/\text{m}^2$  were detected on the surface of unexposed Gobi dust. As for the laboratory-aged samples, both sulfites and sulfates were detected on the surface of the two dusts. Sulfites were found to be formed in higher quantities on the surface of Hagavtn volcanic dust in comparison with Gobi desert dust sample ( $54.4 \pm 6.5 \mu\text{g}/\text{m}^2$  of  $\text{SO}_3^{2-}$  ion for Hagavtn versus  $27.0 \pm 3.2 \mu\text{g}/\text{m}^2$  of  $\text{SO}_3^{2-}$  ion for Gobi desert dust), while the opposite trend was observed for sulfates ( $25.2 \pm 6.1 \mu\text{g}/\text{m}^2$  of  $\text{SO}_4^{2-}$  for Hagavtn and  $53.4 \pm 12.8 \mu\text{g}/\text{m}^2$  of  $\text{SO}_4^{2-}$  for Gobi desert dust).

#### Author contribution

Darya Urupina: conceptualization, methodology, validation, analysis, investigation, writing - original draft, writing - review and editing; Vincent Gaudion: resources; Manolis N. Romanias: conceptualization, review and editing, supervision, funding acquisition; Marie Verrielle: review and editing; Frederic Thevenet: review and editing, supervision, funding acquisition, visualization.



## Declaration of competing interest

The authors declare that they have no known competing financial interests or personal relationships that could have appeared to influence the work reported in this paper.

## Acknowledgments

This work was achieved in the frame of Labex CaPPA, funded by ANR through the PIA under contract ANR-11-LABX-0005-01, and CPER CLIMBIO project, both funded by the Hauts-de-France Regional Council and the European Regional Development Fund (ERDF). This work was supported by the French national program LEFE/INSU within the framework of INVOC-dust project. Darya Urupina acknowledges IMT Lille Douai for funding her PhD.

## References

- Y. Zuo, J. Hoigné, Evidence for photochemical formation of H<sub>2</sub>O<sub>2</sub> and oxidation of SO<sub>2</sub> in authentic fog water, *Science* 260 (1993) 71–73, <https://doi.org/10.1126/science.260.5104.71>.
- D.S. Stevenson, C.E. Johnson, E.J. Highwood, V. Gauci, W.J. Collins, R.G. Derwent, Atmospheric impact of the 1783–1784 Laki eruption: Part I Chemistry modelling, *Atmos. Chem. Phys.* 3 (2003) 487–507, <https://doi.org/10.5194/acp-3-487-2003>.
- E. Ilyinskaya, A. Schmidt, T.A. Mather, F.D. Pope, C. Witham, P. Baxter, T. Jóhannsson, M. Pfeffer, S. Barsotti, A. Singh, P. Sanderson, B. Bergsson, B. McCormick Kilbride, A. Donovan, N. Peters, C. Oppenheimer, M. Edmonds, Understanding the environmental impacts of large fissure eruptions: aerosol and gas emissions from the 2014–2015 Holuhraun eruption (Iceland), *Earth Planet Sci. Lett.* 472 (2017) 309–322, <https://doi.org/10.1016/j.epsl.2017.05.025>.
- H. He, Y. Wang, Q. Ma, J. Ma, B. Chu, D. Ji, G. Tang, C. Liu, H. Zhang, J. Hao, Mineral dust and NO<sub>x</sub> promote the conversion of SO<sub>2</sub> to sulfate in heavy pollution days, *Sci. Rep.* 4 (2014) 4172, <https://doi.org/10.1038/srep04172>.
- A. Sardar, SO<sub>2</sub> emission control and finding a way out to produce sulphuric acid from industrial SO<sub>2</sub> emission, *J. Chem. Eng. Process Technol.* (2015), <https://doi.org/10.4172/2157-7048.1000230>, 06.
- H.T. A/S HQ, Sulfuric acid | H<sub>2</sub>SO<sub>4</sub> | Haldor Topsoe (n.d.) (accessed June 3, 2020), <https://www.topsoe.com/processes/sulfuric-acid>.
- A. Jawad, A. Al-Dallal, Simulation of a wet sulfuric acid process (WSA) for utilization of acid gas separated from Omani natural gas, *Al-Khwarizmi Eng. J.* 9 (2013) 58–69.
- Y. Zuo, Light-induced formation of hydroxyl radicals in fog waters determined by an authentic fog constituent, hydroxymethanesulfonate, *Chemosphere* 51 (2003) 175–179, [https://doi.org/10.1016/S0045-6535\(02\)00803-2](https://doi.org/10.1016/S0045-6535(02)00803-2).
- E.C. Maters, P. Delmelle, M.J. Rossi, P.M. Ayris, Reactive uptake of sulfur dioxide and ozone on volcanic glass and ash at ambient temperature, *J. Geophys. Res.* Atmos. 122 (2017) 10077–10088, <https://doi.org/10.1002/2017JD026993>.
- M. Ullerstam, R. Vogt, S. Langer, E. Ljungstrom, The kinetics and mechanism of SO<sub>2</sub> oxidation by O<sub>3</sub> on mineral dust, *Phys. Chem. Chem. Phys.* 4 (2002) 4694–4699, <https://doi.org/10.1039/b203529b>.
- A.L. Goodman, P. Li, C.R. Usher, V.H. Grassian, Heterogeneous uptake of sulfur dioxide on aluminum and magnesium oxide particles, *J. Phys. Chem. A* 105 (2001) 6109–6120, <https://doi.org/10.1021/jp004423z>.
- E. Harris, B. Sinha, S. Foley, J.N. Crowley, S. Borrmann, P. Hoppe, Sulfur isotope fractionation during heterogeneous oxidation of SO<sub>2</sub> on mineral dust, *Atmos. Chem. Phys.* 12 (2012) 4867–4884, <https://doi.org/10.5194/acp-12-4867-2012>.
- P.M. Ayris, A.F. Lee, K. Wilson, U. Kueppers, D.B. Dingwell, P. Delmelle, SO<sub>2</sub> sequestration in large volcanic eruptions: high-temperature scavenging by tephra, *Geochimica et Cosmochimica Acta.* <https://doi.org/10.1016/j.gca.2013.02.018>, 2013, 110 58–69.
- D. Schmauss, H. Keppler, Adsorption of sulfur dioxide on volcanic ashes, *Am. Mineral.* 99 (2014) 1085–1094, <https://doi.org/10.2138/am.2014.4656>.
- E. Bagnato, A. Aiuppa, A. Bertagnini, C. Bonadonna, R. Cioni, M. Pistolesi, M. Pedone, A. Hoskuldsson, Scavenging of sulphur, halogens and trace metals by volcanic ash: the 2010 Eyjafjallajökull eruption, *Geochem. Cosmochim. Acta* 103 (2013) 138–160, <https://doi.org/10.1016/j.gca.2012.10.048>.
- X. Zhang, G. Zhuang, J. Chen, Y. Wang, X. Wang, Z. An, P. Zhang, Heterogeneous reactions of sulfur dioxide on typical mineral particles, *J. Phys. Chem. B* 110 (2006) 12588–12596, <https://doi.org/10.1021/jp0617773>.
- J.W. Adams, D. Rodriguez, R.A. Cox, The uptake of SO<sub>2</sub> on Saharan dust: a flow tube study, *Atmos. Chem. Phys.* 5 (2005) 2679–2689, <https://doi.org/10.5194/acp-5-2679-2005>.
- T. Kojima, P.R. Buseck, Y. Iwasaka, A. Matsuki, D. Trochline, Sulfate-coated dust particles in the free troposphere over Japan, *Atmos. Res.* 82 (2006) 698–708, <https://doi.org/10.1016/j.atmosres.2006.02.024>.
- C.R. Usher, H. Al-Hosney, S. Carlos-Cuellar, V.H. Grassian, A laboratory study of the heterogeneous uptake and oxidation of sulfur dioxide on mineral dust particles, *J. Geophys. Res.* 107 (2002) 4713, <https://doi.org/10.1029/2002JD002051>.
- D. Urupina, J. Lasne, M.N. Romanias, V. Thiery, P. Dagsson-Waldhauserova, F. Thevenet, Uptake and surface chemistry of SO<sub>2</sub> on natural volcanic dusts, *Atmos. Environ.* 217 (2019) 116942, <https://doi.org/10.1016/j.atmosenv.2019.116942>.
- C.S. Witham, C. Oppenheimer, C.J. Horwell, Volcanic ash-leachates: a review and recommendations for sampling methods, *J. Volcanol. Geoth. Res.* 141 (2005) 299–326, <https://doi.org/10.1016/j.jvolgeores.2004.11.010>.
- T. Wang, Y. Liu, Y. Deng, H. Fu, L. Zhang, J. Chen, Emerging investigator series: heterogeneous reactions of sulfur dioxide on mineral dust nanoparticles: from single component to mixed components, *Environ. Sci.: Nano* 5 (2018) 1821–1833, <https://doi.org/10.1039/C8EN00376A>.
- Y. Zuo, J. Zhan, T. Wu, Effects of monochromatic UV-visible light and sunlight on Fe(III)-Catalyzed oxidation of dissolved sulfur dioxide, *J. Atmos. Chem.* 50 (2005) 195–210, <https://doi.org/10.1007/s10874-005-2813-y>.
- R.C. Sullivan, S.A. Guazzotti, D.A. Sodeman, K.A. Prather, Direct observations of the atmospheric processing of Asian mineral dust, *Atmos. Chem. Phys.* 7 (2007) 1213–1236, <https://doi.org/10.5194/acp-7-1213-2007>.
- Y. Zuo, H. Chen, Simultaneous determination of sulfite, sulfate, and hydroxymethanesulfonate in atmospheric waters by ion-pair HPLC technique, *Talanta* 59 (2003) 875–881, [https://doi.org/10.1016/S0039-9140\(02\)00647-1](https://doi.org/10.1016/S0039-9140(02)00647-1).
- Y. Michigami, K. Ueda, Sulphite stabilizer in ion chromatography, *J. Chromatogr. A* 663 (1994) 255–258, [https://doi.org/10.1016/0021-9673\(94\)85252-9](https://doi.org/10.1016/0021-9673(94)85252-9).
- D. Baratoux, N. Mangold, O. Arnalds, J.-M. Bardintzeff, B. Platevoet, M. Grégoire, P. Pinet, Volcanic Sand in Iceland: diverse origins of aeolian sand deposits revealed at Dyngjúsundur and Lambahraun, Iceland, *Earth Surf. Process. Landforms* 36 (2011) 1789–1808, <https://doi.org/10.1002/esp.2201>.
- X. Wang, M.N. Romanias, F. Thévenet, A. Rousseau, Geocatalytic uptake of ozone onto natural mineral dust, *Catalysts* 8 (2018) 263, <https://doi.org/10.3390/catal8070263>.
- N. Joshi, M.N. Romanias, V. Riffault, F. Thevenet, Investigating water adsorption onto natural mineral dust particles: linking DRIFTS experiments and BET theory, *Aeolian Res.* 27 (2017) 35–45, <https://doi.org/10.1016/j.aeolia.2017.06.001>.
- M.N. Zeineddine, M.N. Romanias, V. Gaudion, V. Riffault, F. Thévenet, Heterogeneous interaction of isoprene with natural Gobi dust, *ACS Earth Space Chem* 1 (2017) 236–243, <https://doi.org/10.1021/acsearthspacechem.7b00050>.
- K. Kovacs, R. McIlwaine, K. Gannon, A.F. Taylor, S.K. Scott, Complex behavior in the Formaldehyde–Sulfite reaction, *J. Phys. Chem. A* 109 (2005) 283–288, <https://doi.org/10.1021/jp0464324>.
- M.N. Zeineddine, M.N. Romanias, V. Riffault, F. Thévenet, Heterogeneous interaction of various natural dust samples with isopropyl alcohol as a probe VOC, *J. Phys. Chem.* (2018), <https://doi.org/10.1021/acs.jpca.8b02034>.
- J. Lasne, M.N. Romanias, F. Thevenet, Ozone uptake by clay dusts under environmental conditions, *ACS Earth Space Chem* 2 (2018) 904–914, <https://doi.org/10.1021/acsearthspacechem.8b00057>.
- O. Arnalds, P. Dagsson-Waldhauserova, H. Olafsson, The Icelandic volcanic aeolian environment: processes and impacts — a review, *Aeolian Res.* 20 (2016) 176–195, <https://doi.org/10.1016/j.aeolia.2016.01.004>.
- D. Kulkarni, I.E. Wachs, Isopropanol oxidation by pure metal oxide catalysts: number of active surface sites and turnover frequencies, *Appl. Catal. Gen.* 237 (2002) 121–137, [https://doi.org/10.1016/S0926-860X\(02\)00325-3](https://doi.org/10.1016/S0926-860X(02)00325-3).
- P.K. Hudson, M.A. Zondlo, M.A. Tolbert, The interaction of methanol, acetone, and acetaldehyde with ice and nitric acid-doped ice: implications for cirrus clouds, *J. Phys. Chem. A* 106 (2002) 2882–2888, <https://doi.org/10.1021/jp012718m>.
- L. Diaz, C.M. Liauw, M. Edge, N.S. Allen, A. McMahon, N. Rhodes, Investigation of factors affecting the adsorption of functional molecules onto gel silicas. 1. Flow microcalorimetry and infrared spectroscopy, *J. Colloid Interface Sci.* 287 (2005) 379–387, <https://doi.org/10.1016/j.jcis.2004.09.039>.
- Y. Sun, G. Zhuang, Y. Wang, X. Zhao, J. Li, Z. Wang, Z. An, Chemical composition of dust storms in Beijing and implications for the mixing of mineral aerosol with pollution aerosol on the pathway, *J. Geophys. Res.: Atmosphere* 110 (2005), <https://doi.org/10.1029/2005JD006054>.
- E. Bagnato, A. Aiuppa, D. Andronico, A. Cristaldi, M. Liotta, L. Brusca, L. Miraglia, Leachate analyses of volcanic ashes from Stromboli volcano: a proxy for the volcanic gas plume composition? *J. Geophys. Res.: Atmosphere* 116 (2011) <https://doi.org/10.1029/2010JD015512>.
- M. Edmonds, C. Oppenheimer, D. Pyle, R. Herd, Rainwater and Ash Leachate Analysis as Proxies for Plume Chemistry at Soufriere Hills Volcano, Montserrat, vol. 213, Geological Society Special Publication, 2003, pp. 203–218, <https://doi.org/10.1144/GSL.SP.2003.213.01.12>.





## Summary

This thesis investigates the interactions of sulfur dioxide (SO<sub>2</sub>) gas with Icelandic Volcanic Dusts. Five natural volcanic dust samples were used for the study: Hagavatn, Mýrdalssandur, Maelifellssandur, Dyngjusandur and Eyjafjallajökull.

The heterogeneous interactions of gas-phase SO<sub>2</sub> with volcanic dusts are investigated using a number of complimentary techniques. Temporal profiles of SO<sub>2</sub> uptake and, more precisely, the steady state uptake coefficients have been determined experimentally. These are important kinetic parameters that can be implemented in models. Mechanisms of formation of various surface species resulting from the interactions of SO<sub>2</sub> with the surface of dusts are proposed. A new method for quantification of surface sulphur species has been developed and validated. This method can now be used both for further laboratory investigations and in field measurements.

It is evidenced that the interactions of SO<sub>2</sub> gas with the volcanic dust is a long continuous process. The products formed on the surface are stable and definitely influence the mineral particle properties. It is evidenced that the interactions of SO<sub>2</sub> gas and volcanic particles are highly influenced by humidity and by UV light. The influence of surface composition also plays an important role especially at levels of humidity equal or lower than 30% RH. This work emphasizes the importance of using relevant natural dust samples in order to study the heterogeneous atmospheric phenomena involving natural solid particles.

## Résumé

Ces travaux de thèse portent sur l'étude des interactions du dioxyde de soufre (SO<sub>2</sub>) gazeux avec des poussières volcaniques islandaises. Ils intègrent cinq échantillons naturels de poussières volcaniques: Hagavatn, Mýrdalssandur, Maelifellssandur, Dyngjusandur and Eyjafjallajökull.

Les interactions hétérogènes entre SO<sub>2</sub> et les poussières volcaniques sont abordées avec plusieurs techniques expérimentales complémentaires. Les profils temporels associés à la capture de SO<sub>2</sub>, caractérisés par les coefficients de capture en régime stationnaire ont été renseignés expérimentalement. Ces paramètres sont des données d'importance pour les modèles atmosphériques. Des mécanismes réactionnels décrivant la formation des espèces de surface résultant de l'interaction de SO<sub>2</sub> avec la surface des poussières sont proposés. Une nouvelle méthode analytique permettant l'extraction et la quantification d'espèces soufrées de surface a été développée et validée. Cette méthode est à présent disponible tant pour l'étude de processus hétérogènes en laboratoire que pour la caractérisation d'échantillons de terrain.

Il a été mis en évidence que l'interaction de SO<sub>2</sub> avec les poussières volcaniques est un processus de long terme. Les produits formés en surface sont stables et influencent les propriétés des particules minérales. Il a été démontré expérimentalement que l'humidité relative présente une influence marquée sur la capture et la transformation de SO<sub>2</sub>. La composition de surface des particules minérales est aussi un élément clé, particulièrement pour des humidités relatives inférieures à 30%. Enfin, ces travaux montrent l'importance d'avoir recours à des échantillons minéraux naturels pour assurer une bonne représentativité des études portant sur les processus atmosphériques hétérogènes impliquant des particules minérales.